Spring 5-15-2016

A Quantitative Genetic Analysis of Craniofacial Variation in Baboons

Jessica Lynn Joganic
Washington University in St. Louis

WASHINGTON UNIVERSITY IN ST. LOUIS

Department of Anthropology

Dissertation Examination Committee:
Erik Trinkaus, Chair
James Cheverud
Allan Larson
Jane Phillips-Conroy
Richard Smith

A Quantitative Genetic Analysis of Craniofacial Variation in Baboons

By
Jessica L. Joganic

A dissertation presented to the
Graduate School of Arts & Sciences
of Washington University in
partial fulfillment of the
requirements for the degree
of Doctor of Philosophy

May 2016
St. Louis, Missouri

TABLE OF CONTENTS

LIST OF FIGURES

LIST OF TABLES

ACKNOWLEDGMENTS

They say it takes a village to raise a child. It takes no less than that to bring a dissertation to fruition. I have an amazing support network of friends, family, mentors, and colleagues. I could not have done this without each and every one of them. My committee members deserve special recognition for the guidance and feedback they have provided me throughout the dissertation completion process. In particular, Jim Cheverud provided me with the essential tools and resources necessary to complete this project, without which none of this would have been possible. Erik Trinkaus was a patient and supportive mentor, and knowing he was always in my corner made all the difference. Finally, Allan Larson's constructive criticism and revisions were essential in helping my drafts mature into a final product.

Completing this research is only one step along my journey through the academic jungle. The only reason I embarked on such an expedition was that John Lynch, Gary Schwartz, Mark Spencer, and Brian Verrelli,.my exceptional undergraduate mentors, saw in me a potential I did not know existed and encouraged my explorations of the natural world.

My dissertation is a component of a much larger collaboration, The HOMININ Project. The early efforts of the co-PIs (Jim Cheverud, Joan Richtsmeier, Jeffrey Rogers, Alan Walker, and Ken Weiss) paved the way for my research. In addition, I must thank the Southwest National Primate Research Center at the Texas Biomedical Research Institute for providing me with the necessary sample of baboons and corresponding genetic map data. Tony Comuzzie, Michael Mahaney, and Charles Peterson were particularly helpful resources.

The National Science Foundation provided funding in the form of a Graduate Research Fellowship and a Doctoral Dissertation Improvement Grant, both of which made my work possible. PEO International and Washington University in St. Louis contributed as well.

I am incredibly thankful for the wonderful members of the Cheverud Lab, my fellow comrades-in-arms: Elizabeth Atkinson, Devin Dobias, Madeline Keleher, Jane Kenney-Hunt, Eliz Norgard-Bean, and Arthur Porto. I would be remiss if I did not particularly and profusely thank Heather Lawson for training me in the ways of SOLAR and all things bioinformatic.

Colleagues at WUSTL contributed substantially to my development as an anthropologist, scientist, and member of The Academy. Although there are many individuals to whom I am indebted, Tab Rasmussen was one of the most important for teaching me how to ask the right questions and that there are more animals to study than just primates. In addition, the administrative staff has earned my gratitude, especially Elaine Beffa for helping me navigate the inanities of Fastlane, Kirsten Jacobson and Kathleen Cook for having all the answers, and Anne Olendorff for working her magic. Malcolm Tobias of the Center for High Performance Computing gave me support where none would, Frank Brooks was absolutely invaluable for having taught me Python, and Kim Trinakus consistently offered the soundest statistical advice.

There are many friends and acquaintances in Saint Louis who have helped me along the way, but I cannot name them all without sacrificing a forest for paper. I would especially like to thank a few: Aaron Bunse and Ali Heller, my photographers par excellence; Kenny Chiou, who provided me with all the pdfs and answers to R; Rachel Dunn, my dissection companion and role model since the beginning; Sarah Lacy, my cohort comrade-in-arms; Blaine Maley and Christopher Shaffer for riding the emotional roller coaster of graduate school with me; Joe Orkin, to whom I am indebted for rescuing me in the 11th hour; Anna Weyher, my fellow traveler on the graduate school journey; John Willman, my intellectual sounding board; Nick Wiltse, for his unerring patience and genuine kindness; Jacob Winter, who kept me grounded and helped me see the forest for the trees. Finally, Louis Wall and I single-handedly kept the local coffee shops in business and Yusuf Daneshyar was there for me when I needed it most.

Words cannot adequately express my gratitude to Ian Anderson, David Chancellor, Yusuf Daneshyar, Doug Munsch, Eric O'Rear, and John Oungst for creating a place for me to call home. Additionally, I must thank Mary Jane Acuña, Marisa Davenport-Shepard, David Nguyen, Natalie Rolwes, and Nick Wiltse for keeping me physically and psychologically healthy.

Erin Dumbauld, Stephanie Gresham, Audrey Martyn, and Kali Rapp are my oldest friends. They have listened to me rant (mostly) and rave (rarely) about monkeys, bones, and graduate school for far too many years. They never judged me for working with flesh-eating beetles or filling my wardrobe with skeleton-patterned apparel. They are beautiful, strong, intelligent women and I am incredibly lucky to call them my friends.

I owe countless cans of tuna to my cats, who were never stingy with their fluffy hugs and sandpaper kisses of support, even though they have only known me recently as The One Who Deposits Food in Our Bowls. My dog deserves all the pets for tirelessly keeping me company, even though that involved a lot of laying around and watching me type.

Finally, without a doubt, my family has been the most important factor in my success: my siblings with mathematical and computer aid and my parents with financial and emotional assistance through 24 years of education. My father instilled in me a curiosity about heads early on that has since become my intellectual passion. I am eternally grateful to my mother for editing countless drafts of manuscripts on esoteric (i.e., boring) topics over the years and for teaching me independence.

Jessica L. Joganic

Washington University in St. Louis

May 2016

Dedicated to my parents
for their unconditional support

ABSTRACT OF THE DISSERTATION

A Quantitative Genetic Analysis of Craniofacial Variation in Baboons

By

Jessica L. Joganic

Doctor of Philosophy in Anthropology

Washington University in St. Louis, 2016

Professor Erik Trinkaus, Chair

This dissertation is an explication of baboon craniofacial variation and its genetic basis. Intraspecific variation is the result of input from and complex interactions among genetic information, functional demands, and developmental processes. The relative effect of each of these on craniofacial variation, as well as the degree of inter-trait covariance, determines whether traits can respond to selection and what that response might look like. Using a sample of pedigreed baboons, I quantify craniofacial variation to address specific questions regarding the distribution and magnitude of phenotypic, genetic, and environmental variation patterns. In addition, I identify regions of the genome containing genetic variants contributing to the production of craniofacial variation. Results demonstrate that the genotype-phenotype map for craniofacial variation in this sample is characterized by patterns of inter-trait correlation that are structured by both functional and developmental relationships. Much of the additive genetic variation is likely pleiotropic and contributes to craniofacial variation regionally, rather than globally. The degree to which regions are affected by this genetic variation lacks patterning, indicating that no one particular region is any more evolvable than others. Finally, after accounting for differences in cranial size among individuals, both the magnitude of genetic correlations and the amount of additive genetic variation decreases, which suggests selection for body size played a major role in craniofacial evolution in baboons.

Our ignorance of how genotypes produce phenotypes is, I believe, the greatest gap in our understanding of the evolutionary process and it is a huge gap indeed.

Douglas J. Futuyuma, 1979

Let Science interrogate the sphinx, let her expose the intricate and delicate mechanism by which the mask is operated, let her even show that the human face, with all its charms, is but the end of a long line of useful improvements upon simple beginnings.

William K. Gregory, 1965

CHAPTER ONE
INTRODUCTION

1.1 Introduction

In an effort to shift the focus of developmental and evolutionary biology from the preformationist paradigm of DNA as "blueprint," Lewontin (2000) wrote:

> There exists, and has existed for a long time, a large body of evidence that demonstrates that the ontogeny of an organism is the consequence of a unique *interaction* [emphasis added] between the genes it carries, the temporal sequence of external environments through which it passes during its life, and random events of molecular interactions within individual cells.

He emphasized the necessity of understanding morphological evolution and phenotypic variation among individuals in light of how genetic variation is modulated through developmental processes and in different environments. The genotype-phenotype map (GP-map)—the complex relationship among genes, environments, and developmental processes that produces an organism—is not 1:1 (Wagner and Zhang, 2011).

Our reluctance to incorporate this truth into research designs contributes to continued inadequacy in explaining phenotypic variation, despite tremendous technological advances in our ability to ascertain genetic variation. Essentially, if we want to know why two individuals of the same population look different from one another, a description of their genetic differences is simply not enough. Gregory Mendel, Charles Darwin, and many other observant individuals have noted a correlation between the appearance of parents and offspring (i.e., that physical characteristics are *heritable*), but we lack a general understanding of the genetic basis for such correlations. Therefore, one of the most important research goals for evolutionary biology and biological anthropology going forward is to explicate the GP-map of fitness-related complex traits (e.g., Mackay, 2001; Eichler et al., 2010).

Change occurs in a group of organisms because there is variation among individuals in a phenotype and some leave more offspring than others, not because each individual

undergoes a parallel developmental transformation during the course of its lifetime (Fracchia and Lewontin, 1964). Understanding this *variational* model of change requires explicating the genetic architecture (i.e., GP-map) of the phenotype in question. In a quantitative genetic framework, variation in complex phenotypes, which do not demonstrate Mendelian inheritance and tend to be normally distributed in a population, is affected by alleles segregating at many genomic loci, each of which has a small effect on the phenotype and is sensitive to environmental variation (Flint and Mackay, 2009). The genetic architecture of a complex phenotype describes how quantitative genetic variation contributes to phenotypic variation within a population and, thus, provides a record of past events of variational change as well as predictions of response to potential future scenarios (Hansen, 2006).

Mammalian crania are composites of many such complex phenotypes. Due to its relatively well-established fossil record and obvious importance for organismal survival and reproduction, the craniofacial complex has been the subject of much evolutionary and developmental biology research. Human crania have been uniquely reorganized to include an enlarged neural vault, a short upright face, and a flexed cranial base (Fig. 1.1), and these trends are well studied in a variety of contexts: structural (e.g., Moss and Young, 1960; Lieberman et al., 2000; Bastir et al., 2008), ontogenetic (e.g., Enlow, 1968; Bastir and Rosas, 2004; Mitteroecker et al., 2004), functional (e.g., Ravosa et al., 2000; Strait et al., 2008), genetic (e.g., Hu and Helms, 1999; Wilkie and Morriss-Kay, 2001), and evolutionary (e.g., Weidenreich, 1947; Rightmire, 1993; Schaefer et al., 2004). However, until the more recent adoption of holistic models for craniofacial evolution (e.g., Ackermann and Cheverud, 2004; Bruner, 2007; Bastir, 2008; Mitteroecker and Bookstein, 2008), these unusual morphologies that define human crania

have been studied largely independent of one another, a practice that hinders our efforts to understand their genetic bases, developmental origins, and evolutionary histories.

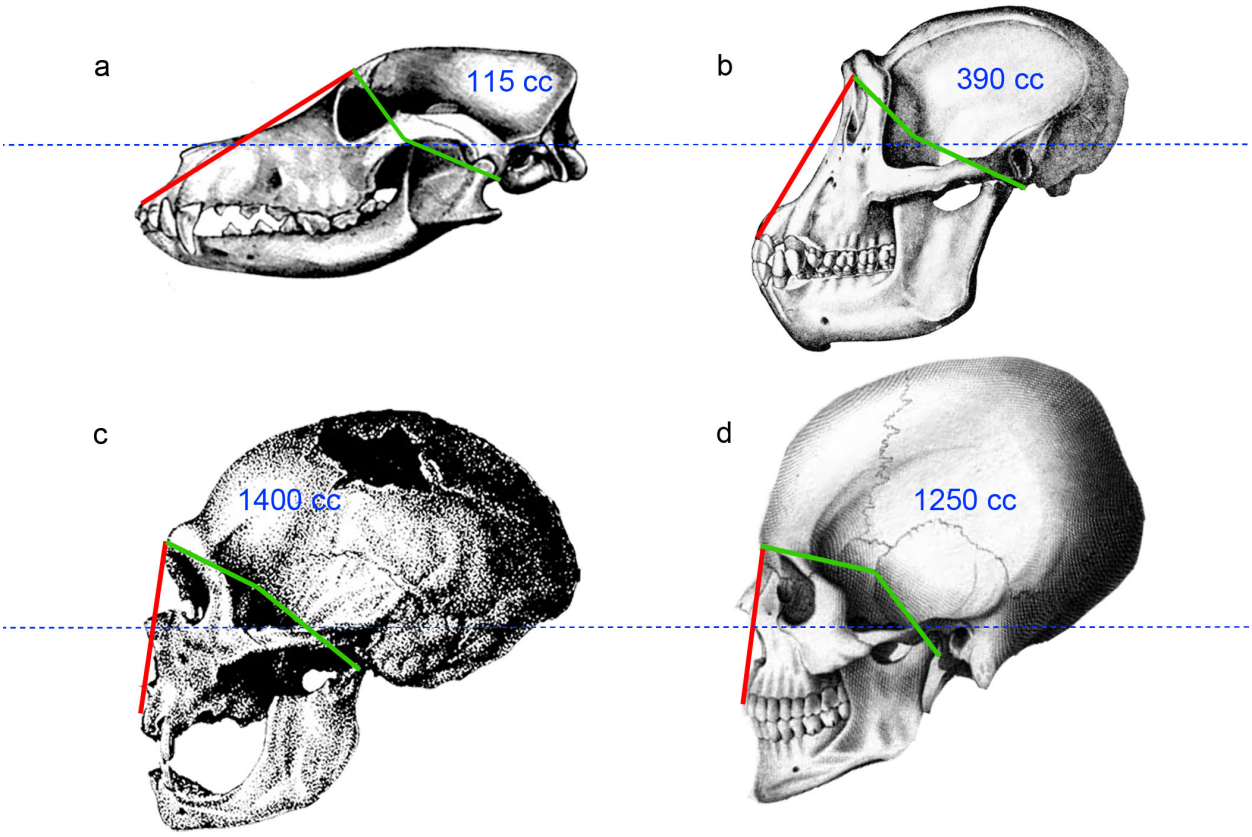

Figure 1.1 The Three Evolutionary Changes that Typify the Human Skull. The first is an increased cranial capacity, indicated here by blue numbers (cubic centimeters, cc). The second is a flexed face, which is typically measured by the angle formed by the intersection of the nasion-prosthion line (red line) and the plane of the Frankfurt horizontal (dashed blue line). The former is a line connecting the point where the internasal suture meets the nasofrontal suture (*nasion*) to the most anterior point in the midline of the maxillary alveolar process (*prosthion*). The latter is a plane passing through the inferior margin of the left orbit (*orbitale*) and the upper margin of both external auditory meati (*porion*). Human crania are characterized by a flexed basicranium, which is measured as the ventral angle between the lines (green lines) connecting nasion to *sella* (the point in the center of the sella turcica, or pituitary fossa) and sella to *basion* (the midpoint on the anterior margin of the foramen magnum). The skulls shown are: (a) dog, *Canis lupus familiaris* (adapted from Romanes, 1910); (b) chimpanzee, *Pan troglodytes* (adapted from Beddard, 1902); (c) Neanderthal, *Homo neanderthalensis* (adapted from Boyle, 1911; cited in Wolpoff, 1980); and (d) human, *Homo sapiens* (adapted from Gordon, 1818). The skull of a dog is provided to represent a non-primate mammal for comparison, but the associated cranial capacity is the average for the grey wolf, *Canis lupus lupus* (Hemmer, 1990).

Many genes have been identified that are both essential for proper craniofacial development and the source of dysmorphology. However, very little is known about the genetic underpinnings of normal craniofacial variation, the material on which selection acts within a framework of variational change. For example, members of the fibroblast growth factor receptor (*FGFR*) gene family induce cell differentiation in developing cranial bones, and point mutations within them can cause premature ossification of cranial sutures, a condition known as craniosynostosis (Wilkie, 1997). However, the potential contribution of these genes to inter-individual craniofacial differences remains a mystery.

The overall objective of this dissertation is to describe and understand the relationship between phenotype and genotype. To do so, I address three main research questions. First, how much does genetic variation contribute to craniofacial variation, and does this contribution differ by anatomical region or scale? Second, what is the relationship between the bony elements surrounding the brain and those supporting the face within different contexts: phenotypic, genetic, developmental, and functional. Lastly, which specific regions of the genome contain this genetic variation, does each genomic region contribute to variation in multiple craniofacial elements, and are individual craniofacial elements affected by genetic variation in multiple genomic regions?

Answering questions such as these requires a large population of interrelated individuals, so such studies cannot easily be conducted in humans or most non-human primates. However, I have curated a large sample of pedigreed non-human primates (baboons, *Papio* spp.) for which genetic data are available, and I have collected morphological data from the sample that allow me to accomplish the goals of this research.

This project unites the fields of genetics and quantitative biology to examine the structure of continuous variation in primate crania and explore its genetic underpinnings. As genetic variation is the basis for evolution, identifying genomic loci underlying trait variation is a necessary step in studying the evolution of complex structures like mammalian crania. Knowledge of this genetic basis and evolutionary history also informs our ability to study the origins of, manage, and treat skull abnormalities and diseases that have clinical and biomedical relevance. Using the information acquired while conducting this research, I formulate hypotheses about both the maintenance of the phenotypic patterns observed in baboon crania and specific candidate genes and regulatory elements that have been involved in their evolution. The hope is that, with increasingly improving genomic resources, genetic techniques, and model primate populations, the work presented in this dissertation can serve as a guide for extending this research into other primate species.

1. 2 Dissertation Outline

Chapter 2 provides a summary of the rationale for utilizing crania to examine evolutionary processes of morphological change and of methods for conducting such research. This chapter includes background information on the baboon model utilized in my research, as well as a brief account of previously conducted research on the phenotypic variation, evolutionary history, and genetic underpinnings of both human and baboon crania. Additionally, I review the specific hypotheses tested in this dissertation. In Chapter 3 I describe general materials used and methods employed in this research. Methods directly related to questions addressed by individual chapters are given in those specific chapters.

Chapter 4 presents estimates of the proportion of heritable craniofacial variation in baboons. I examine the phenotypic and genetic correlations among measures of craniofacial

variation in Chapter 5; doing so can elucidate the role that genetic correlations play in constraining phenotypic evolution, generally, and in affecting the evolvability of baboon crania, specifically. In Chapter 6, I identify regions of the baboon genome likely to contain genetic variants contributing to heritable variation in the craniofacial skeleton. Chapter 7 synthesizes the results from all analyses. It explicates how the results enhance our understanding of: (1) how complex morphological systems evolve, (2) some of the genes responsible for affecting continuous variation in a population of primates, (3) how non-human primate collections can provide robust samples with which to study questions of human evolution, and (4) the selective pressures that may have contributed to shaping some of the craniofacial features we consider to be quintessentially human. Finally, I provide a roadmap for potential next steps to be taken in my research.

CHAPTER TWO
BACKGROUND

2.1 Introduction

With the appearance of chordates possessing a proper brain 525 million years (MY) ago, a protective casing for the organ and its sensory outgrowths (i.e., eyes; vestibulocochlear apparatus; olfactory, auditory, and gustatory nerves; and peripheral nervous system) was necessary. The configuration of early skulls[1], which still largely can be seen in the classes Reptilia, Amphibia, and Osteichthyes today, was complicated as it was composed of many individual bones and cartilages. However, over the past 420 MY of tetrapod evolution, many of the craniofacial bones found in early vertebrates have been progressively eliminated, a phenomenon termed Williston's Law (Gregory, 1965). This resulted in the simplified form exhibited by the class Mammalia today (Fig. 2.1). The processes underlying Williston's Law were able to affect such drastic changes because the bones of the vertebrate head are capable of being modified in both their shape and relationship to one another. Although this trend of craniofacial modification and reorganization is well documented in the fossil record, the processes underlying it are less well understood.

One of our biggest knowledge deficits regarding the craniofacial skeleton is our ignorance of the genetic basis for the production and maintenance of continuous morphological variation. Due to their prevalence, high rates of morbidity, and resulting large impact on global health, much research has been conducted on the underlying genetic mechanisms and developmental origins of craniofacial malformations (CFM). CFMs are among the most common birth defects, with an estimated 35% of congenital anomalies occurring in the head and face

[1] "Skull" refers to the skeleton of the entire head, both lower jaw (mandible) and cranium (face + base + neural vault). Skull applies exclusively to bone but I use "craniofacial" as both a regional and a descriptive term. For the most part, craniofacial and "cranial" are synonymous and I use them interchangeably. However, I preferentially use craniofacial when focusing on aspects of the facial skeleton and/or its relationship to the remainder of the cranium. Occasionally I use "craniodental," but this is almost exclusively in the context of describing paleoanthropology methods in that they focus on analyzing elements of the skeleton that preserve in the fossil record, typically the teeth and denser regions of the skull, such as the mandible, supra-orbital region, and occiput.

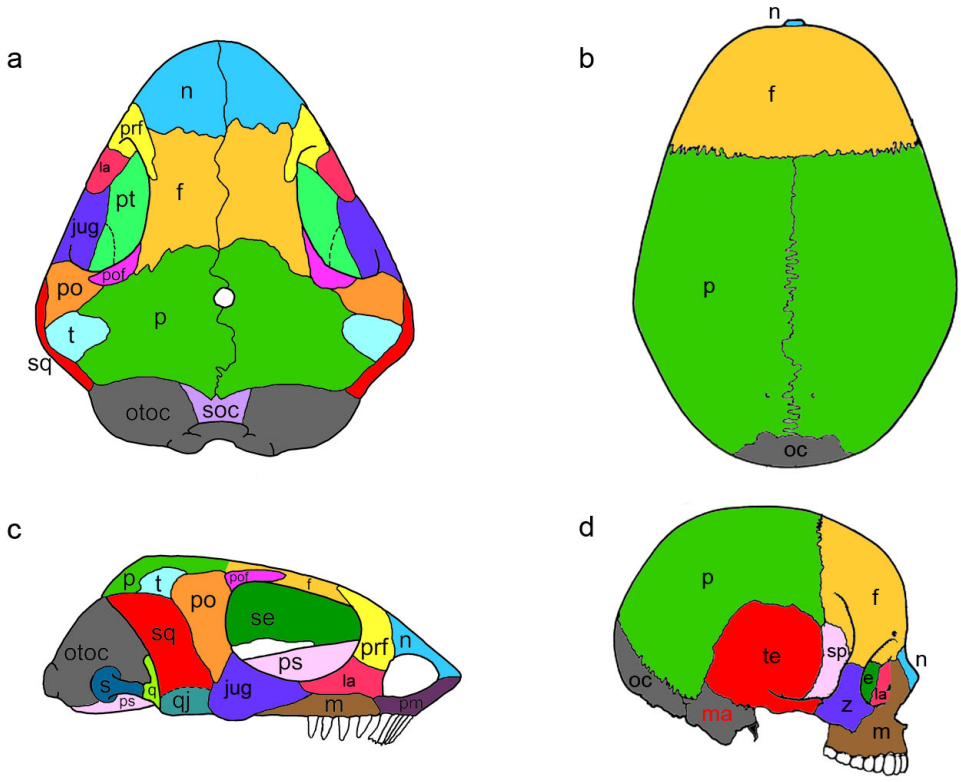

Figure 2.1 Color-Coded Skulls Demonstrating Williston's Law. (a,c) *Batropetes*, a lepospondyl that lived 290-295 MY ago (adapted from Marjanovic and Laurin, 2008) and (b,d) *Homo* (adapted from Aiello and Dean, 2002). Abbreviations: *e*, ethmoid; *f*, frontal; *jug*, jugal (malar); *la*, lacrymal; *ma*, mastoid process *m*, maxilla; *n*, nasal; *oc*, occipital; *otoc*, fusion of prootic, opisthotic, exoccipital, and basioccipital; *p*, parietal; *pm*, premaxilla; *po*, postorbital; *pof*, postfrontal; *prf*, prefrontal; *ps*, parasphenoid; *pt*, pterygoid; *qu*, quadrate; *qj*, quadratojugal; *s*, stapes; *se*, sphenethmoid; *sp*, sphenoid; *soc*, supraoccipital; *sq*, squamosal; *t*, tabular; *te*, temporal; *z*, zygomatic. The mastoid process is colored grey to emphasize its homology with portions of the *otoc*.

(Miettinen et al., 1999). Craniosynostosis (premature fusion of the growing neurocranial bones) and orofacial clefts are the most prevalent CFMs: the incidence of cleft lip and/or palate is 1 in every 600 live births worldwide (WHO, 2002), that of CFMs that do not include orofacial clefts is 1 in 1600 (WHO, 2003), and that of craniosynostosis alone is 1 in ~2500 (Wilkie, 1997). While we have made tremendous progress in the past few decades in understanding the processes of craniofacial development and mal-development, there are still many unanswered questions. For

instance, we do not know if the genes that cause CFMs also contribute to continuous intrapopulation variation. My dissertation research was specifically designed to target this gap in knowledge.

Heads and faces have been fascinating research topics for many years for a variety of reasons. First, primate faces are highly expressive, due to numerous and well-innervated facial muscles (Burrows et al., 2009; see Burrows, 2008 for an excellent review). They are also highly visible, as humans lack the thick facial hair seen in most mammals and the brightly colored facial skin seen in most primates (Santana et al., 2014). Primates are visual specialists (Kremers, 2005), so it comes as no surprise that we are preoccupied with examining the faces around us. Second, our societies are largely structured around attempts to classify objects, conspecifics, and other organisms with which we interact (Bowker and Star, 1999). Our reliance on subtle craniofacial differences to categorize and organize our environments makes sense, given that we have evolved specialized neural components for facial recognition (Parvizi et al., 2012) and recognize faces to the exclusion of other objects from very young ages (Farzin et al., 2012). Finally, for largely anthropocentric reasons, we tend to emphasize the importance of the morphological features we consider to define us as a species over the importance of any other features. Compared to that of other primates, and certainly of other mammals, the organization of and relationship among components of our heads appear unique (see Fig. 1.1).

In the hominin fossil record, the appearance of crania demonstrating various combinations of these characters suggests that hominin cranial evolution is mosaic (Bastir and Rosas, 2005, 2009; Bruner, 2007). In contrast, experimental evidence suggests these characters actually may have co-evolved (Lieberman et al., 2000, 2008; Bastir et al., 2010; Holton et al., 2011). Discerning the nature of the interrelationships among the elements of the

human skull is important for understanding how and why our skulls became different from those of other primates and mammals.

This question has been addressed previously with the use of either morphological or genetic data. Here, I conduct novel research that combines these two lines of evidence into a powerful method for characterizing morphological and genetic variation in the primate cranium. The purpose of this dissertation is to identify genetic variants underlying primate craniofacial variation and evaluate the relationship between patterns of genetic and craniofacial variation. In this chapter, I briefly summarize what is known of craniofacial evolution, describe methods for conducting evolutionary research, and introduce the concept of continuous traits and phenotypic variation. Craniofacial growth, development, and genetic regulation are discussed, particularly in relation to the baboon skull. I then discuss the concepts of morphological integration, modularity, quantitative genetics, and linkage mapping, all of which are employed to address the stated research questions. Finally, I summarize the content of the remainder of the dissertation.

2.2 Craniofacial Diversity

Craniofacial evolution is of interest to many because of the visible breadth of adaptive diversity of cranial form and function (Fig. 2.2), which is all the more impressive for having arisen from evolution's "tinkering" (Jacob, 1977) of elements largely shared by all vertebrates. Elements are shared because conservation of developmental processes has maintained a basic cranial *Bauplan*, or shared assemblage of morphological features (de Beer, 1985), while a complex interplay between genome and environment during development has produced a continuum of intraspecific variation upon which selection can act gradually to modify the skull, or "tinker" in Jacob's (1977) terminology. Arguably, most postcranial elements have changed far less over the past 65 MY, with the possible exception of the distal limb segments: the hands and feet and their homologues. For example, ribs, sacra, femora, and scapulae generally resemble the

Figure 2.2 The Incredible Diversity of Mammalian Craniofacial Morphology. Panels: (a) *Didelphis virginiana*, Order: Didelphimorphia; (b) *Macropus* sp., Diprotodontia; (c) *Dendrohyrax* sp., Hyracoidea; (d) *Dasypus septemcinctus*, Cingulata; (e) *Myotis* sp., Chiroptera; (f) *Panthera leo*, Carnivora; (g) *Tupia glis*, Scandentia; (h) *Lagothrix* sp., Primates; (i) *Agouti paca*, Rodentia; (j) *Oryctolagus cuniculus domesticus*, Lagomorpha; (k) *Eotheroides clavigerum*, Sirenia (photograph permissions: Iyad Zalmout/Michigan-Ann Arbor); (l) *Antidorcas marsupialis*, Artiodactyla; (m) *Caperea marginata*, Cetacea (photograph permissions: Suzann Goldberg/AMNH, O'Leary et al. 2013); (n) *Equus ferus caballus*, Perissodactyla. Unless otherwise stated, photographs by Jessica Joganic. Images not to scale.

homologous elements of other species, even those belonging to orders as distantly related and ecologically divergent as Rodentia and Proboscidea (Fig. 2.3).

One reason for the high degree of evolvability—the ability of a physical structure to change over time in response to environmental stimuli (Houle, 1992; Pigliucci, 2008)—of the mammalian skull is that it houses the overwhelming majority of the sensory systems and thus, is the hard tissue structure through which an organism interacts with and experiences its

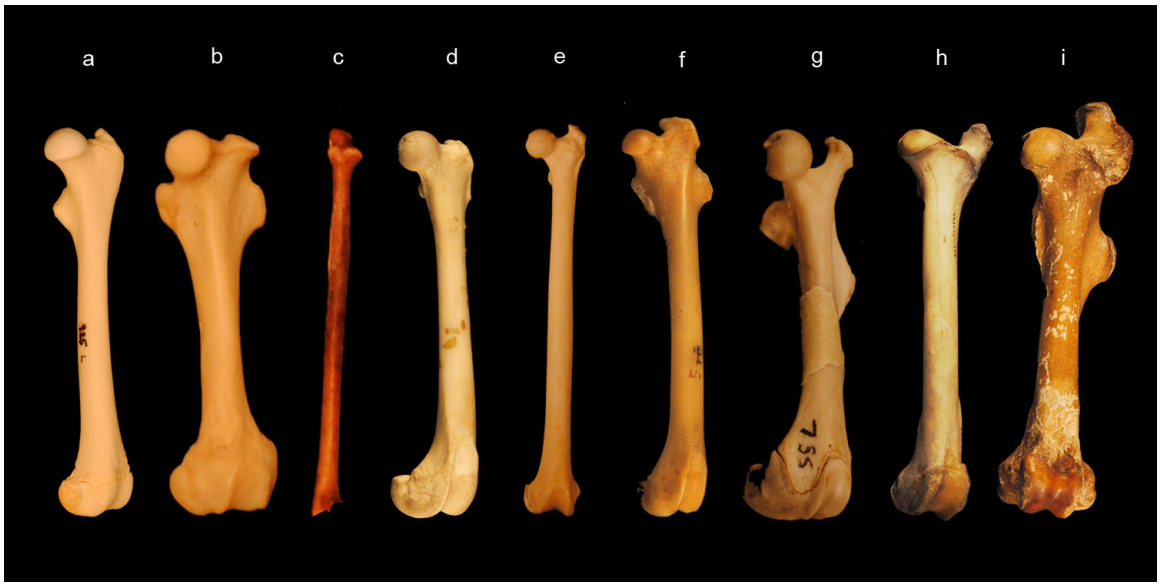

Figure 2.3 The Relative Lack of Morphological Diversity in Mammalian Femora. Despite the very different biomechanical habits among taxa, mammalian femora demonstrate minor evolutionary shape change compared to crania. Panels: (a) *Didelphis virginiana*, Order: Didelphimorphia; (b) *Scalopus aquaticus*, Soricomorpha; (c) *Myotis* sp., Chiroptera; (d) *Neovison vison*, Carnivora; (e) *Colobus guereza*, Primates; (f) *Oryctolagus cuniculus domesticus*, Lagomorpha; (g) *Ondatra zibethicus*, Rodentia; (h) *Antilocapra americana*, Artiodactyla; (i) *Equus africanus asinus*, Perissodactyla. Photographs by Jessica Joganic. Images not to scale.

environment. Consequently, any degree of craniofacial variation among conspecifics has the potential to impact fitness greatly. As long as the variation has a heritable genetic basis—offspring will resemble their parents because the variation can be passed from one generation to the next (Falconer and Mackay, 1996)—elements of the craniofacial skeleton can evolve and, therefore, contribute to species diversification.

Another explanation for the diversity of vertebrate skull forms is that individual elements are integrated, or part of a whole (see *2.5.2 Morphological Integration in the Cranium*). Integration can result from shared developmental origin, a common genetic basis, similarity in function, or any combination of these and other factors. Because complex phenotypes are integrated, modification to any one bony component is likely to affect others (Cheverud, 1982).

As long as the morphological variation is heritable and the result does not have a net negative effect on fitness, adaptive change in one part of the skull can cause a concomitant change in other parts. This concept is called indirect selection (Lande, 1979).

By comparing skull morphology among multiple different taxa that inhabit the same environment or occupy the same ecological niche, we can make inferences about the nature of selective pressures that might produce certain bony configurations. These inferences can be extrapolated back in time, allowing us to form hypotheses about the behavioral regimes and ecological habits of extinct taxa. This can inform us about the evolutionary history of the taxa in question and also increase our general understanding of the morphological adaptation process. However, morphology can change through both direct and indirect selection (as discussed above), neutral evolutionary processes like genetic drift (e.g., Ackermann and Cheverud, 2004; Smith, 2011), and even fail to change or change very little due to the presence of various biological constraints. Therefore, it is important to trace the evolutionary history of such changes. This can be done by examining the fossil record, quantifying inter-trait relationships, and assaying the underlying genetic diversity.

2.2.1 Biological Constraint

Biological constraints are factors that make populations resistant to evolutionary change. One such factor is developmental constraint, which Maynard-Smith and colleagues (1985) define as a “bias on the production of variant phenotypes or a limitation on phenotypic variability caused by the structure, character and composition or dynamics of the developmental system.” In other words, developmental constraints create phenotypes that are canalized, or relatively invariant. Wagner (1988) demonstrates that, even though they limit phenotypic variation, developmental constraints in the presence of phenotypic integration are necessary to facilitate adaptive change

within complex structures, such as vertebrate skulls. This is achieved by concentrating variation with adaptive potential in specific regions of the morphospace for selection to act upon.

Functional constraints limit the range of possible phenotypes to ensure organisms function adequately within their environments. Because organisms are collections of hierarchically-nested, interdependent systems[2], many individual characters are *burdened*, or functionally coupled so that altering one effects both. This concept was developed by Rupert Riedl and attempts to explain the causal mechanisms behind functional and developmental integration in complex structures (see Wagner and Laubichler; 2004; Schoch, 2010). As a result, burdened characters are relatively invariant. For example, all chordates develop a notochord during embryogenesis, even though it is almost universally reduced only to forming the bulk of the nucleus pulposus of the intervertebral discs (Stemple, 2005). The notochord releases the protein sonic hedgehog (*SHH*), which establishes the ventral component of the dorsal-ventral pole in the developing embryo (Echelard et al., 1993). Absence or malformation of the notochord severly hinders proper development in the embryo, and thus, it is a burdened character in chordates.

Both developmental and functional constraints limit the range of phenotypes that can be produced by the genotype, but the final form of biological constraint—stabilizing selection—dictates preferential selection of certain phenotypes, given environmental stability. Stabilizing selection prevents a phenotype from evolving to help ensure organisms remain adapted to a specified niche. A classic example of this is maintainence of the hemoglobin *S* allele in environments where the risk of contracting malaria is high, despite that allele being deleterious

[2] An example of this is that the processes responsible for metabolism and producing ATP (digestive system) affect both the production of neurotransmitters and the excitatory capabilities of neurons (nervous system), which stimulate the muscles (muscular system) of the upper limb (skeletal system) to ingest a sandwich (digestive system).

in non-malarial environments. In contrast, purifying selection removes the allele from those environments where the negative side effects of sickle cell disease far outweigh the risk of malarial infection (Ko et al., 2012).

Properties of a trait that impose biological constraints were often adaptive in the environment in which they initially appeared. However, limiting phenotypic variation can cause phylogenetic inertia, or the tendency for related taxa to share traits because of shared ancestry, rather than adaptation (although the traits themselves may still be adaptive in the taxa). Homoplasy is often the result (see *2.2.4 Methods for Studying Morphological Evolution*), but phylogenetically-informed comparisons among taxa and a thorough understanding of development, function, and integration can often be used to determine its presence.

2.2.2 The Marriage of Morphological and Genetic Methods

Incorporating genetic research into traditional studies of craniofacial morphology is important for three reasons. First, quantitative genetic methods like midparent-offspring regression (see *2.6.5 Methods for Conducting Quantitative Genetic Research*) can determine whether a trait is heritable. Although morphological variation is the result of both genetic and environmental differences among individuals, a trait is not necessarily evolutionarily relevant because that variation is not heritable and, therefore, cannot evolve. For example, prior to establishing hypotheses regarding the adaptive significance of prognathism for increasing gape in cotton-top (*Saguinus oedipus*) relative to saddle-back tamarins (*S. fuscicollis*), Cheverud (1996b) had to first establish that mid-facial length is, indeed, heritable in tamarins.

Second, estimating genetic and phenotypic correlations among traits will resolve the patterns of interdependence within the skull, helping to distinguish between direct and indirect selection; conflating the two can be misleading and inadvertently lend support to flawed adaptive hypotheses. For example, Badyaev and Martin (2000) estimated genetic covariation

patterns in the skull of house finches (*Carpodacus mexicanus*). By establishing that these patterns vary throughout ontogeny, they were able to infer that such ontogenetic variance permitted morphological diversification and compensatory growth for environmental buffering. The authors hypothesized that their results might explain patterns of greater ecological diversity in the species relative to others in the genus.

Finally, identifying genetic variants underlying craniofacial variation provides us with knowledge about some of the molecular pathways that produce a complex morphological structure and allows us to search for genomic signatures of selection, characterize population variation, and test hypotheses about the origin and maintenance of genetic and phenotypic variation. For example, by localizing and characterizing the effect of specific genetic variants on mouse skull characters, Leamy and colleagues (1999) were able to provide support for the genetic independence model, which posits that the phenotypic effects of pleiotropic genes—those having an effect on multiple traits—are limited to groups of integrated traits, which explained the patterns of integration they observed in mouse crania.

2.2.3 Model Organisms in Craniofacial Research

Mice are the traditional mammalian model species and much has been learned about craniofacial growth and development, genetic regulation, and evolution from studying both (inbred and outbred) laboratory lines and natural populations (e.g., Wolf et al., 2005; Hallgrímsson and Lieberman, 2008; Pallares et al., 2014; Maga et al., 2015). The ability to control for environmental heterogeneity, force alleles of interest to fixation via inbreeding, move target genetic sequences onto specific genomic backgrounds, and create knock-out and -in strains makes them an invaluable resource when studying complex phenotypes.

Research on insects, birds, fish, and amphibians has also proven fruitful. For example, transcription factors responsible for body plan segmentation (homeotic/Hox genes), including

development of cranial tissues derived from the branchial arches (see *2.4.1 Craniofacial Embryogenesis*), were first identified in the fruitfly, *Drosophila melanogaster* (see Hughes and Kaufman, 2002 for a good review). Shortly thereafter *Hox* genes were discovered in vertebrates (McGinnis et al., 1984), and cloned in the African clawed toad, *Xenopus levis* (Carrasco et al., 1984), indicating genetic regulation of development, including that of the head, is universal to and highly conserved across taxa diverged for more than 900 MY.

Zebrafish (*Danio rerio*) are ideal for studying craniofacial cellular migrations because differentially stained cells are easily seen through the transparent skin of zebrafish embryos (Mork and Crump, 2015 provide an excellent review of zebrafish research). As a consequence, much has been learned about mammalian ears and jaws from studying the homologous fish pharyngeal arches (see *2.2.4 Methods for Studying Morphological Evolution*). Finally, a series of landmark papers introduced quail-chick chimeras as a method of identifying the embryonic origins of cells composing different craniofacial tissues (e.g., LeDouarin and Tiellet, 1974; Le Lievre et al., 1980; Couly et al., 1993). As a result of their work, we now know skeletal elements located rostral to the notochord (which extends to the sphenoid's sella turcica) are derived from neural crest cells while those caudal to it are paraxial mesoderm in origin (see *2.4.1 Craniofacial Embryogenesis*). This is important for understanding which elements are expected to covary and to be co-affected by genetic variation and developmental perturbation.

In recent years, craniofacial biologists have expanded research into new realms, which has been greatly aided by sequencing of the genomes of non-model organisms, including multiple primate species. One of the more interesting examples is that of the silver fox (*Vulpes vulpes*). Selective breeding experiments for desired behavioral traits have inadvertently produced unexpected changes in the craniofacial skeleton of these foxes that parallel those seen during the domestication of dogs (*Canis lupus familiaris*; Trut et al., 2012). The craniofacial

diversity of dog breeds is extreme, which makes them an excellent taxon in which to study correlated responses to selection and identify candidate genes of major effect on skull form.

Using the Domestic Dog to Answer Evolutionary Questions.

The American Kennel Club recognizes more than 150 dog breeds. The subspecies was domesticated from ancestral populations of the grey wolf (*Canis lupus*), likely around 15,000 years ago (although see Germonpré et al., 2009 and Druzhkova et al., 2013 for evidence possibly placing the event as early as 30,000 years ago), and individual breeds have been artificially selected since then to serve various purposes for humans, from hunting for rats, lions, wolves, and bears to tracking organisms by smell, sight, or sound. As a consequence, the modern dog is an incredibly morphologically diverse species, as evidenced by the degree of both body size and skull shape differences among the various breeds. Dog size can vary in two orders of magnitude (e.g., Chihuahua at 0.5 kg and Great Dane at 50 kg) while the magnitude of cranial diversity is greater between modern breeds than among all wild species in Canidae (Wayne, 1986). Additionally, skull shape differences among dog breeds exceed even the maximal distances observed in species of Carnivora (Drake and Klingenberg, 2010).

The skull morphologies of today's dogs reflect the primary sensory system used by that breed to perform the task for which they were bred historically. Consequently, without even knowing the specifics of a breed's history, one can infer from the form of its skull the traditional job it likely performed. Three main types of skull configurations demonstrate this phenomenon. Sighthounds (e.g., Afghan, Greyhound) tend to have dolichocephalic skulls—the breadth of which is 75-80% shorter than the length—that orient their orbits in such a way to increase their field of vision by up to 20°. Scenthounds (e.g., Beagle, Rhodesian Ridgeback) tend to possess mesaticephalic skulls that are optimized for both sight and smell with a near 1:1 of head to nasal cavity. Finally, catch dogs (e.g., Bulldog, Cane Corso) tend to demonstrate brachycephaly

wherein the breadth of the skull is at least 80% of the length, a configuration built for strength and endurance.

This process of evolutionary inference is most effective when comparisons can be made to the skulls of breeds for which artificial selection histories are known. However, inferences can also be made about historical selective pressures in the absence of breed history. This methodology is powerful and effective in helping elucidate the evolutionary history of extinct taxa as well. With the completion of the dog genome project, we have gained the ability to tie craniofacial shape variation to specific genes (Ostrander and Bustamante, 2012). For example, Schoenebeck et al. (2012) identified a missense mutation in *BMP3* as contributing to the degree of brachycephaly in modern breeds. Bone-morphogenetic proteins (*BMP*s) also contribute to variation in human skulls (see *2.4.4 Summary of Known Craniofacial Genes*), suggesting molecular pathways of craniofacial growth and development have been conserved for ~90 MY.

2.2.4 Methods for Studying Morphological Evolution

The diversity of skull morphology recognized in extant organisms, both within Mammalia and across Vertebrata, highlights the myriad challenges faced by ancestral populations. Most of the mammalian orders are characterized by specific behaviors or phenotypes, many related to the procurement of food resources and often reflected in craniofacial morphology. For example, rodents possess ever-growing incisors for gnawing on hard objects, and carnivores possess carnassials, specialized post-canine teeth for crushing bones and tearing meat (Fig. 2.4). Bats (specifically Microchiropterans) and cetaceans (specifically Odontocetes) have specialized auditory tissues that allow them to utilize biosonar to “visualize” their surroundings and locate prey (Fig. 2.5). In orders where vision is of the utmost importance, such as in Primates, skulls have been modified to enhance visual acuity (e.g., orbital enlargement and convergence, post-orbital closure).

Figure 2.4 Craniodental Adaptations Attributable to Differences in Dietary Niche. Panels: (a) ever-growing incisors in Rodentia (*Erethizum dorsatum*); (b) carnassials in Carnivora (*Canis lupus familiaris*). Photographs by Jessica Joganic.

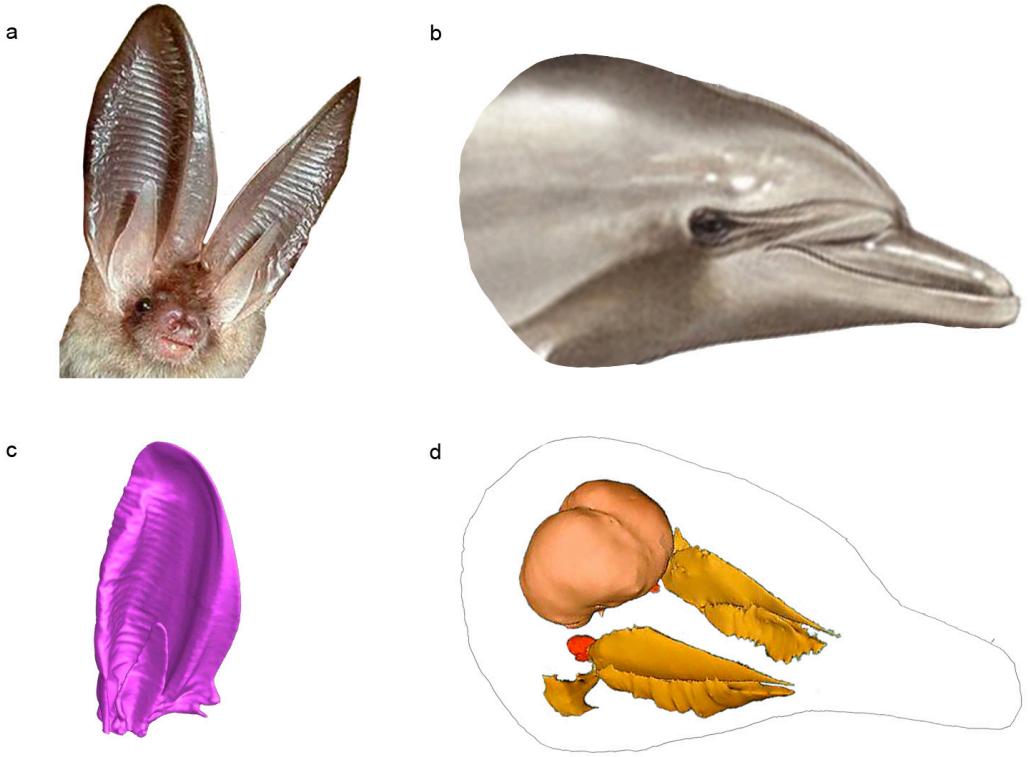

Figure 2.5 Digital Representations of Ear Shape in Bats and Dolphins. Both demonstrate convergence in shape of the auditory tissues due to shared function of echolocation. Panels: (a) Brown long-eared bat (*Plecotus auritus*, Family: Vespertilionidae). Adapted from http://enfo.agt.bme.hu/drupal/node/8246. (b) Common bottlenose dolphin (*Tursiops truncatus*, Family: Delphinidae). Adapted from http://ioniandolphinproject.org/species-guide/common-bottlenose-dolphin/. (c) Digital reconstruction of *Plecotus* pinna. Adapted from Müller et al. (2010). (d) Digital reconstruction of *Tursiops* auditory fats (*yellow*; brain, *pink*; inner ear bones, *red*). Adapted from Ketten and Madin (2005).

However, it is important to remember that present-day morphologies are the result of both adaptive and random processes acting on a population's standing variation (Gould and Lewontin, 1979). As the absence of heritable phenotypic variation precludes selection from acting, understanding the mechanisms by which such variation is produced is as important as exploring evolutionary responses in the phenotype of interest (Wagner, 2014). Biological systems contain historically contingent mechanisms, such as developmental constraints, that suppress or differentially affect the production of variation within a morphological structure (Wagner, 2014). In this way, skull morphology is a manifestation of past selective events that shaped existing population variation, developmental processes that modulate the translation of genetic into phenotypic variation, and unique factors that influence the production of future variation. Traditionally, there are two methods for studying both *how* and *why* skull morphology evolved into its current form, which I describe in greater detail next.

Phylogenetic Comparisons Among Species

Phylogenetic comparative methods are incredibly informative for studying character evolution. The general idea is to compare genetically distinct taxa that have similar ecologies and/or behaviors (Nunn, 2011) to explore the morphospace for a particular phenotype. A morphospace is an *n*-dimensional representation of the possible forms an organismal phenotype can take (Mitteroecker and Huttegger, 2009). A phenotype is any physical characteristic of an organism that can be measured (e.g., humeral length, circulating insulin levels, rates of tissue repair, volume of a copulation call), while a genotype is the underlying genetic makeup of that organism, which contributes to the form or expression of the corresponding phenotype (Lynch and Walsh, 1998). This comparative approach is a sort of "natural experiment" that sheds light on the underlying phenotypic and/or genetic constraints on skull diversification (Robinson and Diamond, 2010); these constraints dictate the limits and surface pattern of a morphospace.

By comparing the ontogeny, morphology, genetic basis, phylogenetic position of a trait, and/or the ecological conditions under which it evolves, one can determine whether two taxa share the same trait due to homology or homoplasy. Homology is the presence of the same trait in two taxa that was also present in their most recent common ancestor (MRCA) while homoplasy is the presence of the same trait in two taxa when their MRCA did not possess that trait (Lankester, 1870; cited in Hall, 2013). In other words, in the former case, similarity is due to common descent and, in the latter, it is due to independent evolution.

Homoplastic traits can be the result of convergence, arising through independent evolution but incorporating different constituent elements to produce a similar resultant structure; parallelism, which is similar to and often confused with convergence[3], but the independently evolved elements forming the homoplastic trait are the same in the various taxa being considered; and atavism, reversion to an ancestral condition (Patterson, 1988; Hall, 2007). If the relationship among elements of a whole is patterned in such a way that selection for one specific character always produces similar concomitant changes in the others (Lande, 1979; Gould and Lewontin, 1979), parallelism will result. This translates to a morphospace that is canalized (Waddington, 1942), or directed along specific trajectories, even if those trajectories are suboptimal (Björklund, 1996; Hansen, 2006).

For example, the homoplastic skull morphology of aardvarks (Order: Tublidentata), pangolins (Order: Pholidota), and anteaters (Order: Pilosa) illustrates the features beneficial for a diet primarily composed of termites and other colonial insects (Fig. 2.6). However, whether

[3] According to Nelson (1978), the most important factor in assessing homology is determining whether the traits are similar due to shared mode of development. This is the first of Patterson's (1982) three tests of homology: similarity, congruence, and conjunction. The congruence test posits that a homology is a synapomorphy and, therefore, any structure not shared by a monophyletic group cannot be a homology (Wiley, 1975). A potential pair of homologous structures fails the conjunction test if they are both discovered within a single organism. According to Patterson (1982), the first two tests can be used to distinguish between cases of parallelism and convergence: structures that pass the similarity test but fail the congruence test are parallelisms while those that fail both tests are convergences.

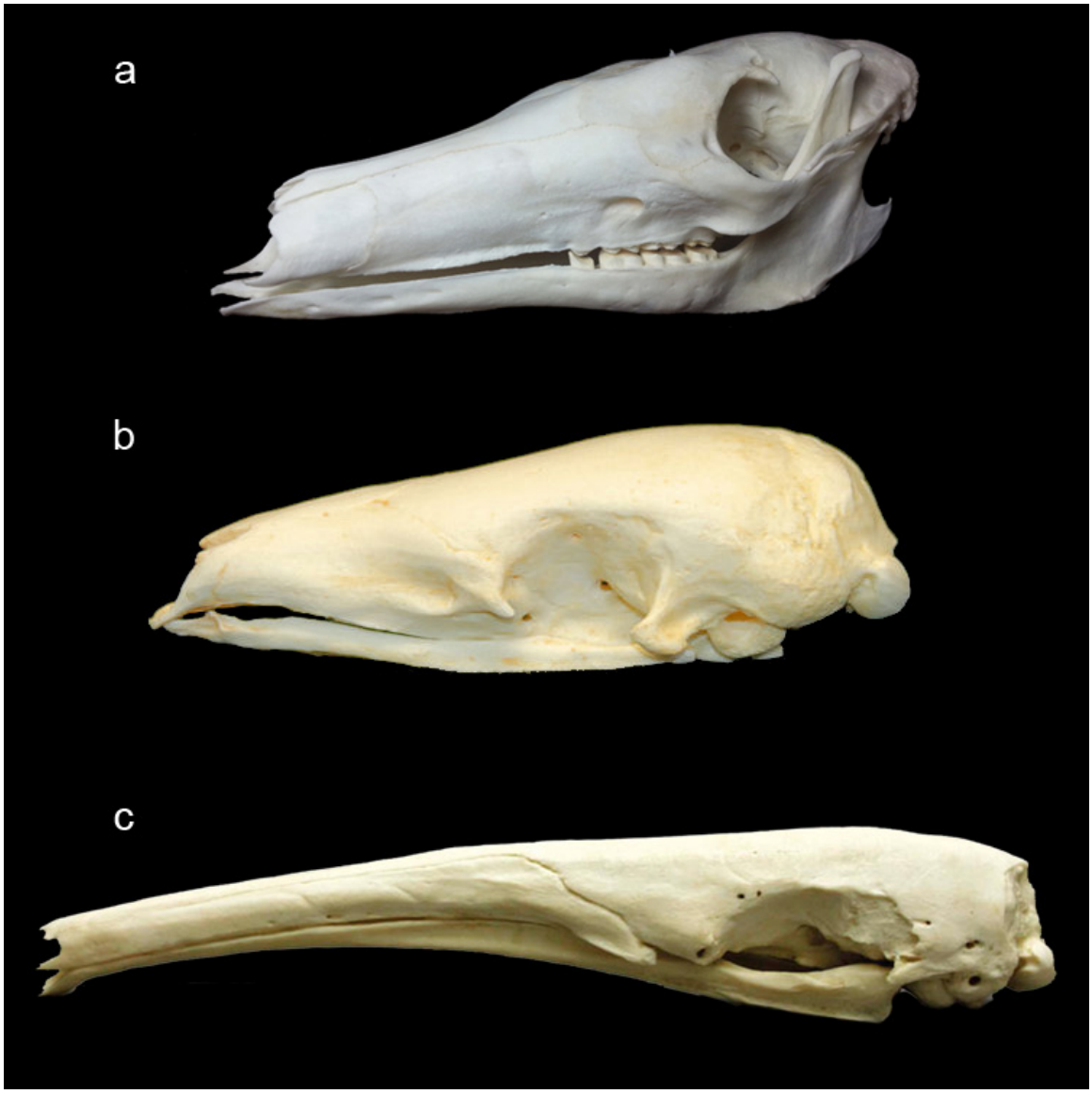

Figure 2.6 Homoplasy of Craniodental Form Due to Shared Dietary Niche. All three taxa exhibit elongated rostra, are partially or completely edentulous, and have greatly reduced orbital regions due to their decreased reliance on vision to aquire their insect prey. Panels: (a) *Orycteropus afer*, Order: Tublidentata. Adapted from: http://www.skullstore.ca/aardvark/. (b) *Manis javonica,* Pholidota. Adapted from: http://www.valleyanatomical.com/catalog/product_info.php?cPath=1_222&products_id=1102&osCsid=nvf2d80naosegcvo9sd6ljr760. (c) *Myrmecophaga tridactyla*, Pilosa. Adapted from: http://www.boneclones.com/BC-011.htm. Images not to scale.

this is a case illustrating convergence, rather than parallelism, cannot be assessed without a detailed study of the specific tissues involved, their embryonic origins, and their relationships to one another in both ancestral and sister taxa. A second example, the monophyletic family of lungless salamanders (Plethodontidae), demonstrates atavism, as some members of the clade revert back to the ancestral condition of persistence of a bipartite premaxilla throughout ontogeny from the derived adaptation of possessing a fused premaxilla that aids in larval feeding (Wake and Larson, 1987).

Homoplasy is a common scourge of the phylogeneticist, whose goal is to reconstruct evolutionary branching patterns, as mistaking homoplastic traits for homologous ones implies a closer relationship between taxa than is actually the case. However, when trying to determine the various conditions under which a specific trait might be adaptive, identifying homoplastic traits may be more informative as there is little risk of confounding adaptive signal with phylogenetic inertia (see Blomberg and Garland, 2002 for a good review of the origin and evolution of this concept), although developmental canalization must still be ruled out (see *2.2.1 Biological Constraint*). For example, similarity in both morphological and behavioral traits of prosimians (Infraclass: Placentalia, Order: Primates) and some phalangerids (Infraclass: Marsupialia, Order: Diprotodontia) has been used to support arguments that the earliest primates filled an ecological niche similar to that occupied by these marsupials: a diet composed of angiosperms and insects that are visually predated in terminal tree branches (Rasmussen and Sussman, 2007). In this way, hypotheses about the selective pressures experienced by populations of extinct taxa can be formed by drawing analogies with the observed phenotypes of extant taxa.

One of the favored methods of distinguishing between these two explanations in a comparative research program is to quantify phenotypic variation in a population and determine

how correlations among characters shape the morphospace. Porto and colleagues (2009) estimated the pattern and magnitude of correlations among measures of skull variation across Mammalia. They discovered that the pattern of craniofacial variation is largely conserved among taxa, but the magnitude of the correlations producing this pattern differs significantly among species. Correlations among characters theoretically have a tremendous impact on phenotypic evolution, as they can bias evolutionary trajectories and constrain the potential for exploration of morphospace. This research demonstrates the utility of the comparative method for addressing questions about how phenotypic evolution proceeds.

Pedigree Analysis Within Populations

The alternative method for studying morphological constraints is to measure them directly within a population. Interdependence of skull measures is quantified as phenotypic covariance. The axes of covariance are the morphological dimensions along which diversification can occur or along which variation is constrained, depending on the effect of that covariance on organismal fitness. Understanding how variation within a complex structure, like a mammalian skull, is patterned is crucial for accurately inferring and reconstructing ecobehavioral environments, both in the present and the past.

Identifying morphological covariance also informs the construction of phylogenies, both within taxa (population trees) and among them (species trees). Certain traits may contain phylogenetic signals (i.e., they evolved only under neutral evolution/genetic drift), while others may retain signatures of selection (i.e., were adapted for a specific purpose), although these are not mutually exclusive scenarios (e.g., Ackermann and Cheverud, 2004). Still others could be evolutionary “hitchhikers” linked to phenotypes under selection but not actually the targets of selection themselves (Barton, 2000). Finally, there are also examples of phenotypes that are

exaptations evolved for a purpose different than that for which they are presently utilized (Gould and Vrba, 1982).

Determining which of these three scenarios, or a combination thereof, is best reflected in the observed patterns of morphological variation is often difficult but necessary for distinguishing among different evolutionary hypotheses. For example, Marroig and colleagues (2004) had difficulty in establishing a clear link between patterns of craniofacial variation in sakis (*Pithecia*, order Primates) and those expected to result from selection on functionally relevant traits and, therefore, concluded genetic drift was likely the main driving force in the genus' diversification.

2.2.5 The Role of Continuous Variation in Evolutionary Process

We have made tremendous progress in the latter part of the 20th and early 21st centuries in understanding the genetic underpinnings and developmental origins of skull morphology (see Sherwood and Duren, 2015 for a good review). However, this knowledge is primarily limited to craniofacial malformations (e.g., cleft lip/palate, hemifacial microsomia, craniosynostosis), particularly those of Mendelian inheritance. Additionally, most of the research producing this knowledge is conducted in model organisms not particularly closely related to humans (e.g., fruitfly, mouse, zebrafish, chicken; Sherwood and Duren, 2015). Very little is known about *continuous* variation in the mammalian skull. In terms of evolution, it is continuous population variation—typically encoded by many genes of small effect (Robertson, 1967) that interact with both each other and the environment—that is important.[4] Consequently, these genes are difficult to identify in genome wide association (GWA) studies, one of the more widely used methods, due to the stringent significance thresholds required to deal with the issue of multiple

[4] Richard Goldschmidt offered an alternative view of the process of morphological evolution with his theory of "hopeful monsters," or saltational evolution. He believed that "the change from species to species is not a change involving more and more additional atomistic changes, but a complete change of the primary pattern or reaction system into a new one, which afterwards may again produce intraspecific variation by micromutation" (Goldschmidt, 1940).

comparisons (Jones et al., 2005; Manolio et al., 2009). They also cannot easily be identified via linkage analyses (see *2.6.5. Methods for Conducting Quantitative Genetic Research*). The large sample sizes of pedigreed families, which in human studies are typically trios and not multi-generational families due to our long life spans and late age at first reproduction, required to provide the power necessary to identify such small gene effects are difficult to achieve (Schork, 1997; Altmüller et al., 2001). Despite these drawbacks, a few studies have successfully estimated the heritability of various craniofacial dimensions (e.g., Harris and Johnson, 1991; Martínez-Abadías et al., 2009; Šešelj et al., 2015) and identified genes putatively underlying human craniofacial variation (e.g., Liu et al., 2012; Fatemifar et al., 2013).

In addition to GWA, another popular methodology used to address questions of phenotypic evolution is genome wide selection scanning (GWSS). In GWSS studies, signatures of selection identified throughout the genome are used to locate genes that demonstrate either more (positive/diversifying selection) or less (negative/purifying selection) variation than a putatively neutrally evolving region (e.g., Chapman et al., 2008; Akey et al., 2010). This represents a bottom-up approach because genes are identified for which the functional link to a phenotype is not well understood or the trait under selection is not known at all (Schork, 1997). Although this characteristic is problematic, such bottom-up approaches have been favored since the completion of the Human Genome Project, and even more so since the online publication of the 1000 Genomes Project, because they are relatively inexpensive and can be completed rather quickly (Nielsen et al., 2005; Oleksyk et al., 2010).

The contrasting method is top-down in that phenotypes of interest are identified *a priori* and the genetic variants contributing to morphological variation are located via linkage or association mapping (Liu, 1998; Zhang et al., 2013). Once identified, these genes can be further interrogated for signatures of selection, linkage, and/or association via fine mapping at that

genomic locus. Because the genomic region being tested is smaller than it would be in most bottom-up analyses, fewer multiple comparisons are performed and less stringent significance thresholds can be set (Nicolae et al., 2005; Donnelly, 2008). Consequently, the power to detect significant deviations from neutrality is increased. Ultimately, this approach can be more informative for evolutionary studies because the genetic variant(s) identified has already been demonstrated to contribute to (or at least be linked to a nearby genetic variant that contributes to) phenotypic variation. Despite the utility of bottom-up methods, they are less popular because they require amassing data from very large samples of pedigreed individuals, which can be expensive, time-consuming, and limiting in the choice of study organism (Risch, 2000). Here, I use a sample of baboons and a top-down approach that combines traditional landmark-based morphometric research with quantitative genetic parameter estimation and linkage mapping to explore morphological and genetic variation in the craniofacial complex.

2.3 Papionina Fossil Record

Certain aspects of their life history and evolution make baboons appropriate animals to use in this project. First, their relatively short interbirth intervals and fast growth rates (Altmann et al., 1977; Smuts and Nicolson, 1989; Hill et al., 2000) ensure adequate sample sizes for conducting quantitative genetic analyses. Second, they make excellent models for examining evolutionary questions due to their extensive fossil record (Jablonski, 1993; Williams et al., 2007) in which are documented trends in craniofacial evolution that can be used to assign character polarity and provide context for the morphological variation observed in my sample. To provide a framework for understanding how primates fit into and differ from the larger picture of mammalian evolution and craniofacial diversity, I briefly summarize the primate fossil record. I then place baboons within this narrative and highlight the trends within the clade that make them particularly interesting to use for craniofacial research.

2.3.1 A Brief Overview of Primate Evolution

Although more research has been conducted on the growth and development of canid, murid, and fish skulls, primate craniofacial morphology has also been studied in an attempt to reconstruct the evolutionary forces that acted upon our order. Primates evolved from small, arboreal mammals during the Paleocene (Van Valen and Sloan, 1965; Johnston and Fox, 1984; Clemens, 2004; Chester et al., 2015) of either North America (Bloch et al., 2007) or Asia (Fu et al., 2002; Beard, 2006). They were called plesiadapiforms (although, see below), resembled tree shrews (order Scandentia; e.g., Sargis, 2004) and/or colugos (order Dermoptera; e.g., Janečka et al., 2007), and behaved much like possums (order Marsupilia; e.g., Rasmussen and Sussman, 2007). These earliest proto-primates had hands and feet adapted to an arboreal lifestyle. One genus, *Carpolestes*, even had hands dexterous enough for grasping and tactility (Bloch and Boyer, 2002; Sargis et al., 2007; Kirk et al., 2008), which likely allowed them to exploit arboreal, fruit/insect-eating niches that were abandoned with the mass extinctions marking the Cretaceous-Tertiary boundary (e.g., Szalay, 1968; Kay and Cartmill, 1977; Eriksson et al., 2000; Sussman et al., 2013).

Primate morphology evolved in a mosaic fashion, which makes fossil classification, character polarity determination, and evolutionary reconstruction difficult. For example, some individuals do not include plesiadapiforms in the primate order because they do not consider postcranial adaptations to an arboreal lifestyle to be enough to merit inclusion (Kay et al., 1990; Beard, 1990) and because plesiadapiform dental morphologies are substantially different from those of early primates (Rose, 1994). The hard-tissue specializations observable in the cranium (e.g., orbital convergence and frontation, post-orbital bar/closure, orbital enlargement) that we associate with primates' increased reliance on vision did not appear in the fossil record until later. The adapids and omomyids of the Eocene were the first "euprimates" because they

demonstrate these orbital autopomorphies, as well as nails instead of claws on their digits, another primate trait (Rose et al., 2012; although see Gingerich, 1990 and Sigé et al., 1990 for arguments that late Paleocene *Altiatlasius* of North Africa and Asia is the earliest euprimate). These two euprimate groups are most likely ancestors of modern day strepsirrhines and tarsiers, respectively (e.g., Simons, 1972; Szalay, 1976; Beard et al., 1988; Dagosto, 1988; although see Schwartz and Tattersall, 1985).

Definitive anthropoids appear in the fossil record in the late Eocene of the Fayum Depression in Egypt (Seiffert et al., 2010a,b; Seiffert, 2012). The oldest family of fossil anthropoids, Parapithecidae, contains genera demonstrating primitive anthropoid features retained by New World monkeys (NWM), which some consider evidence that these taxa likely predate the platyrrhine-catarrhine split (Fleagle and Simons, 1995; Fleagle, 2013). The younger families Oligopithecidae and Propliopithecidae appeared in the Late Eocene and Early Oligocene, respectively. The exact nature of their phylogenetic relationship is debated but they are likely stem catarrhines (Rasmussen and Simons, 1992; Seiffert et al., 2000; Williams et al., 2010; Seiffert, 2012; but see Kay et al., 1997).

The age of the hominoid-cercopithecoid split is debated but recent fossil finds support a molecular divergence date of 25-30 MY ago (Steiper and Young, 2006). The earliest catarrhine fossil genera are *Rukwapithecus* and *Nsungwepithecus*, dated to ~25 MY ago (Stevens et al., 2013). The former is considered a stem hominoid within Proconsuloidea, an extensive superfamily of apes that radiated throughout the Old World in the Late Oigocene-Middle Miocene (e.g., Walker, 1997; Cote et al., 2014). It is the sister taxon to our own superfamily, Hominoidea. Dental morphology of *Nsunwepithecus* aligns it with the Early Miocene family of basal cercopithecoids, Victoriapithecidae (von Koenigswald, 1969; Benefit, 1999; Benefit and McCrossin, 1997; Miller et al., 2009).

Sparse though it is, the Early Miocene fossil record is dominated by victoriapithecids. However, by the Late Miocene cercopithecid fossils become more numerous and more diversified, likely in response to drastic aridification (e.g., Behrensmeyer et al., 1992; Janis, 1993; Cerling et al., 1997; Blue et al., 2006; Seiffert, 2012), as their bilophodont molars and primarily terrestrial locomotor patterns are particularly adapted to these climatic conditions. The more arboreal apes—with thin-enameled teeth adapted to moist, enclosed woodlands of the Early Miocene—did poorly as the forests were replaced with mixed and open environments (e.g., Temerin and Cant, 1983; Behrensmeyer et al., 1992; Michel et al., 2014; Marigó et al., 2014). Ape populations declined as a result of being unable to compete with the more generalist Old World monkey (OWM) genera (Gebo, 2014). The fossil record of one OWM family in particular, Papionina, is directly relevant to the content of this dissertation, so it will be discussed in greater detail below.

Hominins[5] diverged from the clade of surviving hominoids around 7-8 MY ago (Langergraber et al., 2012) and the genus *Homo* appeared ~2 MY ago (e.g., Wood and Collard, 1999; Ferring et al., 2011; Pickering et al., 2011; Leakey et al., 2012; but see Caswell et al., 2008; Villmoare et al., 2015). Hominin fossil specimens display a mosaic of autapomorphic traits, some adaptive and others likely attributable to random evolutionary processes (e.g., Ackermann and Cheverud, 2004; Schroeder et al., 2014). The most commonly cited craniodental autopomorphies of the primate order that are demonstrated to the extreme in *Homo* are: flexed basicranium, relatively enlarged neurocranium, and orthognathic face (see

[5] The term "hominin" has changed meaning over the years so I will clarify the current classification system. All apes are members of the superfamily Hominoidea and are referred to as *hominoids*.Two families exist therein: the great apes (Hominidae, or *hominids*) and the lesser apes (Hylobatidae, the gibbons and siamang). The African great apes belong to the subfamily Homininae while *Pongo* belongs to Ponginae. Within Homininae are the tribes Gorillini for *Gorilla* and Hominini for all other genera. Finally, at the subtribe level are Panina for *Pan* and both Australopithecina and Hominina for members of the human clade. The term *hominin* decribes these last two and refers to all taxa after the split from chimpanzees/ bonobos. As such, taxa need not be ancestral to *Homo sapiens* in order to be classified as hominins.

Fig. 1). These are generally the craniofacial traits that intrigue paleoanthropologists, and much research is focused on questions of *how* they evolved and *why* they are unique to hominins.

2.3.2 Baboon Systematics

Savanna baboons (genus *Papio*, hereafter referred to as baboons) are members of the Papionini tribe (Burnett, 1828), which is composed of six additional genera: *Macaca* (macaques), *Theropithecus* (geladas), *Cercocebus* (terrestrial mangabeys), *Lophocebus* (arboreal mangabeys), *Mandrillus* (mandrills/drills), and the recently described *Rungwecebus* (kipunji). The subtribe including only the African genera is called Papionina (Burnett, 1928), and its evolutionary history is the focus of this section. Traditional cladistic classifications recognize the two mangabeys as sister taxa based on their small body size and shared skeletal morphology (Thorington & Groves, 1970; Szalay & Delson, 1979). However, molecular analyses indicate that *Cercocebus* and *Mandrillus* form a clade to the exclusion of other papionins, meaning that the two large bodied taxa, *Papio* and *Mandrillus*, are not as closely related as morphology would suggest (Fig. 2.7; Disotell et al., 1992; Harris & Disotell, 1998; Harris, 2000).

Because baboons and mandrills/drills are not sister taxa, but both demonstrate large body sizes and distinctively extreme prognathism (a projecting “snout,” or rostrum), these are considered homoplastic characters (Collard & O’Higgins, 2001; Fleagle & McGraw, 2002; O’Higgins & Collard, 2002; Frost et al., 2003; Leigh, 2007). The short branches of the papionin phylogenetic tree (see Fig. 2.7) suggest that the degree of facial projection in papionins has changed both drastically and multiple times in relatively short periods of time. Given the co-occurrence of large body size and long rostra in two different branches within the papionin clade, it seems reasonable to hypothesize that facial length is particularly sensitive to allometric (size-related) changes. Quantifying craniofacial patterns, both in the context of and corrected for

body size variation, in one of these large-bodied taxa may help elucidate the relationship between body and facial size.

2.3.3 Fossil Papionins

One of the greatest strengths of the Cercopithecinae, the subfamily of OWM that includes the papionins, is their ability to adapt to and exploit a wide range of habitats and, in particular, more open and arid ones. The overall trend during the Miocene, the epoch during which the catarrhines began to diversify, was one that demonstrated general trends of climatic aridifcation and grassland expansion (e.g., Behrensmeyer et al., 1992; Janis, 1993; Cerling et al., 1997; Blue et al., 2006; Seiffert, 2012). According to Page et al. (1999), Papionini diverged from the other tribe of cheek-pouch OWMs, the Cercopithecini, 9-10 MY ago. By 7-8 MY ago, the tribe had divided into two lineages: Pan-Eurasian macaques and African papionina (Disotell et al., 1992; Page et al., 1999). Table 2.1 provides a detailed catalogue of the Papionina fossil taxa discussed in this section.

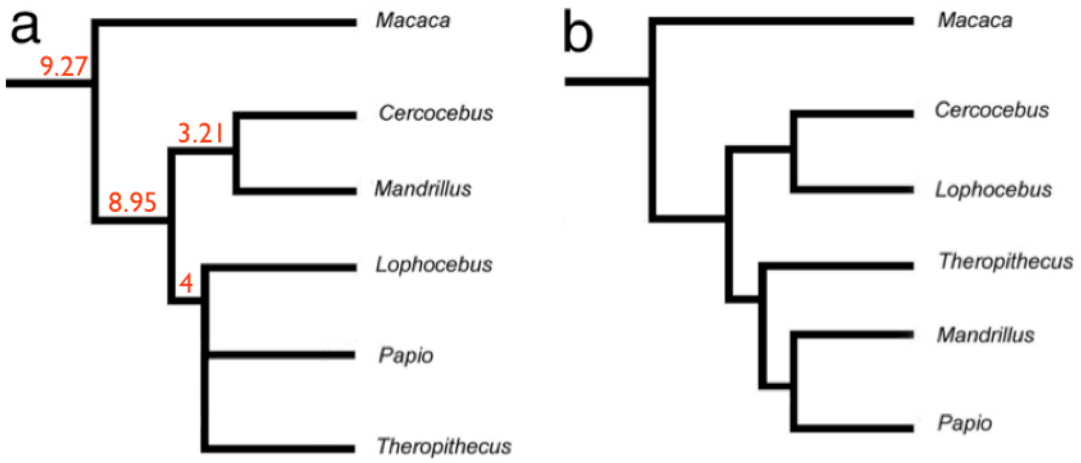

Figure 2.7 Trees of the Papionin Clade. Panels: (A) The current molecular phylogenetic tree (adapted from Gilbert and Rossie, 2007) with divergence dates (Harris, 2000) in millions of years indicated by the red numbers. (B) A morphology-based cladogram of the historically recognized relationship among species.

Papionina specimens dominate the fossil record in Africa during the Plio-Pleistocene (Leakey and Leakey, 1976; Simons and Delson, 1978). Some of this may be preservation bias, as the xeric landscapes on which they lived were ideal for fossil preservation, but it is also reflective of the composition of the faunal communities at the time. Interestingly, most Papionina genera/species recovered from fossil assemblages are not the same as those that exist today. Furthermore, the most dominant genus during the Late Pliocene and Early Pleistocene, *Theropithecus*, has since been drastically reduced in both the number of included species and its geographic range. The specialized montane gramnivore of the Ethiopian highlands, *T. gelada*, is the only remaining taxon. During the Early to Middle Pleistocene, at least four other large-bodied genera were present on the landscape: *Parapapio*, *Gorgopithecus*, *Dinopithecus*, and *Papio*. Only the last survived to the present day and, actually, has increased in both distribution and number of species. Relative to their extinct sister taxa, *Papio* baboons have historically been more omnivorous, drought tolerant, and flexible in their choice of habitat, all of which may have helped them either to outcompete other baboons on the Pleistocene landscape or to take advantage of niches left empty as the others began disappearing from the African faunal communities.

During the reign of the large-bodied Papionina, South Africa was home to the diverse genus *Parapapio*, while *Theropithecus* inhabited East Africa (Jablonski, 2002). Both genera were well adapted for foraging for a variety of seeds and herbaceous vegetation in environments many taxa would find uninhabitable (Jolly, 1970). Fossil and molecular evidence suggest the extant genera are divided into two groups; *Mandrillus* and *Cercocebus* (MC) split from *Theropithecus*, *Papio*, *Lophocebus*, and *Rungwecebus* (TPLR) 6-8 MY ago (Disotell et al., 1992; Page et al., 1999). The most likely stem Papionina was *Parapapio*, or a taxon either ancestral or very similar to it (Jablonski, 2002). The most geographically widespread Papionina

Table 2.1 Catalog of Fossil Baboon Taxa Discovered to Date.

Taxon	Genus	Species	Holotype	Age Range	Localities[b]	Source
Baboon	*Dinopithecus*	*ingens*	SB 7	Plio	SK	Broom, 1937
	Gorgopithecus	*major*	KA 193	Pleisto	KA	Broom, 1940
	Papio	*angusticeps*			KA; T	Freedman, 1957
		hamadryas				Linnaeus, 1758
		h. izodi	AD 992	Pleisto	T; KA; SK; Haasgat Cave	Gear, 1926
		h. robinsoni	SK 555	Pleisto	SK	Freedman, 1957
		h. ursinus	un-numb. partial cranium	Pleisto	Transvaal	Kerr, 1792
	Parapapio	*ado*	BMNH M14940	Plio	LB	Hopwood, 1936
		antiquus	CT 5364	Plio-Pleisto	Taung	Haughton, 1925
		broomi	STS 564	Plio-Pleisto	ST	Jones, 1937
		jonesi	STS 565	Plio-Pleisto	ST	Broom, 1940
		whitei	STS 563	Plio-Pleisto	ST	Broom, 1940
	Pliopapio	*alemui*	ARA-VP-6/933	Plio	Middle Awash	Frost, 2001
Gelada	*Theropithecus*	*baringensis*	KNM-BC 2	Plio	ET; Leba, Angola	R. Leakey, 1969
	T. Omopithecus	*brumpti*	MNHN Omo 001[c] MNHN Omo 002 MNHN Omo 003	Plio	KB; OM	Arambourg, 1947
	T.Theropithecus	*darti*	UWMA MP1 (=M 201, 1326/1)	Plio	M	Broom & Jensen, 1946
		oswaldi delsoni	un-numb. mandible	Middle Pleisto	Punjab, India	Gupta & Sahni, 1981
		o. leakeyi	BMNH M14680	Pleisto	OG	Hopwood, 1934
		o. oswaldi	BMNH M11539[d]	Late Plio/Early Pleisto	Kanjera	Andrews, 1916
Mandrill/Drill	*Soromandrillus*[e]	*quadratirostris*	NME "USNO"	Plio	OM	Iwamoto, 1982
Mangabey	*Cercocebus*	sp. indet.	NMW 4422/ST 624[d] (*C. agilis*)	Late Plio/Early Pleisto	M; KA; ET; OG	É. Geoffroy Saint-Hilaire, 1812
	Lophocebus	sp. indet.	M 15922 & M 18800	Plio-Pleisto	Kanam East	Harrison & Harris, 1996

[a]Frost, 2001; Jablonski, 2002. [b]Only the main fossil localities are given. Abbreviations are: East Turkana (ET), Kromdraai (KA), Koobi Fora (KB), Laetoli (LB), Makapansgat (M), Olduvai (OG), Omo (OM), Sterkfontein (ST), Swartkrans (SK). [c]Syntypes. [d]Lectotype. [e]The taxon was recently placed within the genus *Soromandrillus* (Gilbert, 2013) and may be referred to in older sources by its former genus designation, *Papio*.

taxon was *Theropithecus*, generalists capable of subsisting on large objects (Eck and Jablonski, 1987), fruits and leaves, and grasses and herbaceous material (Benefit and McCrossin, 1990; Cerling et al., 2013) and specialized for dexterous manual foraging (Jablonksi, 1986; Krentz, 1993). The decline of both genera is debated, but in the case of *Theropithecus*, it is likely due to a combination of factors. Geladas are dependent on permanent water sources, making them easy targets for hunting by sympatric hominins (Dunbar, 1993). In addition, their reliance on low-quality resources meant that they had lower basal metabolic rates (BMR) and this, in turn, likely affected social dynamics and reproductive behaviors (Iwamoto, 1993; Lee and Foley, 1993; Martin, 1993). In addition, low BMR constrained the degree of encephalization, which was of further detriment when competing against the relatively larger-brained baboons. (Dunbar, 1993; Lee and Foley, 1993; Jablonski, 2002). The African landscape is now dominated by *Papio*, as it is the genus with the greatest number of species and largest geographic distribution. Unlike geladas, baboons are generalists, able to adapt to heterogeneous environments more easily, which may have played a role in the genus eventually eclipsing *Theropithecus*.

In general, stem Papionina are characterized by male maxillary ridges and maxillary fossae, with the genera of the TPLR clade demonstrating the most extreme examples (Gilbert, 2013). Of the craniodental characteristics that are common to taxa of the MC lineage, the most distinctive are an upward-turned nuchal crest, relatively enlarged premolars, and widely divergent temporal lines (Gilbert, 2013). All Papionina are heavily built, with many taxa having large sagittal crests and laterally flaring zygomatic arches (Simons and Delson, 1978; Jablonski, 2002). Sexual body and canine size dimorphism and extensive allometry are common, especially in *Papio* (Martin, 1993; Frost et al., 2003; Porto et al., 2009; Willmore et al., 2009).

One of the more unusual characteristics of extant *Papio* is the ability of (sub)species to hybridize in the wild, thereby creating clinal genetic variation (Tung et al., 2008; Charpentier et

al., 2012), yet largely maintain phenotypic distinctions such that (sub)species designations are able to be made on the basis of a few characteristic traits (e.g., coat color, relative leg length, facial skin coloring, especially of the eyelids; Williams-Blangero et al., 1990; Jolly, 1993). Interestingly, despite the expectation that selection should impede hybrid individuals, as they should only be partially adapted, or even maladapted, to either parental population's specific environment, natural hybridization is a relatively common observation among baboon groups in the wild, even at the generic level (Jolly et al., 1997). It is unclear whether fossil Papionina behaved similarly, but it is likely that in *Papio* at least, hybridization and introgression have been characteristics of the clade's evolutionary history. Understanding the phenotypic, genetic, and evolutionary effects of these processes is important in the study of speciation, population structure, sympatry, reproductive isolation, and molecular phylogeny. These processes leave identifiable footprints in both the genome and the corresponding patterns of morphological variation. Comparing the phenotypes of purebreds and their hybrid offspring can be a powerful tool for localizing genetic variation contributing to continuous morphological variation (e.g., Ackermann et al., 2006, 2014; Joganic et al., 2012b; Ito et al., 2015).

2.4 Craniofacial Biology

Craniofacial traits are commonly used to infer phylogenetic relationships (e.g., Strait & Grine, 2004; González-José *et al.*, 2008; Gilbert *et al.*, 2009), define taxonomic status (e.g., Wood, 2009; Lockwood & Tobias, 2002), conduct ecomorphological reconstructions (e.g., Heesy, 2008; Figueirido *et al.*, 2009), deduce patterns of trait evolution (e.g., Ravosa *et al.*, 2000; Marroig & Cheverud, 2005), and formulate adaptive hypotheses (e.g., Kay, 1975; Martins, 2000). As crania—along with teeth—are often the only biological materials to survive the fossilization process and be recognized once unearthed, an understanding of the ontogenetic,

genetic, and epigenetic origins of craniofacial variation and the effect of genetic correlations on character evolution is essential for interpreting morphological differentiation.

2.4.1 Craniofacial Embryogenesis

The bones of the skull form by one of two ossification processes: endochondral or intramembranous. As a general rule, the bones of the cranial base that house the auditory and olfactory systems go through a cartilaginous stage, as they are remnants of the early tetrapod chondrocranium composed of the cartilaginous otic and olfactory capsules. These endochondral bones include the: basi- and exoccipital, petrous temporal, most of the sphenoid, ethmoid, and turbinates. Most of the cranial bones are derived from the external calcified dermal plates that protected the neural tissue of our osteichthyes (bony fish) ancestors. As a result, these ossify *in utero* intramembranously (i.e., directly from mesenchyme instead of from a cartilaginous precursor, as in endochondral ossification): frontal, parietal, squamous occipital, squamous temporal, vomer, nasal, lacrimal, palatine, pterygoid plates of the sphenoid, premaxilla, maxilla, zygomatic, and mandible.[6] The remaining bones of the skull (alisphenoid, ear ossicles, and those of the face) are derived from the endoskeleton that supported the gill arches and respiratory muscles of the chondrichthyes, cartilaginous fish that appear in the Devonian Period 419.2 MY ago (Gregory, 1965; de Beer, 1985). *In utero*, these bones originate as pharyngeal arches and later ossify via intramembranous ossification (Kingsley, 1925; Gregory, 1965; Schultze, 1993).

Regardless of how the osseous tissue is formed, the end result is an interlocking matrix of organic collagen impregnated with inorganic calcium salt, hydroxyapatite (Storey, 1972). The collagen provides strength and flexibility while the hydroxyapatite provides support and form. As

[6] The embryonic origin of the mandible is from Meckel's cartilage, a derivative of the ventral portion of the first pharyngeal arch. Despite this, it does not form endochondrally. Rather, mesenchyme surrounding the cartilage condenses and ossifies via intramembranous ossification. Meckel's cartilage forms the primary lower jaw in sharks.

bone tissue has an organic component, it is a living tissue that is constantly modified and replaced throughout the life of the individual in response to diet (e.g., Tieszen and Fagre, 1993; McCrady, 2003; Nielsen, 2004), ambient temperature (e.g., Klein, 1986; Clarke and O'Neil, 1999; Rae et al., 2006; Motyl et al., 2013; Serrat, 2014), mechanical loading (e.g., Bouvier and Hylander, 1981; Duncan and Turner, 1995; Nomura and Takano-Yamamoto, 2000), and health status (e.g., Mensforth et al, 1978; Som et al., 1991). This remodeling is largely regulated by the endocrine and sex hormone (primarily estrogen) systems, which in turn respond to a multitude of internal and external stimuli (e.g., Simpson et al., 1950; Turner et al., 1992; Herring, 1993; Sperber et al., 2010). Therefore, both genetic and epigenetic[7] factors influence the size, shape, and condition of bone tissue throughout the life of an individual.

The embryonic tissue types that develop into the cells that will create and regulate bone growth are derived from one of two sources. Traditionally, it was believed that both the cardiovascular system and all structural tissues in the body (e.g., bone, cartilage, muscle) were derived from the mesoderm, the middle layer of the trilaminar embryonic disc that eventually differentiates and folds into a fetus. However, more recently it has been recognized that the intramembranous bones surrounding the cranial end of the embryonic neural tube (the precursor to the central nervous system) are composed of cells that migrated from the neural crest (Yoshida et al., 2008). Neural crest cells are ectomesenchymal in origin and they invade the space dorsal to the neural tube as it is formed before migrating or being displaced throughout the cranial pole of the embryo, condensing into a variety of different tissue types

[7] The term "epigenetic" refers to a number of different concepts, depending on the context and the individual using the term. The traditional meaning of epigenetics as the role of extrinsic factors on the production of phenotypic variation was born out of Conrad Waddington's experiments with genetic assimilation in *Drosophila* in the 1950's (see Noble, 2015 for an excellent review). The advent of molecular techniques allowing us to study genome methylation and histone modification precipitated a revision of the concept as "a stably heritable phenotype resulting from changes in a chromosome without alterations in the DNA sequence" (Berger et al., 2009). Here, I use epigenetic to encompass both definitions as both contribute to phenotypic variation.

along the way (e.g., Lallier, 1991; Huang et al., 2004; Weston et al., 2004; Ezin et al., 2009; Mishina and Snider, 2014).

Whether mesodermal or neural crest in origin, embryonic cells are initially pluripotent. The mesodermal-derived cells must first differentiate and condense into a disorganized sheet called mesenchyme (Sperber et al., 2010). In contrast, the neural crest cells must first transition from epithelium (which is stationary) to mesenchyme (which is transitory) before they are able to contribute to craniofacial tissues. It is these mesenchymal sheets that undergo either intramembranous or endochondral ossification to form bone. Movement of and interaction among these mesenchymal sheets contributes to final craniofacial form (e.g., Noden, 1988; Wood et al., 1991; Jiang et al., 2002). Additionally, Liu et al. (1997) demonstrated that the bone-forming cells themselves (osteoblasts) are heterogenous in their protein expression patterns, differing even from directly adjacent cells. This suggests that both genetic and epigenetic control of osteogenesis plays an important role in producing and maintaining intraspecific variation of the skull.

2.4.2 The Special Relationship Between Brain and Skull

Perhaps one of the more surprising revelations to emerge from the field of developmental biology was that the growth of the underlying brain plays a very significant role in inducing cranial bone osteogenesis (Zwilling, 1968), and proper development of both brain and cranium is inextricably linked (Richtsmeier et al., 2006). In fact, Zwilling's (1968) studies in chick embryos show that, when a small region of the brain is transplanted, the calvarial bone that overlies that section of the brain *in situ* still forms adjacent to the transplanted region. The complementary test demonstrates that extirpation of a specific region of the chick embryo brain causes a failure of the overlying calvarial bone to form. Additionally, in cases of anencephaly (a neural tube defect causing all of or parts of the brain to be missing) the calvarium does not

develop at all while hydrocephaly (excess cerebral spinal fluid) causes the neurocranium to become greatly inflated (Otto, 1831).

Because the brain grows disproportionately *in utero* and in the first two years of life (Leigh, 2004), the overlying calvarium must be flexible enough to expand in response. This compensatory growth occurs at the sutures, the synarthroses between adjacent cranial bones (Sömmering, 1791, cited in David et al., 1982), until neural expansion ceases, at which point the sutures cease to grow and subsequently ossify. Fibrous bands derived from the dura mater—the falx cerebri, falx cerebelli, and tentorium cerebelli—exert biomechanical forces and biochemical signals that induce appositional growth at the sutural margins (Kokott, 1933, cited in David et al., 1982; Opperman et al., 1993). Anything that interrupts the transmission of these (e.g., genetic mutations, environmental perturbations) has the potential to interrupt or even terminate calvarial expansion, which could have drastic effects on neural functioning as brain growth is regulated by different ontogenetic pathways and, thus, will continue (Otto, 1831; Virchow, 1852, cited in David et al., 1982). This condition of premature sutural fusion is called craniosynostosis and many of the genes of known contribution to craniofacial growth were discovered in studying its etiology. Many of these disease-associated genes, as well as those regulating neural development, likely contribute to craniofacial form, as ontogenetic "disorganisation, in time or space, may lead to craniofacial dysmorphogenesis" (David et al., 1982) and, by extension, normal morphological variation, too.

The shape of the orbits is primarily determined by growth of the eyes, which are extensions of the brain, rather than by masticatory strain or later development of the facial skeleton (Barbeito-Andrés et al., 2016). In fact, orbital growth actually influences growth of the facial skeleton, particularly the midfacial region (Dullemeijer, 1971). In humans the eyes start expanding in size early in the postnatal period and then reach adult interocular distance at age

three and adult size around seven. The many bones comprising the orbit must grow at the sutural margins to accommodate this ocular growth. Over the course of development, orbital bone deposition is induced as a result of growth along the following planes: lengthening of the nasal cartilage grows the maxilla anteriorly, expansion of the brain pushes the anterior cranial fossa and orbital roof anteriorly, inflation of the ethmoid complex pushes the medial orbital walls laterally, and malar development pulls the lateral walls laterally. Concurrently, the cranial base cartilages are compensating for this differential growth in the facial skeleton to maintain or adjust the cranial base angle as needed (Ford, 1956).

Biegert (1963) describes the effect of this interaction among these various developing components—brain, face, and cranial base—as the Spatial Packing Hypothesis (SPH). The SPH highlights the importance of the cranial base as the bridge and mediator between the neuro- and splanchnocrania (Fig. 2.8), giving to it a preeminent role in patterning overall craniofacial form (Ross and Ravosa, 1993; Lieberman et al., 2000, 2008; Parsons et al., 2015). The interaction among brain, face, and cranial base demonstrates the dual nature of the skull in that it is both *modular* and *integrated*.[8] The competing demands of modularity and integration have important consequences for evolutionary change in complex structures as the demands of function and effects of multifactorial developmental pathways can often constrain morphological diversification, although enhancing change along particular evolutionary trajectories can sometimes result as well (Klingenberg, 2008).

The processes and factors controlling and influencing the development of the soft tissue structures of the head and integrating their growth with that of the hard tissue structures are necessarily many. A number of the genetic mechanisms have been identified and will be

[8] Modular structures are composed of groups of morphological units that work and/or grow together somewhat independently of other such groups. To ensure function of the composite structure, congruence among these semi-autonomous groups must be maintained. This is the concept of morphological integration proposed by Olsen and Miller (1958; see *2.5.2 Morphological Integration in the Cranium*).

discussed in greater detail below (see *2.4.4 Summary of Known Craniofacial Genes*) and some of the epigenetic elements have been/will be discussed in this section and the next, but much more remains to be discovered about craniofacial growth and development.

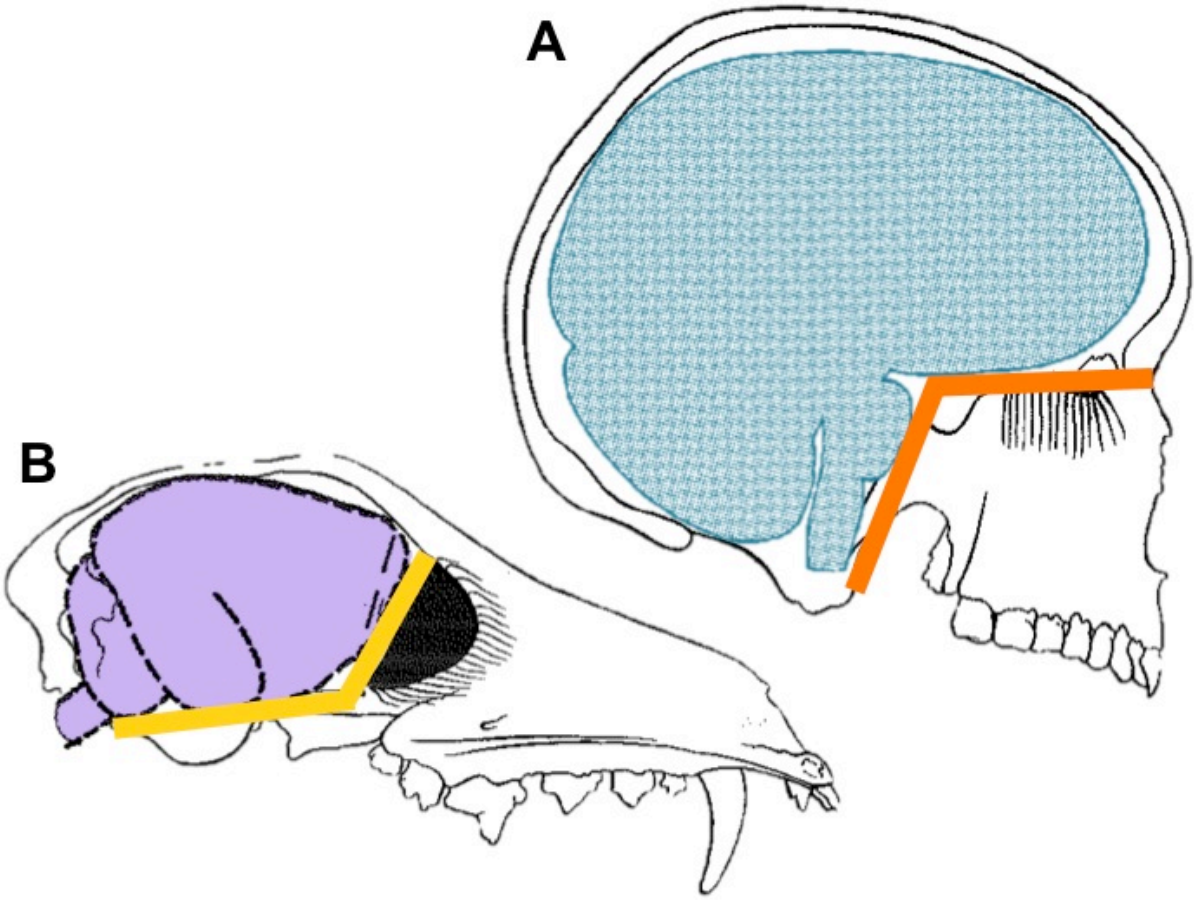

Figure 2.8 The Spatial Packing Hypothesis. The SPH predicts that taxa with greater degrees of encephalization (i.e., brains larger than would be expected for an organism of the same body size) will have a more flexed cranial base, resulting in a face that is hafted onto the neurocranium from underneath. In contrast, most mammals have a retroflexed (greater than 180°) cranial base angle (CBA) and faces that protrude in front of their neurocrania. Panels: (A) Human cranium with brain shown in blue stippling and CBA with orange lines. (B) Canid cranium with brain shown in solid purple and CBA with yellow lines. In both panels, note the difference in orientation of the olfactory nerves (parallel black lines) that results from altering the plane in which the anterior cranial base lies. Adapted from David et al. (1982).

2.4.3 Theories of Craniofacial Growth and Development

The very earliest formulation of a theory describing the process by which bone grows was that of James Couper Brash, which was presented in 1924 as one of five lectures given in a series on orofacial growth. Brash's theory bestows the role of growth solely to the process of displacement via bone remodeling, specifically appositional growth in which bone is selectively added to one surface of a bone and resorbed from the opposite one (Carlson, 2005). For example, the mandibular corpus would lengthen as bone is added to the posterior border of the ramus and removed from its anterior border (called "Hunterian" when describing mandibular growth; Fig. 2.9). Applied to the cranium, this theory dictates that the calvarial bones would increase in size as ectocranial bone is deposited and endocranial bone resorbed. However, this

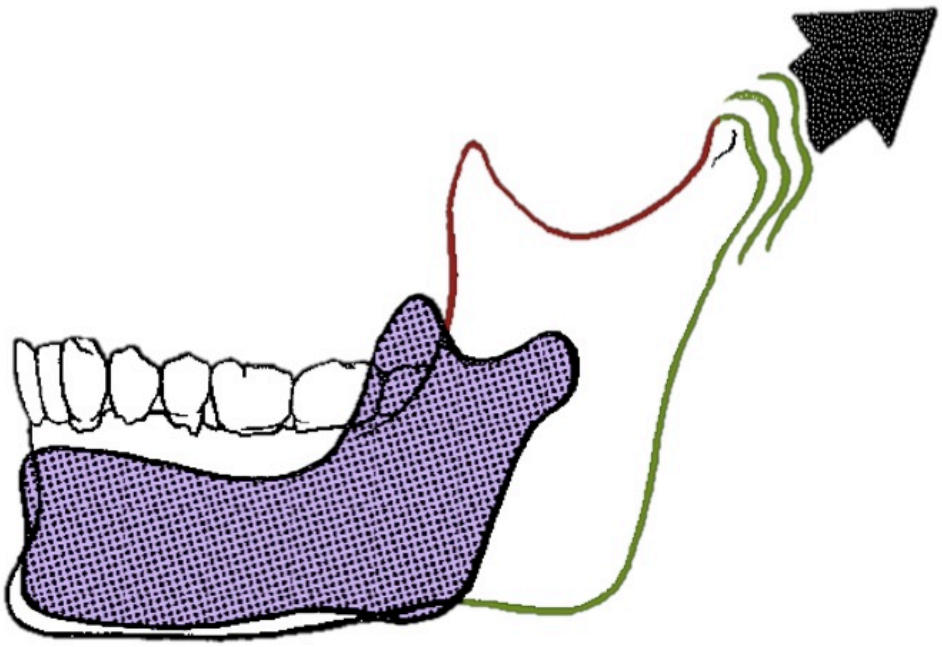

Figure 2.9 A Model of Hunterian Growth of the Mandible. Brash's (1924) theory of craniofacial growth predicted that bone is added to the posterior margin of the mandibular ramus (green outline) and resorbed from its anterior margin (red outline), which increases the size of the mandible in the direction of the black arrow. Over time, this selective appositional growth transforms an infant mandible (purple stippling) into its adult form. Adapted from David et al. (1982).

theory does not provide a role for the unique structures of the sutures and synchondroses between craniofacial bones.

To address this deficiency in Brash's theory, Joseph Weinmann and Harry Sicher developed a sutural theory suggesting that the proliferation and subsequent ossification of connective tissue at the sutural margins dictated growth of the skull and determined its eventual form (Weinmann and Sicher, 1947). Research conducted in the following decades cast doubt on the supremacy of the craniofacial sutures in the growth process because histological studies revealed sutural connective tissue to be only specialized periosteum incapable of actually patterning the growth occurring at them (Baer, 1954; Moss, 1954, 1957).[9] Additionally, sutures are designed to respond to tensile, and not compressive, forces (Crilly, 1972). Displacement involves "pushing" of bony elements to effect growth but, unlike in postcranial epiphyseal joints, compression induces resorption at the site of pressure, rather than deposition (Enlow, 1982).

With these results in mind, James Scott refined Weinmann and Sicher's theory by relegating the sutures to the role of secondary, compensatory growth sites while elevating the cartilaginous nasal septum to the role of most important active and important growth center. Scott (1953, 1958) supported this change by emphasizing the nasal septum's intermediary position between the floor of the anterior cranial base and the roof of the midface (Fig. 2.10). Because of its location, it is the only bone/structure capable of permitting growth and also bridging the two main regions of the skull, the face and the neurocranium. Much of the developmental research conducted in the decades that followed the publication of Scott's theory provided evidence in support of it (Baume, 1961; Latham and Scott, 1970; Kvinnsland, 1973; Siegel, 1979). However, some believe the relative importance of this growth center likely

[9] We now know that, although Weinmann and Sicher were wrong about the sutures themselves patterning neurocranial growth, growth occurring at the sutural margins contributes significantly to final cranial form. As mentioned previously, sutural growth occurs as a response to forces exerted on them directly by the growing brain and indirectly through the associated connective tissues (David et al., 1982).

diminishes postnatally as the face outgrows the ability of the nasal septum to “push” it anteriorly and inferiorly (Babula et al., 1970; Enlow, 1982).

The most likely scenario is that craniofacial growth is multifactorial. Tissue interactions, such as those described by both the cranial suture and nasal septum theories, are one of the most important, but not the only, factors in inducing and directing craniofacial growth. Transplantation procedures in rats (Lacroix, 1951; Felts, 1961; Koski and Mäkinen, 1963) and tissue culture studies (Fell, 1956) demonstrate that, when disjointed from the mandibular ramus, the condylar cartilage cannot maintain proliferation of mesenchymal cells and their differentiation into chondrocytes. Furthermore, the growth that is observed for a short while after transplantation is undirected or even perpendicular to the axis of growth *in situ*. This may be partly explained by the fact that mandibular development is dependent on the presence of movement via articular forces as bone grows in response to periosteal tension (Crilly, 1972). If those forces are not enacted by surrounding tissues and distributed across the periosteum, the result of which is growth induction, bone development will cease. Clearly, the constraint placed on cartilage by connective tissues and adjacent bone is necessary for directional cell proliferation and bone growth (Storey, 1972).

The cranial base synchondroses are more autonomous than the condylar cartilage, but their growth is still not controlled by genetic factors alone (Koski and Rönning, 1970). Therefore, they cannot be considered true “growth centers” *sensu* Baume (1961): “places of endochondral ossification with true tissue separation force.” Growth in the basicranial synchondroses is likely induced by a combination of external factors: the presence of the notochord and other neural elements (e.g., Cohen and Hay, 1971; Carlson, 1973; Lettice et al., 1999), hypoxia (e.g., Wang et al., 2007; Wan et al., 2010), and compressive forces acting across the joint surface (e.g., Enlow, 1982). It is worth noting that dimensional increase in these synchondroses is primarily

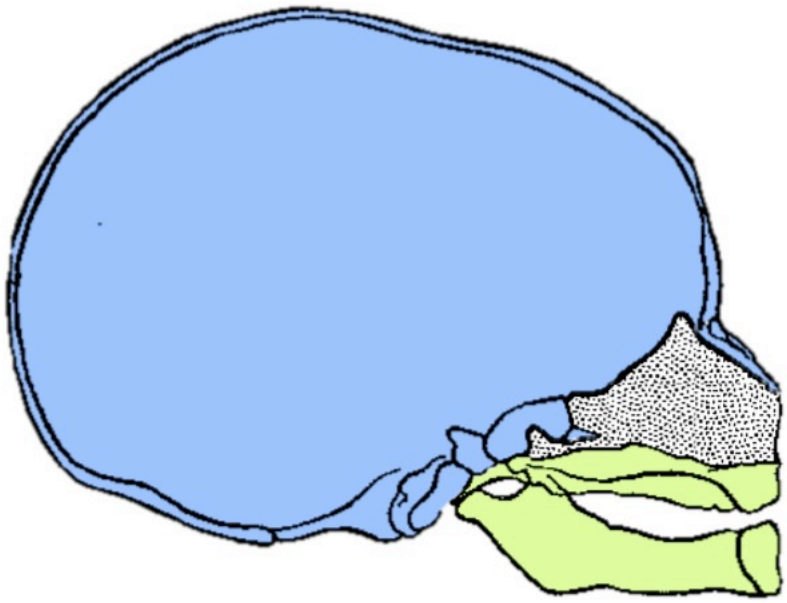

Figure 2.10 The Nasal Septum as a Primary Force in Craniofacial Growth. Scott (1953, 1958) developed a model of craniofacial growth in which growth of the nasal septum cartilage (stippling) pushes the facial skeleton (green) away from the neurocranium (blue), thus patterning craniofacial development. Adapted from David et al. (1982).

asymmetrical, especially in humans, which likely contributes to cranial base flexion (Melsen, 1971; Michejda, 1972; Vilmann, 1972). As such, the cranial base synchondroses can best be considered as bioelastic, pressure-bearing joints (Storey, 1972; Vilmann, 1972). The bony cranial base is a compact region in which a number of critical systems come into contact: prevertebral and postvertebral muscles and ligaments, mandibular and hyoid muscular and ligamentous attachments, the oro- and nasopharynx, caudal portions of the brain, the atlanto-occipital joint, and, potentially most important, the vestibulocochlear system, the horizontal semicircular canals of which must be maintained in a horizontal position (de Beer, 1947; Roberts, 1978; Pozzo et al., 1991). The studies of all three types of craniofacial cartilage (nasal septum, sutures, basicranial synchondroses) demonstrate that the mechanisms of bone growth

cannot operate when separated from their functional environments and, therefore, considering the skull as an integrated structure is imperative to understanding its development and form.

In addition to the necessity of presence of adjacent tissues for directional craniofacial growth, muscle forces acting on the developing structures also play a significant role in influencing skull shape (e.g., Corruccini and Beecher, 1984). Masticatory muscle cross-sectional area is positively associated with craniofacial variation in the transverse plane and negatively with cranial base flexion (van Spronsen et al., 1991). *In vivo* and *in vitro* studies on developing rat skulls demonstrate that mandibular condyles that do not experience strain from the ipsilateral temporalis muscle, whether due to denervation or excision of the muscle, fail to develop proper shape, drastically affecting function in adult individuals (Pratt, 1943; Washburn, 1947; Horwitz and Shapiro, 1951; Avis, 1961). However, removal of the masticatory muscle fibers while still maintaining blood supply to the muscle produces condyles of normal size and shape in most cases (Boyd et al., 1967). This demonstrates that mandibular growth is multifactorial, influenced by both the vascular and muscular systems.

It is worth mentioning that typically the primary focus of ontogenetic studies is on the migration of osteogenic cells to the location of the future tissue, whether bone, cartilage, or muscle, as it relates to form of the adult structure. However, proper tissue relationships must be maintained during development itself, not just in anticipation of adult function. David Enlow (1982) articulated this as the counterpart principle of craniofacial growth—growth of one structure (part) relates geometrically to another (counterpart) and the two must develop in concert to maintain balanced growth. Consequently, it is important to consider the genetic, biomechanical, and hormonal controls of the translocation of tissue cells and the maintenance of functional relationships *throughout* the growth of a structure (Enlow, 1968). These controls are likely to be local in effect, although they could be systemic in origin, and they need not be

the same factors that regulate the genesis of a structure. Alexandre Petrovic developed the Servosystem Theory of craniofacial growth to include the effects of both mechanical stimuli from surrounding tissues and chemical stimuli from systemic hormonal factors in a biofeedback system that stimulates and maintains growth of a structure (Fig. 2.11; Carlson, 2005). Including the further complication of biofeedback in studies of craniofacial growth and development is necessary for developing a holistic understanding of the process.

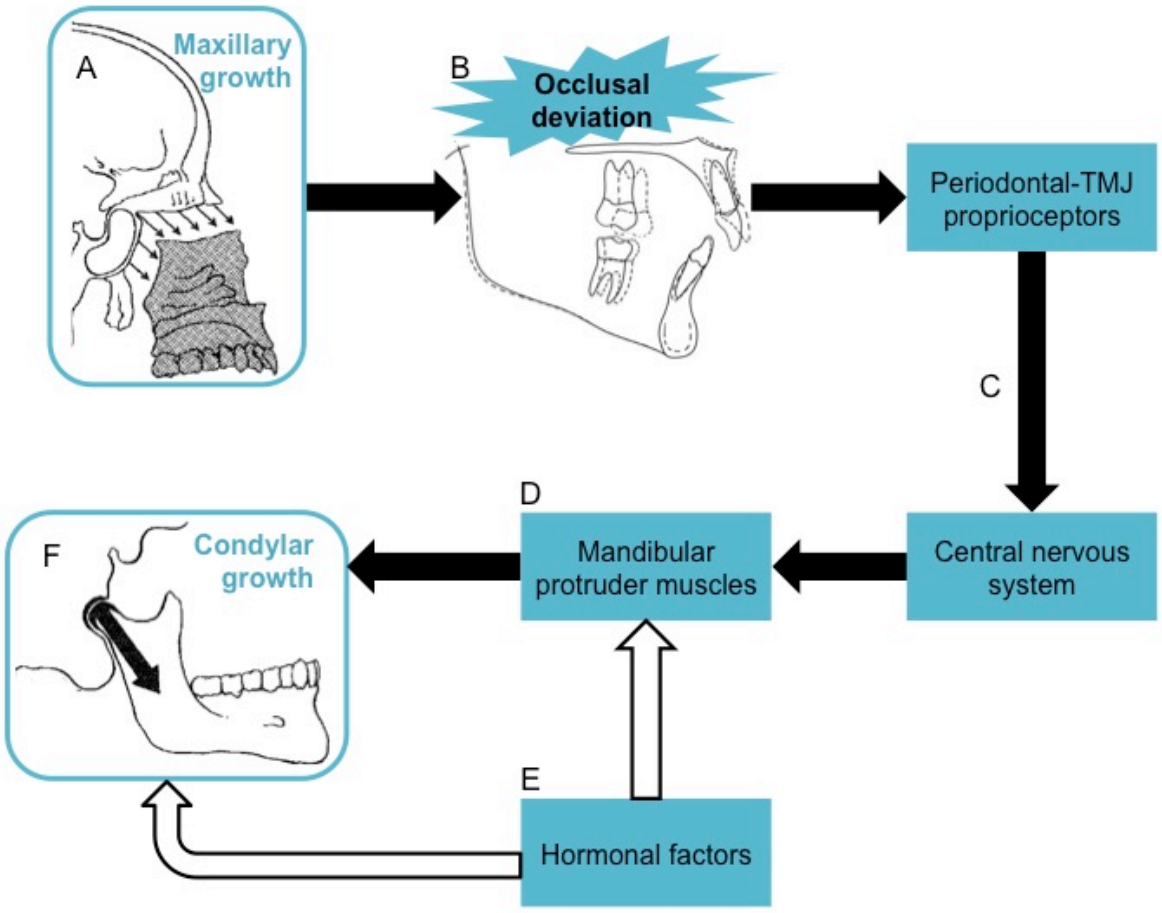

Figure 2.11 Flowchart Illustrating the Servosystem Theory of Craniofacial Growth. Petrovic's (1974) theory is comprised of six components: maxillary growth (A) moves the hard palate anteriorly, causing a slight occlusal deviation between the maxillary and mandibular dentitions (B). Proprioceptors in the periodontium and temporomandibular joints (C) induce tonic action in the muscles that protrude the mandible in an effort to maintain functional occlusion (D). Muscle activity, the displacement of the mandibular condyle due to protraction, and appropriate hormonal controls (E) induce condylar growth (F). Adapted from David et al. (1982), Carlson (2005), and Martinelli et al. (2012).

Enlow's counterpart principle is incorporated into Melvin Moss's (1960, 1962) Functional Matrix Model (FMM), which arose in response to the criticisms of the mid-century craniofacial growth theories. The FMM emphasizes the mutual dependency of craniofacial tissues, positing that growth activity is dependent on maintaining a mechanical equilibrium among the constituent structures that perform an action. If the mandibular condyle (a part) grows out of sync with the temporal glenoid fossa (its counterpart) mastication may be negatively affected. This illustrates Moss's theory that growth of these structures is directed by both the action performed by soft tissues (the functional matrix) to enact a specific function and the presence of their supporting anatomy (the skeletal unit). For example, the *function* of deglutition is performed by the *functional matrix* composed of the supra- and infrahyoid, pharyngeal constrictor, and digastric muscles, which are supported by the hyoid, *the skeletal unit*. The FMM specifically describes craniofacial tissue development early during ontogeny, but the interdependent nature of the skull as a whole is well demonstrated experimentally in adolescent animals as well. Vargervik et al. (1984) determined that requiring oral breathing by preventing nasal breathing in rhesus macaques altered neuromuscular morphology and function of the mandible, tongue, and upper lip relative to control animals. Anterior face height, occlusal plane angles, and malocclusion increased, but some of these changes were reversed after nasal breathing was restored two years later. These results also highlight the phenotypic plasiticity of the skull (Pigliucci, 2001).

Both the counterpart principle and FMM demonstrate a theory put forth by Arthur Koestler (1970), the self-regulating open hierarchic order (SOHO) theory. In his initial description, Koestler applies the SOHO theory to every natural system demonstrating rule-governed behavior: evolution, industry, linguistics, culture, anatomy, the military, watch making, etc. In the present context, the SOHO characterizes the skull as a collection of semiautonomous "holons" that have both self-assertive tendencies in demonstrating their characteristic patterns

of behavior (their “canon”) but also have integrative tendencies in that they are hierarchically aggregated into and function within a systemic whole. Because the basicranial cartilages are able to sustain some growth when transplanted, albeit this growth is reduced in rate and output, some consider them to be holons. They have a canon, their genetically-based growth plan, that can proceed semi-autonomously, but to be truly effective, they function best in aggregate when the environment can direct and modify the canon according to local contingencies. The SOHO theory provides a much-needed alternative to the preexisting stimulus-response (S-R) paradigm in which biology is the result of linear causation. Once it was realized that morphological structures are the products of interactions among genes, both internal and external environmental variables, other such structures, and chance, the S-R model was no longer satisfactory. The SOHO model more adequately incorporates what we have learned about craniofacial growth and development thus far.

Most of these models fail to acknowledge that much of the craniofacial growth process consists of minor adjustments of interacting tissues to differential growth in the “primary” areas on which most craniofacial growth research is focused. Because this compensatory growth is so important for maintaining function and determining final morphology, this failure to account for these “secondary” growth patterns leaves these models incomplete. A theory that more accurately describes the complex process of craniofacial growth and development should account for mechanisms controlling both primary and secondary growth patterns, as well as for interactions between such mechanisms and the growth environment. It is likely that these mechanisms are affected by variation in both specific genes and the regulation of signaling pathways (King and Wilson, 1975; Carroll, 2005). As of now, only the drastic effects that negative mutations within these genes and pathways have on organismal fitness are recognized, but many signaling pathways have been demonstrated to affect certain aspects of

craniofacial growth and development, such as timing of sutural fusion and migration of nasal placodes (Sperber et al., 2010). Therefore, it seems plausible to hypothesize that regulation of such genes and pathways, as well as others as yet unidentified, contribute to within-population normal variation in craniofacial form.

2.4.4 Summary of Known Craniofacial Genes

The skull grows as a result of both cartilage proliferation (chondrogenesis) and forces acting on the craniofacial cartilages and sutures (myogenesis and neurogenesis). Therefore, genes either directly affecting or those involved in pathways that affect these processes have the potential to influence craniofacial growth and development. A number of signaling pathways have been identified that regulate calvarial growth by acting on sutural development (e.g., Kim et al., 1998; Maxson and Ishii, 2008; Martínez-Abadías et al., 2011, 2012; Bonilla-Claudio et al., 2012; Dwivedi et al., 2013; Zhou et al., 2014; see *2.4.2 The special relationship between brain and skull*). The most important include *SHH* (sonic hedgehog), *BMP* (bone morphogenetic protein), *FGF/FGFR* (fibroblast growth factor and receptor), and *TGFβ* (transforming growth factor, beta). Schoenebeck et al. (2012) discovered that *BMP3* contributes to brachycephaly in dogs. A close relative of it, *BMP4*, has been shown to correlate with beak width and depth in *Geospiza* (Darwin's finch; Abzhanov et al., 2004)—*CALM1* (calmodulin 1) affects beak height (Abzhanov et al., 2006)—jaw morphology in *Labeotropheus* and *Metriaclima* (cichlids; Albertson et al., 2003), dental and palatal development in *Mus* (e.g., Jia et al., 2013), and various dysmorphologies in humans, including cleft lip and palate (CLP; e.g., Suzuki et al., 2009) and syn- and polydactyly (e.g., Selever et al., 2004).

Interestingly, it is very likely that genes affecting limb development are involved as well (see preceding sentence). The signaling pathways for cranial and limb development partially overlap; both pathways were probably independently co-opted from pre-existing ancestral ones

(e.g., Rickman and Tickle, 1992; Holland et al., 1995; Schneider et al., 1999). Ancient duplications of pre-existing gene groupings that regulate transcription during embryogenesis also provided an opportunity for processes occurring in pre-chordates to be modified to produce more complicated structures, such as the brain and the skull (e.g., Robinson and Mahon, 1994; Satokata and Maas, 1994; Shimeld and Holland, 2000; Yu et al., 2002; Alappat et al., 2003). Examples of these segmentation gene clusters include *HOX* (homeobox), *MSX* (muscle segment homeobox), *PAX* (paired homeobox), *OTX* (orthodenticle homeobox), and *DLX* (distal-less homeobox).

Not surprisingly, genes and signaling pathways related to the neural tube and to neural crest cell development and migration are critically important for proper craniofacial growth (e.g., Schorle et al., 1996; Chai et al., 2000; Copp and Greene, 2010; Mishina and Snider, 2014). Additionally, genes regulating brain growth almost certainly contribute to craniofacial variation, too. As some of these genes—*ASPM* (abnormal spindle-like microcephaly associated) and *MCPH1* (microcephalin)—have undergone recent positive selection (Evans et al., 2005; Mekel-Bobrov et al., 2005), considering their role in craniofacial growth and development may be a fruitful endeavor.

In addition to genes contributing to normal craniofacial-genesis, a number of genes have been identified that cause congenital defects when mutated. Chief among these genes are *BMP4*, *MSX2*, *FGFR1, -2, -3*, and *TWIST1* (Wilkie, 1997). Having a list of genes known to affect craniofacial growth and development provides a foundation for studying the genetic architecture (see *2.6.6 Going a Step Further: Identifying Quantitative Trait Loci (QTL)*) of normal variation in the cranium, as it is quite possible that the same genes that cause malformations when mutated may also contribute to normal variation. Given that it has already been demonstrated that ancient pathways are reutilized by natural selection in producing evolutionary novelties like a

brain or a skull, genes that are identified in organisms as diverse as zebrafish, fruitflies, mice, and humans are liable to be largely the same as those affecting craniofacial variation in baboons. A more complete list of genes that have been implicated in craniofacial growth, development, and dysgenesis are listed in Table 2.2.

2.4.5 Craniofacial Growth in Papionin Skulls

A decent amount is known about the biology and morphology of rhesus macaques (*Macaca mulatta*), which have been used in studies of craniofacial growth since the 1960s. They are relatively long-lived primates (20-30 years) and, thus, have a growth trajectory that is more delayed than many primates used in biomedical research, which makes it more similar to that of humans. According to extensive longitudinal research by Schneiderman (1992), one of the biggest differences in monkey and human craniofacial growth is that during early human ontogeny the primary focus is on growth of the neurocranium to accommodate the rapidly expanding brain, while in the macaque, the facial skeleton is preeminent (see also Zuckerman, 1926 and Ashton, 1957). However, like humans their skulls continue to grow (up to age seven) even after reaching sexual maturity (around three years for females and four for males; Schneiderman, 1992).Additionally, of the taxa within the papionin family, macaques are considered to retain the most ancestral morphology (e.g., Disotell et al., 1992; Harris, 2000; Tosi et al., 2003; although see Singleton, 2002 who suggests *Papio* conserves the primitive pattern of craniofacial morphology), so it is a good model for understanding papionin evolution.

Enlow (1982) provides a comparison of growth patterns in rhesus macaque and human skulls. The basic growth plan of the monkey skull parallels that of humans with a few important differences related to differences in adult morphology. First, the amount of remodeling that occurs in the mandible and the location of this remodeling determines whether the final form is long, narrow and chinless like a monkey's or short, wide, rounded, and with a chin like a

Table 2.2 Genes Known to Effect Craniofacial Morphogenesis.

Gene	Name	Locus	Associated Malformations	Developmental Role	OMIM
ALX1	aristaless-like homeobox 1	12q21.31	frontonasal dysplasia	forebrain mesenchyme development, neural crest cell migration	601527
ALX4	aristaless-like homeobox 4	11p11.2	craniosynostosis, frontonasal dysplasia, cranium bifidum	calvarial development	605420
BMP4	bone morphogenetic protein 4	14q22-q23	orofacial clefts	mesoderm induction	112262
BMPR1A	bone morphogenetic protein receptor type 1A	10q22.3	bilateral cleft lip/palate	anterior-posterior axis formation, maxillary process mesenchyme proliferation, medial nasal process fusion	601299
COL11A1	collagen type XI, alpha-1	1p21	Marshall/Stickler syndrome, thick calvarium	cartilage collagen fibril formation	120280
COL2A1	collagen type II, alpha-1	12q13.11	achondrogenesis, cleft palate	major collagen synthesized by chondrocytes	120140
DHCR7	7-dehydrocholesterol reductase	11q13.4	cleft palate, craniofacial dysplasia	proper *SHH* function	602858
DLX3	distal-less homeobox 3	17q21	tricho-dento-osseous syndrome	branchial arch mesenchyme development	600525
EPBH3	ephrin receptor B3	3q27.1	palatal clefts	neurite outgrowth inhibitor	601839
EPHB2	ephrin receptor B2	1p36.1-p35	palatal clefts	hindbrain formation	600997
EYA1	eyes absent 1	8q13.3	oto-facio-cervical syndrome	eye, ear, and branchial arch formation	601653
FGFR1	fibroblast growth factor receptor 1	8p11.23-p11.22	Hartsfield, Jackson-Weiss, and Pfeiffer syndromes, trigonocephaly	suture development, neural crest cell migration into branchial arch II	136350
FGFR2	fibroblast growth factor receptor 2	10q26	Apert, Crouzon, Jackson-Weiss, LADD, Pfeiffer, and Saethre-Chotzen syndromes, scaphocephaly, craniofacial-skeletal-dermatologic dysplasia	suture development, osteogenesis of maxilla, mandible, frontal, and ear ossicles	176943
FGFR3	fibroblast growth factor receptor 3	4p16.3	Crouzon, LADD, and Muenke syndromes, thanatophoric dysplasia	chondroprogenitor cell patterning, endochondral ossification	134934
GLI3	Gli-Kruppel family member 3	7p13	craniosynostosis, Greig cephalopolysyndactyly syndrome	osteoblast differentiation during intramembranous ossification	165240
GSC	goosecoid homeobox	14q32.1	nasal cavity aplasia, pharyngeal muscle defects	mandibular and nasal development	138890

HAPLN1	hyaluronan and proteoglycan link protein 1	5q14.3	craniofacial anomalies	gives cartilage its tensile strength and elasticity	115435
HOXA2	homeobox A2	7p15.2	cleft palate	hindbrain segmentation and patterning	604685
HSPG2	heparin sulfate proteoglycan 2	1p36.1-p34	exencephaly	endochondral ossification, cartilage matrix formation	142461
JAG2	jagged 2	14q32	cleft palate, tongue-palatal shelf fusion	craniofacial development	602570
MSX1	muscle segment homeobox 1	4p16.2	orofacial cleft, tooth agenesis	skeletal muscle differentiation	142983
MSX2	muscle segment homeobox 2	5q35.2	craniosynostosis, cleidocranial dysplasia	calvarial osteogenic differentiation	123101
NODAL	nodal growth differentiation factor	10q22.1	holoprosencephaly	left-right axis formation	601265
NOG	noggin	17q22	craniosynostosis	TGFβ downregulation	
PAX3	paired box 3	2q35	craniofacial-deafness-hand syndrome	skeletal myogenesis	606597
PRRX1	paired related homeobox 1	1q24	agnathia-otocephaly complex	pharyngeal arch I patterning	167420
PRRX2	paired related homeobox 2	9q34.1	defects in ear ossicles, cleft mandible, calvarial bone reduction or loss	mandible fibroblast proliferation, inner ear epitheliomesenchymal interactions	604675
RUNX2	runt-related transcription factor 2	6p21	cleidocranial dysplasia	osteoblast differentiation and migration, suture development	600211
SHH	sonic hedgehog	7q36	holoprosencephaly	neural plate development	600725
TBX1	T-box transcription factor 1	22q11.21	velocardiofacial syndrome	vestibulocochlear formation	602054
TCOF1	Treacher Collins-Franceschetti syndrome 1	5q32	Treacher Collins-Franceschetti syndrome	neural crest cell formation and proliferation	606847
TFAP2A	transcription factor activating-enhancer-binding protein (AP) 2 alpha	6p24	branchio-oculo-facial syndrome	cranial closure	107580
TP63	tumor protein 63	3q28	orofacial cleft	epithelial morphogenesis	603273
TWIST1	twist family basic helix-loop-helix (bHLH) transcription factor 1	7p21.2	craniosynostosis	*FGFR* transcription, suture development	601622
WNT3	wingless-type MMTV integration site family, member 3	17q21	tetra-amelia syndrome	primary axis formation	165330

human's. It also explains why macaque incisors meet end-to-end while humans typically have an overbite. To produce the short, upright midface of a human, a significant amount of resorption occurs on the anterior surfaces of the maxillae and zygomatics; these are areas of deposition in the macaque skull. Martinez-Maza et al. (2015) determined these are also areas of deposition during craniofacial growth of chimpanzees and gorillas, both of which are more closely related to humans than are macaques, suggesting the ontogenetic pattern of bone modeling our faces undergo is unique to humans. Also, because the cranial fossae must be much deeper in the human neurocranium to contain our greatly enlarged brains, the amount of resorption on the internal surface of the cranial base is much more extensive in humans than in monkeys. Finally, due to our hypotrophied temporalis muscles, resorption in the infratemporal fossa is unnecessary in humans but must occur in the growing macaque skull to accommodate their relatively larger masticatory muscles.

Less work has been done on other papionin taxa, but Collard and O'Higgins (2001) determined that differences in the faces of the four main papionin genera (*Cercocebus, Lophocebus, Mandrillus, Papio*) are visible in immature individuals.[10] The authors also demonstrate that the craniofacial morphologies of the large-bodied taxa, which are dominated by an elongated rostrum, are homoplastic and evolved in parallel from a macaque-like common ancestor (see also Strasser and Delson, 1987 and Leigh, 2006). It is because of this elongated snout that, in comparison to other anthropoids, baboons consistently have the greatest degree of prognathism: 10-58% more than humans and great apes (Zuckerman, 1926; Fig. 2.12). When examining only large bodied papionins (*Mandrillus*, *Papio*, and *Theropithecus*) and accounting for both sexual dimorphism and allometry, crania of *Papio* are distinct from those of the other

[10]Collard and O'Higgins (2001) interpret this as evidence that interspecific facial differences should not be attributed to the effect of sexual selection. However, there is no reason to assume sexual selection would not affect developmental processes any less so than the resultant phenotypes.

two genera in having a klinorhynchous rostrum and browridges that slope laterally (Shea and Russell, 1986; Delson and Dean, 1993; Frost et al., 2003; although see Russell, 1985), while length of the nasals and prominence of glabella are intermediate (*Mandrillus* has longer nasals and *Theropithecus* has a more prominent glabella; Frost et al., 2003).

According to Collard and O'Higgins (2001), the final adult craniofacial form of the two larger-bodied papionins is produced via an interaction between allometry and an ontogenetic trajectory that diverges from that of the smaller-bodied taxa. This means *Papio* is not simply an enlarged copy of *Lophocebus*, and *Mandrillus* is not just a large *Cercocebus*—although differences in size do explain much of the combined craniofacial variation—as had been implied previously (Freedman, 1963; Jolly, 1970; Disotell, 1994; Harris and Disotell, 1998; Harris, 2000). Singleton (2012) futhered these analyses by conducting developmental simulation studies to

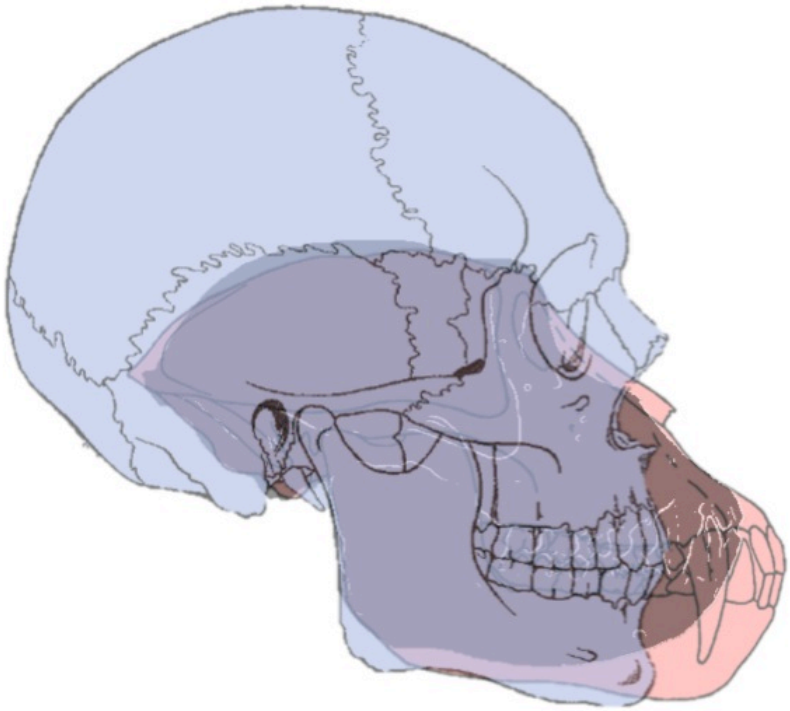

Figure 2.12 Differences in Degree of Midfacial Prognathism. Comparison of the profiles of human (blue), macaque (black), and baboon (pink) skulls. Skulls scaled to the same mandibular ramus width at the margin of the maxillary alveolus. Adapted from David et al. (2012).

compare these ontogenetic trajectories. Her results also suggest that taxon-specific craniofacial morphology is present at very young ages but extends this result to suggest that these species-typical patterns are enhanced by mechanical loading during adolescence. This reflects what laboratory experiments on developmental relationships have revealed: epigenetic interactions play a major role in shaping adult craniofacial form (see *2.4.3 Theories of Craniofacial Growth and Development*).

2.4.6 What is Known About *Papio* Craniofacial Morphology

It has also been demonstrated repeatedly that allometric scaling—shape differences among individuals that are directly related to size differences—is the single largest factor explaining craniofacial shape variation *within* the genus (e.g., Leigh and Cheverud, 1991; O'Higgins and Collard, 2002; Singleton, 2002; Frost et al., 2003; Leigh, 2006; Porto et al., 2009). In other words, many consider male baboons to be "scaled up" versions of their female conspecifics. For example, Freedman (1962) demonstrated that the relative growth rate of the calvarium to the rostrum in both sexes is similar, suggesting that either an extension of the male or a contraction of the female growth trajectory is responsible for the rostrum being relatively longer than the calvarium in adult males as compared to adult females, even though the ratio of the two is the same at birth. Despite such examples, O'Higgins and Collard (2002) suggested that, in addition to being allometric, the cranial growth trajectory in males also diverges from that of females later in development, which alters the shape of their adult cranial forms (see also Leigh, 2009).

This pattern of dual contributing factors to sexual dimorphism in craniofacial morphology appears to be unique to *Papio* and may be related to differences in masticatory muscle mass and dentition (males have much larger canines and a C/P_3 honing complex) that produce

different loadings in the facial skeletons of males as compared to females.[11] Although the fact that male growth trajectories do not diverge from female ones until later, which corresponds to the development of male secondary sexual characteristics like hypertrophied muscles and enlarged canines, it is unclear why other papionins that demonstrate both large degrees of sexual dimorphism and large crania (i.e., *Mandrillus* spp.) do not also follow a similar developmental pattern. More work on the ontogeny of craniofacial sexual dimorphism in non-*Papio* papionina taxa needs to be done and more specimens need to be included in future research designs in order to understand the craniofacial homoplasies in the tribe.

Although the craniofacial growth trajectories of the various baboon (sub)species (*Papio hamadryas anubis, P. h. cynocephalus, P. h. hamadryas, P. h. kindae, P. h. papio,* and *P. h. ursinus*) are similar early in development, morphological differences do distinguish the groups at later ontogenetic stages (e.g., Freedman, 1963; Frost et al., 2003; Leigh, 2006). Among the (sub)species these morphological differences primarily define the robustness of the masticatory system (e.g., width of the rostrum, bizygomatic breadth, basicranial flexion, presence/absence of maxillary and mandibular fossae) and may be related to dietary differences. Frost and colleagues (2003) determined that these subspecific differences in cranial morphology are distributed across sub-Saharan Africa along a stepped cline. Baboons at more northern latitudes have crania that are both broad and less flexed and that also have broad rostra, while the crania of their southern counterparts are more klinorhynch. Additionally, Freedman (1963) demonstrated a geographic cline for overall skull size: smaller individuals (*P. h. kindae*) located on the west side of the continent and larger ones to the east (*P. h. cynocephalus*), south (*P. h. ursinus*), and northeast (*P. h. anubis*) with hybrid zones between adjacent populations.

[11]This may also explain sex-specific differences in the shape of the supraorbital torus, or browridge, as Oyen et al. (1979) suggest changes in patterns of strain on the facial skeleton as a result of the effect of sequentially erupting teeth on masticatory stress loads induces the formation of the supraorbital torus in a cyclic manner.

One of the more unique traits of the genus *Papio* is the ability of groups of sympatric individuals to hybridize. This often results in troops composed of individuals displaying either phenotypes of one of the two parental subspecies or a combination of phenotypes from both parental subspecies (e.g., Maples and McKern, 1967; Dunbar and Dunbar, 1974; Samuels and Altmann, 1986; Jolly et al., 1997, 2011; Alberts and Altmann, 2001). These hybrid individuals are fertile and often display unique behaviors and possess unusual morphologies, such as supernumerary or agenetic teeth (Freedman, 1963; Ackermann et al., 2006; Ackermann, 2010; Ackermann et al., 2014). This causes a problem when attempting to apply the commonly used Biological Species Concept (BSC; Mayr, 1940) to *Papio* populations, as hybrid fertility suggests the existence of only a single baboon species, according to the BSC. However, the appearance of novel phenotypes in hybrids suggests that the parental groups are likely genetically divergent, which makes each parental group consistent with the Phylogenetic Species Concept definition of a species as "the smallest diagnosable cluster of individual organisms within which there is a parental pattern of ancestry and descent" (Cracraft, 1983). According to McKitrik and Zink (1988), the occurrence of hybridization among the parental populations only suggests they are part of a clade, not that they are conspecific—evidence in favor of elevating baboon subspecies to species status.[12]

Despite these taxonomic issues, all baboon populations share a common pattern of sexual dimorphism in craniofacial form that differs only in degree. Male crania can generally be distinguished from those of females by many of the same features that distinguish baboons from other papionins: (1) a more prognathic mid-face, (2) greater sub-nasal height, (3) broader

[12] McKay and Zink (2015) posit an intriguing theory that ground finch (genus *Geospiza*) evolution is better described as Sisyphean, or characterized by varying stages of differentiation that never reach a point of diversification because of a balance between natural selection and introgression. Therefore, the populations should be considered transient ecomorphs of a single species only, *G. magnirostris*. This may be the best model for baboon evolution as well, given the unpredictable, cyclical nature with which baboon populations have diverged and intermittently reconnected to produce a large assortment of hybrid phenotypes and genotypes throughout the Pleistocene and Holocene.

zygomatic roots, (4) greater degree of klinorhynchy, and (5) a deeper and more narrow maxilla (O'Higgins and Collard, 2002). Males and females share a common ontogenetic trajectory and local shape changes in their crania are similar. Leigh and Cheverud (1991) demonstrated that the morphological differences between the sexes are produced by altering growth duration. Female baboons cease growing sooner than males, allowing the males to achieve a greater overall size (see also Leigh, 2009). As allometric scaling plays a major role in baboon craniofacial variation, the result is that male crania look different simply because they are larger. Willmore et al. (2009) suggest evolution of this sexual dimorphism may have been facilitated by differences in the amount of genetic variance in craniofacial traits with males demonstrating more variation than females. However, there is a paucity of research on the genetic underpinnings of baboon craniofacial variation and much more needs to be done before forming any specific hypotheses about papionin craniofacial evolution.

2.5 Patterns of Variation in Skulls

Craniofacial anatomy co-varies spatially within an individual and temporally across both ontogenetic and evolutionary time (Olson and Miller, 1958). These patterns can be assessed to test hypotheses about the underlying functional, phylogenetic, or developmental relationships that structure these morphological patterns and contribute to our knowledge of how adaptive processes create and modify complex structures. Mammalian skulls are very complex in that they house anatomical systems designed to accomplish specific tasks: seeing, hearing, masticating, tasting, swallowing, thinking, and smelling. In answering a number of evolutionary questions, such as how ecology contributes to form (e.g., hyenas incorporate crushed bone into their dietary repertoire so is this why they have large sagittal crests?) or how life history affects development (e.g., because newborn South American opossums, genus *Monodelphis*, are extremely altricial but must be able to acquire milk from their mothers, is that why their mouths

and forelimbs are more developed than their eyes and hindlimbs at birth?), it is tempting to reduce organisms into modules. A larger, more complex structure can be considered modular if its constituent parts are quasi-autonomous and internally unified to the (partial) exclusion of other such parts (Wagner et al., 2007). However, because the structure as a whole must remain adapted to an organism's environment, it should also be considered in a holistic, integrated manner. The implications of these interrelated and complementary views of *modularity* and *morphological integration* for the study of craniofacial anatomy and evolution are discussed below.

2.5.1 Craniofacial Modularity

Modularity is concerned with whether a complex system can be subdivided into relatively independent smaller units, within which the component elements interact primarily with each other and, in doing so, contribute to the greater whole (Klingenberg, 2008). Modules can be formed for a variety of reasons. *Developmental modules* comprise tissues formed via the same molecular pathways, from the same embryonic germ layer, or because they are affected by the same developmental process (e.g., tissue interactions, hormone exposure). They interact as they develop during an individual's ontogeny and affect each other's final forms. The individual components of a *functional module* may not be related developmentally, and could even participate in different developmental modules, but they interact to perform a specific function during the lifespan of an individual. This reinforces the fact that modules are quasi-autonomous in that units of one such module are not precluded from also participating in other such modules (Winther, 2001).

Determining whether modules are congruent within an organism—for instance, if traits that develop together also function together or if traits affected by variation in the same gene(s) vary together in the adult—provides information on how modularity is produced at the biological

level (Wagner et al., 2005; Villmoare et al., 2014). In rare cases, the pathways producing morphological variation are known. More often patterns of variational modularity (Wagner et al., 2007), or the degree to which morphological traits covary (Fig. 2.13), are measured, and from them we infer the unknown biochemical and gene regulatory interaction networks that produce these *variational modules*.

Understanding how genetic variation is translated into and modified by epigenetic factors to produce and structure phenotypic variation is known as genotype-phenotype (GP) mapping (Mezey et al., 2000; Wagner, 1996). The opposite is also true: examining the GP-map (Fig. 2.14) provides information on genetic modularity. Traits within a *genetic module* are ones that

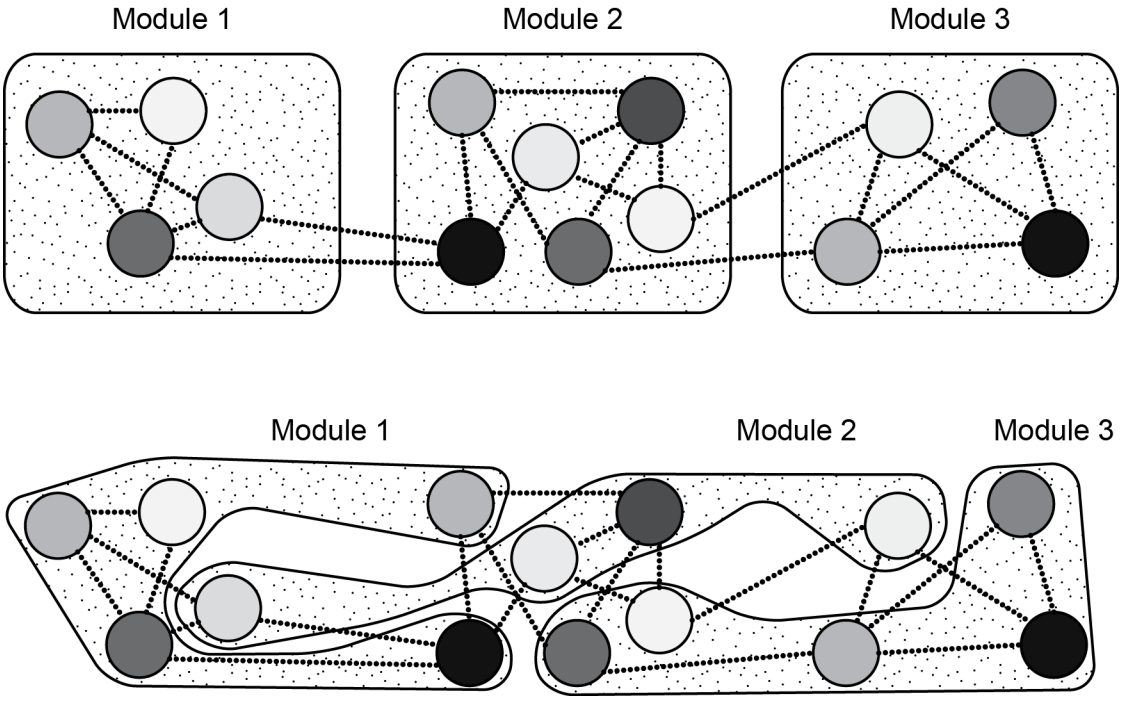

Figure 2.13 Cartoon Diagram of Modularity. Traits are represented by grayscale circles, modules by speckled polygons with rounded corners, and significant correlations as dashed lines. Traits that are correlated are considered integrated. Panels: (top) Module boundaries have been correctly drawn around their traits because there are more correlations between traits within a single module than there are between two adjacent modules. (bottom) The traits and lines of integration are in the exact same locations but the module borders have been redrawn incorrectly because there are now just as many correlations among traits within a module as there are between modules.

are affected by variation in the same gene (i.e., pleiotropy), interactions among genes (i.e., epistasis) that affect multiple traits (Wolf et al., 2005, 2006), or variation in two linked genes, as measured by either genetic linkage within a pedigree or linkage disequilibrium within a population (see *2.6.5 Methods for Conducting Quantitative Genetic Research*). This is important because traits with a common genetic basis are inherited together and, therefore, evolve together (Lande, 1979; Cheverud, 1996a): they are *evolutionary modules*.

Examination of modularity in the skulls of NWM (Marroig and Cheverud, 2001), OWM (Cheverud, 1989; de Oliveira et al., 2009), and hominoids (Ackermann, 2002) suggests that craniofacial variation patterns have remained relatively stable during anthropoid evolution. This is surprising given the diversity in cranial shape and size recognized across Anthropoidea and is likely explained by a conserved genetic basis for craniofacial form (de Oliveira et al., 2009). Factors having a global effect on (overall) craniofacial form are typically under stronger purifying selection while those having local effects, such as those operating solely within one or a few modules, are more likely free to vary (Mitteroecker and Bookstein, 2008). This observation has been used to explain why human heads look so different from those of most other primates: the strength of covariation among craniofacial modules in hominins has been reduced, allowing for the emergence of new patterns and novel factors with purely local effects (Wagner, 2007).

Modularity promotes evolvability—the ability to respond to selection (Houle, 1992; see *2.2 Craniofacial Diversity*). Organizing traits into modules maintains organismal cohesion by constraining traits to covary while allowing evolutionary forces to act simultaneously within modules without causing correlated responses in other distinct modules (Lande, 1979; Klingenberg, 2008). In other words, by definition, in the short run, the effect of interactions among parts within a module will be greater on components that share a module. However, in the long run, the overall effect of parts is an aggregate across modules (Simon, 1962). The.

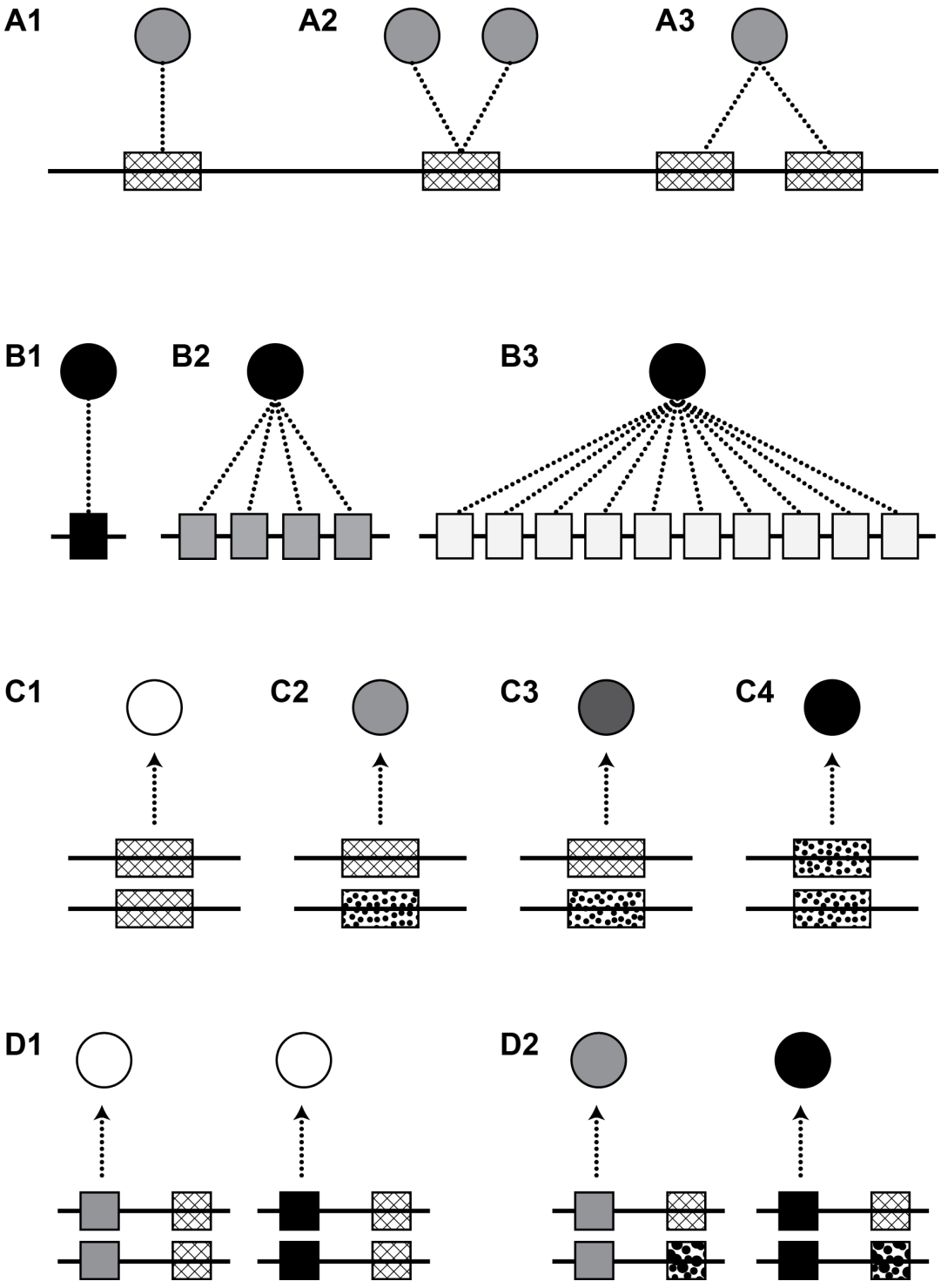
A1
A2
A3
B1
B2
B3
C1
C2
C3
C4
D1
D2

Figure 2.14 Cartoon Diagram of Genotype-Phenotype Map Characteristics. Individuals are represented by circles and their phenotype is a grayscale color, gene effects by dashed lines, chromosomes by horizontal solid lines, and genes by filled rectangles (stacked rectangles in panels C and D are alleles of the same gene so, if each rectangle of the pair has a different fill they demonstrate a heterozygous condition whereas a pair with the same fill demonstrates homozygosity). Panels:
A) What is the relationship between traits and genes? A1: Mendelian, A2: pleiotropy, A3: polygeny.
B) How many genes are involved? B1: monogeny, the gene contributes 100% to the phenotype. B2: oligogeny, each gene contributes 25%. B3: polygeny, each gene contributes 10%.
C) Dominance. C1: white homozygote, C2: heterozygote with no dominance deviation because the phenotype (50% gray) is exactly halfway between the two homozygotes, C3: heterozygote with dominance deviation because of an interaction between the two different alleles causing the trait (75% gray) to be more similar to one of the two homozygotes, C4: black homozygote.
D) Epistasis. D1: Although the genotypes of the two individuals are different at the primary locus (one is homozygous dominant and the other homozygous recessive), the genotype at a linked locus (the hashed-rectangles) masks the effects of the primary locus alleles. D2: Two individuals with the same genotypes at the primary locus as in D1, but being a heterozygote at the linked locus allows the primary locus genotype to dictate the individuals' phenotypes.

result is that, paradoxically, evolvability of a system is proportional to its modularity (Wagner and Altenberg, 1996)

For example, Drake and Klingenberg (2010) determined that, rather than being an integrated whole, dog skulls comprise separate neurocranial and rostral modules. The tissues that comprise these modules are primarily derived from paraxial mesoderm and the neural crest, respectively (Noden and Trainor, 2005; see *2.4.1 Craniofacial Embryogenesis*). Consequently, one possible explanation for the astounding diversity of dog skull shapes is that modularity has permitted genetic modifications to developmental processes differentially affecting these two cell lineages, leading to diversification in how the two modules relate to one another in different breeds.

However, Klingenberg et al. (2004) found that genetic variation affecting multiple dimensions of the mouse mandible was not constrained to affect dimensions contained within the same module. In other words, a single genetic variant was just as likely to affect portions of both the alveolus and the ascending ramus—the two separate modules of the mouse mandible—as it was to affect only the alveolus or only the ascending ramus. This result

complicates the picture but makes sense in light of the fact that, despite a complex structure being modular in design, the individual modules must remain *integrated* enough with one another to still interact synergistically.[13]

2.5.2 Morphological Integration in the Cranium

Interactions among processes that produce subunits within a system contribute to the degree of integration, or covariation, among the different elements. Therefore, an alternative concept of modularity is that it is the pattern of differential intensity of integration across a complex system. As many modules share components (e.g., in primates the roof of the orbit is the floor of the anterior brain case and the floor of the nasal cavity is the roof of the oral cavity), change in one module that may individually increase fitness has the potential of producing a net decrease in fitness through its effect on the function or development of a related module. In a similar manner, systems that are tightly integrated are typically free only to vary along a few morphological axes because change to any portion of the structure results in change to all portions. As a result, constraints are imposed on both the degree of modularity a system can maintain and the extent of its integration to strike a balance between the two.

Determining whether integration patterns are congruent across different organisms can elucidate the selective pressures that were unique to individual taxa, as these patterns affect the evolvability of trait means. Cheverud (1996b) compared patterns of developmental, functional, and genetic integration within cotton-top tamarins (*Saguinus oedipus*) to those within saddle-back tamarins (*S. fuscicollis*) and used the observed pattern of genetic covariance in tamarin crania to reconstruct the differential selection gradients that contributed to changes in trait

[13] It is also possible this result is an artifact of the methods employed by Klingenberg and colleagues (2004). They used Procrustes analysis to quantify morphological variation. However, Garcia et al. (2015) have demonstrated that this practice is problematic because it lacks power to detect modularity patterns. Essentially, local shape variation is redistributed throughout the cranium during the registration process in which a mean landmark configuration is used as the baseline for calculating shape variables such as Procrustes distances and/or residuals.

means. He determined that the gradients were grossly similar, but the minor differential pattern did suggest that *S. oedipus* alone had experienced selection for an increased gape and an emphasis on the anterior dentition.[14]

2.5.3 Morphological Relationships in Baboon Skulls

Although the history of examining morphological relationships among baboon skull parts is not as deep as that of similar research for humans, we have learned a good deal about baboon craniofacial morphology. In comparing patterns of craniofacial variation between papionins, Joganic and colleagues (2012a) determined that the neurocranium of baboons is less globular than that of macaques, being more restricted mediolaterally in the base, and that their orbits are oriented more horizontally, perhaps as a result of the extreme degree of midfacial prognathism. Again, as with the masticatory morphology of *S. oedipus*, polarity for the differences (see Footnote 14) between baboon and macaque crania cannot be established without an outgroup, so it is possible macaques experienced selection for a more globular neurocranium and more vertically oriented orbits. However, because macaques likely retain more ancestral features, the increased body and facial size of baboons being an autapomorphy (see *2.3.2 Baboon Systematics*), and we know that allometric variation is significant in baboon crania (see below), the first scenario is the more likely of the two, at least for the trends in facial morphology.

Most craniofacial variation in baboons is related to differences in scaling, or allometry. Leigh (2006) determined that 76% of baboon craniofacial variation is attributable to ontogenetic allometry, or size-related shape change that occurs as individuals grow and develop. He also compared craniofacial growth trajectories among subspecies and determined that subspecies shared a common growth pattern; it was largely heterochronic changes in developmental timing

[14]The actual polarity of these changes cannot be established and it may well have been *S. fuscicollis* that experienced selective pressure in the opposite direction (see *2.2.2 The Marriage of Morphological and Genetic Methods*).

that produced interspecific craniofacial differences. Because subspecies share growth trajectories—and baboon growth trajectories are dominated by size-related change—it is likely that selection on body size during growth was the most salient aspect of baboon evolution. Despite common growth patterns, some (5%) interspecific differences in form are independent of size, including bizygomatic breath, cranial flexion, and rostral dimensions (Leigh, 2006). One of the most important implications of Leigh's (2006) results is that ontogenetic trajectories are non-linear and differ by sex, perhaps suggesting that craniofacial growth spurts occur at different times in different types of individuals, which influences inferences made from samples of individuals of unknown age.

Leigh (2006) also determined that sexual dimorphism is a major factor explaining craniofacial variation: female crania are relatively wider and they have larger neurocrania and shorter rostra than males. In examining the relationship between genetic and phenotypic variance in craniofacial parameters of demonstrated sexual dimorphism, Willmore et al. (2009) found little evidence to support the theory that sexually dimorphic traits (such as those of the baboon face) should show gene-by-sex interactions or X-linked inheritance patterns relative to traits in the rest of the cranium. The average intersex genetic correlation coefficient was 0.97, indicating that both sexes respond largely the same to selection. Instead, they determined that male genetic variance estimates for craniofacial traits are generally higher than those of females, resulting in increased sexual dimorphism, meaning they respond more readily to selection even if selection is the same across sexes.

Finally, Roseman et al. (2010) examined patterns of genetic covariance in traits from different regions of the baboon skull to determine if any might be better for use in phylogenetic reconstructions and to compare patterns of phenotypic and genetic variation. Prior to the work of Roseman and colleagues (2010), it was assumed that endochondrally ossifying components

of the skull would be better for phylogenetic analysis because they finish growing sooner and, therefore, might be less inclined to deform or remodel in response to masticatory stress (e.g., Corruccini and Beecher, 1984; de Beer, 1985). The logic was that this would make such traits more resistant to evolving in a homoplastic manner as a response to environmental effects. Contrary to expectation, the authors found no support for this assumption, the distribution of genetic effects being randomly distributed throughout the entire cranium. They also determined that patterns of phenotypic and genetic variation are largely similar, a result that echoes similar findings in the crania of macaques (Cheverud, 1982), tamarins (Cheverud, 1995), and a large sample of NWMs (19 species representing 7 genera; Marroig and Cheverud, 2001), suggesting that such patterns are conserved across Primates.

2.6 Quantitative Genetics

Complex traits are assumed to be at least oligogenic—under the influence of a few genes of moderate effect—if not polygenic—under the influence of many genes of small effect (Hill, 2010). Interactions between (1) alleles at a locus, (2) alleles at multiple genes throughout the genome (epistasis), and (3) the genes and the environment in which they act (environmental interactions) also contribute to such phenotypes. Measuring phenotypic values in a population provides an estimate of both the overall mean and variation around this mean, which can then be partitioned into the different sources that contribute to phenotypic variance (V_P):

$$V_P = V_G + V_E + 2cov_{GE} + V_{GE} \quad (2.1)$$

V_G includes variation due to: additive gene effects (V_A), genetic effects that are not heritable (V_D), and interactions between the two (V_I); V_E encompasses sources of variation that arise from differences in the environment across the population; $2cov_{GE}$ represents any correlation between genotypic values and environmental variance; and V_{GE} is the interaction of genetic with environmental variation. For example, variation in human intelligence (V_P) can be attributed to

additive genetic variation (V_A), differences in nutrition (V_E), correlations between the two ($2cov_{GE}$; e.g., children who are judged to be more intelligent are often placed in advanced classes), and interactions between the two (V_{GE}; e.g., some children perform well on standardized tests used to "measure" intelligence while others are affected negatively by such pressure).

To determine the relative significance of the contributions of V_G and V_E to a phenotype's variance, its *heritability* is established. In the most basic of terms, this is simply the ratio V_G/V_P and it describes the extent to which phenotypic variations are determined by genetic variations (broad-sense heritability, H^2) within a generation. Of both greater interest to evolutionary biologists and more importance to this discussion is the narrow-sense heritability (h^2), or the proportion of V_P that is attributable to gene effects passed from parent to offspring (V_A). For the remainder of this dissertation I will use heritability to mean only narrow-sense heritability.

2.6.1 Basic Quantitative Genetic Parameters

For illustrative purposes I will use B and b to represent the alleles at a single biallelic locus. Three genotypes are observable at this locus in frequencies proportional to the population's allele frequencies, given Hardy-Weinburg Equilibrium: BB, Bb, and bb. Each genotype is associated with a genotypic value (by convention, BB = *+a*, bb = *-a*, and Bb = *d*) such that the genotype confers a specific value to the individual's phenotype. The genotypic value halfway between *+a* and *-a* is 0 and this is the value you would expect the Bb genotype to confer as the individual has one copy of each allele. If $d = 0$, the alleles are described as being additive because the relationship among genotypic values is linear and the heterozygote is located at the midpoint between the two homozygote genotypic values. If $d \neq 0$ then the locus is said to exhibit dominance because the two alleles interact such that heterozygotes more closely resemble one of the two homozygotes, rather than being exactly intermediate between them (see Panel C, Fig. 2.14). The sign of *d* determines which allele is the dominant one.

Because dominance deviation is a property of allele *combinations*, it is not transmissible between generations. Only the effects of *individual* alleles can be inherited because each parent contributes only half the genotype. The contribution of an individual allele to a phenotype within a population is its average effect (α_i) which is a function of *a*, *d*, the allele's frequency in the population, and the system of mating. The average effects of the alleles within a parent's gametes will determine how offspring differ from their population mean. The sum of the average effects of the two gene copies present in the diploid genotype is the breeding value (*A*), which is evaluated for all genes whose variation contributes to V_P. The average squared breeding value (V_A) is the numerator for calculating h^2.

Traits with a larger h^2 value will have a greater degree of resemblance between parents and offspring. The slope of offspring *P* on the *P* of a single parent is $\frac{1}{2}h^2$ (one parent provides only half of the offspring's genetic material) whereas the slope = h^2 when the average parental *P* is the independent variable (Fig. 2.15). Siblings, especially full sibs, share common environments, thus biasing h^2 upward by overestimating familial resemblance. There are methods of accounting for this by including relatives of varying closeness.

2.6.2 The Breeder's Equation and its Multivariate Equivalent

In addition to its use for evolutionary time scales, heritability is also an important parameter on shorter time scales as knowledge of breeding values can be used to make informed decisions in selective breeding populations. In fact, early 20th century agribusiness brought science to the art of food production by pioneering quantitative genetic methods (e.g., Hanson and Robinson, 1963; Turner and Young, 1969) and continuing to use them today (Miflin, 2000; Andersson and Georges, 2004). Heritability estimation has been an integral part of endeavors to change a population's characteristics in an efficacious manner. In most cases, this change is to the

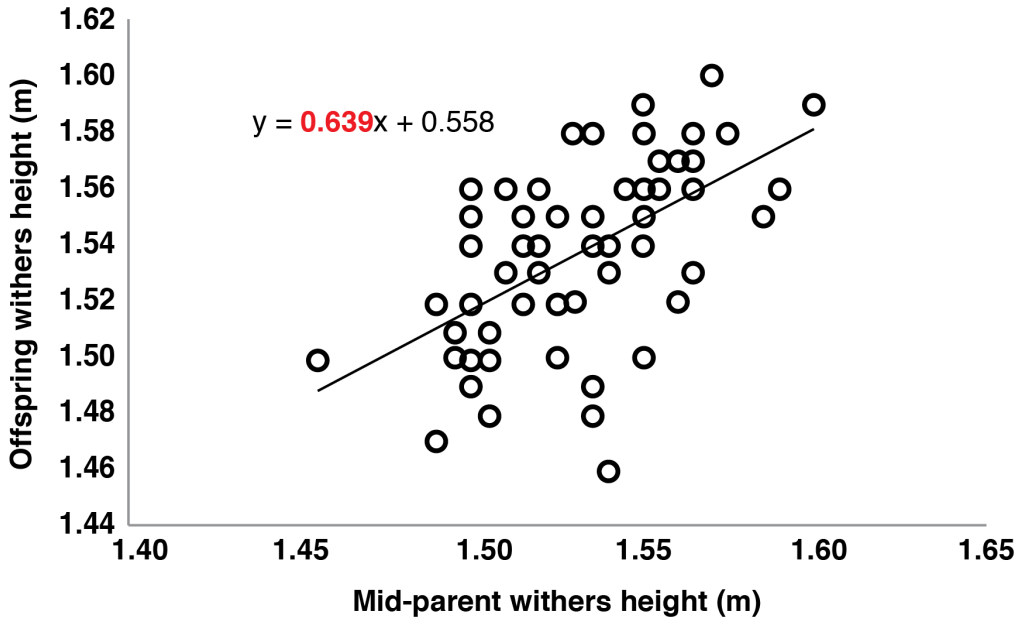

Figure 2.15 Ordinary Least Squares Regression of Offspring on Mid-Parent Values for Height at Withers in Horses (*Equus caballus*). The mean phenotypic value for all offspring of each parental pair is plotted on the Y-axis. The OLS equation is provided and the regression coefficient (*b*) is indicated in bold, red typeface. It is an estimate of the heritability of withers height in this sample ($b = h^2$). Adapted from Oldenbroeck and van der Waaij (2015).

population's mean phenotype, which is symbolized as *R*, the response to selection. As *A* is a major determinant of *P*, the equation describing the impact V_A has on *R* is defined in the Breeder's Equation:

$$R = h^2 S \tag{2.2}$$

where *S* is the force of selection applied to the phenotype in question. This means that, for example, the increase in milk yield (*R*) a dairy farmer is hoping to achieve in his/her next generation of Holsteins by selectively breeding high-yield cows (*S*) is a factor of the magnitude of heritable variation in milk yield. The difference in mean phenotype between the high-yield cows selected for breeding and that of unselected individuals (*S*) and knowledge of a trait's h^2 provides a way to estimate *R*. In an evolutionary sense, this is a valuable attribute of Equation 2.2 if formulating hypotheses about the potential selective forces applied is the goal.

The example used above describes the case in which selection acts upon a single trait. However, the reality is that traits co-vary because their function and developmental pathways are interrelated (see *2.5.2 Morphological Integration in the Cranium)* and are co-inherited because of linkage disequilibrium and pleiotropy (see *2.6.5 Methods for Conducting Quantitative Genetic Research*). The implication of this covariance is that change in one trait will almost always produce a concomitant change in the traits phenotypically and genetically correlated with the true target of selection. To reflect this trait inter-relationship, Lande (1979) proposed a multivariate version of the Breeder's Equation:

$$\boldsymbol{\Delta z = G\beta} \tag{2.3}$$

where **Δz** is a vector of changes in mean trait values, **G** is the additive genetic covariance matrix (explained in greater detail in *2.6.3 The G-matrix and What It's Good For*), and **β** is a vector of selection gradients, or the regression of relative fitness on the phenotype: $\boldsymbol{\beta = P^{-1}S}$. Taking the case of two traits, $\boldsymbol{z_1}$ and $\boldsymbol{z_2}$:

$$\begin{bmatrix} \boldsymbol{\Delta z_1} \\ \boldsymbol{\Delta z_2} \end{bmatrix} = \begin{bmatrix} \boldsymbol{G_{11}} & \boldsymbol{G_{12}} \\ \boldsymbol{G_{21}} & \boldsymbol{G_{22}} \end{bmatrix} \begin{bmatrix} \boldsymbol{\beta_1} \\ \boldsymbol{\beta_2} \end{bmatrix} \tag{2.4}$$

and multiplying through the multivariate Breeder's Equation demonstrates how important genetic covariance is to trait evolution:

$$\boldsymbol{\Delta z_1 = G_{11}\beta_1 + G_{12}\beta_2} \tag{2.5a}$$
$$\boldsymbol{\Delta z_2 = G_{21}\beta_1 + G_{22}\beta_2} \tag{2.5b}$$

Any evolutionary change in a phenotype is the result of both direct selection on that trait—the first term in each equation—as well as indirect selection on any correlated traits—the second term. For this reason, understanding how individual components are correlated with one another, both at the phenotypic and the genetic level, is important to model complex trait evolution (e.g., Mezey et al., 2000; Wagner et al., 2008; Wagner and Zhang, 2011). That is a major goal of this dissertation: to determine trait covariation within the baboon cranium and to

create hypotheses about the significance of this covariation for craniofacial evolution in papionins.

2.6.3 The G-matrix and What It's Good For

The G-matrix is a symmetric matrix with V_A for each trait on the diagonal and additive genetic covariance between traits i and j on the off-diagonal (cov($A_i A_j$)). Estimates of **G** are obtained by measuring phenotypic covariance (cov($P_i P_j$)) in large populations of individuals of known genealogical relationship and comparing the observed value to that expected based on amount of co-ancestry among individuals (Lynch and Walsh, 1998; Falconer and Mackay, 1996). This has been accomplished in a wide variety of animal taxa, ranging from frogs to sheep to guppies (e.g., Lofsvold, 1986; Brodie, 1993; Shaw et al., 1995; Vaez et al., 1996; Reznick et al., 1997; Arnold and Phillips, 1999; Roff and Mousseau, 1999; Cano et al., 2004; Sigurdsson et al., 2009). However, these conditions are rarely met in primates due to relatively long interbirth interval, gestation, and maturation and to reduction in the number of offspring produced per parturition. Hence, the more readily estimated matrix of phenotypic variances and covariances (**P**) is often used as a proxy for **G** (Cheverud, 1988; Roff, 1995, 1996; Waitt & Levin, 1998; Reusch & Blanckenhorn, 1998).

Cheverud and various coauthors estimated both **P** and **G** for the cranium in macaques (Cheverud and Buikstra, 1981; Cheverud 1982) and tamarins (Cheverud, 1996b). These were the first attempts at understanding whether most phenotypic variance is genetic. Resolution for Cheverud's analyses was reduced because sample sizes (both census and effective, see *4.2.4 Sample Size Verus Effective Sample Size (N_e)*) were relatively small and, in the case of the Rhesus macaques (*Macaca mulatta*) on Cayo Santiago, Puerto Rico, only matrilineal heritage was established. This increases standard errors for estimates of h^2, limiting power and efficiency of the estimate. The extended pedigree research design used in this dissertation provides an

opportunity to estimate both **G** and **P** for a primate taxon's craniofacial complex to unprecedented levels of precision. First, all genealogical relationships are known, which provides twice the information about co-inheritance patterns than would be true if only one parent were identifiable. Secondly, the census population size is large enough to ensure that power is sufficiently large to estimate quantitative genetic parameters. Consequently, I have the ability to answer questions about the genetic makeup and evolutionary history of the cranium in a species more closely related to humans than traditional biomedical mouse models. Comparison between my results and corresponding ones for other taxa may provide insight into the general genetic makeup of the mammalian cranium as well as fodder for the development of more targeted research questions about our own evolutionary history.

2.6.4 Genotype-Phenotype Maps

As population-level variation is essential to evolution, understanding the evolutionary history of and potential for future change in a complex structure involves bridging the gap between developmental genetic mechanisms working at the individual level during ontogeny to produce adult phenotypes and the population-level variation in those phenotypes (Hlusko, 2004; Hallgrímsson et al., 2007, 2009; Hlusko and Mahaney, 2009). Quantitative genetics provides a tool for statistically bridging genotype and phenotype, providing a method for both identifying the genes that underlie variation in complex traits and defining the GP-map. This "map" describes how genetic variation at each genomic locus is translated at the phenotypic level through the lenses of development and plasticity. Characteristics of the GP-map include descriptions of:

- pleiotropy: a single gene affecting multiple traits,
- epistasis: genetic variation in one gene influencing the phenotypic effects of other genes,
- polygeny: many genes contributing to a single trait, and
- genetic modularity: non-overlapping suites of genes underlying different trait sets (Zeng et al., 1999; Shao et al., 2008; see Fig. 2.14).

The GP-map details how genetic variation influences phenotypic variation (Debat and David, 2001), how genetic correlations (i.e., the G-matrix) have evolved (Phillips and Arnold, 1999; Steppan et al., 2002), and the potential for genetic variation to yield adaptive change (Altenberg, 1995). For example, traits that are strongly genetically correlated will respond to indirect selection on each other (Lande, 1979; although see Gromko, 1995). If this response by both traits is adaptive, morphological change can occur more quickly than if the traits were uncorrelated and being selected for independently. However, the necessity of maintaining emergent functions of trait complexes means that evolution may be constrained if selection for one trait produces negative effects on a correlated trait. One way to circumvent this antagonism is through morphological redundancy, which may explain the evolution of the complex four-bar linkage system of wrasse (family, Labridae) jaws (Alfaro et al., 2005). Another way would be to develop genetic modularity whereby a set of genes has effects concentrated within a functional complex of characters more so than by chance. Mezey et al. (2000) found evidence for this in the ascending ramus of the mouse mandible—and that this region is independent from the alveolar region—which comprises half of the masticatory system.

2.6.5 Methods for Conducting Quantitative Genetic Research

Genes underlying variation within a complex trait can be identified by: (1) testing candidate genes that have been previously implicated in the etiology of the trait because of knowledge of developmental processes, metabolic pathways, and/or functional analyses or (2) scanning the genomes of a large number of individuals who demonstrate a range of phenotypic variation in the trait. Because the first approach starts with a proposed candidate gene(s), it is considered hypothesis testing. In systems where the anatomy and physiology are well studied, this is an appropriate and preferred approach because power is greater when testing smaller genomic stretches and powerful haplotype tree approaches can be utilized (e.g., Templeton et al., 2005).

In contrast, the second approach makes no assumptions about putative involved biological processes and is hypothesis-generating. The benefit of such an approach is that it identifies previously unidentified genomic loci that can then be tested with more targeted, candidate gene-based approaches (Borecki and Suarez, 2001).

Regardless of methodological specifics, the basic premise underlying all methods of dissecting the genetic basis of complex traits involves demonstrating an association between a locus and the trait. Both linkage and association can be used to test candidate genes and perform genome scans. The available data will determine the type of analysis conducted: association studies identify relevant genetic variants using population data while pedigree studies identify loci that co-segregate with phenotypes within families. If the data and resources are available, both can be used in conjunction to clarify the genetic basis of a trait, as the methods will likely produce complementary, rather than identical, results.

When a pair of alleles appears together more often than expected based on random assortment, given the degree of relatedness among individuals, they are in linkage disequilibrium (LD). Linkage disequilibrium is a violation of Mendel's Law of Independent Assortment, which states that both genes and alleles are split between germ cells at random (i.e., probability = 0.5) during meiosis. The research sample used in my dissertation was derived from a colony of baboons with a unique population history that lends itself well to linkage analysis. Two loci can demonstrate LD if they are physically close on a chromosome—the likelihood of a recombination event splitting a chromosome between loci during meiosis increases with increasing distance between a pair of loci. In other words, recombination is a function of distance between loci. In fact, the unit of measure for recombination is the centiMorgan (cM), which is defined as the distance between two loci for which the expected number of chromosomal crossover events is 1 in 100 per generation.

Production of LD depends on a population's history of mutation, and it is destroyed by recombination. The founder population was a hybrid population of Anubis and yellow baboons, which would produce high levels of LD among genetic loci. Parental type gametes for a pair of genetic loci would contain anubis alleles at both loci (AA) or yellow alleles at both loci (YY), giving complete LD. Independent assortment of the loci would produce the two contrasting gamete types in equal number (AY or YA), destroying the LD. If the loci in LD are genetically closely linked, they will remain in LD for many generations because recombination between them is low. A locus used as a molecular marker will retain LD with a linked locus that effects the phenotypic variation of interest.

Recombination frequency varies across an individual's genome (Sturtevant and Beadle, 1936), between sexes (Morgan, 1914), and among species (e.g., Ptak et al., 2005) so genetic map distances are not equivalent to physical map distances, or the actual number of base pairs along a chromosome. Linkage analysis is performed by measuring phenotypes within families, typically parent-offspring trios but complex pedigrees with many different types of familial relationships can be used as well (Elston and Stewart, 1971), and scanning the species genetic map of marker loci to calculate a LOD score at each locus (Morton, 1955). A LOD score is the logarithm of an odds ratio, the ratio of:

> the probability of observing the specific genotypes in the family given linkage at a particular recombination fraction versus the same probability computed conditional on independent assortment. Thus, high values of the odds ratio would favor the linkage hypothesis, while values close to 1 provide evidence against linkage.
>
> -Borecki and Suarez (2001, p 50)

The control predctions of independent assortment are a function of relatedness and expectations of allele similarity between relative pairs. Greater detail will be provided in Chapter

6, in which methods and results are given that describe how I applied linkage mapping to the questions posed in my research.

Whereas linkage mapping is based on the notion of recombination at a more individual level, association analysis relies on the population-level concept of linkage disequilibrium. If two loci are not linked, and thus are following Mendel's Law of Independent Assortment by randomly assorting into gametes, the frequency of each possible pair of alleles at two or more loci (a haplotype) should be a function of the allele frequencies at each locus. For example, for loci X and Y with allele frequencies p and q at each, the population should contain the following nine genotypes:

1. XXYY = $p_X^2 p_Y^2$
2. XXYy, XXyY = $2p_X^2 p_Y q_y$
3. XxYY, xXYY = $2p_X q_x p_Y^2$
4. XXyy = $p_X^2 q_y^2$
5. XxYy, xXYy, xYyY, XxyY = $4p_X q_x p_Y q_y$
6. xxYY = $q_x^2 p_Y^2$
7. Xxyy, xXyy = $2p_X q_x q_y^2$
8. xxYy, xxyY = $2q_x^2 p_Y q_y$
9. xxyy = $q_x^2 q_y^2$

If the observed frequency of genotypes is greater than expected, the two loci are in LD and, thus, recombination has not yet disassociated the two. The stronger the linkage (i.e., the closer two loci are on a chromosome) the longer LD will persist in a population. Genetic drift, migration, admixture, and rapid population expansion can all affect patterns of LD. Marker loci that demonstrate evidence for linkage/association are not necessarily, and indeed are rarely, the genetic variants that contribute to trait variation. They simply bookmark the stretch of DNA in which this contributory variant (or variants) can be found, meaning the list of genes and regulatory sequences between the linked marker loci is a list of candidate genes to be further tested directly for association with the phenotypic variation.

2.6.6 Going a Step Further: Identifying Quantitative Trait Loci (QTLs)

Advances in next generation sequencing technology since the publication of the draft human genome sequence in 2001 have made it possible to obtain large amounts of genetic data for both non-model organisms and wild populations (Rogers et al., 1999; Joly and Faure, 2015). With the ability to sequence many individuals, we have produced genetic linkage maps for multiple taxa (e.g., O'Brien, 1990; Auton et al., 2012; Liu et al., 2014; Van Oers et al., 2014), providing a key component in the identification of genetic variants responsible for morphological variation. Using these genetic maps and the methods described in *2.6.5 Methods for Conducting Quantitative Genetic Research*, quantitative trait loci (QTLs)—regions containing genetic variation that is correlated with variation in the measured trait of interest—can be located within the genomes of a study population (Lynch and Walsh, 1998). One of the greatest benefits of using a quantitative genetics approach in this manner is that it allows us to work backward from population-level cranial variation to the responsible genetic loci (see discussion on top-down approaches in *2.2.5 The Role of Continuous Variation in Evolutionary Process*). Hypotheses about the evolutionary importance of these genetic variants can then be formulated and subsequently tested in other populations and taxa.

Quantitative genetic methods have identified QTLs affecting craniofacial, mandibular, and dental morphology in the commonly used mammal model, the house mouse (Cheverud et al., 1997; Leamy et al., 1999, 2008; Workman et al., 2002; Ehrich et al., 2003; Cheverud et al., 2004; Klingenberg et al., 2004). Pleiotropic QTLs, a large number of QTLs, variable environmental effects, and a generally small effect size for each QTL are common findings, all of which are in agreement with expectations for the structure of genetic variation underlying continuous traits in complex structures (Lynch and Walsh, 1998; Rogers et al., 1999; Mackay, 2001). Of particular relevance to this project are the results of Pallares and colleagues (2015),

who were able to localize craniofacial variation to numerous QTLs. Futher analysis indicated *Mn1*, a gene integral to proper development of membranous bones, has an unusually large effect on the phenotypic variation. This is incredibly exciting because it is one of the first studies able to provide evidence to suggest that major developmental genes can produce continuous variation without also producing deleterious dysmorphology.

Complementary studies conducted on primates are of greater relevance for addressing specific questions about primate evolution. Sherwood et al. (2008) analyzed the cephalographs of a population of baboons and identified 14 QTLs for specific developmental modules (i.e., cranial face, vault, and base). Similar methods applied to a sample of human cephalographs identified QTLs for 10 traits (Sherwood et al., 2011). Lawson and colleagues (2009) went a step further and localized genetic variation within a previously identified QTL for baboon facial length to a single candidate gene, *HAND2*. Although limited in scope thus far, these studies provide a sample of previously identified QTLs against which I can compare my own results (see Chapter 6). Multiple lines of evidence converging on the same QTL provide support for following up specific candidate genes within that QTL. Such comparisons with published QTLs, as well as with online searches of genomic and gene ontology databases, will be used to provide a short list of positional candidate genes to be tested in future research.

2.6.7 Our Limited Knowledge of Baboon Skull Genetic Architecture

Prior to this study, we knew very little about baboon craniofacial genetic architecture. Of the two studies conducted on baboons examining the genetic basis for craniofacial variation (Sherwood et al., 2008; Lawson et al., 2009), the former used a genetic map of short tandem repeats (STRs; see *3.2.1 Baboon Genetic Map*), and the latter did not have genotype data for the candidate gene in question at the time. Unfortunately, because of the hyper-variable nature of STRs—the number of alleles is almost always more than two—it is difficult to estimate additive,

dominance, and epistatic effects at these loci. The percent of V_P accounted for by the QTL can be calculated, which provides a sense of whether the trait is is mono-, oligo-, or polygenic. This does answer some of the relevant questions regarding a trait's GP-map (how many genes contribute to the craniofacial variation and what is the relative importance of V_A and V_E for V_P), but it does not provide a complete picture of baboon craniofacial genetic architecture. As my research uses the same genetic map as Sherwood et al., 2008, my results share this limitation. However, future research to acquire and analyze single nucleotide polymorphism (SNP) data and construct haplotype trees will be conducted to address this issue. Lawson has the necessary SNP data for such a follow-up study of the QTL she and colleagues (2009) localized, and results are forthcoming (pers. comm.).

2.7 Conclusion

I have presented in this chapter an overview of what is known about craniofacial growth, development, biology, evolution, genetic basis, and inter- and intraspecific variation. What should be obvious is that we have a decent grasp of those topics in a number of organisms, but that there is a dearth of data for non-human primates. Given our interest in human craniofacial evolution and the applications of such knowledge to biomedical problems, much effort is put towards acquiring more and better information about such topics. Genetic and genomic techniques have now advanced to the point where we can conduct parallel research in non-model organisms and, as a consequence, baboons are used in a variety of biomedical research programs. Anthropologists have also conducted a significant amount of research on the morphology, ontogeny, and variation of the baboon craniofacial skeleton. In this dissertation I combine the two lines of inquiry into a unified and multifaceted research project with the intent of quantifying baboon craniofacial variation and its underlying genetic basis. In the next chapter I discuss my sample, general methods, and specific research questions.

CHAPTER THREE
MATERIALS AND METHODS

3.1 Introduction

In this chapter I introduce the study subjects, data collection protocols, and the types of data used in the analyses conducted for this research. The materials and methods described are only those that apply to the data that form the bulk of this dissertation and on which all analyses are conducted. Chapter-specific methods are provided at the beginning of each chapter.

In recent years, morphological variation among primate crania has been studied in many taxa: prosimians (e.g., Viguier, 2004; Bennett and Goswami, 2012; Cuozzo et al., 2013; Baab et al., 2014), platyrrhines (e.g., Marroig and Cheverud, 2005; Cáceres et al., 2014; Meloro et al., 2014; Terhune et al., 2015), colobines (e.g., Koyabu and Endo, 2009, 2010; Ingicco et al., 2011; Stefen and Nadler, 2012), papionins (e.g., Singleton, 2012; Nova Delgado et al., 2014; Dunn et al., 2013; Ito et al., 2014), apes (e.g., Taylor, 2006; Neaux et al., 2013; Pilbrow and Groves, 2013; Villmoare et al., 2014), and humans (e.g., González-José et al., 2008; von Cramon-Taubadel, 2011; Anzelmo et al., 2013; Bastir and Rosas, 2013). Far fewer studies have been able to incorporate genetic information, and many of these analyses are limited to genome scans that look for signatures of selection or sequence conservation followed by *post hoc* attempts to link genetic variation to morphological variation (e.g., Lidral et al., 1997; Boehringer et al., 2011; Roberts et al., 2011; see *2.2.5 The Role of Continuous Variation in Evolutionary Process*). I take the opposite approach in this study, albeit a complementary one. To address questions of morphological variation among primate crania I first quantify that variation in a large sample and then statistically associate it to genetic variation *in those same individuals*. This provides an opportunity to target genetic variation that can be demonstrated to contribute to morphological variation. This chapter describes the materials and methods used to achieve these goals.

3.1.1 Baboons in Biomedical Research

Although the primary goal of this dissertation is to quantify craniofacial and genetic variation in baboons and consider its origin and maintenance in the context of baboon biology, behavior, and ecology, the information gleaned can also contribute to an increased understanding of human craniofacial evolution for two primary reasons: their genetic similarity to humans and the existence of a baboon genetic map. The phylogenetic proximity of baboons and humans is reflected in the high level of DNA sequence identity, both for the genome as a whole and for individual genes (e.g., Caccone and Powell, 1989; Zogopoulos et al., 1999; Doubleday et al., 2009). Although there are gross chromosomal differences, such as inversions and fusions, and more localized differences, like copy-number variation and insertions and deletions (in-dels), the arrangement of genetic loci is largely similar in both the human and baboon genomes (Rogers et al., 2000). This has permitted comparison of syntenic groups—stretches of conserved sequence—and the production of gene maps that provide locations for homologous genes within the genomes of both humans and baboons (Rogers and VandeBerg, 1998; Rogers et al., 2009). These comparisons are almost certainly more relevant than are ones made between humans and rodents, chicks, fish, or flies, the most commonly used model organisms, all of which have been diverged from primates for at least 90 million years. Additionally, the development of a baboon whole-genome linkage map, the first such map for any nonhuman primate species (Rogers et al., 2000; Cox et al., 2006), provides a valuable resource for projecting results from experimental and genetic studies conducted in baboons onto the human genome.

In a more general sense, baboons are often used in the study of complex traits; in fact, they are one of the most widely used primate model organisms. Although their life span (20-30 years in captivity) is shorter—many of their biological processes are accelerated relative to

those of humans—much of their physiology and anatomy is similar to our own, particularly in regards to the cardiovascular system (Mitruka and Bonner, 1976; Cox et al., 2013). For example, baboons respond to high fat, high sugar diets much like we do, developing symptoms that mimic human cardiometabolic syndrome (Higgins et al., 2010). Unlike many other primates, they also experience year-round ovulation and reproductive senescence, menopause, and the associated osteoporotic bone remodeling (Brommage, 2001; Martin et al., 2003). Finally, of special importance to anthropologists is the fact that baboon dental growth ceases upon eruption (Hlusko and Mahaney, 2007) and that adult bones remodel in response to age, diet, disease, and loading (Kammerer et al., 1995; Havill et al., 2013), neither of which is true of rodents, the classic experimental model mammal. Consequently, inferences made from observations of baboon growth and development are often easier to extrapolate to humans than are any drawn from research on other model organisms.

3.2 Materials

My sample was drawn from a colony of baboons (*Papio hamadryas* sspp.)[1] maintained by the Southwest National Primate Research Center (SNPRC) at the Texas Biomedical Research Institute (TBRI) in San Antonio, Texas. The SNPRC maintains between 1,600 and 2,200 baboons at any given time. Roughly 1,200 of these animals are part of a complex pedigree for which family ancestral lines are well documented. The pedigree was founded in 1972 with 200 feral baboons and has since grown to 16,000 individuals across seven generations. It is the largest baboon pedigree in the world. The founders were wild-caught in Kenya along the Tanzanian border in a triangular region bounded by the towns of Ithumba, Kiboko, and Simba

[1]The SNPRC uses Jolly's (1993) nomenclature of classifying all baboon populations as subspecies of the hamadryas baboon. As my sample is derived from the center, their naming convention will be maintained throughout this dissertation (see *2.4.6 What is Known About Papio Craniofacial Morphology* for arguments for and against classifying baboon populations as species or subspecies).

and that overlaps Tsavo East National Park (Maples et al., 1967). At the time, it was noted that baboons in the area did not look like either olive (*P. h. anubis*) or yellow (*P. h. cynocephalus*) baboons, and it has since been confirmed to be a hybrid zone (Fig. 3.1; Samuels and Altmann, 1986; Carpentier et al., 2012). The majority of SNPRC baboons are olive, but some are yellow and many are hybrids or backcrosses of the two. Some hamadryas (*P. h. hamadryas*) and chacma (*P. h. ursinus*) baboons have been introduced into the colony over the years as well, although they have not been crossed with the olive/yellow population.

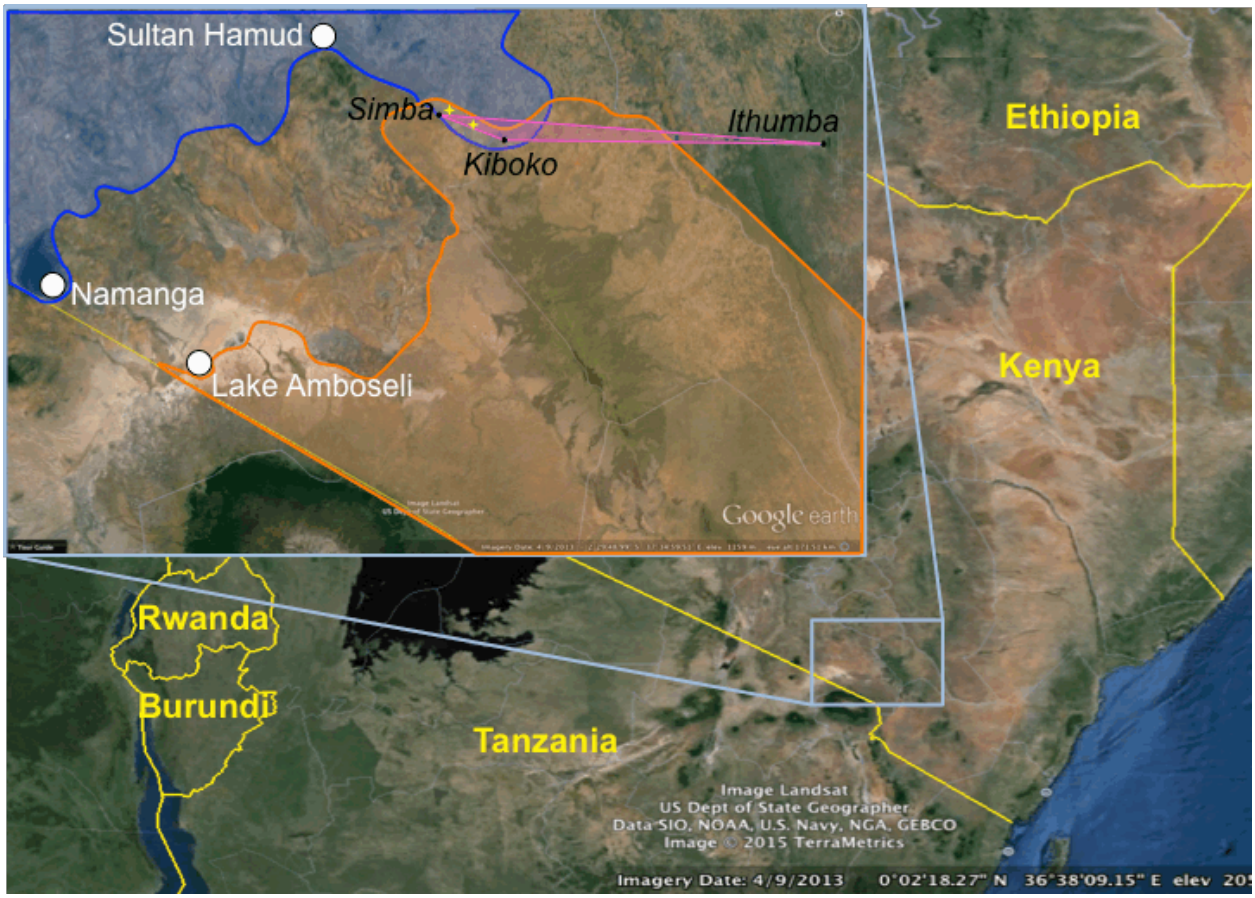

Figure 3.1 Google Earth Landsat Image of Southwestern Kenya. Inset shows a magnified view of the overlapping home ranges of olive (blue outline) and yellow (orange outline) baboons. The region where the SNPRC baboon colony founders were trapped is indicated by the pink triangle. The yellow stars near Simba indicate localities where troops of baboon with hybrid phenotypes were encountered by Maples et al. (1967). Map was created by reconstructing the field notes published in Maples et al. (1967).

Hybridization among these subspecies produces distinct and recognizable craniofacial variation (e.g., both agenesis of and supernumerary teeth, increased overall cranial size, extra sutures). As these trends have been documented elsewhere (see Ackermann et al., 2006) and are not the result of processes producing continuous, intra-population variation, they will not be considered in this dissertation except briefly in passing toward the end of this chapter.

Twelve family lines have been maintained since the foundation of the pedigree by breeding individual males with harems of 10 to 30 females. Each harem is housed in a separate large, outdoor cage to ensure paternity, and males are periodically rotated among neighboring harems in a sequential manner. As a consequence of this breeding strategy, the family lines overlap and, therefore, all individuals can also be linked into one, large multi-generational pedigree. Far fewer males are needed under this husbandry protocol and as such the colony, and therefore the sample used in this dissertation research, contains many more female than male animals.

For the most part, the breeding program has been designed and operated to avoid high levels of inbreeding. This provides an opportunity for the maintenance of high levels of naturally occurring genetic diversity (Dyke et al., 1987), which I discuss in *3.2.1 Baboon Genetic Map*. Occasionally experimental designs call for the production of specific genealogic relationships (e.g., large sibships, half-sibships, or inbred sibships), and inbreeding may be employed in these instances. The remaining animals in the SNPRC colony that are not included in the pedigree are housed in two large, outdoor corrals in which they demonstrate social dynamics (i.e., dominance hierarchies and breeding strategies) typical of wild baboon troops.

3.2.1 Baboon Genetic Map

A whole-genome linkage map for the SNPRC baboons was created (Rogers et al., 2000; Cox et al., 2006) to establish an invaluable resource for identifying genetic contributions to both

disease phenotypes and normal variation. A small sample of the studies from the past five years in which this has been possible include: localization of genomic regions and even genetic variants contributing to variation in adipocyte volume (Bose et al., 2010), immune response (Vinson et al., 2011), cholesterol levels (Karere et al., 2013), cortical folding patterns (Atkinson et al., 2015), and even behavioral traits (Johnson et al., 2015).

As of 2006 (see Cox et al., 2006), the SNPRC baboon linkage map was constructed from genotype data for 984 pedigreed individuals at 284 short tandem repeat (STR) microsatellite markers (Appendix A, Tables A1 and A2). This number has since been increased to 384 markers, of which 7% were designed especially for the baboon genome. The nucleotide sequences for all STRs are available on both the SNPRC website (http://baboon.txbiomedgenetics.org/Bab_Polymorphisms/STRpageBL.php) and GenBank (http://www.ncbi.nlm.nih.gov/gquery/?term=baboon%5Borgn%5D). The average heterozygosity (*H*) is 0.74, which indicates that, on average, a large proportion of individuals is heterozygous at any given marker and that genetic diversity is high in this population. In comparison, Bowcock et al. (1994) used 30 microsatellites for 10 individuals selected from five different continents to estimate $H = 0.64–0.81$ in different human populations. Additionally, Dib et al. (1996) created the Généthon, a human linkage map of 5,264 STRs, and determined that $H = 0.70$. Both of these estimates demonstrate that, despite the large difference in the number of markers used, both the baboon and human genetic maps contain STRs with comparable levels of heterozygosity.

The intermarker distance of the baboon genetic map is 7.2 centiMorgans (cM), which is only slightly smaller than the distance of 8.5 cM in the human genome. This indicates that fewer crossover events in the baboon genome happen during a single generation than in the human genome. More crossover events mean a higher chance for producing gametes with more

variable chromosomes. Despite the fact that relatively few individuals were used to establish the SNPRC colony, the wild genetic diversity from which they were sampled is better maintained than it is in humans. Estimates of inbreeding effective population size in humans using coalescence models vary by type of genetic data used (sexes combined: 9,000–12,000 from protein electrophoresis and 8,000–11,000 from nuclear DNA; females: 3,500–4,600 from mtDNA; Takahata, 1993) and from which population the data are ascertained (sexes combined: ~7,500 for Yoruba and ~3,100 for Japanese, Han Chinese, and United States residents of North and East European ancestry using linkage disequilibrium (LD) data; Tenesa et al., 2007), but all such estimates are much smaller than any estimate made for our closest anthropoid relatives, chimpanzees and bonobos (Yu et al., 2003, sexes combined: *Pan troglodytes troglodytes* 20,100; *P. t. verus* 13,000; *P. paniscus* 12,400; although Eriksson et al., 2006 estimated that of male bonobos to be 700-1,700).

The mean polymorphic information content (PIC)—the probability of a genetic marker providing parent-of-origin information (Botstein et al., 1980; Guo and Elston, 1999)—of this baboon population is 0.72. Simulation studies by Kruglyak (1997) using simple human genealogies suggest that the PIC is a good indicator of the power of a map to detect linkage. A PIC = 0.75 can be expected to identify genomic loci with a linkage (i.e., LOD) score ≈ 4.75, or loci where the presence of linkage is 4.75 times more likely than the observed results being due to chance (see *6.2.1 Linkage Mapping* for a detailed description of linkage analysis and LOD scores). Furthermore, these simulation studies show that STRs with $H = 0.75$ that are spaced 7 cM apart on a human genetic map have a PIC ≈ 0.38. This means the markers on the baboon genetic map, which have the same levels of heterozygosity and equivalent intermarker spacing but a larger PIC, are more informative for pedigree linkage studies than are human markers on a comparable map.

All of these statistics calculated from the baboon genetic map suggest that localization of genomic regions of interest will be feasible, as enough variation exists, and that variation is actually informative. One concern with captive populations is that inbreeding depression and genetic drift can eliminate genetic diversity over time. Low diversity makes it more difficult to identify genetic variation segregating in a pedigree in a pattern similar to that of the phenotypic distribution in the corresponding population. However, the combination of careful husbandry practices, periodic introduction of additional wild caught individuals, and variable founder origin—many of whom were likely hybrids and, thus, had more variable genomes than either parental population while also maintaining LD between markers and loci contributing to V_P (see *2.6.5 Methods for Conducting Quantitative Genetic Research*)—has maintained levels of diversity similar to, if not greater than, those measured in humans. As linkage mapping in humans using microsatellite-based genetic maps has successfully identified genomic regions and putative candidate genes linked to a wide range of phenotypes (see review in Almasy et al., 2015), I expect the same to be possible using the SNPRC baboons.

As the physical locations of these marker loci in the human genome are known and synteny between the human and baboon genomes has been established, putatively orthologous chromosomal regions within the baboon genome can be identified using online human genome browsers, thus facilitating the identification of positional candidate genes. The genomes of both hamadryas (*P. h. hamadryas*; http://pre.ensembl.org/Papio_hamadryas/Info/Index) and olive (*P. h. anubis*; http://useast.ensembl.org/Papio_anubis/Info/Index?redirect=no) baboons have been assembled and are available online, which will also aid positional candidate gene identification.

3.2.2 Sample Processing and Collection Curation

Upon death, each monkey was necropsied by SNPRC veterinarians. Body weight and the weights of various organs was recorded. Typically, the calotte was removed with a bone saw to

extract the animal's brain. However, this was not the case for every specimen in the collection, a consideration discussed in more detail in *3.3.3 Craniofacial Anomalies and Potential Sources of* V_E. The animals included in my sample died between 2000 and 2011. Not all animals that died at the SNPRC in those years were included. Preference was given to animals in the pedigreed portion of the colony and any unusual individuals, one example being a Rhesus macaque–baboon hybrid, or "rheboon" (see Joganic et al., 2012a). After necropsy, the heads of these animals were removed, frozen, and given to Jeff Rogers (JR; Department of Molecular and Human Genetics, Baylor College of Medicine) for storage. James Cheverud (JMC; Department of Biology, Loyola University Chicago) periodically retrieved the specimens from JR and transported them to Washington University in St. Louis (WUSTL) for processing.

Frozen heads were thawed, manually defleshed, and macerated in a warm water bath of 35° C to clean the bone of any remaining adherent tissue. The processing protocol was altered as maceration often leaves bones greasy and with a coating of adiposere. The last ~15% of the collection was placed in a dermestid beetle (*Dermestes maculatus*) colony after being manually defleshed. During the collection curation process, individuals were sequentially assigned a catalogue number beginning with the letter "W" so that each individual is associated with two identifiers, one from the SNPRC and one from WUSTL. Jewelry tags bearing both numbers were attached to the left zygomatic arch of each individual. In almost every case the skull is accompanied by at least one vertebra and often the calotte is separate due to the SNPRC necropsy protocol, as mentioned above. Occasionally an ossified laryngeal cartilage is present as well. All pieces for a single specimen were placed in a box on which both catalogue numbers were written. The collection is on loan to JMC by the SNPRC and, thus, was transported to Loyola University Chicago where it now resides.

The collection contains 992 skulls, of which 689 are female and 303 are male. Seven of the individuals were not CT scanned. Sixteen are of unknown identity due to record discrepancies and two because they were wild-caught animals added in recent years to the colony to diversify the gene pool. Consequently, these 18 individuals are not included in the pedigree. To ensure that the samples used for both the genetic and phenotypic analyses are the same, these animals were omitted from the final sample. All 992 individuals were measured, but only those with both fully erupted M3's and a fused sphenoccipital synchondrosis (usually achieved by 7 years) are considered adult and included in analyses. According to these criteria, 20 individuals are too young to be included in any analyses. An exception was made for two females who have M3's in their crypts but significant wear on M1 and M2 and were chronologically old (15.71 and 25.84 years). The average age of the final sample of 954 adult animals is 18.62 ± 5.9 years (range 6.04–33.70 years) and males in the sample are younger than females ($\bar{X}_F$ = 19.61 ± 5.8, $\bar{X}_M$ = 16.32 ± 5.4, $\bar{X}_{F-M}$ = 3.29, CI = 2.5–4.0, t = 8.24, $P <$ 0.001).

3.3 Methods

Because most of the crania were cut during necropsy, calottes were reattached with radio-translucent modeling clay. In a number of instances, the appearance of false start cuts on the crania permitted approximation of bone lost during necropsy, roughly 1.5 mm. Additionally, for the CT scans (see *3.3.2 Data Collection from Computed Tomography (CT) scans*), radio-translucent tape was used to affix the mandible to each cranium, and cotton batting was placed between the incisors and at each temporomandibular joint to ensure separation between the contiguous skeletal elements in the CT images.

3.3.1 Data Collection from Dry Crania

I collected 3D coordinates for craniometric landmarks from each cranium using a Microscribe MX (Revware Inc., Raleigh, NC) digitizer. Although each specimen includes an associated mandible, only the cranium was measured and analyzed for this dissertation. Twenty-eight landmarks (Fig. 3.2; Table 3.1) were chosen to cover the cranium completely and evenly (Bookstein, 1996), to be easily recognizable across the sample and precisely measured on each

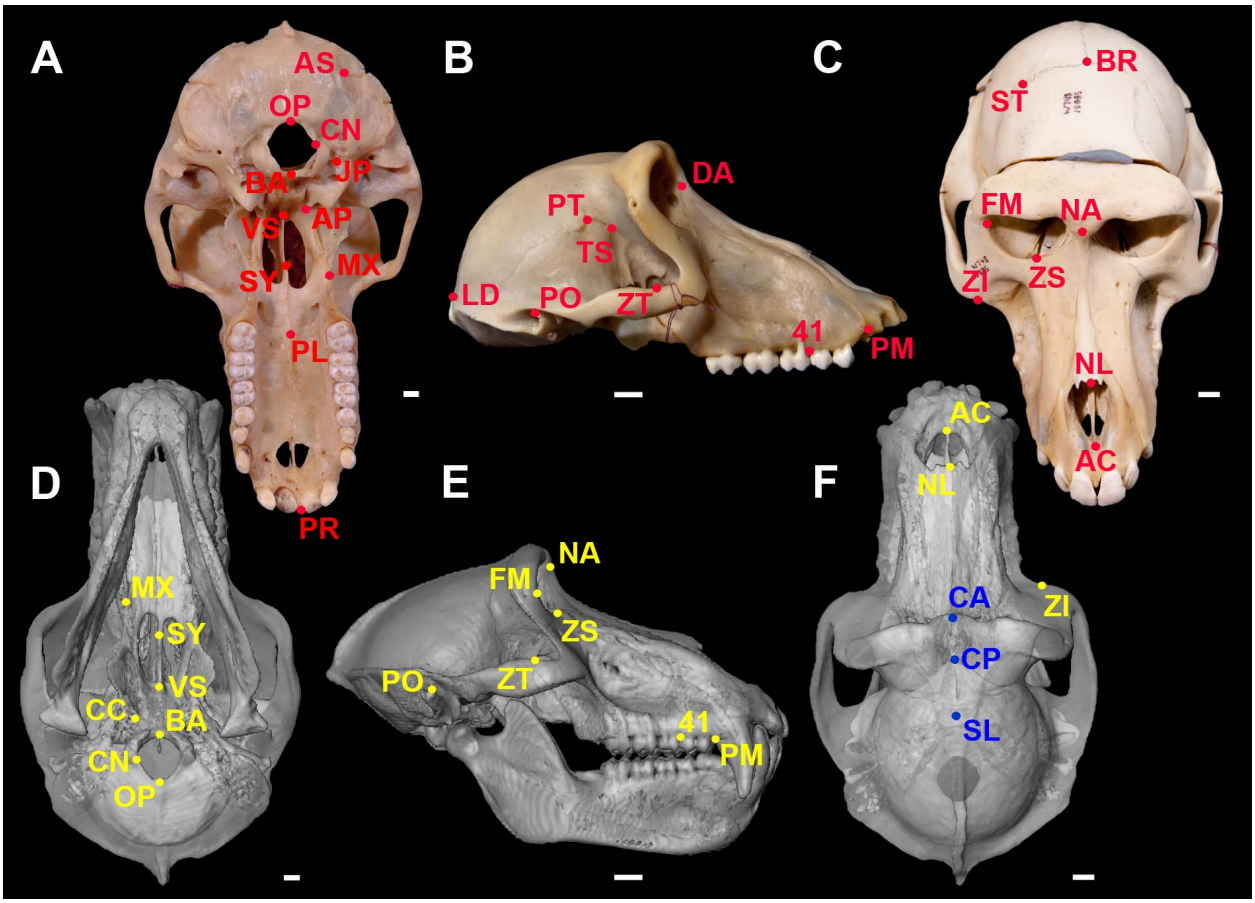

Figure 3.2 Craniometric Landmarks Collected. Panels: (A-C) Landmarks (red dots and letters) collected with a microscribe by JLJ from the dry crania, inferior view (A), right lateral view (B), oblique superior view (C). (D-F) Landmarks (yellow and blue dots and letters) collected digitally by KEW from the CT scans, inferior view (D), right lateral view (E), anterior view (F). Abbreviations correspond to those provided in Table 3.1. Blue landmarks are endocranial while red and yellow landmarks are ectocranial. Only the right side of bilateral landmarks is identified in each of the images. Orbital septum (OB) is not shown. White scale bars are 1 cm. Photos by Aaron Bunse and transparent virtual skulls reconstructed from CT scans by KEW.

Table 3.1 Craniometric Landmarks Measured on the Baboon Crania.

Landmark	Name	Definition[a]	Locat.[b]	Reg.[c]	Miss. (%)[d]	Measur.[e]
acanthion	AC	midline of inferior margin of nasal aperture	M	F	9.00	JLJ, KEW
anterior petrous temporal	AP	most anterior point on inferior petrous temporal	B	B	0.92, 0.51	JLJ
asterion	AS	most superior point on occipitomastoid suture	B	V	0.72, 1.74	JLJ
basion	BA	midline on anterior margin of foramen magnum	M	B	0.31	JLJ, KEW
bregma	BR	intersect. of sagittal and coronal sutures	M	V	0.61	JLJ
carotid canal	CC	most anterolateral point on inferior carotid canal foramen	B	B	0.20, 0.31	KEW
condylion	CN	most posteromedial point on occipital condyle	B	B	3.07, 2.66	JLJ, KEW
crista galli anterior	CA	most anterior point on crista galli crest posterior to orbit	M	F	0.31	KEW
crista galli posterior	CG	most posterior point on crista galli crest posterior to orbit	M	F	0.41	KEW
dacryon	DA	most superior point on lacrimomaxillary suture	B	F	0.41, 0.31	JLJ
frontomalare orbitale	FM	intersect. of frontozygomatic suture and lateral orbital rim	B	F	0.31, 0.51	JLJ, KEW
jugale	JP	most anterior point on occipital jugular notch	B	B	0.51, 0.51	JLJ
lambda	LD	intersect. of sagittal and lambdoid sutures	M	V	0.82	JLJ
maxillary tuberosity	MX	point where inferior palatomaxillary suture crosses M3 midline	B	F	0.72, 0.82	JLJ, KEW
nasale	NL	most inferior point on inter-nasal suture	M	F	2.66	JLJ, KEW
nasion	NA	intersect. of inter-nasal and frontal sutures	M	F	0.41	JLJ, KEW
opisthion	OP	midline on posterior margin of foramen magnum	M	B	7.06	JLJ, KEW
orbital septum	OB	intersect. of orbital septum and medial orbital wall	B	F	0.72, 0.72	JLJ
palatale	PL	most posterior point on palatal surface of inter-maxillary suture	M	F	0.20	JLJ
porion	PO	intersect. of ectotympanic and tympanic petrous	B	V	11.15, 3.99	JLJ, KEW
premaxilla/maxilla junc.	PM	most anterior point on inferior premaxilla-maxillary suture	B	F	12.68, 14.52	JLJ, KEW
premolar/molar junc.	41	most inferior point on alveolus between P4 and M1	B	F	4.40, 4.91	JLJ, KEW
prosthion	PR	most anterior point on lingual surface of max. I1 septum	M	F	14.21	JLJ, KEW
pterion	PT	most inferior point on coronal suture	B	V	3.07, 1.64	JLJ
sella turcica	SL	center of sella turcica	M	F	0.20	KEW
staphylion	SY	most posterior point on vomeropalatal suture	M	F	1.43	JLJ, KEW
stephanion	ST	intersect. of most lateral temporal line and coronal suture	B	V	0.61, 0.61	JLJ
temporosphenoid junc.	TS	most superior point on temporosphenoid suture	B	V	0.20, 0.41	JLJ
vomerosphenoid junc.	VS	most superior point on inter-vomer suture[e]	M	B	0.31	JLJ, KEW
zygomaxillare inferior	ZI	most inferior point on zygomaxillary suture	B	F	0.20, 0.82	JLJ, KEW
zygomaxillare superior	ZS	intersect. of zygomaxillary suture and inferior orbital rim	B	F	0.20, 0.31	JLJ, KEW
zygotemporal junc.	ZT	intersect. of zygotemporal suture and superior zygo. arch	B	F	1.02, 1.74	JLJ, KEW

[a]Adapted from Wilder (1920). [b]Whether the landmark is bilateral (B) or in the midline (M). [c]Region of the skull in which the landmark is located: base (B), face (F), and vault (V). [d]Percent missing data. Bilateral landmarks have a number each for the right and left sides. [e]Individual who measured the landmark on either the dry crania (Jessica Joganic, JLJ) or CT scans (Katherine Willmore, KEW).

specimen, and to capture craniofacial size and shape variation. Most landmarks are of Type I in geometric morphometric nomenclature, or a landmark defined as a local boundary between tissues or elements, such as a sutural intersection or a foramen (e.g., PT and FM; see Table 3.1 for landmark abbreviations). The homology of Type I landmarks among specimens is strongly supported, which is why they are preferred and considered the most useful. A few landmarks are of Type II and are defined geometrically, usually taking the form “greatest curvature of...” or “most inferior point on...” (e.g., SL and AP). There are no Type III landmarks included in this study, which are defined in relation to a nearby element or other landmark.

Many of the animals lived to be very old (max age = 33.70 years), and their cranial bones remodel in response to injury, disease, tooth loss, and old age. Consequently, not all landmarks were collected for each individual and some were affected more than others (e.g., PR and AC). In fact, PR was omitted from all analyses because premaxillary remodeling made it too difficult to identify (Katherine Willmore, pers. comm.). On average, 2.6% of the remaining landmarks are missing from each individual. Euclidean interlandmark distances (EIDs) were calculated between pairs of landmarks (Table 3.2; Fig. 3.3) to provide measures of (1) meaningful biological units, e.g., nasal length or orbital breadth, (2) traits that have been the foci of anthropological research, e.g., cranial base length, or (3) dimensions for the construction of geometric objects, e.g., the cranial vault vs. the face. Cranial base angle was also calculated, as it is of special interest in relation to questions about primate evolution, specifically Biegert’s (1957, 1963; cited in Lieberman et al., 2008) Spatial Packing Hypothesis (see *2.4.2 The Special Relationship Between Brain and Skull*). For bilateral landmarks, the mean of the EIDs from each side of the cranium was used. The side-specific EIDs will be used for future research on directional and fluctuating asymmetry. In the case where landmarks for only one side are present, the corresponding EID for that side is substituted for the mean EID.

Table 3.2 Euclidean Interlandmark Distances (EIDs) Calculated Between Pairs of Craniometric Landmarks.

EID	Abrv	Repeat[a]	Congru[b]	EID	Abrv	Repeat[a]	Congru[b]
acanthion–premax/max junc	ACPM	0.837	0.461	nasale–vomerosphenoid junc	NLVS	0.998	0.940
acanthion–staphylion	ACSY	0.996	0.322	nasion–acanthion	NAAC	0.996	-------
anterior palatal width	PMPM	0.996	-------	nasion–crista galli anterior	NACA	-------	-------
asterion–jugular process	ASJP	0.859	-------	nasion–crista galli posterior	NACP	-------	-------
basion–carotid canal	BACC	-------	-------	nasion–frontomalare orbitale	NAFM	0.995	0.885
basion–opisthion	BAOP	0.925	0.635	nasion–premol/mol junc	NA41	0.995	-------
biasterionic breadth	ASAS	0.802	-------	nasion–vomerosphenoid junc	NAVS	0.954	0.852
bijugal breadth	JPJP	0.963	-------	nasion–zygomax inferior	NAZI	0.974	-------
bipalatal breadth	4141	0.981	0.312	nasion–zygomax superior	NAZS	0.948	0.852
biporionic breadth	POPO	0.991	-------	neurocranial height	BRBA	0.967	-------
bipterionic breadth	PTPT	0.858	-------	neurocranial length	NALD	0.842	-------
bistephanionic breadth	STST	-------	-------	orbital width	DAFM	0.968	-------
bizygomatic breadth	ZTZT	0.998	-------	palatale–staphylion	PLSY	0.960	-------
bregma–asterion	BRAS	0.910	-------	porion–basion	POBA	0.990	0.616
bregma–lambda	BRLD	0.814	-------	premax/max–premol/mol juncs.	PM41	0.860	0.705
bregma–nasion	BRNA	0.978	-------	premol/mol junc–max tuberosity	41MX	0.976	0.891
bregma–pterion	BRPT	0.546	-------	premol/mol junc–zygomax	41ZI	0.977	0.837
cranial base length	NABA	0.986	-------	pterion–asterion	PTAS	0.857	-------
crista galli length	CACP	-------	-------	pterion–lambda	PTLD	0.769	-------
crista galli posterior–sella turcica	CPSL	-------	-------	sella turcica–basion	SLBA	-------	-------
crista galli posterior–zygomax superior	CPZS	-------	-------	sella turcica–carotid canal	SLCC	-------	-------
foramen magnum width	CNCN	0.958	0.778	staphylion–basion	SYBA	0.995	0.579
frontomalare orbitale–premol/mol junc	FMPM	0.992	0.639	staphylion–max tuberosity	SYMX	0.971	-0.358
frontomalare orbitale–sup zygotemp junc	FMZT	0.988	0.893	superior zygotemp junc.–porion	ZTPO	0.946	0.797
frontomalare orbitale–crista galli post	FMCP	-------	-------	sup zygotemp–vomerosphenoid junc	ZTVS	0.997	0.862
frontomalare orbitale–pterion	FMPT	0.769	-------	su zygotemporal junc–zygomax in	ZTZI	0.841	0.560
lambda–asterion	LDAS	0.914	-------	vomerosphenoid junc–basion	VSBA	0.989	0.602
lambda–basion	LDBA	0.989	-------	vomerosphenoid junc-staphylion	VSSY	0.972	-0.510
nasal length	NANL	0.996	0.958	zygomax inferior–max tuberosity	ZIMX	0.876	0.366
nasale–acanthion	NLAC	0.990	0.827	zygomax superior–nasale	ZSNL	0.998	0.883

[a]ICCs calculated from a subset of EIDs that were measured twice by JLJ to assess repeatability. EIDs indicated with a series of dashes were measured exclusively by KEW and duplicate trials were not conducted. [b]ICCs calculated for the EIDs measured by both JLJ and KEW to assess congruence. EIDs indicated with a series of dashes contain at least one craniometric landmark that appeared in only one dataset.

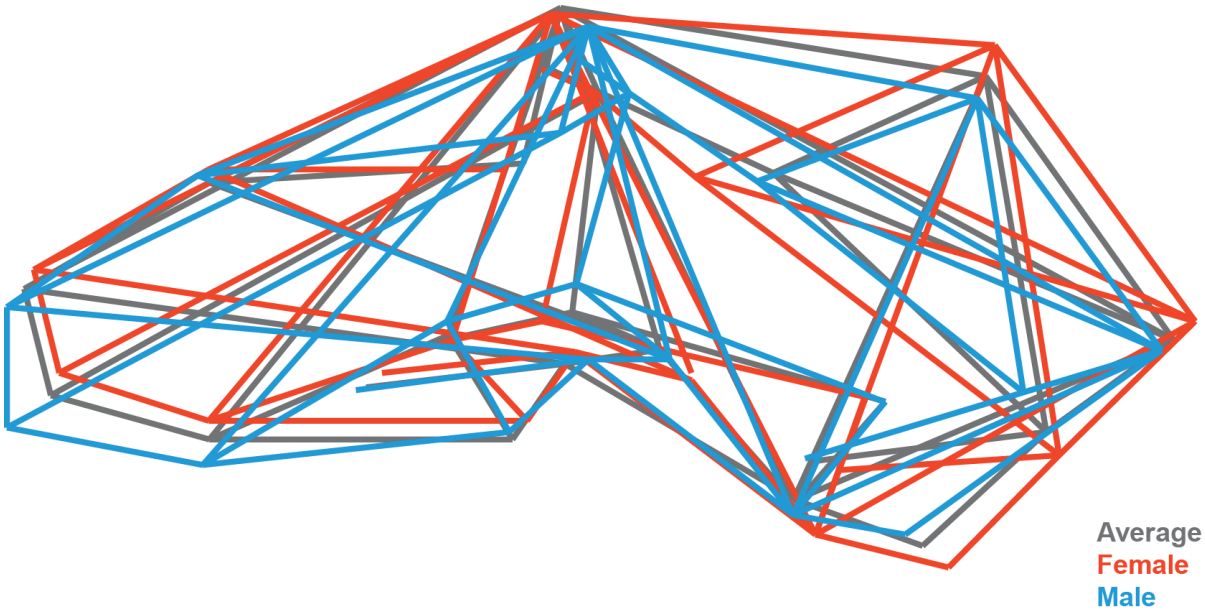

Figure 3.3 Wireframe Meshes of the Euclidean Interlandmark Distances (EIDs). Shown in gray is the mean cranial shape resulting from a Generalized Procrustes Analysis performed in MorphoJ (Klingenberg, 2011). To demonstrate typical dimensions in which the sexes differ, the wireframes of a single female (W076) and male (W065) are provided in red and blue, respectively. General trends include: the snout of males is longer and more klinorhynchous while the cranial vault of females is expanded in every direction.

Bivariate plots for every pair of EIDs were created and examined for influential points, or those that greatly affect the slope of a regression line. Any points suspected to exert undue leverage were omitted. Due to subspecies hybridization, it has been observed that hybrid animals, especially males, often demonstrate values within the tails—typically the right tail due to hybrid vigor presenting as hypermorphosis—of the population distributions (Ackermann et al., 2006, 2014). Because hybrids are not uncommon in this sample, their morphology should not be treated as aberrant. Therefore, only data that were separated from the main distribution by a definitive break, as opposed to simply appearing at its tail ends, were considered outlying. This occurred more often on the right side of the distribution, especially in males. These data were checked for errors in EID calculations, and any mistakes were corrected.

The EID distributions were non-normal for most variables, even after accounting for sex differences, which is an issue for the quantitative genetic parameter estimation, as characters to be analyzed are assumed to be multivariate normal. Typical transformations for normalization of size data (e.g., $\log_{10}$, $\log_e$, square-root) reduce the variance too much to provide accurate information about phenotypic variance, which is ultimately the variable of interest in quantitative genetics. Additionally, the EIDs do not share a common variance pattern, which is also an assumption of the methods used. The amount of variation for any EID is expected to be a factor of both the absolute size of the measurement as well as its relative position in space. For example, cranial length is expected to have a larger variance than bizygomatic breadth because the former is both greater in absolute size (Cardini and Polly, 2013) and captures shape in the plane of greater variance, anteroposterior rather than mediolateral (Goodall, 1991; Klingenberg and McIntyre, 1998; Marcus et al., 2000; Drake and Klingenberg, 2010). Given these issues, all EIDs were standardized to a mean ($\bar{X}$) of zero and standard deviation (s) of one.

3.3.2 Data Collection from Computed Tomography (CT) Scans

All skulls were CT scanned at the Center for Clinical Imaging Research (CCIR) at Washington University School of Medicine. The first 487 specimens were scanned on a machine at a slice thickness of 0.75 mm while the remaining individuals were scanned on the replacement machine at 0.6 mm. Slices were contiguous and taken sequentially for the overall skull. To increase resolution of the inner ear, spiral CT was employed for just the petrous temporal bones. Copies of these scans are stored on CD/DVD at Loyola University Chicago with JMC and in digital format at Pennsylvania State University with Joan Richtsmeier (JTR).

Endocranial volume (ECV) was estimated from the CT scans using Amira 5 (Visage Imaging, Berlin, DEU). The “empty” pixels appearing within those representing the neurocranial bones were segmented on every tenth CT slice and used to interpolate the empty pixels on the

intervening nine slices. Once all relevant pixels were selected, each was transformed into a voxel—a pixel containing a third dimension of depth—by taking into consideration both the interslice and interpixel distances. The interslice distance was either 0.75 or 0.6 mm (see above). A single individual (W185) was scanned on both machines to determine if differences in slice thickness had any effect on ECV estimation. The difference in estimate is less than one cc ($ECV_{0.75}$ = 131.4 cc, $ECV_{0.6}$ = 132.3 cc) and, therefore, negligible.

Interpixel distance is determined by first calculating the reconstruction index (RI) for the slices. The RI is determined by the field of view (FOV), or the area of the scan image included in the digital reconstruction of the object being scanned, and the matrix size of pixels included in the reconstruction, which is set at 512 x 512 for CT scans. Dividing the FOV by 512 provides the RI. FOV size ranged from 10.5–31.7 cm ($\bar{X}_{\mathrm{FOV}}$ = 18.80 ± 0.4 mm) while RI ranged from 0.21–0.62 mm ($\bar{X}_{\mathrm{RI}}$ = 0.37 ± 0.1 mm). The voxel size is then calculated as the product of the squared FOV and the slice thickness. Finally, the number of segmented pixels is summed and multiplied by the voxel size (then divided by 1000) to provide an estimate of the ECV in cubic centimeters.

The CT scans of 16 individuals selected at random were segmented twice (Table 3.3) to calculate an intraclass correlation coefficient (ICC), which provides an estimate of repeatability by comparing the variance of the two trials' measurements to the total amount of variance in the sample as a whole (Weir, 2005; Joganic et al., 2012b). The ICC for ECV was 0.9996 and there was no interaction with either sex ($F = 0.0002$, $P = 0.989$) or age ($F < 0.0001$, $P = 0.995$) of the selected individuals. This indicates that less than 1% of total variance is due to measurement error, and the ECV estimation procedure is very repeatable. Given this precision and the amount of time required to process each CT scan (>20 min), it was decided that only a single ECV estimate would be made for each individual, rather than taking the average of repeated estimates, as is often done when collecting morphological data.

Table 3.3 Repeatability of CT Segmentation and Endocranial Volume (cc) Estimation.

ID	Sex	Age (yrs)	Trial 1	Trial 2
W655	F	21.48	153.8	154.0
W656	F	22.71	137.6	137.2
W657	F	6.45	162.5	162.6
W658	F	16.52	167.0	166.8
W659	M	20.16	181.6	181.7
W660	F	18.47	143.0	143.1
W661	F	9.09	135.1	135.9
W662	F	29.33	159.0	158.9
W663	M	6.67	152.9	152.7
W664	F	27.59	149.4	149.5
W665	F	26.77	134.3	134.4
W666	M	9.31	199.3	198.9
W667	F	14.04	173.9	173.5
W668	M	16.33	169.6	170.6
W872	M	19.99	164.6	164.3
W921	F	19.09	142.6	141.3

In providing an estimate of ECV, CTs should overestimate brain volume—the biological variable of interest for which ECV is only an approximation—because space within the braincase dedicated to meninges and fluids during life of the individual is included in the ECV estimates when segmenting the CT scans. Magnetic resonance (MR) imaging often offers a more accurate estimation of brain size because the various soft tissues within the skull differentially affect the magnetization of protons emitted by the MR machine, allowing neural tissue to be distinguished from non-neural tissue on the resulting scans. To determine the amount of CT overestimation, an additional 72 individuals were also MR scanned at the Research Imaging Center (RIC) at the TBRI while still alive. The MR scans were segmented by Peter Kochunov (RIC, TBRI) using both automatic (Smith, 2002) and manual methods. Brain volume (BV) was then estimated (see Rogers et al., 2007 for details; $\bar{X}_{\mathrm{BV}}$ = 168.3 ± 21 cc). These data were compared to the CT-derived ECV estimates (Table 3.4; $\bar{X}_{\mathrm{ECV}}$ = 160.4 ± 19 cc) on the same animals.

Table 3.4 Comparison of Endocranial Volume (ECV) and Brain Volume (BV) Estimates.

ID[a]	Sex	Age	ECV (cc)	BV (cc)	*d*[b]	ID[a]	Sex	Age	ECV (cc)	BV (cc)	*d*[b]
259	F	14.01	144.0	162.0	-18	540	F	24.68	152.7	159.7	-7
262	F	13.27	141.5	146.6	-5	541	M	18.33	177.8	185.4	-8
285	M	20.53	194.7	206.2	-11	546	F	20.22	131.2	136.3	-5
314	F	13.59	145.8	165.7	-20	548	M	9.39	174.2	179.9	-6
326	F	6.27	150.6	146.0	5	549	M	11.92	193.2	189.0	4
334	F	32.47	152.9	158.7	-6	553	M	18.19	162.0	178.9	-17
336	F	26.61	154.3	158.7	-4	561	F	16.37	154.6	167.2	-13
340	M	16.38	186.9	200.9	-14	568	F	17.08	151.8	156.2	-4
346	M	21.23	185.3	193.9	-9	570	F	27.36	145.4	153.0	-8
349	F	24.88	153.3	164.5	-11	579	F	22.06	138.5	142.9	-4
352	M	17.57	181.4	153.7	28	593	F	21.06	145.5	145.4	0
360	F	7.55	150.3	159.2	-9	599	F	19.17	140.1	143.5	-3
363	M	25.53	171.7	183.7	-12	611	F	16.57	154.6	165.0	-10
376	M	24.55	183.7	189.6	-6	616	M	17.62	168.5	174.9	-6
385	F	13.32	165.4	174.6	-9	621	M	18.00	203.1	215.4	-12
388	F	24.67	141.7	150.0	-8	622	M	18.81	185.5	193.6	-8
390	M	18.93	168.1	183.5	-15	631	F	14.69	143.6	164.1	-20
408	F	27.40	145.7	145.1	1	635	F	15.55	136.9	134.6	2
411	F	11.95	147.0	157.3	-10	636	F	27.59	143.6	149.1	-5
413	F	8.44	145.6	173.4	-28	640	M	20.54	212.4	218.4	-6
417	F	18.85	131.1	137.7	-7	642	M	19.06	177.7	188.1	-10
432	M	15.28	164.9	174.7	-10	644	M	18.06	186.7	199.0	-12
442	F	18.76	144.3	149.8	-6	660	F	18.47	143.0	155.6	-13
447	F	24.20	185.3	188.9	-4	664	F	27.59	149.4	157.8	-8
461	F	28.91	159.0	164.3	-5	670	F	21.84	153.4	159.4	-6
481	F	25.45	147.7	156.2	-8	678	M	20.84	157.4	175.3	-18
501	M	21.73	180.6	172.6	8	680	M	23.88	184.2	191.3	-7
503	M	19.24	188.0	198.9	-11	682	F	14.63	152.8	161.1	-8
511	M	18.94	158.1	173.8	-16	691	F	17.78	151.1	160.2	-9
512	F	23.65	126.6	140.5	-14	693	F	22.32	151.7	162.8	-11
514	F	25.12	139.1	142.5	-3	696	M	18.80	176.5	183.7	-7
517	F	18.50	170.8	175.2	-4	699	M	19.14	162.3	153.2	9
520	F	18.52	142.5	147.2	-5	704	M	19.67	170.3	184.0	-14
527	F	25.50	150.5	150.3	0	710	M	20.07	181.6	193.4	-12
533	M	20.37	176.7	194.4	-18	711	F	23.70	136.8	151.3	-15
538	F	23.76	134.7	137.9	-3	713	M	28.16	191.9	211.3	-19

[a]Identification numbers are those assigned by WUSTL and are proceeded by a "W." [b]Difference between ECV and BV estimates for use in calculation of Bland and Altman's (1999) limits of agreement (LOA).

Inter-method agreement was assessed with Bland and Altman's (1999) limits of agreement (LOA) method, which uses the average and standard deviation of the differences between measurements of the same individual to calculate an interval within which 95% of the observed differences should fall if the two methods produce comparable data. The LOA

calculated for the 72 individuals is a difference (d) of -7.37–23.09 ($\bar{d}$ = 7.86 ± 7.8). The difference in estimated measures calculated from MR and CT scans is outside the LOA for 4 individuals (0.06%, Fig. 3.4). Removing two outliers (W352, W413) did not change the results (5 individuals, or 0.07%, were outside the modified LOA). Therefore, there is agreement between the two imaging techniques.

Unexpectedly, $\bar{X}_{\mathrm{CT}} < \bar{X}_{MR}$, which might be explained by differences in segmentation protocols, assignation of threshold values of radiodensity, or machine settings. This result is completely counter to that expected based on neurocranial biology and, ideally, I would be able to interrogate this discrepancy further. However, I do not have access to the MR scans or Kochunov's measurement protocol. Regardless, the measurement differences between the two are negligible and should not affect interpretation of results regarding ECV as a brain size proxy. Furthermore, as it is the phenotypic *variance* on which quantitative genetic analyses are based, and not central tendencies, estimation of differences among individuals is more important than accurate measurement of the population mean.

Additionally, precision between the two methods was also assessed by regressing CT-derived estimates on MR-derived estimates and calculating the adjusted R^2, the percent of variance in the data explained by the ordinary least-squares model after accounting for the sample size and number of parameters estimated. This method is reminiscent of the measurement of repeatability (the intraclass correlation coefficient) used to partition phenotypic variance into variance within individuals (measurement error or "noise") and between individuals (both environmental and genetic in origin or the "signal"). This is the method used almost exclusively in quantitative genetics (Falconer and MacKay, 1996) and is, therefore, appropriate for these analyses, although LOA specifically addresses the issue of inter-observer error. The model that included all 72 individuals had an R^2 = 0.86, while that with the same two outliers

removed had an R^2 = 0.91. Both models estimated the MR ECV estimate for each animal to be 87-89% of its CT BV, which also suggests that the estimates from MR imaging are unexpectedly larger than those from CT.

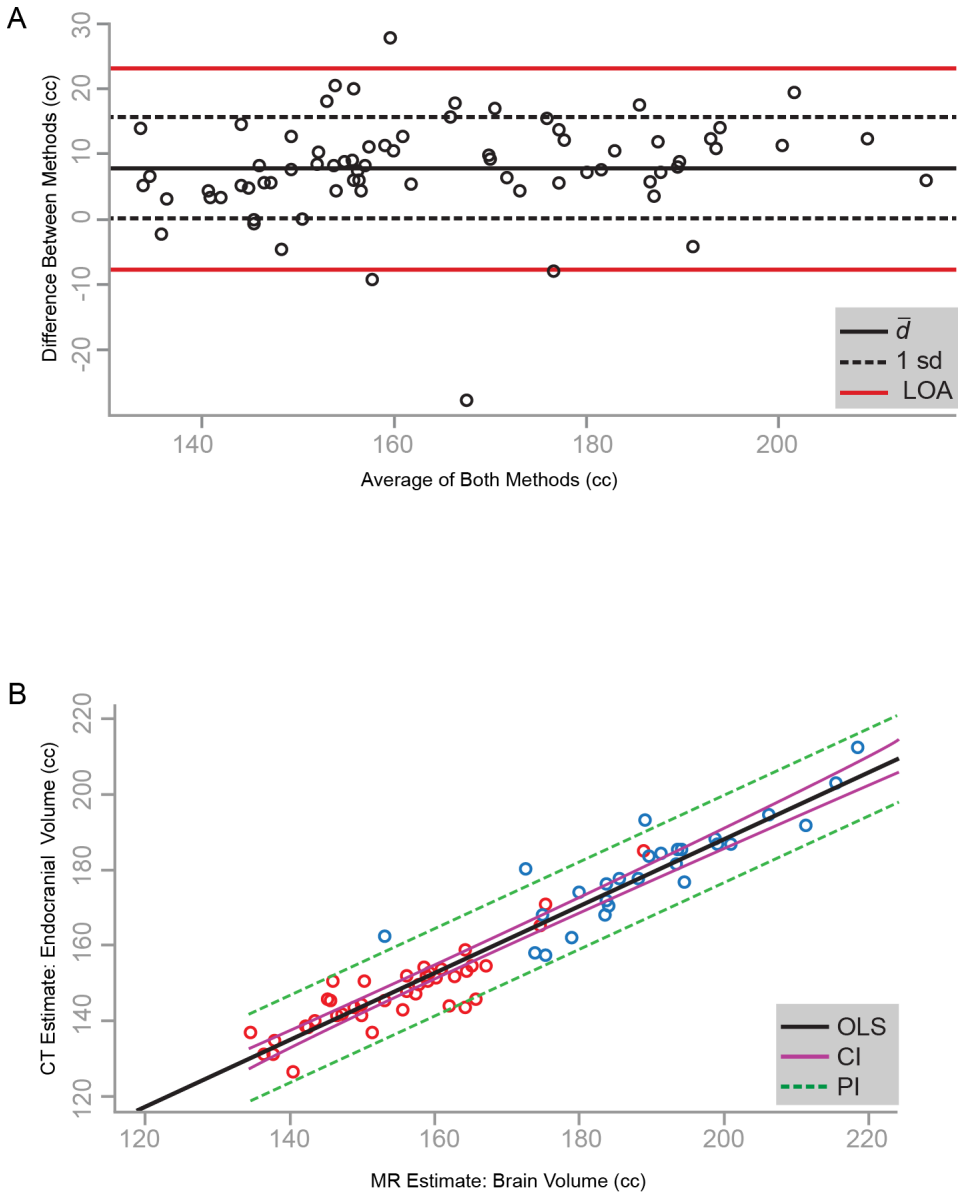

Figure 3.4 Consistency of Baboon Neurocranial Volumes Estimates Between CT and MR Scans. Panels: (A) Bland and Altman's (1999) limits of agreement (LOA; red solid lines) are calculated from the mean pairwise difference (*d*; black solid line) between the CT and MR estimates and the standard deviation (sd; black dashed lines). (B) The ordinary least squares regression (black solid line): ECV = 0.89*BV + 10.3 (SEM = 0.03 cc, R^2 = 0.91). A confidence interval (CI; purple solid lines) and a prediction interval (PI; green dashed lines) are provided.

The scans were also used to capture craniometric landmark data at Pennsylvania State University (PSU) by Katherine Willmore (KEW). In total 21 cranial landmarks were identified on each scan (see Table 3.1 and Fig. 3.2) using eTDIPS, an open-source program for 3D data visualization and segmentation that was jointly developed by the National Institutes of Health Clinical Center and the National University of Singapore (see Willmore et al., 2009 for details). Seventeen of these landmarks were digitized on both the dry crania and CT scans and used to assess the precision of the two methods.

3.3.3 Craniofacial Anomalies and Potential Sources of V_E

In general, V_E is any phenotypic variance that cannot be attributed to genetic sources.[2] In theory, environmental variance can be partitioned into environmental (i.e., biological noise) and measurement-error components. However, practically speaking, doing so requires very specific experimental protocols explicitly designed to tease apart these two sources of V_E. Because this project is concerned with modeling the genetic component of phenotypic variance, V_E need not be considered on such a fine-scale level. The variance-components estimation algorithms simply assume V_E to be uncorrelated within the sample and normally distributed with a mean of zero.

Factors contributing to V_E are varied and numerous. Some are properties of the collection and its curation while others are of the population from which the collection is derived. Over the course of the ~60 years that the SNPRC has been maintaining this baboon colony, husbandry practices have changed and, occasionally, experimental protocols have been administered that alter the diets of adult animals. As any individuals affected ceased craniofacial growth prior to the change in diet, this potential source of variance likely does not affect this

[2] A portion of V_P is also attributable to the effect of gene x environment interaction variance (V_I). Theoretically, V_P can be decomposed into all three types of variance, but this is difficult to do in practice (although, see Ehrich et al., 2005 and Lawson et al., 2010).

project, but changing husbandry practices likely do. Unfortunately, there is no way to know if there has been any effect or how to quantify it. Another concern is that the degree to which individuals are hybrids has generally decreased since the colony's founding. As hybridization has been shown to modify craniofacial traits (e.g., Ackermann et al., 2006, 2014), this variation in the number of hybrids and the extent of their hybridization has the potential to influence results.

There is also variation in individual habits of the animals. For instance, some animals develop idiosyncratic chewing behaviors that modify their oral dimensions. Some individuals demonstrate injuries to be expected within groups of highly social animals with strict dominance hierarchies (e.g., antemortem zygomatic arch breaks and sharp force trauma injuries). Because baboons are very long-lived, even within captivity, it is not unusual to see varying degrees of tooth wear and caries incidence, antemortem tooth loss and associated alveolar bone resorption, and/or general change of bone-surface texture, porosity, and density. All of these factors potentially affect assessment of craniofacial variation within this sample. Conversely, all animals (except those periodically placed on modified experimental diets, none of which were included in this sample) are fed the same Purina monkey chow, meaning that no phenotypic variation due to dietary mastication differences is expected for these animals.

In terms of the skulls themselves, curation protocols changed partway through the skeletonization process. It was discovered that maceration in hot water typically left bones greasy while feeding the heads to dermestid beetle colonies more often did not, so I elected to alter the processing method. It is important to note that, even among the skulls that were skeletonized by the dermestid beetles, there is variation in how dry/greasy the bones are (Fig. 3.5). This is attributable to individual differences in fat content in the tissues still adherent to the bones after defleshing. Bone condition greatly affects the ease with which craniometric

landmarks are identified. Grease on bones often obscures sutures and other important features, making digitizing difficult.

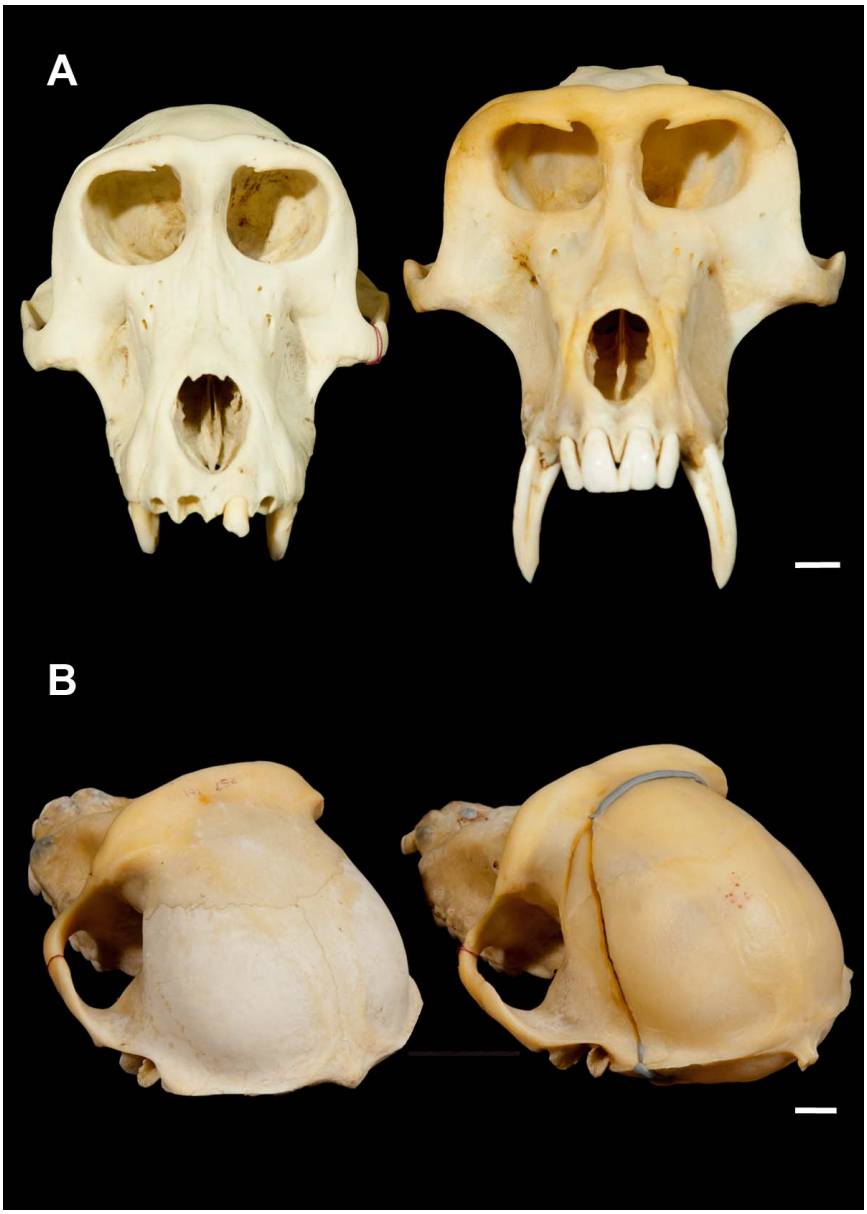

Figure 3.5 Potential Sources of Measurement Error. Panels: (A) Frontal views of a female (left) and male (right) crania demonstrating the gracility of the female relative to the male, in which a wide bizygomatic breadth, large canine fossae, and narrower nasal aperture are visible. (B) Oblique posterior views of a “dry,” complete female cranium (left) and a greasy female cranium that has been reconstructed with modeling clay after necropsy (right). White scale bars are 1 cm. Photographs: Aaron Bunse.

An additional factor of concern regarding processing protocols is that the vast majority of animals had their brains removed at necropsy by way of a circum-calvarial cut. However, the crania of a number of individuals (8%) were left intact and brain tissue was removed during the skeletonization process through the foramen magnum. On average, the necropsy saw removed 0.5 mm of bone during the cutting process. Modeling clay was used to approximate the amount of missing bone (see Fig. 3.5), but these reconstructions were variably successful. Unfortunately, as it is the pattern of craniofacial variation that is of interest and is compared among individuals in order to estimate quantitative genetic parameters and to localize genomic regions potentially contributing to this variation, this particular source of error variance will likely have a larger effect on analyses than most of the other sources. This limitation is acknowledged and was controlled as much as possible.

Age and sex also contributed to error variance (see Fig. 3.5). Male skulls are typically more difficult to digitize, especially the neurocranium. The strain exerted on the ectocranium by the hypertrophied temporalis and nuchal muscles modifies the bone texture, making it ridged instead of smooth, and often remodels the bone to such an extent that sutures are completely obliterated. As hypertrophy of those muscles occurs in response to increasing concentrations of androgens (especially testosterone) during late adolescence (e.g., Kochakian and Tillotson, 1957; Marsh et al., 1998), the difficulty in identifying landmarks also tended to increase with age, particularly in males. Additionally, for unknown reasons, antemortem anterior tooth loss and associated alveolar resorption was more common in older males, which often made the craniometric landmarks PM, AC, and 41 difficult to digitize.

The craniometric landmarks BR, LD, AS, PM (see Table 3.1) were more difficult to digitize than others due to the combination of factors discussed above. Not surprisingly, the EIDs with the lowest repeatability estimates typically contain at least one of these landmarks.

Variation in suture configuration around PT was also of concern. Although catarrhines are said to possess a configuration in which the frontal articulates with the temporal—the parietal and sphenoid articulate in platyrrhines (Ashley-Montagu, 1933; Le Gros Clark, 1959)—patterns of articulation are actually variable in this sample. Others have also noted intraspecific variation of this pattern (e.g., Harrison, 1987; Wang et al. 2006; JMC, pers. comm.).

In addition to the occasional appearance of an ossified laryngeal cartilage, there were two unusual ossification patterns observed. The transverse ligament of the atlas is ossified in 12 individuals, 7♀ and 5♂ (Fig. 3.6). There is anecdotal evidence of this occurring in humans, although it is extremely rare, as there are only six reported cases in the literature (Salcman et al., 1994; Okazaki, 1995; Haraguchi et al., 1996; Hayashi et al., 1998; Sasaji et al., 2011; Desai et al., 2012). The much higher incidence rate in the SNPRC baboons suggests that it may be

Figure 3.6 Examples of Soft Tissue Ossifications that are Not Uncommon in the Collection. Internal view of the anterior and middle cranial fossae (left) with a red arrowhead indicating the ossified anterior falx cerebri. The superior sagittal sinus sulcus is visible as a small, flattened foramen between the inner table and the ossified tissue. Inferior view of the cranial base (right) with yellow arrowheads pointing to the ossified transverse ligament of the atlas. White scale bars are 1 cm. Photographs by Aaron Bunse.

the result of a founder effect. This is supported by the fact that three of the individuals were half-siblings by one father and two by another, there was one avuncular pair, and one individual was the result of multiple generations of consanguineous matings. However, nine of the individuals were F1 progeny,[3] so the trait did not long outlast the effects of genetic drift, and not every offspring of an afflicted individual had an ossified ligament, suggesting the developmental basis is only partially genetic.

A greater number of individuals demonstrated partially ossified anterior falx cerebri, in some cases involving a portion of the superior sagittal sinus. This condition is also rare in humans but more cases of it are published in the literature (e.g., Al-Motabogani et al., 2004; Rangoji et al., 2007; Debnath et al., 2009) and there is even a case report of complete ossification (Tubbs et al., 2006). It is unclear what effect either of these conditions would have had on the individuals, but the co-occurrence of atlanto-occipital and atlanto-axial osteoarthritis in individuals with an ossified transverse ligament suggests that its effects were not benign.

Finally, although not likely to contribute in a meaningful way to error variance but of potential interest to some, a number of individuals in the collection demonstrate congenital dysmorphologies of unknown etiology (Fig. 3.7).

- **W692:** An adult female lacking a right ear canal. The surrounding tissues appear healthy and of normal size and shape, so the most likely cause of the absence is agenesis, possibly due to stapedial artery infarction or first branchial pouch malformations (Gill, 1969; de la Cruz et al., 1985), rather than a syndrome such as Crouzon, Treacher Collins, Pierre Robin, or Goldenhar (Nadol, 2006). Without necropsy records it is impossible to know if her pinna was absent as well, but in humans, congenital atresia of the external

[3] The original wild-caught baboons that were used to found the colony are considered the parental (P0) generation and their offspring are F1's.

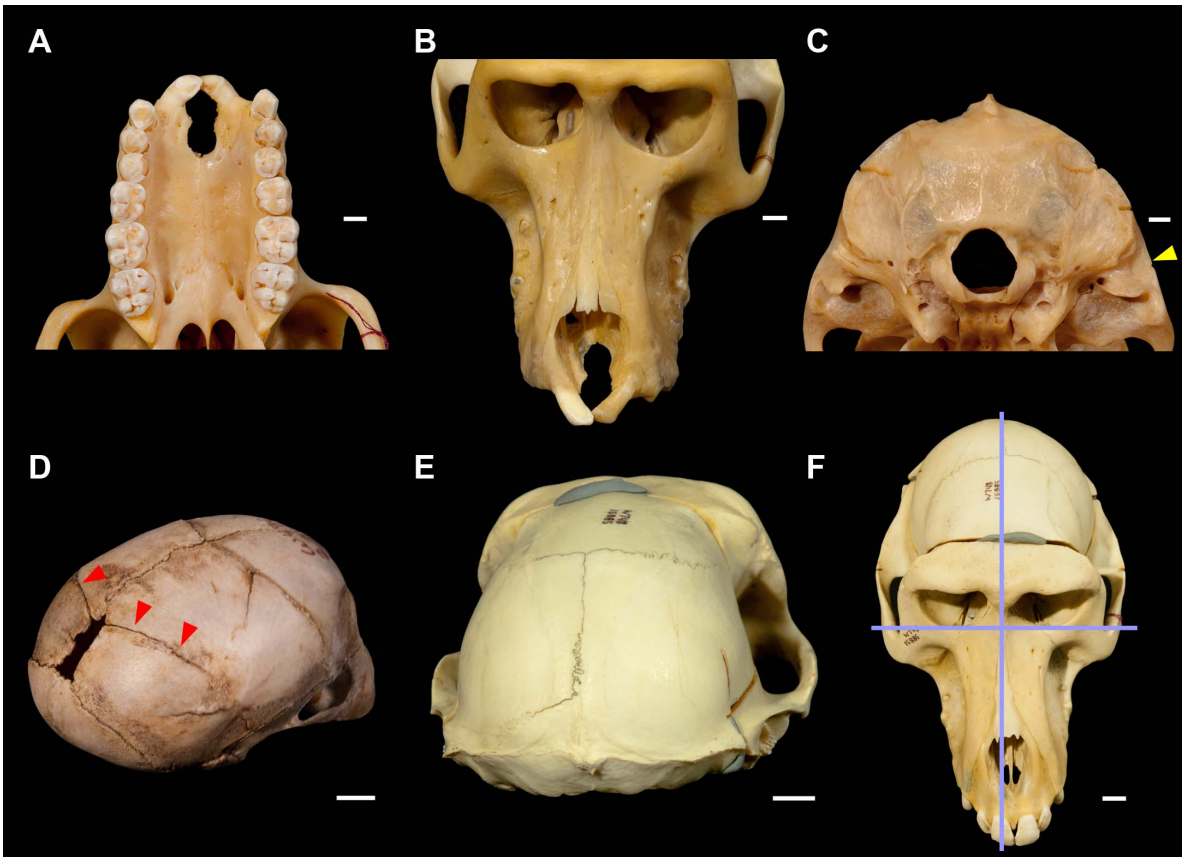

Figure 3.7 Congenital Anomalies Observed in the Curated Collection. Panels: (A) inferior and (B) superior views of a probable Type 0 cleft palate (W216). (C) Agenesis of right ear canal (W692). The yellow arrowhead points to where the right external auditory meatus should be located. (D) Infant cranium (W487) with bilateral intraparietal sutures (red arrowheads). The other lines visible on the right parietal are cracks due to drying and splitting of the delicate dermal bones during the skeletonization process. (E) Posterior and (F) superior views of a case of right lambdoid synostosis (W748). Horizontal and vertical lavender lines demarcate the plane of the inferior orbital margins and a perpendicular midline plane running through nasion. Both the neurocranium and the face are significantly deviated from this midline plane, albeit the latter is much more pronounced in its deviation than the former. White scale bars are 1 cm. Photos: Aaron Bunse.

auditory canal (CAEAC) can occur with or without absence of the pinna as well as with or without malformation of the middle and inner ear structures. CAEAC is observed in 1 in 10,000 human live births (Holmes, 1949), affects the right side more often than the left (Hrdlička, 1933), and is more often seen unilaterally and in males, rather than females (Rosenberger, 1949).

- **W216:** An adult female demonstrating a probable Type 0 facial cleft (Tessier, 1976 and particularly Fig. 3c therein, which closely recapitulates the craniofacial morphology of W216) as the premaxilla is almost entirely absent. A number of individuals have alveolar resorption that extends into the nasal cavity but is non-uniform and asymmetrical, is present with sharp borders, and which alters the gross structure of the bony tissue. This is not the case for W216. The defect is perfectly symmetrical and with rounded edges, and the alveolar bone on both sides just mesial to the most anterior teeth present (canines) is healthy and smooth. The medial incisors are missing, but the lateral ones are extremely angled inferomedially and meet in the midline at their mesial tips, which is also never seen in cases of premaxillary alveolar resorption. It is unknown if the individual also had a cleft lip, and absence of a necropsy report precludes confirmation of this diagnosis, but cleft lip and/or palate have been observed in multiple non-human primate species (e.g., Kraus and Garrett, 1968; Swindler and Merrill, 1971; Goldschmidt et al., 2010).
- **W748:** An adult female with unilateral lambdoid synostosis, but whether this is an isolated case or a symptom of a syndrome is unknown. Absence of other craniofacial abnormalities seems to suggest that it is an isolated case but without access to postcranial remains, a diagnosis cannot be rendered. The prevalence in humans of isolated craniosynostoses is 0.4–1 in 1000 live births, although lambdoid is considered the rarest form of craniosynostosis (Garza and Khosla, 2012).
- **W757:** An adult female with an unfused mental symphysis and a massive soft tissue oronasal tumor of unknown histology.

In terms of dental abnormalities, most are likely the phenotypic manifestation of a hybrid genome and are discussed in Ackermann et al. (2006, 2014). For the sake of completeness, general trends are highlighted here (Fig. 3.8), while readers are referred to Ackermann and

colleagues' works for more detailed explanations. Rotated teeth were visible in at least six individuals and, although molars were more commonly affected, other tooth types were as well. Three individuals had purported ectopic teeth in the walls of their nasal cavities, and quite a few

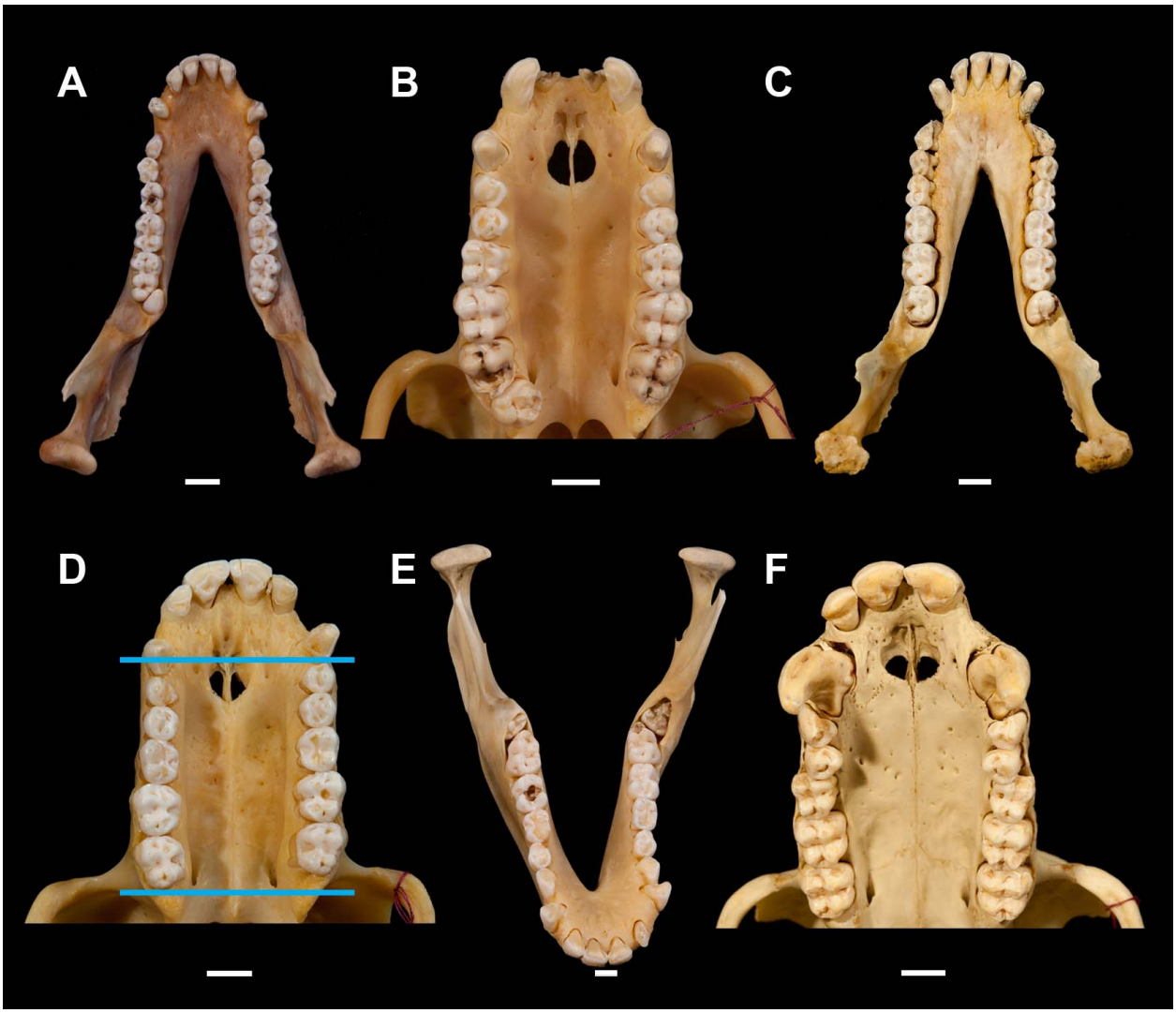

Figure 3.8 Examples of Baboon Dental Anomalies. Panels: (A) Left mandibular supernumerary tooth of unknown type, most closely resembling a small canine. (B) Right maxillary M4 rotated 90° counterclockwise. (C) Bilateral mandibular M4's, the left one being of normal cusp morphology but small in size and the right one showing a reduced number of cusps. (D) Maxillary cheek tooth rows that do not line up. The horizontal blue lines show that the left side is shifted half a tooth forward or the right side is shifted half a tooth back (determining which side is "normal" is impossible) relative to the contralateral side. (E) Bilateral mandibular M4's still in their crypts. There is an abnormal diastema between the left medial and lateral incisors, and the typical diastema between lateral incisor and canine is much larger on the left than on the right side. (F) Agenesis of the left maxillary lateral incisor with crowding of the post-canine teeth, especially of the premolars. White scale bars are 1 cm. Photographs by Aaron Bunse.

had a diastema present between incisor teeth. Both anomalies have been shown to result from disruptions in gene regulation of dental development (Bei, 2009), as would happen within a hybrid genome. At least ten individuals retained deciduous dentition at an adult age while also demonstrating permanent dentition. Dental crowding and tooth displacement are not uncommon in the sample, and neither are supernumerary cusps. Eleven individuals had at least one agenetic tooth, typically an incisor or premolar, and 61 had supernumerary teeth, which were overwhelmingly molars (31% “peg-like”). As these are localized changes within the oral cavity, they are not expected to bias the results of this study. However, any dental modifications that influence occlusal patterns or masticatory function could alter the morphology of associated facial components.

Finally, a number of individuals have supernumerary sutures, also likely the result of hybridization. Intra-parietal (see Fig. 3.6, Panel D) and intra-zygomatic sutures were the most common. This phenomenon has also been observed and discussed by Ackermann et al. (2006, 2014).

3.3.4 Adult Body Weight

Scaling relationships between craniofacial measurements and body size are important to consider in morphological research, particularly for *Papio*, as body size sexual dimorphism is extreme (e.g., Leigh, 2009; Willmore et al., 2009) and contributes significantly to phenotypic correlation structure in the baboon cranium (Porto et al., 2009). By controlling for body size while estimating quantitative genetic parameters and locating QTL (see *4.2.2 Levels of Phenotypic Variation*), I can elucidate the genetic architecture of phenotypic variation in the baboon cranium that is attributable to genetic variants affecting craniofacial variation alone. In order to do so, a proxy measurement for the body size of each individual in the sample must be estimated.

The most common measurement chosen to represent body size is body weight. While body weights are easier to obtain from both live animals (as opposed to skeletal dimensions) and the literature—it is considered a standard measurement to be collected in most research settings—using it as a proxy does have recognized issues. It is extremely sensitive to fluctuations in local environments (reproductive state, seasonality, nutritional fluctuations, pathology, etc.). Additionally, determining the most appropriate age during an individual's life span at which to collect body size measurements varies among taxa, researchers, and studies. "Adult" body mass is an arbitrary designation as the boundaries between relative age classes are fluid and often differ between the sexes, especially during later ontogeny. All of these factors were considered in designing a method to produce an appropriate body-size measurement for the SNPRC baboons.

At the SNPRC, baboons are opportunistically weighed when they walk over a scale that has been embedded in the floor of their enclosure. They are also weighed at any veterinary visits. As a consequence, some individuals have many measurements taken during their lifetimes (maximum = 195) while others do not have any. On average there are 43.5 ± 25 longitudinal body weights for each individual for a total of 42,838 data points. As a side note, both longitudinal and intra-population variance in body weight measurements will be analyzed using these data in a later publication.

Leigh (2009) previously examined data (N = 1,091) from SNPRC baboons, some of which may be included in this sample. Leigh treated his data cross-sectionally and aggregated them into discrete age intervals. Loess regression was used to model growth in body size and 15 other somatic measures. He visually estimated age at growth cessation for all variables. The current analysis builds on that of Leigh (2009) but improves on it in the following ways: (1) more individuals are included in the sample, (2) age is treated in a continuous manner, (3) weight

data are treated as longitudinal, (4) relevant growth parameters are included in the models, and (5) those models are compared on the basis of fit statistics and the best selected accordingly.

Following the methods of O'Mara et al. (2012) and using a script provided by those authors, an iterative piecewise regression (IPR) model was fit to the data in R 3.1.1 (R Core Team, 2014). Piecewise regression models both a quadratic growth curve prior to growth cessation and an asymptotic adult size following growth cessation. The inflection point between the best-fit lines that model the growth and the adult portions of the dataset is the *age of growth cessation*. The birth weight, rate of growth, inflection point, and asymptotic adult size are all parameters included in the model. Similar methods have been used successfully to model bimaturism and ontogeny for a range of primates (e.g., Leigh, 1994; Leigh and Terranova, 1998; Altmann and Alberts, 2005; O'Mara et al., 2012). The strength of the iterative algorithm used here is that it fits all possible models to the data by permuting the inflection point across the full range of the dataset to identify the model that minimizes the sum of squared residuals. After identifying the best fitting model, the best-fit inflection point estimate is used to assign a single body weight to each individual. The body weight recorded at the age closest to the modeled age of growth cessation is selected as the body weight for that individual to be used in further analyses.

Given the sexual dimorphism in body size for adult baboons, sex-specific IPRs were modeled. However, despite the fact that most primate research shows that females cease growth prior to males, and that the male growth rate is often steeper than that of females early in ontogeny (Cheverud et al., 1992; Leigh, 1992, 1996; German et al., 1994; Leigh and Shea, 1996; Setchell et al., 2001), the results of the IPR analysis indicate that the male baboons in this sample reach adult body mass prior to females (Table 3.5, Fig. 3.5). These results are consistent with those of Leigh (2009), who estimated that females achieve adult body mass

(12.09–21.07 kg) during their tenth year and males achieve it during their seventh year (22.67–33.44 kg). Given the inflection points estimated here, the body weight for each male recorded on the day closest to 2801.7 (7.68 years) and for each female the day recorded closest to 3895 (10.67 years) was used in further analyses. In instances where two records were equally close to the growth-cessation estimate, a mean body weight was calculated. Only body weights recorded within two years of the growth-cessation estimate were considered. If an individual did not have a body weight recorded within this four-year period, its weight was scored as missing data. A total of 55 individuals (43♀, 12♂) did not have a body weight record within two years of the age of growth cessation.

My final sample size was 948 baboons (663♀, 285♂). The observed mean male body weight is 29.09 ± 4.1 kg, recorded at an age of 7.78 ± 0.8 years, while the observed mean female body weight is 18.56 ± 3.6 kg, recorded at an age of 10.51 ± 0.9 years. All four of the corresponding IPR estimates are within one standard deviation of these observed means, empirically indicating that the IPR models are good fits to the data.

Table 3.5 Iterative Piecewise Regression Parameters.

Parameter	Female	Male
Sample Sizes		
growing records (N)	16,653	7,609
adult records (N)	9,145	9,411
Regression Statistics		
SSR	201,539	245,454
R^2	0.77	0.84
Parameter Estimates		
duration (years)	10.76	7.68
adult size (kg)	19.15	30.49
regression-based birth size (kg)	0.43	-0.77[a]
mean-based birth size (kg)	1.04	0.09
regression-based growth rate (g/day)	4.81	11.25
mean-based growth rate (g/day)	4.65	10.57

[a]Birth size is derived from the best-fit regression line, which intercepts the vertical axis below the origin in this particular instance.

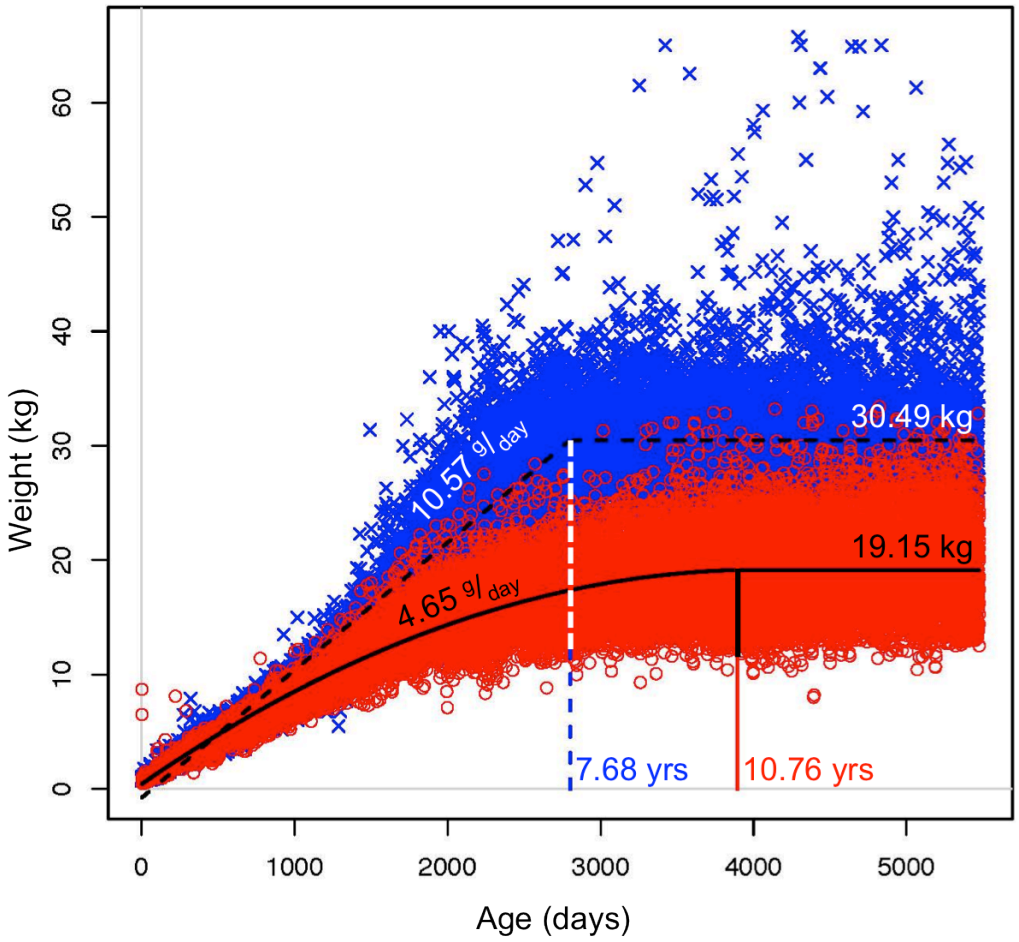

Figure 3.9 Sex-Specific Best-Fit Iterative Piecewise Regression Lines. Regression lines are overlaid on a bivariate plot of longitudinal body weight records for SNPRC male (blue) and female (red) baboons. The sex-specific estimates of growth rate, adult body weight, and age of attainment of adult weight are indicated next to their respective regression lines (see Table 3.5).

3.3.5 Measures of Cranial Size

A variety of methods have been employed for quantifying overall cranial size: centroid size of the landmark coordinate data, geometric mean of the EIDs, ECV or brain size, cranial base length, and the first principal component (PC) from a principal-components analysis (PCA) of the EIDs. Any of these could be applied to the baboon cranium. However, calculating centroid size assumes isometry, or that variation around a 3D landmark is spherical. For the cranium, it has been shown that this is often not the case (e.g., Debat et al., 2000; van der Linde and Houle, 2009; Bookstein, 1996, 2015; see Chapman, 1990 for a detailed discussion of the

related ‘Pinocchio effect’). Because more males than females are missing data (see *3.3.3 Craniofacial Anomalies and Potential Sources of V_E*), calculation of the geometric mean is difficult and, in some cases, impossible. Both ECV and cranial-base length (NABA; see Table 3.2) are variables of interest, so they cannot also be treated as control variables.

Given these limitations, PCA was used to extract the first PC, which is generally considered to contain primarily size-related variation. To do so, residual EIDs (rEIDs) were calculated in SOLAR for every individual for each trait after controlling for body weight and for any additional covariates that significantly structure each EID (sex, age, age^2, sex*age, and/or sex*age^2; see *4.2.2 Levels of Phenotypic Variation* and Table 4.2). A correlation matrix was calculated for every pair of rEIDs using all cases containing values for both rEIDs of each pairwise comparison. PCA was performed on this pairwise correlation matrix ($\mathbf{M}_P$) in Stata 14 (StataCorp, College Station, TX).

The PC1 eigenvalue is 10.22 and accounts for 17% of the variation in M_P. Its loadings were examined to determine which cranial dimensions best quantify size variation in the baboon cranium (Table 3.6; Fig. 3.10). Residual EIDs scoring highest on PC1 capture variation in snout length (ACSY, FMPM, NA41, NAAC, NANL, NLVS, ZSNL), cranial base length (NABA, NAVS), facial hafting (CPZS, FMCP, NACP), and facial breadth (NAZI, ZTVS, ZTZT). To clarify, by facial hafting I mean the angle at which the face attaches to the neurocranium. Joganic et al. (2012b) determined that this is an evolutionarily variable feature of the papionin cranium. The lowest scoring residual EIDs are primarily restricted to the neurocranium (BRLD, BRPT, CPSL, STST) and foramen magnum (BAOP, CNCN). This result suggests that facial variation dominates baboon craniofacial variation above and beyond that which is attributed to the marked facial size sexual dimorphism that characterizes *Papio*, which was accounted for by controlling for sex differences when calculating rEIDs.

Table 3.6 rEID Loadings on PC1.

rEID[a]	N[b]	PC1	rEID[a]	N[b]	PC1	rEID[a]	N[b]	PC1
ACPM	193	0.116	CPZS	177	0.164	NALD	183	0.151
ACSY	255	0.190	CNCN	178	0.035	DAFM	179	0.127
PMPM	296	0.092	FMPM	178	0.192	PLSY	185	0.125
ASJP	182	0.056	FMZT	178	0.134	POBA	173	0.158
BACC	171	0.100	FMCP	178	0.193	PM41	180	0.117
BAOP	131	0.027	FMPT	179	0.114	41MX	195	0.150
ASAS	190	0.108	LDAS	179	0.119	41ZI	180	0.144
JPJP	182	0.105	LDBA	184	0.136	PTAS	179	0.064
4141	176	0.148	NANL	73	0.163	PTLD	178	0.067
POPO	276	0.157	NLAC	197	0.085	SLBA	172	0.037
PTPT	108	0.068	NLVS	201	0.187	SLCC	174	0.060
STST	172	-0.001	NAAC	246	0.185	SYBA	184	0.094
ZTZT	196	0.175	NACA	179	0.153	SYMX	183	0.120
BRAS	178	0.121	NACP	186	0.203	ZTPO	181	0.115
BRLD	186	0.039	NAFM	176	0.163	ZTVS	177	0.175
BRNA	179	0.096	NA41	195	0.193	ZTZI	177	0.040
BRPT	183	0.014	NAVS	180	0.169	VSBA	181	0.071
NABA	177	0.199	NAZI	177	0.192	VSSY	80	0.051
CACP	72	0.048	NAZS	179	0.102	ZIMX	176	0.118
CPSL	717	0.029	BRBA	179	0.099	ZSNL	177	0.183

[a]Particularly high-scoring rEIDs (0.180–0.203) are indicated in orange typeface and low-scoring ones (-0.001–0.04) in light blue. [b]Number of imputed cases.

Because the number of pairwise complete cases is low for some variable pairs, it is possible M_P is unstable, i.e., subject to sampling error. Therefore, a maximum likelihood estimate of the variance/covariance matrix underlying the rEIDs was estimated using the expectation-maximization (EM) algorithm (Truxillo, 2005) in Stata 14. Technically, the estimated matrix is actually a correlation matrix as I standardized the rEIDs on which the estimation was performed. This matrix will be referred to as the imputed correlation matrix ($\mathbf{M}_I$). The EM alternates between an expectation step, in which parameter values are computed with respect to distributions conditioned by both the pattern of missingness in the data and the data themselves, and a maximization step, in which the model parameters are updated with the most recent iteration of the expected values (Schafer, 1997). A solution is obtained once the difference between successive model parameter estimates plateaus.

The EM converged after 287 iterations. A PCA was performed on the resulting $\mathbf{M}_I$, and a dot product was used to compare the first eigenvector to that of the PCA of $\mathbf{M}_P$ (Table 3.7). The angle between the two vectors (θ) is 0.1, which suggests that M_I and M_P are very similar and have nearly identical PC1's (perfect correlation is $\theta = 0$). These results indicate that, contrary to initial concern, $\mathbf{M}_P$ is stable and its PC1 appropriately captures the major axis of variation in rEID values. Ultimately, PC1 of the $\mathbf{M}_I$ was selected, so that the estimated covariance structure used to impute missing data (see below) and to perform the PCA would correspond.

Because only 98 individuals have values for all 60 residual EIDs, component scores could not be calculated for every cranium from the PCA of $\mathbf{M}_I$. Instead, I used multiple

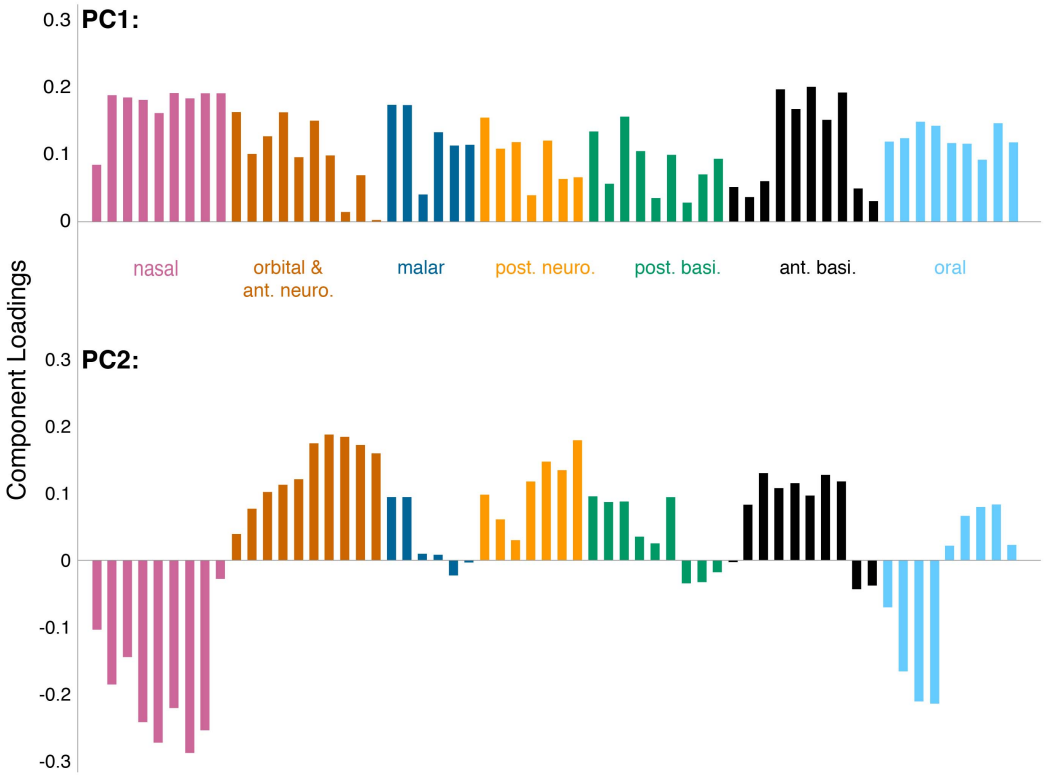

Figure 3.10 PCA Loadings. Standardized loadings for each of the 60 rEIDs on the first two eigenvectors of a PCA performed on the Expectation-Maximization-estimated correlation matrix. The rEIDs are grouped and colored by cranial region: nasal, orbital and anterior neurocranial, malar, posterior neurocranial, posterior basicranial, anterior basicranial, and oral.

imputation to fill holes in the dataset by creating a predictive model that included all the information available in the observed data and any *a priori* knowledge about data structure. I used Expectation Maximization with Bootstrapping (EMB) to impute missing data in the R package Amelia II (Honaker et al., 2011), which combines EM (as discussed above) with traditional Bayesian procedures. The algorithm implemented in Amelia II begins by bootstrapping the set of observed data to produce multiple versions of incomplete data. As is traditional with data that are not burdened with a significant amount of missingness, I chose to bootstrap five datasets (Honaker and King, 2010). EM is then performed on each of the datasets, with starting values for missing data set according to the observed variances in each bootstrap dataset and assuming a covariance of 0. At the convergence of each run of EM, point estimates of sample parameters μ and Σ are obtained and used to impute missing data. The result is five complete datasets that each feature the unaltered observed data combined with imputed data. I then took the mean of each of the five imputed values to create the final dataset (N = 892 and no missing data). To double-check the EMB results, I performed a PCA on the correlation matrix of this final dataset and the results were very similar to those of the PCAs performed on the observed data alone (see Table 3.7).

One benefit to using EMB is that uncertainty in the predictive model is reflected in the degree of variation among the five imputed datasets. An over-imputation technique can be applied to determine how precise the imputed values are. Each of the observed values is treated as missing (i.e., dropped from the analysis), and that "missing" value is then imputed many times, producing a confidence interval for what the observed value would have been had it truly been missing. Plots of the "imputed" estimates against the corresponding observed value were visually inspected to determine how often the confidence intervals cross the $y = x$ line of

Table 3.7 Comparison of PCA Results for Four Different rEID Correlation Matrices.

Correlation Matrix[a]	PC1 (%)[b]	PC2 (%)[b]	PC3 (%)[b]
$\mathbf{M}_P$	10.22 (17)	4.65 (8)	3.58 (6)
$\mathbf{M}_I$ EM	11.28 (19)	4.34 (7)	3.40 (6)
$\mathbf{M}_I$ EMB	11.54 (19)	4.41 (7)	3.40 (6)
$\mathbf{M}_I$ DA	10.27 (18)	4.16 (7)	3.31 (6)

[a]$\mathbf{M}_P$: pairwise complete correl. matrix calculated from observed data, $\mathbf{M}_I$ EM: expectation-maximization estimated correl. matrix, $\mathbf{M}_I$ EMB: correl. matrix of expectation maximization with bootstrap imputed data, $\mathbf{M}_I$ DA: correl. matrix of data augmentation imputed data. [b]Eigenvalue and percent total variance explained by the corresponding eigenvector.

perfect agreement and, thus, how reliable model predictions are. Except for two (POPO and STST), those rEIDs with greater degrees of uncertainty in missing value imputations (N = 29), as indicated by the much wider confidence intervals of the over-imputed values (Fig. 3.11), had small phenotypic variances (range: 1.9–29.3 mm). The remaining 31 rEIDs all had small confidence intervals, although the range of V_P was much greater (7.74–144.43 mm). Because the overwhelming majority of rEIDs with large confidence intervals also had small V_P (Fig. 3.12; $P = 0.002$, $R^2 = 0.15$ and $P < 0.001$, $R^2 = 0.22$ when excluding the two outliers), this suggests that the reliability of the imputation procedure is biased toward measurements with larger variances, which also tend to be those with larger means. However, this bias does not appear to extend to any particular craniofacial region, as the traits with large confidence intervals are dispersed throughout the cranium. So, while some traits may be more difficult to model with a multiple imputation algorithm, neighboring traits may be more accurately imputed, thus helping to maintain a more faithful representation of the cranial covariance structure.

Another diagnostic that was performed to assess model accuracy was to compare the pairwise correlation matrix ($\mathbf{M}_P$) from the observed data to correlation matrices calculated for each of the five imputed datasets ($\mathbf{M}_1$–$\mathbf{M}_5$). Matrices were compared with a Mantel test, which will be described in greater detail in the next chapter. Briefly, the significance of the correlation coefficient between $\mathbf{M}_P$ and each of $\mathbf{M}_1$–$\mathbf{M}_5$ is assessed through a permutation procedure. In all

five cases r = 0.96, which is significant at α = 0.05 for the null hypothesis that the two matrices share a common correlation structure.

A final check of the validity of the imputed data was done by repeating the imputation process in Stata 14 with a more widely known imputation-posterior approach (King et al., 2001), an iterative Monte Carlo Markov Chain (MCMC) procedure that utilizes data augmentation (DA;

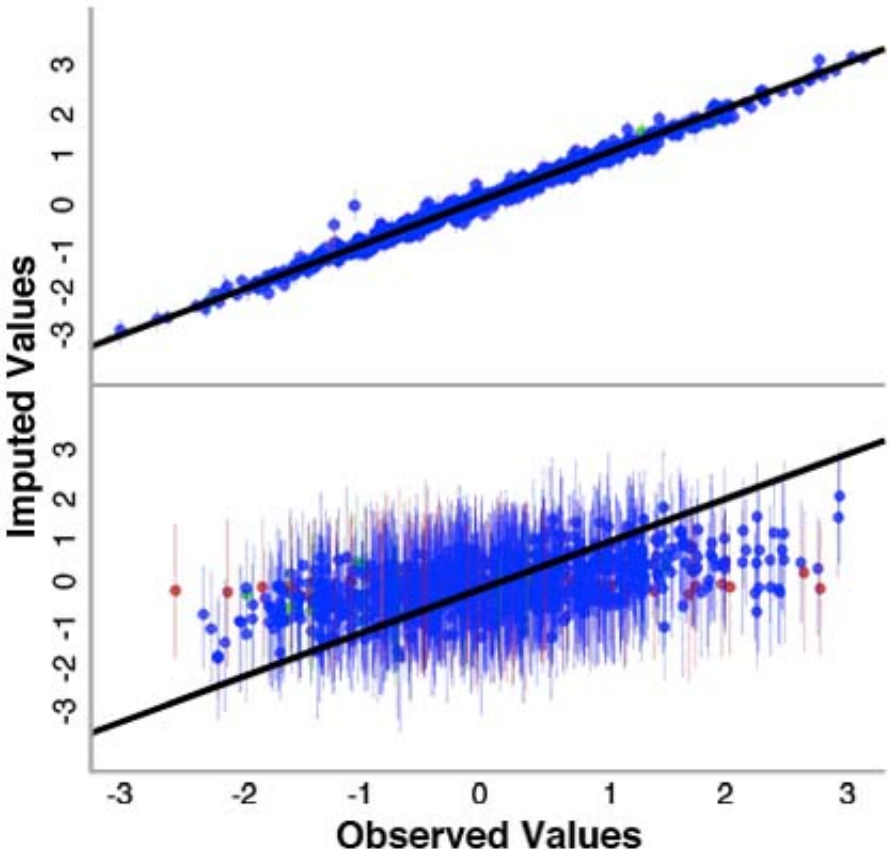

Figure 3.11 Over-Imputation Plots for NALD and BAOP. Plots of over-imputed rEIDs versus their observed values with 90% confidence intervals (CIs) indicated by vertical lines. If an imputation model is a perfect predictor of the true value, all imputations would fall on the line of perfect agreement ($y = x$, the oblique black line). CIs that span the line contain the true observed value. Plots in which a large number of CIs contain the line of perfect agreement suggest the imputation model can more confidently predict the true value of the observation. The colors of the dots and their CIs represents the fraction of covariates observed in the pattern of missingness (blue = 0.0–0.2, green = 0.2–0.4, yellow = 0.4–0.6, orange = 0.6–0.8, red = 0.8–1.0).

Tanner and Wong, 1987; Schafer, 1997). A multivariate normal regression model that assumes a non-monotone (i.e., arbitrary) pattern of missing data and a uniform prior (i.e., all parameter values are equally probable) was selected as the underlying DA model. An initial burn-in period of 100 iterations and a burn-between of 100 iterations between MCMC imputations were specified. The EM-estimated M_I provided the initial starting values for the DA procedure (e.g., Dempster et al., 1977). One of the major differences is that the resulting dataset is composed entirely of imputed values, the observed data having also been replaced by values imputed using M_I. In contrast, the EMB procedure implemented in Amelia II preserves the observed values, filling in only the gaps of missing data. Nevertheless, a PCA of the correlation matrix from the DA imputed data yielded similar results to the previous three PCAs (see Table 3.7). Although these data are not used in further analyses because observed values are no longer included in the imputed dataset, the congruence of the PCA results across the four matrices

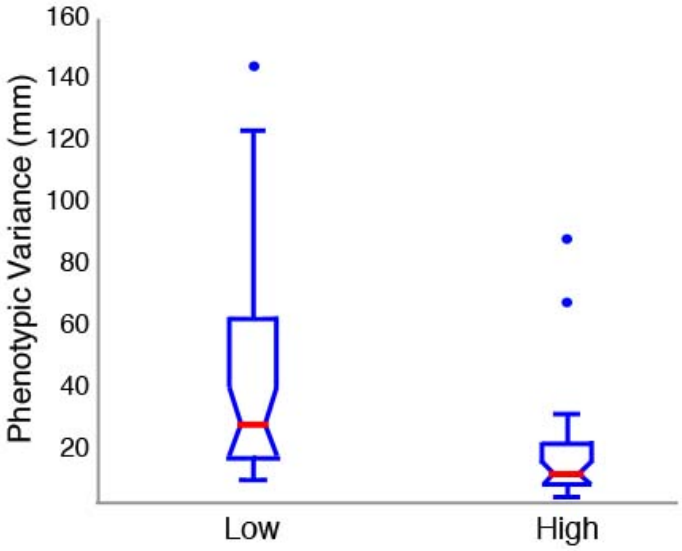

Figure 3.12 The Relationship Between Imputation Uncertainty and V_P. EIDs with a low degree of uncertainty (i.e., the imputation model does a good job of predicting the true observed value according to the over-imputation results) have more V_P than those with a high degree of uncertainty (i.e., the imputation model is less reliable).

suggests that the correlation structure of the observed data is maintained despite the application of complex statistical procedures for solving the missingness issue.

As mentioned previously, the standardized first eigenvector of $\mathbf{M}_I$ was used to calculate PC1 scores for the resulting dataset of EMB-imputed rEIDs. These scores are then used as a covariate to correct EIDs for global cranial size in the quantitative genetic analyses. Scores were standardized to keep the data consistent across analyses, all of which use standardized data to account for differences in variation patterns among the EIDs (see *3.3.1 Data Collection from Dry Crania*). These standardized PC1 scores are then used to estimate quantitative genetic parameters and to map QTLs for cranial dimensions that have been adjusted for both body and cranial size.

Any QTL located for these data that was not previously identified for either the body-size-corrected or uncorrected EIDs should contain genetic variation specifically affecting the region of the skull quantified by that standardized PC1 score. These new QTLs should not contribute to overall cranial size variation, as it has been removed from the analysis, but rather regional shape variation. Making this distinction is important as the effects of allometry are so strong in the baboon cranium and, consequently, the correlations among cranial dimensions are quite high. Consequently, this condition produces a more integrated and less modular cranium (Porto et al., 2009). Identifying QTLs affecting variation at only one of the three scales considered in this project (1–overall body, 2–entire cranium, and 3–localized cranial element; see *4.2.2 Levels of Phenotypic Variation*) will provide us with more and higher-resolution information about the genetic architecture of the baboon cranium.

3.4 Conclusion

The SNPRC baboon skull collection on which these data were measured is a unique and highly valuable collection that can be—and has been (e.g., Willmore et al., 2009; Roseman et al.,

2010; Atkinson et al., 2015)—used to answer a variety of questions regarding variation of complex traits. The research presented in this dissertation is just one of many projects that use the SNPRC sample. In addition to the three mentioned above, some additional specific projects include: a comparison of general patterns of nonmetric trait variation in hybrid and purebred individuals (Ackermann et al., 2006, 2014), an examination of hybrid morphology in the nasal cavity alone (Eichel, 2014), quantification of oral variation in purebreds fed diets of different hardness (Campbell et al., 2015), and an evaluation of changes in oral dimensions after tooth loss (Percival et al., 2010). The remaining chapters of this dissertation detail the results of my project and, at the beginning of each, information regarding methods specific to those chapters.

The next chapter, Chapter 4, presents quantitative genetic analyses: estimation of heritability, genetic correlations, and effective sample sizes, screening of covariates, and proportion of phenotypic variance explained by heritable genetic variation. Details about the program used to analyze the genetic variance components are provided with those results.

Chapter 5 details how phenotypic, genetic, developmental, and functional correlation matrices are created for the analysis of morphological integration and modularity in the baboon cranium. The various permutation methods used to compare these matrices are explained in detail in that chapter. Understanding how variation in the cranium is patterned can aid evolutionary reconstructions, formation of selective hypotheses, studies of craniofacial genesis, and allow for interspecific comparisons with other primates for which similar matrices have been produced.

In the final results chapter, Chapter 6, QTLs are identified for ECV, body size, and EIDs. These phenotypes are analyzed after being corrected for only age and sex and relevant interaction terms, as well as after being additionally corrected for body size and then body and cranium size, as described above (see *3.3.4 Adult body weight* and *3.3.5 Measures of cranial size*). Genetic modularity is assessed by examining patterns of overlapping QTL confidence

intervals. Genes within each QTL are annotated and positional candidate genes identified. Multipoint linkage mapping and gene annotation software are explained therein.

CHAPTER FOUR
RESULTS: HERITABILITY ESTIMATES

4.1 Introduction

Complex traits, such as craniofacial dimensions, are the manifestations of multiple genes (polygeny), interactions among these genes (pleiotropy), and interactions between these genes and the environment. Studying their development and evolution requires knowledge of their underlying genetic architecture by answering questions such as: How many genes are involved? Does each of these genes contribute a lot or a little to variation in the trait? Are the effects of these genes additive or non-additive? Is the trait heritable and if so, how strongly? This last question is of particular importance for three reasons. First, it is paramount for evolutionary biologists to establish whether a trait is significantly heritable. Unless variation in a trait can be passed from parent to offspring, by definition, it cannot evolve. Second, determining the magnitude of the heritability provides information as to whether the trait should even be considered for further genetic and/or genomic research, which can often be time consuming and expensive. Finally, ascertaining a trait's heritability delineates the familial correlation/covariance structure, which improves the constructed etiological model.

Heritability of a trait is estimated by examining the phenotypic correlation between close relatives in relation to their genetic resemblance (Falconer and Mackay, 1996). Charles Darwin pointed out the similarity of close relatives in pigeons, racehorses, and humans, and discussed the importance of surveying this resemblance and its relation to the variation within populations when studying natural selection (Darwin, 1859). Karl Pearson, along with Alice Lee (1903), and Sir Francis Galton (1906) each developed the concept of statistical correlation in conjunction with their respective work on familial resemblance. The concept of heritability was born of the union of these two concepts:

> One of the earliest and most striking successes of the method of correlation was in the biometrical study of inheritance. At a time when nothing was known of the mechanism of inheritance, or of the structure of the germinal material, it was possible by this method to demonstrate the existence of inheritance, and to "measure its intensity"; and this in an organism in which experimental breeding could not be practiced, namely, Man.
>
> (Fisher, 1925, p139)

Upon recognizing this resemblance, Ronald Fisher (1918) and Sewell Wright (1921) each developed methods of describing it by partitioning variance into its constituent components, thus forming the theoretical basis for the field of quantitative genetics.

The earliest application of inheritance was in breeding programs of and research on livestock and plants of commercial value (Derry, 2012; Khatib, 2015). Genetic insights gained by agriculturalists were used to manipulate individual characteristics to increase production yield and insect/disease resistance (e.g., Shull, 1909; Brancourt-Hulmel, 2003; Jauhar, 2006), thus putting quantitative genetic theories into practice (Paul and Kimmelman, 1988). These methods were co-opted in the latter half of the 20th century by evolutionary biologists[1] to address questions of complex trait evolution in model organisms like *Drosophila* and *Mus* (Roff, 1997; Mackay, 2001). It has only been recently that this research has been extended into humans and other primate taxa for which necessary resources for estimating quantitative genetic parameters are largely lacking (e.g., Lande, 1979; Cheverud and Buikstra, 1981; Cheverud, 1996).

Understanding the genetic basis for complex traits allows one to ask questions about their evolutionary history and the relationship between variation patterns within and among

[1] According to Lynch and Walsh (1998), three major developments contributed to the growth of quantitative genetics: (1) Russell Lande's efforts to extend into the realm of evolutionary biology the application of statistical concepts of inheritance to Darwinian selection, which was originally pioneered by Ronald Fisher in the early 20th century; (2) the generation of new statistical techniques and computational resources for estimating variance components in complex pedigrees; and (3) the rapid establishment of molecular methods for ascertaining genetic variation and applying it to identify quantitative trait loci (QTLs). Lande was joined by Steven Arnold, William Atchley, James Cheverud, Douglas Falconer, Michael Lynch, Donald Wade—many of whom composed a group (now referred to as "The Chicago School") of evolutionary biologists who embraced the use of quantitative genetics—in championing the application of quantitative genetic theory to the issue of linking micro- and macroevolutionary processes (Phillips, 2007; Hill and Kirkpatrick, 2010; JM Cheverud, pers. comm.).

species. Marroig and Cheverud (2004) did so in New World monkeys to examine the relative importance of natural selection versus genetic drift in the platyrrhine radiation, and determined that interspecific patterns of craniofacial variation were consistent with genetic drift acting differently in the two species. Roseman et al. (2010) used quantitative genetic methods to assess craniofacial variation and underlying genetic correlations in the baboon cranium, determining that variance is distributed throughout, rather than being concentrated in regions of functional or developmental significance, and that genetic correlations among adjacent traits do impose constraints that could direct evolutionary trajectories. Here, I employ similar methods of measuring resemblance among relatives to determine which craniofacial traits are jointly affected by environmental factors and how genes and the environment interact to produce the range of variation observed in a complex trait.

4.1.1 Research questions

The aim of this chapter is to establish a preliminary understanding of the genetic architecture for the baboon cranium using quantitative genetic methods. For both endocranial volume (ECV) and each of the 60 craniofacial traits (EIDs) the following three questions were answered: (1) Do environmental factors explain any of the trait's phenotypic variance (V_P) and if so, how much? (2) Is the craniofacial trait significantly heritable, and how much of the V_P is explained by additive genetic effects? (3) Has the additive genetic variance (V_A) increased or decreased over time, i.e., what is the effective sample size (N_e) for each trait?

4.2 Materials and Methods

The data used in these analyses consist of endocranial volume (ECV), 60 Euclidean interlandmark distances (EIDs), covariate values, and the baboon genetic map (see Chapter 3).

4.2.1 Quantitative Genetic Parameter Estimation in SOLAR

Heritability is estimated by maximum likelihood variance decomposition (MLVD) with the program Sequential Oligogenic Linkage Analysis Routines (SOLAR v 6.6.2; Almasy and Blangero, 1998). Using the genetic information contained in the baboon pedigree and the phenotypic variance (V_P) reflected in the craniofacial measurements, SOLAR estimates genetic variance (V_G) for each Euclidean interlandmark distance (EID) trait by maximizing the likelihood of the model:

$$\boldsymbol{\Omega} = V_P(\boldsymbol{\Phi} h_r^2 + \boldsymbol{I}\sigma_e^2) \tag{4.1}$$

where $\boldsymbol{\Omega}$ is the pedigree covariance matrix, h_r^2 the residual heritability, $\boldsymbol{\Phi}$ the kinship matrix, $\boldsymbol{I}$ an identity matrix (the *n* x *n* square matrix with ones on the diagonal and zeroes elsewhere), and σ_e^2 the variance in random environmental effects.

- The expected phenotypic covariance between pairs of individuals composes $\boldsymbol{\Omega}$. The matrix elements are calculated according to the equation:

  $$cov(y_1, y_2) = E[(y_1 - \mu)(y_2 - \mu)] \tag{4.2}$$

  where y_i is the phenotypic value for individual *i* for the trait being modeled and μ is the trait grand mean.

- $\boldsymbol{\Phi}$ is composed of Cotterman's (1940) pairwise kinship coefficient (k). Each element (ϕ_{ij}) in the matrix is the probability that an allele selected at random from individual i is identical by descent (IBD) to an allele selected at random from individual j. Two alleles are identical by state (IBS) if they are the same nucleotide in two individuals. That identity can either be due to the same mutation occurring independently in both individuals or to inheritance from a common ancestor (i.e., the alleles are IBD). Some examples of ϕ_{ij} include:

mother-offspring = 0.5, avuncular = 0.25, half-siblings = 0.25, first cousins = 0.125.

- The variable of interest is h_r^2. The portion of V_P attributed to significant model covariates (see *4.2.2 Models of phenotypic variance*) is removed and the proportion of this "residual" V_P (V_R) ascribed to additive genetic variance (i.e., h_r^2) is estimated. The maximization algorithms employed by SOLAR for estimating h_r^2 are more powerful than traditional methods of calculating heritability, such as twin studies and midparent-offspring, parent-offspring, or (half-)sibship regression (Falconer and Mackay, 1996), because variance decomposition includes all ϕ_{ij} in the model (Blangero et al., 2001).
- $\boldsymbol{I}$ is a square matrix of size N x N in which every diagonal element is one and all other elements are zero.
- All baboons are housed in the same environments at the SNPRC and, thus, σ_e^2 is considered to be uncorrelated among individuals. This parameter is held constant in all models such that $e^2 + h_r^2 = 1$. The term e^2 is the proportion of V_R attributable to all sources of variation that are not additive genetic in nature, such as dominance deviation, interaction effects, and environmental variance.

For each EID, a number of models are compared and a likelihood-ratio test conducted between each to assess the best-fit model (i.e., the greatest log-likelihood). Eleven models are tested for each EID[2]:

1. no covariates (NoCov model)
2. h_r^2 is estimated and all covariates are included but age is omitted (NoAge model)
3. h_r^2 is estimated and all covariates are included but sex is omitted (NoSex model)

[2] By definition, body weight and PC1 are fixed in the L2 and L3 models (see next section) so they will always be present in models that include any covariates.

4. h_r^2 is estimated and all covariates are included but age*sex is omitted (NoAgeSex model)
5. h_r^2 is estimated and all covariates are included but age^2 is omitted (NoAge2 model)
6. h_r^2 is estimated and all covariates are included but age^2*sex is omitted (NoAge2Sex model)
7. h_r^2 and the trait mean are estimated and only significant covariates are included (null model)
8. h_r^2 = 0 and all covariates are included (S0 model)
9. h_r^2 = 0 but only significant covariates are included (sporadic model)
10. h_r^2 is estimated, all covariates are included, and the observed trait mean is used (P0 model)
11. h_r^2 is estimated, only significant covariates are included, and the observed trait mean is used (polygenic model)

4.2.2 Levels of phenotypic variation

Three model levels were analyzed to examine phenotypic variation at different scales in baboons. Model 1 examines craniofacial variation as it relates to variation in the entire body due to systemic effects (i.e., sex hormones and ontogenetic changes). Five basic variables were included as potential covariates: sex, age, the interaction between sex and age, the square of age (age^2), and the interaction between sex and age^2. Age^2 was included to account for any non-linear relationships between trait size and age. Only variables significant at the α = 0.10 level (see *4.2.1 Quantitative Genetic Parameter Estimation in SOLAR*) were retained as covariates in the final model maximized to estimate heritability for each EID. The effects measured here include local regional cranial effects, overall cranial size effects, and overall body size effects.

Model 2 narrows the focus by eliminating from consideration any whole-body effects operating on the cranium. Remaining variation would then include the effects of factors contributing to overall cranial size in a manner that is independent of overall body size allometric scaling within the cranium. In addition to the five potential covariates considered in Model 1, adult body weight (see *3.3.4 Adult Body Weight*) is included as a fixed covariate in Model 2. Finally, Model 3 eliminates whole cranium allometric effects, which are particularly strong in

baboons (see *2.4.6 What is Known About Papio Craniofacial Morphology*), by removing the effects of cranial size and size-related shape variation. This is achieved by including each individual's score on principal component one (PC1) from the principal components analysis of standardized residuals from Model 2 (see *3.3.5 Measures of Cranial Size*). Doing so focuses Model 3 on variation in smaller regions of the baboon cranium. These regions likely correspond to functional, developmental, or genetic/evolutionary modules (see *5.3.3 Allometry*).

To determine whether there are any regional patterns in the distribution of h_r^2 and covariate effects, I used the method described by Gonçalves et al. (2008) for performing a joint hierarchical cluster analysis on mixed categorical and continuous data. For every pair of traits i and j, I calculated a Gower's (1971) similarity coefficient (S_{ij}):

$$S_{ij} = \frac{\sum_{k=1}^{p} W_{ijk} S_{ijk}}{\sum_{K=1}^{p} W_{ijk}} \tag{4.3}$$

where K is the number of variables (k = 1, 2, . . ., p), W_{ijk} is a weight of 0 if the variable's value is absent for either trait and 1 if no data are missing, and S_{ijk} is the contribution of variable K to the similarity between the two traits. As none of my data are missing, the W_{ijk} terms drop out and S_{ij} is equal to the sum of S_{ijk}. For categorical data, S_{ijk} = 1 if both traits have the same trait value and S_{ijk} = 0 if their values differ. The equation for continuous data is:

$$S_{ijk} = 1 - \frac{|X_{ik} - X_{jk}|}{R_K} \tag{4.4}$$

where X_{ik} and X_{jk} are the trait's values of K and R_K is its range. For this analysis K = 7. The continuous variables are h_r^2 and V_{cov}, and the categorical ones are bivariate variables for presence/absence of each covariate effect. Although the analysis was conducted for all three models, only the covariates from Model 1 were included, as every trait has (by definition)

significant body and cranial size variation accounted for in Models 2 and 3 and, therefore, these two variables do not contribute to trait similarity. I then used unweighted pair-group method with arithmetic mean (UPGMA) to cluster the S_{ij} matrix and calculated a cophenetic correlation coefficient to determine how faithfully the clustering algorithm captured the variation in the original data. Dendrograms were created from the cophenetic distances produced by the UPGMA algorithm and examined to discern any trends in trait similarity across the cranium. Data visualization and all analyses were conducted in Python using the packages *matplotlib* v1.5.0 (Hunter, 2007), *numpy* v1.10.2 (van der Walt et al., 2011), *pandas* v0.17.1 (McKinney, 2010), *scikit-bio* v0.4.1 (Caporaso, 2013), and *scipy* v0.16.1 (Jones et al., 2015).

4.2.3 V_A and Adjusted h^2_r

Because h_r^2 is a ratio, increases or decreases in its magnitude from one model to the next or among traits can be the result of larger V_A, smaller V_E, or a combination of the two (Houle, 1992). For this reason, V_A was calculated as the product of h_r^2 and V_R to create a metric for comparing relative amounts of genetic variation. For traits in Model 1 that did not have any significant covariates, V_P was used instead of V_R. Ideally, I would be able to calculate the coefficient of additive genetic variation (CV_A), as this is an effective method for allowing "the potential for evolution of different characters to be directly compared, regardless of type (for example morphological characters or life history" (Houle, 1992, cited in Pigliucci, 2008).[3] CV_A is calculated as a ratio of $\sqrt{V_A}$ to the trait mean. However, this cannot be done for traits that have been standardized, as the trait mean is no longer on a meaningful scale (Garcia-Gonzalez et al.,

[3] For Houle (1992), the CV_A is a measure of what he calls *evolvability*. However, evolvability has taken on a variety of different meanings depending on the context and author(s). In the manner in which Houle (1992) refers to it, evolvability is a characteristic of populations and has a meaning similar to that of heritability. Others, such as Wagner and Altenberg (1996), conceptualize evolvability as a property of species in that it describes their *variability*, or the ability of the organismal system to produce new genetic variation through mutation and for that variation to be manifest at the phenotypic level to be selected upon, which is dependent on the structure of the G-P map. The major difference in these two concepts is that the former is concerned with standing variation while the latter includes the potential for the production of additional variation (Pigliucci, 2008).

2012). [4] As such, I was limited to comparisons of V_A to make inferences about the potential for evolution of the mean phenotype.

In theory, heritability ranges from 0-1. However, the traits from which estimates of its value are made are measured with error, which limits the maximum observable heritability estimate. To account for this, the proportion of V_P resulting from measurement error variance is omitted by dividing each h_r^2 by the trait's repeatability to produce the adjusted h_r^2 (h_a^2; see Table 3.2). This also has the effect of standardizing h_r^2 estimates so that they are on a 0-1 scale.

4.2.4 Sample Size Versus Effective Sample Size

A total of 992 baboons were skeletonized for the research collection. I omitted 39 individuals from all analyses because of age, pathology, or unknown identity, resulting in an N = 953. An average of 27 data points were missing from each trait, providing a final sample size for each EID of N = 926 ± 29. Not all individuals in the WUSTL collection are members of the multigenerational pedigree, as a number of them are from other *Papio* subspecies maintained in special sub-populations. Consequently, the sample size for genetic parameter estimation in Model 1 is reduced to N = 812 ± 26. An additional 61 individuals did not have an adult body weight record, which further reduced the sample sizes in Models 2 and 3. Because missing EID data were imputed to calculate PC1 scores (see *3.3.5 Measures of Cranial Size*) to include as a fixed covariate in Model 3, the sample sizes for Models 2 and 3 are the same (N = 765 ± 24).

Because the individuals in this sample are related, their trait values are not independent of each other.[5] This reduces the amount of genetically independent information contained in the

[4] For a scale to be meaningful, both ratios and a value of 0 must be relevant. For example, a length increase of 20 mm is twice that of an increase of 10 mm, while an increase of 0 mm means there was no change in trait value at all. In contrast, 20°F is not twice as warm as 10°F and 0°F does not mean no temperature.

[5] This is analogous to the issue of phylogenetic autocorrelation. Trait similarity is a function of species relatedness so divergence times must be accounted for when using comparative methods. Trait values could be more similar than expected if they were evolving randomly because the trait was inherited from a common ancestor and stabilizing selection has maintained it. Alternatively, trait values could be more divergent than expected because of diversifying

data, but also allows for the estimation of heritability. Including the kinship information contained within the baboon pedigree (**Φ**) accounts for the non-independence of the EID trait values in a manner similar to the inclusion of a phylogenetic covariance matrix in phylogenetic generalized least squares regression (Grafen, 1989). Therefore, despite having a seemingly large sample size ranging from 765 to 812 baboons, the effective sample size (N_e) is the only truly important number for determining the efficiency of quantitative genetic parameter estimates. It measures the effective number of independent individual breeding values used in the analysis. In other words, an effective sample size of 150 for a quantitative genetic analysis is equivalent to estimating typical statistical parameters from a data set of 150 independent data points, even though the number of individuals actually analyzed is much greater. The square of heritability (h^4) and its sampling variance ($\mathrm{V}(h^2)$) are used to calculate N_e for the baboon craniofacial traits (Cheverud, 1996):

$$\mathrm{N}_e = \left[\frac{2h^4}{\mathrm{V}(h^2)}\right] + 1 \tag{4.3}$$

Note that N_e varies by genetic locus and for every phenotype, as evolutionary processes do not act uniformly across the genome.

4.3 Results

Descriptive statistics for ECV and each of the EIDs are provided in Table 4.1 and heritability estimates, calculations of N_e, and results of the covariate screens are in Table 4.2. Every h_r^2 in all three models was significant (Table 4.2), meaning additive genetic variation (V_A) contributes significantly to V_P for all baboon craniofacial traits.

selection in the case of niche partitioning. In fact, Housworth et al. (2004) were able to reformulate the MLVD method that is used in quantitative genetics into the phylogenetic mixed model and apply it to comparative data.

Table 4.1 Descriptive Statistics for Baboon Craniofacial Traits.

Trait	ACPM	ACSY	PMPM	ASJP	BACC	BAOP	ASAS	JPJP	4141	POPO	PTPT	STST	ZTZT	BRAS	BRLD
Mean[a]	21.16	81.08	32.63	39.22	19.76	19.54	60.09	20.89	48.46	77.27	58.44	30.44	96.39	60.47	47.08
SD	2.6	10.2	3.7	3.6	1.6	2.1	5.9	1.9	4.1	8.1	3.0	9.3	9.9	4.1	5.3
Min	16.25	61.56	22.78	28.39	16.29	14.29	44.38	16.48	40.65	64.44	49.40	2.60	79.46	50.74	34.71
Max	29.63	106.64	46.08	49.96	25.08	26.24	82.90	26.59	59.93	102.39	67.69	54.48	122.90	74.73	68.34
N	918	847	799	937	947	876	927	934	937	821	904	943	917	936	931
Trait	**BRNA**	**BRPT**	**NABA**	**CACP**	**CPSL**	**CPZS**	**CNCN**	**FMPM**	**FMZT**	**FMCP**	**FMPT**	**LDAS**	**LDBA**	**NANL**	**NLAC**
Mean	62.51	44.46	80.66	16.77	17.52	41.28	18.01	91.45	35.38	46.22	28.93	38.77	60.83	59.01	33.31
SD	4.1	3.5	6.0	1.9	1.9	3.0	1.4	11.1	3.4	3.7	3.9	5.1	5.8	9.7	4.0
Min	50.33	32.55	68.09	11.39	13.28	34.75	14.51	70.34	28.44	39.69	19.35	28.20	50.54	40.02	23.84
Max	75.50	54.28	99.43	21.66	23.74	50.07	22.43	126.41	46.38	57.18	42.17	56.86	78.48	85.03	45.88
N	935	934	942	941	941	940	938	933	941	937	938	936	932	938	915
Trait	**NLVS**	**NAAC**	**NACA**	**NACP**	**NAFM**	**NA41**	**NAVS**	**NAZI**	**NAZS**	**BRBA**	**NALD**	**DAFM**	**PLSY**	**POBA**	**PM41**
Mean	72.86	89.56	25.37	42.08	37.47	85.26	52.20	62.40	29.84	67.86	101.77	33.54	30.28	46.70	26.96
SD	9.4	12.0	2.8	3.0	2.7	9.9	4.1	5.1	2.4	3.8	6.6	2.2	5.4	4.6	4.4
Min	57.43	66.24	18.41	35.51	31.36	65.14	43.35	52.88	23.21	58.95	88.74	29.40	19.39	38.09	20.34
Max	99.59	124.49	33.35	52.21	45.68	114.40	66.34	78.69	37.50	79.75	127.59	39.72	46.93	58.62	41.31
N	915	858	938	932	941	916	938	936	940	937	933	936	931	944	931
Trait	**41MX**	**41ZI**	**PTAS**	**PTLD**	**SLBA**	**SLCC**	**SYBA**	**SYMX**	**ZTPO**	**ZTVS**	**ZTZI**	**VSBA**	**VSSY**	**ZIMX**	**ZSNL**
Mean	45.10	43.25	55.39	69.93	25.47	27.33	40.20	21.72	47.17	50.50	21.18	30.29	14.45	31.02	49.27
SD	4.0	5.8	3.9	5.0	3.6	2.9	4.2	2.5	5.2	5.2	4.4	3.2	2.6	4.7	8.8
Min	33.54	31.24	46.46	58.44	16.70	21.14	29.51	16.82	36.97	41.71	12.32	22.75	8.16	21.92	31.07
Max	57.76	62.25	68.58	89.66	35.40	35.49	52.97	29.48	64.01	65.47	35.36	40.77	23.46	46.58	72.37
N	915	930	940	939	944	943	932	928	935	940	939	935	933	940	938
Trait	**ECV**		*Stats:*	*Mean*	154.69	*SD*	18.1	*Min*	108.27	*Max*	248.01	*N*	941		

[a]All trait values in mm, except for ECV, which is in cc.

4.3.1 Covariate effects

For Model 1 only sex, age, and their interactions are considered potential covariates but, adult body weight and size-related craniofacial variation are subsequently included in Models 2 and 3, respectively. As the morphological level at which analyses are conducted narrows, the proportion of V_P explained by included covariates (V_{cov}) increases ($\bar{V}_{cov1}$ = 0.039, $\bar{V}_{cov2}$= 0.073, $\bar{V}_{cov3}$ = 0.247; Fig. 4.1), and the amount of residual V_P (V_R) decreases. Because the EIDs were standardized in a sex-specific manner prior to estimating h_r^2, sex does not account for a large proportion of V_P, which is why the estimates of V_{cov} are so low.[6] Contrast these small V_{cov} values with those for ECV, which was analyzed on its original scale because it is normally distributed and is not analyzed in relation to any other trait. Note that a direct comparison cannot be made between ECV and EIDs as their dimensionalities differ (volume vs. linear dimensions), which effects the amount of variance expected (Houle, 1992; Garcia-Gonzalez et al., 2012). In addition, the $\bar{X}$ for ECV is substantially larger than for any EID, and characters with large means are measured with greater accuracy than those with smaller means (Rohlf et al., 1983). This causes a negative relationship between $\bar{X}$ and V_P, thus underestimating V_{cov}.

Examining how the pattern of covariate significance changes for individual EIDs from Models 1-3 sheds light on how variation in the cranium is affected by biological factors related to overall body size, cranial size, and local cranial shape variation. Similarly, evaluating which EIDs are significant for each potential covariate provides insight on how biological processes that differ with sex and age affect the baboon cranium. Including the covariates of adult body weight and the first principal component of the EID correlation matrix in Models 2 and 3, respectively, provides information on allometric effects on craniofacial variation. These observed trends are described in greater detail below.

[6] Roseman and colleagues (2010) estimated $\bar{V}_{cov}$ = 0.526 for unstandardized EIDs in a subset of these baboons.

Covariate: Sex

Not surprisingly, given observed craniofacial sexual dimorphism in baboons (Willmore et al., 2009), sex differences account for a significant proportion of V_P in most EIDs and at all three levels. Interestingly, that number doubled from Model 1 (38%) to 2 (77%) and 3 (85%), suggesting differences in body size—males are almost twice as large as females (Phillips-Conroy and Jolly, 1981; Strum, 1991; Mitani et al., 1996; Smith and Jungers, 1997; Leigh, 2009)—masks craniofacial size- (Model 2) and shape-related (Model 3) variation. Almost all

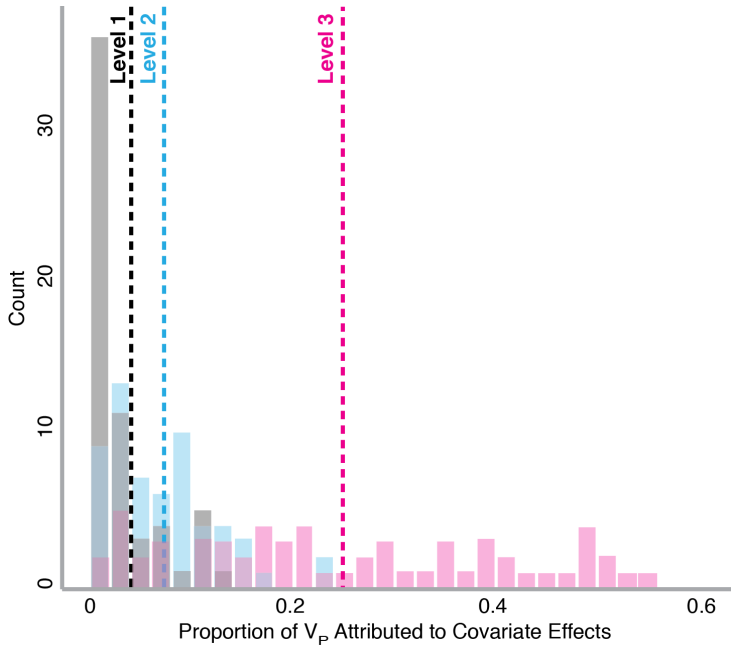

Figure 4.1 Histograms of V_{cov} for Models 1-3. Dashed vertical lines represent the geometric mean for each model.

traits have significant sex-only effects in Model 3 but, surprisingly, some nasal length dimensions do not (covariates for NLAC include AS and for NAAC, A^2S). Upon closer examination it is apparent that, although the trait *means* for nasal length dimensions differ significantly between the sexes (Table 4.3), their localized *variation* does not. This is an interesting result because the larger of the two sexes typically varies more than the smaller (Leutenegger and Cheverud, 1982; Garrick et al., 1989; Hedges and Nowell, 1995; Blows et al.,

Table 4.2 Heritability Estimates, Effective Sample Sizes, and Covariate Screen Results.

	Model 1: Overall					Model 2: Cranial					Model 3: Regional				
Trait	**N**	**N_e**	**h_r^2**	**V_{cov}[a]**	**cov[b]**	**N**	**N_e**	**h_r^2**	**V_{cov}[a]**	**cov[b]**	**N**	**N_e**	**h_r^2**	**V_{cov}[a]**	**cov[b]**
ECV	822	195.9	0.691	40.0	A, S	774	159.9	0.713	42.0	A, S, K	774	228.1	0.746	50.0	A, S, A^2, AS, K, P
ACPM	806	49.5	0.443	5.4	AS, A^2	760	28.9	0.336	13.9	S, AS, K	760	27.5	0.291	28.0	S, AS, K, P
ACSY	741	83.5	0.578	11.4	S, AS, A^2	698	88.8	0.530	4.8	S, K	698	26.4	0.321	48.1	S, AS, K, P
PMPM	697	20.6	0.282	1.3	S, A^2S	657	11.0	0.224	9.6	S, A^2, A^2S, K	657	156.1	0.275	18.3	S, A^2, A^2S, K, P
ASJP	819	61.2	0.384	---	---	771	41.5	0.315	2.6	S, K	771	55.1	0.312	6.8	S, K, P
BACC	830	76.5	0.430	---	---	782	67.7	0.462	3.1	S, K	782	81.8	0.445	14.8	S, K, P
BAOP	770	122.2	0.545	---	---	726	93.5	0.544	0.04	K*	726	89.4	0.532	0.8	K*, P*
ASAS	811	35.6	0.291	0.6	AS	763	43.3	0.322	2.6	S, K	763	30.8	0.270	16.0	S, K, P
JPJP	819	191.4	0.683	2.3	AS	771	177.2	0.657	2.4	S, K	771	168.7	0.641	13.0	S, K, P
4141	824	235.5	0.758	3.3	S, AS, A^2, A^2S	777	175.4	0.747	8.0	S, A^2, A^2S, K	777	108.2	0.659	32.8	S, A^2, A^2S, K, P
POPO	717	122.7	0.624	0.7	S, A^2	677	123.9	0.627	14.2	S, K	677	91.7	0.606	37.0	S, K, P
PTPT	796	81.5	0.444	1.2	AS	750	63.2	0.446	0.1	K*	750	68.0	0.463	6.2	S, K*, P
STST	829	182.6	0.667	0.5	A, AS	781	126.2	0.633	3.9	S, K	781	127.8	0.637	3.8	S, K, P*
ZTZT	803	110.5	0.518	10.8	A, AS, A^2	757	110.1	0.517	22.3	S, AS, A^2, A^2S, K	757	135.5	0.574	49.6	A, S, AS, A^2, A^2S, K, P
BRAS	821	51.3	0.351	0.7	S, A2	775	42.3	0.318	4.5	S, K	775	34.6	0.287	18.9	S, K, P
BRLD	815	19.2	0.211	---	---	767	15.4	0.188	2.4	S, K	767	17.0	0.198	4.3	S, K, P
BRNA	821	86.8	0.524	0.6	A2S	774	81.3	0.507	5.2	S, A^2S, K	774	68.6	0.465	16.2	S, A^2, A^2S, K, P
BRPT	818	58.0	0.427	---	---	770	54.0	0.412	1.4	A, S, K	770	56.7	0.422	1.5	S, K, P
NABA	824	176.1	0.655	3.0	AS, A^2, A^2S	776	113.1	0.599	12.9	S, K	776	82.0	0.509	54.5	S, K, P
CACP	825	20.5	0.250	---	---	778	19.6	0.244	3.0	K*	778	24.3	0.273	2.3	K*, P
CPSL	824	32.5	0.278	11.0	A, S, A^2	776	31.6	0.274	9.8	A, K	776	30.8	0.270	10.4	A, K, P
CPZS	823	86.5	0.523	---	---	776	51.9	0.454	9.4	A, S, A^2, K	776	39.3	0.394	38.0	S, AS, A^2, K, P
CNCN	821	37.7	0.300	0.2	S, A^2, A^2S	775	37.7	0.300	0.3	A, A^2, A^2S, K*	775	40.0	0.309	2.0	A2, A^2S, K*, P
FMPM	822	159.9	0.624	7.5	A, S, AS, A^2, A^2S	775	101.5	0.567	8.9	A, S, AS, A2, A^2S, K	775	153.9	0.612	48.3	A, S, AS, A^2, A^2S, K, P
FMZT	823	147.4	0.599	3.4	AS, A2	775	138.3	0.580	7.4	S, AS, K	775	123.6	0.548	25.6	S, AS, K, P
FMCP	821	147.4	0.599	---	---	775	90.1	0.534	15.5	S, K	775	113.5	0.600	52.0	S, K, P
FMPT	822	142.1	0.588	0.5	AS	774	133.6	0.570	2.4	S, K	774	86.8	0.524	14.5	S, K, P
LDAS	821	45.2	0.329	2.7	S, A^2, A^2S	774	56.3	0.368	8.7	S, A^2, A^2S, K	774	60.0	0.326	21.7	S, A^2S, K, P
LDBA	816	151.4	0.607	1.6	A^2	769	78.6	0.436	17.4	S, K	769	85.9	0.456	35.1	S, K, P
NANL	828	127.4	0.636	---	---	780	122.7	0.624	0.6	K	780	68.5	0.523	29.0	S, K, P
NLAC	803	86.8	0.524	11.0	S, AS, A^2S	756	88.8	0.530	9.6	AS, K	756	103.4	0.501	20.2	AS, K, P
NLVS	800	194.8	0.689	4.0	AS	752	146.8	0.683	5.1	S, K	752	96.2	0.552	42.6	S, K, P
NAAC	751	223.9	0.739	7.7	S, AS, A^2, A^2S	707	232.4	0.753	3.6	A^2S, K	707	168.7	0.641	40.9	A^2S, K, P

NACA	822	114.3	0.602	2.2	A	774	96.9	0.554	6.8	A, S, K	774	67.0	0.402	31.5	S, K, P
NACP	815	93.8	0.545	---	---	767	70.3	0.471	10.0	S, K	767	58.7	0.376	50.8	S, K, P
NAFM	825	220.3	0.733	3.6	AS, A^2	777	212.0	0.719	11.7	AS, K	777	201.6	0.701	41.1	S, K, P
NA41	806	173.4	0.650	8.4	S, AS, A^2, A^2S	758	144.5	0.593	13.3	S, AS, A^2, A^2S, K	758	138.3	0.580	50.7	S, AS, A^2, A^2S, K, P
NAVS	821	124.9	0.551	---	---	773	88.1	0.528	7.9	S, K	773	201.6	0.528	38.4	S, K, P
NAZI	824	142.6	0.589	1.3	AS	776	102.2	0.569	8.3	S, K	776	138.3	0.525	45.5	S, K, P
NAZS	822	129.9	0.562	---	---	774	100.2	0.493	10.4	A, S, K	774	88.1	0.518	16.6	S, K, P
BRBA	822	126.7	0.555	2.2	A^2	774	86.8	0.524	8.9	S, A^2, K	774	87.1	0.504	20.4	S, K, P
NALD	818	44.9	0.375	1.4	AS, A^2	770	22.1	0.260	12.9	S, K	770	84.9	0.284	34.8	S, K, P
DAFM	822	117.3	0.610	2.4	S, AS, A2, A^2S	774	113.5	0.600	7.8	S, K	774	109.4	0.589	27.6	S, K, P
PLSY	815	130.4	0.563	3.3	S, AS, A^2	768	88.1	0.528	40.0	S, K	768	70.6	0.472	22.4	S, K, P
POBA	828	119.6	0.616	6.6	A, S, A^2	780	85.5	0.520	25.0	A, S, K	780	86.2	0.522	47.5	S, K, P
PM41	820	55.3	0.469	1.4	A, S, AS	773	54.2	0.464	1.6	S, AS, K	773	57.7	0.479	17.3	S, AS, K, P
41MX	803	166.6	0.637	12.7	S, AS, A^2	758	122.3	0.623	10.6	AS, A2, K	758	96.6	0.553	35.4	S, AS, A^2, K, P
41ZI	773	154.9	0.614	5.8	A, S, AS, A^2, A^2S	773	109.0	0.588	7.6	A, AS, A^2, A^2S, K	773	108.7	0.587	27.0	A, AS, A^2, A^2S, K, P
PTAS	822	39.1	0.349	---	---	774	32.2	0.316	6.7	A, S, K	774	43.6	0.369	11.9	S, K, P
PTLD	823	59.6	0.433	0.1	S, A^2	775	33.5	0.363	8.5	S, K	775	59.3	0.432	12.9	S, K, P
SLBA	828	86.2	0.522	---	---	781	63.2	0.446	2.5	S, K	781	83.3	0.449	5.5	S, K, P
SLCC	826	50.8	0.399	---	---	779	41.5	0.360	1.9	S, K	779	45.4	0.330	11.5	S, AS, A^2, K, P
SYBA	816	341.6	0.783	0.5	S, A^2S	769	356.6	0.800	2.1	A2S, K	769	213.2	0.721	12.1	K, P
SYMX	817	80.8	0.505	3.4	AS	770	83.2	0.513	5.2	S, K	770	80.4	0.504	20.7	S, K, P
ZTPO	819	28.4	0.296	---	---	772	32.4	0.317	5.9	S, AS, K	772	51.0	0.450	18.3	A, S, AS, A^2S, K, P
ZTVS	823	65.1	0.453	10.2	S, AS, A^2, A^2S	776	75.4	0.488	22.0	S, AS, A^2, A^2S, K	776	100.1	0.563	48.1	S, AS, A^2, A^2S, K, P
ZTZI	823	26.9	0.252	1.5	AS	776	22.0	0.259	2.4	S, AS, K	776	23.8	0.270	3.9	S, AS, K, P
VSBA	819	139.2	0.665	0.04	A2, A^2S	772	110.5	0.666	2.2	S, K	772	100.6	0.635	7.8	S, K, P
VSSY	816	131.3	0.565	---	---	769	94.5	0.547	0.1	K*	769	88.5	0.529	2.9	K*, P
ZIMX	825	27.7	0.256	6.6	A, S, AS, A^2, A^2S	777	11.9	0.140	15.9	A, S, AS, A^2, A^2S, K	777	21.1	0.190	29.2	A, S, AS, A^2, A^2S, K, P
ZSNL	824	129.8	0.642	---	---	776	90.2	0.601	2.5	A^2S, K	776	41.9	0.407	38.0	S, K, P

[a]Percentage of V_P accounted for by significant covariates indicated in the adjacent column. Three dashes indicate traits without a significant contribution from any covariates. [b]Covariates: age (A), sex (S), age-by-sex interaction (AS), age^2 (A^2), age^2-by-sex interaction (A^2S), body weight (K), first eigenvector of the standardized craniofacial shape correlation matrix (P). Covariates that are not significant but are fixed in the model (either K or P) are indicated with an asterisk.

2004), especially in sexually dimorphic traits. That does not appear to be the case with baboons. This may be related to the fact that allometric effects are so strong in the taxon (Porto et al., 2009) that it is merely size, and not the shape, of the snout that is different between males and females. This scenario is supported by the fact that sex-specific variation is not significant for NANL in either Models 1 or 2 or for NAAC and NLAC in Model 2.

Alternatively, or perhaps additionally, the absence of sex effects for nasal length dimensions may be related to the differential effect of trait loadings on the cranial size covariates. EIDs that include the landmarks NA, NL, and AC have some of the highest correlations with PC1 (see Table 3.6). Hence, with the effect of PC1 removed from V_P in Model 3, there is lower V_R for these traits, making it more difficult to partition. However, this may be a less likely explanation as other traits with higher loadings do demonstrate pure sex-effects in Model 3 (e.g., the PC1 loading for NLAC is 0.085 while that for NANL is twice that at 0.163 and sex is a significant covariate for NANL in Model 3)

Table 4.3 Comparison of Nasal Length Dimensions in Males and Females.

	Females		Males		
Trait	**N**	$\bar{X} \pm s$ (mm)	**N**	$\bar{X} \pm s$ (mm)	t^a
NAAC	643	83.4 ± 6	221	107.5 ± 7	50.2
NANL	662	53.5 ± 5	286	71.5 ± 6	49.3
NLAC	658	31.6 ± 3	268	37.8 ± 3	27.4

[a]Test statistic from an unpaired *t* test of sex-specific group means. Differences between group means are statistically significant at $\alpha = 0.05$ for all three traits.

Covariate: Age

Despite omitting immature individuals prior to analysis, age is a significant covariate, albeit rarely. It is possible that some individuals had not completed growth, even after full occlusion of their M3's and fusion of their spheno-occipital synchondrosis, or that cranial dimensions are altered later in life as bone texture and density changes, or both. For example,

STST and PM41 are the only traits with age as a significant covariate for Model 1 but not 2 or 3. Given the fact that young individuals tend to have larger trait values than older ones for both EIDs, this suggests an allometric decrease in the breadth of the cranial vault and length of the canine fossa. In contrast, variation in ZTPO is not significantly explained by age differences for either Model 1 or 2, but it is for 3. This suggests that there are local shape changes to the zygomatic arch with increasing age as older animals have shorter ZTPO. Temporalis muscle hypertrophy increasing the breadth of the zygomatic arch, shifting the zygotemporal junction posteriorly in the process, could account for this result.

Covariate: Age-by-Sex Interaction

Significant age-by-sex interactions indicate that variance in a trait changes at different life stages in females than in males (Fig. 4.2). Some of the most drastic differences in facial anatomy of the male versus female baboon cranium are in snout length, facial breadth, and brain case shape. Ontogenetic research on baboon facial development has demonstrated that male cranial growth trajectories diverge from those of females around 3.5 - 4 years of age and that the duration of this growth is extended into young adulthood past the time when female craniofacial growth has ceased at 5 years (Leigh and Cheverud, 1991; Leigh, 2009). In addition, the surge of sex hormones in males around the time of sexual maturity (~8 years in male baboons; Altmann et al., 1981) increases masticatory muscle and canine size, causing concomitant changes to the facial skeleton as a result. This is reflected by the covariate screen results that show significant interaction effects between age and sex at all three levels of analysis for EIDs related to alveolar and nasal length (e.g., 41MX, NA41, NLAC, PM41), bizygomatic breadth (ZTZT), and midfacial robustness (e.g., 41ZI, FMPM, ZIMX). A handful of craniofacial dimensions are only significant in Model 1 for age-by-sex effects, suggesting that their variation is attributable to sexual dimorphism of body and cranial size. These traits (e.g.,

ASAS, JPJP, NABA) are primarily basicranial, placing them in close proximity to and in a position to be affected by the postcranium (Model 2). In addition, we know that the chondrocranium functions as a "blueprint" for cranial growth (see *2.5.4 Theories of Craniofacial Growth and Development*), so it is not surprising that its V_P is associated—differentially in the two sexes across age cohorts—with overall cranial size (Model 3).

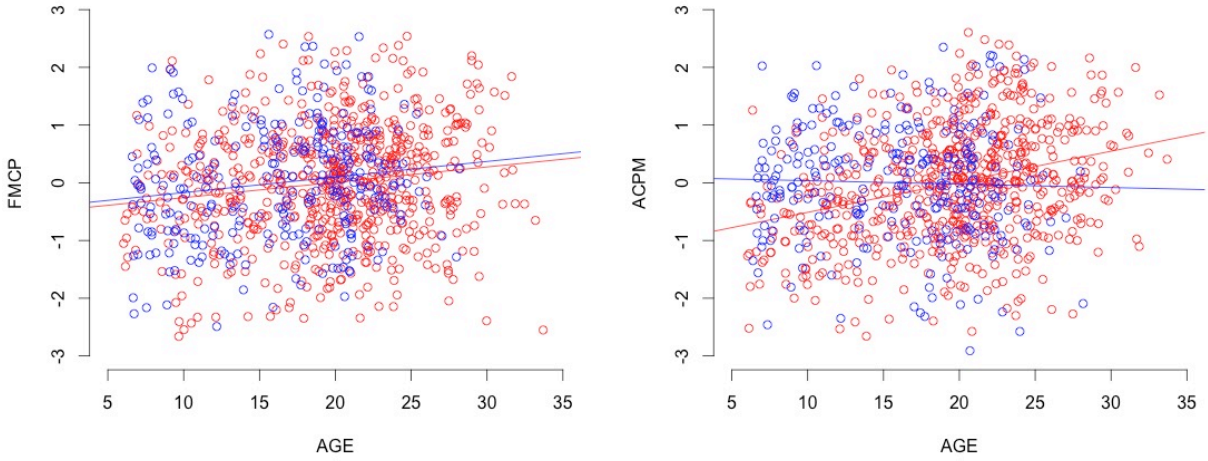

Figure 4.2 Scatterplots of EID Z-Scores with Differences in Covariate Effects. FMCP does not demonstrate a sex-by-age interaction (left) but ACPM does (right). Males are indicated by blue open circles and females by red ones. Sex-specific ordinary least squares best-fit regression lines for each EID regressed on age are indicated by the solid lines (blue for male and red for female.

Covariate: Age^2

Craniofacial variation that increases as individuals develop in early adulthood (6-10 years) and then plateaus or even decreases with maturity (10+ years) shows significant age-squared effects (Fig. 4.3). It is possible that sample sizes at different ages contribute to this trend; the majority of the individuals are of middle age ($\bar{X}$ = 19.60 ± 5.9 and two-thirds are within the range 13.72–25.48 years old). Having a larger sample provides an opportunity to capture more of the phenotypic variation, which could create a nonlinear trend in the data. However, it is unlikely

that this explains age^2 being such a common covariate. Just under half of the traits (45%) show age^2 effects for Model 1, but this number drops precipitously for Models 2 and 3 (22% in both). If sample size were an adequate explanation, age^2 would be a significant covariate at all three levels of analysis.

The more likely scenario is that craniofacial variation is affected more by age-related changes occurring to the body as a whole. A number of studies have demonstrated an increase in V_P and oscillations in V_A and V_E during ontogeny (e.g., Herbert et al., 1979; Atchley and Rutledge, 1980). These trends have been attributed to age-specific in-/activation of genes that vary cellular metabolic activity and chemical composition, which then fluctuate enzyme and hormone levels regulating both cell growth. It seems reasonable to hypothesize that the same process extends into adulthood, affecting the regulation of bone maintenance/remodeling

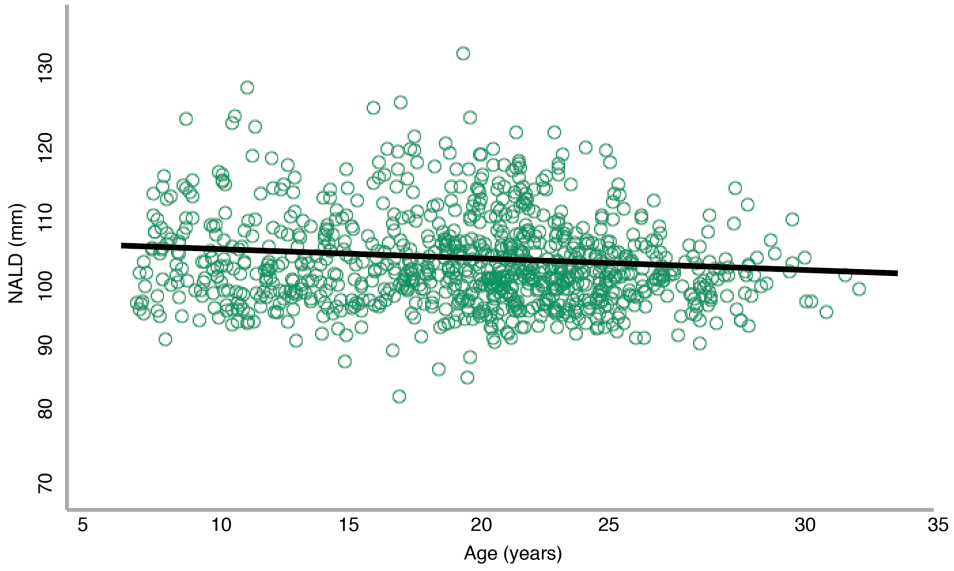

Figure 4.3 A Scatterplot of a Trait that Demonstrates Significant Age^2 Effects. The OLS regression line is shown and has a slight negative slope ($y = -0.14x + 104.3$, $R^2 = 0.01$). Note that, although the trend looks linear, growth data for individuals < 7 years old is not shown.

Covariate: Age^2-By-Sex Interaction

Finally, a small handful of EIDs demonstrate significant age^2-by-sex effects. The number of such traits is constant across levels (Model 1 = 16, Model 2 = 14, Model 3 = 13), and 11 of these traits are common to all three levels. These traits are located across the cranium (e.g., BRNA, CNCN, PMPM, ZTVS), rather than clustered in any one region. This suggests that the magnitude of global craniofacial variation is not constant over chronological time in this sample, and that this temporal trend is different for males and females. This result is congruent with the explanation for age^2 effects (see preceding paragraph), as numerous sex-specific physiological patterns have been uncovered. For example, sex-specific differences in response to prenatal stress alter neural receptor densities in rats, which affects stimulus response throughout the life of the individual (McCormick et al., 1995).

Systemic hormone levels, especially of steroid hormones, differ by sex and affect processes as diverse as metabolism (e.g., Baumgartner et al., 1999; Goodman-Gruen et al., 2000), immune response (e.g., Bouman et al., 2005; Oertelt-Prigione, 2012), behavior (e.g., Collaer et al., 1995; Van Goozen et al., 1995; Gillies and McArthur, 2010), and growth and development (e.g., MacLeod et al., 1991; Pederson et al., 1999). Increased androgen levels in early life differentially affect both bone growth (Clarke and Khosla, 2009) and bone resorption later in life, as the correlation between decreased estrogen levels in human women and increased risk for osteoporosis demonstrates (Vanderschueren et al., 2004). If V_P varies with age as a result of differential gene expression, and those genes affect hormones in males and females differently, or those hormones themselves have different effects on males and females, this could explain observed age^2-by-sex interaction effects.

No Covariates

Interestingly, BAOP does not have any significant covariates at any level. In fact, even adult body weight and PC1 do not explain V_P in the length of the foramen magnum, although these covariates were included in the trait modeling by definition to estimate quantitative genetic parameters in Models 2 and 3. One possible explanation is that variation of the foramen magnum tracks adjacent spinal elements, soft tissues of the neck, and/or demands of the cerebellum and spinal cord. These results suggest BAOP may be an important trait for understanding cranial-postcranial integration. Growth of the medulla oblongata and cervical spinal cord cease early, long before sexual dimorphism is realized in a significant way (see *2.4.6 What is Known About Papio Craniofacial Morphology*), and size of the medulla is not affected by aging processes (Lee et al., 2009; although see Weis et al., 1993) and is larger in males (e.g., Lindenfors et al., 2007; Lee et al., 2009). This explains the lack of age, sex, and their interactions as covariates. One useful application of this is that bony landmarks reflecting the medulla's size could be used as a standard for determining allometric and sexual dimorphism scaling patterns in the cranium (e.g., Deacon, 1988), a much debated topic.

Table 4.4 Estimates of h_a^2 and V_A.

	Level 1: Overall			Level 2: Cranial			Level 3: Regional		
EID[a]	h_r^2	h_a^2	V_A	h_r^2	h_a^2	V_A	h_r^2	h_a^2	V_A
ECV	0.691	0.691	119.8	0.713	0.713	118.8	0.746	0.746	110.5
ACPM	0.443	0.529	0.408	0.336	0.401	0.286	0.291	0.348	0.212
ACSY	0.578	0.580	0.449	0.530	0.532	0.435	0.321	0.322	0.148
PMPM	0.282	0.283	0.261	0.224	0.225	0.196	0.275	0.276	0.217
ASJP	0.384	0.447	0.384	0.315	0.367	0.302	0.312	0.363	0.290
BACC*	0.430	0.463	0.430	0.462	0.498	0.461	0.445	0.479	0.394
BAOP	0.545	0.589	0.544	0.544	0.588	0.535	0.532	0.575	0.519
ASAS	0.291	0.363	0.296	0.322	0.401	0.327	0.270	0.337	0.236
JPJP	0.683	0.709	0.659	0.657	0.682	0.640	0.641	0.666	0.552
4141	0.758	0.773	0.700	0.747	0.761	0.665	0.659	0.672	0.442
POPO	0.624	0.630	0.602	0.627	0.633	0.553	0.606	0.612	0.385
PTPT	0.444	0.517	0.412	0.446	0.520	0.442	0.463	0.540	0.412
STST	0.667	0.687	0.644	0.633	0.652	0.589	0.637	0.656	0.593
ZTZT	0.518	0.519	0.445	0.517	0.518	0.392	0.574	0.575	0.280

BRAS	0.351	0.386	0.336	0.318	0.349	0.300	0.287	0.315	0.229
BRLD	0.211	0.259	0.211	0.188	0.231	0.183	0.198	0.243	0.190
BRNA	0.524	0.536	0.517	0.507	0.518	0.482	0.465	0.475	0.402
BRPT	0.427	0.782	0.425	0.412	0.755	0.384	0.422	0.773	0.393
NABA	0.655	0.664	0.608	0.599	0.608	0.515	0.509	0.516	0.244
CACP*	0.250	0.269	0.250	0.244	0.263	0.239	0.273	0.294	0.261
CPSL*	0.278	0.300	0.243	0.274	0.295	0.240	0.270	0.291	0.224
CPZS*	0.523	0.563	0.523	0.454	0.489	0.417	0.394	0.424	0.255
CNCN	0.300	0.313	0.301	0.300	0.313	0.297	0.309	0.323	0.301
FMPM	0.624	0.629	0.528	0.567	0.572	0.458	0.612	0.617	0.296
FMZT	0.599	0.606	0.564	0.580	0.587	0.520	0.548	0.555	0.396
FMCP*	0.599	0.645	0.597	0.534	0.498	0.456	0.600	0.498	0.300
FMPT	0.588	0.765	0.587	0.570	0.741	0.548	0.524	0.681	0.437
LDAS	0.329	0.360	0.322	0.368	0.403	0.347	0.326	0.357	0.262
LDBA	0.607	0.614	0.554	0.436	0.441	0.377	0.456	0.461	0.318
NANL	0.636	0.639	0.636	0.624	0.627	0.613	0.523	0.525	0.343
NLAC	0.524	0.529	0.435	0.530	0.535	0.434	0.501	0.506	0.374
NLVS	0.689	0.690	0.625	0.683	0.684	0.607	0.552	0.553	0.308
NAAC	0.739	0.742	0.568	0.753	0.756	0.599	0.641	0.644	0.323
NACA*	0.602	0.649	0.650	0.554	0.597	0.515	0.402	0.433	0.283
NACP*	0.545	0.587	0.544	0.471	0.507	0.434	0.376	0.405	0.198
NAFM	0.733	0.737	0.615	0.719	0.723	0.560	0.701	0.705	0.383
NA41	0.650	0.653	0.529	0.593	0.596	0.443	0.580	0.583	0.259
NAVS	0.551	0.578	0.550	0.528	0.553	0.470	0.528	0.553	0.324
NAZI	0.589	0.605	0.551	0.569	0.584	0.498	0.525	0.539	0.280
NAZS	0.562	0.593	0.559	0.493	0.520	0.437	0.518	0.546	0.428
BRBA	0.555	0.574	0.529	0.524	0.542	0.459	0.504	0.521	0.399
NALD	0.375	0.445	0.364	0.260	0.309	0.228	0.284	0.337	0.189
DAFM	0.610	0.630	0.554	0.600	0.620	0.515	0.589	0.608	0.413
PLSY	0.563	0.586	0.511	0.528	0.550	0.461	0.472	0.492	0.342
POBA	0.616	0.622	0.544	0.520	0.525	0.379	0.522	0.527	0.273
PM41	0.469	0.545	0.460	0.464	0.540	0.451	0.479	0.557	0.401
41MX	0.637	0.653	0.539	0.623	0.638	0.507	0.553	0.567	0.335
41ZI	0.614	0.628	0.550	0.588	0.602	0.515	0.587	0.601	0.412
PTAS	0.349	0.407	0.349	0.316	0.369	0.285	0.369	0.431	0.316
PTLD	0.433	0.563	0.426	0.363	0.472	0.330	0.432	0.562	0.376
SLBA*	0.522	0.562	0.521	0.446	0.481	0.423	0.449	0.484	0.421
SLCC*	0.399	0.430	0.400	0.360	0.388	0.355	0.330	0.356	0.298
SYBA	0.783	0.787	0.768	0.800	0.804	0.781	0.721	0.725	0.666
SYMX	0.505	0.520	0.468	0.513	0.528	0.461	0.504	0.519	0.384
ZTPO	0.296	0.313	0.294	0.317	0.335	0.288	0.450	0.476	0.348
ZTVS	0.453	0.454	0.393	0.488	0.489	0.372	0.563	0.565	0.279
ZTZI	0.252	0.300	0.246	0.259	0.308	0.251	0.270	0.321	0.257
VSBA	0.665	0.672	0.647	0.666	0.673	0.643	0.635	0.642	0.585
VSSY	0.565	0.581	0.565	0.547	0.563	0.542	0.529	0.544	0.510
ZIMX	0.256	0.292	0.229	0.140	0.160	0.112	0.190	0.217	0.129
ZSNL	0.642	0.643	0.642	0.601	0.602	0.551	0.407	0.408	0.246

[a]EIDs indicated with an asterisk do not have an associated repeatability estimate with which to adjust their h_r^2 so the geometric mean ($\bar{X}_G$ = 0.929) of the available repeatability estimates was used instead.

4.3.2 Heritability estimates

Heritability of most morphological parameters in vertebrates is estimated to be ~0.40 (e.g., Mousseau and Roff, 1987; Cheverud et al., 1990; Visscher et al., 1991; Cheverud, 1996; Kruuk et al., 2002; Berry et al., 2003; Safari et al., 2005). Adjusted h_r^2 estimates for the baboon craniofacial traits analyzed are consistent with this expectation (Table 4.4).

Average adjusted heritability decreases at each additional level ($\bar{h}_{a1}^2$ = 0.55 ± 0.1, $\bar{h}_{a2}^2$ = 0.52 ± 0.2, $\bar{h}_{a3}^2$ = 0.50 ± 0.1; Fig. 4.4), although these changes are small. This is the result of altering the *proportion* of V_R attributable to V_A by removing variation due to overall and cranial size, respectively (geometric mean: $\bar{V}_{a1}$ = 0.464 ± 1.4, $\bar{V}_{a2}$ = 0.412 ± 1.4, $\bar{V}_{a3}$ = 0.321 ± 1.4). Although the denominator of the heritability equation ($h_r^2 = V_A/V_R$) decreases as the size of V_R is reduced from Model 1 to 3—the inclusion of additional covariates explains more of the V_P—the numerator is also decreased, but to a greater degree, as the net result is a decrease in h_r^2. This indicates that the heritability of overall body size and cranial size is higher than for local size.

One interesting question that arises in regard to relative amounts of V_A is whether it is distributed evenly across the cranium or is higher in some regions. This question is relevant for evolutionary biology as the pattern of apportionment of additive genetic variation provides information on the potential for evolutionary response to selection on cranial traits. This is particularly important for phylogenetic reconstruction, as some have argued that certain traits may be more or less ideal for assessing species relationships (see von Cramen-Taubadel, 2009 for an excellent review). Lieberman (1995) goes so far as to suggest some craniodental characters, primarily those directly affected by the biomechanical stresses of mastication, are more prone to demonstrate homiology: homoplasy as a result of nonheritable environmental factors. Because the cranial base is theoretically unaffected by masticatory stress and completes growth relatively early in ontogeny, many assert that it is more robust to homiology

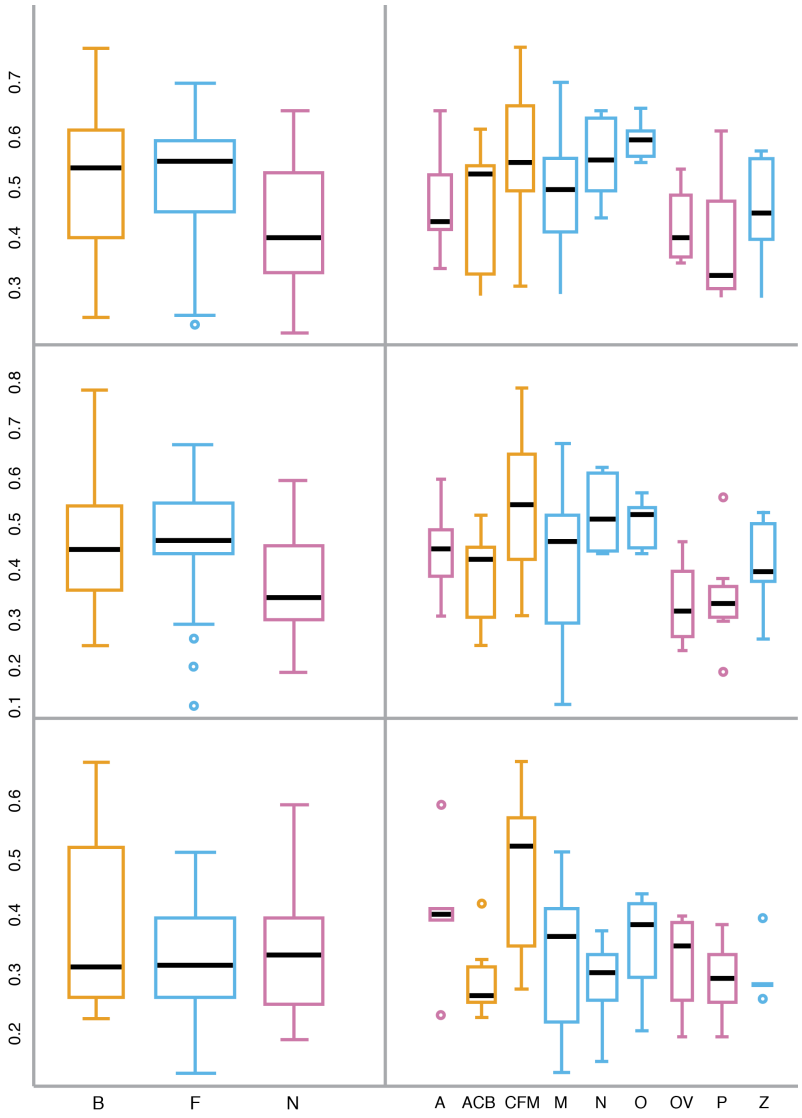

Figure 4.4 Distribution of V_A in Different Regions of the Cranium. General categories are shown on the left and more specific ones on the right (anterior neurocranium, anterior cranial base, circum-foramen magnum, mouth, nose, orbit, overall neurocranium, posterior neurocranium, and zygomatic arch) are colored according to the general category they compose. The three models are shown on each row (1: top, 2: middle, 3: bottom).

and, thus, preferentially carries a phylogenetic signal (e.g., Harvati and Weaver, 2006; Cardini and Elton, 2008). To test this hypothesis, I compared the amount of variation in different regions of the cranium in two ways. First, I constructed the similarity matrix, S_{ij}, from the estimates of heritability and covariate effects. The degree to which the clusters reflected the true relationships among traits did not differ from one model to the next (cophenetic correlation

coefficient: c_1 = 0.41, c_2 = 0.48, c_3 = 0.42). However, no appreciable pattern was observed (Fig. 4.5). This indicates that the effects of additive genetic variation are spread throughout the cranium, rather than being grouped in any particular region. This is not surprising given the interdependent nature of the craniofacial complex, which requires a degree of integration among its constituents. Although individual covariates may differentially affect some traits rather than others, the net effect of both covariate and additive genetic effects are global.

Next, I allocated EIDs to one of three general regions (splanchno-, basi-, and neurocranium) and to one of nine more specific regions corresponding more closely to functional modules such as the orbits or the anterior cranial base (see Fig. 4.4 legend). I compared the amount of V_A in each region but, as is evident from the boxplots in Figure 4.4, V_A did not differ significantly among different regions. However, I did observe a few suggestive patterns. First, for the general cranial categories, the amount of V_A in the neurocranium was less than in the other two in Models 1 and 2, but after correcting for cranial size variation in Model 3, V_A was evenly spread among the three. This indicates that a relatively larger amount of V_A for traits in the face and cranial base is associated with overall cranial size variation, which suggests pleiotropy of genetic variation that contributes variation in overall cranial size and in facial and basicranial form.

Second, cranial base sub-regions (anterior cranial base and circum-foramen magnum) actually had the largest mean values and one of the greatest amounts of variation in V_A estimates for all three models. Consequently, these traits have a greater potential to respond to evolutionary forces, which may actually not make them any better than any other traits for assessing phylogenetic signal.

Third, the traits in categories located most inferoposteriorly (posterior and overall neurocranium and zygomatic arch) tend to have the lowest mean values. These are the traits furthest from the portion of the cranium most affected by growth occurring as a result of sexual

dimorphism in facial length. Given that these sex-specific differences in facial size and shape are likely the product of sexual selection—and traits under sexual selection (i.e., strongly related to fitness) have the highest levels of V_A (Houle, 1992)—it is not surprising that inferoposterior traits would have relatively less V_A.

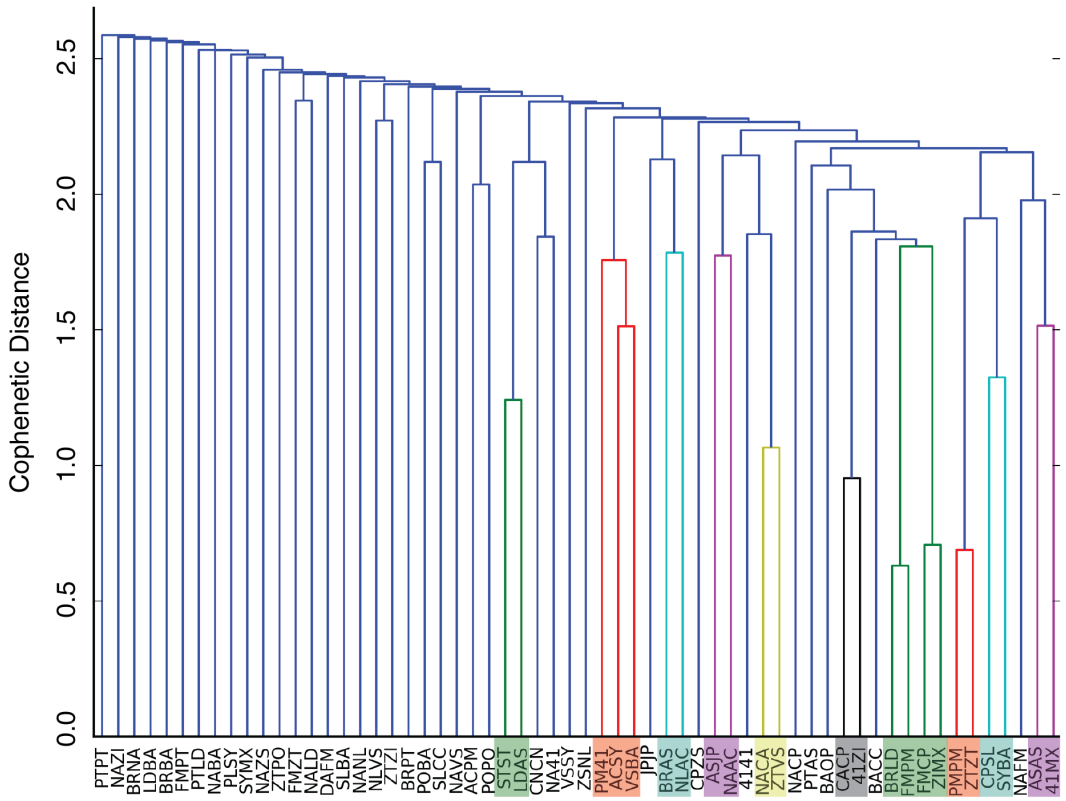

Figure 4.5 Dendrogram of EID Clusters Based on Mixed Categorical and Continuous Data. Except in a few cases, which I have indicated with colored boxes, there are no appreciable clusters and the few pairings or trios that are observed compose traits from very different regions of the cranium (e.g., ASAS and 41MX on the far right). The long branch lengths also suggest the pattern of variation in the data lacks structure as none of the traits are particularly similar to any others.

4.3.3 Effective sample sizes

Finally, N_e's range from 11.0 to 341.6 depending on the trait and the level of analysis (see Table 4.2). The geometric mean N_e in each model is: $\bar{X}_{G1}$ = 88.5 ± 2, $\bar{X}_{G2}$ = 71.1 ± 2, and $\bar{X}_{G3}$ = 68.0 ± 2. Only the reduction in N_e from Models 1 to 2 is significant (ANOVA $F = 3.85$, $P = 0.02$). This

suggests that the genetic variance of body-size variation has a significant impact on craniofacial genetic variance. Given the number of genetic loci (>250) that have been identified that affect body-weight variation in humans (Rankinen et al., 2006), and the fact that at least some if not most of these loci are pleiotropic and/or demonstrate epistasis (e.g., Brockman et al., 2000, Dong et al., 2005; Curran et al., 2013), it is not surprising that regressing out the proportion of V_P due to body size variation (i.e., moving from Model 1 to 2) reduces the V_A (see preceding section). As N_e is dependent on the amount of independent heritable genetic variance (i.e., effective number of breeding values), removing the proportion of phenotypic variation affected by body-size allometry removes the associated genetic information contributed by loci that also affect body-size variation.

4.4 Discussion

The aim of this chapter was to determine how phenotypic variation in the baboon cranium is differentially affected by genetic effects and environmental factors. Additionally, analyses were conducted at three different levels to examine how these effects change as a result of sex, age, and body and cranial size variation. Finally, the distribution of additive genetic variation throughout the cranium was examined to compare the evolutionary potential of different regions and traits. Three different analyses were conducted to address the specific research questions presented.

First, covariate effects were estimated to determine whether environmental factors explain any of the V_P for individual traits and if so, how much. For all EIDs and across all three levels of analysis, the proportion of V_P explained by covariate effects ranged greatly, from 0.04 - 54.6%. The covariates that were significant for the most number of traits include sex, body weight, and cranial size. We have acknowledged for many years that sexual dimorphism and allometry play large roles in patterning phenotypic variation in baboons. Discovering that these

factors significantly interact with genetic variation, each other, and the external environment to affect heritability estimates is exciting because it suggests an ability to identify QTLs that are also sensitive to such factors. It will also contribute to our understanding of morphological response to directional and sexual selection in baboon crania (see Willmore et al., 2009 for an excellent example) and of differences in trait phenotype related to gross size changes.

Second, craniofacial traits were assessed to determine whether they are significantly heritable and how much of the V_P is explained by the net effects of all contributing genetic loci. ECV and all 60 EIDs were heritable in all three models, indicating that craniofacial variation in this population of baboons would be responsive to evolutionary processes operating on heritable genetic variation. Heritability estimates in Model 1 range from 0.211 to 0.783 with a standard deviation (SD) of 0.15. The repeatability of these estimates is determined by comparing their SD to the average standard error (SE), which is 0.07. This indicates that the pattern of distribution of heritability in these baboon crania is about 50% repeatable.[7] In other words, we are able to compare relative degree of heritability among EIDs with a reasonable amount of confidence. Cheverud (1996) conducted the same analysis for two tamarin species but the h_r^2 repeatability was too low (10% for each species and 40% when estimates were pooled between species), which suggests that whether a particular trait was greater than or less than the average h_r^2 (~0.42) was random. In contrast, for this sample the fact that an EID has a larger h_r^2 estimates is a more meaningful statement about its variation being under stronger genetic control and/or it being less responsive to environmental perturbations than a trait with a smaller estimate.

[7] Results for Models 2 and 3 are nearly identical and, thus, not shown here. Although a repeatability of 0.5 seems low—typically only values >0.9 are considered excellent—this estimate must be compared to what has been achieved previously. Due to the difficulty in estimating genetic parameters, we expect repeatability to be much lower than would be acceptable for phenotypic values. The repeatability of previous estimates of genetic parameters in primates has ranged from 0.1-0.4 (Cheverud, 1996).

Determining whether a trait's phenotypic variation is largely influenced by genetic or environmental variation is important knowledge for delineating taxonomic boundaries and selecting characters for both phylogenetic reconstructions and the formation of functional and biomechanical models. Failing to understand the factors that contribute to variation of complex traits and to identify which traits are phenotypically plastic, homoiologous, homoplastic, and/or evolvable can impact the validity of evolutionary models (e.g., Collard and Wood, 2007; von Cramon-Taubadel, 2009; Pino-Bodas et al., 2011). Establishing the genetic architecture of a trait helps alleviate these concerns, and estimating heritability is one of the first steps in doing so (Falconer and Mackay, 1996; Lynch and Walsh, 1998).

However, to answer such evolutionary questions it is not enough to estimate a trait's h_r^2 as it is a dimensionless quantity, the degree of which can be affected by increased V_A, decreased V_E, or both. Rather, it is the absolute amount of V_A that is important. Interestingly, because EIDs were standardized prior to analysis, V_R is largely ~1, meaning that $h_r^2 \cong V_A$ for most traits. So, for this special case, h_r^2 is actually informative for comparisons among cranial regions.

With few exceptions, the amount of V_A reflected in a trait's V_R decreased in Models 2 and 3. This is a significant observation in the context of comparative analyses where some measure of overall size, such as body weight, cranial base length, or femoral length, is often used to correct for both intra- and interspecific allometric effects. My results indicate that the choice of measurement used for standardization and the scale at which trait variation is considered may affect the phylogenetic and selective signals of a trait. A number of researchers have voiced concern about trait selection, arguing either for or against the use of ones in certain cranial regions over others (e.g., Olson, 1981; Harvati and Weaver, 2006; Cardini and Elton, 2008; Roseman et al., 2010), while others have discussed the relative merits of the myriad methods for allometric corrections (e.g., Jungers, 1985), particularly as they are applied (and

often misapplied) statistically. To my knowledge, this dissertation is the first study to suggest caution in trait selection in relation to scaling effects on V_A. Failing to do so could result in inaccurate interpretations as a consequence of conflating the effects of direct selection on one phenotype with indirect selection on those with which it is correlated (trait correlations are provided in Chapter 5). Genetic correlations among traits are maintained through pleiotropy and linkage disequilibrium, and these results (as well as those presented in Chapter 6) suggest that pleiotropy is a definite factor contributing to craniofacial variation in baboons. Most questions asked by evolutionary biologists and biological anthropologists concern the effect of evolutionary forces in producing observed allele frequencies and specific phenotypes, so accounting for and understanding the V_A on which those forces act is necessary.

The lack of sex effects for nasal length traits in Model 3 raises an interesting issue. I chose to correct for cranial size allometry using PC1, rather than with other common variables, such as cranial capacity or cranial base length or centroid size. As an unintended result, traits loading heavily on PC1 had a disproportionate amount of their V_P removed from further analysis. Accurately partitioning V_P becomes more difficult as the amount of V_P is reduced because decomposing it into its constituent elements (V_A, V_E, and V_I) further reduces the variance, making variance component estimation difficult. This will also affect the ability to locate QTLs in Model 3, which will be discussed more in Chapter 6. Despite this complication, I argue that it is important to correct for both body and cranial size to ensure that regional size and shape variation is not conflated with these other causes of variation.

Lastly, N_e was calculated for each trait to determine whether the associated V_A has increased or decreased over time. All calculated N_e were substantially smaller (54-98%) than the analyzed sample sizes (N). However, despite the greatly reduced samples sizes, these data are more robust than in previous studies where primate craniofacial trait quantitative genetic parameters were estimated with much smaller N_e. For example, Cheverud (1996) calculated a

mean N_e of 36 (range: 1.7-161.7) for tamarin craniofacial traits, which is a 93% reduction of the total sample size. A larger N_e reduces the error associated with genetic parameter estimation, providing confidence in these estimates. Calculating the N_e for each craniofacial trait and determining that they are relatively high allows me to assess the power of my research design to localize genetic variants using genome-scanning methods, the results of which are presented in Chapter 6.

4.5 Conclusion

The results of this chapter lay the groundwork for the ones that follow, in which I evaluate the pattern and strength of intertrait associations and perform multipoint linkage mapping analysis to identify QTLs in the baboon genome for ECV and the 60 EIDs. Demonstrating that these traits are heritable was important for two reasons, one conceptual and the other methodological. First, only traits that are heritable can evolve. Evolution, by definition, requires that allele frequencies change over time, which happens as a direct result of differential survival among individuals that vary. This variance must be faithfully transmitted from one generation to the next for it to be meaningful for offspring survival and reproduction and so that it can be used to reconstruct a lineage's history. As this dissertation explores genetic variation in the baboon cranium as it relates to its evolution, demonstrating that features of the cranium are heritable is essential.

Second, linkage mapping can be performed only on traits that are significantly heritable. Traits that are not heritable do not have a significant proportion of their variance attributable to genetic variance that is *passed from parent to offspring*. Their variance may be produced by dominance effects among alleles, epistatic interactions among genes, or epigenetic factors—none of which is heritable—or primarily by the environment. Linkage mapping relies on both the phenotypic and genetic similarity between relatives to identify QTL. Unless genetic variants are IBD, familial resemblance is meaningless.

CHAPTER FIVE
MORPHOLOGICAL INTEGRATION

5.1 Introduction

Olson and Miller (1958) recognized that characters do not evolve independent of one another and, thus, the morphology of an organism must be studied in its totality. Their emphasis on examining associations among morphological traits offers an alternative view of organismal biology from the more traditional reductionist approach of quantifying individuals as a series of linear dimensions (or landmark configurations when using geometric morphometrics). These networks of associations reflect meaningful biological phenomena, such as growth, development, and function (Olson and Miller, 1958), and evolutionary inferences can be drawn from their magnitudes and patterns.

For Olson and Miller (1958), the most meaningful multivariate measure of the nature and intensity of relationships, both among morphological units within an organism and among organisms within a population, is the correlation coefficient, ρ. By first partitioning an organism into discrete morphological units that can be reliably and reproducibly measured and then synthesizing these individual measurements into an array of ρ's (i.e., ρ-groups), the patterns of inter-trait associations can be used as a tool of recognition and interpretation. The utility of this concept of *morphological integration* is that:

> The use of representative measures for a particular system, however, can reveal the underlying order and give a basis for understanding intersystem relationships. Conversely, associations of measures in the absence of knowledge of their biological relationships can lead to recognition of systems and provide clues to their origins and functions as well as to their changes during evolution.
>
> (Olson and Miller, 1958, p 10)

The original work on morphological integration conducted by Miller (1950), Miller and Weller (1952), Olson and Miller (1951), and Olson (1953) compared ρ-groups to F-groups, or arrays of correlation coefficients based on theoretical expectations of shared functional or

developmental properties. This was later extended to include expectations based on underlying genetic basis. In a morphological integration study in rhesus macaque crania, Cheverud (1982) provided evidence to support the quantitative genetic theory prediction that ρ is a result of both genetic and non-genetic environments, as well as their interactions, shared among individuals in a population. This prediction is based on the observations that most evolutionarily-important traits are: (1) polygenic (Lewontin, 1974), (2) byproducts of interactions among both protein-coding and regulatory genes (Mayr, 1976), (3) a consequence of pleiotropy (Wright, 1980), and (4) more affected by genetic correlations than we often acknowledge (Falconer, 1960).

The strength of ρ among various traits is a function of the distribution of V_P over the total morphospace, or the *n*-dimensional range of all possible forms that a structure can take. If variation is concentrated in only a few dimensions of morphospace, forms are more strongly integrated, and change in one trait causes a greater concomitant change in traits with which it is integrated (Klingenberg, 2008). Visually, this would appear as a steep slope on a bivariate plot of raw/log-transformed measurements (Fig. 5.1).

Hallgrímsson and colleagues (2009) frame integration in terms of the propensity of a system to produce correlation, rather than as a simple description of the observable ρ's.[1] This shifts the focus of integration studies from the manifestations of mechanisms for producing covariation to the mechanisms themselves, which is often more meaningful for studying the origin and maintenance of morphological integration. Because "the propensity for traits to covary at a particular level is often due to the association of processes at a lower level" (Klingenberg, 2014), studying patterns of covariation is informative for understanding the contribution of underlying processes to morphological evolution.

[1] This distinction is analogous to that of Wagner and Altenberg (1996) in discussing the difference between variability (a property of a system) and variation (characteristics of a population).

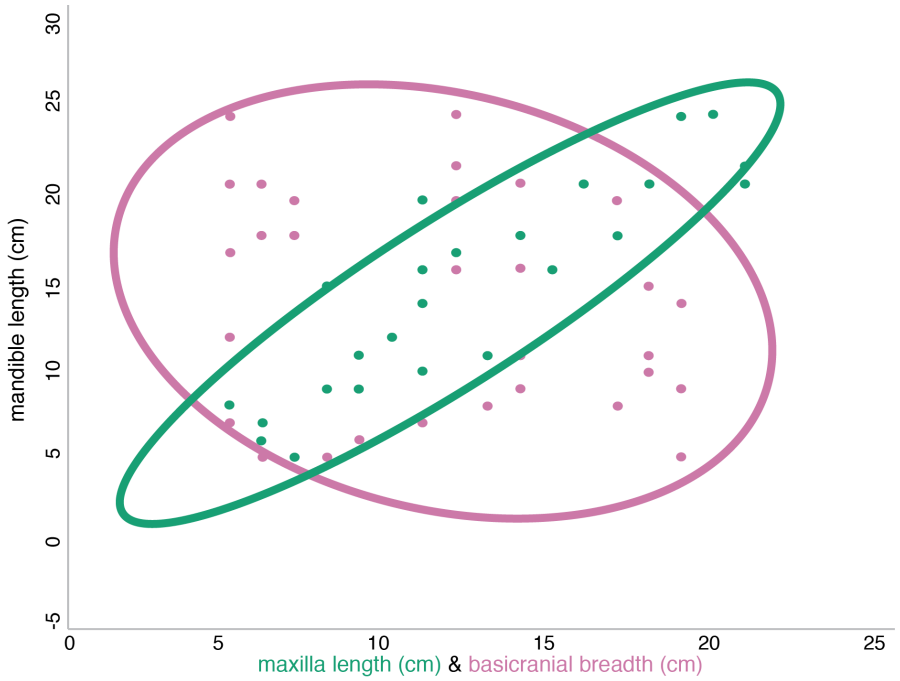

Figure 5.1 Graphical Representation of Morphological Integration. Scatterplots of simulated data drawn with 95% confidence ellipses. Shown in green is a highly integrated pair of traits (maxilla and mandible length), while shown in pink is a pair of traits that is much less integrated (basicranial breadth and mandible length).

5.1.1 Research Questions

In this chapter I perform analyses to determine the correlation structure of V_P in my sample of baboon crania, which can be described in multiple contexts: genetic, developmental, environmental, and functional. I then compare these patterns of inter-trait correlation to address five research questions: (1) Do patterns of modularity in baboon crania closely resemble those expected based on functional and developmental relationships among traits? (2) How closely do phenotypic variation patterns reflect the patterns of the genetic and environmental variation underlying them? (3) Are genotypic patterns of integration reinforced or counteracted by environmental integration? (4) What effect does allometry have on patterns of phenotypic variation? (5) Is morphological integration structured differently in different parts of the cranium?

5.2 Materials and Methods

A number of analytical techniques exist for studying integration (e.g., Magwene, 2001). I chose to use matrix similarity tests because doing so allows me to formulate *a priori* statistical hypotheses. Additionally, matrix similarity test significance is determined with resampling methods that are free of distributional assumptions. To quantify patterns of craniofacial variation in my sample, I estimated pairwise phenotypic, genetic, and environmental correlation coefficients (ρ) for the 60 standardized Euclidean interlandmark distances (EIDs) for all three models that include different combinations of covariates (see *4.2.2 Levels of Phenotypic Variation*) using SOLAR. All analyses were conducted on the computing cluster maintained by the Mallinckrodt Institute of Radiology's Center for High Performance Computing at Washington University School of Medicine.

5.2.1 Correlations

The covariance of any two traits a and b was modeled as an n x n variance/covariance matrix ($\boldsymbol{\Omega}_{ab}$) between all possible pairs of individuals. The matrix elements are calculated using Equation 4.2 while accounting for the effect of covariates determined to be significant for each trait during the heritability estimation conducted in the preceding chapter and then used to maximize the likelihood of the correlation coefficients in the equation:

$$\boldsymbol{\Omega}_{ab} = 2\boldsymbol{\Phi}\rho_G\sigma_{Ga}\sigma_{Gb} + \boldsymbol{I}\rho_E\sigma_{Ea}\sigma_{Eb} \quad (5.1)$$

where $\boldsymbol{\Phi}$ is the kinship matrix and $\boldsymbol{I}$ the identity matrix from Equation 4.1, ρ_G is the genetic correlation between the two traits, and ρ_E is the intertrait correlation due to shared environmental effects on a pair of traits. Both ρ_G and ρ_E are maximum likelihood estimates (Mahaney et al., 1999). A genetic correlation of 1 indicates that the same genes contribute to variance in both traits (i.e., the covariance between two traits is attributable to additive genetic effects) while a correlation of 0 indicates that any phenotypic correlation between the two is

entirely due to shared environmental effects, including all non-additive genetic sources of variation.

Because the relationships between genotypic and environmental variance of a phenotype is additive (see Equation 2.1), the phenotypic correlation between any two traits can be obtained thus (Mahaney et al., 1999):

$$\rho_P = \left[\rho_G\sqrt{h_1^2}\sqrt{h_2^2}\right] + \left[\rho_E\sqrt{1-h_1^2}\sqrt{1-h_2^2}\right] \quad (5.2)$$

where h_i^2 is the maximum likelihood heritability value of trait i as estimated in Chapter 4. I combined all pairwise correlation estimates for each of the three parameters (ρ_P, ρ_G, and ρ_E) into a set of three 60 x 60 matrices. One set (**ρP**$_i$, **ρG**$_i$, and **ρE**$_i$) was created for each of the three covariate models (i), resulting in 9 correlation matrices (Appendix B, Tables B1-B9).

5.2.2 Hypothetical Matrices

Three theoretical connectivity matrices were created to test hypotheses of inter-trait relationships: a developmental matrix (**ρD**) and two functional matrices, one more general and one more specific (**ρF$_G$** and **ρF$_S$**, respectively). Each EID was assigned to one of two tissue types depending on its embryonic origin (Fig. 5.2): neural crest (NC) or paraxial mesoderm (PM). If an EID linked craniometric landmarks on bones originating from both tissue types or one of the two landmarks was located at the intersection of two bones originating from both tissue types (e.g., BRNA), the EID was assigned to a third category (NCPM). Because the sella turcica marks the boundary between pre- and post-sphenoid—the portions of the bone deriving from NC and PM tissues, respectively—any EID containing SL was assigned to NCPM. To create **ρD** (Appendix B, Table B10), this developmental information was considered in a pairwise manner and a value assigned to represent each developmental relationship according to the following scale: 1 = trait pairs with the same embryonic origin; 0.5 = pairs in which both

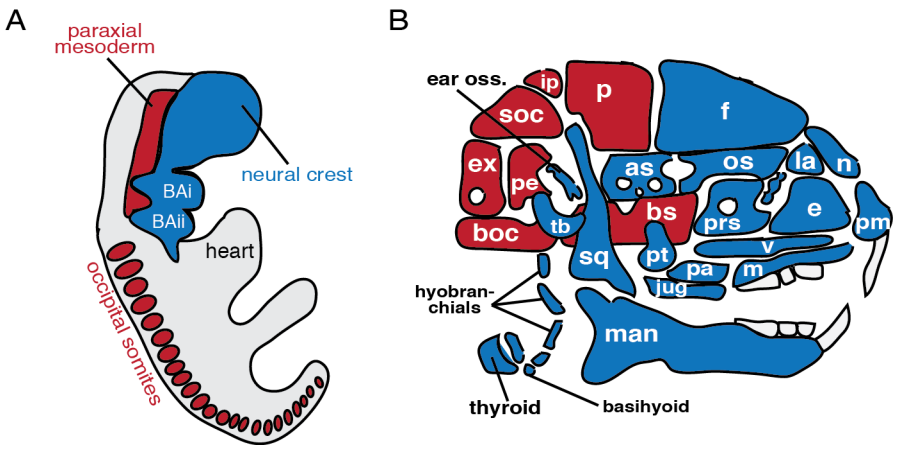

Figure 5.2 Schematic of Embryonic Tissue Types Used to Create the D-Matrix. Paraxial mesoderm is shown in red and neural crest cells in blue. Panels: (A) Lateral view of an E9.5 mouse embryo showing unsegmented paraxial mesoderm in the rostral end, mesoderm-derived occipital somites along the dorsal aspect, and neural crest derived branchial arches I and II (*BAi*, *BAii*). (B) Lateral view of an "exploded" adult mouse skull with bones colored according to embryonic origin. Abbreviations: *as*, alisphenoid; *boc*, basioccipital; *bs*, basisphenoid; *e*, ethmoid; *ex*, exoccipital; *f*, frontal; *ip*, interparietal; *jug*, jugal (malar); *la*, lachrymal; *m*, maxilla; *man*, mandible; *n*, nasal; *os*, orbitosphenoid; *p*, parietal; *pa*, palatine; *pe*, petrosal; *pm*, premaxilla; *prs*, presphenoid; *pt*, pterygoid; *soc*, supraoccipital; *sq*, squamosal; *tb*, tympanic bulla; *v*, vomer. Adapted from Noden and Trainor (2005).

were NCPM; 0.25 = pairs in which one trait was assigned to NCPM and the other to either NC or PM; and 0 = if one trait was derived from NC trait and the other from PM.

A similar process was used to assign traits into general spatial/functional categories: splanchnocranium/face (S), chrondrocranium/base (B), or dermatocranium/neural vault (V). Possible values for ρF_G (Appendix B, Table B11) were 1 (both traits from the same cranial region) or 0 (both traits from different regions). Because dividing the cranium into only the three components typically used to describe the evolutionary origins of the cranium is really reflective of topographic proximity, I created an additional matrix to reflect functional relationships by further subdividing the cranial regions into modules: orbit (O), mouth (M), nose (N), zygoma (Z), anterior vault (A), posterior vault (P), overall vault (V), circum-foramen magnum (CFM, which I also call posterior cranial base), and anterior cranial base (ACB). To create ρF_S (Appendix B, Table B12), trait pairs from the same functional module were assigned 1, those from different

modules but that are located in the same general region were assigned 0.5, and those from different modules that are also in different regions were assigned 0.

5.2.3 Mantel's Test

These predicted patterns of association were compared to the observed correlation matrices to determine whether functional and/or developmental relationships pattern morphological variation. I used Mantel's Test to test the null hypothesis of no relationship between pairs of craniofacial correlation matrices. Mantel's Test (1967) summarizes the pattern of pairwise similarity by calculating a standardized Mantel statistic (r_M), which varies from -1 to 1. A correlation of 1 indicates the two matrices have an identical pattern (although the magnitude of the correlations may still differ), while a correlation of -1 indicates the two are mirror images of one another. If the two matrices are not structurally similar at all, r_M = 0. Correlation magnitude for each matrix is the average ($\bar{r}^2$) of the squared Pearson product moment correlation coefficients that comprise it.

Statistical significance of r_M is assessed through a permutation procedure, which accounts for autocorrelation among the matrix elements. The procedure randomly rearranges one of the two matrices by shuffling both its rows and columns and recalculates r_M after each randomization. This creates an empirical distribution of r_M to address the question: "How often is r_M as larger or larger than its observed value when calculated between any two random matrices of the same dimensions as the test matrices?" If the observed r_M is greater than 95% of the r_M's calculated from randomized matrices, there is evidence to suggest the similarity between the two matrices in question is statistically significant.

To address the research questions (RQ_i), I tested four sets of hypotheses by estimating r_M between pairs of matrices for four models (i) that include different combinations of covariates (see *4.2.2 Levels of Phenotypic Variation*).

(1) RQ_1: Do patterns of modularity in baboon crania closely resemble those expected based on functional and developmental relationships among traits?
   - H_1: The pattern of craniofacial variation in this sample of baboon crania is random with respect to developmental and functional relationships among EIDs.
   - r_M calculated for $\boldsymbol{\rho P}_i$:$\boldsymbol{\rho F_G}$, $\boldsymbol{\rho P}_i$:$\boldsymbol{\rho F_S}$, $\boldsymbol{\rho P}_i$:$\boldsymbol{\rho D}$
   - relative strength of inter-trait correlation within proposed modules as compared to among traits from different modules

(2) RQ_2: How closely do phenotypic variation patterns reflect the patterns of the genetic and environmental variation underlying them?
   - H_2: Craniofacial variation at the population level is not structured in a manner predicted by genetic or environmental variation.
   - r_M calculated for $\boldsymbol{\rho P}_i$:$\boldsymbol{\rho G}_i$ and $\boldsymbol{\rho P}_i$:$\boldsymbol{\rho E}_i$

(3) RQ_3: How much do interactions with environmental conditions alter the patterns of genetic correlation in producing adult crania?
   - H_3: Patterns of genetic and environmental correlation act in a complementary fashion in producing phenotypic integration.
   - r_M calculated for $\boldsymbol{\rho G}_i$:$\boldsymbol{\rho E}_i$

(4) RQ_4: What effect does allometry have on patterns of phenotypic variation?
   - H_4: The relationship among EIDs is the same regardless of whether V_P due to the influence of size-related factors is removed.
   - r_M calculated for $\boldsymbol{\rho P}_{M1}$:$\boldsymbol{\rho P}_{M2}$:$\boldsymbol{\rho P}_{M3}$

5.2.4 Matrix Repeatability and Adjusted r_M

As correlation coefficients are measured from samples of a population, they are estimated with error, which limits the maximum r_M achievable (Cheverud, 1996). This biases interpretations of matrix similarity and necessitates adjusting Mantel correlation coefficients accordingly by factoring in the repeatability (t_i) of both matrices:

$$r_M = r_t\sqrt{t_A t_B} \tag{5.3}$$

where r_M is the observed Mantel correlation coefficient and r_t is the true population correlation coefficient. Equation 5.3 makes it easy to see that an estimated correlation matrix can equal its true population matrix only if it is measured without error. As this is not possible, even if two population matrices were perfectly correlated (i.e., r_t = 1), the maximum correlation between the observed sample matrices is determined by $\sqrt{t_A t_B}$. Consequently, when comparing any two sample correlation matrices between populations, the observed correlation coefficient should be

judged relative to $\sqrt{t_A t_B}$, rather than 1. A matrix's repeatability is calculated according to the equation:

$$t_i = \frac{(V_o - V_e)}{V_o} \tag{5.4}$$

where V_o is the variance among the observed elements of a correlation matrix and V_e is the error variance of estimated correlations. V_o is calculated as the standard deviation of the ρ_i estimates comprising correlation matrix i, and V_e is the average squared standard error of those estimates.

Phenotypic, genetic, and environmental correlation matrices are not independent of each other, as they comprise a part-whole relationship, which further biases correlation estimates among these matrices. Consequently, this additional factor must be taken into consideration when comparing correlation matrices. Equations 5.5 and 5.6 must be applied when comparing **ρG**:**ρE** and **ρG:ρP**, respectively:

$$r_{GE} = \sqrt{(t_G t_E)} - \sqrt{[(1 - t_G)(1 - t_E)]} \tag{5.5}$$

$$r_{GP} = h_r^2 \sqrt{\left(\frac{t_P}{t_G}\right)} + e^2 \sqrt{t_G t_E} - e^2 \sqrt{\left[(1 - t_G)(1 - t_E)\left(\frac{t_P}{t_E}\right)\right]} \tag{5.6}$$

where h_r^2 is the average heritability and e^2 the average environmental variance (1 - h_r^2) of the traits within the correlation matrices.

5.2.5 Hierarchical Clustering of Correlation Matrices

I used hierarchical clustering (Sneath and Sokal, 1963; Johnson, 1967) to answer the final research question (RQ_5): Is morphological integration structured differently in different parts of the cranium? Hierarchical clustering, also called connectivity based clustering, was performed on the distance matrix for $\mathbf{\rho P}_1$, $\mathbf{\rho P}_2$, and $\mathbf{\rho P}_3$ using single-linkage clustering (based on minimum distances between EIDs), complete linkage clustering (similar but based on maximum distances), UPGMA (unweighted pair group method with arithmetic mean, or average link

clustering), and WPGMA (weighted pair group method with arithmetic mean). All hierarchies were formed agglomeratively (aggregating traits into groups based on their individual correlation estimates).

To display the relationships in a useful manner, dendrograms were created. The most appropriate clustering method was selected as the one with the largest cophenetic correlation coefficient, c (Sokal and Rohlf, 1962). This is a measure of how faithfully the cophenetic distance matrix preserves the pairwise distances between the unmodeled data (i.e., it is the correlation coefficient between the original distance matrix and the cophenetic matrix[2]). As in Chapter 4, data visualization and all analyses were conducted in Python.

5.3 Results

Matrices are generally highly repeatable (Table 5.1), with **ρP** being far more so ($\bar{t}_R$ = 0.99) than either **ρG** ($\bar{t}_R$ = 0.46) or **ρE** ($\bar{t}_R$ = 0.55). This is to be expected as phenotypic correlations are measured with much larger sample sizes—estimations of genetic correlations are dependent on N_e, which is almost always much smaller than N—thus reducing their standard errors. V_e is also provided in Table 5.1 and is significantly smaller for **ρP** ($\bar{V}_e$ = 0.001) than for either **ρG** ($\bar{V}_e$ = 0.135) or **ρE** ($\bar{V}_e$ = 0.097). As the observed variance in correlation estimates (V_o) is essentially the same for all correlation matrices (range: 0.19-0.26), it is the greater amount of V_e in genetic correlation estimates that is driving down the repeatability of **ρG**. This will make it difficult to estimate ρ_G, but should not greatly affect comparisons of patterns of genetic correlation.

In terms of the correlation estimates themselves, they are highest in **ρG** in both Models 1 and 2 (Table 5.1; Fig. 5.3), which reflects a bias due to small sample size that inflates r^2 values (Hill and Thompson, 1979; Cheverud, 1988). As sample sizes for **ρG** are smallest, genetic

[2] A cophenetic matrix is composed of cophenetic distances, which can be thought of as either (1) the length of the branches connecting two objects in a dendrogram or (2) the height of the node connecting two branches within a dendrogram. It is a measure of how similar two objects have to be in order to be grouped into the same cluster.

Table 5.1 Repeatability of Correlation Matrices. Estimates of matrix repeatability (t_R), observed variance (V_o) and average error variance (V_e) of the matrix elements, average (r) and squared average (r^2) correlations are provided for phenotypic (**ρP**), genetic (**ρG**), and environmental (**ρE**) correlation matrices for all three covariate models.

Matrix	t_R	V_o	V_e	r	r^2
Model 1					
ρP	0.99	0.19	0.001	0.20	0.039
ρG	0.47	0.23	0.124	0.27	0.071
ρE	0.53	0.21	0.097	0.12	0.013
Model 2					
ρP	0.99	0.21	0.001	0.19	0.034
ρG	0.47	0.25	0.135	0.23	0.053
ρE	0.57	0.23	0.099	0.13	0.017
Model 3					
ρP	0.99	0.20	0.001	0.02	0.0002
ρG	0.44	0.26	0.145	0.02	0.0003
ρE	0.55	0.21	0.094	0.01	0.0001

correlation estimates are biased, and it is more likely that the **ρG** and **ρE** are actually very similar to one another.

Correlations drop precipitously for all three matrices in Model 3 (all < 0.001; Fig. 5.4). This is mainly due to a contraction of the range of values (Fig. 5.5), suggesting that the strength of inter-trait association is strongly influenced by cranial size variation. Growth of the rostrum, especially during later ontogeny (see *2.4.5 Craniofacial Growth in Papionin Skulls*), is a primary driving force of allometric change in baboon crania. As I suggested in the preceding chapter, correcting for cranial size using PC1 likely preferentially removed variation in the midface. If baboon craniofacial variation is influenced substantially by nasal growth, traits in other regions of the cranium must be correlated in some manner with those in the midface. Therefore, removing a disproportionate amount of nasal variation by correcting for PC1 might explain the drastic difference in average r^2 between Models 2 and 3.

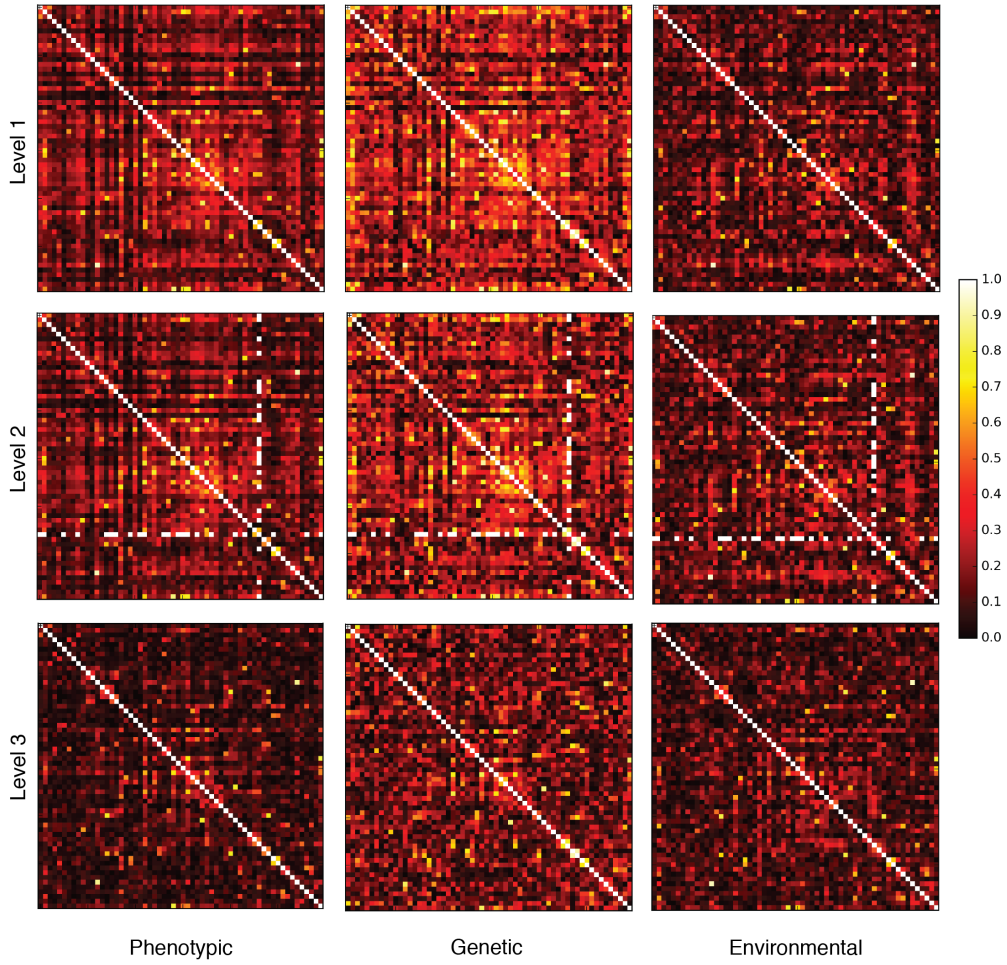

Figure 5.3 Correlation Matrix Heat Maps. For the sake of simplicity, the absolute value of the correlation coefficient was used for plotting. Black is $\rho = 0$ and white is $\rho = 1$. Columns depict the types of correlations (phenotypic, genetic, and environmental) and rows depict the analysis models (overall, cranial, and regional). Two major trends are apparent. First, there is a general impression that the middle column (**ρG**) is lighter and, thus, has higher correlations. This is a statistical artifact and is discussed more in the text. Second, the heat maps get darker from top to bottom, indicating correlations become weaker as allometric variation is removed.

5.3.1 Morphological Integration

The morphological integration results shown in Table 5.2 also demonstrate an interesting pattern in nasal variation. I compared the relative strength of correlations within proposed modules to that of correlations among all other traits in the cranium. For example, the average

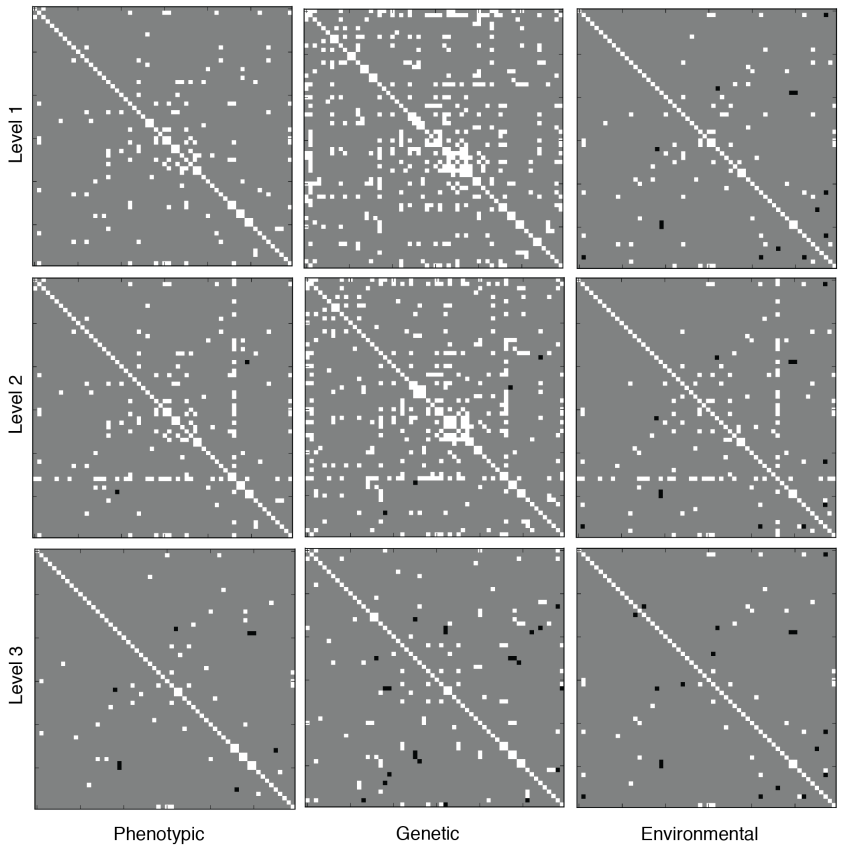

Figure 5.4 Grayscale Correlation Matrix Heat Maps. To illustrate general trends between levels of analysis and types of correlation, all correlation coefficients were rounded so that black is $\rho = -1$, gray is $\rho = 0$, and white is $\rho = 1$. This easily demonstrates the general decrease in correlatation coefficients as allometric variation is removed (i.e., white squares are filled in with gray or even black). The layout is the same as in Figure 5.3.

ρ_P among all EIDs when both traits are classified as nasal traits was calculated for Model 1 (0.56, N = 8) and compared to the average ρ_P for all other traits (0.17, N = 52). Contrast that to the average ρ_P for oral traits (0.21, N = 7) relative to all others (0.18, N = 53). The average correlation among EIDs in the nasal region is, by far, the largest of any region. The orbit and zygomatic arch demonstrate higher degrees of correlation among their constituent elements, too. This suggests that rostral shape variation (mostly length as most traits are in the sagittal plane) is more highly integrated than that in the rest of the cranium. Genetic correlations are

generally largest, phenotypic correlations smallest, and environmental correlations are in between but much more similar to ρ_P. These average correlations are virtually identical in Models 1 and 2 but disappear in Model 3 in all but the traits in the anterior half of the cranium, including nasal, orbital, zygomatic, and anterior cranial vault regions (Fig. 5.6).

This differential pattern in distribution of correlations from the ventral to the dorsal aspects of the cranium is unexpected. Cheverud (1996) found evidence for integration among traits characterizing the cranial vault as a whole (i.e., those within both my anterior and posterior cranial vault regions) and among those of the cranial base (i.e., my anterior and posterior cranial base regions) in tamarins, which he had predicted based on the difference in developmental origin of the vault and base. This discovery is mirrored in other New World monkeys (Marroig and Cheverud, 2001) and macaques (Cheverud, 1982). In contrast, I found that correlations within these modules fit a model in which both were divided into anterior and posterior halves

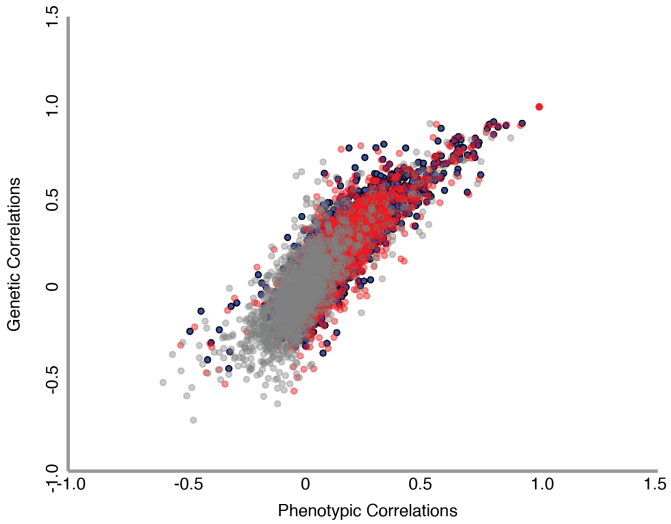

Figure 5.5 Scatterplot of Genetic Correlations on Phenotypic Correlations. The range of both genetic and phenotypic correlations is reduced between Models 1 (blue filled circles) and 2 (red filled circles) relative to Model 3 (gray filled circles). This demonstrates that craniofacial variation is greatly affected by patterns of both phenotypic and genetic integration with cranial size variation, which was removed in Model 3.

Table 5.2 Morphological Integration in the Baboon Cranium. Average correlation among trait pairs within a single developmental/functional region compared to that for all other traits not in that region (provided in parentheses).

Region[a]	Phenotypic	Genetic	Environmental
Model 1			
Nasal	0.56 (0.18)	0.65 (0.25)	0.41 (0.10)
Oral	0.21 (0.18)	0.34 (0.25)	0.09 (0.10)
Orbital	0.39 (0.18)	0.48 (0.25)	0.25 (0.10)
Zygomatic	0.38 (0.18)	0.48 (0.25)	0.32 (0.10)
ACB	0.17 (0.18)	0.28 (0.25)	0.09 (0.10)
PCB	0.19 (0.18)	0.32 (0.25)	0.02 (0.10)
Base[b]	0.15 (0.19)	0.22 (0.26)	0.07 (0.11)
AV	0.24 (0.18)	0.33 (0.25)	0.16 (0.10)
PV	0.20 (0.18)	0.26 (0.25)	0.17 (0.10)
Vault[b]	0.14 (0.19)	0.20 (0.27)	0.09 (0.10)
Model 2			
Nasal	0.55 (0.17)	0.62 (0.21)	0.45 (0.11)
Oral	0.21 (0.17)	0.32 (0.22)	0.14 (0.12)
Orbital	0.38 (0.17)	0.46 (0.22)	0.26 (0.11)
Zygomatic	0.36 (0.17)	0.44 (0.22)	0.31 (0.11)
ACB	0.16 (0.17)	0.24 (0.22)	0.09 (0.12)
PCB	0.18 (0.17)	0.31 (0.22)	0.01 (0.12)
Base[b]	0.14 (0.18)	0.19 (0.23)	0.08 (0.13)
AV	0.24 (0.17)	0.31 (0.22)	0.17 (0.12)
PV	0.17 (0.17)	0.20 (0.22)	0.15 (0.12)
Vault[b]	0.13 (0.18)	0.16 (0.23)	0.10 (0.12)
Model 3			
Nasal	0.32 (-0.01)	0.32 (0)	0.33 (-0.01)
Oral	0.01 (0)	0.07 (0)	-0.01 (0)
Orbital	0.17 (0)	0.20 (0)	0.15 (-0.01)
Zygomatic	0.20 (0)	0.29 (0)	0.16 (0)
ACB	0.07 (0)	0.15 (0)	0.01 (0)
PCB	0.11 (0)	0.21 (0)	0 (0)
Base[b]	0 (0)	0.01 (0)	0 (0)
AV	0.21 (0)	0.28 (0)	0.16 (0)
PV	0.06 (0)	0.06 (0)	0.06 (0)
Vault[b]	0.01 (0)	0.01 (0)	0.01 (-0.01)

[a]Regional abbreviations: anterior cranial base (ACB), posterior cranial base (PCB), anterior vault (AV), posterior vault (PV). [b]ACB and PCB EIDs were combined to form the "Base" and AV and PV traits were combined to form the "Vault."

better than if each module was considered as a whole (see Table 5.2). In fact, the only groupings for which correlations among every other trait were higher than for within the group were the base and the vault when each was considered as a whole. It may be that the influence

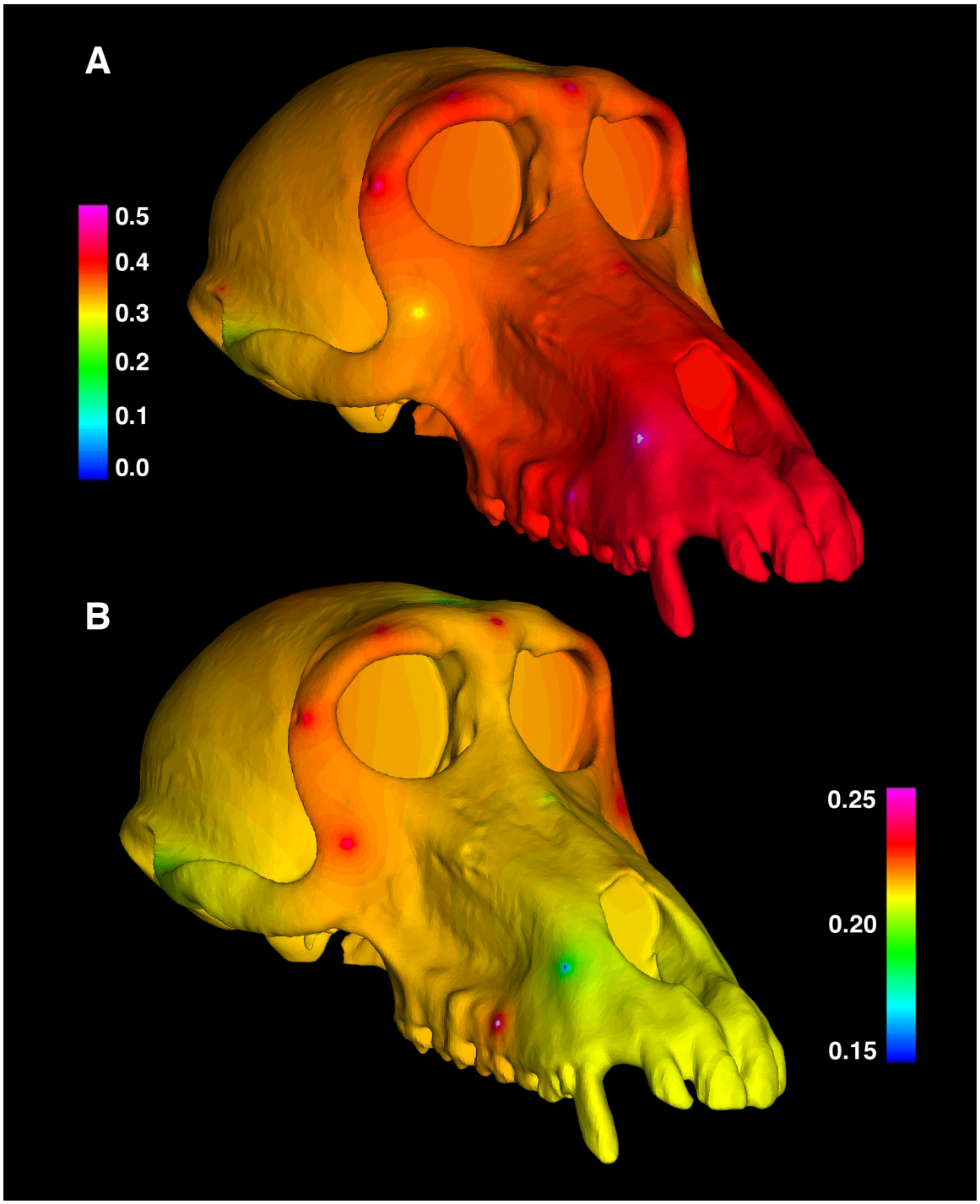

Figure 5.6 Heuristic Depiction of Morphological Integration in Baboon Crania. Heat maps have been reflected onto volume renderings of CT scans to show the differential distribution of genetic correlation coefficients throughout baboon crania (Model 1, panel A) and the change in those patterns that result from removing body size variation and cranial size variation (Model 3, panel B). Note that the color scales are different in the two panels.

of midfacial variation on neighboring regions acts on a gradient that has contributed to a partial disassociation of the ventral from the dorsal aspects of the cranium.

The results of Mantel's Test between **ρP** and three different connectivity matrices (**D**, $\mathbf{F_g}$, and $\mathbf{F_s}$) that were designed to reflect expected relationships among traits based on developmental and functional interactions echo the results discussed above (Table 5.3). Correlation estimates (r_M) are nearly identical in Models 1 and 2 but correcting for cranial size variation destroys those patterns in relation to developmental (r_M = 0.06) and general functional (r_M = 0.17) expectations. However, r_M estimated for the correlation of **ρP** with $\mathbf{F_s}$ is essentially constant from one model to the next. This suggests that, although the pattern of inter-trait association on a large scale is greatly determined by cranial size variation, local patterns are maintained, even after removing the effects of PC1. In fact, it may be that cranial size variation is so influential that it masks regional sources of variation unless accounted for.

Table 5.3 General Patterns of Morphological Integration in Baboon Crania. Mantel's correlation coefficient between **P** and developmental (**D**) and functional (**F**) correlation matrices for three covariate models.

Comparison	Model 1	Model 2	Model 3
ρP vs **D**	0.25	0.23	0.06
ρP vs $\mathbf{F_g}$	0.29	0.26	0.17
ρP vs $\mathbf{F_s}$	0.32	0.28	0.26

5.3.2 The GP-Map

One of the more exciting aspects of being able to estimate **ρP**, **ρG**, and **ρE** from the same sample is the opportunity to interrogate how genotype maps to phenotype by comparing correlation patterns (Table 5.4). All Mantel's test results are statistically significant at the 0.001 level. **ρP** and **ρG** correlations are high for all three models, suggesting that phenotypic and genetic variation follow similar patterns across the cranium. The same is true of correlations

Table 5.4 Matrix Comparison of Correlations Among ρG, ρP, and ρE. Observed correlations were produced with a Mantel's test and theoretical maxima by incorporating estimates of each matrix's repeatability.

Comparison	Observed Correlation	Theoretical Maximum
Model 1		
ρP vs. **ρG**	0.83	0.66
ρP vs. **ρE**	0.68	0.54
ρG vs. **ρE**	0.34	-0.01
Model 2		
ρP vs. **ρG**	0.83	0.65
ρP vs. **ρE**	0.79	0.59
ρG vs. **ρE**	0.49	0.03
Model 3		
ρP vs. **ρG**	0.65	0.61
ρP vs. **ρE**	0.71	0.53
ρG vs. **ρE**	0.34	-0.01

between **ρP** and **ρE**, while the correlations between **ρG** and **ρE** are substantially less than expected based on their negative error correlation. The correlations among matrices remain largely constant from Model 1 to 2 but the correlation between **ρP** and **ρG** drops in Model 3. This means that the relationship describing how genetic correlations among traits manifest as phenotypic correlations is altered with the reduction in V_A in Model 3.

5.3.3 Allometry

Finally, the correlation between $\boldsymbol{\rho P}_1$ and $\boldsymbol{\rho P}_2$ = 0.85, that between $\boldsymbol{\rho P}_1$ and $\boldsymbol{\rho P}_3$ = 0.66, and that between $\boldsymbol{\rho P}_2$ and $\boldsymbol{\rho P}_3$ = 0.60. The repeatabilities of these matrices give the maximum r_M that can be realized when comparing them, so r_M should be should be compared to t_i. For all three correlations, the maximum is 0.99 (i.e., 1), which means that they can be judged relative to one another, and the decrease in r_M from Models 1-3 is meaningful. This suggests that removing allometric variation in the additional models alters the pattern of phenotypic correlation among traits.

The hierarchical cluster analysis performed on **ρP** supports this result (Fig. 5.7). The correlation estimates in Model 1 cluster into six main groups, reflecting the somewhat modular structure of the cranium. However, that structure breaks down in Models 2 and 3, indicating that correlations within modules are largely the result of allometric variation. In other words, traits located within the same module tend to respond to the effects of allometry in a similar manner.

5.4 Discussion

Matrix repeatability is high, but it does limit the maximum observable matrix correlations. Consequently, r_M must be evaluated in relation to these maxima. Doing so indicates that measures of phenotypic variation and covariation provide some insight into the genetic relationships among traits as well, the estimation of which is much more laborious and often not possible for a given population. This result has now been demonstrated in multiple primate taxa, both platyrrhines and catarrhines (e.g., Cheverud, 1982, 1995), and adds to our understanding of craniofacial variation within our order as a whole. If this pattern is taken as the expectation for primates, any significant deviation from this pattern merits explanation.

Although the overall *patterns* of phenotypic correlation among traits are congruent with expectations based on functional and developmental relationships, the *strength* of these patterns is somewhat contrary to what might be expected based on the hypothesis that cranial regions that develop earlier, such as the cranial base, should demonstrate higher levels of phenotypic integration than regions that grow for longer periods of time or later during ontogeny, such as the face. However, I found that the magnitude of $\bar{\rho}_P$ was highest in the rostrum, which continues growth late into adolescence and early adulthood. However, the regions with the second highest $\bar{\rho}_P$ are the orbits, which grow early under the influence of neural growth, and the zygomatic arches, which are subjected to the strains of masticatory loading. Consequently, both of the regions would be expected to have high degrees of intra-trait correlation.

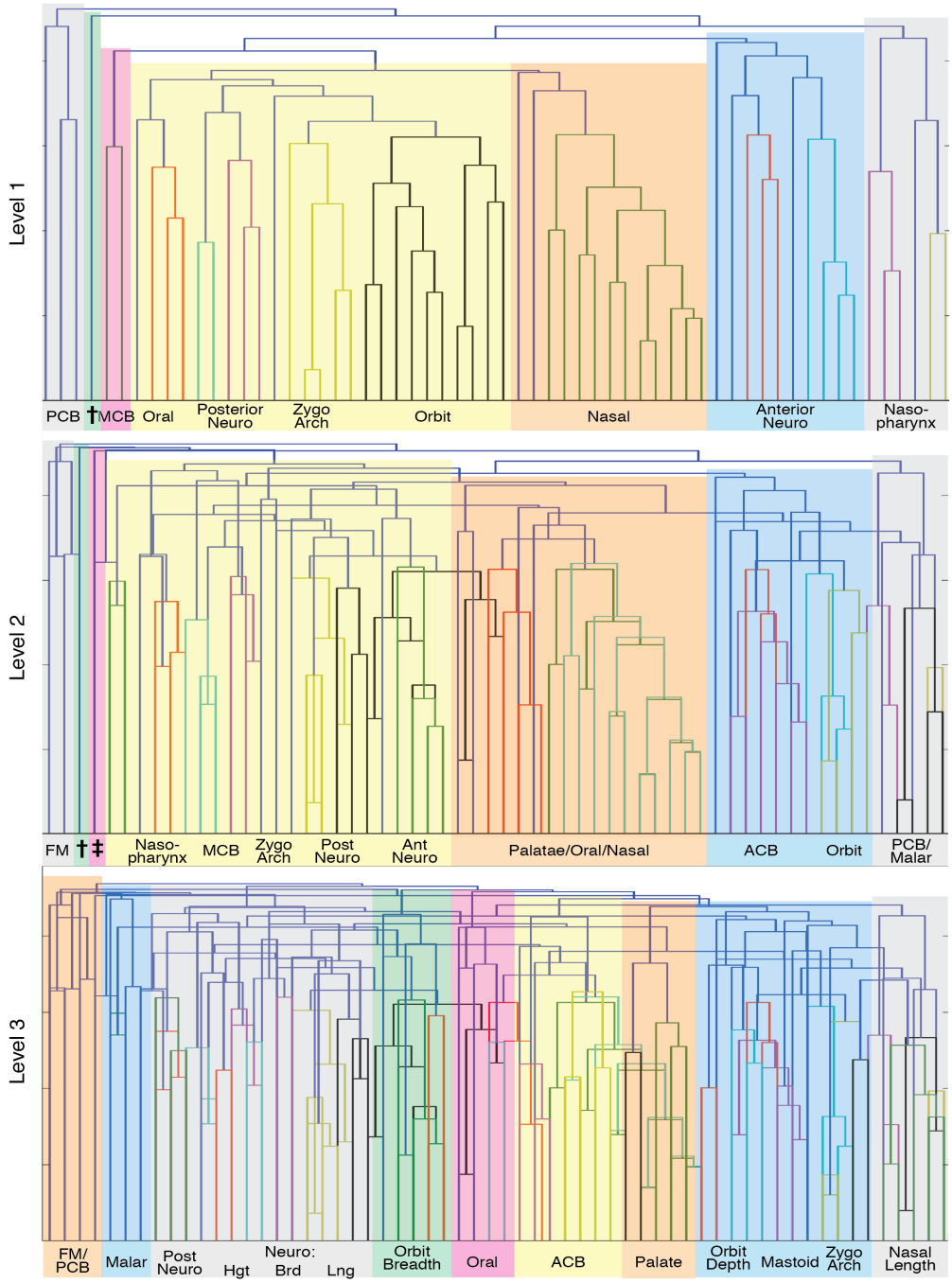

Figure 5.7 Comparison of ρP-Matrix Dendrograms. UPGMA hierarchical clustering was performed on **ρP** for Models 1-3 to compare the effect of correcting for different covariates on the phenotypic correlation pattern. Branches are color-coded to group EIDs with similar ρ_P estimates and transparent colored boxes enclose relatively distinct nodes and included branches. Abbreviations: *ACB*, anterior cranial base; *brd*, breadth; *FM*, foramen magnum; *hgt*, height; *lng*, length; *MCB*, middle cranial base; *neuro*, neurocranium; *PCB*, posterior cranial base; †, CACP; ‡, STST. See text for corresponding cophenetic correlation coefficients.

Due to the change in patterns of integration between Models 2 and 3, in addition to the change in how genetic correlations manifest as phenotypic correlations, any results from morphological integration studies will be highly dependent on the methods used to analyze morphological data. Systemic differences in the manner in which phenotypic variation is treated prior to analysis in the use of traditional interlandmark distances versus geometric morphometric landmark configurations alter the associations among traits, which can lead to a difference in interpretation, even if the data are collected from the same individuals.

5.5 Conclusion

These results should be considered in conjunction with those of the next chapter, which presents the results of linkage mapping to identify quantitative trait loci. Both analyses endeavor to explicate how genetic variation manifests as phenotypic variation in the baboon cranium. Here I have examined patterns pertaining to the net effect of additive genetic and environmental variation in producing morphological variation. Next, I partition that genetic variation and localize it to regions of the baboon genome (QTLs). Although individual QTL effects cannot be estimated with the data analyzed in this dissertation, the goal is to examine general trends in the structure of that genetic variation and its distribution across the genome.

CHAPTER SIX
RESULTS: LINKAGE MAPPING

6.1 Introduction

After establishing the heritability of a trait (see Chapter 4), it is possible to identify the location of the genetic variants that contribute to its phenotypic variance (V_P). These genetic variants can be identified because they are co-inherited with genetic markers, or chromosomal segments that vary in a population and contain information about patterns of relatedness among individuals. When the pattern of co-segregation is examined at the level of pedigrees, it is called linkage analysis, while association analyses study such patterns at the population level (Falconer and Mackay, 1996). These are complementary methods with one goal: to implicate a particular locus in the generation of V_P (or the etiology of a disease in the case of biomedical research) by demonstrating that the same locus is associated with the trait of interest. Regions of the genome that demonstrate evidence for such co-segregation are called quantitative trait loci (QTLs).

Drosophila geneticists in the early 20th-century established the foundations for the analysis of co-segregation within families. In 1911 Thomas Hunt Morgan proposed the mechanism by which Mendel's Law of Independent Assortment is sometimes violated: genes located close together on the same chromosome are often not randomly sorted into gametes (Borecki and Suarez, 2001). A few years earlier, Frans Janssens empirically demonstrated that one set of an individual's paired chromosomes "crosses-over" while the other does not, resulting in one chromosome that faithfully replicates that of the parent and one that is a novel recombination thereof (Koszul et al., 2012). Alfred Sturtevant combined these two important ideas in 1913 to produce the very first genetic map (described in Borecki and Suarez, 2001) and Fernandus Payne (1918) conducted the first linkage mapping analysis a few years later. Increased computational capabilities and the development of resources for organisms other than fruitflies in the intervening century has allowed us to extend the usefulness of linkage

mapping (e.g., Blangero and Almasy, 1997 and Rogers et al., 2000 in the case of baboons), but the basic premise as I apply it in this chapter to the analysis of baboon craniofacial variation remains the same.

The power of a research design to identify QTLs is a function of the trait's genetic architecture (especially the amount of heritable variation), sample characteristics (its size and the nature of relations among individuals), the QTL's effect size (its heritability), and the nature of the genetic markers used (their number, distribution, and degree of variability in the sample; Rogers et al., 1999). Analytical methods are currently such that we can expect to locate QTLs that are responsible for 10-15% of a trait's V_P in samples of humans and non-human primates (Williams and Blangero, 1999) and for < 5% in model organisms (see *2.2.3 Model Organisms in Craniofacial Research*). As complex traits like the craniofacial skeleton are expected to be the result of variation in many genes of small effect (i.e., polygeny), or a few genes of moderate effect (i.e., oligogeny), as well as the contribution of environmental effects, I can expect to explain only a portion—the oligogenic portion—of the phenotypic variation I measured in my sample of baboon crania.

6.1.1 Research Questions

This chapter presents the methods used to identify QTLs for baboon craniofacial variation and to create lists of positional candidate genes for future research. Specific questions addressed include: (1) Where in the baboon genome is there evidence for genetic variation contributing to variation in craniofacial dimensions? (2) Are linkage signals distributed throughout the baboon genome or clustered in specific regions? (3) Do individual traits have many QTLs, and does the region of the cranium in which a trait is located affect the number of QTLs that map to it? (4) Does controlling for allometric variation change the number of QTLs for a trait? (5) Is there evidence for pleiotropy in baboon craniofacial variation?

6.2 Materials and Methods

The data used in this chapter consist of 60 Euclidean interlandmark distances (EIDs), endocranial volume (ECV), the baboon genetic map, multipoint and two-point linkage files (see below), and the pedigree of Southwest National Primate Research Center (SNPRC) baboons (see Chapter 3 for more detailed descriptions of the traits used and the genetic map).

6.2.1 Linkage Mapping

I identified relevant QTLs for each EID and for ECV in SOLAR using maximum likelihood variance decomposition (MLVD) for complex pedigrees (Almasy et al., 1996). This method estimates the proportion of genetic variance (V_G) attributable to genetic variation around a marker (short tandem repeats, STR) as a function of expected covariance ($\boldsymbol{\Omega}$) among relatives based on the degree of relatedness:

$$\boldsymbol{\Omega} = \sum_{i=1}^{n} \widehat{\boldsymbol{\Pi}}_i \sigma_{qi}^2 + 2\boldsymbol{\Phi}\sigma_g^2 + \mathbf{I}\boldsymbol{\sigma_e^2} \quad (6.1)$$

where $\widehat{\boldsymbol{\Pi}}_i$ is a matrix with elements (π_{ijk}) that indicate the predicted proportion of genes shared IBD (π) between two individuals (j and k) at the i-th QTL (i = 1 to n) linked to an STR marker locus, σ_{qi}^2 is the additive genetic variance due to the i-th QTL, $\boldsymbol{\Phi}$ is the kinship matrix derived from the pedigree, σ_g^2 is the additive genetic variance contributed by unspecified loci in the genome (i.e., not the QTL in question), $\mathbf{I}$ is an identity matrix, and σ_e^2 is the environmental variance (Almasy and Blangero, 1998; Lynch and Walsh, 1998).

- The expected phenotypic covariances among relatives contained in $\boldsymbol{\Omega}$ are calculated as in Equation 4.2. MLVD assumes that that the phenotype (y_j) of each individual (j) is given by the equation:

$$y_i = \mu + \sum_{i=1}^{n} q_{ji} + \hat{\beta} x_j + g_j + e_j \quad (6.2)$$

where μ is the grand trait mean, q_{ji} is the effect of each QTL, $\hat{\beta}$ is a vector of estimated regression coefficients (see *4.3.1 Covariate effects*) associated with the vector (x) of covariate values, g is the additive polygenic effect (i.e., effects of other, unspecified genetic variants), and e is the residual.

- $\widehat{\mathbf{\Pi}}_i$ is a function of the IBD probability matrix ($\mathbf{\Pi}_m$) at each STR marker, and the correlation between the proportion of alleles IBD (π) at the marker (m) and at the QTL (q): $\rho(\pi_m \pi_q)$. A locus with a significant signal is not assumed to be the exact location of the genetic variant contributing to the observed phenotypic variance. Rather, the responsible genetic variant is located close enough to be linked to the location of the signal, i.e., the two tend to be inherited together (co-segregate).

  For every one of the 384 STR markers there is an estimated $\mathbf{\Pi}_m$ (these are called two-point linkage files, see *6.2.1 Linkage Mapping*). There are also multipoint linkage files, which provide a $\mathbf{\Pi}_m$ at every 1 cM along the genetic map. Genotypes for every individual were directly assayed only at each of the 384 STR markers (which are spaced an average of 7.2 cM apart, see *3.2.1 Baboon Genetic Map*), but genotypes were imputed in between markers based on the probability of a crossover event (1% per cM), the genotypes at the two flanking markers, and the pedigree structure.

  Locating QTLs using the two-point linkage files (twopoint mapping) provides a very general idea of what is going on in the genome, while the picture depicted using the multipoint linkage files (multipoint mapping) is much more nuanced. Markers are sometimes far apart, and it is impossible to determine the exact peak of a QTL that falls between two markers when using two-point linkage files. Mapping with the imputed genotype scores between markers typically reduces the area to target in follow-up

analyses. This is easiest to observe by comparing a plot of two-point mapping results to those of multipoint mapping using the same phenotype (Fig. 6.1).

- σ_{qi}^2 and σ_g^2 sum to h^2_r, which was estimated according to the methods described in Chapter 4. Essentially σ_g^2 is the portion of h^2_r that remains after accounting for the effects of a specific QTL. Typically, the likelihood of Equation 6.1 is first maximized with a single σ_{qi}^2 term, but additional models can be maximized that allow for multiple QTLs. In most cases, the simplest model (only a σ_{q1}^2 term) is the most appropriate. However, occasionally two loci in close proximity yield significant results. In such a scenario, a second QTL is included in the model (a σ_{q2}^2 term is added). If the model with 2 QTLs does not significantly improve the fit of the model, the second "peak" is deemed an artifact of the primary QTL. If the model with two σ_{qi}^2 terms is a better fit, both QTLs are retained. Another way to think about σ_{qi}^2 is as the population variance of g_{ji} from Equation 6.2. The proportion of V_P contributed by each QTL (h^2_{qi}) can be calculated as:

$$h_{qi}^2 = \sigma_{qi}^2(1 - h_{cv}^2) \quad (6.3)$$

  where (1 - h_{cv}^2) is the proportion of V_P that remains after accounting for covariate effects (see *4.3.1 Covariate Effects*).
- The matrices $\mathbf{\Phi}$ and $\mathbf{I}$, as well as σ_e^2, are calculated as described in *4.2.1 Quantitative Genetic Parameter Estimation in SOLAR*.

As in heritability estimation (see Chapter 4), three analyses were conducted for ECV and every EID: Model 1 (Overall), in which only age, sex, age*sex, age^2, and age^2*sex were potential covariates; Model 2 (Cranial), in which body weight (kg; see *3.3.4 Adult Body Weight*) was added as a potential covariate; and Model 3 (Regional), in which the standardized first principal component (PC1) of the correlation matrix between all EIDs (see *3.3.5 Measures of Cranial*

Size) was also added as a potential covariate. The covariates deemed significant for each trait (see *4.3.1 Covariate Effects*) were included in the linkage mapping conducted in this chapter.

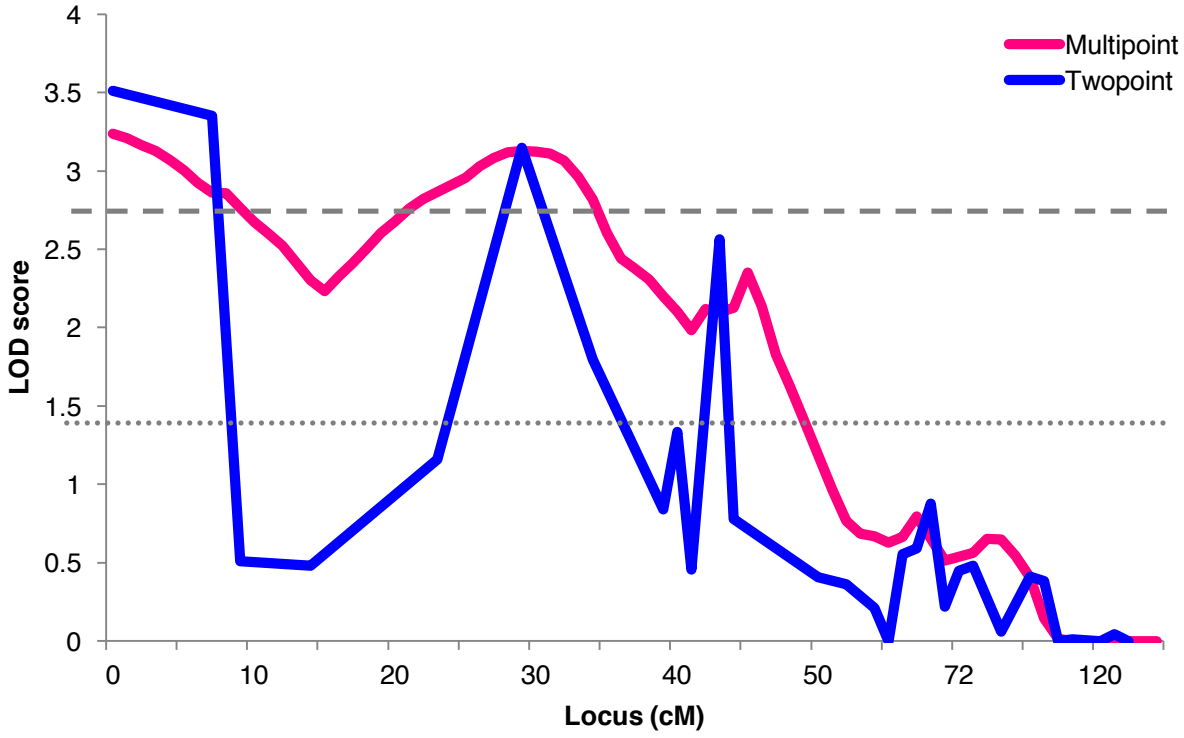

Figure 6.1 Twopoint vs. Multipoint Linkage Mapping. Comparison of linkage mapping results for PLSY (Model 3) on HSA6 using only STR marker genotypes (blue line) and using genotypes imputed every 5 cM (pink line). The horizontal dotted line delineates the $P < 0.10$ threshold and the dashed line $P < 0.05$.

Multipoint

When conducting multipoint linkage analyses in SOLAR, every trait is assumed to be multivariate normal. Blangero (1995) demonstrated that likelihood estimates of variance component effect sizes are robust to violations of this assumption. In addition, I used standardized trait values (see *3.3.1 Data Collected from Dry Crania*) to help meet distributional assumptions, so my analyses should yield consistent parameter estimates. The likelihood of the parameters $(\mu, \hat{\beta}, \sigma_{qi}^2, \sigma_g^2, \sigma_e^2)$ given the vectors of individual-trait values (y_i) and the matrix of covariates $(\boldsymbol{X})$ is maximized in SOLAR. Two models are fit: a null model that is restricted to

assuming there is not a QTL contributing to V_P linked to locus i (i.e., $\sigma^2_{qi} = 0$) and a model that acknowledges the potential for such a linkage (i.e., σ^2_{qi} is estimated). The $\log_{10}$ likelihood of the two models is then compared with a likelihood ratio test and a likelihood of odds (LOD) score (Morton, 1955) is calculated:

$$\text{LOD}_i = \log_{10}\left[\frac{\max l_r(\mathbf{z})}{\max l(\mathbf{z},c)}\right] \quad (6.4)$$

where $\max l_r(\mathbf{z})$ is the maximum of the likelihood of the null model and $\max l(\mathbf{z}, c)$ the maximum of the likelihood function given a QTL at i (Lynch and Walsh, 1998).

Model fitting is repeated sequentially across the genome at a set interval (calculating the LOD once at each locus is termed a pass, and the entire process of conducting multiple passes to determine the locations of all QTLs is called a scan). In the first pass, a LOD score is calculated every 5 cM (i.e., using $\mathbf{\Pi}_o, \mathbf{\Pi}_5, \mathbf{\Pi}_{10}$, etc.), and if the LOD passes a designated threshold, a second pass is performed every 1 cM around a potential peak. The program's default sets that threshold to LOD ≥ 0.588. However, as a compromise between thoroughness and efficiency (one scan for one trait takes ~16 hours) I chose LOD ≥ 1.0. If the LOD at a locus was greater than a predetermined cut-off (similar to the use of $\alpha = 0.05$ in traditional null hypothesis significance testing), I considered this to be evidence for linkage.

LOD scores were originally used by Morton (1955) to assess the likelihood of obtaining the observed data (y_i and $\boldsymbol{X}$) if the locus in question is linked to a QTL as compared to the likelihood of obtaining the data purely by chance. Larger LOD scores favor the presence of linkage. For example, LOD = 3.0 indicates that there is a 1000:1 chance that the results are not due to chance, i.e., there is likely a QTL present. In traditional linkage analyses, significance is arbitrarily set at LOD ≥ 3.0. However, when using sequential MLVD in complex pedigrees, this criterion is overly conservative (Blangero and Almasy, 1997). Instead, Sherwood et al. (2008)

used extensive simulations to establish genome-wide thresholds for evidence of significant linkage (LOD ≥ 2.75, $P = 0.05$) and suggestive linkage (LOD ≥ 1.53, $P = 0.10$).

Multi-QTL

In a few cases, two or more loci in close proximity have LOD ≥ 1.53. Such a result indicates one of three things. First, it is possible that there are adjacent genetic variants, both of which contribute to the V_P, but I lack the power to resolve the single, larger QTL into two or more smaller, linked QTL. For example, Palleres et al. (2014) localized 8 SNPs accounting for 1.5% of V_P in mouse crania (26 SNPs total were identified and accounted for a total of 12.6% of the V_P) to a region of mouse (MMU) chromosome 8, which is syntenic to HSA16. In this QTL they identified 19 candidate genes; all other QTL had <5 candidate genes. They hypothesized that this region of HSA16 could be a hotspot for genes affecting craniofacial variation in mammals. Second, a genetic variant is located in the center of a large QTL (between the two "peaks"), but none of the intervening markers are informative and so there is a dearth of linkage information in that portion of the genome. Finally, it is possible that one of the multiple additional peaks is a false positive. Without additional analysis, such as fine-mapping using single nucleotide polymorphism (SNP) markers, it is impossible to distinguish between these three scenarios.

In these situations, it was necessary to conduct a second pass of the chromosome on which the potential QTLs were identified. In such cases, an additional model was maximized in which the QTL with highest LOD is fixed in the model (σ^2_{q1}) and a second QTL-specific additive genetic variance term (σ^2_{q2}) is estimated conditional on the value of the first such term. This reduces the appearance of false positives because it more accurately estimates effect sizes and maximizes the signal-to-noise ratio of true linkage. In other words, multi-QTL models help eliminate false linkage.

Two-point

An important thing to keep in mind is that genetic maps only span a portion of each chromosome. 0 cM on a genetic map represents the genomic locus of the first marker used, and the genetic map ends at the location of the last marker used (which is why including more markers, especially in those proximal and distal regions, can increase the length of the genetic map, even though the physical size of the chromosome is not altered). 0 cM does not correspond to 0 basepair (bp), the most proximal bp of the chromosome. As a consequence, there is a portion of every chromosome (typically composed largely of the telomeres) that is not included in the genetic map. Depending on the location of the genetic map's first and last markers on that chromosome, this portion can be very large. Because there is no linkage information past the ends of the genetic map, there is no evidence for (or against) the presence of a QTL. Although a functional genetic variant may, indeed, exist toward the ends of the chromosome, there is no way to localize what or where the peak multipoint-LOD score is. In some cases, an increase in LOD scores toward the beginning or end of the genetic map may be a spurious result simply as a consequence of the reduced information present in the region.

One way to gain additional information about whether such a pattern is spurious is to examine two-point LOD scores in the region. Although multipoint mapping is more efficient at detecting linkage (Ashton and Wilson, 1986), two-point linkage scores will be locus-specific and so will provide evidence for linkage to a specific marker (sometimes markers are located in-between two adjacent cMs so that the multipoint scan will not test direct linkage to a marker). If the pattern of LOD scores toward the most telomeric ends of the genetic map are similar in both the multipoint and two-point scans, this is evidence that a QTL could exist past the final markers. Given the limitations of modeling genetic effects in these uninformative chromosomal regions, more confidence should be placed in evidence for linkage in the central portions of the

genetic map. Without additional information, such as the inclusion of additional markers or fine-mapping with SNP markers, I would be cautiously optimistic about such results.

The amount of data is reduced with two-point mapping. Depending on the number of markers genotyped on a chromosome, there may actually be very few linkage models maximized relative to the number maximized in a multipoint scan, which is based on the total length of the chromosome's genetic map. For example, the genetic map of human chromosome (HSA) 9, which is orthologous to baboon chromosome/PHA 15) is 136 cM long, so 27 multipoint linkage models will be maximized if the interval selected is every 5 cM. However, there are only 13 STR markers on HSA9. In contrast, HSA8 (PHA8) is 138 cM long, so 27 multipoint linkage models will also be maximized, but it has 20 STR markers.

Pleiotropy

Finally, one of the exciting advantages of using SOLAR to implement sequential linkage scans is that models can be extended to include a pleiotropy term (see Fig. 2.14, Panel A2). To test whether two traits share a QTL, a model including both traits is maximized and a QTL-specific genetic correlation (ρ_Q) is estimated. Significance of ρ_Q is determined by comparing the $\log_{10}$ likelihood of a model in which $\rho_Q = 0$ to that of a model where ρ_Q is estimated. If the latter model is a better fit, this is evidence that a single QTL contributes to V_P of both traits. Otherwise, the more likely explanation is coincident linkage due to two or more closely located genetic variants.

Additionally, a matrix of estimated ρ_Q terms (**Q**) can be constructed and compared to a corresponding matrix for phenotypic (ρ_P) and genetic (ρ_G) correlations: the **P** and **G** matrices, respectively. Matrix correlations are calculated, and associated significance values are simulated using a Mantel test, as was done for the **P**, **G**, **F**, **D**, and **E** matrices in Chapter 4. I used the R package "ade4" to conduct Mantel tests between matrices.

Unfortunately, this is an incredibly computationally intense analysis as pairwise scans of all traits mapping to the same QTL must be conducted and each scan takes ~20 hours. As assessing the entire pleiotropic profile of baboon craniofacial variation is not a goal of this dissertation, a single locus was randomly selected and evaluated for the presence of pleiotropy. This will demonstrate whether pleiotropy is a general feature of the GP-map I aim to construct in this dissertation. I summarize the results of the single pleiotropy test below, but a full profile of the pleiotropic effects baboon craniofacial will be addressed in a subsequent publication.

6.2.2 Candidate Gene Determination and Prioritization

The order of operations for these analyses are: (1) conduct one multipoint linkage scan for each trait; (2) if applicable, conduct an additional twopoint or multi-QTL scan; (3) assess pleiotropy and construct support intervals for each QTL; (4) determine the physical positions of the proximal and distal extents of each QTL; (5) assess the relevance of each annotated gene within the QTL support interval for the trait in question; and (6) construct a list of candidate genes. I have described the methods for accomplishing the first two operations and will now discuss the remaining ones.

Constructing QTL support intervals (SIs)

A QTL "peak" is identified in a linkage scan as the locus with the locally highest LOD. To establish an SI around this peak that roughly corresponds to a typical 95% confidence interval constructed from the sample size and standard deviation of a statistical parameter, a 1-LOD drop is established (Lander and Botstein, 1989). This means the proximal locus with LOD = $LOD_{peak} - 1$ and the distal locus with LOD = $LOD_{peak} + 1$ is identified. For example, if the LOD score at locus 95 cM on PHA5 is 2.86, this would be significant evidence for the presence of a genetic variant affecting the phenotype of interest in the vicinity of 95 cM. The proximal confidence limit of the QTL would be at the first locus with LOD ≤ 1.86 (say at 61 cM) and the

distal one would be the corresponding locus distal to the peak (say at 120 cM). The result would be a 59 cM-wide QTL with a peak at 95 cM.

In cases where multiple traits map to loci within 20 cM of each other on the same chromosome, tests for pleiotropy were conducted according to a modification of the procedure performed by Cheverud (2001):

1. Calculate a weight (ω_i) for the i-th trait from the LOD at its individual peak locus (LOD_i):

$$\omega_i = \frac{\mathrm{LOD}_i}{\sum_{i=1}^{n} \mathrm{LOD}_i} \tag{6.5}$$

2. Sum the weighted individual peak loci (cM_i) to obtain the pleiotropic peak (cM_P):

$$cM_P = \sum_{i=1}^{n} cM_i * \omega_i \tag{6.6}$$

3. Determine the LOD score of each trait at the pleiotropic peak (LOD_{Pi}) and use the difference between that LOD score and the LOD score of the trait at its local peak to calculate a chi-square statistic with degrees of freedom (df) equal to the number of traits minus one:

$$\chi^2 = \sum_{i=1}^{n} \mathrm{LOD}_i - \mathrm{LOD}_{Pi} \tag{6.7}$$

A χ^2 < the critical value (CV_{df}) fails to reject the null hypothesis that the traits are affected by a single pleiotropic QTL, rather than individual single-trait QTLs.

Translating Genetic Map into Physical Map Positions

Once the limits of each QTL have been established according to the 1-LOD drop convention, the proximal and distal markers that flank the QTL must be identified. Those genetic map markers closest to the cM that defines the extent of the QTL are selected. Often the closest marker falls within the SI. In these cases, the first marker beyond the SI is selected. This is an extremely conservative practice that ensures the genetic variant responsible for the signal is

contained within the QTL limits. Using the example from the preceding section of a QTL at PHA5 95 cM, the closest proximal marker to 61 cM is D4S3248 at 60.7 cM and the closest distal marker is D4S2374 at 122.9 cM. Therefore, these two markers would define the extent of this QTL.

Because most of the baboon genetic map markers originate from the human genome, their physical positions can be determined by searching the marker name in the UCSC Genome Browser (https://genome.ucsc.edu/; Appendix A, Table A1). Returning to our hypothetical QTL from the previous paragraph, PHA5 is orthologous to HSA4. The proximal marker, D4S3248, is 200,346 bp long and starts at bp 59,055,737 on HSA4 while the distal one, D4S2374, is 200,292 bp long and ends at bp 178,235,115. Therefore, a genetic variant at any point in this 119 megabase (Mb) interval could be the one contributing to population-level variation in the phenotype. The genetic variant(s) could be a point mutation (single nucleotide polymorphim, SNP), an insertion-deletion mutation (indel), or even a larger structural change like copy-number variation (CNV) or an inversion. In the case of STR markers that were unable to be located in the UCSC Genome Browser, the flanking polymerase chain reaction (PCR) primers were queried against the human genome (build GRCh38 released December 2013) using the National Center for Biotechnology Information (NCBI) Basic Local Alignment Search Tool (BLAST; http://blast.ncbi.nlm.nih.gov/Blast.cgi; Appendix A, Table A2). I was unable to localize the markers designed specifically for the baboon genome, so they were omitted and any QTL SI defined by such a marker was widened to include the next closest identifiable marker.

Gene Ontology (GO)

QTLs that contained at least one trait whose LOD passed the stringent threshold (LOD ≥ 2.75) are heretofore called significant QTLs (Sig-QTL). Those with 1.53 ≤ LOD < 2.75 are considered

suggestive (i.e., are significant at α = 0.10). A list of the Refseq genes contained within each such significant QTL was obtained from the NCBI Genome database (http://www.ncbi.nlm.nih.gov/projects/genome/guide/human/index.shtml). Genes identified in other species for which no human ortholog is yet available (i.e., HGNC gene symbols beginning with "LOC"), all open reading frames (i.e., HGNC gene symbols containing "orf"), and all micro-RNAs (i.e., HGNC gene symbols beginning with "MIR") were omitted. The abridged list (“QTL Gene Set,” Q-set) was submitted to the GO Enrichment Analysis tool on the GO Consortium website (http://geneontology.org/), which uses the Protein ANnotation THrough Evolutionary Relationship (PANTHER) classification system (Mi et al., 2012, 2013) and multi-species annotations to describe gene products in terms of their biological processes, cellular components, and molecular functions (Ashburner et al., 2015; The Gene Ontology Consortium, 2015). An enrichment analysis compares the frequency of genes annotated with a specific GO term in the submitted list (the sample frequency) to the frequency of such genes in the entire database (the background frequency). After accounting for multiple testing with a Bonferroni correction, a list of over- and underrepresented GO terms is provided for the gene sample.

Examining enrichment of GO terms will indicate whether there are any patterns in the types of gene products contained within the QTLs. For example, do genomic regions harboring variants related to craniofacial variation encode genes preferentially involved in tissue development or those that code for regulatory elements rather than cellular structural components? An important question regarding morphological evolution is whether change in complex structures is a result of novel gene function or differential regulation of existing gene products (King and Wilson, 1975).

Genes Implicated in Previous Research

Because each QTL often contains hundreds or thousands of genes, regulatory element binding sites, splice sites, etc., additional information is needed to whittle down the list of potential candidates to a manageable size for follow-up analysis. One way to do this is to cross-reference the list of genes contained within a QTL to a list of genes of known function compiled from the literature and/or online databases. I created a list of 317 such genes ("Craniofacial Gene Set," C-set; Table 6.1) from Wilkie and Morriss-Kay (2001), Maga et al. (2015), and the Online Mendelian Inheritance in Man (OMIM; http://www.omim.org) database. Genes from the craniofacial gene set that are also present in QTLs may be more likely to affect craniofacial variation if mutated or up-/down-regulated.

ToppGene Suite

An additional gene list analysis toolkit based on enrichment assessments is the ToppGene Suite (https://toppgene.cchmc.org), a set of four online tools for candidate gene annotation and *in silico* prioritization (Chen et al., 2009). Essentially, the suite is designed to assess the functional annotation profile of a set of known genes ("Training Set", Tr-set) and rank genes within a list of QTL genes ("Test Set", Te-set) by probabilistic similarity to the functional annotation profile, thus prioritizing additional genes that may be good candidates for follow-up analysis (e.g., Maga et al., 2015).

Similar to the GO enrichment analysis, ToppFun categorizes the Tr-set according to a variety of criteria, including involvement in human phenotypes and disease, biological processes, cellular components, and molecular functions. ToppGene then assigns each Te-set gene a series of fuzzy-logic based similarity measures by comparing its functional annotation to that of the training set genes. A composite score is determined from a meta-analysis of the individual similarity measures and a *P*-value calculated from random resampling of the whole

genome. The result is a table that lists Te-set genes by their associated *P*-values. ToppGene analysis is based on functional similarity between Tr- and Te-sets. The last two tools are ToppNet, which is similar to ToppGene but uses protein-protein interaction networks in its analysis rather than functional annotations, and ToppGenet, which includes additional information derived from the protein interactome.

Because I endeavored to prioritize additional positional candidate genes for my craniofacial QTLs, and not to assess their roles in producing morphological variation, I only used ToppFun and ToppGene. As the Tr- and Te-sets must be non-overlapping, the genes common to both C- and Q-sets were omitted from the C-set to produce the Tr-set (Table 6.1). The ToppGene result tables were examined to identify the five most significant genes not already present in the Q-set.

6.3 Results

A large number of QTLs were discovered within each of the three levels of analysis (Models 1-3), most of which explain the expected 10-15% of each trait's V_P (see Williams and Blangero, 1999). Most of these QTLs were merely suggestive ($P < 0.10$), but ~12% were significant. In the following sections, I analyze attributes of the QTLs, such as their gene content and the traits to whose V_P they contribute. I also examine their patterns of distribution throughout the genome, paying particular attention to any overlap among the QTL SIs constructed for multiple traits, as this is indicative of a shared genetic basis. Traits that share a common genetic basis are more likely to evolve together and, therefore, evaluating the degree of pleiotropy among craniofacial traits can help establish hypotheses about correlated evolution in the papionin clade. First, I will apply the linkage mapping results to the research questions I stated at the beginning of this chapter (see *6.1.1 Research Questions*).

6.3.1 Addressing my research questions

Where in the baboon genome is there evidence for genetic variation contributing to variation in craniofacial dimensions?

I localized linkage signals for ≥ 1 analytical model (see *4.2.2 Levels of Phenotypic Variation*) for 57 of the 61 traits (ECV + 60 EIDs; Appendix E, Table E1). I will refer to these as individual-trait peaks to distinguish them from the QTLs, which combine multiple individual-trait peaks in most instances. Peaks with 1.53 ≤ LOD < 2.75 are termed suggestive and those with LOD ≥ 2.75, significant. If an individual-trait peak was not located in all three models, I examined the LOD score at the peak locus in the models for which no peak was observed. A LOD ≥ 1.3 was considered evidence for linkage in the additional model as well.[1] This resulted in 460 individual-trait peaks (μ = 2.07 ± 0.6 LOD), of which 45 are significant. The highest LOD = 5.29 for POBA (Model 3) at PHA3 189 cM. Individual-trait peaks explain 0.142 ± 0.05 of the residual phenotypic variance (i.e., peak-specific heritability, h^2_q) with the minimum value for NAFM (Model 1) at PHA4 61 cM (h^2_q = 0.060) and maximum for POPO (Model 3) at PHA3 151 cM (h^2_q = 0.605).

I was unable to localize craniofacial variation at any level of analysis to the baboon genetic map for 4141, BRAS, FMPT, or NAZI and at least one level for an additional five traits: POPO (Model 2), PTPT (Model 3), SYBA (Model 1), ZIMX (Model 1), ZTPO (Models 2 and 3). The amount of V_P determines the ability to identify linkage peaks (chi-square test of V_P for traits with no peaks and all others pooled for having at least one peak: χ^2 = 130.3, df = 59, $P <$ 0.001). The average amount of V_P for all 60 EIDs is 48.6 ± 92 mm (Fig. 6.2), but the average amount for EIDs for which no individual-trait peaks were identified is 21.2 ± 12 mm, while that for EIDs with at least one peak is 52.4 ± 97 mm.

In a few cases, multiple individual-trait peaks for a single trait were identified very close together on the same chromosome. For example, peaks were present for JPJP (Model 2) on

[1] The genome-wide threshold corresponding to $P < 0.05$ is LOD ≥ 2.75, but an uncorrected threshold of LOD ≥ 1.3 can be used when testing linkage at only a single locus: $\log_{10}(0.05) = 1.3$.

Table 6.1 HGNC Gene Symbols for Craniofacial Related Genes.

Genes Retained for ToppGene Training Set						
ABCC11	*CDON*	*EVC2*	*GSC*	*NIPBL*	*PVRL1*	*SMARCA4*
ACTA1	*CHD7*	*EXT2*	*HESX1*	*NME1*	*RAB23*	*SMARCB1*
ADAMTS2	*CHRD*	*EYA1*	*HLA-B*	*NME2*	*RAI1*	*SMARCE1*
ALX1	*CHRNA5*	*FANCA*	*HMX1*	*OTX2*	*RARA*	*SNAI1*
ALX4	*CMT1A*	*FGD1*	*HRAS*	*PAH*	*RARB*	*SOX10*
AMER1	*CNGA3*	*FGF4*	*HSPG2*	*PAX6*	*RARG*	*STIL*
ANK2	*COL11A2*	*FGFR1*	*IDUA*	*PAX9*	*RAX*	*STRA6*
ANKH	*COL1A1*	*FGFR3*	*IFT43*	*PCSK6*	*RB1*	*TBX1*
AP1S2	*COL9A1*	*FKRP*	*IGF1R*	*PEPD*	*RBBP8*	*TBX22*
APOA1	*COL9A2*	*FLNA*	*INPP5E*	*PEX13*	*RBPJ*	*TCF4*
APOE	*CREBBP*	*FMR1*	*IRF6*	*PEX14*	*RECQL4*	*TFAP2B*
ARID1A	*CRLF1*	*FNDC3B*	*JAG1*	*PEX16*	*RHAG*	*TGFA*
ARID1B	*CUL7*	*FOLR1*	*JAG2*	*PEX2*	*RHCE*	*TGFB3*
ARSA	*CYBB*	*FOXO3*	*KMT2B*	*PHF6*	*RHD*	*TGFBR2*
ARX	*DCX*	*FOXA2*	*LDLR*	*PHF8*	*RTN4R*	*TGIF1*
ASXL1	*DDB2*	*FOXC2*	*LHX1*	*PIBF1*	*RUNX2*	*TH*
ATL1	*DHCR7*	*FRAS1*	*LTBP3*	*PIEZO2*	*SALL1*	*TP63*
ATP1A3	*DLK1*	*FREM1*	*MAOA*	*PINK1*	*SALL4*	*TSC1*
ATP2A1	*DLX3*	*FREM2*	*MAP2K2*	*PITX2*	*SAT1*	*TSHZ1*
ATP7A	*DMD*	*FSHR*	*MASP1*	*PKP1*	*SC5D*	*TTR*
ATRX	*DOCK6*	*FTO*	*MBTPS2*	*PLAG1*	*SEC23A*	*UPF3B*
B3GLCT	*EBP*	*GAN*	*MECP2*	*PLCB4*	*SH3BP2*	*VSX1*
BMP2	*ECE1*	*GCH1*	*MED12*	*POLR1C*	*SHOX*	*VSX2*
BMP4	*EFNB1*	*GDF5*	*MID1*	*POLR1D*	*SIX1*	*WRN*
BMP7	*ELANE*	*GDF6*	*MMP2*	*PORCN*	*SIX3*	*ZDHHC9*
BTK	*EOGT*	*GLI2*	*MSX1*	*PRM1*	*SIX5*	*ZIC2*
C1QA	*EPHB2*	*GNAS*	*MSX2*	*PRNP*	*SKI*	*ZMPSTE24*
C3	*EPHB3*	*GNPTAB*	*MTMR2*	*PRRX2*	*SLC2A1*	
CALM1	*ERCC2*	*GNRHR*	*MYH9*	*PSEN1*	*SLC35D1*	
CAV3	*ERF*	*GPC3*	*NF1*	*PTPRF*	*SLC9A6*	
CBS	*ESCO2*	*GRHL3*	*NHS*	*PTPRS*	*SMAD2*	
Genes Omitted because They are Contained within the QTLs						
AANAT	*COL3A1*	*FBN1*	*HAPLN1*	*PAX3*	*SCN4A*	*TLR4*
ABCA4	*COLEC11*	*FCGR1A*	*HOXA1*	*PITX1*	*SF3B4*	*TMC6*
ADAR	*CPN1*	*FGF8*	*HOXA2*	*PLOD3*	*SGCE*	*TP53*
AKAP9	*CRP*	*FGFR2*	*IFT122*	*POR*	*SHH*	*TPM2*
ALX3	*CYP19A1*	*FOXE1*	*KCNJ2*	*PRKRA*	*SLC26A2*	*TPM3*
ARHGAP31	*CYP2C19*	*FOXL2*	*KMT2D*	*PRRX1*	*SOD1*	*TWIST1*
BMPR1A	*DLX5*	*FRZB*	*KRAS*	*PTCH1*	*SOS1*	*UROS*
BRAF	*DLX6*	*GABRA1*	*KRT10*	*PYCR1*	*SOX9*	*VCL*
CHDH	*DRD3*	*GABRB3*	*KRT17*	*RBP4*	*SPTA1*	*VDR*
CHRNA1	*DPYD*	*GABRG2*	*LHX8*	*RET*	*TCF12*	*WDR35*
CHST14	*EDN1*	*GJA1*	*LMNA*	*RHO*	*TCOF1*	*WNT1*
CHST3	*EFNA4*	*GLI3*	*MYH8*	*ROR2*	*TDGF1*	*WNT3*
COL11A1	*EFTUD2*	*GLRA1*	*NODAL*	*RUNX1*	*TFAP2A*	*WNT9B*
COL1A2	*ERCC6*	*GNAI3*	*PAFAH1B1*	*SATB2*	*TFR2*	*ZEB2*
COL2A1	*ETFDH*	*GRIP1*	*PAX2*	*SCN1A*	*TGFBR1*	

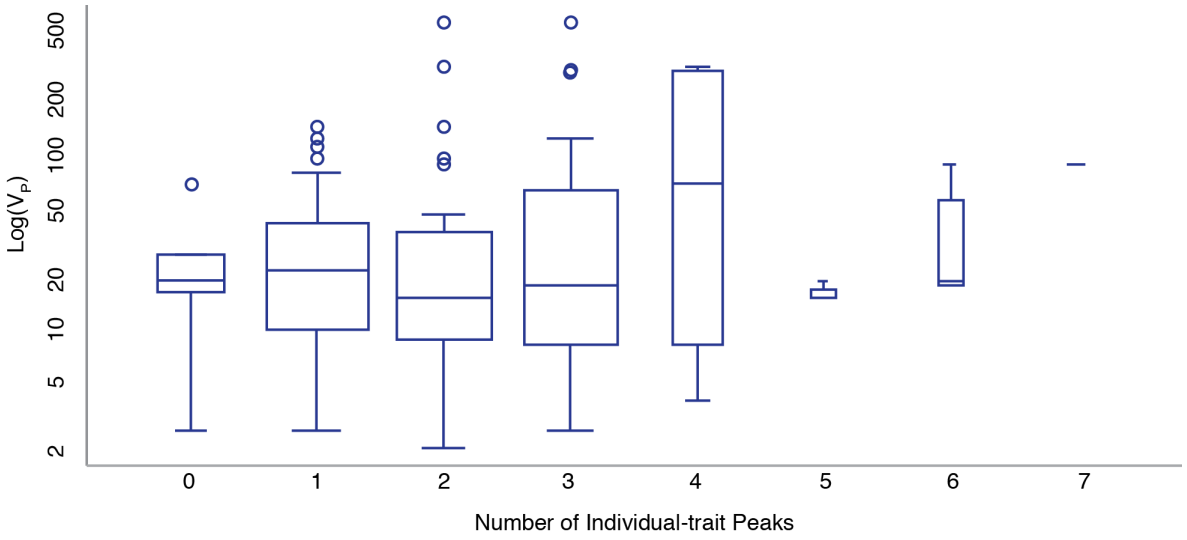

Figure 6.2 Boxplot of V_P of Traits with 0-7 Individual-trait Peaks. Box width is scaled to sample size, the horizontal bar inside the box gives the median value, the upper and lower hinges represent the first and third quartile, respectively, and the whiskers extend to 1.5 x IQR (interquartile range). Open circles indicate outlying data. The y-axis is on a log-10 scale.

HSA6 at both 105 and 124 cM. In such cases, I conducted a multi-QTL test, in which a second scan on the chromosome was conditioned on one of the two peaks to determine whether the other was simply an artifact. For JPJP (Model 2), the multi-QTL test revealed that the peak at 105 cM was spurious. Sometimes, the most likely linkage model was the one in which both peaks were included. For example, both 59 and 92 cM on HSA7_21 remained significant in a multi-QTL model for ZTZT (Model 3). Consequently, I report that the individual-trait peak was at 76 cM, the weighted-average of the two peaks.

If any individual-trait peaks were located within 10 cM of the beginning or end of the genetic map for a chromosome, I performed a twopoint linkage scan, which tests linkage models only at the exact location of an STR marker. If the LOD score at the first or last marker on that chromosome's map was also ≥ 1.53, I kept the individual-trait peak as suggestive of a genetic variant located between beyond that marker, likely in the portion of the chromosome not covered by the genetic map. For example, this occurred for CACP (Model 2) on HSA5 at 7 cM.

The closest STR is D5S208 at 9.7 cM, for which the LOD = 1.86. However, the twopoint results often suggested that an individual-trait peak near the beginning/end of the genetic map was spurious. For instance, this happened for CPZS (Model 1) on HSAX at 34 cM as the LOD for MMLXS37 at 33.6 cM was 0.64.

Based on the degree of overlap among individual-trait peaks, I identified 69 QTLs (Table 6.2) and tested whether the presence of a single pleiotropic QTL explained the presence of multiple overlapping individual-trait peaks according to the method of Cheverud (2001) explained above. The QTLs are named for the craniofacial skeleton (*Cfs*) and designated according to the baboon chromosome on and the order in which they are located, starting from the genetic map's proximal end. Every chromosome had at least one QTL (maximum: 5, mode: 4). Specific QTLs were not defined for the X-chromosome as all individual-trait peak SIs were largely overlapping and, thus, distinguishing among the most likely QTL boundaries was pointless. Any QTL containing an individual-trait peak with LOD ≥ 2.75 was considered a Sig-QTL and included in candidate gene analyses; there are 24 such Sig-QTLs on 13 chromosomes.

Of the 69 QTLs, 47 had at least two traits mapping to it. Whether a QTL is pleiotropic is not a function of chromosome length (χ^2= 66.4, df = 66, P = 0.46), number of traits mapping to the same chromosome (χ^2 = 15.7, df = 11, P = 0.15), or total number of QTLs on that chromosome (χ^2 = 7.0, df = 4, P = 0.13). This indicates that the occurrence of pleiotropy is not random, but possibly due to a feature of that particular locus—perhaps the presence of a gene or cluster of genes with more general craniofacial, rather than trait-specific, effects. This possibility is supported by the fact that pleiotropic QTLs involve traits from various regions of the cranium, such as *Cfs3.2*, which explains variation in CPZS (orbit), BRNA (anterior neurocranium), FMCP (orbit), NACP (anterior cranial base), POPO (posterior neurocranium),

Table 6.2 QTL Characteristics.

Name	HSA[a]	QTL (range)[b]	Traits (LOD)[c]	Proximal STR (cM)[d]	Distal STR (cM)[d]	Genomic Size[e]	Genes
Cfs1.1	1	51 (35-68)	2 (FMPM: 1.92)	D1S548 (0)	D1S2896 (75)	94.3	1824
Cfs1.2	1	79 (60-125)	4 (NA41: 2.99)*	D1S550 (59.9)	D1S533 (133.5)	124.9	2143
Cfs1.3	1	104 (86-136)	4 (NANL: 2.78)*	D1S1675 (85.5)	D1S518 (137.1)	77.9	1512
Cfs1.4	1	129 (114-175)	8 (FMPM: 2.61)	D1S213 (110)	D1S304 (176.6)	77.7	1305
Cfs1.5	1	192 (158-203)	2 (CPZS: 1.82)	D1S194 (152)	---	83.6	1479
Cfs2.1	3	14 (0-28)	1 (BRBA: 1.95)	---	D3S3591 (30.8)	8.2	71
Cfs2.2	3	31 (13-58)	2 (CPSL: 3.46)*	D3S3045 (11.6)	D3S1229 (71.9)	63.6	941
Cfs2.3	3	58 (24-90)	3 (NAZS: 3.34)*	D3S1267 (22.6)	D3S1309 (90.7)	17.9	330
Cfs2.4	3	96 (60-126)	2 (NLVS: 3.31)*	D3S1227 (52.2)	D3S1768 (119.4)	42.6	788
Cfs3.1	7_21	73 (25-115)	9 (ZTZT: 4.62) *	D21S167 (20.4)	D7S496 (117.5)	147.1	2225
Cfs3.2	7_21	125 (82-145)	8 (POPO: 3.10)*	D7S1830 (69.4)	D7S794 (148)	122.8	2023
Cfs3.3	7_21	172 (135-196)	7 (POBA: 5.29)*	D7S680 (129.8)	---	32.4	715
Cfs4.1	6	17 (0-41)	5 (PLSY: 3.42)*	---	D6S405 (41.3)	67.6	1563
Cfs4.2	6	34 (15-60)	6 (DAFM: 2.10)	D6S276 (14.1)	D6S311 (69.7)	88.3	1692
Cfs4.3	6	67 (40-90)	2 (NAFM: 2.28)	D6S1048 (39.6)	D6S1608 (95.1)	56.5	567
Cfs4.4	6	111 (73-135)	5 (BRNA: 2.89)*	D6S311 (69.7)	---	49.9	680
Cfs5.1	4	33 (18-39)	1 (STST: 1.94)	D4S1582 (3.4)	D4S400 (47.2)	34.8	331
Cfs5.2	4	62 (55-80)	2 (ZTVS: 2.20)	D4S2931 (54.9)	D4S2365 (82.1)	64.3	801
Cfs5.3	4	120 (90-135)	3 (NA41: 2.85)*	D4S2365 (82.1)	---	60.4	668
Cfs6.1	5	12 (0-45)	1 (CACP: 1.57)	---	D5S647 (52)	67.1	709
Cfs6.2	5	56 (30-69)	1 (POBA: 2.01)	D5S208 (9.7)	D5S1466 (69.8)	100.9	1080
Cfs6.3	5	80 (46-112)	1 (CPZS: 2.92)*	D5S418 (40.1)	D5S1465 (117.8)	122.2	1598
Cfs6.4	5	112 (100-130)	1 (ASJP: 1.97)	D5S210 (98.5)	D5S429 (132)	27.0	343
Cfs7.1	14_15	16 (0-32)	3 (STST: 3.12)*	---	D15S644 (39.5)	64.1	940
Cfs7.2	14_15	40 (25-56)	3 (BRLD: 2.68)	MML7S16 (21.5)	D14S261 (64.7)	77.6	1190
Cfs7.3	14_15	60 (46-85)	2 (NLVS: 2.22)	D14S261 (64.7)	D14S277 (93.1)	52.4	1016
Cfs7.4	14_15	89 (60-125)	7 (NA41: 2.66)	D15S519 (49.6)	D14S985 (127.7)	157.8	2099
Cfs7.5	14_15	128 (105-144)	2 (BRNA: 2.66)	D14S61 (95)	---	31.3	763
Cfs8.1	8	18 (0-35)	4 (BRNA: 2.50)	---	MML8S35 (43.3)	25.6	479
Cfs8.2	8	43 (25-60)	1 (ASJP: 1.77)	MML8S30 (23.4)	D8S285 (64)	39.1	554
Cfs8.3	8	68 (46-86)	2 (NLVS: 2.55)	MML8S35 (43.3)	D8S208 (92.7)	77.3	1009
Cfs8.4	8	91 (75-129)	1 (FMCP: 1.71)	D8S260 (68.8)	---	84.3	1061
Cfs9.1	10	30 (0-40)	3 (LDBA: 3.10)*	---	GGAT1A4 (50.7)	74.5	1051
Cfs9.2	10	86 (58-114)	2 (BRBA: 2.88)*	D10S611 (34.7)	---	106.5	1642
Cfs9.3	10	125 (105-125)	2 (41ZI: 1.96)	D10S1230 (90.8)	---	12.9	219

Cfs10.1	20_22	81 (62-100)	2 (STST: 2.20)	D20S112 (60.1)	D20S897 (100.1)	46.8	827
Cfs10.2	20_22	117 (93-134)	6 (FMPM: 2.44)	MML10S36 (91)	---	25.9	549
Cfs11.1	12	5 (0-15)	2 (ZTZI: 2.75)*	---	D12S364 (21.6)	13.8	419
Cfs11.2	12	47 (25-65)	6 (NAFM: 3.36)*	D12S364 (21.6)	D12S375 (66.7)	40.9	579
Cfs11.3	12	65 (55-85)	4 (DAFM: 2.73)	D12S297 (55.2)	D12S318 (87.4)	50.5	850
Cfs11.4	12	100 (75-114)	5 (NABA: 2.67)	D12S375 (66.7)	MML11S8 (114.7)	73.6	1257
Cfs11.5	12	127 (113-127)	1 (ZTPO: 1.91)	D12S342 (109)	---	8.0	141
Cfs12.1	2q	31 (4-104)	1 (ECV: 1.65)	D2S295 (0)	D2S1363 (106.4)	98.9	1717
Cfs12.2	2q	63 (50-84)	3 (NAVS: 3.59)*	D2S150 (47.8)	D2S434 (90.6)	78.1	954
Cfs12.3	2q	94 (79-117)	7 (STST: 3.59)*	D2S115 (78.1)	D2S2176 (117.3)	35.0	555
Cfs12.4	2q	136 (131-146)	3 (NAVS: 3.55)*	D2S2338 (125.8)	---	6.0	143
Cfs13.1	2p	19 (0-37)	2 (PTAS: 2.86)*	---	D2S119 (44.5)	43.9	639
Cfs13.2	2p	90 (50-104)	3 (VSSY: 1.85)	D2S391 (44.5)	---	47.2	779
Cfs14.1	11	13 (0-44)	1 (BAOP: 2.30)	---	D11S904 (44.8)	50.9	1390
Cfs14.2	11	75 (55-80)	1 (NLAC: 2.26)	D11S1329 (55.7)	D11S925 (100.9)	52.5	889
Cfs14.3	11	94 (81-130)	1 (NACP: 1.83)	D11S1366 (75)	---	38.2	650
Cfs14.4	11	138 (129-145)	1 (NAVS: 1.68)	D11S968 (123.2)	---	1.2	27
Cfs15.1	9	0 (0-15)	1 (NAFM: 1.61)	---	D9S922 (23.2)	7.6	95
Cfs15.2	9	37 (10-48)	2 (BRBA: 1.93)	D9S152 (0)	D9S285 (48)	15.5	151
Cfs15.3	9	62 (49-76)	4 (PTLD: 3.43)*	D9S285 (48)	D9S1798 (79.3)	107.6	1523
Cfs15.4	9	124 (109-134)	2 (NANL: 1.81)	D9S1818 (100.7)	---	4.3	183
Cfs15.5	9	134 (115-134)	1 (PMPM: 1.61)	D9S1818 (100.7)	---	4.3	183
Cfs16.1	17	23 (11-35)	1 (PTAS: 2.75)*	MML16S5 (0)	D17S1803 (42.9)	11.6	403
Cfs16.2	17	61 (30-94)	2 (NANL: 1.88)	D17S796 (20.7)	MML16S12 (118.1)	71.1	1911
Cfs16.3	17	120 (88-160)	3 (STST: 2.82)*	D17S800 (87.1)	---	31.2	919
Cfs17.1	13	42 (15-64)	3 (FMZT: 1.84)	D13S139 (6.4)	MML17S15 (71.5)	70.8	818
Cfs18.1	18	15 (0-30)	1 (NACA: 2.34)	---	D18S456 (33.1)	33.7	330
Cfs18.2	18	38 (24-41)	2 (ASAS: 1.78)	D18S869 (21.2)	D18S72 (47.1)	24.0	425
Cfs19.1	19	16 (9-45)	1 (SLBA: 2.13)	MML19S37 (0)	MML19S8 (48.1)	19.2	483
Cfs19.2	19	41 (25-65)	1 (NACP: 1.59)	D19S226 (23.1)	D19S180 (80.8)	38.9	1428
Cfs19.3	19	85 (41-104)	2 (POPO: 2.68)	MML19S35 (35.9)	D19S418 (88.1)	31.1	1386
Cfs19.4	19	104 (95-104)	2 (LDBA: 2.16)	D19S418 (88.1)	---	3.6	204
Cfs20.1	16	54 (20-84)	2 (PMPM: 2.66)	D16S423 (0)	D16S505 (88.7)	75.8	1298
Cfs20.2	16	83 (62-106)	2 (NAZS: 2.13)	D16S320 (62.2)	---	31.0	536

[a]Syntenic human chromosome number. [b]Location of the QTL's peak and its confidence interval, given in cM units. [c]Number of traits mapping to each chromosome and the trait with the highest LOD score for that QTL. Significant LODs are indicated by an asterisk. [d]Name of the microsatellite marker flanking the QTL support interval and its genetic map location in cM units. [e]Size of the QTL in millions of basepairs (Mb).

LDAS (posterior neurocranium), and ACSY (snout). Alternatively (although these two scenarios are not mutually exclusive), the propensity for a particular QTL to be pleiotropic may be a function of the trait(s) mapping to it. These possibilities are addressed more directly in research question 3.

One thing I noted is that the QTLs located on baboon chromosomes that are fusions of syntenic human chromosomes (PHA3/HSA7_21, PHA7/HSA14_15, and PHA10/HSA20_22) are more likely to be pleiotropic for a larger-than-average number of traits. The average number of traits per QTL is 2.8 but the number of traits for the QTLs on these three fusion chromosomes is typically above average (*Cfs3.1*: 9, *Cfs3.2*: 8, *Cfs3.3*: 7, *Cfs7.1*: 3, *Cfs7.2*: 3, *Cfs7.3*: 2, *Cfs7.4*: 7, *Cfs10.1*: 2, *Cfs10.2*: 6). There may be an association between large-scale rearrangements such as chromosome fission/fusions and either the ability to localize linkage signals—a function of sample characteristics, as mentioned above—or the accrual of genetic variation that happens to be relevant for intrapopulation craniofacial variation.

Are linkage signals distributed throughout the baboon genome or clustered in specific regions?

I tested whether QTL signals were clumped along a chromosome and, thus, likely to be the result of a "hot spot" for craniofacial variation. Based on the length of each chromosome and the number of QTLs mapping to it, I determined the expected location of each QTL under the assumption of no clumping. The expected and observed locations are nearly identical (Pearson's $\rho = 0.94$; Fig. 6.3). Although the QTLs themselves are not clumped, the linkage signal of each may still be attributed to a clump of craniofacial-related genes. The only way to distinguish between a single genetic variant and multiple ones as the cause of such a signal is through association mapping on a finer scale. This typically requires SNP data, but as my data are from microsatellite markers, I am unable to test such hypotheses with my data.

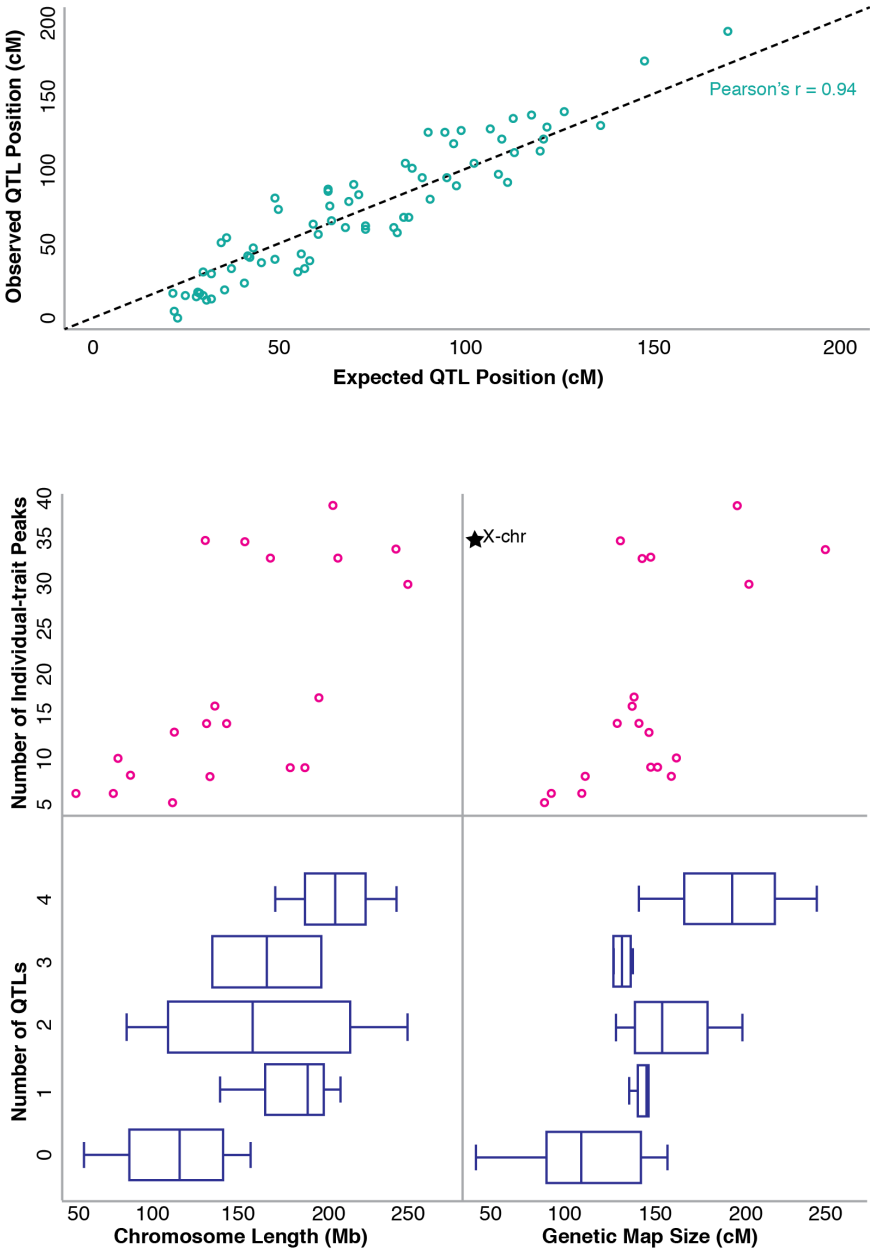

Figure 6.3 Relationship Among the Number and Location of Linkage Signals and the Size of Individual Chromosomes. Panels: (top) Observed QTL locations are plotted against the expected locations under the assumption of random distribution along a chromosome (i.e., not clumped together). The dashed line represents the line of identity (x = y). (bottom) Chromosomal length using two different means of quantification is plotted on the x-axis and the number of linkage signals associated with each chromosome (both those for each of the 61 traits individually and the QTLs given in Table 6.2) is plotted on the y-axis. A black star highlights the unexpectedly small genetic map size of the X-chromosome, given the number of individual-trait peaks that map to it.

Having determined that QTLs are distributed evenly along a chromosome, I tested whether linkage signals were more likely to be found on certain chromosomes over others. Shorter chromosomes tend to have fewer associated linkage signals, both individual-trait peaks and Sig-QTLs, regardless of whether quantifying size by physical (Mb) or genetic map (cM) lengths (see Fig. 6.3), suggesting a linkage signal is equally likely to be located on any particular chromosome. The r^2 values from ordinary least squares (OLS) regressions adjusted for sample size are:

- number of Sig-QTL ~ chromosome length (Mb): 0.39 ($P = 0.002$)
- number of Sig-QTL ~ genetic map length (cM): 0.08 ($P = 0.13$)
- number individual-trait peaks ~ chromosome length (Mb): 0.39 ($P = 0.002$)
- number individual-trait peaks ~ genetic map length (cM): 0.36 ($P = 0.003$)

Generally, if a chromosome contains only either one or three Sig-QTLs (PHA2, 5, 7, 9, 15), it is ~150 cM (range: 125-145) long. However, most of the chromosomes with only one Sig-QTL (PHA5 and 7) are longer than expected (~200 Mb); most of the chromosomes of a similar length have four Sig-QTLs. Finally, the shortest chromosomes, both in terms of their physical and genetic map sizes, are those to which no Sig-QTLs and few individual-trait peaks were localized. The most obvious exception to these general trends is that the X-chromosome has a greater number of individual-trait peaks localized to it than expected for the size of its genetic map. Despite the small size of its map, its physical length is no different than that of any other chromosome with 43 individual-trait peaks.

Do individual-traits have a lot of QTLs and does the region of the cranium in which a trait is located affect the number of QTLs that map to it?

On average, each EID has 3 QTLs, only half of which are significant (Appendix E, Table E1). BRNA has the most number of QTLs (7), five of which are significant. ECV has a large number of QTLs as well (5), but only two are significant.

The location and range of each QTL and the traits that map to each are shown in Appendix C, Figure C1. I parsed the EIDs into different types of descriptive categories (anatomical plane and regions at two different scales) to examine the relationship between such categories and trait variability and number of individual-trait peaks identified (Fig. 6.4). Traits in the sagittal plane (anteroposterior measurements) are not any more variable than those in the transverse (mediolateral) or coronal (superoinferior) planes (OLS adj. $r^2 = 0.02$, $P = 0.08$), despite geometric morphometric data that suggest otherwise (e.g., Debat et al., 2000; Bookstein, 2015). Similar numbers of individual-trait peaks are discovered in each ($\chi^2 = 20.6$, df = 14, $P = 0.10$).

EIDs can be parsed into one of three general craniofacial regions: neural vault, basicranium, and face. V_P varies significantly by region (OLS adj. $r^2 = 0.06$, $P = 0.002$): basicranial traits are less variable (11.5 ± 10 mm) than either facial (75.3 ± 123 mm) or neural (30.9 ± 21 mm) ones. Despite this difference, an approximately equal number of individual-trait peaks were identified in each region ($\chi^2 = 21.0$, df = 14, $P = 0.09$).

Finally, the three general craniofacial regions can be further subdivided into more regional “modules”: overall, anterior, and posterior neurocranium; anterior cranial base and circum-foramen magnum; and oral, nasal, orbital, and zygomatic arch. Modules differ in their degree of variability (OLS adj. $r^2 = 0.45$, $P < 0.001$) with both nasal and zygomatic arch traits being more variable than any of the others (OLS adj. $r^2 = 0.36$, $P < 0.001$). The number of individual-trait peaks identified differed by module ($\chi^2 = 111.5$, df = 56, $P < 0.001$) but, despite nasal and zygomatic arch traits being more variable than any others, a similar number of peaks (median = 2 ± 1) were identified for those two categories compared to all other categories ($\chi^2 = 6.0$, df = 7, $P = 0.53$). Interestingly, fewer individual-trait peaks were identified for anterior

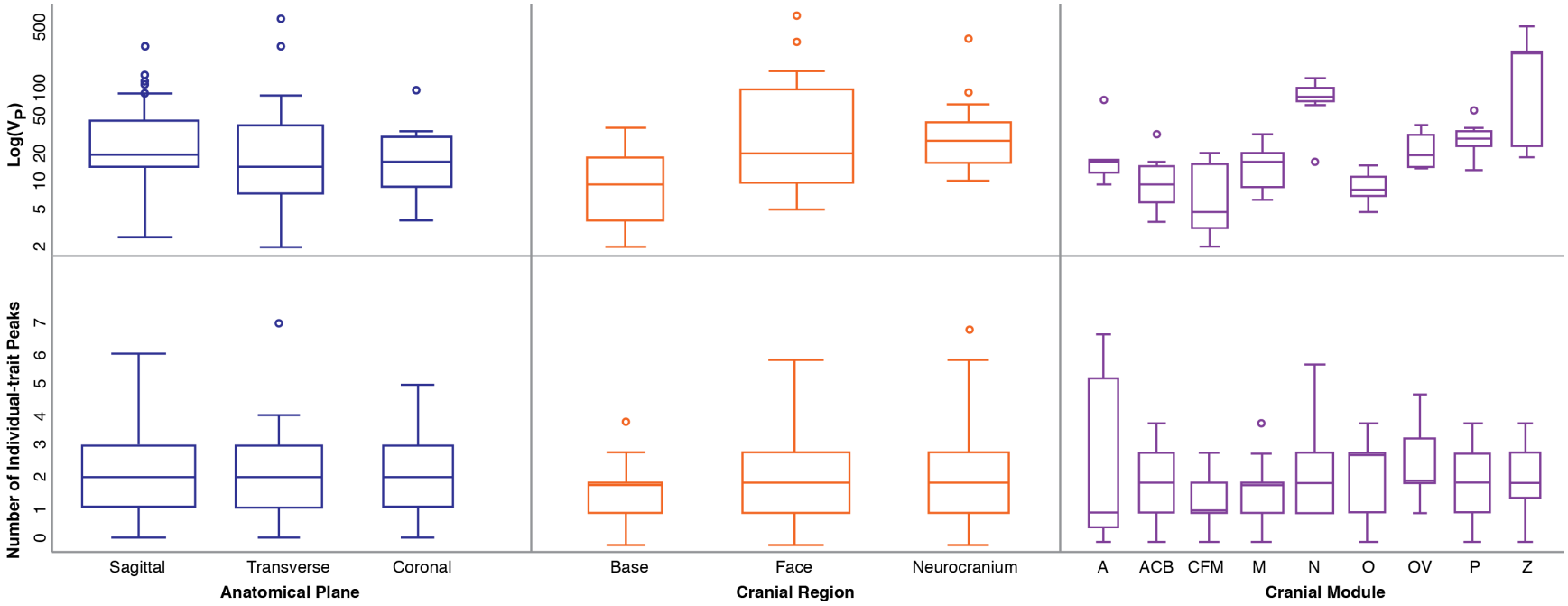

Figure 6.4 Boxplots of the Relationship Between Trait Location and Linkage Signal. Phenotypic variance (top row) and number of individual-trait peaks (bottom row) for cranial measurements grouped by different criteria. The left column groups an EID by the anatomical plane in which it is measured, the middle column by the general cranial region, and the right column by specific cranial module (A: anterior neurocranium, ACB: anterior cranial base, CFM: circum-foramen magnum, M: oral, N: nasal, O: orbital, OV: global neurocranium, P: posterior neurocranium, Z: zygomatic arch). Boxes are defined as described in the Figure 6.2 legend.

neurocranial EIDs (χ^2 = 47.4, df = 7, $P < 0.001$), but the variation in number of peaks discovered for each trait was much higher (median: 1 ± 3).

Does controlling for allometric variation change the number of QTLs for a trait?
In general, controlling for allometric variation, both by including body weight and PC1 as covariates in linkage models, does not increase the number of suggestive or significant individual-trait peaks identified (χ^2 = 5.94, df = 14, P = 0.98; Fig. 6.5). A major exception is STST, which has 3 individual-trait peaks at Model 1(2 of which are significant) and 7 each for Models 2 and 3 (3 of which are significant at each level). It is also the only trait with 7 peaks identified at any level. BRNA also demonstrates an unusual pattern in that it maps to 5 (Model 2) or 6 (Models 1 and 3) different individual-trait peaks, but the only one with LOD ≥ 2.75 is on HSA6/PHA4 for Model 2. Those individual-trait peaks correspond to 7 different QTL, 5 of which are significant, the largest number of Sig-QTL for any trait (the median number of Sig-QTL is 1 ± 1).

Is there evidence for pleiotropy in baboon craniofacial variation?
As mentioned previously, there are 69 QTLs. Of these, 51 are linked to variation in at least two traits (median = 2 ± 2). The most number of traits linked to any single QTL is nine, or 10 if you include PC1 (*Cfs3.1*). The two chromosomes with the largest number of pleiotropic QTLs (5) are PHA1 and PHA7; PHA6 has no pleiotropic QTL. If multiple traits map to the same QTL, they tend to be in similar regions of the cranium (e.g., *Cfs1.2* contains the peaks of 4 traits, all of which capture variation in rostrum length) or in similar planes (e.g., *Cfs7.1* contains the peaks of 3 traits, all of which are breadth measurements in the coronal plane).

I randomly selected a pleiotropic QTL (*Cfs4.1*) to estimate QTL-specific genetic correlation coefficients (ρ_Q) using SOLAR. There are five Model 2 traits that map to this QTL: ASAS, PLSY, POBA, SYMX, and VSSY. Correlation coefficients are provided in Table 6.3 as a

phenotypic correlation matrix (**P**), a genetic correlation matrix (**G**), a QTL-specific genetic correlation matrix (**Q**), and an environmental correlation matrix (**E**). The correlation coefficient between **P**-**G** is 0.898 (P_{sim} = 0.03), **G**-**E** is 0.805 (P_{sim} = 0.02), **G**-**Q** is 0.864 (P_{sim} = 0.02), and **P**-**Q** is 0.780 (P_{sim} = 0.04). These results suggest that phenotypic correlation patterns among these 5 traits are very similar to genetic correlations and that these genetic correlations are due, at least in part, to the pleiotropic genetic variant(s) at *Cfs4.1*. In other words, the effects of the genetic variant(s) linked to variation at the QTL's peak locus (17 cM) are the same as the overall pattern of genetic correlation. That pattern derives, at least in part, from the allelic effects at this locus.

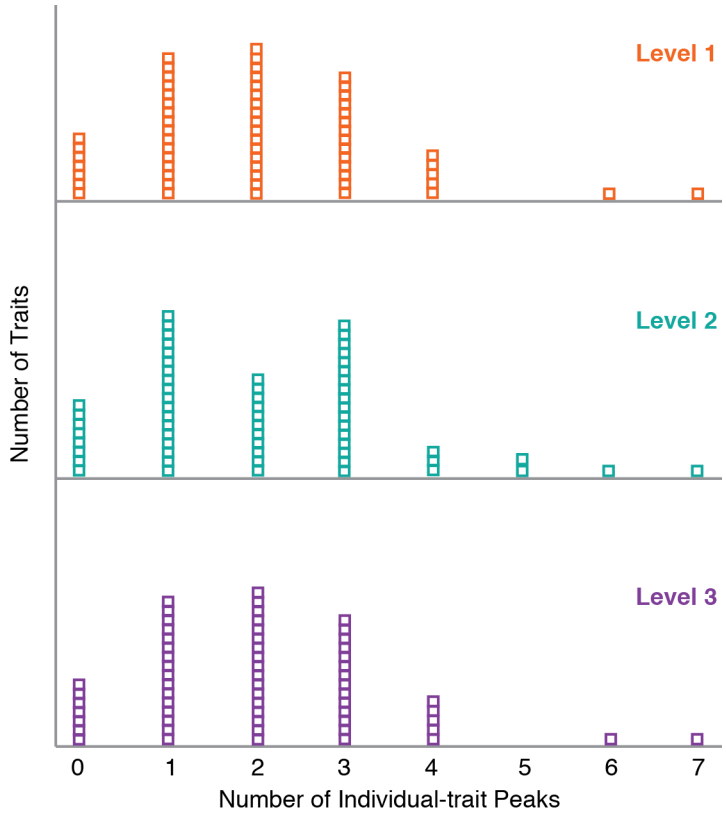

Figure 6.5 Frequency Distributions of the Number of Individual-Trait Peaks Identified. Each square represents a single trait. Only peaks with LOD ≥ 1.53 are included.

Table 6.3 Pleiotropy Matrix Correlations. Phenotypic (**P**), genetic (**G**), QTL-specific genetic (**Q**), and environmental (**E**) matrices compared to examine signals of pleiotropy at *Cfs4.1*.

P	PLSY	ASAS	SYMX	VSSY	POBA
PLSY	1	0.0543	0.5802	-0.3251	0.1248
ASAS	0.0543	1	0.1079	0.0314	0.2970
SYMX	0.5802	0.1079	1	-0.3055	0.1389
VSSY	-0.3251	0.0314	-0.3055	1	0.0183
POBA	0.1248	0.2970	0.1389	0.0183	1
G	PLSY	ASAS	SYMX	VSSY	POBA
PLSY	1	0.0541	0.4950	-0.1276	0.0512
ASAS	0.0541	1	0.1437	0.0235	0.4853
SYMX	0.4950	0.1437	1	-0.0907	0.0268
VSSY	-0.1276	0.0235	-0.0907	1	-0.0063
POBA	0.0512	0.4853	0.0268	-0.0063	1
Q	PLSY	ASAS	SYMX	VSSY	POBA
PLSY	1	0.1929	0.6797	-0.3221	-0.0792
ASAS	0.1929	1	0.1035	0.0084	1.0000
SYMX	0.6797	0.1035	1	-1.0000	-0.6848
VSSY	-0.3221	0.0084	-1.0000	1	-0.0510
POBA	-0.0792	1.0000	-0.6848	-0.0510	1
E	PLSY	ASAS	SYMX	VSSY	POBA
PLSY	1	0.0566	0.6726	-0.5569	0.2062
ASAS	0.0566	1	0.0861	0.0389	0.1855
SYMX	0.6726	0.0861	1	-0.5500	0.2602
VSSY	-0.5569	0.0389	-0.5500	1	0.0464
POBA	0.2062	0.1855	0.2602	0.0464	1

The linkage signal is significantly large for two of the five traits (VSSY LOD_6 = 3.25, VSSY LOD_{25} = 2.88, PLSY LOD_0 = 3.42, PLSY LOD_{33} = 2.89, where the subscript denotes the individual-trait peak locus), so genetic variation at *Cfs4.1* plays a large role in the patterns of V_P for these traits. The LOD score for SYMX is also significant (2.90 at 20 cM) once cranial size variation is controlled (i.e., for Model 3). Taken together, these traits quantify the size and shape of the bones of the nasopharynx, so it is not surprising that they are affected in a similar manner by genetic variation at this locus. The ρ_Q between SYMX and VSSY is -1, meaning that genetic variation at this locus causes one trait's values to increase in size while the other's decreases. The correlation between PLSY and VSSY is also negative, although not as much so (-0.322),

while that between PLSY and SYMX is 0.680. Taken together, these results indicate that the effect of *Cfs4.1* is to increase the length and breadth of the palate in concert while also shortening the distance between the palate and the cranial base (and vice versa). As both POBA and ASAS are measures of posterior cranial breadth, it is not surprising that their $\rho_Q = 1$. For the most part, the variation at *Cfs4.1* has the opposite effect on the nasopharyngeal and posterior neurocranial region ($\rho_Q = -0.68$ for POBA:SYMX).

The correlation between **G** and **E** suggests that genetic and environmental correlations also vary in the same direction so that the allelic effects of genetic variation at *Cfs4.*1 are in the same direction as the effect of environmental factors. All five traits are located on the inferior surface of the cranium (ASAS defines the nuchal ridge, which is located much more inferiorly on the neurocranium than in other taxa), and both ASAS and POBA describe the breadth of the cranial base surrounding the foramen magnum. Therefore, these results suggest that environmental variation—epigenetic, developmental, functional, or otherwise—affects the bones of the nasopharynx and those of the posterior cranial fossa in concert with genetic variation contributed by *Cfs4.1*.

6.3.2 GO Enrichment Analysis and Overrepresentation Test

Results of the Enrichment Analysis are presented in Table 6.4. Of the top 21 most overrepresented gene annotations in the Q-Set, 11 are involved in developmental processes, largely structure morphogenesis. The protein class is dominated by nucleic acid binding and receptor proteins. The most common pathway in which Q-set genes are involved is *Wnt* signaling, specifically in the regulation of cadherin (41% of these *Wnt*-pathway-related genes are associated with cadherin).

Table 6.4 Gene Annotations of the Q-Set. Results of the Gene Ontology (GO) and PANTHER (PC) Enrichment Analysis and Overrepresentation Tests.

Enrichment Analysis Annotations[a]	Accession Number	Fold Enrichment[b]
keratinization	GO: 0031424	2.32
cell-cell adhesion	GO: 0098609	1.37
cell adhesion	GO: 0007155	1.28
biological adhesion	GO: 0022610	1.28
cellular response to O_2-containing compound	GO: 1901701	1.26
movement of cell or subcellular component	GO: 0006928	1.25
response to nitrogen compound	GO: 1901698	1.25
tissue development	GO: 0009888	1.23
locomotion	GO: 0040011	1.21
response to O_2-containing compound	GO: 1901700	1.21
organ development	GO: 0048513	1.21
cellular developmental process	GO: 0048869	1.20
cell differentiation	GO: 0030154	1.20
system development	GO: 0048731	1.19
nervous system development	GO: 0007399	1.19
single-organism developmental process	GO: 0044767	1.19
developmental process	GO: 0032502	1.19
anatomical structure development	GO: 0048856	1.19
anatomical structure morphogenesis	GO: 0009653	1.19
positive regulation of molecular function	GO: 0044093	1.18
multicellular organismal development	GO: 0007275	1.18
Overrepresentation Test Annotations	**Accession Number**	**N (%)[c]**
Molecular Function		
binding	GO: 0005488	1,982 (31.5)
catalytic activity	GO: 0003824	1,894 (30.1)
Biological Process		
metabolic process	GO: 0008152	2,887 (24.9)
cellular process	GO: 0009987	2,516 (21.7)
Cellular Component		
cell part	GO: 0044464	1,129 (38.4)
organelle	GO: 0043226	669 (22.7)
Protein Class		
nucleic acid binding	PC: 00171	792 (11.8)
receptor	PC: 00197	627 (9.4)
Pathway		
Wnt signaling [cadherin][d]	PC: 00057 [PC: 01440]	146 (6.1) [61 (40.9)]
chemokine/cytokine signaling	PC: 00031	105 (4.4)

[a]Only the top 21 categories are provided, but an additional 35 were also significant with $P < 0.05$. Categories that are particularly relevant given the phenotypes are indicated in red typeface. [b]Determined using the binomial test to compare the observed distribution of annotations to the expected distribution drawn at random from the genome. [c]Number of genes with the annotation and proportion of all such annotated genes in the database that are observed in the Q-set. [d]Within the *Wnt* signaling pathway, genes involved in the regulation of cadherin are overrepresented.

6.3.3 Candidate Genes

According to the NCBI Genome database, there is an average of 899 genes (range: 27-2,225) within each QTL. The lists of genes contained within each Sig-QTL were filtered to remove non-coding element and duplicates from where Sig-QTL SIs overlap. The final list, the Q-set, is provided in Appendix D, Table D1. I chose to look at the number of genes within QTLs in two different ways: by comparing that number to both the length of the QTL and the number of genes found in total on the QTL's chromosome (the number of genes on a chromosome is not dependent on its length: OLS adj. $r^2 = 0.08$, $P = 0.10$). First, the number of genes contained in a QTL is a function of its genomic size (OLS adj. $r^2 = 0.61$, $P < 0.001$). Two QTLs deviate from this pattern (Fig. 6.6): *Cfs7.3* appears to be gene-poor (1,016) given its size (157.8 Mb) while *Cfs7.4* appears to be gene-rich (2,099) for a similarly sized QTL (31.3 Mb). Removing the QTLs that do not contain traits with a LOD ≥ 2.75 does not change this pattern (OLS adj. $r^2 = 0.88$, $P < 0.001$). Second, the number of genes contained in a QTL is also a function of the number of genes on the chromosome (OLS adj. $r^2 = 0.21$, $P = 0.01$). Taken together, these results suggest that the distribution of genes across the genome is not random but that the proportion of genes in each QTL remains largely constant. Genetic variants linked to craniofacial variation in this sample of baboons are located in regions of the genome that are neither particularly gene dense nor sparse, although the discovery of a number of pleiotropic QTL indicates that such genetic variation itself may be grouped.

The list of 317 craniofacial genes (the C-set; see Table 6.1) was compared to the Q-set to determine if there was any overlap. Of the 24 Sig-QTLs, 22 of them contained at least one C-set gene (Table 6.5); *Cfs1.2* even contained 15! It was not surprising which of the Sig-QTLs I was unable to identify C-set genes for, as both had gene lists that were among the smallest of any Sig-QTL (*Cfs11.1* = 276, *Cfs12.4* = 71, $\mu = 1040 \pm 596$, median = 930). The 102 genes that

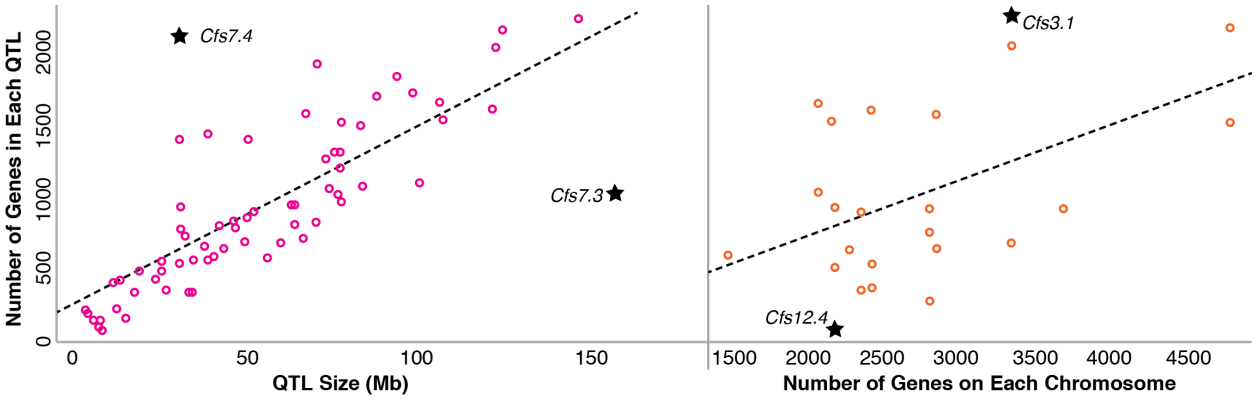

Figure 6.6 Relationship of QTL Size and Chromosome Size to QTL Gene Number. The number of genes in each QTL as determined from the NCBI Genome website plotted against both the size of each chromosome (left panel) and the number of genes on each chromosome (right panel). Black stars indicate deviations from the pattern. *Cfs7.4* has many more genes within each QTL than expected while *Cfs7.3* has far fewer, given the size of PHA7. *Cfs3.1* appears to be gene-rich and *Cfs12.4* gene-poor, based on the number of genes located on chromosomes PHA3 and PHA12, respectively. All QTL are plotted in the left panel but only the Sig-QTLs are shown in the right panel.

represented the union of the C- and Q-sets were removed from the C-set to create the Tr-set for a ToppFun analysis. As a proof of concept, I examined the ToppFun results (Table 6.6) to ensure the ToppGene Suite correctly classifies them as craniofacial-related genes.

The Q-set was submitted to ToppGene as the Te-set. Many additional genes were identified by ToppGene as priority candidates. Of the 102 genes that were omitted from the Tr-set for being present in the Q-set, only 27 of them recurred as one of the top five priority genes, meaning that an additional 93 genes were identified that were not previously known to be potentially related to craniofacial variation (see Table 6.5).

6.4 Discussion

Having now identified QTLs for baboon craniofacial variation, I can compare the locations of my linkage signals to those of published QTLs (Table 6.7). A handful of my QTLs correspond to some of those identified by Palleres et al. (2014) in mice and Sherwood et al. (2008, 2011) in baboons and humans, respectively. Leamy et al. (1999) and Kenney-Hunt et al.

Table 6.5 Candidate Genes for All Sig-QTLs

QTL	N[a]	Culled from Literature[b] & OMIM	ToppGene Prioritized[c]
Cfs1.2	1372	*ABCA4, ADAR, ALX3,* ***COL11A1****, CRP, DPYD, EFNA4, FCGR1A, GNAI3, LHX8, LMNA, PRRX1, SF3B4, SPTA1, TPM3*	*NOTCH2, NRAS, APOA2, NTRK1, TBX15*
Cfs1.3	993	*ADAR, CRP, FCGR1A, PRRX1, SF3B4, SPTA1, TPM3*	*NRAS, NOTCH2, APOA2, NTRK1, ATP1A2*
Cfs2.2	563	*ARHGAP31,* ***DRD3****, FOXL2, IFT122, RHO*	*AGTR1, GSK3B, ADCY5, TF, DRD3*
Cfs2.3	209	*FOXL2,* ***IFT122****,* ***RHO***	*ADCY5, TF, EPHB1, GATA2, PIK3CB*
Cfs2.4	550	*CHDH, TDGF1*	*CTNNB1, SMARCC1, DAG1, PRKCD, CACNA1D*
Cfs3.1	1268	*AKAP9, COL1A2,* ***GLI3****, HOXA1, HOXA2, PLOD3, POR, RUNX1, SGCE, TFR2, TWIST1*	*EGFR, ACTB, APP, DLX5, CD36*
Cfs3.2	1247	*AKAP9,* ***BRAF****, COL1A2,* ***GLI3****, HOXA1, HOXA2, PLOD3, POR, SGCE, TFR2*	*EGFR, MET, CAV1, DLX5, CD36*
Cfs3.3	471	***BRAF****,* ***SHH***	*NOS3, SMO, PAX4, LEP, TRIM24*
Cfs4.1	527	***EDN1****,* ***TFAP2A***	*FOXC1, SOX4, E2F3, DTNBP1, BMP6*
Cfs4.4	356	*GJA1*	*T, HDAC2, PEX3, ENPP1, LAMA2*
Cfs5.3	313	*ETFDH*	*HAND2, CASP3, GRIA2, GUCY1A3, FBXW7*
Cfs6.3	914	*GABRA1, GABRG2, GLRA1, HAPLN1, PITX1, SLC26A2, TCOF1*	*MEF2C, APC, NR3C1, FGF10, GRIA1*
Cfs7.1	485	*CHST14,* ***CYP19A1****,* ***FBN1****, GABRB3,* ***TCF12***	*LIPC, FGF7, THBS1, ADAM10, BUB1B*
Cfs9.1	590	*CHST3, ERCC6,* ***NODAL****,* ***RET***	*ITGB1, GATA3, KCNMA1, CDK1, CUBN*
Cfs9.2	1035	***BMPR1A****, CHST3, CPN1, CYP2C19, ERCC6,* ***FGF8****,* ***FGFR2****, PAX2, NODAL, RET, RBP4, UROS, VCL*	*TCF7L2, PTEN, FAS, ITGB1, CHUK*
Cfs11.1	276	---	*CACNA1C, TNFRSF1A, GRIN2B, A2M, CCND2*
Cfs11.2	355	***COL2A1****,* ***GRIP1****, KMT2D,* ***KRAS****,* ***VDR***	*LRRK2, SCN8A, GRIN2B, WNT1, PTHLH*
Cfs12.2	525	*CHRNA1, COL3A1, FRZB, PRKRAH, SATB2, SCN1A, ZEB2*	*STAT1, LRP2, CASP8, CREB1, ERBB4*

Cfs12.3	336	***PAX3**, SATB2*	*CASP8, CREB1, FN1, ERBB4, IRS1*
Cfs12.4	71	---	*HDAC4, GPC1, TWIST2, COL6A3, PER2*
Cfs13.1	317	*COLEC11, DLX5, DLX6, **SOS1**, WDR35*	*APOB, ADAM17, NCOA1, ALK, DNMT3A*
Cfs15.3	853	*FOXE1, **PTCH1**, ROR2, **TGFBR1**, TLR4, TPM2*	*CDKN2A, ABCA1, GNAQ, KLF4, NTRK2*
Cfs16.1	289	*MYH8, **PAFAH1B1**, **TP53***	*SLC2A4, YWHAE, DLG4, PFN1, TRPV1*
Cfs16.3	627	*AANAT, EFTUD2, KCNJ2, SCN4A, KRT10, KRT17, PYCR1, **SOX9**, TMC6, WNT3, WNT9B*	*STAT3, BRCA1, GRB2, ACTG1, MAPT*

[a]Number of genes within the QTL SI used as the ToppGene test set (Te-set). [b]Wilkie and Morriss-Kay, 2001 and Maga et al., 2015. [c]Top five novel genes most functionally similar to those in the ToppGene training set (Tr-set). All genes are significant at $\alpha < 0.01$. Only genes not already in the Tr-set are listed. Any Tr-set genes that were listed in ToppGene's top five appear in bold typeface in the third column.

(2008) mapped craniofacial traits in mice, but I was unable to compare my QTLs to theirs due to differences in how results were presented. As QTLs identified by Palleres et al. (2014) likely correspond to a few of mine, it is possible the same is true of Leamy et al. (1999) and Kenney-Hunt et al. (2008).

A number of QTLs explain variation in exclusively one region of the cranium. For example, only traits in the neurocranium (ECV, BRNA, NABA, JPJP) map to *Cfs4.4*. In some cases, all the traits mapping to a particular locus are measured in the same plane. *Cfs7.1* appears to explain variation in craniofacial breadth (ASAS, STST, PTPT) while length measurements (NALD, NLVS) map to *Cfs8.3*. These associations between a QTL and only a very specific subset of the traits could be used to target a specific QTL if one were interested in a particular phenotype, thus reducing the list of potential candidate genes drastically. In contrast, the X-chromosome harbors variation contributing to 35 different craniofacial measurements representing all regions of the cranium. Any genetic variant on the X-

Table 6.6 ToppFun Functional Enrichment Results. 317 craniofacial genes identified on OMIM and/or from previous publications[a].

Molecular Function	N (%)[b]	Biological Process	N (%)[b]
sequence-specific DNA binding	68 (8.3)	organ morphogenesis	123 (13.4)
regulatory region nucleic acid binding	54 (9.6)	embryonic morphogenesis	103 (17.9)
regulatory region DNA binding	54 (9.6)	skeletal system development	91 (19.7)
transcription regulatory region DNA binding	52 (9.4)	embryo development	122 (11.3)
transcription factor activity, sequence-specific DNA binding	75 (6.3)	tissue development	145 (8.1)
Pathway	**N (%)[b]**	**Human Phenotype**	**N (%)[b]**
neural crest differentiation	24 (23.8)	palate abnormality	132 (25.3)
cancer pathways	35 (10.7)	orbit abnormality	166 (19.2)
cancer proteoglycans	23 (10.2)	oral cleft	100 (31.7)
extracellular matrix organization	25 (9.5)	mouth abnormality	186 (16.6)
TGF-β signaling pathway	14 (17.5)	oral cavity abnormality	176 (17.5)
Cellular Component	**N (%)[b]**	**Disease**	**N (%)[b]**
transcription factor complex	30 (9.3)	craniofacial abnormalities	66 (44.3)
neuron part	54 (4.8)	craniosynostoses	8 (72.7)
extracellular matrix	30 (7.1)	congenital heart defects	12 (37.5)
membrane raft	24 (8.6)	holoprosencephaly	8 (61.5)
neuron projection	45 (4.8)	cleft palate	12 (31.6)

[a]Wilkie and Morriss-Kay, 2001; Maga et al., 2015. [b]Number of Tr-set genes thus annotated and the proportion that these genes comprise of the total number of genes with that annotation in the database.

chromosome (as well as the Y, although that was not included in any analyses) has the potential to demonstrate dosage effects and genomic imprinting, which may have interesting implications for sex-related craniofacial variation.

I conducted a *post hoc* linkage scan for adult body weight (KG) and principal component 1 (PC1), which were used as covariates when mapping the EIDs and ECV. I localized three peaks for KG and four for PC1 (Table 6.8). All seven correspond to one of my QTLs. The four PC1 QTLs are highly pleiotropic. Additionally, the traits that map to the same QTLs as PC1 all have high, positive loadings on PC1 (see Table 3.6). For the most part, the lists of traits for these QTLs are dominated by Model 1 measurements. This supports my assertion that correcting for PC1 in Model 3 may have preferentially removed more variation in some regions of the skull than others (see *4.4 Discussion*). I observed an interesting pattern at one of the KG QTLs (*Cfs12.4*). The linkage signal for two of the traits

Table 6.7 Comparison of QTLs Identified in this Study to Published Ones.

Published QTL	Published Traits[a]	Organism Traits Markers	Human Ortholog(s)	My QTL	My Traits[b]	Source
Mus chr17: 30615222-31231411	PC1: BA, BR, NA, PO, PT, ST, ZI, ZS, ZT	Mouse Cranial PCs SNPs	6 & 21	*Cfs4.1*	ASAS, PLSY, POBA, SYMX, VSSY	Palleres et al., 2014[c]
Mus chr11: 51241312-51391312	PC18: AS, BA, OP, PM, PO, ZI, ZS, ZT		5	*Cfs6.4*	ASJP	
Mus chr8: 90136634-95150348	PC18: AS, BA, OP, PM, PO, ZI, ZS, ZT		16	*Cfs20.2*	BACC, FMPM, JPJP, 41MX, 41ZI	
Mus chr5: 62131920-62659428	PC14: AS, BR, DA, NA, PO, ST, ZI, ZS, ZT		X	distal X	BRNA, BRPT, CNCN, CPZS, NA41, NACP, NANL, PM41, STST, ZSNL	
Papio chr16: 54cM	NAPR	Baboon EIDs STRs	17	*Cfs16.2*	NANL, ZSNL	Sherwood et al., 2008
Homo 3p21.31-p14.1	lower facial height angle	Human EIDs STRs	3	*Cfs2.3*	NLAC, NAZS, PM41	Sherwood et al., 2011[d]
Homo 6q16.1-q21	posterior facial height angle		6	*Cfs4.3*	NAFM, ZTVS	
Homo 12q13.11-q21.31	NABA		12	*Cfs11.3*	CACP, DAFM, NAFM, NLVS	

[a]Trait abbreviations as in Table 3.1. [b]Although all traits mapping to each QTL are listed, those that are more likely to correspond to the published QTL signal are in red typeface. [c]Published QTLs are given in basepairs. The craniometric landmarks that appear to load most heavily on each PC upon examination of Procrustes distance wireframes (see published Supp. Fig. 5) are listed with their associated PCs. [d]These cephalometric angles are defined as lower facial height: nasale medium columella (i.e., AC) to center of the mandible (center of the mandibular ramus) to soft tissue pogonion (i.e., mental eminence) and posterior facial height: nasion to the pterygomaxillary fissure to gonion.

that share this QTL with KG (NABA and NACA) was observable only for Model 1, which suggests this locus may include a genetic variant that operates globally, rather than on the cranium specifically.

6.4.1 Pleiotropy

One way to infer pleiotropy indirectly is to examine the distribution of linkage signals across the genetic map (e.g., Kenney-Hunt et al., 2008). Signals that tend to cluster may suggest the existence of a single or a few pleiotropic genes or of a number of closely located genes that act on individual traits alone. As pleiotropy and epistasis are proposed mechanisms underlying morphological integration and modularity, it is expected that morphological integration will be produced and maintained by genetic correlations (i.e., genetic integration), thereby eventually contributing to evolutionary integration as the genes are more likely to be co-inherited (Klingenberg, 2008). This evolutionary integration, in turn, helps to maintain the functionality of the traits affected by variation at any locus at which linkage signals cluster. Therefore, genetically integrated traits would be expected to be part of the same functional and/or developmental module. This theory is called the genetic independence model and Leamy et al. (1999) demonstrate evidence corroborating it in craniofacial growth in mice. One prediction of the model is that a genetic variant should affect phenotypic values of traits within the same module more so than those of traits in different modules.

The ρ_Q patterns at *Cfs4.1* partially support this prediction in that traits of the nasopharynx are affected similarly by genetic variation at this pleiotropic locus (although the effect is antagonistic between palatal dimensions and the height of the posterior nasal opening), as are traits of the posterior cranial fossa. However, *Cfs4.1* does contribute to variation in both the nasopharyngeal and posterior neurocranial traits, and it is hard to envision how the two sets of traits could belong to the same module. The ρ_P patterns support this, as phenotypic

Table 6.8 Linkage Mapping Analysis of Body and Cranial Size.

Trait	N	h^2 (se)	covariates (h^2_{cv})[a]
KG	787	0.443 (0.07)	A, S, AS, A^2 (65.1)
PC1	787	0.661 (0.08)	--- (---)

Trait	Human Ortholog	LOD Score	Peak Locus (SI)	h^2q	QTL Name
KG	2q	1.51	125 (118-137)	0.106	*Cfs12.4*
	3	1.91	24 (7-37)	0.139	*Cfs2.2*
	14_15	1.75	95 (79-104)	0.144	*Cfs7.4*
PC1	1	2.13	146[b] (117-172)	0.242	*Cfs1.4*
	7_21	2.90	76 (63-101)	0.150	*Cfs3.1*
	7_21	2.91	120 (105-128)	0.150	*Cfs3.2*
	12	1.81	39 (27-61)	0.119	*Cfs11.2*

[a]Covariate symbols as in Table 4.2. Traits without significant covariates are indicated with a series of three dashes. Percentage V_P accounted for by significant covariates. [b]This locus is actually the weighted average of a peak at 130 cM (LOD = 2.13) and 161 cM (LOD = 2.07). Both peaks were significant in a multi-QTL scan, suggesting the linkage signal actually lies between these two peaks. The SI is a 1-LOD-drop proximal to 130 cM and distal to 161 cM. The LOD score and h^2_q estimate are given for the peak with the higher LOD score.

correlations are higher between traits of the nasopharynx (PLSY:SYMX = 0.580, PLSY:VSSY = -0.325, VSSY:SYMX = -0.306) and between traits of the posterior cranial fossa (POBA:ASAS = 0.297) than they are between a trait from each region (e.g., POBA:VSSY = 0.018, ASAS:PLSY = 0.054). Despite this, the pleiotropic variation at *Cfs4.1* does affect all traits, helping to maintain the patterns of correlation (phenotypic, genetic, and environmental) among them.

6.4.2 Prioritized Candidate Genes

The overabundance of development-related annotations in the Q-set is consistent with expectations based on the linkages of the loci with craniofacial variation. A number of the annotations even specifically reference morphogenesis and development of anatomical structures and systems. To gauge whether these results are particularly exceptional, I also submitted a list of the 1,223 genes contained within the Sig-QTLs to which ECV maps (*Cfs4.4* and *Cfs15.3*) to the GO Enrichment Analysis. The first 20 overrepresented biological processes (all with >5 fold enrichment) involve various components of the immune system (results not shown). These 1,223 genes are a subset of the Q-set and were included in the original analysis, too. The fact that the results for the entire Q-set are not biased toward immune system

annotations as well suggests that the prevalence of development-related annotations is significant, as there must be enough present to counter-balance the universal and high degree of enrichment of immune-related genes.

The overabundance of genes annotated as being involved in the *Wnt* signaling pathway is noteworthy. This pathway is involved in neural crest cell development in zebrafish and mice (e.g., Ikeya et al., 1997; Lewis et al., 2004; Mani et al., 2010) and osteoblast development and osteoclast differentiation in mice (e.g., Glass et al., 2005; Hu et al., 2005). Perturbations to the pathway manifest as craniofacial and brain malformations (e.g., Brault et al., 2001; Huelsken and Birchmeier, 2001; Alexander et al., 2014; Kurosaka et al., 2014). The enrichment of these genes within Sig-QTL suggests that the *Wnt* signaling pathway may also be important for non-pathological, continuous intrapopulation variation and would be a good place to start looking for explanatory variants.

Of the 102 genes that overlapped the C- and Q-sets, only 27 were prioritized by ToppGene as likely candidates. This does not mean the remaining 75 are not related to craniofacial variation, as they were identified by previous researchers for contributing in some way to craniofacial growth and development. Rather, it may be the case that these genes are less important for explaining variation in this sample of baboons. Linkage and association signals are entirely dependent on sample characteristics, which is why it is so important to account for population structure in mapping studies (e.g., Pritchard et al., 2000). There are known craniofacial genes that are not contained within the SIs of any QTLs I identified. For example, *FGFR3* plays a critical role in craniofacial growth and development (Wilkie et al., 1997) and causes craniosynostosis when mutated (Wilkie, 1997). It is located at HSA16p16.3. The closest individual-trait peak (for STST) is 8.8 Mb away, too far for *FGFR3* to be considered a viable candidate gene.

A number of possibilities exist that explain why no traits map to the proximal end of HSA4. First, I may not have the power to identify such a linkage signal. I was able to locate 460 individual-trait peaks, but I certainly missed some signals due to lack of statistical power, which fluctuated across scans. Reduction in statistical power for some scans was observable in that a significant locus for a trait at one level of analysis sometimes did not pass either the significant or suggestive threshold when incorporating a different set of covariates. For example, none of the individual-trait LOD scores for *Cfs4.2* pass the stringent threshold, so it was not included in candidate gene prioritization and GO analyses. However, an important craniofacial-related gene, *RUNX2* (Wilkie and Morriss-Kay, 2001), is located within 6 cM of *Cfs4.2*'s peak. Despite this issue, the sample of SNPRC baboons that I used has more statistical power than any other primate sample previously analyzed. This is indicated by the relatively large effective sample sizes for each trait (N_e; see *4.3.3 Effective sample size*). It is also possible that genetic variation in some craniofacial genes (like *FGFR3*) is not segregating in the SNPRC baboons and, thus, does not contribute to intrapopulation craniofacial variation. Alternatively, such genes may contribute to V_P but their effect sizes may be too small (<10%) to identify in complex pedigrees of outbred populations with the statistical methods and computational resources currently available (e.g., Hill, 2010; Walsh, 2014).

I identified 93 genes that, to my knowledge, are not often implicated as contributing to craniofacial variation, either pathological or continuous. Examining the genes on that list in greater detail is a much more manageable task than starting with the 11,453 genes in the Q-set, and certainly more so than starting with the ~20,000 in the entire (human) genome. One possible approach to studying the genetic basis for complex traits is to start with a list, such as the C-set, and perform a genome wide association study. However, it is difficult to link it to craniofacial variation. The benefit of having performed linkage mapping on traits measured in a

population for which genetic data are available is that when the list of potential candidate genes is narrowed, the genes that are omitted are those that do not demonstrate evidence of being involved in the production of that population's V_P.

ToppGene prioritizes Te-set genes by functional similarity to the Tr-set. According to the ToppFun results, the Tr-set genes are best categorized as regulatory sequences, meaning that the 93 genes identified by ToppGene as priorities are likely to be regulatory in nature. This is significant because evidence from researchers like Chen and Rajewsky (2006), Haygood et al., (2007), and McLean et al. (2011) supports King and Wilson's (1975) hypothesis that genetic variation in regulatory pathways can have drastic effects on phenotypes, thus explaining the disjunction between morphological differences between some sister taxa being large-scale while genetic differences are very minor. Obtaining SNP data for my sample in the regions of these genes and associating them to V_P would provide further opportunities to test King and Wilson's theory.

6.4.3 Study Design Limitations

A number of the limitations that I discuss below are known issues with linkage mapping techniques, MLVD, and aspects of my experimental design that were unavoidable, while others I discovered in the course of conducting these analyses.

Interval Size

In general, linkage analyses narrow the search for contributory genetic variants only to large regions (multiple Mb in size), which potentially contain hundreds of genes (Borecki and Suarez, 2001). Association mapping has more resolution than linkage mapping does (although false positives are more of a problem), but it requires ascertaining more of a population's genetic diversity, such as would be possible with SNP genotypes. For example, Sherwood and colleagues (2011) located 10 QTLs for human craniofacial shape using STR genotypes. On

average, each QTL was 70 cM and contained 146 genes (range: 30-363). In contrast, Norgard et al. (2008) conducted a similar study in mice for a single trait, long bone length, using SNP genotypes. They located 70 QTLs, each of which was 12.8 cM in size; a subset of the QTL that were pleiotropic (22 in total) contained an average of 106 genes each (range: 37-298).

One strategy that maximizes resource usage is initial linkage mapping using microsatellites (often less expensive on a genome-wide scale, although the cost of SNP-chips is decreasing rapidly) to discover large QTLs, followed by association mapping in these regions of interest using SNPs to narrow down the SIs to target specific candidate genes. Now that I have identified multiple QTLs for baboon craniofacial variation, I can select the most promising for additional association mapping to achieve better resolution for identifying potential functional variants.

Effect Size

Although more complicated models that include the potential for epistasis, gene-by-environment interactions, oligogenic inheritance, and covariates have been developed and successfully implemented in linkage analysis routines, one major drawback that remains is that we almost certainly cannot detect genes of small effect (i.e., those contributing to polygenic inheritance). This partially explains why so much heritable genetic variation remains unidentified, an issue many refer to as the problem of “missing heritability” (e.g., Manolio et al., 2009; Eichler et al., 2010), although a significant factor there is our inability to account for phenotypic plasticity and the myriad ways in which gene products interact with other gene products and environmental conditions. Perhaps we will solve this issue in the future, but for now, we must be content with identifying genes of intermediate effect. The results of my linkage analysis are no different than expected; I was able to localize QTLs explaining ~14% of the craniofacial variation in my sample.

Outbred Populations

My sample of baboons is derived from an outbred population, rather than a recombinant inbred-line (RIL) cross, as is often used in experimental laboratory settings. QTL mapping in RILS is considerably easier as linkage disequilibrium is at a maximum in the first generation progeny (F_1) of crossed inbred lines, and every member of the population is *informative*. An individual is informative if it is heterozygous at both the QTL and the marker to which it is linked (Lynch and Walsh, 1998). Every F_1 individual is heterozygous for (*i*) all fixed differences between the two parental populations and (*ii*) some of the variable loci (at a probability equal to the allele frequencies at that locus). Thus, given that both marker loci and QTLs are either *i* or *ii*, every individual in the population is informative. Unfortunately, members of an outbred population are potentially non-informative because they might be heterozygous at only the marker locus, only the linked QTL, or neither (see *4.2.4 Sample Size Versus Effective Sample Size*).

An additional difficulty is that the pattern of allele segregation may vary across the population (or in this case, among sire-lines in the pedigree): marker locus allele *M* may be linked to QTL allele *Q* in one individual and allele q in another (Lynch and Walsh, 1998). This obscures the patterns of co-segregation used to identify QTLs. One method for exploring the effect of this scenario on the results presented here is by replicating linkage scans within each sire-line separately.

Z-Score Standardization

One limitation specific to my research design is the use of standardized EID values. Transforming the traits in this way constrains the standard deviations (~1.0), which can make it difficult to estimate genetic parameters because (1) variance is even smaller (when sd < 1.0) as it is a squared term of sd, and (2) variance becomes even smaller as it is decomposed into its constituent components ($\sigma^2_{qi}, \sigma^2_g, \sigma^2_e$; Michael Mahaney, pers. comm.). This can be seen in the

occasional occurrence of convergence errors, where SOLAR gets “stuck” on a relatively flat likelihood surface and is unable to determine which is the most likely solution. This happened rarely but for whatever reason, locus 132 cM on HSA1/PHA1 demonstrated convergence errors on a few passes. In the event that this occurred, two-point mapping was conducted for that trait and the LOD scores for the markers immediately up- and downstream of this locus were examined (upstream: D1S306 at 124.1 cM, downstream: D1S533 at 133.5 cM). The twopoint results suggest that these convergence errors at 132 cM were not an issue, as neither marker ever demonstrated linkage in these cases.

MLE Method

The application of maximum likelihood to the estimation of model parameters is a powerful method for dealing with complex pedigrees. The alternative, Analysis of Variance (ANOVA), cannot jointly decompose variance among relatives of different class (i.e., parent-offspring, half-sibships, and avuncular relationships cannot be combined in the same ANOVA model). It also requires relatively balanced sample sizes for each class of individual, a requirement that is difficult to achieve in non-experimental settings (Lynch and Walsh, 1998). MLE methods can handle unbalanced research designs and complex pedigrees but are computationally intensive, and it is assumed that all fixed effects, such as the population mean, are known without error, which can provide biased estimates of effect sizes.

It is also possible that the final MLE solution is only a local maximum as it would be impossible to evaluate the likelihood of every possible parameter combination. This issue can be addressed by repeating the maximization using different starting parameters to determine if each replicate maximization converges on the same result. Due to the computational demands of my project (MLE for the results presented in Chapters 4, 5, and 6 took a total of 7,306 hours, or 304 days), I did not explicitly conduct such repeated analyses. However, the triplicate

research design provided a test of sorts in that the parameters were, by definition, different for each MLE procedure. Models 1-3 were allowed to include different combinations of covariates (i.e., different values of μ)—thus, the residual observed data with which the expected covariance matrices ($\boldsymbol{\Omega}$) were created differed—and had different h^2 estimates (i.e., σ_g^2 and σ_e^2 were different). Additionally, some measurements were purposefully modified duplicates of one another (for example, NANL and NLAC are roughly equivalent to NAAC) so their results could be compared. They are very similar, particularly those of NANL and NAAC.

6.4.4 Twopoint Linkage Mapping

In rare cases, results for two-point scans were different from those of a corresponding multipoint scan. For instance, the multipoint results for NAVS (Model 3) on HSA2q initially indicated a linkage signal at 139 cM. As this is very close to the end of the chromosome's genetic map (146 cM), I conducted a twopoint scan, too. The LOD (0.92) for the closest marker (D2S2338 at 125.8 cM) did not pass the suggestive threshold, suggesting that the multipoint peak was an artifact of being at the end of the genetic map. However, two other markers (D2S433 at 92.2 cM and D2S206 at 116.5 cM) both had suggestive LOD scores (1.57 and 1.74, respectively). I chose to err on the side of caution and ignore the linkage signal entirely, but it is possible that there is a peak in the range of 92.2-116.5 cM, as suggested by the twopoint results.

A result such as the one I obtained for NAVS (Model 3) typically occurs because the number of informative individuals scored at each marker differs as a function of allele frequencies (Lynch and Walsh, 1998). Because two-point mapping only uses the two observed data points (genotypes at each marker flanking the interval in question), results can be unreliable when those data points demonstrate very different patterns (Fulker et al., 1995). In contrast, multipoint mapping estimates genotypes throughout an interval for every pair of relatives, thus increasing the amount of information used to estimate model parameters.

Multipoint methods provide more power and increased precision in locating QTL peaks, particularly in cases where the QTL is located in an area of low information and when allele frequencies differ between adjacent markers (Almasy and Blangero, 1998). Ideally, both sets of results would correspond for every trait, which occurred for the majority of EIDs. Extensive simulations by both Fulker and colleagues (1995) and Almasy and Blangero (1998) indicate that multipoint approaches are both powerful and robust, so for the few instances where the two-point and multipoint mapping results differed, I placed more confidence in the multipoint results or ignored the signal entirely, as I did with NAVS (Model 3).

6.5 Conclusion

In this chapter I identified locations within the baboon genome that are significantly correlated with craniofacial variation in a population of pedigreed baboons. I condensed the 460 individual-peak loci into 69 QTLs, 24 of which were significant with $P < 0.05$ (i.e., LOD ≥ 2.75). Most of the QTLs are pleiotropic and contribute to variation in multiple traits that quantify different regions of the cranium. The SIs of these QTLs include ~11,500 genes and I prioritized 120 positional candidate genes using gene ontology annotations and the functional profiles of genes known to regulate craniofacial development and/or cause craniofacial malformations when mutated.

Producing a list of prioritized positional candidate genes provides a foundation on which to design association mapping studies in an effort to discover functional genetic variants contributing to craniofacial variation in this population and to estimate their allelic effect sizes. Identifying and annotating such variants further clarifies the genetic architecture of baboon craniofacial variation. Although we should not necessarily expect GP-maps to be orthologous between species, using knowledge about the genomic regions contributing to baboon craniofacial variation allows us to formulate testable hypotheses for species that lack similar genetic, genomic, and phenotypic data.

CHAPTER SEVEN
DISCUSSION

7.1 Introduction

This study had three main objectives: (1) to quantify craniofacial variation in baboons, (2) to describe the patterns of how that variation is structured, and (3) to identify regions of the genome that are likely to contain genetic variation that contributes to it. I completed these objectives by skeletonizing and microscribing a sample of 985 pedigreed baboons. To address the second objective, I calculated linear distances among the landmark data and assessed the nature and degree of morphological integration in those dimensions. Finally I estimated the proportion of variation in each measurement attributable to additive genetic effects and mapped those effects to the baboon genetic map.

In this chapter I will review the specific questions I addressed and hypotheses I tested in Chapters 4-6. I will then discuss how my findings fit into the larger picture of craniofacial development and the evolution of complex traits, and end with a discussion of some important caveats to keep in mind. I argue that this research highlights the necessity of considering both inter-trait correlations and the relative contribution of additive genetic and environmental variation when studying complex phenotypes. Doing so should be a priority in biological anthropology and evolutionary biology. Accurately modeling a phenotype's genetic architecture allows for making informed interpretations of interspecific diversification and patterns of growth and development.

7.2 Review of Research Questions and Results

I estimated endocranial volume (ECV) and calculated 60 Euclidean interlandmark distances (EIDs) to quantify craniofacial variation in baboons. These EIDs reflect variation in the nasal, oral, and orbital complexes; the zygomatic arch; the anterior and posterior neural vault; and the anterior and posterior cranial base. Their phenotypic variation differs by age and sex and with body and cranial size (i.e., demonstrates allometric effects). By analyzing these traits in

conjunction with the baboon genetic map, I was able to address the following research questions.

7.2.1 The Contribution of Genetic Variation to Craniofacial Variation

In Chapter 4 I estimate the heritability of these 61 traits, determine the effect of covariates—such as sex, age, and the interaction between sex and age—on trait variation, and determine effective sample sizes (N_e) for each trait.

What are the effects of allometry and covariate factors on a trait's V_P?

Because the EIDs were standardized prior to analysis, much of the sex and age-by-sex related variation was eliminated prior to analysis. Only adult individuals were included in analyses so there was little age-related variation. However, ECV was analyzed in raw units (cm^3, or cc), as it was normally distributed and did not need to be compared to any other traits that might have different distributional properties. A large proportion of ECV variation was attributable to covariate effects: 40-50% depending on the model. If the pattern of covariate effects on ECV is any guide to that of other craniofacial traits, and there is no reason to assume that error variance associated with age and sex would affect volumetric dimensions differently than linear measurements that capture the same structural variation, it can be inferred that covariates account for a significant amount of the variation in baboon crania. This is supported by the results of Roseman et al. (2010) who showed that, across 46 linear craniofacial dimensions in a subsample of this same population of baboons, an average of 53% of the trait variation (on their original measurement scale, mm) was explained by covariates, primarily age and sex.

The amount of phenotypic variation explained by covariates (i.e., V_{cov}) increases when first body size and then cranial size variation is eliminated. This is to be expected as previous research (e.g., O'Higgins and Collard, 2002; Singleton, 2002; Frost et al., 2003; Leigh, 2006) has demonstrated that scaling effects in baboons, as well as other large-bodied papionins, is an

important source of intraspecific craniofacial variation. Removing the portion of phenotypic variation attributable to allometric effects and analyzing patterns of variation in the residual variation (V_R) that was masked by size-related variation allows for the examination of local, small-scale variation. This variation likely corresponds to the influence of developmental and functional demands on individual craniofacial units, such as those envisioned by Moss in his Functional Matrix Model (Moss and Young, 1960; Moss, 1962).

Are craniofacial traits heritable and how much of the V_P is explained by additive genetic effects?

For all 61 traits, a significant proportion of V_R demonstrates additive genetic effects. After adjusting for trait repeatability, estimates of heritability are ~0.5, which is moderately high and congruent with estimations of morphological traits for most taxa thus studied (Mousseau and Roff, 1987). These estimates decrease when traits are corrected for body and cranial size variation, and this reduction is due to a decrease in the amount of V_A, rather than a relative increase in the amount of V_E. This indicates that genetic variation influencing body and/or cranial size also contributes to variation in craniofacial shape and, thus, provides evidence for the effects of pleiotropy in baboon crania.

What is the relationship between V_A and V_P, or what is the N_E for each trait?

Determining N_e for a trait is an additional method of assessing the significance of genetic parameters, which will always be estimated with a greater degree of error than their phenotypic counterparts. Phenotypic variances/covariances and correlations are estimated by using every individual measured ($N \leq 953$, depending on the trait), but redundant genetic information is contained in the distribution of trait variation due to the fact that individuals are related to one another (therefore sharing some portion of their genes and causing the data to be non-independent). Consequently, the sample sizes from which genetic parameters are estimated

(N_e) are much lower, on the order of a 90% reduction in size in this sample. This means that the repeatability of genetic correlation estimates will be much lower and the standard errors much higher. This affects the accuracy of the estimates, but not the determination of the pattern of inter-trait relationship, as will be discussed below.

7.2.2 The Relationships Among Regions of the Cranium in Different Contexts

In Chapter 5 I estimated pairwise genetic correlations among EIDs for three different covariate models: accounting for only sex, age, and interaction effects; additionally accounting for the effect of body size variation; and then also accounting for cranial size variation. I compared the observed correlation patterns to those expected on the basis of developmental and functional relationships under the working hypothesis that traits that develop together or interact with one another to perform a function will be more highly correlated, or integrated, than those with which they do not interact, either developmentally or functionally.

Do patterns of modularity in baboon crania closely resemble those expected based on functional and developmental relationships among traits?

The correlation between the matrix of phenotypic correlations and connectivity matrices designed to reflect expected patterns of integration are generally high in Models 1 and 2. However, only phenotypic correlations among various regional modules (e.g., among just the traits comprising the orbit) are maintained after correcting for cranial size variation in Model 3. Modules in the ventral portion of the cranium (e.g., nasal, orbital, zygomatic, and anterior neural vault) tend to be more highly integrated than others.

What effect does allometry have on patterns of phenotypic variation?

Omitting body-size variation in Model 2 does not alter the magnitude of phenotypic or genetic correlations, but omitting cranial size variation in Model 3 reduces both. It also alters the pattern of phenotypic correlation and the manner in which genotype maps to phenotype. These results

indicate that allometric variation has a very strong influence on overall patterns of craniofacial integration. One major implication of this is that results of a study that corrects for allometric variation related to overall cranial size differences will likely produce different results than one that does not or corrects only for overall body-size differences. This should be kept in mind when conducting and evaluating studies of morphological integration.

7.2.3 The Location and Structure of Craniofacial-Related Genetic Variation in the Baboon Genome

In the final results chapter, Chapter 6, I performed linkage mapping of the EIDs and ECV to the baboon genetic map using maximum likelihood variance decomposition. I identified regions of the genome, or quantitative trait loci (QTLs), containing STR markers linked to genetic variants that significantly contribute to a portion of V_P. Finally, I determined which gene ontology annotations were most commonly represented in these QTLs.

Where are QTLs located within the baboon genome?

I identified a total of 384 linkage signals for ECV and 56 of the EIDs. On average, these signals accounted for 12% of the V_R for a trait, which is consistent with the current expectation of being able to identify linkage signals for oligogenes (e.g., Borecki and Suarez, 2001). A number of these signals coincide with those identified for other traits, so they were considered evidence for a single QTL with additive genetic effects on multiple traits. There were 69 such QTLs, of which 24 were significant with $P < 0.05$. Most QTLs affected variation in at least two traits. Larger chromosomes contain more linkage signals, and more of the QTLs on larger chromosomes affect multiple traits.

How many QTLs do individual traits have and how does that vary across cranial regions?

Most traits map to 3 QTLs, half of which are significant. Basicranial traits are less variable on average but this does not affect the number of linkage signals identified for such traits. Nasal

and zygomatic traits are more variable than any others, but again, this has no effect on linkage-mapping results. There is a greater variance, but a lower average, in number of linkage peaks localized for anterior neural vault traits, with seven individual-trait peaks for bi-stephanionic breadth (the most of any other trait) and 0 for the distance between bregma and asterion. In other words, the ability to localize heritable genetic variation to specific regions of the genome in the same region of the cranium depends on whether that variation is contributing to variation in the sagittal or coronal planes in this case.

Do different QTLs contribute to allometric variation and size-corrected variation?
The overall number of linkage signals does not vary when taking into account body and cranial size variation. However, for specific regions, allometric variation does mask some signals (i.e., more peaks are identified in Models 2 and 3) or signals cannot be identified for some size-independent variation (i.e., significant peaks in Models 1 and 2 disappear once size variation is removed).

Is there evidence for pleiotropy in baboon crania?
Based on the pattern of distribution of individual-trait linkage signals, I inferred that a number of QTLs contribute to variation in multiple EIDs. In some cases, these EIDs characterize variation in the same craniofacial component. For example, the first QTL identified on baboon chromosome three (*Cfs3.1*) explains variation in nine different EIDs, as well as PC1, and eight of those EIDs characterize variation in the region of the cranium connecting the upper face and anterior cranial vault: width and depth of the orbits, the angle at which the face is hafted onto the vault, and size of the infratemporal fossa. As PC1 also maps to the same locus, genetic variation that increases global cranial size appears also to alter the shape of the posterior face and its relationship to the anterior cranial base. In other cases, only variation in a single trait maps to a QTL, such as all four QTLs on baboon chromosome 14.

Additionally, I was able to test individual-trait variation against a model of pleiotropy by estimating additive genetic variation common to pairs of traits and linked to *Cfs4.1*. For all five traits, which characterize variation in both the nasopharynx and posterior basicranial breadth, additive genetic correlations specifically attributable to shared variation at *Cfs4.1* are significant. This indicates that, not only are these traits phenotypically correlated but, they are genetically correlated, and this is due partly to the pleiotropic effects of genetic variants within *Cfs4.1*.

What types of genes characterize the QTLs to which craniofacial variation maps?
In combination, the genes contained within the support intervals (SIs) of the QTLs that I identified are characterized as being overrepresented by those involved in tissue and organ development, particularly in regard to the *Wnt* signaling pathway. None of the QTLs in particular are gene rich or gene poor, as the number of genes within an SI is a function of its size.

Of the 24 significant QTLs (Sig-QTLs), 22 of them contain at least one gene that is known to be involved in craniofacial embryogenesis or to cause structural deformities with gain- or loss-of-function mutations. I used GO and PANTHER classifications to characterize a list of these known craniofacial genes according to their involvement in particular pathways, preferential contribution to molecular signaling versus cellular structure, and association with particular biological processes. The annotations of all genes within my QTLs were then compared to this list of characters to determine if they more closely match the subset of annotations than would be expected if a sample of similar size were drawn at random from the genome. Finally, I used this list to help identify genes that closely match those characteristics, as they should be priorities for future targeted candidate gene research.

7.3 Discussion Points

Recently, there has been a move away from studying forms to studying the processes that underlie their production and, especially, the production of their variation (Rolian and Willmore,

2009). The research presented in my dissertation combines the fields of quantitative genetics and evolutionary biology in a first attempt at providing a holistic view of craniofacial variation in baboons. The sample curated and measured in the course of completing this dissertation is an amazing and valuable resource that can be put to use answering multiple questions, from the contribution of heritable variation to osseous changes associated with periodontal disease (Miley et al., 2011) to the structural patterns of cerebral gyrification (Atkinson et al., 2015).

Most of the phenotypes studied by biological anthropologists are complex in that they are continuous, polygenic in nature, generally normally distributed within a population, and affected by pleiotropy, epistasis, environmental variation, and interactions between genetic and environmental variation. The only way to study such traits is with quantitative genetic methods. For this study, I quantified morphological variation using linear dimensions, but there are multiple ways to do so.

What is important about whichever method is selected for assessing V_P is the recognition that such measurements need to be considered in relation to others to obtain the maximum amount of biologically meaningful information from the results. For example, the QTL I selected for pleiotropy analysis, *Cfs4.1*, explains variation in 5 EIDs: PLSY, ASAS, SYMX, VSSY, and POBA. Rather than examine the effects of this locus on the traits individually, I chose to consider the traits that represent variation in an anatomical structure, and then to examine the effects of the locus on the structure(s). PLSY, VSSY, and SYMX are dimensions that describe the length and breadth of the posterior hard palate (PLSY and SYMX, respectively) and height of the nasal choanae (VSSY). Together, they quantify variation in the nasopharynx. Examination of the genetic correlations among them indicates that variation at *Cfs4.1* affects palatal and nasal dimensions in an inverse manner: the same genetic variant(s) cause the palate to become wider and longer but the height of the posterior nasal aperture to

diminish. Including the final two EIDs, both of which describe breadth of the posterior cranial base, completes the picture. The same genetic variant(s) also affects the nuchal region, but in such a way that the breadth of the palate and of the basicranium are inversely related. Considering the effect of this locus on the traits as a whole and the structures that they represent provides a more meaningful interpretation of the results and indicates that the most meaningful question to ask is what the selective pressure might be that would affect variation in both the nasopharynx and the nuchal region jointly, rather than on the specific EIDs themselves.

7.3.1 A Cautionary Tale of Allometry and Morphological Integration

One of the most important inferences to be drawn from this research—and one that is supported by results in all three chapters, which is remarkable because they describe three very different types of analyses—is that individual aspects of the cranium cannot be evaluated in isolation. As indicated in Chapter 5, traits are integrated at the phenotypic level, and even more so at the genetic level. This genetic correlation is the result of genetic variation that affects both the patterns and magnitude of inter-trait association. The results presented in Chapter 6 suggest that, in a number of cases, these genetic correlations are attributable to QTLs that have a joint effect on multiple dimensions of craniofacial variation. Whether this genetic variation is the result of single genes with pleiotropic effects or multiple genes in linkage disequilibrium remains to be seen and cannot be determined with these data. Based on the patterns of change in inter-trait correlations, the relative amount of V_A, and the number of QTLs identified in each covariate model, much of this genetic variation likely affects craniofacial variation through the mechanism of acting on body and cranial size variation.

As a result of these allometric effects, it is even more important to consider the *relationships* among traits within a complex structure, such as the cranium. Because of the tendency for allometric variation to mask all other sources, it is common practice to attempt to

eliminate this allometric variation.[1] However, depending on the question being asked, this may not be a wise decision, and in fact, it often produces biased results. For instance, Garcia and colleagues (2015) demonstrate that the use of popular geometric morphometric techniques to "correct" for size greatly increases the probability of making a Type II error because doing so makes it difficult to identify patterns of modularity, even when they truly exist in the data. Geometric morphometric methods, such as Procrustes superimposition, tend to destroy correlation patterns in complex structures by averaging variation across measurements to create a "consensus" (mean) shape and then evaluating individual variation in relation to this sample average shape. This likely explains results such as those of Martínez-Abadías et al. (2009), who suggested that human crania are actually highly integrated, so that change in any one portion of the structure causes concomitant changes in all others. This is contrary to the results of most other studies, which support the premise that the unique configuration of the human craniofacial complex is a result of the breakdown in more global patterns of integration and a rearrangement of the constituent elements to produce our odd-looking crania (e.g., Lieberman 2008, 2011).

Based on the results of my research I argue that, whenever possible, allometric variation should be acknowledged, quantified, and then both omitted from and included in analyses so that results can be compared and the presence and degree of bias can be determined. Valuable information can be gleaned from comparing the results of both analyses. For example, in Chapter 4 I estimate heritabilities for EIDs that are corrected for only sex, age, and interaction effects (Model 1) and then also include body and cranial size as additional covariates (Model 3). If I had only estimated parameters using the latter, I would not be able to determine that: (a)

[1] This is evident in the extensive literature on allometric scaling, which has been widely studied in mammals, especially primates (see the excellent edited volume by Jungers, 1985), and the common practice of automatically performing a Procrustes superimposition on geometric morphometric landmark configurations (see Richtsmeier et al., 2002 for an explanation of the pitfalls associated with using such techniques).

there is a decrease in the $\bar{h}_a^2$ estimates and (2) this is the result of a reduction in V_A, which suggests at least some of the variation in baboon crania is influenced by genetic variants that contribute to allometric variation. In theory, these genetic variants would not be identified in linkage analyses from which size variation was omitted and, therefore, molecular evidence for a potentially important aspect of baboon craniofacial evolution would be missed. Of course, if one is solely interested in regional or even trait-specific variation, then accounting for other sources of variation may be preferred.

Although this is not a new argument, it is an important one to belabor and revisit anew upon occasion. Two major questions in regard to patterns of trait covariation are: Is it sufficient to estimate phenotypic correlations as a substitute for genetic correlations and call it a day? Can we assume that the pattern and/or magnitude of genetic correlations remain constant among species or through time? The former issue is sometimes called "Cheverud's Conjecture," and there is mixed evidence to support it (e.g., Lofsvold, 1986; Roff, 1995), while the latter involves the computationally intense intra-specific comparison of **G**-matrices and adaptive landscapes (see Steppan et al., 2002 and Arnold et al., 2008 for descriptions of methods for doing so). Simply describing patterns of morphological integration is not enough; understanding processes producing integration is also necessary. As correlations among traits bias both the direction of evolutionary change and the ability of a trait to respond to selection (i.e., it's evolvability), studying organismal evolution necessitates understanding integration-producing processes (Hallgrímsson et al., 2002).

Finally, in addition to modeling trait evolution by including inter-trait correlations, it is necessary to establish a trait's heritability to determine if it is evolutionarily salient. For example, if metabolic comparisons among sympatric species of mammals are being used to answer questions about life-history evolution, using a trait like presence/absence of lactation is useless.

It has a heritability of 0 because the trait is not variable within mammalian species. A more realistic example is that using a trait whose variation is primarily the result of environmental variation, rather than additive genetic variation (i.e., it's $h^2 \sim 0$), is also not informative for evolutionary questions. Not understanding the basis for phenotypic variation in a trait can result in creating inaccurate adaptive models or inferences from empirical data.

7.3.2 Caveats

There are a few issues that must be discussed pertaining to the analyses conducted herein. First of all, I emphasize that the results of any quantitative genetic analysis are *specific to the population* in which they are conducted (Flint and Mott, 2001). The estimate of additive genetic variation that is obtained from a sample is the net result of alleles at every locus that contributes to phenotypic variation. As such, it is dependent on both the alleles segregating within a population and the population structure itself. Results obtained in one subsample may not be representative of the entire population and, therefore, replication in multiple populations and across many study designs is necessary.

Because it is an additive *genetic effect* and not an individual *gene* that is being mapped, results can be misleading. For example, a linkage signal could be the result of either a single quantitative trait nucleotide (QTN, the nucleotide that contributes to quantitative trait variation; Lyman et al., 1999) or QTNs in multiple linked genes in close proximity. A single large effect might be the result of two much smaller ones such that, if one variant were to be fixed in a subsample of the population, the effect of the second would not be enough to be detected by linkage. Alternatively, two genes located close together might have opposite genetic effects such that they cancel each other out, also making it impossible to identify a linkage signal. As the old adage goes, absence of evidence (in this case) is not necessarily evidence of absence.

Congruence of evidence from studies using different samples, phenotypes, and methods of ascertaining variation provides additional support for the location of specific QTLs, which can be used as a method of selecting the QTLs and candidate genes to prioritize. As the size and number of QTLs identified in such studies is sometimes daunting—even if they do represent a drastic reduction when compared to the entire genome—ancillary information is often necessary for distinguishing among prospective candidates. For example, in Chapter 6 I point out that some of my traits are similar to those measured in other studies and map to eight of my QTLs that are homologous to regions on the chromosomes of the other organisms in these studies. This may be cause to focus on these QTLs for follow-up. Depending on the study design (e.g., in GWA studies where multiple comparison is a large problem), confidence in having correctly identified a QTL is only obtained with analyses conducted in multiple independent samples.

The issue of moving from QTL to QTN and then demonstrating causality of those QTNs is certainly not a trivial task (e.g., Flint and Mott, 2001). The effect of the QTL must be large enough that the SI is relatively small so that high-density population genetic data can be obtained. Once an appropriate QTL has been selected, SNP data must be obtained for the region, allelic effects estimated for each SNP, and haplotypes constructed. The sample used (either population or pedigree) determines the type of analysis used to demonstrate concordance between genotype and phenotype. However, that correlation is not enough. The QTN(s) must be validated by functional studies, such as are done with complementation tests or through mutagenesis. One of the few success stories for isolating QTNs is in commercial dairy cows. Mutations *DGAT1* and *ABCG2* have been successfully identified as QTNs for milk fat and protein concentrations. However, identification of the QTN in *ABCG2* took 10 years once the QTL was discovered (Cohen-Zinder et al., 2005), while that in *DGAT1* took 4 (Winter et al., 2002).

Despite the limitations of linkage analyses in regard to the specificity of results to the population sampled and the difficulty in then identifying QTNs, the results of a QTL analysis can be used as a hypothesis to test in another population, particularly a wild population if the original result was obtained from a laboratory sample, which represents a small sampling of the total V_A in the taxon.

7.4 Conclusion

Synthesizing these results provides an emerging picture of the genotype-phenotype map (GP-map) underlying craniofacial variation in at least this sample of baboons. The next steps to enhance the resolution to this GP-map could take a few different forms. First, obtaining more nuanced genetic markers, such as SNPs instead of STRs, would allow for the reduction in QTL size through fine-mapping of the regions identified here. By obtaining SNP genotypes for all individuals in the sample and conducting association mapping, which is based on patterns of linkage disequilibrium, the length of most QTLs would be reduced by many Mbs. The hope is that the number of genes within these smaller intervals would be on the order of a few hundred, rather than over a thousand in many cases.

Additionally, comparative analyses using alignments of published draft genomes from multiple primate species to estimate rates of molecular evolution among species within only these QTL intervals seriously reduces the multiple testing burden carried by genome-wide scans. Identifying genetic variants that differ among species, or even those that are polymorphic within species if population data can be obtained, could be an additional method of prioritizing candidate genes. Although genetic variants that are important for species diversification are not necessarily the same as those producing intraspecific variation, the obvious link between heritable genetic variation and evolution by selection provides reason to consider this a suitable starting place.

Although identifying QTNs may not currently be realistic, as the effort required to follow a candidate gene through to demonstration of causality is often cost prohibitive and time intensive, doing so has the potential to expand our understanding of the pattern and process by which morphological variation is produced and maintained. One of the major questions in developmental biology is the relative contribution of molecular variation, either in regulatory pathways or of structural components, to phenotypic variation. The seemingly large degree of interspecific phenotypic diversity has not proven to be reflected by correspondingly large amounts of genetic differentiation among closely related species. This observed disparity has been suggested by some to be the result of genetic mutations in regulatory elements (King and Wilson, 1975), which have the potential to affect a great number of bodily systems, particularly if they act early in the developmental processes.

I propose that the genetic variation underlying craniofacial variation is more likely to be in regulatory elements than in structural genes. Such intraspecific regulatory variation would explain my results: why removing the effects of cranial size variation from V_P (a) reduces the relative amount of V_A among EIDs and (b) diminishes the magnitude and alters the patterns of morphological integration; and why (c) the annotations of the genes contained within the QTL SIs are overrepresented by involvement in regulatory pathways (*Wnt* in particular) and (d) 40% of the genes known to affect craniofacial embryogenesis that also happen to be located within Sig-QTLs are either regulatory or directly involved in a regulatory pathway, despite the fact that mutations in structural proteins are far easier to identify and to validate. Structural size differences, such as those that are accounted for in Model 3, result from variation in the amount of growth-regulating proteins. So if, as my results suggest, a substantial portion of craniofacial variation in baboons is correlated with allometric variation, then a correspondingly substantial portion of craniofacial variation in baboons is likely attributable to regulatory differences.

CHAPTER EIGHT
WORKS CITED

Abzhanov A, Protas M, Grant BR, Grant PR, Tabin CJ. 2004. *Bmp4* and morphological variation of beaks in Darwin's finches. *Science* 305:1462-5.

Abzhanov A, Protas M, Grant BR, Grant PR, Tabin CJ. 2006. The calmodulin pathway and evolution of elongated beak morphology in Darwin's finches. *Nature* 442:563-7.

Ackermann RR. 2002. Patterns of covariation in the hominoid craniofacial skeleton: implications for paleoanthropological models. *J Hum Evol* 43:167-87.

Ackermann RR. 2010. Phenotypic traits of primate hybrids: recognizing admixture in the fossil record. *Evol Anthropol* 19:258-70.

Ackermann RR, Cheverud JM. 2002. Morphological integration in primate evolution. In: Pigliucci M, Preston K, eds. Phenotypic integration: studying the ecology and evolution of complex phenotypes. Oxford, GBR: Oxford University Press. p 302-19.

Ackermann RR, Cheverud JM. 2004. Detecting genetic drift versus selection in human evolution. *Proc Natl Acad Sci U S A* 101:17946-51.

Ackermann RR, Rogers J, Cheverud JM. 2006. Identifying the morphological signatures of hybridization in primate and human evolution. *J Hum Evol* 51:632-45.

Ackermann RR, Schroeder L, Rogers J, Cheverud JM. 2014. Further evidence for phenotypic signatures of hybridization in descendant baboon populations. *J Hum Evol* 76:54-62.

Aiello L, Dean C. 2002. An introduction to human evolutionary anatomy. 6th ed. London, GBR: Academic Press.

Akey JM, Ruhe AL, Akey DT, Wong AK, Connelly CF, Madeoy J, Nicholas TJ, Neff MW. 2010. Tracking footprints of artificial selection in the dog genome. *Proc Natl Acad Sci U S A* 107:1160-5.

Al-Motabagani M, Haroun H, Meguid EA. 2004. Calcification and ossification of the convexity of the falx cerebri and related subdural space in human cadavers. *Neurosci* 9:261-4.

Alappat S, Zhang ZY, Chen YP. 2003. *Msx* homeobox gene family and craniofacial development. *Cell Res* 13:429-42.

Alberts SC, Altmann J. 2001. Immigration and hybridization patterns of yellow and anubis baboons in and around Amboseli, Kenya. *Am J Primatol* 53:139-54.

Albertson RC, Streelman JT, Kocher TD. 2003. Directional selection has shaped the oral jaws of Lake Malawi cichlid fishes. *Proc Natl Acad Sci U S A* 100:5252-7.

Alexander C, Piloto S, Le Pabic P, Schilling TF. 2014. *Wnt* signaling interacts with *Bmp* and *Edn1* to regulate dorsal-ventral patterning and growth of the craniofacial skeleton. *PLoS Genet* 10:e1004479.

Alfaro ME, Bolnick DI, Wainwright PC. 2005. Evolutionary consequences of many-to-one mapping of jaw morphology to mechanics in labrid fishes. *Am Nat* 165:140-54.

Almasy L, Blangero J. 1998. Multipoint quantitative-trait linkage analysis in general pedigrees. *Am J Hum Genet* 62:1198-1211.

Almasy L, Kos MZ, Blangero J. 2015. Linkage mapping: localizing the genes that shape human variation. In: Duggirala R, Almasy L, Williams-Blangero S, Paul SFD, Kole C, eds. Genome mapping and genomics in human and non-human primates. Berlin, DEU: Springer-Verlag. p 33-52.

Altmann J, Alberts SC. 2005. Growth rates in a wild primate population: ecological influences and maternal effects. *Behav Ecol Sociobiol* 57:490-501.

Altmann J, Altmann S, Hausfater G. 1981. Physical maturation and age estimates of yellow baboons, *Papio cynocephalus*, in Amboseli National Park, Kenya. *Am J Primatol* 1:389-99.

Altmann J, Altmann SA, Hausfater G, McCuskey SA. 1977. Life history of yellow baboons: physical development, reproductive parameters, and infant mortality. *Primates* 18:315-30.

Altmüller J, Palmer LJ, Fischer G, Scherb H, Wjst M. 2001. Genomewide scans of complex human diseases: true linkage is hard to find. *Am J Hum Genet* 69:936-50.

Altenberg L. 1995. Genome growth and the evolution of the genotype-phenotype map. In: Banzhaf W, Eeckman FH, eds. Evolution and Biocomputation: computational models of evolution. Berlin, DEU: Springer-Verlag. p. 205-59.

Andersson L, Georges M. 2004. Domestic-animal genomics: deciphering the genetics of complex traits. *Nat Rev Genet* 5:202-12.

Andrews CW. 1916. Note on a new baboon (*Simopithecus oswaldi*, gen. et sp. nov.) from the Pliocene of British East Africa. *Ann Mag Nat Hist Zool Bot Geol* 18:410-9.

Anzelmo M, Barbeito-Andrés J, Ventrice F, Pucciarelli HM, Sardi ML. 2013. Ontogenetic patterns of morphological variation in the ectocranial human vault. *Anat Rec* 296:1008-15.

Arambourg C. 1947. Mission scientifique à l'Omo, vol. 1, géologie, anthropologie. Paris: Muséum national d'histoire naturelle.

Arnold SJ, Bürger R, Hohenlohe PA, Ajie BC, Jones AG. 2008. Understanding the evolution and stability of the G-matrix. *Evol* 62:2451-61.

Arnold SJ, Phillips PC. 1999. Hierarchical comparison of genetic variance-covariance matrices. II. coastal-inland divergence in the garter snake, *Thamnophis elegans*. *Evol* 53:1516-27.

Ashburner M, Ball CA, Blake JA, Botstein D, Butler H, Cherry JM, Davis AP, Dolinski K, Dwight SS, Eppig JT, Harris MA, Hill DP, Issel-Tarver L, Kassarskis A, Lewis S, Matese JC, Richardson JE, Ringwald M, Rubin GM, Sherlock G. 2000. Gene ontology: toll for the unification of biology. *Nat Genet* 25:25-9.

Ashley-Montagu MF. 1933. The anthropological significance of the pterion in the Primates. *Am J Phys Anthropol* 18:159-336.

Ashton EH. 1957. Age changes in the basicranial axis of the Anthropoidea. *Proc Zool Soc Lond* 129:61-74.

Ashton CE, Wilson SR. 1986. Two-point versus multipoint linkage analysis: a statistical view. *Genet Epidemiol* 3:S113-6.

Atchley WR, Rutledge JJ. 1980. Genetic components of size and shape. I. dynamics of components of phenotypic variability and covariability during ontogeny in the laboratory rat. *Evol* 34:1161-73.

Atkinson EG, Rogers J, Mahaney MC, Cox LA, Cheverud JM. 2015. Cortical folding of the primate brain: an interdisciplinary examination of the genetic architecture, modularity, and evolvability of a significant neurological trait in pedigreed baboons (genus *Papio*). *Genet* 200:651-65.

Auton A, Fledel-Alon A, Pfeifer S, Venn O, Ségurel L, street T, Leffler EM, Bowden R, Aneas I, Broxholme J, Humburg P, Iqbal Z, Lunter G, Maller J, Hernandez RD, Melton C, Venkat A, Nobrega MA, Bontrop R, Myers S, Donnelly P, Prezeworski M, McVean G. 2012. A fine-scale chimpanzee genetic map from population sequencing. *Science* 336:193-8.

Avis V. 1961. The significance of the angle of the mandible: an experimental and comparative study. *Am J Phys Anthropol* 19:55-61.

Baab KL, Perry JMG, Rohlf J, Jungers WL. 2014. Phylogenetic, ecological, and allometric correlates of cranial shape in Malagasy lemuriforms. *Evol* 68:1450-68.

Babula Jr WJ, Smiley GR, Dixon AD. 1970. The role of the cartilaginous nasal septum in midfacial growth. *Am J Orthod* 58:250-63.

Badyaev AV, Martin TE. 2000. Individual variation in growth trajectories: phenotypic and genetic correlations in ontogeny of the house finch (*Carpodacus mexicanus*). *J Evol Biol* 13:290-301.

Baer MJ. 1954. Patterns of growth of the skull as revealed by vital staining. *Hum Biol* 26:80-126.

Barbeito-Andrés J, Anzelmo M, Ventrice F, Pucciarelli HM, Sardi ML. 2016. Morphological integration of the orbital region in a human ontogenetic sample. *Anat Rec* 299:70-80.

Barton NH. 2000. Genetic hitchhiking. *Philos Trans R Soc Lond B Biol Sci* 355:1553-62.

Bastir M. 2008. A systems-model for the morphological analysis of integration and modularity in human craniofacial evolution. *J Anthropol Sci* 86:37-58.

Bastir M, Rosas A. 2004. Facial heights: evolutionary relevance of postnatal ontogeny for facial orientation and skull morphology in humans and chimpanzees. *J Hum Evol* 47:359-81.

Bastir M, Rosas A. 2005. Hierarchical nature of morphological integration and modularity in the human posterior face. *Am J Phys Anthropol* 128:26-34.

Bastir M, Rosas A. 2009. Mosaic evolution of the basicranium in Homo and its relation to modular development. *Evol Biol* 36:57-70.

Bastir M, Rosas A. 2013. Cranial airways and the integration between the inner and outer facial skeleton in humans. *Am J Phys Anthropol* 152:287-93.

Bastir M, Rosas A, Lieberman DE, O'Higgins P. 2008. Middle cranial fossa anatomy and the origin of modern humans. *Anat Rec* 291:130-40.

Bastir M, Rosas A, Stringer C, Cuétara JM, Kruszynski R, Weber GW, Ross CF, Ravosa MJ. 2010. Effects of brain and facial size on basicranial form in human and primate evolution. *J Hum Evol* 58:424-31.

Baume LJ. 1961. Principles of cephalofacial development revealed by experimental biology. *Am J Orthod* 47:881-901.

Baumgartner RN, Waters DL, Morley JE, Patrick P, Montoya GD, Garry PJ. 1999. Age-related changes in sex hormones affect the sex difference in serum leptin independently of changes in body fat. *Metab* 48:378-84.

Beard KC. 1990. Gliding behavior and palaeoecology of the alleged primate family Paromomyidae (Mammalia, Dermoptera). *Nature* 345:340-1.

Beard KC. 2006. Mammalian biogeography and anthropoid origins. In: Lehman SM, Fleagle JG, eds. Primate biogeography: progress and prospects. New York, NY: Springer US. p 439-67.

Beard KC, Dagosto M, Gebo DL, Godinot M. 1988. Interrelationships among primate higher taxa. *Nature* 331:712-4.

Beddard F. 1902. The Cambridge natural history: vol X, Mammalia. Codicote, GBR: Wheldon & Wesley.

Behrensmeyer AK, Hook RW, Badgley CE, Boy JA, Chapman RE, Dodson P, Gastaldo RA, Graham RW, Martin LD, Olsen PE, Spicer RA, Taggart RE, Wilson MVH. 1992. Paleoenvironmental contexts and taphonomic modes. In: Behrensmeyer AK, Damuth JD, DiMichele WA, Potts R, Sues HD, Wing SL, eds. Terrestrial ecosystems through time: evolutionary paleoecology of terrestrial plants and animals. Chicago, IL: University of Chicago Press. p 15-136.

Bei M. 2009. Molecular genetics of tooth development. *Curr Op Genet Develop* 19:504-10.

Benefit BR. 1999. Victoriapithecus: the key to the Old World monkey and catarrhine origins. *Evol Anthropol* 7:155-74.

Benefit BR, McCrossin ML. 1990. Diet, species diversity and distribution of African fossil baboons. *Kroeber Anthropol Soc Papers* 71-72:77-93.

Benefit BR, McCrossin ML. 1997. Earliest known Old World monkey skull. *Nature* 388:368-71.

Bennett CV, Goswami A. 2012. Morphometric analysis of cranial shape in fossil and recent euprimates. *Anat Res Int* 2012:1-7.

Berger SL, Kouzarides T, Shiekhattar R, Shilatifard A. 2009. An operational definition of epigenetics. *Genes Dev* 23:781-3.

Berry DP, Buckley F, Dillon P, Evans RD, Rath M, Veerkamp RF. 2003. Genetic parameters for body condition score, body weight, milk yield, and fertility estimated from using random regression models. *J Dairy Sci* 86:3704-17.

Biegert J. 1963. The evaluation of characteristics of the skull, hands, and feet for primate taxonomy. In: Washburn SL, eds. Classification and human evolution. Chicago, IL: Aldine Publishing Company.

Björklund M. 1996. The importance of evolutionary constraints in ecological time scales. *Evol Ecol* 10:423-31.

Bland JM, Altman DG. 1999. Measuring agreement in method comparison studies. *Stat Methods Med Res* 8:135-60.

Blangero J. 1995. Multivariate oligogenic linkage analysis of quantitative traits in general pedigrees. *Am J Hum Genet* 57:A11.

Blangero J, Almasy L. 1997. Multipoint oligogenic linkage analysis of quantitative traits. *Genet Epidemiol* 14:959-64.

Blangero J, Williams JT, Almasy L. 2001. Variance component methods for detecting complex trait loci. *Adv Genet* 41:151-81.

Bloch JI, Boyer DM. 2002. Grasping primate origins. *Science* 298:1606-10.

Bloch JI, Silcox MT, Boyer DM, Sargis EJ. 2007. New Paleocene skeletons and the relationship of plesiadapiforms to crown-clade primates. *Proc Natl Acad Sci U S A* 104:1159-64.

Blomberg SP, Garland Jr. T. 2002. Tempo and mode in evolution: phylogenetic inertia, adaptation and comparative methods. *J Evol Biol* 6:899-910.

Blows MW, Chenoweth SF, Hine E. 2004. Orientation of the genetic variance-covariance matrix and the fitness surface for multiple male sexually selected traits. *Am Nat* 163:329-40.

Blue KT, McCrossin ML, Benefit BR. 2006. Terrestriality in a Middle Miocene context: *Victoriapithecus* from Maboko, Kenya. In: Ishida H, Tuttle R, Pickford M, Ogihara N, Nakatsukasa M, eds. Human origins and environmental backgrounds. Dordrecht, NLD: Springer. p 45-58.

Boehringer S, van der Lijn F, Liu F, Günther M, Sinigerova S, Nowak S, Ludwig KU, Herberz R, Klein S, Hofman A, Uitterlinden AG, Niessen WJ, Breteler MMB, van der Lugt A, Würtz RP, Nöthen MM, Horsthemke B, Wieczorek D, Mangold E, Kayser M. 2011. Genetic determination of human facial morphology: links between cleft-lips and normal variation. *Eur J Hum Genet* 19:1192-7.

Bonilla-Claudio M, Wang J, Bai Y, Klysik E, Selever J, Martin JF. 2012. *Bmp* signalling regulates a dose-dependent transcriptional program to control facial skeletal development. *Dev* 139:709-19.

Bookstein FL. 1996. Combining the tools of geometric morphometrics. In: Marcus LF, Corti M, Loy A, Naylor GJ, Slice DE, eds. Advances in morphometrics. New York, NY: Plenum Press. p 131-51.

Bookstein FL. 2015. The relation between geometric morphometrics and functional morphology, as explored by Procrustes interpretation of individual shape measures pertinent to function. *Anat Rec* 298:314-27.

Borecki IB, Suarez BK. 2001. Linkage and association: basic concepts. In: Rao DC, Province MA. Genetic dissection of complex traits. San Diego, CA: Academic Press. p 45-66.

Bose T, Voruganti VS, Tejero ME, Proffit JM, Cox LA, VandeBerg JL, Mahaney MC, Rogers J, Freeland-Graves JH, Cole SA, Comuzzie AG. 2010. Identification of a QTL for adipocyte volume and of shared genetic effects with aspartate aminotransferase. *Biochem Genet* 48:538-47.

Botstein D, White RL, Skolnick M, Davis RW. 1980. Construction of a genetic linkage map in man using restriction fragment length polymorphisms. *Am J Hum Genet* 32:314-31.

Bouman A, Heineman MJ, Faas MM. 2005. Sex hormones and the immune response in humans. *Hum Reprod Update* 11:411-23.

Bouvier M, Hylander WL. 1981. Effect of bone strain on cortical bone structure in macaques (*Macaca mulatta*). *J Morphol* 167:1-12.

Bowcock AM, Ruiz-Linares A, Tomfohrde, Minch E, Kidd JR, Cavalli-Sforza LL. 1994. High resolution of human evolutionary trees with polymorphic microsatellites. *Nature* 368:455-7.

Bowker GC, Star SL. 1999. Sorting things out: classification and its consequences. Cambridge, MA: MIT Press.

Boyd TG, Castelli WA, Huelke DF. 1967. Removal of the temporalis muscle from its origin: effects on the size and shape of the coronoid process. *J Dent Res* 46:997-1001.

Brancourt-Hulmel M, Doussinault G, Lecomte C, Bérard P, Le Buanex B, Trottet M. 2003. Genetic improvement of agronomic traits of winter wheat cultivars released in France from 1946 to 1992. *Crop Sci* 43:37-45.

Brash JC. 1924. The growth of the jaws and palate. In: The growth of jaws, normal and abnormal, in health and disease. London, GBR: Dental Board of the United Kingdom. p 23-66.

Brault V, Moore R, Kutsch S, Ishibashi M, Rowitch DH, McMahon AP, Sommer L, Boussadia O, Kemler R. 2001. Inactivation of the β-catenin gene by *Wnt1-Cre*-mediated deletion results in dramatic brain malformation and failure of craniofacial development. *Develop* 128:1253-64.

Brockmann GA, Kratzsch J, Haley CS, Renne U Schwerin M, Karle S. 2000. Single QTL effects, epistasis, and pleiotropy account for two-thirds of the phenotypic F_2 variance of growth and obesity in DU6i x DBA/2 mice. *Genome Res* 10:1941-57.

Brodie III ED. 1993. Homogeneity of the genetic variance-covariance matrix for antipredator traits in two natural populations of the garter snake *Thamnophis ordinoides*. *Evol* 47:844-54.

Brommage R. 2001. Perspectives on using nonhuman primates to understand the etiology and treatment of postmenopausal osteoporosis. *J Musculoskel Neuron Interact* 1:307-25.

Broom R. 1936. A new fossil baboon from the Transvaal. *Ann Transvaal Mus* 18:393-6.

Broom R. 1937. On some new Pleistocene mammals from limestone caves of the Transvaal. *S Afr J Sci* 33:750-68.

Broom R. 1940. The South African Pleistocene cercopithecid apes. *Ann Transvaal Mus* 20:89-100.

Broom R, Jensen JS. 1946. A new fossil baboon from the caves at Potgietersrust. *Ann Transvaal Mus* 20:337-40.

Bruner E. 2007. Cranial shape and size variation in human evolution: structural and functional perspectives. *Childs Nerv Syst* 23:1357-65.

Burnett G. 1828. Illustrations of the manupeda, or apes and their allies; being the arrangement of the quadrumana or anthropomorphous beasts indicated in outline. *Q J Sci Lit Art* 25:300-7.

Burrows AM. 2008. The facial expression musculature in primates and its evolutionary significance. *BioEssays* 30:212-25.

Burrows AM, Waller BM, Parr LA. 2009. Facial musculature in the rhesus macaque (*Macaca mulatta*): evolutionary and functional contexts with comparisons to chimpanzees and humans. *J Anat* 215:320-34.

Caccone A, Powell JR. 1989. DNA divergence among hominoids. *Evol* 43:925-42.

Cáceres N, Meloro C, Carotenuto F, Passaro F, Sponchiado J, Melo GL, Raia P. 2014. Ecogeographical variation in skull shape of capuchin monkeys. *J Biogeogr* 41:501-12.

Campbell PM, Campbell ML, Muzzall E. 2015. Occlusopalatal landmark variation among savanna baboons fed different diets. *Am J Phys Anthropol* 156:S100.

Cano JM, Laurila A, Palo J, Merillä J. 2004. Population differentiation in G matrix structure due to natural selection in *Rana temporaria*. *Evol* 9:2013-20.

Caporaso JG. 2013. scikit-bio: core bioinformatics data structures and algorithms in Python. https://github.com/biocore/scikit-bio.

Cardini A, Elton S. 2008. Does the skull carry a phylogenetic signal? evolution and modularity in the guenons. *Biol J Linn Soc* 93:813-34.
Cardini A, Polly PD. 2013. Larger mammals have longer faces because of size-related constraints on skull form. *Nat Commun* 4:1-7.

Carlson DS. 2005. Theories of craniofacial growth in the postgenomic era. *Semin Orthod* 7:172-83.

Carlson EC. 1973. Intercellular connective tissue fibrils in the notochordal epithelium of the early chick embryo. *Am J Anat* 136:77-90.

Carpentier MJE, Fontaine MC, Cherel E, Renoult JP, Jenkins T, Benoit L, Barthès N, Alberts SC, Tung J. 2012. Genetic structure in a dynamic baboon hybrid zone corroborates behavioral observations in a hybrid population. *Molec Ecol* 21:715-31.

Carrasco AE, McGinnis W, Gehring WJ, De Robertis EM. 1984. Cloning of an *X. laevis* gene expressed during early embryogenesis coding for a peptide region homologous to *Drosophila* homeotic genes. *Cell* 37:409-14.

Carroll SB. 2005. Evolution at two levels: on genes and form. *PLoS Biol* 3:e245.

Caswell JL, Mallick S, Richter DJ, Neubauer J, Schirmer C, Gnerre S, Reich D. 2008. Analysis of chimpanzee history based on genome sequence alignments. *PLoS Genet* 4:e1000057.

Cerling TE, Harris JM, MacFadden BJ, Leakey MG, Quade J, Eisenmann V, Ehleringer JR. 1997. Global vegetation change through the Miocene/Pliocene boundary. *Nature* 389:153-8.

Cerling TE, Chritz KL, Jablonski NG, Leakey MG. 2013. Diet of *Theropithecus* from 4 to 1 Ma in Kenya. *Proc Nat Acad Sci U S A* 110:10507-12.

Chai Y, Jiang X, Ito Y, Bringas Jr. P, Han J, Rowitch DH, Soriano P, McMahon AP, Sucov HM. 2000. Fate of the mammalian cranial neural crest during tooth and mandibular morphogenesis. *Dev* 127:1671-9.

Chapman MA, Pashley CH, Wenzler J, Hvala J, Tang S, Knapp SJ, Burke JM. 2008. A genomic scan for selection reveals candidates for genes involved in the evolution of cultivated sunflower (*Helianthus annuus*). *Plant Cell* 20:2931-45.

Chapman RE. 1990. Conventional Procrustes approaches. In: Rohlf FJ, Bookstein FL, eds. Proceedings of the Michigan morphometrics workshop. Ann Arbor, MI: The University of Michigan Museum of Zoology. p 251-67.

Charpentier MJE, Fontaine MC, Cherel E, Reoult JP, Jenkins T, Benoit L, Barthès N, Alberts SC, Tung J. 2012. Genetic structure in a dynamic baboon hybrid zone corroborates behavioural observations in a hybrid population. *Molec Ecol* 21:715-31.

Chen J, Bardes EE, Aronow BJ, Jegga AG. 2009. ToppGene Suite for gene list enrichment analysis and candidate gene prioritization. *Nucl Acids Res* 37:W305-11.

Chen K, Rajewsky N. 2006. Natural selection on human microRNA binding sites inferred from SNP data. *Nat Genet* 38:1452-6.

Chester SGB, Bloch JI, Boyer DM, Clemens WA. 2015. Oldest known euarchontan tarsals and affinities of Paleocene *Purgatorius* to primates. *Proc Natl Acad Sci U S A* 112:1487-92.

Cheverud JM. 1982. Phenotypic, genetic, and environmental morphological integration in the cranium. *Evol* 36:499-516.

Cheverud JM. 1988. A comparison of genetic and phenotypic correlations. *Evol* 42:958-68.

Cheverud JM. 1989. A comparative analysis of morphological variation patterns in the papionins. *Evol* 43:1737-47.

Cheverud JM. 1995. Morphological integration in the saddle-back tamarin (*Saguinus fuscicollis*) cranium. *Am Nat* 145:63-89.

Cheverud JM. 1996a. Developmental integration and the evolution of pleiotropy. *Am Zool* 36:44-50.

Cheverud JM. 1996b. Quantitative genetic analysis of cranial morphology in the cotton-top (*Saguinus oedipus*) and saddle-back (*S. fuscicollis*) tamarins. *J Evol Biol* 9:5-42.

Cheverud JM. 2001. The genetic architecture of pleiotropic relations and differential epistasis. In: Wagner GP, ed. The character concept in evolutionary biology. San Diego, CA: Academic Press. p 411-33.

Cheverud JM, Buikstra JE. 1981. Quantitative genetics of skeletal nonmetric traits in the rhesus macaques on Cayo Santiago. I. single trait heritabilities. *Am J Phys Anthropol* 54:43-9.

Cheverud JM, Buikstra JE. 1981. Quantitative genetics of skeletal nonmetric traits in the rhesus macaques on Cayo Santiago. II. phenotypic, genetic, and environmental correlations between traits. *Am J Phys Anthropol* 54:51-8.

Cheverud JM, Falk D, Vannier M, Konigsberg L, Helmkamp RC, Hildebolt C. 1990. Heritability of brain size and surface features in rhesus macaques (*Macaca mulatta*). *J Hered* 81:51-7.

Cheverud JM, Routman E, Irschick D. 1997. Pleiotropic effects of individual gene loci on mandibular morphology. *Evol* 51:2004-14.

Cheverud JM, Ehrich TH, Vaughn TT, Koreishi SF, Linsey RB, Pletscher LS. 2004. Pleiotropic effects on mandibular morphology II: differential epistasis and genetic variation in morphological integration. *J Exp Zool B Mol Dev Evol* 302:424-35.

Cheverud JM, Wilson P, Dittus WPJ. 1992. Primate population studies at Polonnaruwa. III. Somatometric growth in a natural population of toque macaques (*Macaca sinica*). *J Hum Evol* 23:51-77.

Clarke BL, Khosla S. 2009. Androgens and bone. *Steroids* 74:296-305.

Clarke MR, O'Neil JAS. 1999. Morphometric comparison of Chinese-origin and Indian-derived rhesus monkeys (*Macaca mulatta*). *Am J Primatol* 47:335-46.

Clemens WA. 2004. *Purgatorius* (Plesiadaiformes, Primates?, Mammalia) a Paleocene immigrant into northeastern Montana: stratigraphic occurrences and incisor proportions. *Bull Carnegie Mus Nat Hist* 36:3-13.

Cohen AM, Hay ED. 1971. Secretion of collagen by embryonic neuroepithelium at the time of spinal cord-somite interaction. *Dev Biol* 26:578-605.

Collaer ML, Hines M. 1995. Human behavioral sex differences: a role for gonadal hormones during early development? *Psychol Bull* 118:55-107.

Collard M, O'Higgins P. 2001. Ontogeny and homoplasy in the papionin monkey face. *Evol Dev* 3:322-331.

Collard M, Wood B. 2007. Hominin homoiology: an assessment of the impact of phenotypic plasticity on phylogenetic analyses of humans and their fossil relatives. *J Hum Evol* 52:573-84.

Copp AJ, Greene NDE. 2010. Genetics and development of neural tube defects. *J Pathol* 220:217-30.

Corruccini RS, Beecher RM. 1984. Occlusofacial morphological integration lowered in baboons raised on soft diet. *J Craniofac Genet Dev Biol* 4:135-42.

Cote S, Malit N, Nengo I. 2014. Additional mandibles of *Rangwapithecus gordoni*, an early Miocene catarrhine from the Tinderet localities of western Kenya. *Am J Phys Anthropol* 153:341-52.

Cotterman CW. 1940. A calculus for statistico-genetics. Dissertation: Ohio State University.

Couly GF, Coltey PM, Le Douarin NM. 1993. The triple origin of skull in higher vertebrates: a study in quail-chick chimeras. *Dev* 117:409-29.

Cox LA, Mahaney MC, VandeBerg JL, Rogers J. 2006. A second-generation genetic linkage map of the baboon (*Papio hamadryas*) genome. *Genomics* 88:274-81.

Cox LA, Comuzzie AG, Havill LM, Karere GM, Spradling KD, Mahaney MC, Nathanielsz PW, Nicolella DP, Shade RE, Voruganti S, VandeBerg JL. 2013. Baboons as a model to study genetics and epigenetics of human disease. *ILAR J* 54:106-21.

Cracraft J. 1983. Species concepts and speciation analysis. In: Johnston RF, ed. Current Ornithology, vol. 1. New York City, NY: Plenum Press. p 159-87.

Crilly RG. 1972. Longitudinal overgrowth of chicken radius. *J Anat* 112:11-18.

Cuozzo FP, Rasoazanabary E, Godfrey LR, Sauther ML, Youssouf IA, LaFleur MM. 2013. Biological variation in a large sample of mouse lemurs from Amboasary, Madagascar: implications for interpreting variation in primate biology and paleobiology. *J Hum Evol* 64:1-20.

Curran JE, McKay DR, Winkler AM, Olvera RL, Carless MA, Dyer TD, Kent Jr JW, Kochunov P, Sprooten E, Knowles EE, Comuzzie AG, Fox PT, Almasy L, Duggirala R, Blangero J, Glahn DC. 2013. Identification of pleiotropic genetic effects on obesity and brain anatomy. *Hum Hered* 75:136-43.

Dagosto M. 1988. Implications of postcranial evidence for the origin of euprimates. *J Hum Evol* 17:35-56.

Darwin CR. 1859. On the origin of species by means of natural selection, or the preservation of favoured races in the struggle for life. London, GBR: John Murray.

David DJ, Poswillo D, Simpson D. 1982. The craniosynostoses: causes, natural history, and management. Berlin, DEU: Springer-Verlag.

de Beer GR. 1947. How animals hold their heads. *Proc Linn Soc Lond* 159:125-39.

de Beer GR. 1985. The development of the vertebrate skull. Chicago, IL: The University of Chicago Press.

de la Cruz A, Linthicum FH, Luxford WM. 1985. Congenital atresia of the external auditory canal. *Laryngoscope* 95:421-7

de Oliveira FB, Porto A, Marroig G. 2009. Covariance structure in the skull of Catarrhini: a case of pattern stasis and magnitude evolution. *J Hum Evol* 56:417-30.

Deacon TW. 1988. Human brain evolution: II. embryology and brain allometry. In: Jerison JH, Jerison I, eds. Intelligence and evolutionary biology. Berlin, DEU: Springer Berlin Heidelberg. p 383-415.

Debat V, Alibert P, David P, Paradis E, Auffray JC. 2000. Independence between developmental stability and canalization in the skull of the house mouse. *Proc R Soc Lond B Biol Sci* 267:423-30.

Debat V, David P. 2001. Mapping phenotypes: canalization, plasticity and developmental stability. *Trends Ecol Evol* 16:555-61.

Debnath J, Satija L, George RA, Vaidya A, Sen D. 2009. Computed tomography demonstration of unusual ossification of the falx cerebri: a case report. *Surg Radiol Anat* 31:211-3.

Delson E. 1975. Evolutionary history of the Cercopithecidae. *Contrib Primatol* 5:167-217.

Delson E, Dean D. 1993. Are *Papio baringensis* R. Leakey, 1969, and *P. quadratirostris* Iwamoto, 1982, species of *Papio* or *Theropithecus*? In: Jablonski N, ed. *Theropithecus*: the rise and fall of a primate genus. Cambridge, MA: Cambridge University Press. p 125-56.

Derry ME. 2012. Art and science in breeding: creating better chickens. Toronto, CAN: University of Toronto Press.

Desai SD, Shaik HS, Shepur MP, Thomas ST, Mavishettar GF, Haseena S. 2012. Ossification of transverse ligament of atlas. *Indican J Med Healthcare* 1:82-4.

Dib C, Fauré S, Fizames C, Samson D, Drouot N, Vignal A, Millasseau P, Marc S, Kazan J, Seboun E, Lathrop M, Gyapay G, Morissette J, Weissenbach J. 1996. A comprehensive genetic map of the human genome based on 5,264 microsatellites. *Nature* 380:152-4.

Disotell TR. 1994. Generic level relationships of the Papionini (Cercopithecoidea). *Am J Phys Anthropol* 94:47-57.

Disotell TR, Honeycutt RL, Ruvolo M. 1992. Mitochondrial DNA phylogeny of the Old-World monkey tribe Papionini. *Mol Biol Evol* 9:1-13.

Dong C, Li WD, Li D, Price RA. 2005. Interaction between obesity-susceptibility loci in chromosome regions 2p25-p24 and 13q13-q21. *Eur J Hum Genet* 13:102-8.

Donnelly P. 2008. Progress and challenges in genome-wide association studies in humans. *Nature* 456:728-31.

Doubleday AF, Kaestle FA, Cox LA, Birnbaum S, Mahaney MC, Havill LM. 2009. LRP5 sequence and polymorphisms in the baboon. *J Med Primatol* 38:97-106.

Drake AG, Klingenberg CP. 2010. Large-scale diversification of skull shape in domestic dogs: disparity and modularity. *Am Nat* 175:289-301.

Druzhkova AS, Thalmann O, Trifonov VA, Leonard JA, Vorobieva NV, Ovodov ND, Graphodatsky AS, Wayne RK. 2013. Ancient DNA analysis affirms the canid from Altai as a primitive dog. *PLoS One* 8:e57754.

Dullemeijer P. 1971. Comparative ontogeny and cranio-facial growth. In: Moyers RE, Krogman WM. Cranio-facial growth in man: proceedings of a conference on genetics, bone biology, and analysis of growth data. New York, NY: Pergamon Press. p 45-75.

Dunbar RIM. 1993. Socioecology of the extinct theropiths: a modelling approach. In: Jablonski NG, ed. *Theropithecus*: the rise and fall of a genus. Cambridge, MA: Cambridge University Press. p 465-86.

Dunbar RIM, Dunbar P. 1974. On hybridization between *Theropithecus gelaga* and *Papio anubis* in the wild. *J Hum Evol* 3:187-92.

Duncan RL, Turner CH. 1995. Mechanotransduction and the functional response of bone to mechanical strain. *Calcif Tissue Int* 57:344-58.

Dunn J, Cardini A, Elton S. 2013. Biogeographic variation in the baboon: dissecting the cline. *J Anat* 223:337-52.

Dwivedi PP, Grose RH, Filmus J, Hii CST, Xian CJ, Anderson PJ, Powell BC. 2013. Regulation of bone morphogenetic protein signalling and cranial osteogenesis by Gpc1 and Gpc3. *Bone* 55:367-76.

Dyke B, Gage TB, VandeBerg JL, King RH, Mamelka PM, Cheng M, Goodwin WJ. 1987. Decision making in genetic management of primate breeding colonies. *Genetica* 73:137-44.

Echelard Y, Epstein DJ, St-Jacques B, Shen L, Mohler J, McMahon JA, McMahon AP. 1993. Sonic hedgehog, a member of a family of putative signaling molecules, is implicated in the regulation of CNS polarity. *Cell* 75:1417-30.

Eck GG, Jablonski NG. 1987. The skull of *Theropithecus brumpti* compared with those of other species of the genus *Theropithecus*. In: Coppens Y, Howell FC, eds. Les Faunes Plio-Pléistocènes de la Basse Vallée de l'Omo (Éthiopie), Tome 3, Cercopithecidae de la formation de Shungura. Paris, FRA: Editions du Centre National de la Recherche Scientifique. p 11-122.

Ehrich TH, Hrbek T, Kenney-Hunt JP, Pletscher LS, Wang B, Semenkovich CF, Cheverud JM. 2005. Fine-mapping gene-by-diet interactions on chromosome 13 in a LG/J x SM/J murine model of obesity. *Diabetes* 54:1863-72.

Ehrich TH, Vaughn TT, Koreishi SF, Linsey RB, Pletscher LS, Cheverud JM. 2003. Pleiotropic effects on mandibular morphology I. developmental morphological integration and differential dominance. *J Exp Zool B Mol Dev Evol* 296:58-79.

Eichel K. 2014. Identification of hybridization in the nasal cavity of baboon hybrids, *Papio anubis x P. cynocephalus*, as an analogue for Neanderthal and anatomically modern human hybrids. Thesis: University of Waterloo.

Eichler EE, Flint J, Gibson G, Kong A, Leal SM, Moore JH, Nadeau JH. 2010. Missing heritability and strategies for finding the underlying causes of complex disease. *Nat Rev Genet* 11:446-50.

Elston RC, Stewart J. 1971. A general model for the genetic analysis of pedigree data. *Hum Hered* 21:523-42.

Enlow DH. 1968. The human face: an account of the postnatal growth and development of the craniofacial skeleton. New York, NY: Harpers & Row.

Enlow DH. 1982. Handbook of facial growth. Philadelphia, PA: W. B. Saunders Company.

Eriksson J, Siedel H, Lukas D, Kayser M, Erler A, Hashimoto C, Hohmann G, Boesch C, Vigilant L. 2006. Y-chromosome analysis confirms highly sex-biased dispersal and suggests a low male effective population size in bonobos (*Pan pnasicus*). *Molec Ecol* 15:939-49.

Eriksson O, Friis EM, Löfgren P. 2000. Seed size, fruit size, and dispersal systems in angiosperms from the Early Cretaceous to the Late Tertiary. *Am Nat* 156:47-58.

Evans PD, Gilbert SL, Mekel-Bobrov N, Vallender EJ, Anderson JR, Vaez-Azizi L, Tishkoff SA, Hudson RR, Lalhn BT. 2005. *Microcephalin*, a gene regulating brain size, continues to evolve adaptively in humans. *Science* 309:1717-20.

Ezin AM, Fraser SE, Bronner-Fraser M. 2009. Fate map and morphogenesis of presumptive neural crest and dorsal neural tube. *Dev Biol* 330:221-36.

Falconer DS, Mackay TFC. 1996. Introduction to Quantitative Genetics. 4th ed. Essex, GBR: Pearson Education Limited.

Farzin F, Hou C, Norcia AM. 2012. Piecing it together: infants' neural responses to face and object structure. *J Vis* 12:1-14.

Fatemifar G, Hoggart CJ, Paternoster L, Kemp JP, Prokopenko I, Horikoshi M, Wright VJ, Tobias JH, Richmond S, Zhurov AI, Toma AM, Pouta A, Taanila A, Sipila K, Lähdesmäki R, Pillas D, Geller F, Feenstra B, Melbye M, Nohr EA, Ring SM, St Pourcain B, Timpson NJ, Smith GD, Jarvelin MR, Evans DM. 2013. Genome-wide association study of primary tooth eruption identifies pleiotropic loci associated with height and craniofacial distances. *Hum Mol Genet* 22:3807-17.

Fell HB. 1956. Skeletal development in tissue culture. In: Bourne GH, ed. The biochemistry and physiology of bone. New York, NY: Academic Press. p 401-41.

Felts WJL. 1961. *In vivo* implantation as a technique in skeletal biology. *Int Rev Cytol* 12:243-302.

Ferring R, Oms O, Agustí J, Berna F, Nioradze, Shelia T, Tappen M, Vekua A, Zhvania D, Lordkipanidze D. 2011. Earliest human occupations at Dmanisi (Georgian Caucasus) dated to 1.85-1.78 Ma. *Proc Natl Acad Sci U S A* 108:10432-6.

Figueirido B, Palmqvist P, Pérez-Claros JA. 2009. Ecomorphological correlates of craniodental variation in bears and paleobiological implications for extinct taxa: an approach based on geometric morphometrics. *J Zool* 277:70-80.

Fisher RA. 1918. The correlation between relatives on the supposition of Mendelian inheritance. *Proc R Soc Edinb Nat Environ* 52:399-433.

Fisher RA. 1925. The correlation coefficient. Statistical methods for research workers. Edinburgh, GBR: Oliver and Boyd. p 138-75.

Fleagle JG. 2013. Primate adaptation and evolution. New York, NY: Academic Press.

Fleagle JG, McGraw WS. 2002. Skeletal and dental morphology of African papionins: unmasking a cryptic clade. *J Hum Evol* 42:267-292.

Fleagle JG, Simons EL. 1995. Limb skeleton and locomotor adaptations of *Apidium phiomense*, an Oligocene anthropoid from Egypt. *Am J Phys Anthropol* 97:235-89.

Flint J, Mackay TF. 2009. Genetic architecture of quantitative traits in mice, flies and humans. *Genome Res* 19:723-33.

Flint J, Mott R. 2001. Finding the molecular basis of quantitative traits: successes and pitfalls. *Nat Rev Genet* 2:437-44.

Ford HER. 1956. The growth of the foetal skull. *J Anat* 90:63-72.

Fracchia J, Lewontin RC. 1999. Does culture evolve? *Hist Theory* 38:52-78.

Freedman L. 1957. The fossil Cercopithecoidea of South Africa. *Ann Transvaal Mus* 23:8-262.

Freedman L. 1962. Growth of muzzle length relative to calvaria length in *Papio*. *Growth* 26:117-28.

Freedman L. 1963. A biometric study of *Papio cynocephalus* skulls from Northern Rhodesia and Nyasaland. *J Mammal* 44:24-43.

Frost SR. 2001. Fossil Cercopithecidae of the Afar Depression, Ethiopia: species, systematics and comparison to the Turkana Basin. Ph.D dissertation: The City University of New York.

Frost SR, Marcus LF, Bookstein FL, Reddy DP, Delson E. 2003. Cranial allometry, phylogeography, and systematics of large-bodied papionins (Primates: Cercopithecinae) inferred from geometric morphometric analysis of landmark data. *Anat Rec A Discov Mol Cell Evol Biol* 275:1048-1072.

Fu JF, Wang JW, Tong YS. 2002. The new discovery of the Plesiadapiformes from the early Eocene of Wutu Bason, Shandong Province. *Vertebrata PalAsiatica* 40:219-27.

Fulker DW, Cherny SS, Cardon LR. 1995. Multipoint interval mapping of quantitative trait loci, using sib pairs. *Am J Hum Genet* 56:1224-33.

Galton F. 1906. The measurement of resemblance. *Sci Am* 62:25898.

Garcia G, de Oliveira FB, Marroig G. 2015. Modularity and morphometrics: error rates in hypothesis testing. bioRxiv doi: http://dx.doi.org/10.1101/030874.

Garcia-Gonzalez F, Simmons LW, Tomkins JL, Kotiaho JS, Evans JP. 2012. Comparing evolvabilities: common errors surrounding the calculation and use of coefficients of additive genetic variation. *Evol* 66:2341-9.

Garrick DJ, Pollak EJ, Quaas RL, Van Vleck LD. 1989. Variance heterogenetity in direct and maternal weight traits by sex and percent purebred for Simmental-sired calves. *J Anim Sci* 67:2515-28.

Garza RM, Khosla RK. 2012. Nonsyndromic craniosynostosis. *Semin Plast Surg* 26:53-63.

Gear JHS. 1926. A preliminary account of the baboon remains from Taungs. *S Afr J Sci* 23:731-47.

Gebo, DL. 2014. Primate comparative anatomy. Baltimore, MD: Johns Hopkins University Press.

The Gene Ontology Consortium. 2015. Gene Ontology Consortium: going forward. *Nucl Acids Res* 43:D1049-56.

Geoffroy Saint-Hilaire É. 1812. Tableau des quadrumanes ou de animaux composant le premier ordre de la classe des mammifères. *Annales Muséum d'Histoire Naturelle Paris* 19:85-122.

German RZ, Hertweck DW, Sirianni JE, Swindler DR. 1994. Heterchrony and sexual dimorphism in the pigtailed macaque (*Macaca nemestrina*). *Am J Phys Anthropol* 93:373-80.

Germonpré M, Sablin MV, Stevens RE, Hedges REM, Hofreiter M, Stiller M, Després VR. 2009. Fossil dogs and wolves from Paleolithic sites in Belgium, the Ukraine and Russia: osteometry, ancient DNA and stable isotopes. *J Archaeol Sci* 36: 473-90.

Gilbert CC. 2013. Cladistic analysis of extant and fossil African papionins using craniodental data. *J Hum Evol* 64:399-433.

Gilbert CC, Frost SR, Strait DS. 2009. Allometry, sexual dimorphism, and phylogeny: a cladistic analysis of extant African papionins using craniodental data. *J Hum Evol* 57:298-320.

Gilbert CC, Rossie JB. 2007. Congruence of molecules and morphology using a narrow allometric approach. *Proc Natl Acad Sci U S A* 104:11910-11914.

Gill NW. 1969. Congenital atresia of the ear: a review of the surgical findings in 83 cases. *J Laryngol Otol* 83:551-87.

Gillies GE, McArthur S. 2010. Estrogen actions in the brain and the basis for differential action in men and women: a case study for sex-specific medicines. *Pharmacol Rev* 62:155-98.

Gingerich PD. 1990. African dawn for primates. *Nature* 346:411.

Glass II DA, Bialek P, Ahn JD, Starbuck M, Patel MS, Clevers H, Taketo MM, Long F, McMahon AP, Lang RA, Karsenty G. 2005. Canonical *Wnt* signaling in differentiated osteoblasts controls osteoclast differentiation. *Develop Cell* 8:751-64.

Goldschmidt B, Lopes CAA, Moura M, Nogueira DM, Gonçalves MAB, Fasano DM, Andrade MCR, Nascimento LWF, Marinho AM. 2010. Cleft lip and palate associated with other malformations in a Neotropical primate (*Saimiri ustus*). *J Am Assoc Lab Anim Sci* 49:357-60.

Goldschmidt R. 1940. The material basis of evolution. New Have, CT: Yale University Press.

Gonçalves LSA, Rodrigues R, Amaral Júnior AT, Karasawa M, Sudré CP. 2008. Comparison of multivariate statistical algorithms to cluster tomato heirloom accessions. *Genet Mol Res* 7:1289-97.

González-José R, Bortolini MC, Santos FR, Bonatto SL. 2008. The peopling of America: craniofacial shape variation on a continental scale and its interpretation from an interdisciplinary view. *Am J Phys Anthropol* 137:175-87.

González-José R, Escapa I, Neves WA, Cúneo R, Mucciarelli HM. 2008. Cladistic analysis of continuous modularized traits provides phylogenetic signals in *Homo* evolution. *Nature* 453:775-778.

Goodall C. 1991. Procrustes methods in the statistical analysis of shape. *J R Stat Soc Series B Stat Methodol* 53:285-339.

Goodman-Gruen D, Barrett-Connor E. 2000. Sex differences in the association of endogenous sex hormone levels and glucose tolerance status in older men and women. *Diabetes Care* 23:912-8.

Gordon J. 1818. Engravings of the skeleton of the human body. Edinburgh, GBR: Blackwood Publishing.

Gould SJ, Lewontin RC. 1979. The spandrels of San Marco and the Panglossian paradigm: a critique of the adaptationist programme. *Proc R Soc Lond B Biol Sci* 205:581-98.

Gould SJ, Vrba ES. 1982. Exaptation—a missing term in the science of form. *Paleobiol* 8:4-15.

Gower JC. 1971. General coefficient of similarity and some of its properties. *Biomet* 27:857-74.

Grafen A. 1989. The phylogenetic regression. *Philos Trans R Soc Lond B Biol Sci* 326:119-57.

Gregory WK. 1965. Our face from fish to man. New York, NY: Capricorn Books.

Gromko MH. 1995. Unpredictability of correlated response to selection: pleiotropy and sampling interact. *Evol* 49:685-93.

Guo X, Elston RC. 1999. Linkage information content of polymorphic genetic markers. *Hum Hered* 49:112-8.

Gupta VJ, Sahni A. 1981. Theropithecus delsoni, a new cercopithecine species from the Upper Siwaliks of India. *Bull Indian Geol Assoc* 14:69-71.

Hall BK. 2007. Homplasy or homology: dichotomy or continuum? *J Hum Evol* 473-9.

Hall BK. 2013. Homology, homoplasy, novelty, and behavior. *Dev Psychobiol* 55:4-12.

Hallgrímsson B, Lieberman DE. 2008. Mouse models and the evolutionary developmental biology of the skull. *Integr CompBiol* 48:373-84.

Hallgrímsson B, Lieberman DE, Liu W, Ford-Hutchinson AF, Jirik FR. 2007. Epigenetic interactions and the structure of phenotypic variation in the cranium. *Evol Dev* 9:76-91.

Hallgrímsson B, Jamniczky H, Young NM, Rolian C, Parsons TE, Boughner JC, Marcucio RS. 2009. Deciphering the palimpsest: studying the relationship between morphological integration and phenotypic covariation. *Evol Biol* 36:355-76.

Hallgrímsson B, Willmore K, Hall BK. 2002. Canalization, developmental stability, and morphological integration in primate limbs. *Yrbk Phys Anthropol* 45:131-58.

Hansen TF. 2006. The evolution of genetic architecture. *Annu Rev Ecol Evol Syst* 37:123-57.

Hanson WD, Robinson HF. 1963. Statistical genetics and plant breeding: a symposium and workshop. Washington, DC: National Academy of Sciences-National Research Council.

Haraguchi K, Yamaki T, Kurokawa Y, Ohtaki M, Ibayashi Y, Yede T, Tanabe S, Hashi K. 1996. A case of calcification of the cervical ligamentum flavum. *Shinkei Geka* 24:69-73.

Harris EE. 2000. Molecular systematics of the Old World monkey tribe Papionini: analysis of the total available genetic sequences. *J Hum Evol* 38:235-256.

Harris EE, Disotell TR. 1998. Nuclear gene trees and the phylogenetic relationships of the mangabeys (Primates: Papionini). *Mol Biol Evol* 15:892-900.

Harris EF, Johnson MG. 1991. Heritability of craniometric and occlusal variables: a longitudinal sib analysis. *Am J Ortho Dentofac Orthop* 99:258-68.

Harrison T. 1987. The phylogenetic relationships of the early catarrhine primates: a review of the current evidence. *J Hum Evol* 16:41-80.

Harrison T. 2011. Cercopithecids (Cercopithecidae, Primates). In: Harrison T, ed. Paleontology and geology of Laetoli: human evolution in context; vol 2: fossil hominins and the associated fauna. Dordrecht, NLD: Springer. p 83-139.

Harrison T, Harris EE. 1996. Plio-Pleistocene cercopithecids from Kanam East, western Kenya. *J Hum Evol* 30:539-61.

Harvati K, Weaver TD. 2006. Human cranial anatomy and the differential preservation of population history and climate signatures. *Anat Rec A Discov Mol Cell Evol Biol* 288:1225-33.

Haughton RH. 1925. A note on the occurrence of a species of baboon in limestone deposits near Taungs. *Trans Roy Soc S Afr* 12:68.

Havill LM, Allen MR, Harris JAK, Levine SM, Coan HB, Mahaney MC, Nicolella DP. 2013. Intracortical bone remodeling variation shows strong genetic effects. *Calcif Tissue Int* 93:472-80.

Hayashi T, Hirose Y, Sagoh M, Murakami H. 1998. Ossification of transverse ligament of the atlas associated with atlanto-axial dislocation—case report. *Neurologia Medico-Chirurgica* 38:425-8.

Haygood R, Fedrigo O, Hanson B, Yokoyama KD, Wray GA. 2007. Promoter regions of many neural- and nutrition-related genes have experienced positive selection during human evolution. *Nat Genet* 39:1140-4.

Hedges LV, Nowell A. 1995. Sex differences in mental test scores, variability, and numbers of high-scoring individuals. *Science* 269:41-5.

Heesy CP. 2008. Ecomorphology of orbit orientation and the adaptive significance of binocular vision in primates and other mammals. *Brain Behav Evol* 71:54-67.

Hemmer, H. 1990. Domestication: the decline of environmental appreciation, 2nd ed. New York, NY: Cambridge University Press.

Herbert JG, Kidwell JF, Chase HB. 1979. The inheritance of growth and form in the mouse. IV. Changes in the variance components of weight, tail length and tail width during growth. *Growth* 43:36-46.

Herring SW. 1993. Epigenetic and functional influences on skull growth. In: Hanken J, Hall BK, eds. The skull, vol. 1: development. Chicago, IL: The University of Chicago Press. p 153-206.

Higgins PB, Bastarrachea RA, Lopez-Alvarenga JC, Garcia-Forey M, Proffitt JM, Voruganti VS, Tejero ME, Mattern V, Haack K, Shade RE, Cole SA, Comuzzie AG. 2010. Eight week exposure to a high sugar high fat diet results in adiposity gain and alterations in metabolic biomarkers in baboons (*Papio hamadryas* sp.). *Cardiovasc Diabetol* 9:71.

Hill WG. 2010. Understanding and using quantitative genetic variation. *Philos Trans R Soc Lond B Biol Sci* 365:73-85.

Hill WG, Kirkpatrick M. 2010. What animal breeding has taught us about evolution. *Ann Rev Ecol Evol Syst* 41:1-19.

Hill RA, Lycett JE, Dunbar RIM. 2000. Ecological and social determinants of birth intervals in baboons. *Behav Ecol* 11:560-4.

Hlusko LJ. 2004. Integrating the genotype and phenotype in hominid paleontology. *Proc Natl Acad Sci U S A* 101:2653-7.

Hlusko LJ, Mahaney MC. 2007. A multivariate comparison of dental variation in wild and captive populations of baboons (*Papio hamadryas*). *Arch Oral Biol* 52:195-200.

Hlusko LJ, Mahaney MC. 2009. Quantitative genetics, pleiotropy, and morphological integration in the dentition of *Papio hamadryas*. *Evol Biol* 36:5-18.

Holland ND, Holland LZ, Kozmik Z. 1995. An amphioxus Pax gene, AmphiPax-1, expressed in embryonic endoderm, but not in mesoderm: implications for the evolution of class I paired box genes. *Mol Mar Biol Biotechnol* 4:206-14.

Holmes EM. 1949. The microtic ear. *Arch Otolarynol* 49: 243-65.

Holton NE, Franciscus RG, Marshall SD, Southard TE, Nieves MA. 2011. Nasal septal and premaxillary developmental integration: implications for facial reduction in *Homo*. *Anat Rec* 294:68-78.

Honaker J, King G. 2010. What to do about missing values in time-series cross-section data. *Am J Polit Sci* 54:561-81.

Honaker J, King G, Blackwell M. 2011. Amelia II: a program for missing data. *J Stat Softw* 45:1-47.

Hopwood AT. 1934. New fossil mammals from Olduvai, Tanganyika Territory. *Ann Mag Nat Hist Ser 10* 14:546-50.

Hopwood AT. 1936. New and little-known fossil mammals from the Pleistocene of Kenya Colony and Tanganyika Territory. *Ann Mag Nat Hist Ser 10* 17:636-41.

Horwitz S, Shapiro HH. 1951. Modifications of the mandibular architecture following removal of the temporalis muscle in the rat. *J Dent Res* 30:276-80.

Houle D. 1992. Comparing evolvability and variability of quantitative traits. *Genet* 130:195-204.

Housworth EA, Martins EP, Lynch M. 2004. The phylogenetic mixed model. *Am Nat* 163:84-96.

Hrdlička A. 1933. Seven prehistoric American skulls with complete absence of external auditory meatus. *Am J Phys Anthropol* 17:355-77.

Hu D, Helms JA. 1999. The role of Sonic hedgehog in normal and abnormal craniofacial morphogenesis. *Dev* 126:4873-84.

Hu H, Hilton MJ, Tu X, Yu K, Ornitz DM, Long F. 2005. Sequential roles of Hedgehog and *Wnt* signaling in osteoblast development. *Develop* 132:49-60.

Huang X, Saint-Jeannet JP. 2004. Induction of the neural crest and the opportunities of life on the edge. *Dev Biol* 275:1-11.

Huelsken J, Birchmeier W. 2001. New aspects of *Wnt* signaling pathways in higher vertebrates. *Curr Opin Genet Dev* 11:547-53.

Hughes CL, Kaufman TC. 2002. Hox genes and the evolution of the arthropod body plan. *Evol Dev* 4:459-99.

Hunter JD. 2007. Matplotlib: a 2D graphics environment. *Comput Sci Eng* 9:90-5.

Ikeya M, Lee SMK, Johnson JE, McMahon AP, Takada S. 1997. *Wnt* signalling required for expansion of neural crest and CNS progenitors. *Nature* 389:966-70.

Ingicco T, Balzeau A, Callou C, Fitriana YS. 2011. Brief communication: a cranial morphometric assessment of the taxonomic affinities of *Trachypithecus auratus* (E. Geoffroy, 1812 primates: Colobinae) with a reassessment of the *T. auratus* type specimen. *Am J Phys Anthropol* 146:306-12.

Ito T, Kawamoto Y, Hamada Y, Nishimura TD. 2015. Maxillary sinus variation in hybrid macaques: implications for the genetic basis of craniofacial pneumatization. *Biol J Linn Soc* 115:333-47.

Ito T, Nishimura T, Takai M. 2014. Ecogeographical and phylogenetic effects on craniofacial variation in macaques. *Am J Phys Anthropol* 154:27-41.

Iwamoto M. 1982. A fossil baboon skull from the Lower Omo Basin, Southwest Ethiopia. *Primates* 23:533-41.

Iwamoto M. 1993. Food digestion and energetic conditions in *Theropithecus gelada*. In: Jablonski NG, ed. *Theropithecus*: the rise and fall of a genus. Cambridge, MA: Cambridge University Press. p 453-63.

Jablonski NG. 1986. The hand of *Theropithecus brumpti*. In: Proceedings of the 10th congress of the International Primatological Society, vol. 1, primate evolution. Cambridge, MA: Cambridge University Press. p 173-82.

Jablonski NG. 1993. Theropithecus: the rise and fall of a primate genus. New York, NY: Cambridge University Press.

Jablonski NG. 2002. Fossil Old World monkeys: the late Neogene radiation. In: Hartwig WC, ed. The primate fossil record. New York, NY: Cambridge University Press. p 255-300.

Jacob F. 1977. Evolution and tinkering. *Science* 196:1161-6.

Janečka JE, Miller W, Pringle TH, Wiens F, Zitzmann A, Helgen KM, Springer MS, Murphy WJ. 2007. Molecular and genomic data identify the closest living relative of primates. *Science* 318:792-4.

Janis CM. 1993. Tertiary mammal evolution in the context of changing climates, vegetation, and tectonic events. *Annu Rev Ecol Syst* 24:467-500.

Jauhar PP. 2006. Modern biotechnology as an integral supplement to conventional plant breeding: the prospects and challenges. *Crop Sci* 46:1841-59.

Jia S, Zhou J, Gao Y, Baek JA, Martin JF, Lan Y, Jiang R. 2013. Roles of Bmp4 during tooth morphogenesis and sequential tooth formation. *Dev* 140:423-32.

Jiang X, Iseki S, Maxxson RE, Sucov HM, Morriss-Kay GM. 2002. Tissue origins and interactions in the mammalian skull vault. *Dev Biol* 241:106-16.

Joganic JL, Willmore KE, Richtsmeier JT, Rogers J, Cheverud JM. 2012a. Ligers and tigons and pizzlies, oh my!: the morphological consequences of intergeneric hybridization in the cranium of a rheboon (*Macaca mulatta x Papio hamadryas*). *Am J Phys Anthropol* 147:S175.

Joganic JL, Willmore KE, Roseman CC, Richtsmeier JT, Rogers J, Cheverud JM. 2012b. Comparative quantitative genetic analysis of cranial capacity and craniofacial morphology in two closely related primate species. In: Wang Q, ed. Bones, genetics, and behavior of rhesus macaques: *Macaca mulatta* of Cayo Santiago and beyond. New York, NY: Springer-Verlag. p 37-59.

Johnson SC. 1967. Hierarchicagl clustering schemes. *Psychometrika* 2:241-54.

Johnson Z, Brent L, Alvarenga JC, Comuzzie AG, Shelledy W, Ramirez S, Cox L, Mahaney MC, Huang Y, Mann JJ, Kaplan JR, Rogers J. 2015. Genetic influences on response to novel objects and dimensions of personality in *Papio* baboons. *Behav Genet* 45:215-27.

Johnston PA, Fox RC. 1984. Paleocene and Late Cretaceous mammals from Saskatchewan, Canada. *Palaeontographica A* 186:163-222.

Jolly CJ. 1970. The seed-eaters: a new model of hominind differentiation based on a baboon analogy. *Man* 5:5-26.

Jolly CJ. 1993. Species, subspecies, and baboon systematics. In: Kimbel WH, Martin LB, eds. Species, species concepts, and primate evolution. New York, NY: Plenum Press. p 67-107.

Jolly CJ. 2001. A proper study for mankind: analogies from the Papionin monkeys and their implications for human evolution. *Am J Phys Anthropol* 33:S177-204.

Jolly CJ, Burrell AS, Phillips-Conroy JE, Bergey C, Rogers J. 2011. Kinda baboons (*Papio kindae*) and grayfoot chacma baboons (*P. ursinus griseipes*) hybridize in the Kafue river valley, Zambia. *Am J Primatol* 73:291-303.

Jolly CJ, Woolley-Barker T, Beyene S, Disotell TR, Phillips-Conroy JE. 1997. Intergeneric hybrid baboons. *Intl J Primatol* 18:597-627.

Joly D, Faure D. 2015. Next-generation sequencing propels environmental genomics to the front line of research. *Hered* 114:429-30.

Jones TR. 1937. A new fossil primate from Sterkfontein, Krugersdorp, Transvaal. *S Afr J Sci* 33:709-28.

Jones E, Oliphant E, Peterson P, et al. 2001-2015. SciPy: open source scientific tools for Python. http://www.scipy.org.

Jones R, Pembrey M, Golding J, Herrick D. 2005. The search for genotype/phenotype associations and the phenome scan. *Paediatr Perinat Epidemiol* 19:264-75.

Jungers WL. 1985. Size and scaling in primate biology. New York, NY: Plenum Press.

Kammerer CM, Sparks ML, Rogers J. 1995. Effects of age, sex, and heredity on measures of bone mass in baboons (*Papio hamadryas*). *J Med Primatol* 24:236-42.

Karere GM, Glenn JP, Birnbaum S, Rainwater DL, Mahaney MC, VandeBerg JL, Cox LA. 2013. Identification of candidate genes encoding an LDL-C QTL in baboons. *J Lipid Res* 54:1776-85.

Kay RF. 1975. The functional adaptations of primate molar teeth. *Am J Phys Anthropol* 43:195-216.

Kay RF, Cartmill M. 1977. Cranial morphology and adaptations of *Palaechthon nacimienti* and other Paromomyidae (Plesiadapoidea, ? Primates), with a description of a new genus and species. *J Hum Evol* 6:19-53

Kay RF, Ross C, Williams BA. 1997. Anthropoid origins. *Science* 275:797-804.

Kay RF, Thorington RW, Houde P. 1990. Eocene plesiadapiform shows affinities with flying lemurs not primates. *Nature* 345:342-4.

Kenney-Hunt JP, Wang B, Norgard EA, Fawcett G, Falk D, Pletscher SL, Jarvis JP, Roseman C, Wolf J, Cheverud JM. 2008. Pleiotropic patterns of quantitative trait loci for 70 murine skeletal traits. *Genet* 178:2275-88.

Kerr R. 1792. The animal kingdom, or zoological system, of the celebrated Sir Charles Linnaeus. Edinburgh, GBR: A. Strahan.

Ketten D, Madin K. 2005. How to see what whales hear: biomedical imaging reveals news insights into marine mammal ears. *Oceanus* 43:59-63.

Khatib H. 2015. Molecular and quantitative animal genetics. Hoboken, NJ: John Wiley & Sons.

Kim HJ, Rice DPC, Kettunen PJ, Thesleff I. 1998. *FGF*-, *BMP*- and *SHH*-mediated signaling pathways in the regulation of suture morphogenesis and calvarial bone development. *Dev* 125:1241-51.

King G, Honaker J, Joseph A, Scheve K. 2001. Analyzing incomplete political science data: an alternative algorithm for multiple imputation. *Am Pol Sci Rev* 95:46-69.

King MC, Wilson AC. 1975. Evolution at two levels in humans and chimpanzees. *Science* 188:107-16.

Kingsley JS. 1925. The vertebrate skeleton from the developmental standpoint. Philadelphia, PA: P. Blakiston's Son & Co.

Kirk EC, Lemelin P, Hamrick MW, Boyer DM, Bloch JI. 2008. Intrinsic hand proportions of euarchontans and other mammals: implications for the locomotor behavior of plesiadapiforms. *J Hum Evol* 55:278-99.

Klein RG. 1986. Carnivore size and Quaternary climatic change in southern Africa. *Quaternary Res* 26:153-70.

Klingenberg CP. 2008. Morphological integration and developmental modularity. *Ann Rev Ecol Evol Syst* 39:115-32.

Klingenberg CP. 2011. MorhoJ: an integrated software package for geometric morphometrics. *Molec Ecol Resour* 11:353-7.

Klingenberg CP. 2014. Studying morphological integration and modularity at multiple levels: concepts and analysis. *Philos Trans Roy Soc Lond B Biol Sci* **369**:20130249.

Klingenberg CP, Leamy LJ, Cheverud JM. 2004. Integration and modularity of quantitative trait locus effects on geometric shape in the mouse mandible. *Genet* 166:1909-21.

Klingenberg CP, McIntyre GS. 1998. Geometric morphometrics of developmental instability: analyzing patterns of fluctuating asymmetry with Procrustes methods. *Evol* 52:1363-75.

Ko WY, Gomez F, Tishkoff SA. 2012. Evolution of human erythrocyte-specific genes involved in malaria susceptibility. In: Singh RS, Xu J, Kulathinal RJ, eds. Rapidly evolving genes and genetic systems. Oxford, GBR: Oxford University Press. p 223-34.

Kochakian CD, Tillotson C. 1957. Influence of several C19 steroids on the growth of individual muscles of the guinea pig. *Endocrinol* 60:607-18.

Koestler A. 1970. Beyond atomism and holism: the concept of the holon. *Perspect Biol Med* 13:131-54.

Koski K, Mäkinen L. 1963. Growth potential of transplanted components of the mandibular ramus of the rat. I. *Suomen Hammaslääkäriseuran Toimituksia* 60:209-17.

Koski K, Rönning O. 1970. Growth potential of intracerebrally transplanted cranial base synchondroses in the rat. *Arch Oral Biol* 15:1107-8.

Koszul R, Meselson M, Van Doninck K, Vandenhaute J, Zickler D. 2012. The centenary of Janssens's chiasmatype theory. *Genet* 191:309-17.

Koyabu DB, Endo H. 2009. Craniofacial variation and dietary adaptations of African colobines. *J Hum Evol* 56:525-36.

Koyabu DB, Endo H. 2010. Craniodental mechanics and diet in Asian colobines: morphological evidence of mature seed predation and sclerocarpy. *Am J Phys Anthropol* 142:137-48.

Kraus BS, Garrett WS. 1968. Cleft palate in a marmoset: report of a case. *Cleft Palate J* 5:340-5.

Kremers J. 2005. The primate visual system: a comparative approach. Chichester, GBR: John Wiley & Sons.

Krentz HB. 1993. Postcranial anatomy of extant and extinct species of *Theropithecus*. In: Jablonski NG, ed. *Theropithecus*: the rise and fall of a genus. Cambridge, MA: Cambridge University Press. p 383-422.

Kruglyak L. 1997. The use of a genetic map of biallelic markers in linkage studies. *Nature Genet* 17:21-4.

Kruuk LEB, Slate J, Pemberton JM, Brotherstone S, Guinness F, Clutton-Brock T. 2002. Antler size in red deer: heritability and selection but no evolution. *Evol* 56:1683-95.

Kurosaka H, Iulianella A, Williams T, Trainor PA. 2014. Disrupting hedgehog and *WNT* signaling interactions promotes cleft lip pathogenesis. *J Clin Invest* 124:1660-71.

Kvinnsland S. 1973. Growth in height of autotransplanted nasal septum in the rat, its correlation to increase in height of the upper face. *Acta Odontol Scand* 31:317-22.

Lacroix P. 1951. The organization of bones. London, GBR: Churchill.

Lallier TE. 1991. Cell lineage and cell migration in the neural crest. *Ann NY Acad Sci* 615:158-71.

Lande R. 1979. Quantitative genetic analysis of multivariate evolution, applied to brain:body size allometry. *Evol* 33:402-16.

Lander ES, Botstein D. 1989. Mapping Mendelian factors underlying quantitative traits using RFLP linkage maps. *Nat Genet* 4:5-6.

Langergraber KE, Prüfer K, Rowney C, Boesch C, Crockford C, Fawcett K, Inoue E, Inoue-Muruyama M, Mitani JC, Muller MN, Robbins MM, Schubert G, Stoinski TS, Viola B, Watts D, Wittig RM, Wrangham RW, Zuberbühler K, Pääbo S, Vigilant L. 2012. Generation times in wild chimpanzees and gorillas suggest earlier divergence times in great ape and human evolution. *Proc Natl Acad Sci U S A* 109:15716-21.

Latham RA, Scott JH. 1970. A newly postulated factor in the early growth of the human middle face and the theory of multiple assurance. *Arch Oral Biol* 15:1097-1100.

Lawson HA, Willmore KE, Cox L, Mahaney M. 2009. Using comparative genomics to improve understanding of hominid craniofacial evolution. *Am J Phys Anthropol* 138:S173.

Lawson HA, Zelle KM, Fawcett GL, Wang B, Pletscher LS, Maxwell TJ, Ehrich TH, Kenney-Hunt JP, Wolf JB, Semenkovich CF, Cheverud JM. 2010. Genetic, epigenetic, and gene-by-diet interaction effects underlie variation in serum lipids in a LG/J x SM/J murine model. *J Lipid Res* 51:2976-84.

Le Gros Clark WE. 1959. The antecedents of man. Edinburgh, GBR: Edinburgh University Press.

Le Douarin NM, Teillet MAM. 1974. Experimental analysis of the migration and differentiation of neuroblasts of the autonomic nervous system and of neuroectodermal mesenchymal derivatives, using a biological cell marking technique. *Dev Biol* 41:162-84.

Le Lievre CS, Schweizer GG, Ziller CM, Le Douarin NM. 1980. Restrictions of developmental capabilities in neural crest cell derivatives as tested by *in vivo* transplantation experiments. *Dev Biol* 77:362-78.

Leakey REF. 1969. New Cercopithecidae from the Chemeron Beds of Lake Baringo, Kenya. *Fossil Vert Afr* 1:395-405.

Leakey MG, Leakey REF. 1976. Further Cercopithecinae (Mammalia, Primates) from the Plio/Pleistocene of East Africa. *Fossil Vertebrates Afr* 4:121-46.

Leakey MG, Spoor F, Dean MC, Feibel CS, Antón SC, Kiarie C, Leakey LN. 2012. New fossils from Koobi Fora in northern Kenya confirm taxonomic diversity in early *Homo*. *Nature* 488: 201-4.

Leamy LJ, Klingenberg CP, Sherratt E, Wolf JB, Cheverud JM. 2008. A search for quantitative trait loci exhibiting imprinting effects on mouse mandible size and shape. *Hered* 101:518-26.

Leamy LJ, Routman EJ, Cheverud JM. 1999. Quantitative trait loci for early- and late-developing skull characters in mice: a test of the genetic independence model of morphological integration. *Am Nat* 153:201-14.

Lee PC, Foley RA. 1993. Ecological energetics and extinction of giant gelada baboons. In: Jablonski NG, ed. *Theropithecus*: the rise and fall of a genus. Cambridge, MA: Cambridge University Press. p 487-98.

Lee NJ, Park IS, Koh IS, Jung TW, Rhyu IJ. 2009. No volume difference of medulla oblongata between young and old Korean people. *Brain Res* 1276:77-82.

Leigh SR. 1992. Patterns of variation in the ontogeny of primate body size dimorphism. *J Hum Evol* 23:27-50.

Leigh SR. 1994. Ontogenetic correlates of diet in anthropoid primates. *Am J Phys Anthropol* 94:499-522.

Leigh SR. 1996. Evolution of human growth spurts. *Am J Phys Anthropol* 101:455-74.

Leigh SR. 2004. Brain growth, life history, and cognition in primate and human evolution. *Am J Primatol* 62:139-64.

Leigh SR. 2006. Cranial ontogeny of *Papio* baboons (*Papio hamadryas*). *Am J Phys Anthropol* 130:71-84.

Leigh SR. 2007. Homoplasy and the evolution of ontogeny in papionin primates. *J Hum Evol* 52:536-558.

Leigh SR. 2009. Growth and development of baboons. In: VandeBerg JL, Williams-Blangero S, Tardif SD, eds. The baboon in biomedical research. New York, NY: Springer. p 57-88.

Leigh SR, Cheverud JM. 1991. Sexual dimorphism in the baboon facial skeleton. *Am J Phys Anthropol* 84:193-208.

Leigh SR, Shah NF, Buchanan LS. 2003. Ontogeny and phylogeny in papionin primates. *J Hum Evol* 45:285-316.

Leigh SR, Shea BT. 1996. Ontogeny of body size variation in African apes. *Am J Phys Anthropol* 99:43-65.

Leigh SR, Terranova CJ. 1998. Comparative perspectives on bimaturism, ontogeny, and dimorphism in lemurid primates. *Intl J Primatol* 19:723-41.

Lettice LA, Purdie LA, Carlson GJ, Kilanowski F, Dorin J, Hill RE. 1999. The mouse bagpipe gene controls development of axial skeleton, skull, and spleen. *Proc Natl Acad Sci U S A* 96:9695-700.

Leutenegger W, Cheverud JM. 1982. Correlates of sexual dimorphism in primates: ecological and size variability. *Intl J Primatol* 3:387-402.

Lewis JL, Bonner J, Modrell M, Ragland JW, Moon RT, Dorsky RI, Raible DW. 2004. Reiterated *Wnt* signaling during zebrafish neural crest development. *Develop* 131:1299-1308.

Lewontin R. 1974. The genetic basis of evolutionary change. New York City, NY: Columbia University Press.

Lewontin R. 2000. The triple helix: gene, organism, and environment. Cambridge, MA: Harvard University Press.

Lidral AC, Murray JC, Buetow KH, Basart AM, Schearer H, Shiang R, Naval A, Layda E, Magee K, Magee W. 1997. Studies of the candidate genes *TGFB2*, *MSX1*, *TGFA*, and *TGFB3* in the etiology of cleft lip and palate in the Philippines. *Cleft Palate Craniofac J* 34:1-6.

Lieberman DE. 1995. Testing hypotheses about recent human evolution from skulls: integrating morphology, function, development, and phylogeny. *Curr Anthropol* 36:159-97.

Lieberman DE, Hallgrímsson B, Liu W, Parsons TE, Jamniczky HA. 2008. Spatial packing, cranial base angulation, and craniofacial shape variation in the mammalian skull: testing a new model using mice. *J Anat* 212:720-35.

Lieberman DE, Pearson OM, Mowbray KM. 2000. Basicranial influence on overall cranial shape. *J Hum Evol* 38:291-315.

Lieberman DE, Ross CF, Ravosa MJ. 2000. The primate cranial base: ontogeny, function, and integration. *Yrbk Phys Anthropol* 43:117-69.

Lindenfors P, Nunn CL, Barton RA. 2007. Primate brain architecture and selection in relation to sex. *BMC Biol* 5:20.

Linnaeus C. 1758. Systema naturae per regna tria naturae, secundam classes, ordines, genera, species cum characteribus, synonymis, locis. Stockholm, SWE: Laurentii Sylvii.

Liu BH. 1998. Statistical genomics: linkage, mapping, and QTL analysis. Boca Raton, FL: CRC Press.

Liu F, Malaval L, Aubin JE. 1997. The mature osteoblast phenotype is characterized by extensive plasticity. *Exp Cell Res* 232:97-105.

Liu EY, Morgan AP, Chesler EJ, Wang W, Churchill GA, de Villena FPM. 2014. Hig-resolution sex-specific linkage maps of the mouse reveal polarized distribution of crossovers in male germline. *Genet* 197:91-106.

Liu F, van der Lijn F, Schurmann C, Zhu G, Chakravarty MM, Hysi PG, Wollstein A, Lao O, de Bruijne M, Ikram MA, van der Lugt A, Rivadeneira F, Uitterlinden AG, Hofman A, Niessen WJ, Homuth G, de Zubicaray G, McMahon KL, Thompson PM, Daboul A, Puls R, Hegenscheid K, Bevan L, Pausova Z, Medland SE, Montgomery GW, Wright MJ, Wicking C, Boehringer S, Spector TD, Paus T, Martin NG, Biffar R, Kayser M. 2012. A genome-wide association study identifies five loci influencing facial morphology in Europeans. *PLoS Genet* 8:e1002932.

Lockwood CA, Tobias PV. 2002. Morphology and affinities of new hominin cranial remains from Member 4 of the Sterkfontein Formation, Gauteng Province, South Africa. *J Hum Evol* 42:389-450.

Lofsvold D. 1986. Quantitative genetics of morphological differentiation in *Peromyscus*. I. tests of the homogeneity of genetic covariance structure among species and subspecies. *Evol* 40:559-73.

Lynch M, Walsh B. 1998. Genetics and analysis of quantitative traits. Sunderland, MA: Sinauer Associates, Inc.

Mackay TFC. 2001. The genetic architecture of quantitative traits. *Annu Rev Genet* 35:303-39.

Mackay TFC, Stone EA, Ayroles JF. 2009. The genetics of quantitative traits: challenges and prospects. *Nat Rev Genet* 10:595-77.

MacLeod JN, Pampori NA, Shapiro BH. 1991. Sex differences in the ultradian pattern of plasma growth hormone concentrations in mice. *J Endocrinol* 131:395-9.

Maga AM, Navarro N, Cunningham ML, Cox TC. 2015. Quantitative trait loci affecting the 3D skull shape and size in mouse and prioritization of candidate genes *in-silico*. *Front Phsyiol* 6:92.

Magwene PM. 2001. New tools for studying integration and modularity. *Evol* 55:1734-45.

Mahaney MC, Blangero J, Rainwater DL, Mott GE, Comuzzie AG, MacCluer JW, VandeBerg JL. 1999. Pleiotropy and genotype by diet interaction in a baboon model for atherosclerosis: a

multivariate quantitative genetic analysis of HDL subfractions in two dietary environments. *Arterioscler Thromb Vasc Biol* 19:1134-41.

Mani P, Jarrell A, Myers J, Atit R. 2010. Visualizing canonical *Wnt* signaling during mouse craniofacial development. *Develop Dynam* 239:354-63.

Manolio TA, Collins FS, Cox NJ, Goldstein DB, Hindorff LA, Hunter DJ, McCarthy MI, Ramos EM, Cardon LR, Chakravarti A, Cho JH, Guttmacher AE, Kong A, Kruglyak L, Mardis E, Rotimi CN, Slatkin M, Valle D, Whittemore AS, Boehnke M, Clark AG, Eichler EE, Gibson G, Haines JL, Mackay TFC, McCarroll SA, Visscher PM. 2009. Finding the missing heritability of complex disease. *Nature* 461:747-53.

Mantel N. 1967. The detection of disease clustering and a generalized regression approach. *Cancer Res* 27:209-20.

Maples WR, McKern MA, McKern TW. 1967. A preliminary report on classification of the Kenya baboon. In: Vagtborg H, ed. The baboon in medical research vol II: proceedings of the second international symposium on the baboon and its use as an experimental animal. Austin, TX: University of Texas Press. p 13-22.

Marcus LF, Hingst-Zaher E, Zaher H. 2000. Application of landmark morphometrics to skulls representing the orders of living mammals. *Hystrix* 11:27-47.

Marigó J, Susanna I, Minwer-Barakat R, Madurell-Malapeira J, Moyà-Solà S, Casanovas-Vilar I, Robles JM, Alba DM. 2014. The primate fossil record in the Iberian Peninsula. *J Iberian Geol* 40:179-211.

Marjanovic D, Laurin M. 2008. A reevaluation of the evidence supporting an unorthodox hypothesis on the origin of extant amphibians. *Contrib Zool* 77:149-99.

Marroig G, Cheverud JM. 2001. A comparison of phenotypic variation and covariation patterns and the role of phylogeny, ecology, and ontogeny during cranial evolution of New World monkeys. *Evol* 55:2576-600.

Marroig G, Cheverud JM. 2004. Did natural selection or genetic drift produce the cranial diversification of Neotropical monkeys? *Am Nat* 163:417-28.

Marroig G, Cheverud JM. 2005. Size as a line of least evolutionary resistance: diet and adaptive morphological radiation in New World monkeys. *Evol* 59:1128-42.

Marroig G, Cheverud JM. 2005. Size as a line of least evolutionary resistance: diet and adaptive morphological radiation in New World monkeys. *Evol* 59:1128-1142.

Marroig G, De Vivo M, Cheverud JM. 2004. Cranial evolution in sakis (*Pithecia*, Platyrrhini) II: evolutionary processes and morphological integration. *J Evol Biol* 17:144-55.

Marsh JD, Lehmann MH, Ritchie RH, Gwathmey JK, Green GE, Schiebinger RJ. 1998. Androgen receptors mediate hypertrophy in cardiac myocytes. *Circulat* 98:256-61.

Martin RD. 1993. Allometric aspects of skull morphology in *Theropithecus*. In: Jablonski NG, ed. *Theropithecus*: the rise and fall of a genus. Cambridge, MA: Cambridge University Press. p 273-98.

Martin LJ, Carey KD, Comuzzie AG. 2003. Variation in menstrual cycle length and cessation of menstruation in captive raised baboons. *Mech Ageing Dev* 124:865-71.

Martinelli FL, Reale CS, Bolognese AM. 2012. Class II malocclusion with dep overbite: a sequential approach. *Dent Press J Orthod* 17:76-82.

Martínez-Abadías N, Esparza M, Sjøvold T, González-José R, Santos M, Hernández M. 2009. Heritability of human cranial dimensions: comparing the evolvability of different cranial regions. *J Anat* 214:19-35.

Martínez-Abadías N, Esparza M, Sjøvold T, González-José R, Santos M, Hernández M, Klingenberg CP. 2011. Pervasive genetic integration directs the evolution of human skull shape. *Evol* 66:1010-23.

Martínez-Abadías N, Heuzé Y, Wang Y, Jabs EW, Aldridge K, Richtsmeier JT. 2011. *FGF*/*FGFR* signaling coordinates skull development by modulating magnitude of morphological integration: evidence from Apert Syndrome mouse models. *PLoS One* 6:e26425.

Martínez-Abadías N, Mitteroecker P, Parsons TE, Esparza M, Sjøvold T, Rolian C, Richtsmeier JT, Hallgrímsson B. 2012. The developmental basis of quantitative craniofacial variation in humans and mice. *Evol Biol* 39:554-67.

Martinez-Maza C, Freidline SE, Strauss A, Nieto-Diaz M. 2015. Bone growth dynamics of the facial skeleton and mandible in *Gorilla gorilla* and *Pan troglodytes*. *Evol Biol* (early online edition).

Martins EP. 2000. Adaptation and the comparative method. *Trends Ecol Evol* 15:296-299.

Maxson R, Ishii M. 2008. The *Bmp* pathway in skull vault development. In: Rice DP, ed. Craniofacial sutures: development, disease and treatment. Basel, CHE: Karger 12:197-208.

Maynard Smith J, Burian R, Kauffman S, Alberch P, Campbell J, Goodwin B, Lande R, Raup D, Wolpert L. 1985. Developmental constraints and evolution. *Q Rev Biol* 60:265-87.

Mayr E. 1940. Speciation phenomena in birds. *Am Nat* 74:249-78.

Mayr E. 1976. Evolution and the diversity of life. Cambridge, MA: Harvard Press.

McCormick CM, Smythe JW, Sharma S, Meaney MJ. 1995. Sex-specific effects of prenatal stress on hypothalamic-pituitary-adrenal responses to stress and brain glucocorticoid receptor density in adult rats. *Dev Brain Res* 84:55-61.

McCrady S. 2003. Response surface analysis of rat bone composition changes by dietary calcium and silicon. Thesis: University of Wisconsin-Stout.

McGinnis W, Garber RL, Wirz J, Kuroiwa A, Gehring WJ. 1984. A homologous protein-coding sequence in *Drosophila* homeotic genes and its conservation in other metazoans. *Cell* 37:403-8.

McKay BD. Zink RM. 2015. Sisyphean evolution in Darwin's finches. *Biol Rev* 90:689-98.

McKinney W. 2010. Data structures for statistical computing in python. In: van der Walt S, Millman J, eds. Proceedings of the 9th Python in Science Conference. http://conference.scipy.org/proceedings/scipy2010/mckinney.html. p 51-6.

McKitrik MC, Zink RM. 1988. Species concepts in ornithology. *Condor* 90:1-14.

McLean CY, Reno PL, Pollen AA, Bassan AI, Capellini TD, Guenther C, Indjeian VB, Lim X, Menke DB, Schaar BT, Wenger AM, Bejerano G, Kingsley DM. 2011. Human-specific loss of regulatory DNA and the evolution of human-specific traits. *Nature* 471:216-9.

Mekel-Bobrov N, Gilbert SL, Evans PD, Vallender EJ, Anderson JR, Hudson RR, Tishkoff SA, Lahn BT. 2005. Ongoing adaptive evolution of *ASPM*, a brain size determinant in *Homo sapiens*. *Science* 309:1720-2.

Meloro C, Cáceres N, Carotenuto F, Passaro F, Sponchiado J, Melo GL, Raia P. 2014. Ecogeographical variation in skull morphology of howler monkeys (Primates: Atelidae). *Zool Anz* 253:345-59.

Melsen B. 1971. The postnatal growth of the cranial base in *Macaca rhesus* analyzed by the implant method. *Tandlaegebladet* 75:1320-9.

Mensforth RP, Lovejoy CO, Lallo JW, Armelagos GJ. 1978. The role of constitutional factors, diet, and infectious disease in the etiology of porotic hyperostosis and periosteal reactions in prehistoric infants and children. *Med Anthropol* 2:1-59.

Mezey JG, Cheverud JM, Wagner GP. 2000. Is the genotype-phenotype map modular?: a stastistical approach using mouse quantitative trait loci data. *Genet* 156:305-11.

Mi H, Muruganujan A, Casagrande JT, Thomas PD. 2012. PANTHER in 2013: modeling the evolution of gene function, and other gene attributes, in the context of phylogenetic trees. *Nucleic Acids Res* 41:377-86.

Mi H, Muruganujan A, Casagrande JT, Thomas PD. 2013. Large-scale gene function analysis with the PANTHER classification system. *Nat Protoc* 8:1551-66.

Michejda M. 1972. The role of basicranial synchondroses in flexure processes and ontogenetic development of the skull base. *Am J Phys Anthropol* 37:143-50.

Michel LA, Peppe DJ, Lutz JA, Driese SG, Dunsworth HM, Harcourt-Smith WEH, Horner WH, Lehmann T, Nightingale S, McNulty KP. 2014. Remnants of an ancient forest provide ecological context for Early Miocene fossil apes. *Nat Commun* 5:3236.

Miettinen PJ, Chin JR, Shum L, Slavkin HC, Shuler CF, Derynck R, Werb Z. 1999. Epidermal growth factor receptor function is necessary for normal craniofacial development and palate closure. *Nature Genet* 22:69-73.

Miflin B. Crop improvement in the 21st century. 2000. *J Exp Bot* 51:S1-8.

Miley DD, Baumgartner MH, Cheverud JM, Roseman CC, Rogers J, McLeod DE, Reyes E, Hildebolt CF. 2011. Heritability of alveolar bone loss from periodontal disease in a baboon population. A population study. *J Periodontol* 82:575-80.

Miller RL. 1950. Biometrical analysis of skull morphology. Unpublished doctoral thesis. University of Chicago.

Miller ER, Benefit BR, McCrossin ML, Plavcan JM, Leakey MG, El-Barkooky AN, Hamdan MA, Abdel Gawad MK, Hassan SM, Simons EL. 2009. Systematics of early and middle Miocene Old World monkeys. *J Hum Evol* 57:195-211.

Miller RL, Weller JM. 1952. Significant comparisons in paleontology. *J Paleontol* 26:993-96.

Mishina Y, Snider TN. 2014. Neural crest cell signaling pathways critical to cranial bone development and pathology. *Exp Cell Res* 325:138-47.

Mitani JC, Gros-Louis J, Richards AF. 1996. Sexual dimorphism, the operational sex ratio, and the intensity of male competition in polygynous primates. *Am Nat* 147:966-80.

Mitteroecker P, Bookstein F. 2008. The evolutionary role of modularity and integration in the hominoid cranium. *Evol* 62-4: 943-58.

Mitteroecker P, Gunz P, Bernhard M, Schaefer K, Bookstein FL. 2004. Comparison of cranial ontogenetic trajectories among great apes and humans. *J Hum Evol* 46:679-98.

Mitteroecker P, Huttegger SM. 2009. The concept of morphospaces in evolutionary and developmental biology: mathematics and metaphors. *Biol Theory* 4:54-67.

Mitruka BM, Bonner MJ. 1976. Uniquely useful animal species for biomedical research. In: Mitruka BM, Rawnsley HM, Vadehra DV, eds. Animals for medical research: models for the study of human disease. New York, NY: John Wiley & Sons. p 523-80.

Morgan TH. 1914. No crossing over in the male of *Drosophila* of genes in the second and third pairs of chromosomes. *Biol Bull* 26:195-204.

Mork L, Crump G. 2015. Zebrafish craniofacial development: a window into early patterning. *Curr Top Dev Biol* 115:235-69.

Morton NE. 1955. Sequential tests for the detection of linkage. *Am J Hum Genet* 7:277-318.

Moss ML. 1954. Growth of the calvaria in the rat: the determination of osseous morphology. *Am J Anat* 94:333-61.

Moss ML. 1957. Experimental alteration of sutural area morphology. *Anat Rec* 127:569-89.

Moss ML. 1960. Functional analysis of human mandibular growth. *J Prost Dent* 10:1149-59.

Moss ML. 1962. The functional matrix. In: Kraus B, Reidel R, eds. Vistas in orthodontics. Philadelphia, PA: Lea & Feibeger. p 85-98.

Moss ML, Young RW. 1960. A functional approach to craniology. *Am J Phys Anthropol* 18:281-92.

Moss ML. 1962. The functional matrix. In: Kraus BS, Riedel RA, eds. Vistas of orthodontics. Philadelphia, PA: Lea and Febiger. p 85-98.

Mousseau TA, Roff DA. 1987. Natural selection and the heritability of fitness components. *Heredity* 181-97.

Motyl KJ, Bishop KA, DeMambro VE, Bornstein SA, Le P, Kawai M, Lotinun S, Horowitz MC, Baron R, Bouxsein ML, Rosen CJ. 2013. Altered thermogenesis and impaired bone remodeling in *Misty* mice. *J Bone Miner Res* 28:1885-97.

Müller R, Lu H, Buck JR. 2010. Sound-diffracting flap in the ear of a bat generates spatial information. *Phys Rev Lett* 100:108701.

Nadol Jr JB. 2006. Histology and histopathology of the temporal bone. In: Van de Water TR, Staecker H, eds. Otolaryngology: basic science and clinical review. New York, NY: Thieme. p 283-312.

Neaux D, Guy F, Gilissen E, Coudyzer W, Vignaud P, Ducrocq S. 2013. Facial orientation and facial shape in extant great apes: a geometric morphometric analysis of covariation. *PLoS One* 8:e57026.

Nelson GJ. 1978. Ontogeny, phylogeny, paleontology and the biogenetic law. *Syst Zool* 27:324-45.

Nicolae D, Cox NJ, Lester LA, Schneider D, Tan Z, Billstrand C, Kuldanek S, Donfack J, Kogut P, Patel NM, Goodenbour J, Howard T, Wolf R, Koppelman GH, White SR, Parry R, Postma DS, Meyers D, Bleecker ER, Hunt JS, Solway J, Ober C. 2005. Fine mapping and positional

candidate studies identify *HLA-G* as an asthma susceptibility gene on chromosome 6p21. *Am J Hum Genet* 76:349-57.

Nielsen FH. 2004. Dietary fat composition modifies the effect of boron on bone characteristics and plasma lipids in rats. *Biofactors* 20:161-71.

Nielsen R, Bustamante C, Clark AG, Glanowski S, Sackton TB, Hubisz MJ, Fledel-Alon A, Tanenbaum DM, Civello D, White TJ, Sninsky JJ, Adams MD, Cargill M. 2005. A scan for positively selected genes in the genomes of humans and chimpanzees. *PLoS Biol* 3:e170.

Noble D. 2015. Conrad Waddington and the origin of epigenetics. *J Exp Biol* 218:816-8.

Noden DM. 1988. Interactions and fates of avian craniofacial mesenchyme. *Dev* 103:S121-40.

Noden DM, Trainor PA. 2005. Relations and interactions between cranial mesoderm and neural crest populations. *J Anat* 207: 575-601.

Nomura S, Takano-Yamamoto T. 2000. Molecular events caused by mechanical stress to bone. *Matrix Biol* 19:91-6.

Norgard RA, Roseman CC, Fawcett GL, Pavličev M, Morgan CD, Pletscher LS, Wang B, Cheverud JM. 2008. Identification of quantitative trait loci affecting murine long bone length in a two-generation intercross of LG/J and SM/J mice. *J Bone Min Res* 23:887-95.

Nova Delgado M, Gamarra B, Nadal J, Mercadal O, Olesti O, Guàrdia J, Pérez- Pérez A, Galbany J. 2014. Dental shape variability in cercopithecoid primates: a model for the taxonomic attribution of macaques from Roman archaeological contexts. *Folia Primatol* 85:361-78.

Nunn CL. 2011. The comparative approach in evolutionary anthropology and biology. Chicago, IL: The University of Chicago Press.

O'Brien SJ. 1990. Genetic maps: locus maps of complex genomes. Cold Spring Harbor, NY: Cold Spring Harbor Laboratory Press.

Oertelt-Prigione S. 2012. The influence of sex and gender on the immune response. *Autoimmun Rev* 11:479-85.

O'Higgins P, Collard M. 2002. Sexual dimorphism and facial growth in papionin monkeys. *J Zool Lond* 257:255-272.

Okazaki K. 1995. Anatomical study of the ligaments in the occipito-atlanto-axial complex. *Nippon Seikeigeka Gakkai Zasshi* 69:1259-67.

Oldenbroeck K, van der Waaij L. 2015. Textbook animal breeding and genetics for BSc students. Centre for Genetic Resources, the Netherlands; Animal Breeding and Genomics Centre: https://wiki.groenkennisnet.nl/display/TAB/Textbook+Animal+Breeding+and+Genetics.

O'Leary MA, Bloch JI, Flynn JJ, Gaudin TJ, Giallombardo A, Giannini, Goldberg SL, Kraatz BP, Luo ZX, Meng J, Ni X, Novacek MJ, Perini FA, Randall ZS, Rougier GW, Sargis EJ, Silcox MT, Simmons NB, Spaulding M, Velazco PM, Weksler M, Wible JR, Cirranello AL. 2013. The placental mammal ancestor and the Post-K-Pg radiation of placentals. *Science* 339:662-7.

Oleksyk TK, Smith MW, O'Brien SJ. 2010. Genome-wide scans for footprints of natural selection. *Philos Trans R Soc Lond B Biol Sci* 365:185-205.

Olson EC. 1953. Integrating factors in amphibian skulls. *J Geol* 61:557-68.

Olson EC, Miller RL. 1951. A mathematical model applied to a study of the evolution of species. *Evol* 9:75-83.

Olson EC, Miller RL. 1958. Morphological integration. Chicago, IL: The University of Chicago Press.

Olson TR. 1981. Basicranial morphology of the extant hominoids and Pliocene hominids: the new material from the Hadar Formation, Ethiopia and its significance in early human evolution and taxonomy. In: Stringer CB, ed. Aspects of human evolution. London, GBR: Taylor and Francis. p 99-128.

O'Mara MT, Gordon AD, Catlett KK, Terranova CJ, Schwartz GT. 2012. Growth and the development of sexual size dimorphism in lorises and galagos. *Am J Phys Anthropol* 147:11-20.

Opperman LA, Sweeney TM, Redmon J, Persing JA, Ogle RC. 1993. Tissue interactions with underlying dura mater inhibit osseous obliteration of developing cranial sutures. *Dev Dyn* 198:312-22.

Ostrander EA, Bustamante CD. 2012. Genetics of morphological traits in the domestic dog. In: Ostrander EA, Ruvinsky A, eds. The genetics of the dog. Cambridge, MA: CAB International. p 359-74.

Otto AW. 1831. A compendium of human and comparative pathological anatomy. London, GBR: B. Fellowes.

Oyen OJ, Walker AC, Rice RW. 1979. Craniofacial growth in olive baboons (*Papio cynocephalus anubis*): browridge formation. *Growth* 43:174-87.

Page SL, Chiu C, Goodman M. 1975. Molecular phylogeny of Old World monkeys (Cercopithecidae) as inerred from gamma-globin DNA seqeuces. *Mol Phylogenet Evol* 13:348-59.

Pallares LF, Carbonetto P, Gopalakrishnan S, Parker CC, Ackert-Bicknell CL, Palmer AA, Tautz D. 2015. Mapping of craniofacial traits in outbred mice identifies major developmental genes involved in shape determination. *PLoS Genet* 11:e1005607.

Pallares LF, Harr B, Turner LM, Tautz D. 2014. Use of a natural hybrid zone for genomewide association mapping of craniofacial traits in the house mouse. *Molec Ecol* 23:5756-70.

Parsons TE, Downey CM, Jirik FR, Hallgrimsson B, Jamniczky HA. 2015. Mind the gap: genetic manipulation of basicranial growth within synchondroses modulates calvarial and facial shape in mice through epigenetic interactions. *PLoS One* 10:e0118355.

Parvizi J, Jacques C, Foster BL, Withoft N, Rangarajan V, Weiner KS, Grill-Spector K. 2012. Electrical stimulation of human fusiform face-selective regions distorts face perception. *J Neurosci* 32:14915-20.

Patterson C. 1982. Morphological characters and homology. In: Joysey KA, Friday AE, eds. Systematic association special volume 21: problems of phylogenetic reconstruction. London, GBR: Academic Press. p 21-74.

Patterson C. 1988. Homology in classical and molecular biology. *Mol Biol Evol* 5:603-25.

Paul DB, Kimmelman BA. 1988. Mendel in America: theory and practice, 1900-1919. Philadelphia, PA: University of Pennsylvania Press.

Payne F. 1918. The effect of artificial selection on bristle number in *Drosophila ampelophila* and its interpretation. *Proc Natl Acad Sci U S A* 4:55-8.

Pearson K, Lee A. 1903. On the laws of inheritance in man: I. inheritance of physical characters. *Biometrika* 2:357-462.

Pederson L, Kremer M, Judd J, Pascoe D, Spelsberg TC, Riggs BL, Oursler MJ. 1999. Androgens regulate bone resorption activity of isolated osteoclasts *in vitro*. *Proc Natl Acad Sci U S A* 96:505-10.

Percival C, Wilmore K, Chimera M, Sirivunnabood S, Rogers J, Cheverud JM, Buchanan A, Weiss K, Richtsmeier J. 2010. Morphological changes associated with tooth loss and alveolar resorption in male baboons. *Am J Phys Anthropol* 141:S187.

Petrovic A. 1974. Control of postnatal growth of secondary cartilages of the mandible by mechanisms regulating occlusion. cybernetic model. *Trans Eur Orthod Soc* 69-75.

Phillips PC. 2007. What maintains genetic variation in natural populations? A commentary on ‘The maintainence of genetic variability by mutation in a polygenic character with linked loci’ by Russell Lande. *Genet Res* 89:371-2.

Phillips PC, Arnold SJ. 1999. Hierarchical comparison of genetic variance-covariance matrices. I. using the Flury hierarchy. *Evol* 53:1506-15.

Phillips-Conroy JE, Jolly CJ. 1981. Sexual dimorphism in two subspecies of Ethiopian baboons (*Papio hamadryas*) and their hybrids. *Am J Phys Anthropol* 56:115-29.

Pickering R, Dirks PHG, Jinnah Z, de Ruiter DJ, Churchill SE, Herries AIR, Woodhead JD, Hellstrom JC, Berger LR. 2011. *Australopithecus sediba* at 1.977 Ma and implications for the origins of the genus *Homo*. *Nature* 333:1421-3.

Pigliucci M. 2001. Phenotypic plasticity: beyond nature and nurture. Baltimore, MD: John Hopkins University Press.

Pigliucci M. 2008. Is evolvability evolvable? *Nat Rev Genet* 9:75-82.

Pilbrow V, Groves C. 2013. Evidence for divergence in populations of bonobos (*Pan paniscus*) in Lomami-Lualaba and Kasai-Sankuru regions based on preliminar analysis of craniodental variation. *Intl J Primatol* 34:1244-60.

Pino-Bodas R, Burgaz AR, Martín MP, Lumbsch HT. 2011. Phenotypical plasticity and homoplasy complicate species delimitation in the *Cladonia gracilis* group (Cladoniaceae, Ascomycota). *Org Divers Evol* 11:343-55.

Porto A, de Oliveira FB, Shirai LT, De Conto V, Marroig G. 2009. The evolution of modularity in the mammalian skull I: morphological integration patterns and magnitudes. *Evol Biol* 36:118-35.

Pozzo T, Berthox A, Lefort L, Vitte E. 1991. Head stabilization during various locomotor tasks in humans. II. patients with bilateral peripheral vestibular defects. *Exp Brain Res* 85:208-17.

Pratt LW. 1943. Experimental masseterectomy in the laboratory rat. *J Mamm* 24:204-11.

Pritchard JK, Stephens M, Rosenberg NA, Donnelly P. 2000. Association mapping in structured populations. *Am J Hum Genet* 67:170-81.

Ptak SE, Hinds DA, Koehler K, Nickel B, Patil N, Ballinger DG, Przeworski M, Frazer KA, Pääbo S. 2005. Fine-scale recombination patterns differ between chimpanzees and humans. *Nat Genet* 37:429-434.

R Core Team. 2014. R: a language and environment for statistical computing. Vienna: R Foundation for Statistical Computing. http://www.R-project.org/.

Rae TC, Viðarsdóttir US, Jeffery N, Steegmann Jr AT. 2006. Developmental response to cold stress in cranial morphology of *Rattus*: implications for the interpretation of climatic adaptation in fossil hominins. *Proc Biol Sci* 273:2605-10.

Rankinen T, Zuberi A, Chagnon YC, Weisnagel SJ, Argyropoulos G, Walts B, Pérusse L, Bouchard C. 2006. The human obesity gene map: the 2005 update. *Obesity* 14:529-644.

Rao SR, Rao TR, Ovchinnikov N, McRae A, Rao AVC. 2007. Unusual isolated ossification of falx cerebri: a case report. *Neuroanat* 6:54-5.

Rasmussen DT, Simons EL. 1992. Paleobiology of the oligopithecines, the earliest known anthropoid primates. *Int J Primatol* 13:477-508.

Rasmussen DT, Sussman RW. 2007. Parallelisms among primates and possums. In: Ravosa MJ, Dagosto M, eds. Primate origins: adaptations and evolution. New York, NY: Spring US. p 775-803.

Ravosa MJ, Noble VE, Hylander WL, Johnson KR, Kowalski EM. 2000. Masticatory stress, orbital orientation and the evolution of the primate postorbital bar. *J Hum Evol* 38:667-93.

Ravosa MJ, Vinyard CJ, Hylander WL. 2000. Stressed out: masticatory forces and primate circumorbital form. *Anat Rec* 261:173-175.

Reusch T, Blanckenhorn WU. 1998. Quantitative genetics of the dung fly *Sepsis cynipsea*: Cheverud's conjecture revisited. *Hered* 81:111-9.

Rice TK, Borecki IB. Familial resemblance and heritability. In: Rao DC, Province MA. Genetic dissection of complex traits. San Diego, CA: Academic Press. p 35-44.

Richtsmeier JT, Aldridge K, DeLeon VB, Panchal J, Kane AA, Marsh JL, Yan P, Cole III TM. 2006. Phenotypic integration of neurocranium and brain. *J Exp Zool B Mol Dev Evol* 306:360-78.

Richtsmeier JT, Deleon VB, Lele SR. 2002. The promise of geometric morphometrics. *Yrbk Phys Anthropol* 45:63-91.

Rickman JM, Tickle C. 1992. Epithelial-mesenchymal interactions in the outgrowth of imb buds and facial primordia in chick embryos. *Dev Biol* 154:299-308.

Rightmire GP. 1993. Variation among early *Homo* crania from Olduvai Gorge and the Koobi Fora region. *Am J Phys Anthropol* 90:1-33.

Risch NJ. 2000. Searching for genetic determinants in the new millennium. *Nature* 405: 847-56.

Roberts TD. 1978. Neurophysiology of postural mechanisms. London, GBR: Butterworths.

Roberts RB, Hu Y, Albertson RC, Kocher TD. 2011. Craniofacial divergence and ongoing adaptation via the hedgehog pathway. *Proc Natl Acad Sci U S A* 108:13194-9.

Robertson A. 1967. The nature of quantitative genetic variation. In: Brink A, ed. Heritage from Mendel. Madison, WI: University of Wisconsin Press. p 265–80.

Robinson GW, Mahon KA. 1994. Differential and overlapping expression domains of *Dlx-2* and *Dlx-3* suggest distinct roles for *Distal-less* homeobox genes in craniofacial development. *Mech Dev* 48:199-215.

Robinson JA, Diamond J. 2010. Natural experiments of history. Cambridge, MA: Harvard University Press.

Roff DA. 1995. The estimation of genetic correlations from phenotypic correlations: a test of Cheverud's conjecture. *Hered* 74:481-90.

Roff DA. 1996. The evolution of genetic correlations: an analysis of patterns. *Evol* 50:1392-1403.

Roff DA. 1997. Evolutionary quantitative genetics. New York, NY: Chapman and Hall.

Roff DA, Mousseau TA. 1999. Does natural selection alter genetic architecture? An evaluation of quantitative genetic variation among populations of *Allonemobiussocius* and *A. fasciatus*. *J Evol Biol* 12:361-9.

Rogers J, Kochunov P, Lancaster J, Shelledy W, Glahn D, Blangero J, Fox P. 2007. Heritability of brain volume, surface area and shape: an MRI study in an extended pedigree of baboons. *Hum Brain Mapp* 28:576-83.

Rogers J, Mahaney MC, Almasy L, Comuzzie AG, Blangero J. 1999. Quantitative trait linkage mapping in anthropology. *Yrbk Phys Anthropol* 42:127-51.

Rogers J, Mahaney MC, Cox LA. 2009. The development and status of the baboon genetic linkage map. In: VandeBerg JL, Williams-Blangero S, Tardif SD, eds. The baboon in biomedical research. New York, NY: Springer-Verlag. p 1-19.

Rogers J, Mahaney MC, Witte SM, Nair S, Newman D, Wedel S, Rodriguez LA, Rice KS, Slifer SH, Perelygin A, Slifer M, Palladino-Negro P, Newman T, Chambers K, Joslyn G, Parry P, Morin PA. 2000. A genetic linkage map of the baboon (*Papio hamadryas*) genome based on human microsatellite polymorphisms. *Genomics* 67:237-47.

Rogers J, VandeBerg JL. 1998. Gene maps of nonhuman primates. *ILAR J* 39:145-52.

Rohlf FJ, Gilmartin AJ, Hart G. 1983. The Kluge-Kerfoot phenomenon—a statistical artifact. *Evol* 37:180-202.

Rolian C, Willmore KE. 2009. Morphological integration at 50: patterns and processes of integration in biological anthropology. *Evol Biol* 36:1-4.

Romanes GJ. 1910. Darwin, and after Darwin: an exposition of the Darwinian theory and a discussion of post-Darwinian questions. Chicago, IL: Open Court Publishing Company.

Rose KD. 1994. The earliest primates. *Evol Anthropol* 3:159-73.

Rose KD, Chew AE, Dunn RH, Kraus MJ, Fricke HC, Zack SP. 2012. Earliest Eocene mammalian fauna from the Paleocene-Eocene thermal maximum at Sand Creek Divide, southern Bighorn Basin, Wyoming. *University of Michigan Papers on Paleontology* 36:1-122.

Roseman CC, Willmore KE, Rogers J, Hildebolt C, Sadler BE, Richtsmeier JT, Cheverud JM. 2010. Genetic and environmental contributions to variation in baboon cranial morphology. *Am J Phys Anthropol* 143:1-12.

Rosenberger AL. 1977. *Xenothrix* and ceboid phylogeny. *J Hum Evol* 6:461-81.

Rosenberger HC. 1949. Surgery for congenital atresia, with report of a case. *Ann Otol Rhinol Laryngol* 58:798-808.

Ross CF, Ravosa MJ. 1993. Basicranial flexion, relative brain size, and facial kyphosis in nonhuman primates. *Am J Phys Anthropol* 91:305-24.

Russell MD. 1985. The supraorbital torus: “a most remarkable peculiarity.” *Curr Anthropol* 26:337-60.

Safari E, Fogarty NM, Gilmour AR. 2005. A review of genetic parameter estimates for wool, growth, meat and reproduction traits in sheep. *Livestock Produc Sci* 92:271-289.

Salcman M, Khan A, Symonds DA. 1994. Calcium pyrophosphate arthropathy of the spine: case report and review of the literature. *Neurosurg* 34:915-8.

Samuels A, Altmann J. 1986. Immigration of a *Papio anubis* male into a group of *Papio cynocephalus* baboons and evidence for an *anubis-cynocephalus* hybrid zone in Amboseli, Kenya. *Int J Primatol* 7:131-8.

Santana SE, Dobson SD, Diogo R. 2014. Plain faces are more expressive: comparative study of facial colour, mobility and musculature in primates. *Biol Lett* 10:20140275.

Sargis EJ. 2004. New views on tree shrews: the role of tupaiids in primate supraordinal relationships. *Evol Anthropol* 13:56-66.

Sargis EJ, Boyer DM, Bloch JI, Silcox MT. 2007. Evolution of pedal grasping in Primates. *J Hum Evol* 53:103-7.

Satokata I, Maas R. 1994. *Msx1* deficient mice exhibit cleft palate and abnormalities of craniofacial and tooth development. *Nature* 6:348-56.

Schafer JL. 1997. Analysis of incomplete multivariate data. Boca Raton, FL: Chapman & Hall/CRC.

Schaefer K, Mitteroecker P, Gunz P, Bernhard M, Bookstein FL. 2004. Craniofacial sexual dimorphism patterns and allometry among extant hominids. *Ann Anat* 186:471-8.

Schneider RA, Hu D, Helms JA. 1999. From head to toe: conservation of molecular signals regulating limb and craniofacial morphogenesis. *Cell Tissue Res* 296:103-9.

Schneiderman ED. 1992. Facial growth in the rhesus monkey. Princeton, NJ: Princeton University Press.

Schoch RR. 2010. Riedl's burden and the body plan: selection, constraint, and deep time. *J Exp Zool B Mol Dev Evol* 314:1-10.

Schoenebeck JJ, Hutchinson SA, Byers A, Beale HC, Carrington B, Faden DL, Rimbault M, Decker B, Kidd JM, Sood R, Boyko AR, Fondon III JW, Wayne RK, Bustamante CD, Ciruna B, Ostrander EA. 2012. Variation in *BMP3* contributes to dog breed skull diversity. *PLoS Genet* 8:e1002849.

Schork NJ. 1997. Genetics of complex disease: approaches, problems, and solutions. *Am J Respir Crit Care Med* 156:S103-9.

Schorle H, Meier P, Buchert M, Jaenisch R, Mitchell PJ. 1996. Transcription factor *AP-2* essential for cranial closure and craniofacial development. *Nature* 381:235-8.

Schroeder L, Roseman CC, Cheverud JM, Ackermann RR. 2014. Characterizing the evolutionary path(s) to early *Homo*. *PLoS One* 9:e114307.

Schultze HP. 1993. Patterns of diversity in the skulls of jawed fishes. In: Hanken J, Hall BK, eds. The skull, vol. 2: patterns of structural and systematic diversity. Chicago, IL: The University of Chicago Press. p 189-254.

Schwartz JH, Tattersall I. 1985. Evolutionary relationships of living lemurs and lorises (Mammalia, Primates) and their potential affinities with European Eocene Adapidae. *Pap Am Mus Nat Hist* 60:1-100.

Scott JH. 1953. The cartilage of the nasal septum: a contribution to the study of facial growth. *Br Dent J* 95:37-43.

Scott JH. 1958. The cranial base. *Am J Phys Anthropol* 16:319-48.

Seiffert ER. 2012. Early primate evolution in Afro-Arabia. *Evol Anthropol* 21:239-53.

Seiffert ER, Simons EL, Boyer DM, Perry JMG, Ryan TM, Sallam HM. 2010a. A fossil primate of uncertain affinities from the earliest Late Eocene of Egypt. *Proc Natl Acad Sci U S A* 107:9712-7.

Seiffert ER, Simons EL, Fleagle JG. 2000. Anthropoid humeri from the Late Eocene of Egypt. *Proc Natl Acad Sci U S A* 97:10062-7.

Seiffert ER, Simons EL, Fleagle JG, Godinot M. 2010b. Paleogene anthropoids. In: Saunders WJ, Werdelin K, eds. Cenozoic mammals of Africa. Berkeley, CA: University of California Press. p 369-91.

Selever J, Liu W, Lu MF, Behringer RR, Martin JF. 2004. *Bmp4* in limb bud mesoderm regulates digit pattern by controlling AER development. *Dev Biol* 276:268-79.

Serrat MA. 2014. Environmental temperature impact on bone and cartilage growth. *Compr Physiol* 4:621-55.

Šešelj M, Duren DL, Sherwood RJ. 2015. Heritability of the human craniofacial complex. *Ant Rec* 298:1535-47.

Setchell JM, Lee PC, Wicking EJ, Dixson AF. 2001. Growth and ontogeny of sexual size dimorphism in the mandrill (*Mandrillus sphinx*). *Am J Phys Anthropol* 115:349-60.

Shao H, Burrage LC, Sinasac DS, Hill AE, Ernest SR, O'Brien W, Courtland HW, Jepsen KJ, Kibry A, Kulbokas EJ, Daly MJ, Broman KW, Lander ES, Nadeau JH. 2008. Genetic architecture of complex traits: large phenotypic effects and pervasive epistasis. *Proc Natl Acad Sci U S A* 105:19910-4.

Shaw FH, Shaw RG, Wilkinson GS, Turelli M. 1995. Changes in genetic variances and covariances: G whiz! *Evol* 49:1260-7.

Shea BT, Russell MD. 1986. On skull form and the supraorbital torus in primates. *Curr Anthropol* 27:257-60.

Sherwood RJ, Duren DL, Havill LM, Rogers J, Cox LA, Towne B, Mahaney MC. 2008. A genomewide linkage scan for quantitative trait loci influencing the craniofacial complex in baboons (*Papio hamadryas* spp.). *Genet* 180:619-28.

Sherwood RJ, Duren DL, Mahaney MC, Blangero J, Dyer TD, Cole SA, Czerwinski SA, Chumlea WMC, Siervogel RM, Choh AC, Nahhas RW, Lee M, Towne B. 2011. A genome-wide linkage scan for quantitative trait loci influenceing the craniofacial complex in humans (*Homo sapiens sapiens*). *Anat Rec* 294:664-75.

Sherwood RJ, Duren DL. 2015. Variation, genetics, and evolution of the primate craniofacial complex. In: Duggirala R, Almasy L, Williams-Blangero S, Paul SFD, Kole C, eds. Genome mapping and genomics in human and non-human primates. Berlin, DEU: Springer-Verlag. p 259-75.

Shimeld SM, Holland PWH. 2000. Vertebrate innovations. *Proc Nat Acad Sci U S A* 97:4449-52.

Shull GH. 1909. A pure-line method in corn breeding. *J Hered* os-5:51-8.

Siegel MI. 1979. A longitudinal study of facial growth in *Papio cynocephalus* after resection of the cartilaginous nasal septum. *J Med Primatol* 8:122-7.

Sigé B, Jaeger JJ, Sudre J, Vianey-Liaud M. 1990. *Altiatlasius koulchii* n. gen. et sp., primate omomyidé du Paléocène supérieur du Maroc, et les origins des Euprimates. *Palaeontographica A* 214:31-56.

Sigurdsson A, Banos G, Phillipsson J. 1996. Estimation of genetic (co)variance components for international evaluation of dairy bulls. *Acta Agr Scand A-An* 46:129-36.

Simon HA. 1962. The architecture of complexity. *Proc Am Philos Soc* 106:467-82.

Simons EL. 1972. *Primate evolution*. New York:, NY Macmillan.

Simons EL, Delson E. 1978. Cercopithecidae and Parapithecidae. In: Maglio VJ, Cooke HBS, eds. Evolution of African mammals. Cambridge, MA: Harvard University Press. p 100-19.

Simpson ME, Asling CW, Evans HM. 1950. Some endocrine influences on skeletal growth and differentiation. *Yale J Biol Med* 23:1-27.

Singleton M. 2002. Patterns of cranial shape variation in the Papionini (Primates: Cercopithecinae). *J Hum Evol* 42:547-578.

Singleton M. 2012. Postnatal cranial development in papionin primates: an alterantive model for hominin evolutionary development. *Evol Biol* 39:499-520.

Smith HF. 2011. The role of genetic drift in shaping modern human cranial evolution: a test using microevolutionary modeling. *Int J Evol Biol* 2011:145262.

Smith SM. 2002. Fast robust automated brain extraction. *Hum Brain Mapp* 17:143-55.

Smith RJ, Jungers WL. 1997. Body mass in comparative primatology. *J Hum Evol* 32:523-59.

Smuts B, Nicolson N. 1989. Reproduction in wild female olive baboons. *Am J Primatol* 19:229-46.

Sneath HA, Sokal RR. 1963. Principles of numerical taxonomy: the principles and practice of numerical classification. San Francisco, CA: Freeman.

Sokal RR, Rohlf FJ. 1962. The comparison of dendrograms by objective methods. *Taxon* 11:33-40.

Som PM, Lawson W, Lidov MW. 1991. Simulated aggressive skull base erosion in response to benign sinonasal disease. *Radiol* 180:755-9.

Sperber GH, Sperber SM, Guttmann GD. 2010. Craniofacial embryogenetics and development. Shelton, CT: People's Medical Publishing House.

Stefen C, Nadler T. 2012. Comparative cranial morphology of douc langurs (*Pygathrix cinerea, P. nemaeus, P. nigripes*). *Vietnam J Primatol* 2:7-24.

Steiper ME, Young NM. 2006. Primate molecular divergence dates. *Mol Phylogenet Evol* 41:384-94.

Stemple DL. 2005. Structure and function of the notochord: an essential organ for chordate development. *Dev* 132: 2503-12.

Steppan SJ, Phillips PC, Houle D. 2002. Comparative quantitative genetics: evolution of the G matrix. *Trends Ecol Evol* 17:320-7.

Stevens NJ, Seiffert ER, O'Connor PM, Roberts EM, Schmitz MD, Krause C, Gorscak E, Ngasala S, Hieronymus TL, Temu J. 2013. Palaeontological evidence for an Oligocene divergence between Old World monkeys and apes. *Nature* 497:611-4.

Storey E. 1972. Growth and remodeling of bone and bones. *Am J Orthod* 62:142-65.

Strait DS, Grine FE. 2004. Inferring hominoid and early hominid phylogeny using craniodental characters: the role of fossil taxa. *J Hum Evol* 47:399-452.

Strait DS, Wright BW, Richmond BG, Ross CF, Dechow PC, Spencer MA, Wang Q. 2008. Craniofacial strain patterns during premolar loading: implications for human evolution. In: Vinyard C, Ravosa MJ, Wall C, eds. Primate craniofacial function and biology. New York, NY: Springer Science+Business Media. p 173-98.

Strasser E, Delson E. 1987. Cladistic analysis of cercopithecid relationships. *J Hum Evol* 16:81-99.

Strum SC. 1991. Weight and age in wild olive baboons. *Am J Primatol* 25:219-37.

Sturtevant AH, Beadle GW. 1936. The relations of inversions in the X chromosome of *Drosophila melanogaster* to crossing over and disjunction. *Genet* 21:554-604.

Sussman RW, Rasmussen DT, Raven PH. 2013. Rethinking primate origins again. *Am J Primatol* 75:95-106.

Suzuki S, Marazita ML, Cooper ME, Miwa N, Hing A, Jugessur A, Natsume N, Shimozato K, Ohbayashi N, Suzuki Y, Niimi T, Minami K, Yamamoto M, Altannamar TJ, Erkhembaatar T, Furukawa H, Daack-Hirsch S, L'Heureux J, Brandon CA, Weinberg SM, Neiswanger K, Deleyiannis FWB, de Salamanca JE, Vieira AR, Lidral AC, Martin JF, Murray JC. 2009. Mutations in *BMP4* are associated with subepithelial, microform, and overt cleft lip. *Am J Hum Genet* 84:406-11.

Swindler DR, Merrill OM. 1971. Spontaneous cleft lip and palate in a living nonhuman primate, *Macaca mulatta*. *Am J Phys Anthropol* 34:435-9.

Szalay FS. 1968. The beginnings of primates. *Evol* 22:19-36.

Szalay FS. 1976. Systematics of the Omomyidae (Tarsiiformes, Primates) taxonomy, phylogeny, and adaptations. *Bull Am Mus Nat Hist* 156:157-450.

Szalay FS, Delson E. 1979. Evolutionary History of the Primates. New York: Academic Press.

Takahata N, Nei M. 1993. Allelic genealogy under overdominant and frequency-dependent selection and polymorphism of major histocompatibility complex loci. *Genetics* 124:967-78.

Tanner MA, Wong WH. 1987. The calculation of posterior distributions by data augmentation. *J Am Stat Assoc* 82:528-50.

Tatosuro S, Kawahara C, Matsumoto F. 2011. Ossification of transverse ligament of atlas causing cervical myelopathy: a case report and review of the literature. *Case Rep Med* 238748.

Taylor AB. 2006. Size and shape dimorphism in great ape mandibles and implications for fossil species recognition. *Am J Phys Anthropol* 129:82-98.

Temerin LA, Cant JGH. 1983. The evolutionary divergence of Old World monkeys and apes. *Am Nat* 122:335-51.

Templeton AR, Maxwell T, Posada D, Stengård JH, Boerwinkle E, Sing CF. 2005. Tree scanning: a method for using haplotype trees in phenotype/genotype association studies. *Genet* 169:441-53.

Tenesa A, Navarro P, Hayes BJ, Duffy DL, Clarke GM, Goddard ME, Visscher PM. 2007. Recent human effective population size estimated from linkage disequilibrium. *Genome Res* 17:520-6.

Terhune CE, Cooke SB, Otárola-Castillo E. 2015. Form and function in the platyrrhine skull: a three-dimensional analysis of dental and TMJ morphology. *Anat Rec* 298:29-47.

Tessier P. 1976. Anatomical classification of facial, cranio-facial and latero-facial clefts. *J Maxillofac Surg* 4:69-92.

Thorington Jr. RW, Groves CP. 1970. An annotated classification of the Cercopithecoidea. In: Napier JR, Napier PH, eds. Old World monkeys: evolution, systematics and behavior. New York, NY: Academic Press. p 629-647.

Tieszen LL, Fagre T. 1993. Effect of diet quality and composition on the isotopic composition of respiratory CO2, bone collagen, bioapatite, and soft tissues. In: Lambert JB, Grupe G, eds. Prehistoric human bone: archaeology at the molecular level. Berlin, DEU: Springer-Verlag. p 121-55.

Tosi AJ, Disotell TR, Morales JC, Melnick DJ. 2003. Cercopithecine Y-chromosome data provide a test of competing morphological evolutionary hypotheses. *Mol Phylogenet Evol* 27:510-21.

Trut LN, Oskina IN, Kharlamova AV. 2012. Experimental studies of early canid domestication. In: Ostrander EA, Ruvinsky A, eds. The genetics of the dog. Cambridge, MA: CAB International. p 12-37.

Truxillo C. 2005. Maximum likelihood parameter estimation with incomplete data. *Proc Thirtieth Ann SAS® Users Group Int Conf*. Paper: 111-30.

Tubbs RS, Kelly DR, Lott R, Salter EG, Oakes WJ. 2006. Complete ossification of the human falx cerebri. *Clin Anat* 19:147-50.

Tung J, Charpentier MJE, Garfield DA, Altmann J, Alberts SC. 2008. Genetic evidence reveals temporal change in hybridization patterns in a wild baboon population. *Molec Ecol* 17:1998-2011.

Turner RT, Backup P, Sherman PJ, Hill E, Evans GL, Spelsberg TC. 1992. Mechanism of action of estrogen on intramembranous bone formation: regulation of osteoblast differentiation and activity. *Endocrinol* 131:883-9.

Turner HN, Young SSY. 1969. Quantitative genetics of sheep breeding. South Melbourne, AUS: Macmillan Co. of Australia.

Vaez TR, Nicolas FW, Raadsma HW. 1996. REML estimates of variance and covariance components for production traits in Australian Merino sheep, using an animal model. 1. body weight from birth to 22 months. *Aust J Agr Res* 47:1235-49.

van der Linde K, Houle D. 2009. Inferring the nature of allometry from geometric data. *Evol Biol* 36:311-22.

van der Walt S, Colbert SC, Varoquaux G. 2011. The NumPy array: a structure for efficient numerical computation. *Comput Sci Eng* 13:22-30.

Van Goozen SHM, Cohen-Kettenis PT, Gooren LJG, Frijda NH, Van de Poll NE. 1995. Gender differences in behavior: activating effects of cross-sex hormones. *Psychoneuroendocrinology* 20:343-63.

van Spronsen PH, Weijs WA, Valk J, Prahl-Andersen B, van Ginkel FC. 1991. Relationships between jaw muscle cross-sections and craniofacial morphology in normal adults, studied with magnetic resonance imaging. *Eur J Orthod* 13:351-61.

Van Valen L, Sloan RE. 1965. The earliest primates. *Science* 150:743-5.

Vanderschueren D, Vandenput L, Boonen S, Lindberg MK, Bouillon R, Ohlsson C. 2004. Androgens and bone. *Endocr Rev* 25:389-425.

Vargervik K, Miller AJ, Chierici G, Harvold E, Tomer BS. 1984. Morphologic response to changes in neuromuscular patterns experimentally induced by altered modes of respiration. *Am J Orthod* 85:115-24.

Viguier B. 2004. Functional adaptations in the craniofacial morphology of Malagasy primates: shape variations associated with gumnivory in the family Cheirogaleidae. *Ann Anat* 186:495-501.

Villmoare BA, Dunmore C, Kilpatrick S, Oertelt N, Depew MJ, Fish JL. 2014. Craniofacial modularity, character analysis, and the evolution of the premaxilla in early African hominins. *J Hum Evol* 77:143-54.

Villmoare B, Kimbel WH, Seyoum C, Campisano CJ, DiMaggio EN, Rowan J, Braun DR, Arrowsmith JR, Reed KE. 2015. Early *Homo* at 2.8 Ma from Ledi-Geraru, Afar, Ethiopia. *Science* 347:1352-5.

Vilmann H. 1972. Osteogenesis in the basioccipital bone of the Wistar albino rat. *Scand J Dent Res* 80:410-21.

Vinson A, Curran JE, Johnson MP, Dyer TD, Moses EK, Blangero J, Cox LA, Rogers J, Havill LM, VandeBerg JL, Mahaney MC. 2011. Genetical genomics of Th1 and Th2 immune response in a baboon model of atherosclerosis risk factors. *Atherosclerosis* 217:387-94.

Visscher PM, Thompson R, Hill WG. 1991. Estimation of genetic and environmental variances for fat yield in individual herds and an investigation into heterogeneity of variance between herds. *Livestock Produc Sci* 28:273-90.

von Cramon-Taubadel N. 2009. Revisiting the homoiology hypothesis: the impact of phenotypic plasticity on the reconstruction of human population history from craniometric data. *J Hum Evol* 57:179-90.

von Cramon-Taubadel N. 2011. Global human mandibular variation reflects differences in agricultural and hunter-gatherer subsistence strategies. *Proc Natl Acad Sci U S* A 108:19546-51.

von Koenigswald GHR. 1969. Miocene Cercopithecoidea and Oreopithecoidea from the Miocene of East Africa. In: Leakey LSB, ed. Fossil vertebrates of Africa, vol 1. London, GBR: Academic Press. p 39-51.

Waddington CH. 1942. Canalization of development and the inheritance of acquired characters. *Nature* 150:563-5.

Wagner GP. 1988. Significance of developmental constraints for phenotypic evolution by natural selection. In: de Jong G, ed. Population genetics and evolution. Berlin, DEU: Springer-Verlag. p 222-9.

Wagner GP. 1996. Homologues, natural kinds and the evolution of modularity. *Amer Zool* 36:36-43.

Wagner GP. 2007. The developmental genetics of homology. *Nat Rev Genet* 8:473-9.

Wagner GP. 2014. The intellectual challenge of morphological evolution: a case for variational structuralism. In: Wagner GP, ed. Homology, genes, and evolutionary innovation. Oxford, GBR: Princeton University Press. p 7-38.

Wagner GP, Altenberg L. 1996. Complex adaptations and the evolution of evolvability. *Evol* 50:967-76.

Wagner GP, Kenney-Hunt JP, Pavlicev M, Peck JR, Waxman D, Cheverud JM. 2008. Pleiotropic scaling of gene effects and the 'cost of complexity.' *Nat* 452:470-3.

Wagner GP, Laubichler MD. 2004. Rupert Riedl and the re-synthesis of evolutionary and developmental biology: body plans and evolvability. *J Exp Zool B Mol Dev Evol* 302:92-102.

Wagner GP, Mezey J, Calabretta R. 2005. Natural selection and the origin of modules. In: Callebaut W, Rasskin-Gutman D, eds. Modularity: understanding the development and evolution of complex natural systems. Cambridge, MA: The MIT Press. p 33-50.

Wagner GP, Pavlicev M, Cheverud JM. 2007. The road to modularity. *Nat Rev Genet* 8:921-31.

Wagner GP, Zhang J. 2011. THe pleiotropic structure of the genotype-phenotype map: the evolvability of complex organisms. *Nat Rev Genet* 12:204-13.

Waitt DE, Levin DA. 1998. Genetic and phenotypic correlations in plants: a botanical test of Cheverud's conjecture. *Hered* 80:310-9.

Wake DB, Larson A. 1987. Multidimensional analysis of an evolving lineage. *Science* 238:42-8.

Walker A. 1997. *Proconsul* function and phylogeny. In: Begun DR, Ward CV, Rose MD, eds. Function, phylogeny, and fosssils: Miocene Hominoid evolution and adaptations. New York, NY: Plenum Press. p 209-24.

Walsh B. 2014. Special issues on advances in quantitative genetics: introduction. *Hered* 112:1-3

Wan C, Shao J, Gilbert SR, Riddle RC, Long F, Johnson RS, Schipani E, Clemens TL. 2010. Role of HIF-1α in skeletal development. *Ann N Y Acad Sci* 1192:322-6.

Wang Q, Opperman LA, Havill LM, Carlson DS, Dechow PC. 2006. Inheritance of sutural pattern at the pterion in rhesus monkey skulls. *Anat Rec* 228A:1042-9.

Wang Y, Wan C, Deng L, Liu X, Cao X, Gilbert SR, Bouxsein ML, Faugere MC, Guldberg RE, Gerstenfeld LC, Haase VH, Johnson RS, Schipani E, Clemens TL. 2007. The hypoxia-inducible factor α pathway couples angiogenesis to osteogenesis during skeletal development. *J Clin Invest* 117:1616-26.

Washburn SL. 1947. The relation of the temporal muscle to the form of the skull. *Anat Rec* 99:239-48.

Wayne RK. 1986. Cranial morphology of domestic and wild canids: the influence of development on morphological change. *Evol* 40:243-61.

Weidenreich F. 1947. The trend of human evolution. *Evol* 1:221-36.

Weinmann JP, Sicher H. 1947. Bones and bones: fundamentals in bone biology. St. Louis, MO: C.V. Mosby Co.

Weir JP. 2005. Quantifying test-retest reliability using the intraclass correlation coefficient and the *SEM*. *J Strength Cond Res* 19:231-40.

Weis S, Kimbacher M, Wenger E, Neuhold. 1993. Morphometric analysis of the corpus callosum using MR: correlation of measurements with aging in healthy individuals. *Am J Neuroradiol* 14:637-45.

Weston JA, Yoshida H, Robinson V, Nishikawa S, Fraser ST, Nishikawa S. 2004. Neural crest and the origin of ectomesenchyme: neural fold heterogeneity suggest an alternative hypothesis. *Dev Dyn* 229:118-30.

Wilder HH. 1920. A laboratory manual of anthropometry. Philadelphia, PA: P. Blakiston's Son & Co.

Wiley EO. 1975. Karl R. Popper, systematics, and classification: a reply to Walter Bock and other evolutionary taxonomists. *Syst Zool* 24:233-43.

Williams AB, Kay RF, Kirk EC. 2010. New perspectives on anthropoid origins. *Proc Natl Acad Sci U S A* 107:4797-804.

Williams FL, Ackermann RR, Leigh SR. 2007. Inferring Plio-Pleistocene southern African biochronology from facial affinities in *Parapapio* and other fossil papionins. *Am J Phys Anthropol* 132:163-74.

Williams JT, Blangero J. 1999. Asymptotic power of likelihood-ratio tests for detecting quantitative trait loci using the COGA data. *Genet Epidemiol* 17:S397-402.

Williams-Blangero S, Vandeberg JL, Blangero J, Konigsberg L, Dyke B. 1990. Genetic differentiation between baboon subspecies: relevance for biomedical research. *Am J Primatol* 20:67-81.

Willmore KE, Roseman CC, Rogers J, Richtsmeier JT, Cheverud JM. 2009. Genetic variation in baboon craniofacial sexual dimorphism. *Evol* 63:799-806.

Wilkie AOM. 1997. Craniosynostosis: genes and mechanisms. *Hum Molec Genet* 6:1647-56.

Wilkie AOM, Morris-Kay GM. 2001. Genetics of craniofacial development and malformation. *Nat Genet* 2:458-68.

Wilkie TA, Gubbels S, Schwartz J, Richman JM. 1997. Expression of fibroblast growth factor receptors (*FGFR1*, *FGFR2*, *FGFR3*) in the developing head and face. *Develop Dyn* 210:41-52.

Winther RG. 2001. Varieties of modules: kinds, levels, origins, and behaviors. *J Exp Zool B Mol Dev Evol* 291:116-29.

Wolf JB, Leamy LJ, Routman EJ, Cheverud JM. 2005. Epistatic pleiotropy and the genetic architecture of covariation within early and late-developing skull trait complexes in mice. *Genet* 171:683-94.

Wolf JB, Pomp D, Eisen EJ, Cheverud JM, Leamy LJ. 2006. The contribution of epistatic pleiotropy to the genetic architecture of covariation among polygenic traits in mice. *Evol Dev* 8:468-76.

Wolpoff MH. 1980. Paleoanthropology. New York, NY: Random House.

Wood A, Ashurst DE, Corbett A, Thorogood P. 1991. The transient expression of type II collagen at tissue interfaces during mammalian craniofacial development. *Dev* 111:955-68.

Wood BA. 2009. Where does the genus *Homo* begin, and how would we know? In: Grine FE, Fleagle JG, Lealey RE, eds. The first humans - origin and early evolution of the genus *Homo*: contributions from the third Stony Brook human evolution symposium and workshop October 3-October 7, 2006. Dordrecht, NLD: Springer. p 17-28.

Wood B, Collard M. 1999. The human genus. *Science* 284:65-71.

Workman MS, Leamy LJ, Routman EJ, Cheverud JM. 2002. Analysis of quantitative trait locus effects on the size and shape of mandibular molars in mice. *Genet* 160:1573-86.

World Health Organization (WHO). 2002. Global strategies to reduce the health-care burden of craniofacial anomalies: report of WHO meetings on international collaborative research on craniofacial anomalies. Geneva, CHE: World Health Organization.

World Health Organization (WHO). 2003. Global registry and database on craniofacial anomalies: report of a WHO registry meeting on craniofacial anomalies. Mossey P, Castilla E, eds. Geneva, CHE: World Health Organization.

Wright S. 1921. Systems of mating. I. the biometric relations between parent and offspring. *Genet* 6:111-23.

Wright S. 1980. Genic and organismic selection. *Evol* 34:825-43.

Yoshida T, Vivatbutsiri P, Morriss-Kay G, Saga Y, Iseki S. 2008. Cell lineage in mammalian craniofacial mesenchyme. *Mech Dev* 125:797-808.

Yu JK, Holland ND, Holland LZ. 2002. An amphioxus winged helix/forkhead gene, *AmphiFoxD*: insights into vertebrate neural crest evolution. *Dev Dyn* 225:289-7.

Yu N, Jensen-Seaman MI, Chemnick L, Kidd JR, Deinard AS, Ryder O, Kidd KK, Li WH. 2003. Low nucleotide diversity in chimpanzees and bonobos. *Genet* 164:1511-8.

Zeng ZB, Kao CH, Basten CJ. 1999. Estimating the genetic architecture of quantitative traits. *Genet Res* 74:279-89.

Zhang D, Cheng H, Hu Z, Wang H, Kan G, Liu C, Yu D. 2013. Fine mapping of a major flowering time QTL on soybean chromosome 6 combining linkage and association analysis. *Euphytica* 191:23-33.

Zhou H, Zou S, Lan Y, Fei W, Jiang R, Hu J. 2014. *Smad7* modulates *TGFβ* signalling during cranial suture development to maintain suture patency. *J Bone Min Res* 29:716-24.

Zogopoulos G, Nathanielsz P, Hendy GN, Goodyear CG. 1999. The baboon: a model for the study of primate growth hormone receptor gene expression during development. *J Molec Endocrinol* 23:67-75.

Zuckerman S. 1926. Growth-changes in the skull of the baboon, *Papio porcarius*. *Proc Zool Soc Lond* 96:843-73.

Zwilling E. 1968. Morphogenetic phases in development. *Dev Biol Suppl* 2:184-207.

APPENDIX A
BABOON GENETIC MAP MARKERS

Table A1 Location of the baboon genetic map's STR markers in the human genome (GRCh38).

Marker Name	Baboon Ortholog	Locus (cM)	Cytogenetic Band[a]	Proximal (bp)[a]	Distal (bp)[a]
D1S548	1	0	1p36.23	7282686	7483060
PHA1S1	1	28.3	---	---	---
D1S2130	1	39.4	1p34.2	41251814	41452146
D1S515	1	51.9	1p31.3	63776599	63976855
D1S192	1	57.7	1p31.1	70920506	71120993
D1S550	1	59.9	1p31.1	73663622	73863923
D1S207	1	65.1	1p31.1	81977665	82177918
D1S2896	1	75	1p21.2	101406920	101607288
D1S248	1	79.2	1p21.1-p13.3	106512298	106712623
D1S1675	1	85.5	1p13.2	114097495	114297767
D1S506	1	100.8	1q23.1	156775604	156975849
D1S213	1	110	1q41	223529162	223729272
D1S306	1	124.1	1q32.1	201335825	201536138
D1S533	1	133.5	1q31.3	193988802	194189095
D1S518	1	137.1	1q31.1	187481048	187681403
D1S215	1	142.7	1q25.2	179559400	179759678
D1S194	1	152	1q23.3-q24.1	165368005	165658266
D1S1656	1	160.5	1q42.2	230669450	230869763
D1S304	1	176.6	1q43	241025181	241225592
D2S323	13	0	2p25.3	2002389	2202748
D2S2243	13	13.6	2p25.1	9038289	9238540
D2S131	13	19.7	2p24.3	13127414	13327740
D2S387	13	25	2p24.1	19042676	19243030
D2S144	13	30.3	2p23.3	25177302	25378170
D2S146	13	33.8	2p23.2	29269207	29469482
D2S119	13	44.5	2p21	43746844	43947107
D2S391	13	47.9	2p21	46084229	46284626
D2S169	13	66.1	2p12	78319980	78520242
D2S135	13	90.5	2q12.1	104794986	104995148
D2S95	12	0	2q14.3	127396458	127596715
D2S114	12	39.1	2q21.2	133467485	133667919
D2S1326	12	46.7	2q22.1	139065436	139265733
D2S150	12	47.8	2q22.1	139705839	139906200
D2S122	12	51.8	---	---	---
D2S1399	12	54.7	2q22.3	147352480	147552875
D2S156	12	63.4	2q24.2	159692269	159892587
D2S382	12	65.8	2q24.3	165011260	165211653
D2S326	12	67.9	2q31.1	172132061	172332379
PHA12S1	12	74.5	---	---	---
D2S425	12	76.7	2q32.3	194296196	194496536
D2S115	12	78.1	2q33.1	198005509	198205848
D2S434	12	90.6	2q35	217611751	217812086
D2S433	12	92.2	2q35	218800964	219001344
D2S163	12	93.4	2q35	219827551	220027876
D2S377	12	96.1	2q36.1	220859056	221059355
D2S126	12	96.9	2q36.1	221052194	221252557

D2S102	12	98.7	2q36.1	222036576	222236871
D2S360	12	100.4	2q36.1	222730810	222931169
D2S133	12	102.3	2q36.1	223670237	223870560
D2S351	12	103.8	2q36.2	224754905	224955152
D2S1363	12	106.4	2q36.3	226064872	226265168
D2S2354	12	106.9	2q36.3	226384509	226584905
D2S1333	12	107	2q36.3	226064695	226265323
D2S2276	12	114.3	2q37.1	231253864	231454211
D2S2344	12	114.3	2q37.1	232479807	232680221
D2S206	12	116.5	2q37.1	232743065	232943451
D2S2176	12	117.3	2q37.1	232782923	232983277
D2S2338	12	125.8	2q37.2-q37.3	236226751	236427100
D3S1251	2	0	3q11.2	94458164	94658444
D3S3045	2	11.6	3q13.12	107171010	107371314
D3S1267	2	22.6	3q21.1	123224356	123424541
D3S1252	2	26.9	3p25.1	13800105	14000379
D3S3591	2	30.8	3p26.1-p25.3	8044070	8244413
D3S1300	2	46.3	3p14.2	60424174	60624438
D3S1227	2	52.2	3p21.1	53875022	54075168
D3S1229	2	71.9	3q26.2	170552519	170752673
D3S1268	2	77.5	3q26.1	164102224	164302626
D3S1309	2	90.7	3q23	140907472	141107845
D3S1211	2	113.6	3p23	30925335	31125589
D3S1768	2	119.4	3p22.3	34482838	34683138
D4S2925	5	0	4p16.2	4791456	4991672
D4S1582	5	3.4	4p16.1	10599833	10800146
D4S230	5	23.9	4p15.1	28537731	28738088
D4S188	5	28.5	4p15.1	33003246	33203506
D4S1627	5	34.2	4p13	44076769	44277090
D4S414	5	38.3	4q22.1	91417510	91617878
PHA5S8	5	40.1	---	---	---
PHA5S6	5	45.3	---	---	---
D4S400	5	47.2	4q21.22	81953697	82153865
PHA5S1	5	49.5	---	---	---
D4S2958	5	51.5	4q21.1	75793383	75993671
D4S2456	5	51.7	---	---	---
D4S2931	5	54.9	4q13.3	71197478	71397621
D4S416	5	57.8	4q13.2	65659390	65859652
D4S1645	4	59.7	6p21.31	35514993	35715319
D4S3248	5	60.7	4q13.1	59055737	59256082
PHA5S7	5	64.2	---	---	---
PHA5S5	5	67.7	---	---	---
PHA5S4	5	73.9	---	---	---
PHA5S3	5	74.5	---	---	---
PHA5S9	5	75.9	---	---	---
PHA5S2	5	79.5	---	---	---
D4S2365	5	82.1	4q28.2	129765088	129965444
D4S413	5	99.4	4q32.1	157332003	157532332
D4S1626	5	103.9	4q32.2	161652052	161852382
D4S1636	5	108.3	4q32.3	165491885	165692008
D4S243	5	112.8	4q33	169822334	170022569
D4S2374	5	122.9	4q34.3	178034824	178235115
D4S1554	5	132.8	4q35.1	183667417	183867742
D5S406	6	0	5p15.32	4893930	5094254
D5S208	6	9.7	5p15.31	8886393	9086542
D5S111	6	33.9	5p13.3	33123285	33323541
D5S418	6	40.1	5p13.1	39915665	40116072

D5S647	6	52	5q12.3	66851322	67051713
D5S424	6	57.4	5q13.3	76761894	76962227
D5S806	6	60.1	5q14.1-q14.2	82097482	82297857
D5S1466	6	69.8	5q21.3	109583847	109784192
D5S178	6	86.5	5q31.3	142211863	142412018
D5S658	6	94.2	5q31.3	140893302	141093682
D5S210	6	98.5	5q31.3-q32	144988696	145188988
D5S519	6	106.2	5q33.1	150502966	150703070
D5S1465	6	117.8	5q34	161886794	162087132
D5S1458	6	125.9	5q34	168048732	168249016
D5S429	6	132	5q35.1	171813555	172013916
D6S259	4	0	6p23	14635717	14836004
D6S422	4	6.5	6p22.3	20269806	20470118
D6S1663	4	8.8	6p22.3	22502533	22702906
D6S276	4	14.1	6p22.3	24085574	24285941
D6S291	4	23.1	6p21.31	36197737	36397945
D6S271	4	28.7	6p21.1	43433080	43633455
D6S1280	4	33.5	6p12.3	48782204	48982514
D6S402	4	38.7	6q11.1	62155495	62355893
D6S1048	4	39.6	6q11.2-q12	62671845	62872127
D6S405	4	41.3	6q12	67382153	67582417
D6S1718	4	42.7	6q13	69828997	70029320
D6S493	4	44.2	6q13	72600081	72800447
D6S482	4	49.6	6q15	89925895	89826016
D6S1013	4	52.1	6q16.1	93683356	93883649
D6S501	4	53.5	6q16.1	97283742	97484090
D6S1028	4	55.2	6q16.3	101969166	102169498
PHA4S2	4	58.9	---	---	---
PHA4S1	4	65.4	---	---	---
PHA4S3	4	67.7	---	---	---
D6S311	4	69.7	6q24.3	148268577	148468885
PHA4S4	4	71.8	---	---	---
PHA4S5	4	74.1	---	---	---
D6S1040	4	85.1	6q23.1	130564593	130764874
D6S1608	4	95.1	6q22.31	120490207	120690534
D6S266	4	103.3	6q21	113261440	113461754
D6S404	4	106.3	6q21	111519146	111719459
D6S1698	4	108.9	6q21	110894500	111094827
MML4S17	4	122.5	---	---	---
D6S503	4	126.8	6q27	167689168	167889484
MML4S14	4	130.9	---	---	---
D21S1446	3	0	21q22.3	46517671	46709983
D21S167	3	20.4	21q22.2	39473544	39673716
D21S1258	3	32.9	21q21.3	27347362	27547742
PHA3S1	3	59.3	---	---	---
D7S1830	3	69.4	7p12.1	51587146	51787507
D7S817	3	86.7	7p14.3	31996708	32197031
D7S2534	3	95.7	7p15.3-p15.2	25449652	25649986
D7S493	3	97.5	7p15.3	21554472	21865715
D7S821	3	105.7	7q21.3	96328189	96528484
D7S2204	3	114	7q21.11	78397528	78597834
D7S669	3	114.6	7q21.11	78143119	78343441
D7S496	3	117.5	7q22.3	107414241	107614405
D7S480	3	124.9	7q31.31-q31.32	121224967	121425211
D7S466	3	125.6	7q31.32	121940602	122140872
D7S680	3	129.8	7q31.33	126937788	127138175
D7S794	3	148	7q35	143926547	144126849

D7S1826	3	159.2	7q36.1	150826982	151027303
D7S559	3	170.7	7q36.3	156580177	156780681
MML8S18	8	0	---	---	---
MML8S19	8	9.5	---	---	---
D8S351	8	14.4	8p23.1	8819390	9019645
D8S1106	8	16.7	8p22	12878350	13078640
MML8S29	8	21.6	---	---	---
MML8S30	8	23.4	---	---	---
D8S298	8	32.6	8p21.3	21804335	22004634
MML8S35	8	43.3	---	---	---
MML8S22	8	46.7	---	---	---
PHA8S1	8	48	---	---	---
D8S278	8	48.9	8p12	32590799	32791140
D8S268	8	55	8p11.21	41289974	41490248
D8S285	8	64	8q12.1	56054498	56254823
D8S260	8	68.8	8q12.2	60809222	61009535
D8S251	8	78.3	8q21.13	78213497	78413812
D8S1119	8	83.5	8q21.3	86059648	86259992
D8S208	8	92.7	8q22.3	102636951	102837111
D8S266	8	112.2	8q24.13	125583062	125783414
D8S557	8	119.6	8q24.22	131977970	132178263
D8S1100	8	125.8	8q24.23	135974232	136174566
D9S152	15	0	9q21.32	83390737	83590935
D9S922	15	23.2	9q21.31	80253368	80453683
D9S178	15	40.9	9p24.2	4021246	4221694
D9S268	15	45.8	9p23	12956168	13156563
D9S156	15	47.1	9p22.3	16144093	16344322
D9S285	15	48	9p22.3	15977947	16178223
D9S265	15	52.4	9p21.3	25358359	25558676
D9S910	15	57.2	9q22.33	98761459	98961794
D9S261	15	63.2	9q31.2	107972860	108173189
D9S934	15	71.2	9q33.1	118233378	118433898
D9S1798	15	79.3	9q33.3	126310101	126510407
D9S1818	15	100.7	9q34.2	134143504	134343863
D9S905	15	116.1	9q34.3	136880745	137081103
D10S179	9	0	10p15.1	5449268	5649428
D10S1707	9	16.4	10p13	13689653	13889908
D10S197	9	33.1	10p12.1	26137952	26338224
D10S611	9	34.7	10p12.1	27258464	27458826
GGAT1A4	9	50.7	10q22.3	78852252	79052566
D10S1432	9	54.1	10q22.1	72799455	72999833
D10S192	9	70.6	10q24.31	100576443	100776773
D10S1230	9	90.8	10q26.12	120883121	121083399
D10S1655	9	107.3	10q26.3	129057646	129257985
D11S4162	14	0	11q13.4	71164701	71365086
D11S1975	14	4.1	11q13.3-q13.4	70456970	70657253
D11S987	14	11	11q13.2	68025874	68225982
D11S4203	14	36.2	11p13	35691823	35892172
D11S4200	14	39.6	11p13	34730962	34931329
D11S904	14	44.8	11p14.2	26558968	26759252
D11S1349	14	54.4	11p15.4-p15.3	11630955	11831308
D11S1329	14	55.7	11p15.4	10595304	10795650
D11S1338	14	56.5	11p15.4	5866682	6067038
D11S916	14	57.4	11q13.4	73518755	73719015
D11S1902	14	59.3	11q13.4-q13.5	75412262	75612551
D11S1352	14	62.4	11q14.1	79013213	79213570
D11S2002	14	62.9	11q14.1	80154338	80354618

D11S1366	14	75	11q21	96878478	97078805
D11S925	14	100.9	11q23.3	120857502	121057837
MML14S10	14	114.8	---	---	---
MML14S11	14	122.4	---	---	---
D11S968	14	123.2	11q25	133848481	134048722
D12S372	11	0	12p13.32	3377967	3578554
D12S93	11	6.7	12p13.32-p13.31	5121677	5321974
D12S364	11	21.6	12913.1	13580369	13780706
PHA11S2	11	29.2	---	---	---
PHA11S3	11	49.4	---	---	---
D12S85	11	52.2	12q13.11	46842904	47043079
D12S297	11	55.2	12q13.13	52119058	52319505
PHA11S4	11	58.2	---	---	---
D12S75	11	64.7	12q14.3	66497951	66498078
D12S375	11	66.7	12q15	68450939	68651271
PHA11S5	11	78.8	---	---	---
PHA11S6	11	82.5	---	---	---
D12S318	11	87.4	12q23.2	102436334	102636605
D12S84	11	93.4	12q23.3-q24.11	108528291	108728534
D12S86	11	103	12q24.23	118632517	118832697
MML11S6	11	104.6	---	---	---
D12S342	11	109	12q24.31-q24.32	125299294	125499706
MML11S8	11	114.7	---	---	---
MML17S11	17	0	---	---	---
D13S139	17	6.4	13q13.3	39090138	3929269
D13S318	17	27.6	13q21.33	69901454	70101795
D13S170	17	35.3	13q31.1	80434959	80635243
D13S317	17	37.3	13q31.1	82047898	82248179
D13S167	17	44.7	13q31.3	93923872	94124235
D13S280	17	56.8	13q33.1	102795654	102996021
MML17S15	17	71.5	---	---	---
D15S165	7	0	15q13.2-q13.3	30868347	31068674
MML7S16		21.5	---	---	---
D15S220	7	27.2	15q21.2	51681671	51882106
D15S644	7	39.5	15q22.31	63894318	64094693
D15S108	7	39.9	15q22.31	64792258	64992503
D15S216	7	44.7	15q23	69611416	69811755
D15S519	7	49.6	---	---	---
D14S261	7	64.7	14q11.2	20272229	20742545
D14S72	7	65.7	14q11.2	20802829	21003192
D14S264	7	68.8	14q12	24710713	24910976
D14S306	7	76.4	14q21.1	37758878	37959246
D14S66	7	84.9	14q22.3	56483898	56684157
D14S277	7	93.1	14q24.2	72460597	72660954
D14S61	7	95	14q24.3	75768898	75969197
D14S291	7	110.3	14q32.11	90703421	90903893
D14S985	7	127.7	14q32.2-q32.31	100730199	100930478
D16S423	20	0	16p13.3	5893140	6093468
D16S403	20	32.5	16p12.2	22926330	23126502
D16S411	20	49.1	16q12.1	49602823	49803086
D16S320	20	62.2	16q21	57873375	58073526
D16S503	20	68.8	16q21	63464884	63665231
D16S3106	20	74.9	16q22.2	72053720	72254065
D16S505	20	88.7	16q23.2-q23.3	81540658	81740962
MML16S5	16	0	---	---	---
PHA16S1	16	8.5	---	---	---
D17S796	16	20.7	17p13.2	6248202	6448455

D17S804	16	33.7	17p13.1	9862059	10062380
D17S1803	16	42.9	17p12	12560920	12761252
D17S620	16	55.4	17p11.2	17576358	17776820
D17S1824	16	63.5	17q11.2	28232926	28433201
D17S1290	16	77.4	17q22	58154036	58354369
D17S800	16	87.1	17q21.2	40800006	41000374
D17S934	16	91.3	17q21.31	44880138	45080488
MML16S12	16	118.1	---	---	---
MML16S10	16	138.3	---	---	---
D18S453	18	0	18p11.21	12814784	13014962
D18S1153	18	7.1	18p11.22	10033111	10233451
D18S869	18	21.2	18q11.2	22403477	22602762
D18S456	18	33.1	18q12.1	33482613	33682946
D18S74E	18	35.1	---	---	---
D18S451	18	36.9	18q12.2	37858182	38058522
D18S475	18	37.8	18q12.2	37623478	37823807
D18S72	18	47.1	18q21.1	46248697	46449027
PHA18S1	18	52.3	---	---	---
D18S1156	18	56.3	18q21.2	53142525	53342940
FIC1	18	58.9	18q21.31	57646429	57803095
D18S849	18	59.9	18q21.31	57797346	57997656
D18S1117	18	61.6	18q21.32	58780595	58980899
D18S1155	18	62.8	18q21.32	59296429	59496789
D18S38	18	64.4	18q21.32	60778348	60978585
D18S42	18	68.5	18q21.33	63656786	63856967
D18S537	18	70.5	18q22.1	65036462	65236763
D18S499	18	78.8	---	---	---
MML19S37	19	0	---	---	---
MML19S38	19	6.1	---	---	---
D19S391	19	9.6	19p13.2	8453653	8654016
MML19S40	19	13	---	---	---
MML19S41	19	15.3	---	---	---
D19S226	19	23.1	19p13.12	14422588	14622979
D19S714	19	26.3	19p13.12	15517322	15717596
MML19S35	19	35.9	---	---	---
D19S431	19	43.9	19q12-q13.11	31730641	31931001
MML19S8	19	48.1	---	---	---
DM-19	19	64	---	---	---
D19S180	19	80.8	19q13.42	53146384	53346790
D19S418	19	88.1	19q13.42	60237646	60237997
D22S1043	10	0	---	---	---
D22S304	10	16.9	22q12.3	34874694	35074804
D22S280	10	28.7	22q12.3	32713386	32913714
D22S419	10	38.5	22q11.23-q12.1	25447247	25647623
D22S420	10	46.8	22q11.1-q11.21	17279336	17479699
MML10S34	10	50.8	---	---	---
MML10S14	10	56.1	---	---	---
D20S112	10	60.1	20p12.1	17235293	17435643
MML10S31	10	64.7	---	---	---
D20S189	10	69.1	20p12.2	11093159	11293524
MML10S32	10	72	---	---	---
D20S194	10	75.7	20p12.3	6062049	6262493
D20S482	10	77.3	20p13	4425602	4625820
D20S116	10	78	20p13	3972544	4172950
MML10S29	10	79.2	---	---	---
MML10S13	10	80.2	---	---	---
MML10S35	10	80.9	---	---	---

D20S181	10	84.8	20p13	3091866	3292248
MML10S36	10	91	---	---	---
D20S897	10	100.1	20q13.13	50555608	50755979
MML10S6	10	107	---	---	---
D20S100	10	115.1	20q13.2	55638997	55839249
D20S171	10	122.6	20q13.32	59132834	59333236
MMLXS21	X	0	---	---	---
DXS207	X	1.1	Xp22.2	15310896	15511212
MMLXS22	X	1.5	---	---	---
DXS1683	X	2.7	Xp22.11	22149128	22349281
DXS989	X	3.6	Xp22.11	23066288	23266537
MMLXS4	X	4.9	---	---	---
MMLXS26	X	10	---	---	---
DXS6810	X	11.3	Xp11.3	42959354	43159713
MMLXS28	X	15	---	---	---
MMLXS8	X	16.9	---	---	---
MMLXS10	X	19	---	---	---
MMLXS32	X	20.1	---	---	---
MMLXS17	X	21.2	---	---	---
DXS1196	X	22.3	Xq21.31	87333592	87533855
MMLXS35	X	25.8	---	---	---
DXS6804	X	29.8	Xq23	112769360	112969687
MMLXS36	X	33.2	---	---	---
MMLXS37	X	33.6	---	---	---
MMLXS15	X	36	---	---	---
MMLXS14	X	36.9	---	---	---
DXS102	X	39	Xq27.1	139201208	139401354
MMLXS16	X	40.6	---	---	---

[a]Markers indicated with a series of three dashes could not be located in the UCSC Genome Database with a simple search of the marker name. Instead, they were BLAST'ed to the human genome (GRCh38; see Table A2).

Table A2 Baboon Genetic Map STR Markers Identified in the Human Reference Sequence (GRCh38) Using BLAST.

GRCh38	Marker Name	Forward Primer	Reverse Primer	Proximal (bp)[a]	Distal (bp)[a]
1	PHA1S1	AGTGGATCGATAGATTGACAGATG	TCAGGTGACAGCCAAGTCAATTCA	---	---
2q	PHA12S1	CATTCAATCACCACTCACTCAC	ACTCGTCTCCAGCTTGACAGAG	---	---
4	D4S2456	AACCAAACTGTTTTTATTCTACCG	AGTGCATGTCTCCCAGTGTT	75450627	75451154
4	PHA5S1	TATTTTTCATTGAGCCCAGGAG	GGGCTTTGAAGTCTGCAATTTTAAG	---	---
4	PHA5S2	GAAGATTTGGAGGCATAGCTCAC	ATGTCATCATACTTGTAACCCAAAG	---	---
4	PHA5S3	ATAAGGTTGATAAGCCAGTTGCTC	TTAAGTATAGAACCCTGGAAGCAGT	---	---
4	PHA5S4	TGAACCAAAATTTCTTACTGCCTTA	ATGGCAGCTTTGTGGATCTTTTAT	---	---
4	PHA5S5	CCCATGCCTCTTTAGAAACATAACA	CTCTCATCCCAGGAATTTCACTGAC	---	---
4	PHA5S6	GTAGACAACAATACAGAATTCCCAA	GTTTAAAATATGTGGCTTCTAACG	---	---
4	PHA5S7	AACAGTTCTGGGAGCTTGCACACAT	TGGCACCAAATACCTGATTGCTCT	---	---
4	PHA5S8	CCAGCTTAAGTATAGATCGATTGAC	CGACTTACTGGTGGATAAAATTGTC	---	---
4	PHA5S9	CAGTCCTTCCCCATAACAACAC	CAATAGCGTGCCTAGGTACAAAGTT	---	---
6	MML4S14	CAGCTTGGGTGAGATTCCAT	GTTTCAGGCAAAGGCCATAC	169597932	
6	MML4S17	GTCAGTTGCACAAGGCAGAA	AAGGACCCAGAGCTGTCTCA	166295889	
6	PHA4S1	AAGCTTCAGAGAACTTTATTATGGG	TCAACCTGGACGTGACCTTCAGAAC	---	---
6	PHA4S2	GTGGGAATCCAAAGAGACTTCTCAT	TTTAGTATTTCTTGTGTATTGGGTC	---	---
6	PHA4S3	CCAGATCAGCTGCTCTTTACTGTGC	CTCGTTTTCTCCTGGTGTTTCCTGT	---	---
6	PHA4S4	GGGCTATGCTATCATCAGCTTC	TTAGAGGGACAAAACCAACATGAGA	---	---
6	PHA4S5	ACCTTCAACCATGTGTAGTAGACCC	GGAGGTAGAAGAGCAAGAGGC	---	---
7	PHA3S1	AAGTCCTGGAATTACAAGCGTGAG	TTCAAGGCTGCAATGAGCCATTAT	---	---
8	MML8S18	TCTGCCTTTGGAGACACTCA	TGTGGGCAATGCATACTTGT	2585376	2585838
8	MML8S19	AGTTGCCAAATGAAGCCAAT	AAGTCAGCAGGCAAACCATT	6557603	6557758
8	MML8S22	AAAGCCATTGGCCTACACAT	TGGTCCTGAGCAAAGTGATG	29823705	29823906
8	MML8S29	ATCTTTCCTCTCTCTCCTCACTTTC	TTGGGGAGATGATGTCAATG	16271484	16271633
8	MML8S30	AAGGGAATCCCAAAAGTTCC	TGGAGGTTTTGATTTCAGCA	17128198	17128578
8	MML8S35	TGCCAGAACCCCTAAATCAC	GCCAGAATGACAGCCTTCTC	25583551	25583928
8	PHA8S1	CTCCCAACATTATACAGTTTCTGG	ACTGTGTCACAGGTACGTCCTCAA	---	---
11	MML14S10	GGCTGTGACAGTGGTGAGAA	CACTTTCCCATGCATTTCCT	129285013	129284831
11	MML14S11	GTGCCATGAGTTTGCAGAGA	CCTAGGCCTCTGTTCCTCCT	133948595	133948825
12	D2S122	CAGATTAACTTTCTGCCAGAGAG	GAGTGCCCTAGATGGAAGGT	132974998	144573882
12	MML11S6	ATGTGTGTGTGCATGTGAGC	TGCATGAGCTCTTAGCACCT	122562251	122562655
12	MML11S8	CCCTCTGGGTGTTCATTTGT	GGGGTTCAGGCATTTAAGGT	127294654	127294806
12	PHA11S1	---	---	---	---
12	PHA11S2	CTGGCAGACATTTGGCTTATT	GCCCCTTTGAGTCATTCTAC	---	---
12	PHA11S3	CACTTGACCCCACTAGCCTTATG	ATACTTGCCTGTGCGAATATGGAA	---	---
12	PHA11S4	GCGATAAAGTGAGACCCTGTCTAA	GAATTCCTGACCTCAGTTGATCCA	---	---
12	PHA11S5	GCCTTCAAGTATTCTCTGATTGGA	AAATGGCCTGGACATGATTA	---	---

12	PHA11S6	CCACTACCCCAACACACAACTATA	CCTTGAACACTCCCGAAAT	---	---
13	MML17S11	CAAAGGCTGGGAGATGACTC	TGGCCAGCTTGTTCTAGGTT	32959717	32959926
13	MML17S15	CCTACCTTGGCTGGTGACAT	GCTGAGCTAAATGGCTTCTCC	109841028	109841458
13	MML17S9	CTGTAGACTTTATCCCTGACTTACTG	ACAGGGTTGAAAAGCAGCAT	27726806	27727132
14_15	D15S519	GGTCAAAGTGGCTGTGTAAGGA	TTTAAATGGGTGAATGTATGGTG	74779545	74779561
14_15	MML7S16	ATCCCAACCCTACAGCAGTG	CAGGATCACGGAGGAGGTTA	45141724	---
17	MML16S10	AAGGCCTTTCATATGCCAAA	ACTGATGCTGGAAACTCTAACCA	80728374	80728524
17	MML16S12	TGTGCTTCCAGGGATAAAGG	CAATCCCAACCTTTGCACTT	77350354	77350684
17	MML16S5	ACCATTCCTCCAGAGTGGTG	TGGTAGGAGGGTGCTTATGG	1146155	1146363
17	PHA16S1	CAAACTTTGGCGTAGGTCAGAC	GGGATCACATAGATAGTAGAGACA	---	---
18	D18S499	AGATTACCCAGAAATGAGATCAG	GAAAATGTAGAAGTGAGTCACCT	58810897	58811296
18	D18S74E	AGTAATGGTCCAGGCCCTGG	GACCGGAATATCTGATTACT	---	---
18	PHA18G1	TTCCAGTTCAGAGTTCGGTTGA	AAGAAAGCGTTGCAGTCCTTAT	---	---
18	PHA18S1	GCTGGGGATGGATCTGG	CCTCAGCCTCCCAAGTAG	---	---
19	DM-19	CTTCCCAGGCCTGCAGTTTGCCCATC	GAACGGGGCTCGAAGGGTCCTTGTAGC	---	---
19	MML19S35	GAGGAGAAGAGATGGGGACA	GGGGTGGGTAGATGGAGAAA	29118044	29118063
19	MML19S37	TGATGACTTCCCCAGAGCTT	CCCTGGAACTGTGGTTTGTT	14119118	14119102
19	MML19S38	GGAGAGGTTCAGATGGGAGA	TCTGCTCACCTTGACTCGTG	12768732	12768712
19	MML19S40	TCTGCCTGCCTATCCTTGTT	TCCACAATACGCTGAGTGCT	9851373	9851393
19	MML19S41	ACATCCCCATACCCCAATCT	TGGCATGGGAGAAAGAGAGA	10595815	10595831
19	MML19S8	CCTCATGTGATTCTGGGAGA	CTGCGGGGAGAATTTTACTG	33344982	33344963
20_22	D22S1043	CCTCTTGGCTCTAACAGCAA	AGCAAGACCCTGTCTCAAGA	42148505	42148602
20_22	MML10S13	TAGGAGTTCTGTGGGCTTGG	AATGCCTGAGAATGCTGGAG	672274	672474
20_22	MML10S14	CCTGCCCCTCCTTCTTATTT	TCCAATGGGGTATGATTTGG	19406045	19406261
20_22	MML10S29	TGCCTTCTCTCCTGCTGTTT	CTGGAGATGCTGGAGGGTAA	2032058	2032273
20_22	MML10S31	AACATGGTTAAATGCAAGGAA	TCTGCCTTCAATCAAAAGTGA	14536518	14536727
20_22	MML10S32	ACCACATGCTCTGTTGCTGA	TGGAAGGATTCAGCTTTGCT	7936237	7936613
20_22	MML10S33	TGTTCCTCAAACCCTTGTCC	TCTCAACCCCCTCCAGAAC	674639	674774
20_22	MML10S34	AGGACAAGCCAACCAGAAGA	CACAAGGGGTGTTCCTGACT	25065983	25066451
20_22	MML10S35	TGTTCCTCCTATGTTTCTTATTTCC	CCACAGCAAGGGTCTTATGG	31289309	31289537
20_22	MML10S36	TTTTCTCCTCCCCTCTGGTT	GAAAATGGGCTGCTCTGAAA	38577547	38577775
20_22	MML10S6	GGGGTCTGAGAAGACCTCTG	CCTCGCATGGTGATCAGAC	39558909	39559073
X	MMLXS10	TGGCTTGTCCTTTGAAATCC	AAAGATGCGCTGACATTCCT	71393195	71393443
X	MMLXS14	CAGCTGATGCCTGTTTTCAA	CAACCTGCCAAACAAATCAA	137878032	137878420
X	MMLXS15	ATGTCTGGCAAAGGTGCAG	AAAAGAAAAGTATTTCCTTGAGACATT	136177074	136177048
X	MMLXS16	AATGCTGGAAACGCTTTGAT	CAAATGGACAAATGGGAAGG	148135973	148136207
X	MMLXS17	TGAAAGTCGTTGTGGGGAGT	AACCAAAGTCTGAGCTTTTTGC	85493036	85493212
X	MMLXS21	TTATCATCCCTTGCCTGTGG	ACCCTGCTTTTCCCAGAACT	5261460	5261738
X	MMLXS22	CAGAAACACTCCCCTGTGCT	CCTTGCTGAAGAGAGCCTGT	19252500	19252694
X	MMLXS26	TCAAAATCAGCCACATGGAA	TGCCCTTTTTAAATCCAAGG	41887164	41887562

X	MMLXS27	GATGACTGTGACCTGCCTCA	AAGCGGGCATCTTCTTCTTC	48060016	48060405
X	MMLXS28	CTTCCGTCCATCCTTCCTTT	TGAAATTGCCCATGAGTCAG	50722625	50722744
X	MMLXS32	TCCCACCTCCTAAACACAGG	CCTGTTCAGTGAATAAATCTTTGATG	74922160	74922385
X	MMLXS35	TCAGTGGAGCTCAGCCTTTT	TGCAGGTCTTGTAGCTGGTTT	99462632	99462883
X	MMLXS36	TCTCCGGAGTGACATTTTCC	GTAGGGCAGACGGTTTTGAA	119115107	119115456
X	MMLXS37	TTGGTGTAAAAGCCTTCAAGC	GGCATCTTTTGAGTGGGAAC	124463642	124463962
X	MMLXS4	TTTCCCCACAAACTTGCATT	TTTTTGAACTCTTGACTTGCAGTT	29936362	29936584
X	MMLXS8	TTGCTGTGATACCCATGAGC	CACATTACCTGGGCCAAGAC	57576931	57577126

[a]Markers indicated with a series of three dashes do not have recorded primer sequences and/or could not be located in the UCSC Genome Database using the BLAST search engine.

Table B1 Genetic Correlation Matrix for Model 1.

	ACPM	ACSY	PMPM	ASJP	BACC	BAOP	ASAS	JPJP	4141	POPO	PTPT	STST	ZTZT	BRAS	BRLD	BRNA	BRPT
ACPM	1.000	0.621	0.813	0.318	0.178	0.213	0.290	0.326	0.645	0.441	0.475	0.003	0.315	0.353	0.399	0.608	0.475
ACSY	0.621	1.000	0.248	0.139	0.311	0.212	0.375	0.227	0.423	0.476	0.017	-0.066	0.397	0.336	0.264	0.312	0.082
PMPM	0.813	0.248	1.000	0.104	-0.076	0.369	0.161	0.105	0.696	0.237	0.170	-0.230	0.232	0.383	0.635	0.239	0.094
ASJP	0.318	0.139	0.104	1.000	0.184	0.175	0.437	-0.080	0.308	0.226	0.131	-0.123	0.310	0.203	0.240	0.344	0.192
BACC	0.178	0.311	-0.076	0.184	1.000	0.136	0.492	0.529	0.214	0.534	0.118	-0.012	0.511	0.207	0.136	0.326	0.004
BAOP	0.213	0.212	0.369	0.175	0.136	1.000	0.230	0.289	0.326	0.143	-0.042	-0.235	0.161	0.128	-0.125	0.124	-0.023
ASAS	0.290	0.375	0.161	0.437	0.492	0.230	1.000	0.513	0.388	0.633	-0.050	-0.151	0.546	0.539	-0.140	0.406	0.062
JPJP	0.326	0.227	0.105	-0.080	0.529	0.289	0.513	1.000	0.187	0.377	0.077	0.083	0.272	0.080	0.048	0.274	0.115
4141	0.645	0.423	0.696	0.308	0.214	0.326	0.388	0.187	1.000	0.379	0.159	-0.094	0.514	0.445	0.200	0.481	-0.005
POPO	0.441	0.476	0.237	0.226	0.534	0.143	0.633	0.377	0.379	1.000	0.149	0.166	0.608	0.318	0.034	0.469	0.135
PTPT	0.475	0.017	0.170	0.131	0.118	-0.042	-0.050	0.077	0.159	0.149	1.000	0.518	0.060	0.218	0.093	0.331	0.477
STST	0.003	-0.066	-0.230	-0.123	-0.012	-0.235	-0.151	0.083	-0.094	0.166	0.518	1.000	-0.070	0.121	-0.016	0.240	0.475
ZTZT	0.315	0.397	0.232	0.310	0.511	0.161	0.546	0.272	0.514	0.608	0.060	-0.070	1.000	0.434	0.181	0.305	-0.102
BRAS	0.353	0.336	0.383	0.203	0.207	0.128	0.539	0.080	0.445	0.318	0.218	0.121	0.434	1.000	0.563	0.282	0.094
BRLD	0.399	0.264	0.635	0.240	0.136	-0.125	-0.140	0.048	0.200	0.034	0.093	-0.016	0.181	0.563	1.000	-0.030	0.043
BRNA	0.608	0.312	0.239	0.344	0.326	0.124	0.406	0.274	0.481	0.469	0.331	0.240	0.305	0.282	-0.030	1.000	0.519
BRPT	0.475	0.082	0.094	0.192	0.004	-0.023	0.062	0.115	-0.005	0.135	0.477	0.475	-0.102	0.094	0.043	0.519	1.000
NABA	0.603	0.655	0.395	0.458	0.499	0.153	0.500	0.226	0.401	0.413	0.049	-0.094	0.466	0.280	-0.018	0.479	0.082
CACP	0.565	0.427	0.461	0.453	-0.299	0.223	0.156	-0.196	-0.166	-0.082	-0.139	-0.256	-0.245	-0.093	0.026	0.281	0.188
CPSL	0.009	0.093	-0.203	-0.077	0.314	0.079	-0.029	0.001	-0.129	0.089	0.088	0.220	0.079	-0.017	-0.168	0.223	0.201
CPZS	0.575	0.599	0.334	0.310	0.264	0.317	0.540	0.251	0.507	0.443	0.080	-0.104	0.437	0.261	0.132	0.345	-0.047
CNCN	0.005	0.087	0.013	0.056	0.412	0.610	0.170	0.317	0.233	0.089	0.061	0.017	0.020	-0.148	-0.205	0.128	0.129
FMPM	0.378	0.673	0.354	0.262	0.124	0.261	0.085	0.166	0.385	0.295	-0.012	-0.216	0.244	0.163	0.268	0.258	0.029
FMZT	0.373	0.326	0.254	0.355	0.227	0.099	0.352	0.163	0.246	0.263	0.046	0.118	0.570	0.435	0.140	0.330	0.046
FMCP	0.579	0.554	0.246	0.279	0.299	0.213	0.520	0.327	0.419	0.430	0.081	-0.040	0.509	0.388	0.225	0.482	0.099
FMPT	0.323	0.316	0.304	0.125	0.181	0.234	0.332	0.103	0.456	0.243	0.262	-0.217	0.344	0.536	0.060	0.259	-0.389
LDAS	0.209	0.399	0.380	0.009	0.171	0.211	0.686	0.216	0.369	0.539	-0.086	-0.205	0.515	0.730	0.015	0.338	-0.136
LDBA	0.443	0.286	0.488	0.470	0.255	0.317	0.413	0.015	0.244	0.405	0.113	-0.121	0.400	0.445	0.360	0.492	0.076
NANL	0.332	0.694	0.227	0.209	0.068	0.277	0.280	0.199	0.264	0.335	-0.076	-0.200	0.232	0.141	0.112	0.084	-0.181
NLAC	0.261	0.570	0.251	0.206	0.049	0.275	0.043	0.072	0.340	0.129	0.022	-0.259	0.188	0.091	0.142	0.190	0.094
NLVS	0.485	0.791	0.214	0.128	0.264	0.090	0.360	0.316	0.258	0.370	-0.053	-0.068	0.342	0.416	0.141	0.210	0.063
NAAC	0.328	0.732	0.175	0.206	0.169	0.313	0.231	0.239	0.327	0.330	0.043	-0.154	0.293	0.272	0.207	0.152	-0.043
NACA	0.448	0.441	0.139	0.220	0.322	0.191	0.594	0.393	0.540	0.469	0.085	-0.052	0.494	0.296	-0.066	0.298	-0.080
NACP	0.712	0.664	0.414	0.403	0.307	0.232	0.634	0.279	0.496	0.522	0.023	-0.150	0.437	0.266	-0.108	0.556	0.160
NAFM	0.500	0.538	0.257	0.222	0.261	0.224	0.390	0.404	0.314	0.451	0.377	-0.010	0.416	0.258	-0.048	0.393	0.135
NA41	0.443	0.587	0.441	0.295	0.198	0.282	0.262	0.291	0.377	0.370	0.161	-0.112	0.310	0.223	0.181	0.361	0.080
NAVS	0.488	0.574	0.272	0.216	0.150	0.143	0.305	0.176	0.288	0.208	0.186	0.140	0.163	0.137	-0.118	0.434	0.286
NAZI	0.393	0.584	0.294	0.276	0.256	0.193	0.493	0.308	0.317	0.402	0.181	-0.134	0.448	0.229	-0.141	0.469	0.079
NAZS	0.210	0.269	0.200	0.065	0.227	0.243	0.287	0.236	0.135	0.360	0.312	0.055	0.216	0.154	0.027	0.167	0.147
BRBA	0.458	0.291	0.236	0.565	0.286	0.111	0.198	-0.101	0.172	0.172	0.305	0.239	0.283	0.345	0.359	0.632	0.430
NALD	0.795	0.509	0.722	0.511	0.371	0.186	0.339	0.240	0.562	0.450	0.188	-0.114	0.371	0.479	0.532	0.668	0.334
DAFM	0.450	0.586	0.188	0.316	0.157	0.171	0.222	0.250	0.247	0.345	0.356	-0.061	0.457	0.023	0.174	0.313	0.181
PLSY	0.430	0.659	0.182	0.059	0.099	0.058	0.122	0.112	0.221	0.216	0.005	0.087	0.227	0.154	0.232	0.169	0.015
POBA	0.525	0.426	0.349	0.560	0.582	0.191	0.531	0.381	0.390	0.790	0.058	-0.074	0.629	0.237	0.267	0.364	0.103
PM41	0.561	0.610	0.248	0.157	0.229	0.240	0.317	0.273	0.470	0.258	0.162	-0.077	0.151	0.184	0.036	0.166	0.193
41MX	0.340	0.577	0.436	0.136	0.272	0.246	0.167	0.232	0.463	0.360	0.035	-0.030	0.210	0.268	0.241	0.353	0.051
41ZI	0.319	0.444	0.345	0.262	0.118	0.165	0.007	0.211	0.232	0.365	-0.012	-0.084	0.171	0.193	0.474	0.231	0.047
PTAS	0.249	0.133	0.098	0.477	0.152	0.171	0.234	0.112	0.243	0.172	-0.254	0.067	0.145	0.205	0.549	0.251	0.419
PTLD	0.518	0.227	0.461	0.350	0.188	0.079	0.076	0.149	0.091	0.219	-0.016	0.089	0.092	0.206	0.636	0.339	0.608
SLBA	0.499	0.430	0.604	0.462	0.296	-0.114	-0.105	-0.042	0.423	0.033	0.012	-0.195	0.263	-0.016	0.326	0.250	-0.019
SLCC	0.509	0.409	0.417	0.405	0.547	0.062	0.231	0.329	0.599	0.207	0.127	-0.262	0.334	0.001	-0.052	0.358	-0.143
SYBA	0.165	0.269	0.182	0.053	0.327	0.121	0.239	0.184	0.236	0.315	-0.208	-0.084	0.337	0.372	-0.010	0.030	-0.147
SYMX	0.387	0.480	0.124	0.065	0.136	-0.036	0.164	0.080	0.232	0.167	-0.037	-0.012	0.327	0.315	0.202	0.219	-0.056
ZTPO	0.131	0.321	0.134	-0.048	0.235	0.267	0.147	-0.090	0.419	0.076	-0.216	-0.129	0.366	0.118	-0.003	0.176	-0.249
ZTVS	0.374	0.530	0.232	0.251	0.455	0.140	0.489	0.275	0.510	0.527	-0.026	-0.040	0.910	0.466	0.200	0.390	-0.057
ZTZI	0.104	0.198	-0.164	0.142	0.305	0.156	0.185	0.025	0.299	-0.025	0.034	-0.102	0.538	0.098	-0.136	0.060	-0.317
VSBA	0.253	0.301	0.206	0.266	0.490	0.044	0.413	0.116	0.224	0.383	-0.264	-0.224	0.455	0.198	0.067	0.028	-0.274
VSSY	0.045	0.078	0.216	-0.026	-0.056	0.126	0.004	0.127	0.035	0.000	-0.014	-0.080	0.010	0.316	-0.069	0.174	0.068
ZIMX	0.775	0.488	0.774	0.304	0.071	0.141	0.108	-0.069	0.358	0.340	0.072	-0.041	0.399	-0.042	0.132	0.510	0.241
ZSNL	0.478	0.730	0.377	0.287	0.131	0.169	0.355	0.291	0.370	0.397	-0.140	-0.155	0.323	0.388	0.291	0.207	-0.173

	NABA	CACP	CPSL	CPZS	CNCN	FMPM	FMZT	FMCP	FMPT	LDAS	LDBA	NANL	NLAC	NLVS	NAAC	NACA	NACP
ACPM	0.603	0.565	0.009	0.575	0.005	0.378	0.373	0.579	0.323	0.209	0.443	0.332	0.261	0.485	0.328	0.448	0.712
ACSY	0.655	0.427	0.093	0.599	0.087	0.673	0.326	0.554	0.316	0.399	0.286	0.694	0.570	0.791	0.732	0.441	0.664
PMPM	0.395	0.461	-0.203	0.334	0.013	0.354	0.254	0.246	0.304	0.380	0.488	0.227	0.251	0.214	0.175	0.139	0.414
ASJP	0.458	0.453	-0.077	0.310	0.056	0.262	0.355	0.279	0.125	0.009	0.470	0.209	0.206	0.128	0.206	0.220	0.403
BACC	0.499	-0.299	0.314	0.264	0.412	0.124	0.227	0.299	0.181	0.171	0.255	0.068	0.049	0.264	0.169	0.322	0.307
BAOP	0.153	0.223	0.079	0.317	0.610	0.261	0.099	0.213	0.234	0.211	0.317	0.277	0.275	0.090	0.313	0.191	0.232
ASAS	0.500	0.156	-0.029	0.540	0.170	0.085	0.352	0.520	0.332	0.686	0.413	0.280	0.043	0.360	0.231	0.594	0.634
JPJP	0.226	-0.196	0.001	0.251	0.317	0.166	0.163	0.327	0.103	0.216	0.015	0.199	0.072	0.316	0.239	0.393	0.279
4141	0.401	-0.166	-0.129	0.507	0.233	0.385	0.246	0.419	0.456	0.369	0.244	0.264	0.340	0.258	0.327	0.540	0.496
POPO	0.413	-0.082	0.089	0.443	0.089	0.295	0.263	0.430	0.243	0.539	0.405	0.335	0.129	0.370	0.330	0.469	0.522
PTPT	0.049	-0.139	0.088	0.080	0.061	-0.012	0.046	0.081	0.262	-0.086	0.113	-0.076	0.022	-0.053	0.043	0.085	0.023
STST	-0.094	-0.256	0.220	-0.104	0.017	-0.216	0.118	-0.040	-0.217	-0.205	-0.121	-0.200	-0.259	-0.068	-0.154	-0.052	-0.150
ZTZT	0.466	-0.245	0.079	0.437	0.020	0.244	0.570	0.509	0.344	0.515	0.400	0.232	0.188	0.342	0.293	0.494	0.437
BRAS	0.280	-0.093	-0.017	0.261	-0.148	0.163	0.435	0.388	0.536	0.730	0.445	0.141	0.091	0.416	0.272	0.296	0.266
BRLD	-0.018	0.026	-0.168	0.132	-0.205	0.268	0.140	0.225	0.060	0.015	0.360	0.112	0.142	0.141	0.207	-0.066	-0.108
BRNA	0.479	0.281	0.223	0.345	0.128	0.258	0.330	0.482	0.259	0.338	0.492	0.084	0.190	0.210	0.152	0.298	0.556
BRPT	0.082	0.188	0.201	-0.047	0.129	0.029	0.046	0.099	-0.389	-0.136	0.076	-0.181	0.094	0.063	-0.043	-0.080	0.160
NABA	1.000	0.256	0.175	0.548	0.221	0.311	0.382	0.617	0.363	0.352	0.466	0.239	0.254	0.564	0.335	0.655	0.804
CACP	0.256	1.000	0.397	0.194	0.014	0.240	0.028	0.098	-0.084	-0.098	0.129	0.225	0.329	0.213	0.315	-0.295	0.271
CPSL	0.175	0.397	1.000	0.196	0.310	0.283	0.202	0.162	0.031	0.079	0.194	0.107	-0.003	0.289	0.225	-0.235	0.073
CPZS	0.548	0.194	0.196	1.000	0.168	0.388	0.415	0.759	0.466	0.355	0.288	0.365	0.266	0.593	0.457	0.622	0.732
CNCN	0.221	0.014	0.310	0.168	1.000	-0.042	0.025	-0.053	-0.034	-0.139	-0.060	-0.028	-0.020	-0.031	0.035	0.049	-0.048
FMPM	0.311	0.240	0.283	0.388	-0.042	1.000	0.391	0.298	0.101	0.200	0.345	0.779	0.608	0.527	0.881	0.229	0.377
FMZT	0.382	0.028	0.202	0.415	0.025	0.391	1.000	0.416	0.278	0.362	0.419	0.231	0.339	0.241	0.337	0.369	0.390
FMCP	0.617	0.098	0.162	0.759	-0.053	0.298	0.416	1.000	0.523	0.425	0.328	0.235	0.317	0.544	0.357	0.730	0.806
FMPT	0.363	-0.084	0.031	0.466	-0.034	0.101	0.278	0.523	1.000	0.621	0.484	0.230	0.092	0.236	0.298	0.515	0.454
LDAS	0.352	-0.098	0.079	0.355	-0.139	0.200	0.362	0.425	0.621	1.000	0.626	0.257	0.064	0.453	0.335	0.544	0.532
LDBA	0.466	0.129	0.194	0.288	-0.060	0.345	0.419	0.328	0.484	0.626	1.000	0.289	0.200	0.295	0.408	0.250	0.395
NANL	0.239	0.225	0.107	0.365	-0.028	0.779	0.231	0.235	0.230	0.257	0.289	1.000	0.193	0.636	0.918	0.150	0.377
NLAC	0.254	0.329	-0.003	0.266	-0.020	0.608	0.339	0.317	0.092	0.064	0.200	0.193	1.000	0.213	0.552	0.106	0.311
NLVS	0.564	0.213	0.289	0.593	-0.031	0.527	0.241	0.544	0.236	0.453	0.295	0.636	0.213	1.000	0.611	0.424	0.606
NAAC	0.335	0.315	0.225	0.457	0.035	0.881	0.337	0.357	0.298	0.335	0.408	0.918	0.552	0.611	1.000	0.238	0.479
NACA	0.655	-0.295	-0.235	0.622	0.049	0.229	0.369	0.730	0.515	0.544	0.250	0.150	0.106	0.424	0.238	1.000	0.820
NACP	0.804	0.271	0.073	0.732	-0.048	0.377	0.390	0.806	0.454	0.532	0.395	0.377	0.311	0.606	0.479	0.820	1.000
NAFM	0.636	0.187	0.094	0.479	0.073	0.263	0.201	0.459	0.208	0.249	0.181	0.170	0.267	0.416	0.274	0.495	0.607
NA41	0.395	0.254	0.229	0.493	0.002	0.904	0.477	0.434	0.279	0.297	0.477	0.751	0.472	0.431	0.849	0.371	0.530
NAVS	0.723	0.072	0.179	0.465	-0.200	0.277	0.190	0.529	0.203	0.288	0.260	0.167	0.220	0.602	0.335	0.619	0.695
NAZI	0.488	0.016	0.026	0.524	-0.146	0.495	0.503	0.464	0.301	0.391	0.378	0.524	0.305	0.473	0.599	0.589	0.649
NAZS	0.380	-0.003	0.031	0.234	-0.024	0.155	0.145	0.264	0.225	0.269	0.227	0.252	0.082	0.182	0.321	0.420	0.398
BRBA	0.522	0.233	0.401	0.098	0.078	0.194	0.341	0.280	0.280	0.183	0.703	0.076	0.143	0.260	0.209	0.049	0.250
NALD	0.565	0.235	-0.075	0.488	0.032	0.415	0.313	0.609	0.400	0.368	0.774	0.285	0.282	0.357	0.374	0.448	0.567
DAFM	0.593	0.129	0.050	0.429	0.127	0.337	0.262	0.441	0.071	-0.058	0.081	0.273	0.363	0.467	0.330	0.378	0.470
PLSY	0.401	0.187	0.044	0.237	-0.127	0.566	0.354	0.316	0.093	0.179	0.149	0.431	0.390	0.407	0.541	0.349	0.404
POBA	0.618	0.128	0.109	0.327	0.106	0.442	0.355	0.412	0.215	0.337	0.636	0.496	0.139	0.411	0.418	0.415	0.484
PM41	0.410	0.228	0.318	0.321	0.266	0.250	0.144	0.196	0.178	0.341	0.278	0.351	0.397	0.497	0.450	0.282	0.253
41MX	0.363	0.185	0.190	0.487	0.102	0.824	0.361	0.531	0.228	0.225	0.303	0.518	0.509	0.444	0.590	0.361	0.491
41ZI	0.323	0.172	0.238	0.398	-0.196	0.799	0.246	0.389	0.166	0.046	0.332	0.630	0.291	0.443	0.662	0.318	0.439
PTAS	0.216	0.130	-0.181	0.131	0.111	0.300	0.286	0.166	-0.437	-0.040	0.097	0.061	0.226	0.178	0.122	0.067	0.100
PTLD	0.167	0.185	-0.113	0.122	0.083	0.287	0.142	0.290	-0.346	0.009	0.366	0.122	0.174	0.178	0.187	-0.011	0.134
SLBA	0.638	0.116	-0.232	0.066	0.235	0.229	0.147	0.149	0.168	-0.314	0.302	0.119	0.325	0.165	0.116	0.172	0.155
SLCC	0.685	-0.021	-0.122	0.365	0.220	0.135	0.157	0.303	0.323	-0.095	0.245	-0.048	0.234	0.180	0.036	0.441	0.404
SYBA	0.575	0.036	0.311	0.436	0.330	0.305	0.210	0.381	0.252	0.335	0.227	0.242	0.196	0.464	0.297	0.268	0.384
SYMX	0.349	0.142	-0.285	0.238	-0.284	0.291	0.346	0.314	0.170	0.280	0.185	0.329	0.239	0.368	0.383	0.313	0.388
ZTPO	0.233	-0.155	-0.036	0.262	0.011	0.278	0.222	0.318	0.241	0.261	0.051	0.299	0.172	0.360	0.279	0.199	0.168
ZTVS	0.474	-0.279	0.148	0.444	0.023	0.261	0.486	0.619	0.325	0.509	0.406	0.185	0.238	0.501	0.318	0.537	0.503
ZTZI	0.062	0.033	0.312	0.267	0.213	0.071	0.333	0.052	0.236	0.185	0.056	-0.189	0.292	-0.079	-0.037	-0.035	-0.082
VSBA	0.566	0.062	0.096	0.151	0.423	0.238	0.240	0.071	0.200	0.206	0.206	0.313	0.086	0.159	0.237	0.198	0.221
VSSY	0.057	0.167	0.365	0.426	0.070	0.298	0.089	0.314	0.227	0.250	0.209	0.152	0.144	0.417	0.256	0.049	0.264
ZIMX	0.436	0.364	0.052	0.359	-0.196	0.505	0.234	0.448	0.169	0.182	0.516	0.345	0.360	0.417	0.475	0.182	0.476
ZSNL	0.430	0.369	0.309	0.392	-0.127	0.776	0.297	0.382	0.322	0.400	0.419	0.898	0.187	0.745	0.828	0.223	0.521

	NAFM	NA41	NAVS	NAZI	NAZS	BRBA	NALD	DAFM	PLSY	POBA	PM41	41MX	41ZI	PTAS	PTLD	SLBA	SLCC
ACPM	0.500	0.443	0.488	0.393	0.210	0.458	0.795	0.450	0.430	0.525	0.561	0.340	0.319	0.249	0.518	0.499	0.509
ACSY	0.538	0.587	0.574	0.584	0.269	0.291	0.509	0.586	0.659	0.426	0.610	0.577	0.444	0.133	0.227	0.430	0.409
PMPM	0.257	0.441	0.272	0.294	0.200	0.236	0.722	0.188	0.182	0.349	0.248	0.436	0.345	0.098	0.461	0.604	0.417
ASJP	0.222	0.295	0.216	0.276	0.065	0.565	0.511	0.316	0.059	0.560	0.157	0.136	0.262	0.477	0.350	0.462	0.405
BACC	0.261	0.198	0.150	0.256	0.227	0.286	0.371	0.157	0.099	0.582	0.229	0.272	0.118	0.152	0.188	0.296	0.547
BAOP	0.224	0.282	0.143	0.193	0.243	0.111	0.186	0.171	0.058	0.191	0.240	0.246	0.165	0.171	0.079	-0.114	0.062
ASAS	0.390	0.262	0.305	0.493	0.287	0.198	0.339	0.222	0.122	0.531	0.317	0.167	0.007	0.234	0.076	-0.105	0.231
JPJP	0.404	0.291	0.176	0.308	0.236	-0.101	0.240	0.250	0.112	0.381	0.273	0.232	0.211	0.112	0.149	-0.042	0.329
4141	0.314	0.377	0.288	0.317	0.135	0.172	0.562	0.247	0.221	0.390	0.470	0.463	0.232	0.243	0.091	0.423	0.599
POPO	0.451	0.370	0.208	0.402	0.360	0.172	0.450	0.345	0.216	0.790	0.258	0.360	0.365	0.172	0.219	0.033	0.207
PTPT	0.377	0.161	0.186	0.181	0.312	0.305	0.188	0.356	0.005	0.058	0.162	0.035	-0.012	-0.254	-0.016	0.012	0.127
STST	-0.010	-0.112	0.140	-0.134	0.055	0.239	-0.114	-0.061	0.087	-0.074	-0.077	-0.030	-0.084	0.067	0.089	-0.195	-0.262
ZTZT	0.416	0.310	0.163	0.448	0.216	0.283	0.371	0.457	0.227	0.629	0.151	0.210	0.171	0.145	0.092	0.263	0.334
BRAS	0.258	0.223	0.137	0.229	0.154	0.345	0.479	0.023	0.154	0.237	0.184	0.268	0.193	0.205	0.206	-0.016	0.001
BRLD	-0.048	0.181	-0.118	-0.141	0.027	0.359	0.532	0.174	0.232	0.267	0.036	0.241	0.474	0.549	0.636	0.326	-0.052
BRNA	0.393	0.361	0.434	0.469	0.167	0.632	0.668	0.313	0.169	0.364	0.166	0.353	0.231	0.251	0.339	0.250	0.358
BRPT	0.135	0.080	0.286	0.079	0.147	0.430	0.334	0.181	0.015	0.103	0.193	0.051	0.047	0.419	0.608	-0.019	-0.143
NABA	0.636	0.395	0.723	0.488	0.380	0.522	0.565	0.593	0.401	0.618	0.410	0.363	0.323	0.216	0.167	0.638	0.685
CACP	0.187	0.254	0.072	0.016	-0.003	0.233	0.235	0.129	0.187	0.128	0.228	0.185	0.172	0.130	0.185	0.116	-0.021
CPSL	0.094	0.229	0.179	0.026	0.031	0.401	-0.075	0.050	0.044	0.109	0.318	0.190	0.238	-0.181	-0.113	-0.232	-0.122
CPZS	0.479	0.493	0.465	0.524	0.234	0.098	0.488	0.429	0.237	0.327	0.321	0.487	0.398	0.131	0.122	0.066	0.365
CNCN	0.073	0.002	-0.200	-0.146	-0.024	0.078	0.032	0.127	-0.127	0.106	0.266	0.102	-0.196	0.111	0.083	0.235	0.220
FMPM	0.263	0.904	0.277	0.495	0.155	0.194	0.415	0.337	0.566	0.442	0.250	0.824	0.799	0.300	0.287	0.229	0.135
FMZT	0.201	0.477	0.190	0.503	0.145	0.341	0.313	0.262	0.354	0.355	0.144	0.361	0.246	0.286	0.142	0.147	0.157
FMCP	0.459	0.434	0.529	0.464	0.264	0.280	0.609	0.441	0.316	0.412	0.196	0.531	0.389	0.166	0.290	0.149	0.303
FMPT	0.208	0.279	0.203	0.301	0.225	0.280	0.400	0.071	0.093	0.215	0.178	0.228	0.166	-0.437	-0.346	0.168	0.323
LDAS	0.249	0.297	0.288	0.391	0.269	0.183	0.368	-0.058	0.179	0.337	0.341	0.225	0.046	-0.040	0.009	-0.314	-0.095
LDBA	0.181	0.477	0.260	0.378	0.227	0.703	0.774	0.081	0.149	0.636	0.278	0.303	0.332	0.097	0.366	0.302	0.245
NANL	0.170	0.751	0.167	0.524	0.252	0.076	0.285	0.273	0.431	0.496	0.351	0.518	0.630	0.061	0.122	0.119	-0.048
NLAC	0.267	0.472	0.220	0.305	0.082	0.143	0.282	0.363	0.390	0.139	0.397	0.509	0.291	0.226	0.174	0.325	0.234
NLVS	0.416	0.431	0.602	0.473	0.182	0.260	0.357	0.467	0.407	0.411	0.497	0.444	0.443	0.178	0.178	0.165	0.180
NAAC	0.274	0.849	0.335	0.599	0.321	0.209	0.374	0.330	0.541	0.418	0.450	0.590	0.662	0.122	0.187	0.116	0.036
NACA	0.495	0.371	0.619	0.589	0.420	0.049	0.448	0.378	0.349	0.415	0.282	0.361	0.318	0.067	-0.011	0.172	0.441
NACP	0.607	0.530	0.695	0.649	0.398	0.250	0.567	0.470	0.404	0.484	0.253	0.491	0.439	0.100	0.134	0.155	0.404
NAFM	1.000	0.375	0.644	0.595	0.542	0.181	0.370	0.889	0.402	0.403	0.319	0.372	0.296	0.137	0.053	0.297	0.432
NA41	0.375	1.000	0.392	0.712	0.362	0.263	0.536	0.363	0.555	0.469	0.147	0.772	0.812	0.245	0.312	0.141	0.119
NAVS	0.644	0.392	1.000	0.555	0.521	0.301	0.369	0.573	0.431	0.405	0.293	0.350	0.382	0.017	0.106	0.195	0.238
NAZI	0.595	0.712	0.555	1.000	0.521	0.124	0.406	0.514	0.474	0.444	0.234	0.503	0.412	0.154	0.077	0.115	0.301
NAZS	0.542	0.362	0.521	0.521	1.000	0.047	0.264	0.348	0.163	0.191	0.193	0.178	0.266	-0.053	0.110	-0.122	-0.020
BRBA	0.181	0.263	0.301	0.124	0.047	1.000	0.621	0.154	0.197	0.521	0.151	0.319	0.317	0.171	0.370	0.496	0.263
NALD	0.370	0.536	0.369	0.406	0.264	0.621	1.000	0.401	0.299	0.580	0.301	0.442	0.465	0.524	0.627	0.481	0.442
DAFM	0.889	0.363	0.573	0.514	0.348	0.154	0.401	1.000	0.475	0.352	0.137	0.350	0.260	0.244	0.223	0.370	0.403
PLSY	0.402	0.555	0.431	0.474	0.163	0.197	0.299	0.475	1.000	0.246	0.188	0.437	0.436	0.162	0.153	0.280	0.235
POBA	0.403	0.469	0.405	0.444	0.191	0.521	0.580	0.352	0.246	1.000	0.175	0.409	0.511	0.346	0.406	0.423	0.484
PM41	0.319	0.147	0.293	0.234	0.193	0.151	0.301	0.137	0.188	0.175	1.000	0.076	-0.088	0.010	0.147	0.122	0.320
41MX	0.372	0.772	0.350	0.503	0.178	0.319	0.442	0.350	0.437	0.409	0.076	1.000	0.837	0.286	0.259	0.131	0.085
41ZI	0.296	0.812	0.382	0.412	0.266	0.317	0.465	0.260	0.436	0.511	-0.088	0.837	1.000	0.374	0.319	0.063	-0.008
PTAS	0.137	0.245	0.017	0.154	-0.053	0.171	0.524	0.244	0.162	0.346	0.010	0.286	0.374	1.000	0.882	0.413	0.278
PTLD	0.053	0.312	0.106	0.077	0.110	0.370	0.627	0.223	0.153	0.406	0.147	0.259	0.319	0.882	1.000	0.287	0.026
SLBA	0.297	0.141	0.195	0.115	-0.122	0.496	0.481	0.370	0.280	0.423	0.122	0.131	0.063	0.413	0.287	1.000	0.737
SLCC	0.432	0.119	0.238	0.301	-0.020	0.263	0.442	0.403	0.235	0.484	0.320	0.085	-0.008	0.278	0.026	0.737	1.000
SYBA	0.302	0.254	0.142	0.153	0.177	0.222	0.147	0.224	-0.016	0.198	0.444	0.244	0.146	0.135	-0.018	0.174	0.236
SYMX	0.315	0.501	0.345	0.578	0.200	0.146	0.405	0.339	0.542	0.228	-0.001	0.315	0.289	0.268	0.181	0.317	0.380
ZTPO	0.078	0.279	0.043	0.239	-0.236	-0.025	0.306	0.179	0.164	0.225	-0.084	0.246	0.079	0.043	0.045	0.321	0.416
ZTVS	0.373	0.311	0.360	0.453	0.139	0.290	0.454	0.410	0.296	0.524	0.126	0.313	0.162	0.228	0.212	0.208	0.285
ZTZI	0.124	0.044	-0.352	0.094	-0.028	-0.065	-0.022	0.276	0.079	0.112	0.138	-0.039	-0.223	-0.239	-0.280	0.162	0.144
VSBA	0.193	0.154	-0.160	0.099	0.036	0.248	0.237	0.177	0.097	0.347	0.297	0.129	0.097	0.079	0.002	0.500	0.514
VSSY	0.038	0.295	0.149	0.130	0.067	0.082	0.081	-0.011	-0.095	0.009	0.218	0.313	0.263	0.053	-0.007	-0.239	-0.193
ZIMX	0.282	0.627	0.464	0.373	0.012	0.439	0.566	0.346	0.666	0.425	-0.048	0.508	0.490	0.090	0.353	0.477	0.416
ZSNL	0.272	0.689	0.325	0.494	0.205	0.289	0.410	0.308	0.447	0.540	0.439	0.623	0.691	0.196	0.136	0.153	0.005

	SYBA	SYMX	ZTPO	ZTVS	ZTZI	VSBA	VSSY	ZIMX	ZSNL
ACPM	0.165	0.387	0.131	0.374	0.104	0.253	0.045	0.775	0.478
ACSY	0.269	0.480	0.321	0.530	0.198	0.301	0.078	0.488	0.730
PMPM	0.182	0.124	0.134	0.232	-0.164	0.206	0.216	0.774	0.377
ASJP	0.053	0.065	-0.048	0.251	0.142	0.266	-0.026	0.304	0.287
BACC	0.327	0.136	0.235	0.455	0.305	0.490	-0.056	0.071	0.131
BAOP	0.121	-0.036	0.267	0.140	0.156	0.044	0.126	0.141	0.169
ASAS	0.239	0.164	0.147	0.489	0.185	0.413	0.004	0.108	0.355
JPJP	0.184	0.080	-0.090	0.275	0.025	0.116	0.127	-0.069	0.291
4141	0.236	0.232	0.419	0.510	0.299	0.224	0.035	0.358	0.370
POPO	0.315	0.167	0.076	0.527	-0.025	0.383	0.000	0.340	0.397
PTPT	-0.208	-0.037	-0.216	-0.026	0.034	-0.264	-0.014	0.072	-0.140
STST	-0.084	-0.012	-0.129	-0.040	-0.102	-0.224	-0.080	-0.041	-0.155
ZTZT	0.337	0.327	0.366	0.910	0.538	0.455	0.010	0.399	0.323
BRAS	0.372	0.315	0.118	0.466	0.098	0.198	0.316	-0.042	0.388
BRLD	-0.010	0.202	-0.003	0.200	-0.136	0.067	-0.069	0.132	0.291
BRNA	0.030	0.219	0.176	0.390	0.060	0.028	0.174	0.510	0.207
BRPT	-0.147	-0.056	-0.249	-0.057	-0.317	-0.274	0.068	0.241	-0.173
NABA	0.575	0.349	0.233	0.474	0.062	0.566	0.057	0.436	0.430
CACP	0.036	0.142	-0.155	-0.279	0.033	0.062	0.167	0.364	0.369
CPSL	0.311	-0.285	-0.036	0.148	0.312	0.096	0.365	0.052	0.309
CPZS	0.436	0.238	0.262	0.444	0.267	0.151	0.426	0.359	0.392
CNCN	0.330	-0.284	0.011	0.023	0.213	0.423	0.070	-0.196	-0.127
FMPM	0.305	0.291	0.278	0.261	0.071	0.238	0.298	0.505	0.776
FMZT	0.210	0.346	0.222	0.486	0.333	0.240	0.089	0.234	0.297
FMCP	0.381	0.314	0.318	0.619	0.052	0.071	0.314	0.448	0.382
FMPT	0.252	0.170	0.241	0.325	0.236	0.200	0.227	0.169	0.322
LDAS	0.335	0.280	0.261	0.509	0.185	0.206	0.250	0.182	0.400
LDBA	0.227	0.185	0.051	0.406	0.056	0.206	0.209	0.516	0.419
NANL	0.242	0.329	0.299	0.185	-0.189	0.313	0.152	0.345	0.898
NLAC	0.196	0.239	0.172	0.238	0.292	0.086	0.144	0.360	0.187
NLVS	0.464	0.368	0.360	0.501	-0.079	0.159	0.417	0.417	0.745
NAAC	0.297	0.383	0.279	0.318	-0.037	0.237	0.256	0.475	0.828
NACA	0.268	0.313	0.199	0.537	-0.035	0.198	0.049	0.182	0.223
NACP	0.384	0.388	0.168	0.503	-0.082	0.221	0.264	0.476	0.521
NAFM	0.302	0.315	0.078	0.373	0.124	0.193	0.038	0.282	0.272
NA41	0.254	0.501	0.279	0.311	0.044	0.154	0.295	0.627	0.689
NAVS	0.142	0.345	0.043	0.360	-0.352	-0.160	0.149	0.464	0.325
NAZI	0.153	0.578	0.239	0.453	0.094	0.099	0.130	0.373	0.494
NAZS	0.177	0.200	-0.236	0.139	-0.028	0.036	0.067	0.012	0.205
BRBA	0.222	0.146	-0.025	0.290	-0.065	0.248	0.082	0.439	0.289
NALD	0.147	0.405	0.306	0.454	-0.022	0.237	0.081	0.566	0.410
DAFM	0.224	0.339	0.179	0.410	0.276	0.177	-0.011	0.346	0.308
PLSY	-0.016	0.542	0.164	0.296	0.079	0.097	-0.095	0.666	0.447
POBA	0.198	0.228	0.225	0.524	0.112	0.347	0.009	0.425	0.540
PM41	0.444	-0.001	-0.084	0.126	0.138	0.297	0.218	-0.048	0.439
41MX	0.244	0.315	0.246	0.313	-0.039	0.129	0.313	0.508	0.623
41ZI	0.146	0.289	0.079	0.162	-0.223	0.097	0.263	0.490	0.691
PTAS	0.135	0.268	0.043	0.228	-0.239	0.079	0.053	0.090	0.196
PTLD	-0.018	0.181	0.045	0.212	-0.280	0.002	-0.007	0.353	0.136
SLBA	0.174	0.317	0.321	0.208	0.162	0.500	-0.239	0.477	0.153
SLCC	0.236	0.380	0.416	0.285	0.144	0.514	-0.193	0.416	0.005
SYBA	1.000	-0.031	0.367	0.303	0.212	0.689	0.547	-0.064	0.338
SYMX	-0.031	1.000	0.427	0.414	0.214	0.012	-0.077	0.456	0.317
ZTPO	0.367	0.427	1.000	0.517	0.220	0.152	0.218	0.388	0.345
ZTVS	0.303	0.414	0.517	1.000	0.467	0.262	0.121	0.474	0.330
ZTZI	0.212	0.214	0.220	0.467	1.000	0.279	-0.039	0.033	-0.183
VSBA	0.689	0.012	0.152	0.262	0.279	1.000	-0.091	-0.075	0.362
VSSY	0.547	-0.077	0.218	0.121	-0.039	-0.091	1.000	0.095	0.243
ZIMX	-0.064	0.456	0.388	0.474	0.033	-0.075	0.095	1.000	0.463
ZSNL	0.338	0.317	0.345	0.330	-0.183	0.362	0.243	0.463	1.000

Table B2 Genetic Correlation Matrix for Model 2.

	ACPM	ACSY	PMPM	ASJP	BACC	BAOP	ASAS	JPJP	4141	POPO	PTPT	STST	ZTZT	BRAS	BRLD	BRNA	BRPT
ACPM	1.000	0.555	0.831	0.290	0.122	0.185	0.277	0.367	0.607	0.273	0.523	0.020	0.241	0.225	0.329	0.600	0.404
ACSY	0.555	1.000	-0.074	0.031	0.241	0.188	0.327	0.224	0.391	0.361	-0.033	0.013	0.298	0.300	0.233	0.241	0.073
PMPM	0.831	-0.074	1.000	-0.020	-0.065	0.448	0.121	0.140	0.659	-0.134	0.171	-0.154	0.047	0.228	0.507	0.126	-0.021
ASJP	0.290	0.031	-0.020	1.000	0.129	0.209	0.406	-0.075	0.227	0.155	0.126	-0.059	0.242	0.107	0.222	0.319	0.136
BACC	0.122	0.241	-0.065	0.129	1.000	0.040	0.498	0.512	0.232	0.552	0.103	0.013	0.501	0.191	0.094	0.275	-0.061
BAOP	0.185	0.188	0.448	0.209	0.040	1.000	0.195	0.268	0.348	0.121	0.018	-0.247	0.144	0.126	-0.039	0.113	-0.003
ASAS	0.277	0.327	0.121	0.406	0.498	0.195	1.000	0.537	0.395	0.657	-0.014	-0.155	0.545	0.546	-0.205	0.341	-0.051
JPJP	0.367	0.224	0.140	-0.075	0.512	0.268	0.537	1.000	0.161	0.390	0.068	0.119	0.272	0.057	0.043	0.251	0.095
4141	0.607	0.391	0.659	0.227	0.232	0.348	0.395	0.161	1.000	0.292	0.219	-0.043	0.492	0.429	0.135	0.456	-0.034
POPO	0.273	0.361	-0.134	0.155	0.552	0.121	0.657	0.390	0.292	1.000	0.185	0.320	0.562	0.264	-0.039	0.369	0.146
PTPT	0.523	-0.033	0.171	0.126	0.103	0.018	-0.014	0.068	0.219	0.185	1.000	0.490	0.133	0.197	0.117	0.306	0.448
STST	0.020	0.013	-0.154	-0.059	0.013	-0.247	-0.155	0.119	-0.043	0.320	0.490	1.000	-0.022	0.176	-0.048	0.254	0.518
ZTZT	0.241	0.298	0.047	0.242	0.501	0.144	0.545	0.272	0.492	0.562	0.133	-0.022	1.000	0.387	0.180	0.276	-0.189
BRAS	0.225	0.300	0.228	0.107	0.191	0.126	0.546	0.057	0.429	0.264	0.197	0.176	0.387	1.000	0.493	0.217	0.053
BRLD	0.329	0.233	0.507	0.222	0.094	-0.039	-0.205	0.043	0.135	-0.039	0.117	-0.048	0.180	0.493	1.000	-0.080	0.041
BRNA	0.600	0.241	0.126	0.319	0.275	0.113	0.341	0.251	0.456	0.369	0.306	0.254	0.276	0.217	-0.080	1.000	0.467
BRPT	0.404	0.073	-0.021	0.136	-0.061	-0.003	-0.051	0.095	-0.034	0.146	0.448	0.518	-0.189	0.053	0.041	0.467	1.000
NABA	0.512	0.620	0.344	0.428	0.458	0.101	0.455	0.156	0.350	0.278	0.062	-0.032	0.398	0.200	-0.106	0.454	0.038
CACP	0.590	0.433	0.412	0.411	-0.306	0.094	0.056	-0.247	-0.258	-0.246	-0.174	-0.122	-0.441	-0.215	0.033	0.225	0.201
CPSL	-0.195	-0.035	-0.239	-0.159	0.314	0.061	-0.160	-0.042	-0.252	0.055	0.083	0.273	0.110	-0.048	-0.191	0.186	0.218
CPZS	0.513	0.593	0.257	0.252	0.279	0.258	0.485	0.241	0.444	0.337	0.104	-0.021	0.415	0.213	0.129	0.244	-0.123
CNCN	-0.129	0.027	0.138	0.050	0.365	0.584	0.093	0.276	0.322	0.121	0.072	0.010	-0.002	-0.081	-0.203	0.108	0.188
FMPM	0.275	0.574	0.069	0.262	0.076	0.215	0.072	0.181	0.339	0.195	-0.046	-0.105	0.167	0.089	0.273	0.153	-0.051
FMZT	0.360	0.268	0.187	0.381	0.217	0.125	0.413	0.177	0.237	0.215	0.050	0.091	0.555	0.376	0.090	0.267	0.000
FMCP	0.524	0.561	0.163	0.187	0.318	0.169	0.485	0.313	0.418	0.277	0.075	-0.004	0.474	0.353	0.240	0.375	-0.023
FMPT	0.379	0.330	0.392	0.084	0.186	0.270	0.350	0.061	0.511	0.201	0.229	-0.269	0.374	0.535	0.069	0.235	-0.460
LDAS	0.095	0.332	0.185	-0.074	0.257	0.146	0.741	0.207	0.381	0.448	-0.063	-0.139	0.481	0.724	-0.119	0.188	-0.203
LDBA	0.371	0.188	0.305	0.498	0.271	0.318	0.409	-0.009	0.228	0.245	0.129	-0.076	0.334	0.426	0.336	0.456	0.027
NANL	0.345	0.636	0.109	0.234	0.080	0.241	0.296	0.262	0.258	0.311	-0.045	-0.106	0.178	0.157	0.158	-0.020	-0.214
NLAC	0.199	0.495	0.117	0.212	-0.007	0.284	0.010	0.077	0.307	0.045	0.003	-0.275	0.157	0.041	0.166	0.176	0.163
NLVS	0.512	0.779	0.113	0.099	0.285	0.032	0.372	0.357	0.248	0.293	-0.017	0.003	0.356	0.416	0.140	0.179	0.043
NAAC	0.320	0.704	-0.015	0.225	0.125	0.290	0.221	0.256	0.309	0.268	0.069	-0.110	0.277	0.255	0.261	0.077	-0.031
NACA	0.398	0.421	0.126	0.167	0.272	0.243	0.562	0.408	0.520	0.389	0.100	-0.069	0.501	0.290	-0.093	0.294	-0.114
NACP	0.709	0.665	0.382	0.370	0.298	0.157	0.572	0.281	0.434	0.333	0.005	-0.095	0.407	0.232	-0.100	0.514	0.132
NAFM	0.417	0.485	0.179	0.130	0.211	0.212	0.286	0.359	0.331	0.403	0.436	0.087	0.388	0.193	0.005	0.410	0.159
NA41	0.375	0.493	0.207	0.249	0.128	0.245	0.189	0.255	0.334	0.229	0.134	-0.017	0.214	0.114	0.159	0.247	-0.006
NAVS	0.519	0.559	0.295	0.178	0.135	0.083	0.255	0.183	0.270	0.123	0.214	0.183	0.177	0.115	-0.127	0.453	0.302
NAZI	0.370	0.537	0.198	0.241	0.229	0.180	0.464	0.324	0.297	0.340	0.214	-0.094	0.415	0.155	-0.164	0.439	0.054
NAZS	0.206	0.208	0.125	0.062	0.189	0.201	0.188	0.204	0.111	0.299	0.385	0.117	0.210	0.119	0.058	0.203	0.214
BRBA	0.373	0.261	0.125	0.611	0.290	0.089	0.215	-0.161	0.187	0.122	0.335	0.270	0.267	0.347	0.327	0.595	0.380
NALD	0.755	0.420	0.547	0.470	0.314	0.226	0.227	0.222	0.491	0.276	0.201	-0.090	0.295	0.425	0.518	0.668	0.330
DAFM	0.165	0.489	-0.091	0.125	0.062	0.084	0.099	0.113	0.158	0.238	0.328	0.130	0.375	-0.085	0.177	0.261	0.144
PLSY	0.297	0.583	-0.047	-0.058	0.033	-0.021	0.022	0.085	0.147	0.113	-0.039	0.232	0.129	0.085	0.165	0.095	-0.014
POBA	0.343	0.220	0.023	0.406	0.595	0.196	0.514	0.356	0.345	0.772	0.053	0.089	0.584	0.118	0.125	0.249	0.051
PM41	0.493	0.597	0.320	0.053	0.249	0.242	0.291	0.299	0.497	0.220	0.112	0.026	0.043	0.202	-0.126	0.060	0.130
41MX	0.245	0.483	0.116	0.046	0.141	0.262	0.014	0.196	0.361	0.185	-0.081	0.016	0.094	0.177	0.206	0.326	0.008
41ZI	1.000	1.000	0.017	0.261	0.065	1.000	-0.030	0.218	1.000	0.213	-0.036	-0.027	0.126	0.071	1.000	1.000	1.000
PTAS	0.055	-0.010	-0.191	0.478	0.138	0.160	0.181	0.107	0.131	0.036	-0.269	0.192	-0.011	0.094	0.512	0.244	0.486
PTLD	0.365	0.052	0.079	0.296	0.100	0.068	-0.134	0.124	-0.146	0.027	-0.032	0.233	-0.092	0.079	0.618	0.274	0.657
SLBA	0.458	0.384	0.580	0.441	0.210	-0.109	-0.200	-0.101	0.368	-0.105	-0.023	-0.249	0.138	-0.255	0.289	0.279	-0.073
SLCC	0.495	0.339	0.508	0.346	0.508	0.043	0.194	0.310	0.595	0.178	0.116	-0.248	0.225	-0.084	-0.135	0.382	-0.197
SYBA	0.142	0.288	0.165	0.034	0.349	0.102	0.245	0.210	0.219	0.244	-0.187	-0.061	0.323	0.374	-0.022	0.002	-0.164
SYMX	0.347	0.396	-0.030	0.024	0.142	-0.141	0.158	0.082	0.276	0.075	-0.045	0.088	0.266	0.272	0.159	0.192	-0.090
ZTPO	-0.078	0.136	-0.042	-0.123	0.199	0.187	0.078	-0.139	0.332	-0.016	-0.318	0.010	0.238	0.077	-0.071	0.111	-0.254
ZTVS	0.144	0.391	-0.097	0.040	0.425	0.046	0.467	0.214	0.420	0.437	-0.001	0.129	0.897	0.421	0.065	0.256	-0.154
ZTZI	-0.020	-0.009	-0.268	0.132	0.307	0.102	0.166	0.014	0.299	-0.028	0.058	-0.018	0.498	0.067	-0.205	0.009	-0.331
VSBA	0.122	0.273	0.144	0.283	0.501	0.045	0.375	0.066	0.183	0.339	-0.303	-0.216	0.384	0.107	0.028	-0.051	-0.319
VSSY	0.117	0.120	0.269	-0.019	-0.023	0.141	0.057	0.176	0.069	0.001	0.066	-0.042	0.019	0.391	-0.004	0.175	0.075
ZIMX	0.786	0.421	0.625	0.071	-0.058	-0.150	-0.107	-0.242	0.282	0.073	-0.009	0.163	0.153	-0.327	-0.031	0.623	0.270
ZSNL	0.481	0.681	0.257	0.306	0.158	0.199	0.395	0.387	0.364	0.348	-0.076	-0.072	0.315	0.416	0.330	0.146	-0.215

	NABA	CACP	CPSL	CPZS	CNCN	FMPM	FMZT	FMCP	FMPT	LDAS	LDBA	NANL	NLAC	NLVS	NAAC	NACA	NACP
ACPM	0.512	0.590	-0.195	0.513	-0.129	0.275	0.360	0.524	0.379	0.095	0.371	0.345	0.199	0.512	0.320	0.398	0.709
ACSY	0.620	0.433	-0.035	0.593	0.027	0.574	0.268	0.561	0.330	0.332	0.188	0.636	0.495	0.779	0.704	0.421	0.665
PMPM	0.344	0.412	-0.239	0.257	0.138	0.069	0.187	0.163	0.392	0.185	0.305	0.109	0.117	0.113	-0.015	0.126	0.382
ASJP	0.428	0.411	-0.159	0.252	0.050	0.262	0.381	0.187	0.084	-0.074	0.498	0.234	0.212	0.099	0.225	0.167	0.370
BACC	0.458	-0.306	0.314	0.279	0.365	0.076	0.217	0.318	0.186	0.257	0.271	0.080	-0.007	0.285	0.125	0.272	0.298
BAOP	0.101	0.094	0.061	0.258	0.584	0.215	0.125	0.169	0.270	0.146	0.318	0.241	0.284	0.032	0.290	0.243	0.157
ASAS	0.455	0.056	-0.160	0.485	0.093	0.072	0.413	0.485	0.350	0.741	0.409	0.296	0.010	0.372	0.221	0.562	0.572
JPJP	0.156	-0.247	-0.042	0.241	0.276	0.181	0.177	0.313	0.061	0.207	-0.009	0.262	0.077	0.357	0.256	0.408	0.281
4141	0.350	-0.258	-0.252	0.444	0.322	0.339	0.237	0.418	0.511	0.381	0.228	0.258	0.307	0.248	0.309	0.520	0.434
POPO	0.278	-0.246	0.055	0.337	0.121	0.195	0.215	0.277	0.201	0.448	0.245	0.311	0.045	0.293	0.268	0.389	0.333
PTPT	0.062	-0.174	0.083	0.104	0.072	-0.046	0.050	0.075	0.229	-0.063	0.129	-0.045	0.003	-0.017	0.069	0.100	0.005
STST	-0.032	-0.122	0.273	-0.021	0.010	-0.105	0.091	-0.004	-0.269	-0.139	-0.076	-0.106	-0.275	0.003	-0.110	-0.069	-0.095
ZTZT	0.398	-0.441	0.110	0.415	-0.002	0.167	0.555	0.474	0.374	0.481	0.334	0.178	0.157	0.356	0.277	0.501	0.407
BRAS	0.200	-0.215	-0.048	0.213	-0.081	0.089	0.376	0.353	0.535	0.724	0.426	0.157	0.041	0.416	0.255	0.290	0.232
BRLD	-0.106	0.033	-0.191	0.129	-0.203	0.273	0.090	0.240	0.069	-0.119	0.336	0.158	0.166	0.140	0.261	-0.093	-0.100
BRNA	0.454	0.225	0.186	0.244	0.108	0.153	0.267	0.375	0.235	0.188	0.456	-0.020	0.176	0.179	0.077	0.294	0.514
BRPT	0.038	0.201	0.218	-0.123	0.188	-0.051	0.000	-0.023	-0.460	-0.203	0.027	-0.214	0.163	0.043	-0.031	-0.114	0.132
NABA	1.000	0.185	0.106	0.532	0.130	0.246	0.345	0.593	0.303	0.256	0.372	0.213	0.230	0.567	0.286	0.659	0.795
CACP	0.185	1.000	0.331	0.117	-0.103	0.184	-0.066	0.087	-0.134	-0.195	0.062	0.188	0.300	0.179	0.268	-0.301	0.257
CPSL	0.106	0.331	1.000	0.095	0.314	0.225	0.097	0.019	-0.075	0.018	0.046	0.108	-0.073	0.234	0.238	-0.317	-0.048
CPZS	0.532	0.117	0.095	1.000	0.097	0.313	0.404	0.758	0.473	0.286	0.220	0.354	0.215	0.616	0.455	0.637	0.714
CNCN	0.130	-0.103	0.314	0.097	1.000	-0.086	-0.025	-0.048	-0.119	-0.079	-0.039	-0.011	-0.020	0.002	0.004	0.096	-0.017
FMPM	0.246	0.184	0.225	0.313	-0.086	1.000	0.371	0.217	0.085	0.107	0.302	0.755	0.550	0.509	0.863	0.171	0.331
FMZT	0.345	-0.066	0.097	0.404	-0.025	0.371	1.000	0.393	0.249	0.302	0.399	0.237	0.310	0.258	0.351	0.386	0.373
FMCP	0.593	0.087	0.019	0.758	-0.048	0.217	0.393	1.000	0.553	0.384	0.219	0.182	0.324	0.553	0.345	0.729	0.791
FMPT	0.303	-0.134	-0.075	0.473	-0.119	0.085	0.249	0.553	1.000	0.578	0.503	0.235	0.013	0.247	0.292	0.514	0.442
LDAS	0.256	-0.195	0.018	0.286	-0.079	0.107	0.302	0.384	0.578	1.000	0.575	0.212	-0.008	0.421	0.256	0.480	0.420
LDBA	0.372	0.062	0.046	0.220	-0.039	0.302	0.399	0.219	0.503	0.575	1.000	0.292	0.162	0.302	0.401	0.209	0.340
NANL	0.213	0.188	0.108	0.354	-0.011	0.755	0.237	0.182	0.235	0.212	0.292	1.000	0.141	0.603	0.902	0.133	0.355
NLAC	0.230	0.300	-0.073	0.215	-0.020	0.550	0.310	0.324	0.013	-0.008	0.162	0.141	1.000	0.190	0.498	0.123	0.325
NLVS	0.567	0.179	0.234	0.616	0.002	0.509	0.258	0.553	0.247	0.421	0.302	0.603	0.190	1.000	0.614	0.433	0.621
NAAC	0.286	0.268	0.238	0.455	0.004	0.863	0.351	0.345	0.292	0.256	0.401	0.902	0.498	0.614	1.000	0.228	0.463
NACA	0.659	-0.301	-0.317	0.637	0.096	0.171	0.386	0.729	0.514	0.480	0.209	0.133	0.123	0.433	0.228	1.000	0.833
NACP	0.795	0.257	-0.048	0.714	-0.017	0.331	0.373	0.791	0.442	0.420	0.340	0.355	0.325	0.621	0.463	0.833	1.000
NAFM	0.606	0.154	-0.015	0.482	0.050	0.202	0.184	0.446	0.172	0.167	0.145	0.106	0.267	0.375	0.225	0.519	0.617
NA41	0.286	0.117	0.206	0.396	-0.058	0.895	0.438	0.330	0.256	0.163	0.385	0.729	0.434	0.380	0.848	0.336	0.453
NAVS	0.727	0.034	0.134	0.438	-0.203	0.269	0.198	0.500	0.156	0.212	0.242	0.120	0.246	0.602	0.323	0.637	0.702
NAZI	0.437	-0.058	-0.049	0.481	-0.191	0.471	0.509	0.399	0.241	0.298	0.334	0.501	0.320	0.434	0.605	0.558	0.613
NAZS	0.354	-0.113	0.074	0.182	-0.024	0.141	0.183	0.219	0.203	0.158	0.194	0.233	0.121	0.111	0.305	0.481	0.382
BRBA	0.491	0.264	0.255	0.086	0.026	0.178	0.329	0.244	0.248	0.159	0.704	0.120	0.098	0.327	0.209	-0.043	0.228
NALD	0.477	0.174	-0.174	0.404	0.037	0.315	0.208	0.544	0.388	0.191	0.745	0.224	0.297	0.300	0.350	0.428	0.532
DAFM	0.498	-0.044	-0.040	0.263	0.081	0.197	0.164	0.331	0.028	-0.102	-0.105	0.149	0.304	0.358	0.231	0.338	0.323
PLSY	0.377	0.212	-0.045	0.206	-0.196	0.521	0.277	0.267	0.077	0.096	0.002	0.395	0.309	0.376	0.501	0.332	0.392
POBA	0.515	-0.015	0.066	0.128	0.089	0.260	0.240	0.248	0.208	0.257	0.514	0.449	-0.059	0.317	0.331	0.294	0.278
PM41	0.317	0.217	0.224	0.252	0.229	0.185	0.040	0.154	0.146	0.396	0.184	0.334	0.334	0.456	0.420	0.202	0.199
41MX	0.283	0.094	0.188	0.446	0.103	0.787	0.308	0.476	0.242	0.022	0.231	0.426	0.500	0.379	0.550	0.378	0.469
41ZI	0.250	0.097	1.000	0.332	1.000	1.000	0.198	0.341	0.169	1.000	1.000	0.566	1.000	1.000	1.000	0.271	1.000
PTAS	0.227	0.158	-0.174	0.067	0.235	0.250	0.211	0.067	-0.522	-0.214	-0.004	0.023	0.279	0.118	0.092	0.059	0.132
PTLD	0.045	0.078	-0.051	-0.105	0.209	0.120	-0.001	0.097	-0.443	-0.243	0.209	0.012	0.205	0.054	0.123	-0.094	-0.039
SLBA	0.653	0.081	-0.309	0.037	0.124	0.182	0.091	0.089	0.201	-0.486	0.287	0.057	0.322	0.160	0.072	0.155	0.127
SLCC	0.684	-0.084	-0.208	0.338	0.136	0.060	0.119	0.259	0.321	-0.106	0.261	-0.077	0.200	0.178	-0.041	0.422	0.378
SYBA	0.628	-0.107	0.323	0.451	0.358	0.319	0.256	0.393	0.234	0.292	0.178	0.248	0.239	0.478	0.311	0.327	0.387
SYMX	0.328	0.221	-0.428	0.232	-0.314	0.194	0.318	0.331	0.179	0.241	0.132	0.224	0.199	0.347	0.300	0.268	0.402
ZTPO	0.124	-0.243	-0.053	0.123	0.067	0.170	0.146	0.210	0.178	0.204	-0.038	0.216	0.142	0.223	0.190	0.200	0.153
ZTVS	0.335	-0.560	0.213	0.268	-0.013	0.100	0.367	0.511	0.276	0.523	0.172	0.056	0.179	0.462	0.240	0.508	0.344
ZTZI	-0.002	-0.106	0.236	0.256	0.252	0.021	0.376	0.027	0.139	0.168	0.034	-0.133	0.258	-0.168	-0.052	-0.010	-0.054
VSBA	0.602	0.030	0.064	0.199	0.350	0.220	0.221	0.076	0.183	0.127	0.118	0.366	0.024	0.200	0.238	0.209	0.224
VSSY	0.062	0.034	0.376	0.392	0.150	0.320	0.147	0.314	0.236	0.258	0.251	0.107	0.220	0.406	0.266	0.109	0.266
ZIMX	0.310	0.370	-0.122	0.211	-0.288	0.342	-0.004	0.392	0.192	0.032	0.374	0.173	0.208	0.424	0.363	0.094	0.421
ZSNL	0.438	0.355	0.281	0.410	-0.062	0.760	0.343	0.368	0.388	0.351	0.442	0.903	0.143	0.719	0.824	0.233	0.525

	NAFM	NA41	NAVS	NAZI	NAZS	BRBA	NALD	DAFM	PLSY	POBA	PM41	41MX	41ZI	PTAS	PTLD	SLBA	SLCC
ACPM	0.417	0.375	0.519	0.370	0.206	0.373	0.755	0.165	0.297	0.343	0.493	0.245	1.000	0.055	0.365	0.458	0.495
ACSY	0.485	0.493	0.559	0.537	0.208	0.261	0.420	0.489	0.583	0.220	0.597	0.483	1.000	-0.010	0.052	0.384	0.339
PMPM	0.179	0.207	0.295	0.198	0.125	0.125	0.547	-0.091	-0.047	0.023	0.320	0.116	0.017	-0.191	0.079	0.580	0.508
ASJP	0.130	0.249	0.178	0.241	0.062	0.611	0.470	0.125	-0.058	0.406	0.053	0.046	0.261	0.478	0.296	0.441	0.346
BACC	0.211	0.128	0.135	0.229	0.189	0.290	0.314	0.062	0.033	0.595	0.249	0.141	0.065	0.138	0.100	0.210	0.508
BAOP	0.212	0.245	0.083	0.180	0.201	0.089	0.226	0.084	-0.021	0.196	0.242	0.262	1.000	0.160	0.068	-0.109	0.043
ASAS	0.286	0.189	0.255	0.464	0.188	0.215	0.227	0.099	0.022	0.514	0.291	0.014	-0.030	0.181	-0.134	-0.200	0.194
JPJP	0.359	0.255	0.183	0.324	0.204	-0.161	0.222	0.113	0.085	0.356	0.299	0.196	0.218	0.107	0.124	-0.101	0.310
4141	0.331	0.334	0.270	0.297	0.111	0.187	0.491	0.158	0.147	0.345	0.497	0.361	1.000	0.131	-0.146	0.368	0.595
POPO	0.403	0.229	0.123	0.340	0.299	0.122	0.276	0.238	0.113	0.772	0.220	0.185	0.213	0.036	0.027	-0.105	0.178
PTPT	0.436	0.134	0.214	0.214	0.385	0.335	0.201	0.328	-0.039	0.053	0.112	-0.081	-0.036	-0.269	-0.032	-0.023	0.116
STST	0.087	-0.017	0.183	-0.094	0.117	0.270	-0.090	0.130	0.232	0.089	0.026	0.016	-0.027	0.192	0.233	-0.249	-0.248
ZTZT	0.388	0.214	0.177	0.415	0.210	0.267	0.295	0.375	0.129	0.584	0.043	0.094	0.126	-0.011	-0.092	0.138	0.225
BRAS	0.193	0.114	0.115	0.155	0.119	0.347	0.425	-0.085	0.085	0.118	0.202	0.177	0.071	0.094	0.079	-0.255	-0.084
BRLD	0.005	0.159	-0.127	-0.164	0.058	0.327	0.518	0.177	0.165	0.125	-0.126	0.206	1.000	0.512	0.618	0.289	-0.135
BRNA	0.410	0.247	0.453	0.439	0.203	0.595	0.668	0.261	0.095	0.249	0.060	0.326	1.000	0.244	0.274	0.279	0.382
BRPT	0.159	-0.006	0.302	0.054	0.214	0.380	0.330	0.144	-0.014	0.051	0.130	0.008	1.000	0.486	0.657	-0.073	-0.197
NABA	0.606	0.286	0.727	0.437	0.354	0.491	0.477	0.498	0.377	0.515	0.317	0.283	0.250	0.227	0.045	0.653	0.684
CACP	0.154	0.117	0.034	-0.058	-0.113	0.264	0.174	-0.044	0.212	-0.015	0.217	0.094	0.097	0.158	0.078	0.081	-0.084
CPSL	-0.015	0.206	0.134	-0.049	0.074	0.255	-0.174	-0.040	-0.045	0.066	0.224	0.188	1.000	-0.174	-0.051	-0.309	-0.208
CPZS	0.482	0.396	0.438	0.481	0.182	0.086	0.404	0.263	0.206	0.128	0.252	0.446	0.332	0.067	-0.105	0.037	0.338
CNCN	0.050	-0.058	-0.203	-0.191	-0.024	0.026	0.037	0.081	-0.196	0.089	0.229	0.103	1.000	0.235	0.209	0.124	0.136
FMPM	0.202	0.895	0.269	0.471	0.141	0.178	0.315	0.197	0.521	0.260	0.185	0.787	1.000	0.250	0.120	0.182	0.060
FMZT	0.184	0.438	0.198	0.509	0.183	0.329	0.208	0.164	0.277	0.240	0.040	0.308	0.198	0.211	-0.001	0.091	0.119
FMCP	0.446	0.330	0.500	0.399	0.219	0.244	0.544	0.331	0.267	0.248	0.154	0.476	0.341	0.067	0.097	0.089	0.259
FMPT	0.172	0.256	0.156	0.241	0.203	0.248	0.388	0.028	0.077	0.208	0.146	0.242	0.169	-0.522	-0.443	0.201	0.321
LDAS	0.167	0.163	0.212	0.298	0.158	0.159	0.191	-0.102	0.096	0.257	0.396	0.022	1.000	-0.214	-0.243	-0.486	-0.106
LDBA	0.145	0.385	0.242	0.334	0.194	0.704	0.745	-0.105	0.002	0.514	0.184	0.231	1.000	-0.004	0.209	0.287	0.261
NANL	0.106	0.729	0.120	0.501	0.233	0.120	0.224	0.149	0.395	0.449	0.334	0.426	0.566	0.023	0.012	0.057	-0.077
NLAC	0.267	0.434	0.246	0.320	0.121	0.098	0.297	0.304	0.309	-0.059	0.334	0.500	1.000	0.279	0.205	0.322	0.200
NLVS	0.375	0.380	0.602	0.434	0.111	0.327	0.300	0.358	0.376	0.317	0.456	0.379	1.000	0.118	0.054	0.160	0.178
NAAC	0.225	0.848	0.323	0.605	0.305	0.209	0.350	0.231	0.501	0.331	0.420	0.550	1.000	0.092	0.123	0.072	-0.041
NACA	0.519	0.336	0.637	0.558	0.481	-0.043	0.428	0.338	0.332	0.294	0.202	0.378	0.271	0.059	-0.094	0.155	0.422
NACP	0.617	0.453	0.702	0.613	0.382	0.228	0.532	0.323	0.392	0.278	0.199	0.469	1.000	0.132	-0.039	0.127	0.378
NAFM	1.000	0.321	0.614	0.566	0.509	0.187	0.362	0.896	0.368	0.341	0.259	0.332	0.290	0.091	0.004	0.292	0.408
NA41	0.321	1.000	0.346	0.698	0.357	0.170	0.428	0.247	0.510	0.284	0.076	0.740	0.783	0.159	0.128	0.046	0.002
NAVS	0.614	0.346	1.000	0.518	0.491	0.295	0.362	0.499	0.441	0.299	0.187	0.365	1.000	0.029	0.082	0.246	0.259
NAZI	0.566	0.698	0.518	1.000	0.512	0.089	0.330	0.427	0.430	0.334	0.129	0.471	0.390	0.124	-0.053	0.088	0.266
NAZS	0.509	0.357	0.491	0.512	1.000	0.055	0.270	0.330	0.120	0.136	0.080	0.198	0.304	-0.045	0.111	-0.152	-0.063
BRBA	0.187	0.170	0.295	0.089	0.055	1.000	0.595	0.051	0.138	0.432	0.053	0.251	0.292	0.166	0.292	0.494	0.252
NALD	0.362	0.428	0.362	0.330	0.270	0.595	1.000	0.283	0.163	0.411	0.100	0.391	0.461	0.497	0.603	0.484	0.397
DAFM	0.896	0.247	0.499	0.427	0.330	0.051	0.283	1.000	0.435	0.148	0.119	0.241	1.000	0.080	0.077	0.237	0.278
PLSY	0.368	0.510	0.441	0.430	0.120	0.138	0.163	0.435	1.000	0.074	0.145	0.351	0.410	0.053	0.020	0.244	0.160
POBA	0.341	0.284	0.299	0.334	0.136	0.432	0.411	0.148	0.074	1.000	0.177	0.190	1.000	0.154	0.167	0.229	0.363
PM41	0.259	0.076	0.187	0.129	0.080	0.053	0.100	0.119	0.145	0.177	1.000	0.030	-0.154	-0.110	0.028	0.024	0.288
41MX	0.332	0.740	0.365	0.471	0.198	0.251	0.391	0.241	0.351	0.190	0.030	1.000	0.823	0.232	0.107	0.068	-0.018
41ZI	0.290	0.783	1.000	0.390	0.304	0.292	0.461	1.000	0.410	1.000	-0.154	0.823	1.000	0.329	0.185	1.000	-0.102
PTAS	0.091	0.159	0.029	0.124	-0.045	0.166	0.497	0.080	0.053	0.154	-0.110	0.232	0.329	1.000	0.904	0.360	0.216
PTLD	0.004	0.128	0.082	-0.053	0.111	0.292	0.603	0.077	0.020	0.167	0.028	0.107	0.185	0.904	1.000	0.163	-0.135
SLBA	0.292	0.046	0.246	0.088	-0.152	0.494	0.484	0.237	0.244	0.229	0.024	0.068	1.000	0.360	0.163	1.000	0.719
SLCC	0.408	0.002	0.259	0.266	-0.063	0.252	0.397	0.278	0.160	0.363	0.288	-0.018	-0.102	0.216	-0.135	0.719	1.000
SYBA	0.302	0.253	0.176	0.182	0.167	0.265	0.117	0.157	-0.007	0.183	0.449	0.193	0.096	0.193	-0.094	0.189	0.275
SYMX	0.283	0.421	0.326	0.550	0.138	0.203	0.311	0.299	0.474	0.096	-0.060	0.217	0.249	0.200	0.046	0.302	0.319
ZTPO	-0.017	0.140	-0.003	0.125	-0.268	-0.114	0.158	0.112	0.060	-0.032	-0.177	0.138	0.009	-0.040	-0.055	0.167	0.310
ZTVS	0.293	0.111	0.339	0.329	0.094	0.204	0.209	0.301	0.202	0.334	0.071	0.078	-0.027	-0.017	-0.102	-0.087	0.050
ZTZI	-0.027	-0.022	-0.438	0.076	-0.082	-0.020	-0.212	0.151	-0.060	-0.027	0.005	-0.191	-0.319	-0.266	-0.369	0.072	0.046
VSBA	0.188	0.130	-0.128	0.122	0.044	0.252	0.177	0.104	0.079	0.385	0.269	0.032	1.000	0.130	-0.108	0.491	0.516
VSSY	0.047	0.291	0.147	0.144	0.078	0.133	0.105	-0.023	-0.119	-0.030	0.229	0.338	0.272	0.058	-0.027	-0.247	-0.172
ZIMX	0.259	0.462	0.548	0.192	-0.202	0.379	0.492	0.236	0.768	-0.009	-0.123	0.385	0.304	-0.134	0.063	0.378	0.268
ZSNL	0.229	0.667	0.309	0.485	0.203	0.369	0.371	0.193	0.395	0.486	0.402	0.547	1.000	0.129	-0.034	0.110	-0.014

	SYBA	SYMX	ZTPO	ZTVS	ZTZI	VSBA	VSSY	ZIMX	ZSNL
ACPM	0.142	0.347	-0.078	0.144	-0.020	0.122	0.117	0.786	0.481
ACSY	0.288	0.396	0.136	0.391	-0.009	0.273	0.120	0.421	0.681
PMPM	0.165	-0.030	-0.042	-0.097	-0.268	0.144	0.269	0.625	0.257
ASJP	0.034	0.024	-0.123	0.040	0.132	0.283	-0.019	0.071	0.306
BACC	0.349	0.142	0.199	0.425	0.307	0.501	-0.023	-0.058	0.158
BAOP	0.102	-0.141	0.187	0.046	0.102	0.045	0.141	-0.150	0.199
ASAS	0.245	0.158	0.078	0.467	0.166	0.375	0.057	-0.107	0.395
JPJP	0.210	0.082	-0.139	0.214	0.014	0.066	0.176	-0.242	0.387
4141	0.219	0.276	0.332	0.420	0.299	0.183	0.069	0.282	0.364
POPO	0.244	0.075	-0.016	0.437	-0.028	0.339	0.001	0.073	0.348
PTPT	-0.187	-0.045	-0.318	-0.001	0.058	-0.303	0.066	-0.009	-0.076
STST	-0.061	0.088	0.010	0.129	-0.018	-0.216	-0.042	0.163	-0.072
ZTZT	0.323	0.266	0.238	0.897	0.498	0.384	0.019	0.153	0.315
BRAS	0.374	0.272	0.077	0.421	0.067	0.107	0.391	-0.327	0.416
BRLD	-0.022	0.159	-0.071	0.065	-0.205	0.028	-0.004	-0.031	0.330
BRNA	0.002	0.192	0.111	0.256	0.009	-0.051	0.175	0.623	0.146
BRPT	-0.164	-0.090	-0.254	-0.154	-0.331	-0.319	0.075	0.270	-0.215
NABA	0.628	0.328	0.124	0.335	-0.002	0.602	0.062	0.310	0.438
CACP	-0.107	0.221	-0.243	-0.560	-0.106	0.030	0.034	0.370	0.355
CPSL	0.323	-0.428	-0.053	0.213	0.236	0.064	0.376	-0.122	0.281
CPZS	0.451	0.232	0.123	0.268	0.256	0.199	0.392	0.211	0.410
CNCN	0.358	-0.314	0.067	-0.013	0.252	0.350	0.150	-0.288	-0.062
FMPM	0.319	0.194	0.170	0.100	0.021	0.220	0.320	0.342	0.760
FMZT	0.256	0.318	0.146	0.367	0.376	0.221	0.147	-0.004	0.343
FMCP	0.393	0.331	0.210	0.511	0.027	0.076	0.314	0.392	0.368
FMPT	0.234	0.179	0.178	0.276	0.139	0.183	0.236	0.192	0.388
LDAS	0.292	0.241	0.204	0.523	0.168	0.127	0.258	0.032	0.351
LDBA	0.178	0.132	-0.038	0.172	0.034	0.118	0.251	0.374	0.442
NANL	0.248	0.224	0.216	0.056	-0.133	0.366	0.107	0.173	0.903
NLAC	0.239	0.199	0.142	0.179	0.258	0.024	0.220	0.208	0.143
NLVS	0.478	0.347	0.223	0.462	-0.168	0.200	0.406	0.424	0.719
NAAC	0.311	0.300	0.190	0.240	-0.052	0.238	0.266	0.363	0.824
NACA	0.327	0.268	0.200	0.508	-0.010	0.209	0.109	0.094	0.233
NACP	0.387	0.402	0.153	0.344	-0.054	0.224	0.266	0.421	0.525
NAFM	0.302	0.283	-0.017	0.293	-0.027	0.188	0.047	0.259	0.229
NA41	0.253	0.421	0.140	0.111	-0.022	0.130	0.291	0.462	0.667
NAVS	0.176	0.326	-0.003	0.339	-0.438	-0.128	0.147	0.548	0.309
NAZI	0.182	0.550	0.125	0.329	0.076	0.122	0.144	0.192	0.485
NAZS	0.167	0.138	-0.268	0.094	-0.082	0.044	0.078	-0.202	0.203
BRBA	0.265	0.203	-0.114	0.204	-0.020	0.252	0.133	0.379	0.369
NALD	0.117	0.311	0.158	0.209	-0.212	0.177	0.105	0.492	0.371
DAFM	0.157	0.299	0.112	0.301	0.151	0.104	-0.023	0.236	0.193
PLSY	-0.007	0.474	0.060	0.202	-0.060	0.079	-0.119	0.768	0.395
POBA	0.183	0.096	-0.032	0.334	-0.027	0.385	-0.030	-0.009	0.486
PM41	0.449	-0.060	-0.177	0.071	0.005	0.269	0.229	-0.123	0.402
41MX	0.193	0.217	0.138	0.078	-0.191	0.032	0.338	0.385	0.547
41ZI	0.096	0.249	0.009	-0.027	-0.319	1.000	0.272	0.304	1.000
PTAS	0.193	0.200	-0.040	-0.017	-0.266	0.130	0.058	-0.134	0.129
PTLD	-0.094	0.046	-0.055	-0.102	-0.369	-0.108	-0.027	0.063	-0.034
SLBA	0.189	0.302	0.167	-0.087	0.072	0.491	-0.247	0.378	0.110
SLCC	0.275	0.319	0.310	0.050	0.046	0.516	-0.172	0.268	-0.014
SYBA	1.000	0.030	0.372	0.265	0.224	0.692	0.551	-0.275	0.342
SYMX	0.030	1.000	0.292	0.351	0.115	0.024	-0.051	0.542	0.233
ZTPO	0.372	0.292	1.000	0.377	0.317	0.071	0.250	0.281	0.266
ZTVS	0.265	0.351	0.377	1.000	0.391	0.137	0.104	0.165	0.211
ZTZI	0.224	0.115	0.317	0.391	1.000	0.290	-0.010	-0.234	-0.184
VSBA	0.692	0.024	0.071	0.137	0.290	1.000	-0.086	-0.319	0.424
VSSY	0.551	-0.051	0.250	0.104	-0.010	-0.086	1.000	-0.064	0.245
ZIMX	-0.275	0.542	0.281	0.165	-0.234	-0.319	-0.064	1.000	0.350
ZSNL	0.342	0.233	0.266	0.211	-0.184	0.424	0.245	0.350	1.000

Table B3 Genetic Correlation Matrix for Model 3.

	ACPM	ACSY	PMPM	ASJP	BACC	BAOP	ASAS	JPJP	4141	POPO	PTPT	STST	ZTZT	BRAS	BRLD	BRNA	BRPT
ACPM	1.000	0.108	0.751	0.171	-0.206	0.005	-0.084	0.142	0.304	-0.218	0.487	-0.018	-0.138	-0.138	0.246	0.426	0.437
ACSY	0.108	1.000	-0.466	-0.324	-0.313	-0.091	-0.218	-0.173	-0.182	-0.197	-0.289	-0.086	-0.349	-0.239	0.068	-0.202	0.039
PMPM	0.751	-0.466	1.000	-0.064	-0.153	0.339	-0.051	-0.015	0.568	-0.376	0.180	-0.248	-0.109	0.167	0.499	0.002	0.000
ASJP	0.171	-0.324	-0.064	1.000	0.008	0.128	0.286	-0.231	0.022	-0.065	0.084	-0.072	0.098	-0.031	0.188	0.216	0.139
BACC	-0.206	-0.313	-0.153	0.008	1.000	-0.088	0.324	0.411	-0.016	0.465	0.044	-0.018	0.356	0.000	0.017	0.059	-0.082
BAOP	0.005	-0.091	0.339	0.128	-0.088	1.000	0.048	0.195	0.272	-0.025	-0.058	-0.246	-0.037	-0.041	-0.112	0.005	-0.026
ASAS	-0.084	-0.218	-0.051	0.286	0.324	0.048	1.000	0.410	0.061	0.473	-0.126	-0.199	0.335	0.379	-0.380	0.088	-0.091
JPJP	0.142	-0.173	-0.015	-0.231	0.411	0.195	0.410	1.000	-0.054	0.245	-0.005	0.127	0.058	-0.113	-0.049	0.071	0.082
4141	0.304	-0.182	0.568	0.022	-0.016	0.272	0.061	-0.054	1.000	0.010	0.109	-0.092	0.215	0.197	0.003	0.213	-0.095
POPO	-0.218	-0.197	-0.376	-0.065	0.465	-0.025	0.473	0.245	0.010	1.000	0.094	0.326	0.332	-0.016	-0.297	0.151	0.181
PTPT	0.487	-0.289	0.180	0.084	0.044	-0.058	-0.126	-0.005	0.109	0.094	1.000	0.457	0.048	0.167	0.106	0.244	0.447
STST	-0.018	-0.086	-0.248	-0.072	-0.018	-0.246	-0.199	0.127	-0.092	0.326	0.457	1.000	-0.060	0.167	-0.069	0.253	0.507
ZTZT	-0.138	-0.349	-0.109	0.098	0.356	-0.037	0.335	0.058	0.215	0.332	0.048	-0.060	1.000	0.137	0.092	-0.008	-0.242
BRAS	-0.138	-0.239	0.167	-0.031	0.000	-0.041	0.379	-0.113	0.197	-0.016	0.167	0.167	0.137	1.000	0.474	0.003	0.070
BRLD	0.246	0.068	0.499	0.188	0.017	-0.112	-0.380	-0.049	0.003	-0.297	0.106	-0.069	0.092	0.474	1.000	-0.168	0.057
BRNA	0.426	-0.202	0.002	0.216	0.059	0.005	0.088	0.071	0.213	0.151	0.244	0.253	-0.008	0.003	-0.168	1.000	0.521
BRPT	0.437	0.039	0.000	0.139	-0.082	-0.026	-0.091	0.082	-0.095	0.181	0.447	0.507	-0.242	0.070	0.057	0.521	1.000
NABA	0.103	-0.002	0.176	0.265	0.221	-0.137	0.003	-0.214	-0.170	-0.199	-0.077	-0.098	-0.031	-0.302	-0.274	0.132	0.018
CACP	0.602	0.473	0.494	0.397	-0.294	0.012	0.015	-0.301	-0.325	-0.290	-0.119	-0.155	-0.493	-0.201	0.060	0.203	0.220
CPSL	-0.302	-0.220	-0.330	-0.191	0.279	0.023	-0.265	-0.096	-0.389	-0.081	0.056	0.268	0.050	-0.107	-0.207	0.116	0.222
CPZS	0.149	0.028	0.070	0.083	0.001	0.083	0.122	-0.006	0.065	-0.011	0.034	-0.095	0.073	-0.183	0.003	-0.080	-0.160
CNCN	-0.190	-0.167	0.207	0.042	0.377	0.538	0.053	0.259	0.354	0.125	0.092	-0.015	-0.054	-0.113	-0.172	0.085	0.202
FMPM	-0.165	0.135	-0.059	0.074	-0.252	0.006	-0.399	-0.105	-0.092	-0.218	-0.179	-0.194	-0.326	-0.238	0.175	-0.229	-0.077
FMZT	0.062	-0.239	0.004	0.268	-0.004	-0.006	0.199	-0.020	-0.128	-0.055	-0.039	0.082	0.380	0.181	-0.007	0.040	-0.020
FMCP	0.195	-0.091	-0.024	-0.008	0.049	-0.011	0.157	0.085	-0.013	-0.164	-0.019	-0.086	0.172	0.010	0.146	0.056	-0.061
FMPT	0.096	-0.186	0.205	-0.085	-0.026	0.189	0.111	-0.116	0.353	-0.077	0.148	-0.319	0.104	0.345	-0.069	0.023	-0.542
LDAS	-0.272	-0.144	0.082	-0.270	0.049	0.016	0.650	0.037	0.114	0.230	-0.142	-0.187	0.248	0.630	-0.250	-0.029	-0.218
LDBA	0.145	-0.442	0.210	0.423	0.088	0.224	0.209	-0.211	-0.044	-0.031	0.089	-0.104	0.125	0.242	0.285	0.302	0.031
NANL	-0.101	0.255	-0.106	0.059	-0.257	0.098	-0.072	0.043	-0.173	-0.005	-0.159	-0.204	-0.235	-0.172	0.027	-0.408	-0.286
NLAC	-0.003	0.326	0.055	0.113	-0.178	0.188	-0.282	-0.101	0.035	-0.208	-0.075	-0.296	-0.106	-0.135	0.115	-0.019	0.147
NLVS	0.114	0.423	-0.284	-0.225	-0.087	-0.173	-0.104	0.146	-0.327	-0.145	-0.209	-0.016	-0.123	0.048	-0.055	-0.249	-0.002
NAAC	-0.195	0.326	-0.337	0.015	-0.292	0.164	-0.256	-0.029	-0.202	-0.197	-0.122	-0.188	-0.266	-0.175	0.121	-0.357	-0.097
NACA	-0.102	-0.323	-0.178	-0.111	-0.015	0.084	0.249	0.225	0.188	0.026	-0.025	-0.120	0.156	-0.117	-0.414	-0.013	-0.156
NACP	0.460	0.032	0.263	0.220	-0.106	-0.030	0.265	-0.023	-0.033	-0.127	-0.145	-0.221	-0.105	-0.323	-0.401	0.278	0.136
NAFM	0.042	-0.042	-0.017	-0.118	-0.093	0.056	-0.116	0.173	-0.054	0.090	0.408	0.087	0.023	-0.168	-0.155	0.139	0.165
NA41	-0.105	-0.105	-0.049	0.036	-0.246	0.057	-0.294	-0.022	-0.121	-0.231	0.029	-0.065	-0.312	-0.266	0.041	-0.112	-0.031
NAVS	0.186	0.092	0.131	-0.028	-0.194	-0.111	-0.290	-0.085	-0.174	-0.302	0.158	0.175	-0.305	-0.282	-0.273	0.217	0.354
NAZI	-0.077	-0.078	-0.060	0.040	-0.102	-0.014	0.111	0.097	-0.170	-0.095	0.121	-0.155	0.028	-0.256	-0.337	0.162	0.030
NAZS	-0.076	-0.177	0.019	-0.081	0.003	0.095	-0.095	0.068	-0.194	0.077	0.359	0.106	-0.054	-0.120	-0.039	0.008	0.226
BRBA	0.164	-0.190	0.036	0.548	0.140	-0.037	-0.057	-0.343	-0.098	-0.117	0.297	0.281	0.073	0.189	0.266	0.487	0.403
NALD	0.613	-0.252	0.469	0.389	0.057	0.029	-0.258	-0.041	0.146	-0.225	0.151	-0.150	-0.078	0.177	0.577	0.551	0.410
DAFM	-0.175	0.192	-0.179	-0.063	-0.169	-0.071	-0.269	-0.096	-0.178	-0.006	0.271	0.117	0.092	-0.357	0.090	0.003	0.142
PLSY	-0.050	0.293	-0.244	-0.264	-0.255	-0.207	-0.375	-0.113	-0.231	-0.251	-0.162	0.221	-0.276	-0.215	0.074	-0.162	-0.036
POBA	-0.039	-0.411	-0.012	0.269	0.466	0.017	0.237	0.161	-0.024	0.670	-0.028	0.050	0.373	-0.144	0.041	-0.022	0.055
PM41	0.233	0.329	0.247	-0.085	0.077	0.090	0.043	0.131	0.286	-0.047	0.036	-0.029	-0.319	0.005	-0.195	-0.193	0.144
41MX	-0.169	0.071	-0.090	-0.187	-0.173	0.102	-0.383	-0.042	0.011	-0.176	-0.204	-0.034	-0.331	-0.126	0.104	0.044	-0.037
41ZI	-0.057	-0.022	-0.132	0.093	-0.253	-0.009	-0.408	-0.007	-0.237	-0.077	-0.119	-0.067	-0.252	-0.206	0.464	-0.098	0.004
PTAS	-0.031	-0.229	-0.058	0.437	0.084	0.046	0.073	0.032	-0.030	-0.074	-0.253	0.159	-0.094	0.069	0.498	0.177	0.482
PTLD	0.340	-0.034	0.197	0.263	0.068	-0.017	-0.209	0.072	-0.240	-0.058	-0.007	0.175	-0.134	0.096	0.623	0.231	0.654
SLBA	0.393	0.191	0.590	0.392	0.131	-0.173	-0.361	-0.236	0.237	-0.259	-0.047	-0.254	-0.013	-0.365	0.261	0.169	-0.074
SLCC	0.348	-0.114	0.468	0.272	0.437	-0.051	0.022	0.189	0.458	0.021	0.066	-0.261	0.015	-0.246	-0.153	0.228	-0.198
SYBA	-0.262	-0.142	-0.032	-0.141	0.181	0.045	-0.023	0.071	-0.066	0.033	-0.324	-0.091	0.035	0.169	-0.140	-0.290	-0.222
SYMX	0.087	0.055	-0.176	-0.128	-0.075	-0.330	-0.138	-0.098	-0.003	-0.251	-0.127	0.063	-0.001	0.069	0.093	0.001	-0.103
ZTPO	-0.264	-0.232	0.025	-0.168	0.118	0.043	-0.133	-0.297	0.204	-0.214	-0.320	-0.061	0.100	-0.029	-0.038	-0.036	-0.262
ZTVS	-0.316	-0.098	-0.188	-0.166	0.235	-0.168	0.183	-0.040	0.119	0.213	-0.089	0.109	0.829	0.220	-0.018	-0.049	-0.158
ZTZI	-0.083	-0.139	-0.144	0.143	0.312	0.050	0.135	-0.026	0.250	-0.073	0.076	-0.043	0.580	0.077	-0.198	-0.047	-0.306
VSBA	-0.167	-0.048	0.042	0.195	0.414	-0.015	0.225	-0.062	0.001	0.214	-0.385	-0.251	0.243	-0.097	-0.055	-0.266	-0.356
VSSY	-0.057	-0.177	0.131	-0.107	-0.155	0.099	-0.128	0.083	-0.120	-0.177	0.006	-0.054	-0.172	0.295	-0.068	0.050	0.059
ZIMX	0.698	0.181	0.622	0.032	-0.214	-0.334	-0.423	-0.496	-0.069	-0.247	-0.019	0.069	-0.129	-0.520	0.007	0.400	0.314
ZSNL	0.009	0.131	-0.042	0.137	-0.300	0.060	-0.050	0.122	-0.147	-0.040	-0.281	-0.216	-0.203	0.046	0.235	-0.312	-0.313

	NABA	CACP	CPSL	CPZS	CNCN	FMPM	FMZT	FMCP	FMPT	LDAS	LDBA	NANL	NLAC	NLVS	NAAC	NACA	NACP
ACPM	0.103	0.602	-0.302	0.149	-0.190	-0.165	0.062	0.195	0.096	-0.272	0.145	-0.101	-0.003	0.114	-0.195	-0.102	0.460
ACSY	-0.002	0.473	-0.220	0.028	-0.167	0.135	-0.239	-0.091	-0.186	-0.144	-0.442	0.255	0.326	0.423	0.326	-0.323	0.032
PMPM	0.176	0.494	-0.330	0.070	0.207	-0.059	0.004	-0.024	0.205	0.082	0.210	-0.106	0.055	-0.284	-0.337	-0.178	0.263
ASJP	0.265	0.397	-0.191	0.083	0.042	0.074	0.268	-0.008	-0.085	-0.270	0.423	0.059	0.113	-0.225	0.015	-0.111	0.220
BACC	0.221	-0.294	0.279	0.001	0.377	-0.252	-0.004	0.049	-0.026	0.049	0.088	-0.257	-0.178	-0.087	-0.292	-0.015	-0.106
BAOP	-0.137	0.012	0.023	0.083	0.538	0.006	-0.006	-0.011	0.189	0.016	0.224	0.098	0.188	-0.173	0.164	0.084	-0.030
ASAS	0.003	0.015	-0.265	0.122	0.053	-0.399	0.199	0.157	0.111	0.650	0.209	-0.072	-0.282	-0.104	-0.256	0.249	0.265
JPJP	-0.214	-0.301	-0.096	-0.006	0.259	-0.105	-0.020	0.085	-0.116	0.037	-0.211	0.043	-0.101	0.146	-0.029	0.225	-0.023
4141	-0.170	-0.325	-0.389	0.065	0.354	-0.092	-0.128	-0.013	0.353	0.114	-0.044	-0.173	0.035	-0.327	-0.202	0.188	-0.033
POPO	-0.199	-0.290	-0.081	-0.011	0.125	-0.218	-0.055	-0.164	-0.077	0.230	-0.031	-0.005	-0.208	-0.145	-0.197	0.026	-0.127
PTPT	-0.077	-0.119	0.056	0.034	0.092	-0.179	-0.039	-0.019	0.148	-0.142	0.089	-0.159	-0.075	-0.209	-0.122	-0.025	-0.145
STST	-0.098	-0.155	0.268	-0.095	-0.015	-0.194	0.082	-0.086	-0.319	-0.187	-0.104	-0.204	-0.296	-0.016	-0.188	-0.120	-0.221
ZTZT	-0.031	-0.493	0.050	0.073	-0.054	-0.326	0.380	0.172	0.104	0.248	0.125	-0.235	-0.106	-0.123	-0.266	0.156	-0.105
BRAS	-0.302	-0.201	-0.107	-0.183	-0.113	-0.238	0.181	0.010	0.345	0.630	0.242	-0.172	-0.135	0.048	-0.175	-0.117	-0.323
BRLD	-0.274	0.060	-0.207	0.003	-0.172	0.175	-0.007	0.146	-0.069	-0.250	0.285	0.027	0.115	-0.055	0.121	-0.414	-0.401
BRNA	0.132	0.203	0.116	-0.080	0.085	-0.229	0.040	0.056	0.023	-0.029	0.302	-0.408	-0.019	-0.249	-0.357	-0.013	0.278
BRPT	0.018	0.220	0.222	-0.160	0.202	-0.077	-0.020	-0.061	-0.542	-0.218	0.031	-0.286	0.147	-0.002	-0.097	-0.156	0.136
NABA	1.000	0.228	0.034	0.097	0.133	-0.414	-0.048	0.181	-0.076	-0.258	0.061	-0.380	-0.149	0.052	-0.468	0.270	0.523
CACP	0.228	1.000	0.338	0.107	-0.045	0.204	-0.102	0.120	-0.204	-0.237	0.072	0.148	0.277	0.126	0.201	-0.514	0.307
CPSL	0.034	0.338	1.000	-0.006	0.297	0.172	0.043	-0.055	-0.151	-0.048	-0.009	0.040	-0.121	0.194	0.179	-0.519	-0.295
CPZS	0.097	0.107	-0.006	1.000	0.140	-0.193	0.102	0.596	0.219	-0.109	-0.068	-0.062	-0.055	0.248	-0.104	0.316	0.447
CNCN	0.133	-0.045	0.297	0.140	1.000	-0.078	-0.080	-0.104	-0.195	-0.123	-0.076	-0.007	-0.023	-0.085	-0.091	0.047	-0.105
FMPM	-0.414	0.204	0.172	-0.193	-0.078	1.000	0.045	-0.445	-0.308	-0.308	-0.012	0.584	0.393	0.022	0.720	-0.497	-0.424
FMZT	-0.048	-0.102	0.043	0.102	-0.080	0.045	1.000	0.082	0.036	0.088	0.225	-0.061	0.085	-0.146	-0.010	0.047	-0.027
FMCP	0.181	0.120	-0.055	0.596	-0.104	-0.445	0.082	1.000	0.335	-0.004	-0.076	-0.379	0.033	0.119	-0.378	0.473	0.596
FMPT	-0.076	-0.204	-0.151	0.219	-0.195	-0.308	0.036	0.335	1.000	0.437	0.358	-0.059	-0.218	-0.119	-0.085	0.286	0.165
LDAS	-0.258	-0.237	-0.048	-0.109	-0.123	-0.308	0.088	-0.004	0.437	1.000	0.421	-0.120	-0.243	0.050	-0.192	0.189	-0.002
LDBA	0.061	0.072	-0.009	-0.068	-0.076	-0.012	0.225	-0.076	0.358	0.421	1.000	0.046	-0.043	-0.017	0.042	-0.142	0.042
NANL	-0.380	0.148	0.040	-0.062	-0.007	0.584	-0.061	-0.379	-0.059	-0.120	0.046	1.000	-0.136	0.266	0.819	-0.474	-0.397
NLAC	-0.149	0.277	-0.121	-0.055	-0.023	0.393	0.085	0.033	-0.218	-0.243	-0.043	-0.136	1.000	-0.200	0.353	-0.259	-0.073
NLVS	0.052	0.126	0.194	0.248	-0.085	0.022	-0.146	0.119	-0.119	0.050	-0.017	0.266	-0.200	1.000	0.178	-0.143	0.096
NAAC	-0.468	0.201	0.179	-0.104	-0.091	0.720	-0.010	-0.378	-0.085	-0.192	0.042	0.819	0.353	0.178	1.000	-0.498	-0.348
NACA	0.270	-0.514	-0.519	0.316	0.047	-0.497	0.047	0.473	0.286	0.189	-0.142	-0.474	-0.259	-0.143	-0.498	1.000	0.637
NACP	0.523	0.307	-0.295	0.447	-0.105	-0.424	-0.027	0.596	0.165	-0.002	0.042	-0.397	-0.073	0.096	-0.348	0.637	1.000
NAFM	0.290	0.161	-0.100	0.137	0.009	-0.344	-0.210	0.064	-0.189	-0.225	-0.198	-0.377	-0.023	-0.121	-0.382	0.162	0.308
NA41	-0.417	0.119	0.153	-0.125	-0.110	0.806	0.133	-0.347	-0.088	-0.277	0.063	0.535	0.216	-0.293	0.707	-0.300	-0.250
NAVS	0.483	0.067	0.076	0.056	-0.259	-0.264	-0.166	0.149	-0.214	-0.196	-0.045	-0.448	-0.044	0.250	-0.279	0.336	0.476
NAZI	-0.139	-0.098	-0.151	0.029	-0.307	0.040	0.275	-0.109	-0.106	-0.105	0.045	0.129	0.029	-0.112	0.226	0.172	0.213
NAZS	0.089	-0.146	0.031	-0.113	-0.055	-0.185	-0.030	-0.066	0.005	-0.076	0.014	-0.021	-0.061	-0.245	0.035	0.308	0.158
BRBA	0.307	0.253	0.219	-0.212	-0.003	-0.123	0.159	-0.029	0.067	-0.078	0.638	-0.188	-0.054	0.048	-0.165	-0.428	-0.123
NALD	0.067	0.242	-0.279	0.043	-0.002	-0.129	-0.094	0.251	0.084	-0.169	0.638	-0.246	0.038	-0.320	-0.261	-0.021	0.190
DAFM	0.203	-0.011	-0.119	-0.049	0.078	-0.149	-0.162	-0.014	-0.292	-0.402	-0.439	-0.163	0.103	-0.007	-0.193	0.005	-0.086
PLSY	-0.023	0.214	-0.167	-0.179	-0.284	0.271	0.005	-0.203	-0.232	-0.210	-0.334	0.104	0.119	-0.062	0.204	-0.035	-0.036
POBA	0.110	0.020	-0.014	-0.418	0.091	-0.120	-0.078	-0.248	-0.115	-0.027	0.325	0.140	-0.318	-0.217	-0.153	-0.174	-0.227
PM41	-0.117	0.242	0.155	-0.066	0.242	-0.091	-0.288	-0.264	-0.133	0.225	-0.035	0.093	0.177	0.148	0.076	-0.266	-0.249
41MX	-0.282	0.066	0.137	0.071	0.060	0.639	-0.007	0.070	-0.041	-0.336	-0.120	0.073	0.312	-0.126	0.237	-0.080	-0.011
41ZI	-0.220	0.064	0.156	-0.073	-0.290	0.687	-0.082	-0.069	-0.094	-0.492	0.004	0.347	0.090	0.064	0.441	-0.134	-0.042
PTAS	0.128	0.225	-0.183	0.009	0.262	0.186	0.128	-0.016	-0.721	-0.304	-0.064	-0.103	0.211	-0.067	-0.108	-0.134	0.017
PTLD	-0.058	0.164	-0.056	-0.138	0.240	0.096	-0.075	0.046	-0.587	-0.285	0.171	-0.076	0.169	-0.117	-0.024	-0.239	-0.140
SLBA	0.685	0.087	-0.360	-0.120	0.120	-0.015	-0.052	-0.115	0.068	-0.631	0.187	-0.130	0.226	-0.086	-0.225	-0.023	-0.021
SLCC	0.635	-0.063	-0.293	0.174	0.130	-0.232	-0.076	0.008	0.165	-0.291	0.118	-0.364	0.055	-0.234	-0.466	0.248	0.230
SYBA	0.447	-0.180	0.291	0.205	0.331	-0.028	0.020	0.099	0.052	0.071	-0.080	-0.039	0.029	0.229	-0.016	0.072	0.022
SYMX	-0.019	0.234	-0.556	-0.066	-0.370	-0.108	0.101	0.051	-0.047	0.008	-0.084	-0.092	0.012	-0.021	-0.027	-0.094	0.052
ZTPO	-0.073	-0.086	-0.124	0.002	0.129	0.098	-0.023	0.110	-0.029	0.059	-0.141	0.079	0.074	-0.057	-0.091	-0.064	-0.113
ZTVS	-0.171	-0.590	0.155	-0.159	-0.048	-0.313	0.078	0.158	-0.057	0.319	-0.134	-0.381	-0.041	0.047	-0.257	0.149	-0.252
ZTZI	-0.025	-0.017	0.212	0.318	0.271	-0.005	0.380	0.039	0.113	0.160	0.025	-0.174	0.241	-0.323	-0.124	-0.153	-0.252
VSBA	0.521	-0.006	0.027	-0.003	0.339	-0.021	0.062	-0.180	0.038	-0.070	-0.065	0.232	-0.118	-0.076	-0.006	-0.010	-0.050
VSSY	-0.198	-0.001	0.364	0.273	0.125	0.169	0.024	0.182	0.147	0.151	0.148	-0.080	0.116	0.327	0.125	-0.092	0.056
ZIMX	0.003	0.445	-0.200	-0.082	-0.235	0.217	-0.251	0.100	-0.127	-0.177	0.223	-0.097	0.104	0.054	0.035	-0.287	0.098
ZSNL	-0.254	0.371	0.213	-0.196	-0.156	0.520	-0.023	-0.241	0.063	-0.046	0.199	0.831	-0.205	0.355	0.619	-0.528	-0.165

	NAFM	NA41	NAVS	NAZI	NAZS	BRBA	NALD	DAFM	PLSY	POBA	PM41	41MX	41ZI	PTAS	PTLD	SLBA	SLCC
ACPM	0.042	-0.105	0.186	-0.077	-0.076	0.164	0.613	-0.175	-0.050	-0.039	0.233	-0.169	-0.057	-0.031	0.340	0.393	0.348
ACSY	-0.042	-0.105	0.092	-0.078	-0.177	-0.190	-0.252	0.192	0.293	-0.411	0.329	0.071	-0.022	-0.229	-0.034	0.191	-0.114
PMPM	-0.017	-0.049	0.131	-0.060	0.019	0.036	0.469	-0.179	-0.244	-0.012	0.247	-0.090	-0.132	-0.058	0.197	0.590	0.468
ASJP	-0.118	0.036	-0.028	0.040	-0.081	0.548	0.389	-0.063	-0.264	0.269	-0.085	-0.187	0.093	0.437	0.263	0.392	0.272
BACC	-0.093	-0.246	-0.194	-0.102	0.003	0.140	0.057	-0.169	-0.255	0.466	0.077	-0.173	-0.253	0.084	0.068	0.131	0.437
BAOP	0.056	0.057	-0.111	-0.014	0.095	-0.037	0.029	-0.071	-0.207	0.017	0.090	0.102	-0.009	0.046	-0.017	-0.173	-0.051
ASAS	-0.116	-0.294	-0.290	0.111	-0.095	-0.057	-0.258	-0.269	-0.375	0.237	0.043	-0.383	-0.408	0.073	-0.209	-0.361	0.022
JPJP	0.173	-0.022	-0.085	0.097	0.068	-0.343	-0.041	-0.096	-0.113	0.161	0.131	-0.042	-0.007	0.032	0.072	-0.236	0.189
4141	-0.054	-0.121	-0.174	-0.170	-0.194	-0.098	0.146	-0.178	-0.231	-0.024	0.286	0.011	-0.237	-0.030	-0.240	0.237	0.458
POPO	0.090	-0.231	-0.302	-0.095	0.077	-0.117	-0.225	-0.006	-0.251	0.670	-0.047	-0.176	-0.077	-0.074	-0.058	-0.259	0.021
PTPT	0.408	0.029	0.158	0.121	0.359	0.297	0.151	0.271	-0.162	-0.028	0.036	-0.204	-0.119	-0.253	-0.007	-0.047	0.066
STST	0.087	-0.065	0.175	-0.155	0.106	0.281	-0.150	0.117	0.221	0.050	-0.029	-0.034	-0.067	0.159	0.175	-0.254	-0.261
ZTZT	0.023	-0.312	-0.305	0.028	-0.054	0.073	-0.078	0.092	-0.276	0.373	-0.319	-0.331	-0.252	-0.094	-0.134	-0.013	0.015
BRAS	-0.168	-0.266	-0.282	-0.256	-0.120	0.189	0.177	-0.357	-0.215	-0.144	0.005	-0.126	-0.206	0.069	0.096	-0.365	-0.246
BRLD	-0.155	0.041	-0.273	-0.337	-0.039	0.266	0.577	0.090	0.074	0.041	-0.195	0.104	0.464	0.498	0.623	0.261	-0.153
BRNA	0.139	-0.112	0.217	0.162	0.008	0.487	0.551	0.003	-0.162	-0.022	-0.193	0.044	-0.098	0.177	0.231	0.169	0.228
BRPT	0.165	-0.031	0.354	0.030	0.226	0.403	0.410	0.142	-0.036	0.055	0.144	-0.037	0.004	0.482	0.654	-0.074	-0.198
NABA	0.290	-0.417	0.483	-0.139	0.089	0.307	0.067	0.203	-0.023	0.110	-0.117	-0.282	-0.220	0.128	-0.058	0.685	0.635
CACP	0.161	0.119	0.067	-0.098	-0.146	0.253	0.242	-0.011	0.214	0.020	0.242	0.066	0.064	0.225	0.164	0.087	-0.063
CPSL	-0.100	0.153	0.076	-0.151	0.031	0.219	-0.279	-0.119	-0.167	-0.014	0.155	0.137	0.156	-0.183	-0.056	-0.360	-0.293
CPZS	0.137	-0.125	0.056	0.029	-0.113	-0.212	0.043	-0.049	-0.179	-0.418	-0.066	0.071	-0.073	0.009	-0.138	-0.120	0.174
CNCN	0.009	-0.110	-0.259	-0.307	-0.055	-0.003	-0.002	0.078	-0.284	0.091	0.242	0.060	-0.290	0.262	0.240	0.120	0.130
FMPM	-0.344	0.806	-0.264	0.040	-0.185	-0.123	-0.129	-0.149	0.271	-0.120	-0.091	0.639	0.687	0.186	0.096	-0.015	-0.232
FMZT	-0.210	0.133	-0.166	0.275	-0.030	0.159	-0.094	-0.162	0.005	-0.078	-0.288	-0.007	-0.082	0.128	-0.075	-0.052	-0.076
FMCP	0.064	-0.347	0.149	-0.109	-0.066	-0.029	0.251	-0.014	-0.203	-0.248	-0.264	0.070	-0.069	-0.016	0.046	-0.115	0.008
FMPT	-0.189	-0.088	-0.214	-0.106	0.005	0.067	0.084	-0.292	-0.232	-0.115	-0.133	-0.041	-0.094	-0.721	-0.587	0.068	0.165
LDAS	-0.225	-0.277	-0.196	-0.105	-0.076	-0.078	-0.169	-0.402	-0.210	-0.027	0.225	-0.336	-0.492	-0.304	-0.285	-0.631	-0.291
LDBA	-0.198	0.063	-0.045	0.045	0.014	0.638	0.638	-0.439	-0.334	0.325	-0.035	-0.120	0.004	-0.064	0.171	0.187	0.118
NANL	-0.377	0.535	-0.448	0.129	-0.021	-0.188	-0.246	-0.163	0.104	0.140	0.093	0.073	0.347	-0.103	-0.076	-0.130	-0.364
NLAC	-0.023	0.216	-0.044	0.029	-0.061	-0.054	0.038	0.103	0.119	-0.318	0.177	0.312	0.090	0.211	0.169	0.226	0.055
NLVS	-0.121	-0.293	0.250	-0.112	-0.245	0.048	-0.320	-0.007	-0.062	-0.217	0.148	-0.126	0.064	-0.067	-0.117	-0.086	-0.234
NAAC	-0.382	0.707	-0.279	0.226	0.035	-0.165	-0.261	-0.193	0.204	-0.153	0.076	0.237	0.441	-0.108	-0.024	-0.225	-0.466
NACA	0.162	-0.300	0.336	0.172	0.308	-0.428	-0.021	0.005	-0.035	-0.174	-0.266	-0.080	-0.134	-0.134	-0.239	-0.023	0.248
NACP	0.308	-0.250	0.476	0.213	0.158	-0.123	0.190	-0.086	-0.036	-0.227	-0.249	-0.011	-0.042	0.017	-0.140	-0.021	0.230
NAFM	1.000	-0.216	0.351	0.237	0.361	-0.102	-0.039	0.857	0.053	-0.041	-0.085	-0.082	-0.058	-0.049	-0.107	0.131	0.203
NA41	-0.216	1.000	-0.195	0.432	0.108	-0.159	-0.016	-0.144	0.240	-0.124	-0.350	0.574	0.681	0.031	0.065	-0.203	-0.341
NAVS	0.351	-0.195	1.000	0.141	0.339	0.066	0.001	0.260	0.140	-0.104	-0.171	-0.049	0.073	-0.053	0.023	0.105	0.057
NAZI	0.237	0.432	0.141	1.000	0.339	-0.253	-0.119	0.105	0.110	-0.097	-0.298	0.103	0.054	-0.004	-0.170	-0.148	0.001
NAZS	0.361	0.108	0.339	0.339	1.000	-0.135	0.026	0.166	-0.113	-0.115	-0.139	-0.081	0.097	-0.130	0.072	-0.276	-0.238
BRBA	-0.102	-0.159	0.066	-0.253	-0.135	1.000	0.481	-0.187	-0.098	0.254	-0.162	-0.008	0.093	0.103	0.238	0.431	0.120
NALD	-0.039	-0.016	0.001	-0.119	0.026	0.481	1.000	-0.055	-0.219	0.116	-0.239	0.033	0.165	0.536	0.699	0.450	0.247
DAFM	0.857	-0.144	0.260	0.105	0.166	-0.187	-0.055	1.000	0.237	-0.144	-0.126	-0.064	-0.125	-0.003	0.038	0.115	0.105
PLSY	0.053	0.240	0.140	0.110	-0.113	-0.098	-0.219	0.237	1.000	-0.294	-0.167	0.090	0.212	-0.073	-0.056	0.112	-0.062
POBA	-0.041	-0.124	-0.104	-0.097	-0.115	0.254	0.116	-0.144	-0.294	1.000	-0.085	-0.156	0.088	0.100	0.192	0.106	0.195
PM41	-0.085	-0.350	-0.171	-0.298	-0.139	-0.162	-0.239	-0.126	-0.167	-0.085	1.000	-0.330	-0.430	-0.128	0.060	-0.074	0.157
41MX	-0.082	0.574	-0.049	0.103	-0.081	-0.008	0.033	-0.064	0.090	-0.156	-0.330	1.000	0.742	0.111	0.029	-0.113	-0.279
41ZI	-0.058	0.681	0.073	0.054	0.097	0.093	0.165	-0.125	0.212	0.088	-0.430	0.742	1.000	0.231	0.126	-0.113	-0.342
PTAS	-0.049	0.031	-0.053	-0.004	-0.130	0.103	0.536	-0.003	-0.073	0.100	-0.128	0.111	0.231	1.000	0.908	0.323	0.183
PTLD	-0.107	0.065	0.023	-0.170	0.072	0.238	0.699	0.038	-0.056	0.192	0.060	0.029	0.126	0.908	1.000	0.134	-0.130
SLBA	0.131	-0.203	0.105	-0.148	-0.276	0.431	0.450	0.115	0.112	0.106	-0.074	-0.113	-0.113	0.323	0.134	1.000	0.707
SLCC	0.203	-0.341	0.057	0.001	-0.238	0.120	0.247	0.105	-0.062	0.195	0.157	-0.279	-0.342	0.183	-0.130	0.707	1.000
SYBA	-0.004	-0.147	-0.170	-0.244	-0.033	0.063	-0.298	-0.104	-0.327	-0.157	0.262	-0.107	-0.191	0.058	-0.216	0.072	0.122
SYMX	-0.011	0.154	0.061	0.377	-0.058	0.031	0.056	0.089	0.314	-0.202	-0.349	-0.096	0.019	0.144	0.014	0.197	0.153
ZTPO	-0.215	-0.027	-0.176	-0.105	-0.436	-0.210	0.066	0.032	-0.137	-0.140	-0.217	-0.015	-0.163	0.051	0.105	0.162	0.264
ZTVS	-0.111	-0.389	-0.042	-0.122	-0.161	-0.028	-0.226	0.072	-0.111	0.070	-0.226	-0.308	-0.398	-0.063	-0.030	-0.248	-0.203
ZTZI	-0.085	-0.073	-0.486	0.042	-0.108	-0.030	-0.261	0.138	-0.134	-0.051	-0.001	-0.237	-0.449	-0.166	-0.286	0.075	0.051
VSBA	-0.047	-0.150	-0.464	-0.175	-0.120	0.112	-0.115	-0.078	-0.176	0.197	0.106	-0.206	-0.178	0.044	-0.175	0.437	0.436
VSSY	-0.145	0.146	-0.027	-0.059	-0.038	0.022	-0.074	-0.190	-0.311	-0.248	0.105	0.219	0.141	-0.022	-0.078	-0.314	-0.272
ZIMX	-0.064	0.287	0.340	-0.158	-0.408	0.284	0.361	0.052	0.645	-0.125	-0.234	0.219	0.172	-0.020	0.224	0.388	0.188
ZSNL	-0.438	0.317	-0.340	-0.059	-0.144	0.075	-0.173	-0.276	-0.056	0.137	0.115	0.158	0.449	-0.031	-0.155	-0.126	-0.459

	SYBA	SYMX	ZTPO	ZTVS	ZTZI	VSBA	VSSY	ZIMX	ZSNL
ACPM	-0.262	0.087	-0.264	-0.316	-0.083	-0.167	-0.057	0.698	0.009
ACSY	-0.142	0.055	-0.232	-0.098	-0.139	-0.048	-0.177	0.181	0.131
PMPM	-0.032	-0.176	0.025	-0.188	-0.144	0.042	0.131	0.622	-0.042
ASJP	-0.141	-0.128	-0.168	-0.166	0.143	0.195	-0.107	0.032	0.137
BACC	0.181	-0.075	0.118	0.235	0.312	0.414	-0.155	-0.214	-0.300
BAOP	0.045	-0.330	0.043	-0.168	0.050	-0.015	0.099	-0.334	0.060
ASAS	-0.023	-0.138	-0.133	0.183	0.135	0.225	-0.128	-0.423	-0.050
JPJP	0.071	-0.098	-0.297	-0.040	-0.026	-0.062	0.083	-0.496	0.122
4141	-0.066	-0.003	0.204	0.119	0.250	0.001	-0.120	-0.069	-0.147
POPO	0.033	-0.251	-0.214	0.213	-0.073	0.214	-0.177	-0.247	-0.040
PTPT	-0.324	-0.127	-0.320	-0.089	0.076	-0.385	0.006	-0.019	-0.281
STST	-0.091	0.063	-0.061	0.109	-0.043	-0.251	-0.054	0.069	-0.216
ZTZT	0.035	-0.001	0.100	0.829	0.580	0.243	-0.172	-0.129	-0.203
BRAS	0.169	0.069	-0.029	0.220	0.077	-0.097	0.295	-0.520	0.046
BRLD	-0.140	0.093	-0.038	-0.018	-0.198	-0.055	-0.068	0.007	0.235
BRNA	-0.290	0.001	-0.036	-0.049	-0.047	-0.266	0.050	0.400	-0.312
BRPT	-0.222	-0.103	-0.262	-0.158	-0.306	-0.356	0.059	0.314	-0.313
NABA	0.447	-0.019	-0.073	-0.171	-0.025	0.521	-0.198	0.003	-0.254
CACP	-0.180	0.234	-0.086	-0.590	-0.017	-0.006	-0.001	0.445	0.371
CPSL	0.291	-0.556	-0.124	0.155	0.212	0.027	0.364	-0.200	0.213
CPZS	0.205	-0.066	0.002	-0.159	0.318	-0.003	0.273	-0.082	-0.196
CNCN	0.331	-0.370	0.129	-0.048	0.271	0.339	0.125	-0.235	-0.156
FMPM	-0.028	-0.108	0.098	-0.313	-0.005	-0.021	0.169	0.217	0.520
FMZT	0.020	0.101	-0.023	0.078	0.380	0.062	0.024	-0.251	-0.023
FMCP	0.099	0.051	0.110	0.158	0.039	-0.180	0.182	0.100	-0.241
FMPT	0.052	-0.047	-0.029	-0.057	0.113	0.038	0.147	-0.127	0.063
LDAS	0.071	0.008	0.059	0.319	0.160	-0.070	0.151	-0.177	-0.046
LDBA	-0.080	-0.084	-0.141	-0.134	0.025	-0.065	0.148	0.223	0.199
NANL	-0.039	-0.092	0.079	-0.381	-0.174	0.232	-0.080	-0.097	0.831
NLAC	0.029	0.012	0.074	-0.041	0.241	-0.118	0.116	0.104	-0.205
NLVS	0.229	-0.021	-0.057	0.047	-0.323	-0.076	0.327	0.054	0.355
NAAC	-0.016	-0.027	-0.091	-0.257	-0.124	-0.006	0.125	0.035	0.619
NACA	0.072	-0.094	-0.064	0.149	-0.153	-0.010	-0.092	-0.287	-0.528
NACP	0.022	0.052	-0.113	-0.252	-0.252	-0.050	0.056	0.098	-0.165
NAFM	-0.004	-0.011	-0.215	-0.111	-0.085	-0.047	-0.145	-0.064	-0.438
NA41	-0.147	0.154	-0.027	-0.389	-0.073	-0.150	0.146	0.287	0.317
NAVS	-0.170	0.061	-0.176	-0.042	-0.486	-0.464	-0.027	0.340	-0.340
NAZI	-0.244	0.377	-0.105	-0.122	0.042	-0.175	-0.059	-0.158	-0.059
NAZS	-0.033	-0.058	-0.436	-0.161	-0.108	-0.120	-0.038	-0.408	-0.144
BRBA	0.063	0.031	-0.210	-0.028	-0.030	0.112	0.022	0.284	0.075
NALD	-0.298	0.056	0.066	-0.226	-0.261	-0.115	-0.074	0.361	-0.173
DAFM	-0.104	0.089	0.032	0.072	0.138	-0.078	-0.190	0.052	-0.276
PLSY	-0.327	0.314	-0.137	-0.111	-0.134	-0.176	-0.311	0.645	-0.056
POBA	-0.157	-0.202	-0.140	0.070	-0.051	0.197	-0.248	-0.125	0.137
PM41	0.262	-0.349	-0.217	-0.226	-0.001	0.106	0.105	-0.234	0.115
41MX	-0.107	-0.096	-0.015	-0.308	-0.237	-0.206	0.219	0.219	0.158
41ZI	-0.191	0.019	-0.163	-0.398	-0.449	-0.178	0.141	0.172	0.449
PTAS	0.058	0.144	0.051	-0.063	-0.166	0.044	-0.022	-0.020	-0.031
PTLD	-0.216	0.014	0.105	-0.030	-0.286	-0.175	-0.078	0.224	-0.155
SLBA	0.072	0.197	0.162	-0.248	0.075	0.437	-0.314	0.388	-0.126
SLCC	0.122	0.153	0.264	-0.203	0.051	0.436	-0.272	0.188	-0.459
SYBA	1.000	-0.259	0.214	-0.055	0.170	0.639	0.506	-0.545	0.030
SYMX	-0.259	1.000	0.161	0.142	0.084	-0.192	-0.215	0.378	-0.229
ZTPO	0.214	0.161	1.000	0.314	0.372	-0.043	0.137	0.255	0.037
ZTVS	-0.055	0.142	0.314	1.000	0.438	-0.115	-0.074	0.000	-0.374
ZTZI	0.170	0.084	0.372	0.438	1.000	0.272	-0.044	-0.187	-0.352
VSBA	0.639	-0.192	-0.043	-0.115	0.272	1.000	-0.185	-0.476	0.285
VSSY	0.506	-0.215	0.137	-0.074	-0.044	-0.185	1.000	-0.220	0.075
ZIMX	-0.545	0.378	0.255	0.000	-0.187	-0.476	-0.220	1.000	0.027
ZSNL	0.030	-0.229	0.037	-0.374	-0.352	0.285	0.075	0.027	1.000

Table B4 Environmental Correlation Matrix for Model 1.

	ACPM	ACSY	PMPM	ASJP	BACC	BAOP	ASAS	JPJP	4141	POPO	PTPT	STST	ZTZT	BRAS	BRLD	BRNA	BRPT
ACPM	1.000	0.225	0.472	0.040	0.056	-0.117	0.163	-0.017	0.082	-0.011	-0.106	-0.114	0.223	0.113	0.010	-0.148	-0.194
ACSY	0.225	1.000	0.243	-0.038	0.005	-0.084	0.081	0.158	0.014	0.051	0.044	-0.248	0.093	0.041	-0.069	0.029	-0.096
PMPM	0.472	0.243	1.000	0.176	0.211	-0.192	0.187	0.151	0.320	0.213	0.136	-0.010	0.281	0.112	-0.138	0.145	0.020
ASJP	0.040	-0.038	0.176	1.000	0.082	-0.137	0.424	0.116	-0.076	0.142	0.080	0.016	0.155	-0.144	0.000	0.151	0.029
BACC	0.056	0.005	0.211	0.082	1.000	-0.161	-0.031	0.278	0.271	0.067	0.179	-0.028	0.206	0.083	0.004	-0.054	0.054
BAOP	-0.117	-0.084	-0.192	-0.137	-0.161	1.000	-0.041	-0.212	-0.363	0.056	0.017	0.022	-0.122	-0.122	0.120	-0.046	-0.052
ASAS	0.163	0.081	0.187	0.424	-0.031	-0.041	1.000	-0.003	0.024	0.205	0.180	0.107	0.222	0.183	0.056	-0.058	0.055
JPJP	-0.017	0.158	0.151	0.116	0.278	-0.212	-0.003	1.000	0.105	0.098	0.251	-0.094	0.138	0.262	-0.003	-0.079	-0.056
4141	0.082	0.014	0.320	-0.076	0.271	-0.363	0.024	0.105	1.000	0.109	0.166	0.004	0.262	0.065	0.121	-0.194	0.054
POPO	-0.011	0.051	0.213	0.142	0.067	0.056	0.205	0.098	0.109	1.000	0.323	-0.088	0.486	0.303	0.143	0.016	0.086
PTPT	-0.106	0.044	0.136	0.080	0.179	0.017	0.180	0.251	0.166	0.323	1.000	0.134	0.324	0.288	0.143	0.257	0.442
STST	-0.114	-0.248	-0.010	0.016	-0.028	0.022	0.107	-0.094	0.004	-0.088	0.134	1.000	-0.105	0.112	0.013	0.047	0.187
ZTZT	0.223	0.093	0.281	0.155	0.206	-0.122	0.222	0.138	0.262	0.486	0.324	-0.105	1.000	0.227	0.149	0.172	0.191
BRAS	0.113	0.041	0.112	-0.144	0.083	-0.122	0.183	0.262	0.065	0.303	0.288	0.112	0.227	1.000	0.420	-0.367	0.012
BRLD	0.010	-0.069	-0.138	0.000	0.004	0.120	0.056	-0.003	0.121	0.143	0.143	0.013	0.149	0.420	1.000	-0.283	0.006
BRNA	-0.148	0.029	0.145	0.151	-0.054	-0.046	-0.058	-0.079	-0.194	0.016	0.257	0.047	0.172	-0.367	-0.283	1.000	0.448
BRPT	-0.194	-0.096	0.020	0.029	0.054	-0.052	0.055	-0.056	0.054	0.086	0.442	0.187	0.191	0.012	0.006	0.448	1.000
NABA	0.020	0.050	0.182	0.004	0.246	-0.323	-0.023	0.175	0.204	0.206	0.130	-0.085	0.303	0.273	0.159	-0.020	0.029
CACP	-0.061	-0.027	-0.057	-0.061	0.273	-0.118	0.039	0.246	0.267	0.015	0.051	0.031	0.188	0.034	-0.040	-0.084	-0.061
CPSL	0.086	0.088	0.047	0.132	-0.041	-0.081	-0.054	0.052	0.009	0.009	-0.024	-0.020	0.022	0.014	0.043	0.086	-0.019
CPZS	0.010	-0.103	0.210	0.054	0.206	-0.213	0.052	0.172	0.165	0.065	0.130	0.061	0.280	0.182	0.077	0.045	0.088
CNCN	0.061	0.111	0.009	0.068	0.270	0.158	-0.041	0.188	-0.039	-0.010	-0.079	-0.133	0.040	0.095	0.036	-0.010	-0.077
FMPM	0.145	0.384	0.132	0.024	0.111	-0.171	0.229	0.141	0.066	0.157	0.105	-0.043	0.368	0.066	-0.062	0.092	-0.013
FMZT	-0.042	0.064	0.159	0.082	0.061	-0.139	0.108	0.086	0.069	0.276	0.295	-0.104	0.340	0.091	-0.032	0.165	0.122
FMCP	0.069	0.054	0.325	0.111	0.248	-0.153	0.110	0.069	0.348	0.432	0.262	-0.051	0.585	0.203	0.068	0.201	0.161
FMPT	-0.047	-0.046	0.037	0.094	0.134	-0.019	-0.049	0.149	-0.164	0.090	0.123	-0.024	0.152	-0.069	0.053	0.119	-0.438
LDAS	0.182	0.139	0.134	-0.261	0.081	-0.096	0.548	0.120	0.149	0.193	0.179	-0.007	0.211	0.491	-0.089	-0.077	0.088
LDBA	0.074	0.171	0.165	0.191	0.147	-0.209	0.056	0.303	0.338	0.223	0.014	-0.252	0.378	0.360	-0.053	0.082	0.086
NANL	-0.149	0.154	-0.058	-0.070	0.196	-0.170	0.019	0.075	-0.129	-0.044	0.042	0.023	0.101	-0.024	-0.107	0.020	0.080
NLAC	0.230	0.250	0.138	-0.019	0.178	-0.084	0.135	0.152	-0.023	0.015	0.067	0.110	0.043	0.056	0.031	0.014	0.021
NLVS	0.078	0.623	0.144	-0.074	0.105	-0.016	0.032	0.051	0.031	0.150	0.047	-0.212	0.153	-0.076	-0.055	0.031	-0.093
NAAC	0.040	0.546	0.135	-0.016	0.055	-0.090	0.041	0.019	-0.178	-0.034	-0.051	-0.115	0.048	-0.172	-0.127	0.071	0.038
NACA	-0.045	-0.107	0.233	0.096	-0.073	-0.085	-0.103	-0.207	-0.121	0.156	0.168	-0.011	0.123	0.228	0.237	0.178	0.169
NACP	-0.097	-0.043	0.148	0.041	0.137	-0.173	0.030	0.102	0.139	0.158	0.200	-0.023	0.287	0.280	0.168	0.113	0.059
NAFM	0.098	0.151	0.358	0.037	0.201	-0.091	0.158	-0.077	0.325	0.366	0.038	0.043	0.489	0.261	0.182	0.093	0.060
NA41	-0.020	0.258	-0.022	0.047	0.132	-0.195	0.154	0.086	0.014	0.133	-0.016	-0.152	0.347	0.094	-0.002	-0.004	-0.073
NAVS	0.081	0.065	0.138	0.095	0.176	-0.109	0.078	0.195	0.149	0.392	0.012	-0.235	0.419	0.306	0.190	0.097	-0.002
NAZI	0.106	0.109	0.190	0.110	0.182	-0.045	0.091	0.163	0.226	0.294	0.187	0.090	0.402	0.243	0.217	-0.091	0.058
NAZS	0.122	0.075	0.103	0.059	0.017	0.088	0.082	0.038	0.099	0.207	0.032	-0.045	0.275	0.127	0.094	0.080	0.028
BRBA	-0.028	-0.089	0.114	0.054	0.215	-0.334	0.083	0.312	0.251	0.253	0.198	0.132	0.301	0.595	0.193	-0.121	0.166
NALD	-0.019	0.102	0.036	0.065	0.029	0.062	0.047	0.038	0.058	0.275	0.220	-0.073	0.356	0.279	0.784	0.234	0.107
DAFM	0.056	-0.088	0.278	-0.135	0.206	-0.024	0.135	0.021	0.323	0.339	0.069	0.085	0.330	0.251	-0.033	0.088	0.093
PLSY	-0.045	0.650	0.066	-0.061	0.032	-0.137	0.034	0.105	0.001	0.053	0.007	-0.281	0.144	0.031	-0.090	0.082	-0.058
POBA	0.144	0.158	0.153	0.000	0.069	0.029	0.186	0.034	0.244	0.662	0.335	-0.037	0.459	0.234	0.092	0.143	0.106
PM41	0.083	0.111	0.344	0.060	0.077	-0.011	0.106	-0.064	0.347	0.157	0.036	-0.023	0.183	0.137	0.051	-0.020	-0.060
41MX	0.005	0.379	-0.103	-0.076	-0.029	-0.217	0.107	-0.088	-0.151	0.047	0.018	-0.211	0.312	-0.010	-0.045	0.052	-0.095
41ZI	0.099	0.277	-0.141	-0.075	-0.087	-0.070	0.313	0.013	-0.016	-0.029	0.099	-0.143	0.293	-0.064	-0.109	0.029	-0.094
PTAS	0.128	0.193	0.175	0.260	0.115	-0.148	-0.163	0.186	0.120	0.315	0.064	-0.002	0.267	0.325	0.070	0.259	0.178
PTLD	-0.038	0.050	-0.038	0.047	0.003	0.066	0.099	-0.003	0.259	0.264	0.241	-0.016	0.339	0.275	0.683	0.188	0.477
SLBA	-0.127	-0.234	-0.145	-0.218	0.150	0.052	0.157	0.087	0.030	0.091	0.112	0.131	0.105	0.092	-0.026	-0.147	0.037
SLCC	-0.112	-0.186	0.059	-0.107	0.422	0.036	0.063	0.155	-0.056	0.146	0.146	0.188	0.110	0.200	0.058	-0.121	0.084
SYBA	0.018	-0.331	0.149	0.027	0.186	-0.233	-0.015	-0.114	0.246	-0.040	0.209	-0.131	0.052	-0.285	-0.015	0.075	0.125
SYMX	-0.079	0.573	0.112	0.026	0.127	-0.111	0.118	0.285	0.080	0.243	0.116	-0.122	0.221	0.080	-0.043	0.073	0.043
ZTPO	0.142	0.189	0.128	0.133	0.199	-0.172	0.036	0.304	0.091	0.308	0.163	-0.153	0.303	0.288	0.103	0.206	0.195
ZTVS	0.172	0.019	0.229	0.083	0.240	-0.062	0.216	0.184	0.256	0.536	0.329	-0.144	0.946	0.186	0.125	0.129	0.169
ZTZI	-0.060	-0.030	0.162	0.164	0.178	-0.194	-0.071	0.120	-0.093	0.155	-0.009	-0.047	0.084	0.059	0.024	0.046	0.100
VSBA	-0.101	0.095	0.120	-0.032	0.174	-0.299	-0.088	0.010	0.096	-0.137	0.258	0.110	-0.069	-0.057	-0.115	0.057	0.114
VSSY	0.005	-0.544	-0.018	0.067	0.116	0.102	0.069	-0.067	0.178	0.137	0.046	-0.030	0.154	-0.158	0.083	0.034	0.076
ZIMX	0.056	0.067	-0.028	0.058	0.155	-0.088	0.236	0.182	0.320	0.192	0.196	-0.103	0.546	0.246	0.096	0.138	0.039
ZSNL	-0.060	0.352	0.013	-0.097	0.083	-0.047	0.017	-0.118	-0.166	0.038	0.126	-0.166	0.077	-0.192	-0.157	0.033	0.133

	NABA	CACP	CPSL	CPZS	CNCN	FMPM	FMZT	FMCP	FMPT	LDAS	LDBA	NANL	NLAC	NLVS	NAAC	NACA	NACP
ACPM	0.020	-0.061	0.086	0.010	0.061	0.145	-0.042	0.069	-0.047	0.182	0.074	-0.149	0.230	0.078	0.040	-0.045	-0.097
ACSY	0.050	-0.027	0.088	-0.103	0.111	0.384	0.064	0.054	-0.046	0.139	0.171	0.154	0.250	0.623	0.546	-0.107	-0.043
PMPM	0.182	-0.057	0.047	0.210	0.009	0.132	0.159	0.325	0.037	0.134	0.165	-0.058	0.138	0.144	0.135	0.233	0.148
ASJP	0.004	-0.061	0.132	0.054	0.068	0.024	0.082	0.111	0.094	-0.261	0.191	-0.070	-0.019	-0.074	-0.016	0.096	0.041
BACC	0.246	0.273	-0.041	0.206	0.270	0.111	0.061	0.248	0.134	0.081	0.147	0.196	0.178	0.105	0.055	-0.073	0.137
BAOP	-0.323	-0.118	-0.081	-0.213	0.158	-0.171	-0.139	-0.153	-0.019	-0.096	-0.209	-0.170	-0.084	-0.016	-0.090	-0.085	-0.173
ASAS	-0.023	0.039	-0.054	0.052	-0.041	0.229	0.108	0.110	-0.049	0.548	0.056	0.019	0.135	0.032	0.041	-0.103	0.030
JPJP	0.175	0.246	0.052	0.172	0.188	0.141	0.086	0.069	0.149	0.120	0.303	0.075	0.152	0.051	0.019	-0.207	0.102
4141	0.204	0.267	0.009	0.165	-0.039	0.066	0.069	0.348	-0.164	0.149	0.338	-0.129	-0.023	0.031	-0.178	-0.121	0.139
POPO	0.206	0.015	0.009	0.065	-0.010	0.157	0.276	0.432	0.090	0.193	0.223	-0.044	0.015	0.150	-0.034	0.156	0.158
PTPT	0.130	0.051	-0.024	0.130	-0.079	0.105	0.295	0.262	0.123	0.179	0.014	0.042	0.067	0.047	-0.051	0.168	0.200
STST	-0.085	0.031	-0.020	0.061	-0.133	-0.043	-0.104	-0.051	-0.024	-0.007	-0.252	0.023	0.110	-0.212	-0.115	-0.011	-0.023
ZTZT	0.303	0.188	0.022	0.280	0.040	0.368	0.340	0.585	0.152	0.211	0.378	0.101	0.043	0.153	0.048	0.123	0.287
BRAS	0.273	0.034	0.014	0.182	0.095	0.066	0.091	0.203	-0.069	0.491	0.360	-0.024	0.056	-0.076	-0.172	0.228	0.280
BRLD	0.159	-0.040	0.043	0.077	0.036	-0.062	-0.032	0.068	0.053	-0.089	-0.053	-0.107	0.031	-0.055	-0.127	0.237	0.168
BRNA	-0.020	-0.084	0.086	0.045	-0.010	0.092	0.165	0.201	0.119	-0.077	0.082	0.020	0.014	0.031	0.071	0.178	0.113
BRPT	0.029	-0.061	-0.019	0.088	-0.077	-0.013	0.122	0.161	-0.438	0.088	0.086	0.080	0.021	-0.093	0.038	0.169	0.059
NABA	1.000	0.205	0.174	0.237	0.150	0.129	0.268	0.387	0.137	0.114	0.350	0.088	0.001	0.277	0.089	0.122	0.379
CACP	0.205	1.000	-0.180	0.331	0.072	0.078	0.110	0.267	0.077	0.037	0.016	0.065	-0.061	0.090	-0.036	-0.510	0.405
CPSL	0.174	-0.180	1.000	0.025	0.079	0.045	-0.040	-0.033	0.019	-0.071	0.071	0.094	0.184	-0.017	0.063	0.175	-0.076
CPZS	0.237	0.331	0.025	1.000	0.079	0.292	0.108	0.531	0.074	0.108	0.209	0.147	0.109	0.024	-0.070	0.137	0.518
CNCN	0.150	0.072	0.079	0.079	1.000	0.099	-0.005	0.175	0.169	0.081	0.271	0.162	0.192	0.193	0.177	0.016	0.167
FMPM	0.129	0.078	0.045	0.292	0.099	1.000	0.123	0.277	0.099	0.191	0.140	0.493	0.279	0.383	0.581	0.164	0.245
FMZT	0.268	0.110	-0.040	0.108	-0.005	0.123	1.000	0.271	0.154	0.051	0.077	0.188	-0.121	0.144	0.136	0.015	0.155
FMCP	0.387	0.267	-0.033	0.531	0.175	0.277	0.271	1.000	0.191	0.228	0.459	-0.032	0.014	0.098	-0.137	0.309	0.659
FMPT	0.137	0.077	0.019	0.074	0.169	0.099	0.154	0.191	1.000	-0.076	0.008	-0.069	-0.088	0.157	-0.212	-0.077	0.040
LDAS	0.114	0.037	-0.071	0.108	0.081	0.191	0.051	0.228	-0.076	1.000	0.444	0.111	0.089	0.107	0.018	0.021	0.116
LDBA	0.350	0.016	0.071	0.209	0.271	0.140	0.077	0.459	0.008	0.444	1.000	0.019	0.001	0.088	-0.074	0.290	0.297
NANL	0.088	0.065	0.094	0.147	0.162	0.493	0.188	-0.032	-0.069	0.111	0.019	1.000	-0.011	0.521	0.626	0.079	0.069
NLAC	0.001	-0.061	0.184	0.109	0.192	0.279	-0.121	0.014	-0.088	0.089	0.001	-0.011	1.000	0.022	0.357	0.072	0.033
NLVS	0.277	0.090	-0.017	0.024	0.193	0.383	0.144	0.098	0.157	0.107	0.088	0.521	0.022	1.000	0.512	-0.080	0.046
NAAC	0.089	-0.036	0.063	-0.070	0.177	0.581	0.136	-0.137	-0.212	0.018	-0.074	0.626	0.357	0.512	1.000	-0.115	-0.190
NACA	0.122	-0.510	0.175	0.137	0.016	0.164	0.015	0.309	-0.077	0.021	0.290	0.079	0.072	-0.080	-0.115	1.000	0.472
NACP	0.379	0.405	-0.076	0.518	0.167	0.245	0.155	0.659	0.040	0.116	0.297	0.069	0.033	0.046	-0.190	0.472	1.000
NAFM	0.366	0.061	0.060	0.121	0.118	0.342	0.051	0.526	0.035	0.238	0.327	0.022	0.204	0.068	0.189	0.145	0.279
NA41	0.307	0.037	0.102	0.095	0.132	0.581	0.207	0.099	0.053	0.124	0.076	0.474	0.182	0.324	0.715	-0.049	-0.006
NAVS	0.738	0.089	0.126	0.221	0.297	0.158	0.307	0.445	0.211	0.163	0.413	0.164	0.056	0.383	0.090	0.271	0.423
NAZI	0.456	0.078	0.145	0.124	0.128	0.379	0.450	0.200	0.049	0.132	0.182	0.236	0.163	0.131	0.425	-0.035	0.034
NAZS	0.420	-0.020	0.011	0.086	0.203	0.025	0.163	0.223	0.028	0.093	0.100	-0.063	0.192	0.152	0.088	-0.003	0.086
BRBA	0.507	-0.021	0.075	0.263	0.077	-0.001	0.148	0.357	-0.064	0.238	0.520	-0.077	0.074	-0.102	-0.215	0.344	0.272
NALD	0.327	-0.014	0.142	0.153	0.082	0.124	0.131	0.258	0.163	-0.050	0.155	-0.040	0.051	0.114	0.043	0.303	0.315
DAFM	0.073	0.060	0.041	0.169	-0.001	0.194	-0.001	0.459	-0.009	0.307	0.208	-0.177	0.005	-0.098	-0.192	0.178	0.303
PLSY	0.068	0.002	0.134	0.157	0.043	0.363	-0.099	0.129	0.152	0.127	0.207	0.145	0.022	0.374	0.266	-0.131	-0.012
POBA	0.100	0.068	-0.038	0.196	-0.098	0.137	0.125	0.502	0.140	0.287	0.174	-0.181	0.110	0.028	-0.051	0.196	0.302
PM41	0.186	0.104	-0.085	0.279	0.047	0.476	0.053	0.357	0.056	0.105	0.127	0.092	0.059	0.103	-0.087	0.146	0.346
41MX	0.016	0.017	0.082	-0.133	-0.022	0.315	0.016	-0.082	0.071	0.085	-0.055	0.101	0.024	0.330	0.268	-0.132	-0.073
41ZI	-0.041	0.176	-0.058	0.061	0.013	0.403	0.015	0.068	0.062	0.165	-0.142	0.127	0.151	0.109	0.178	-0.060	0.120
PTAS	0.437	0.051	0.193	0.167	0.091	0.024	0.241	0.323	-0.235	-0.092	0.404	0.071	-0.005	0.119	0.131	0.260	0.344
PTLD	0.236	-0.043	0.140	0.167	0.017	0.014	0.109	0.227	-0.291	0.022	0.187	-0.021	0.066	0.018	0.043	0.331	0.257
SLBA	0.170	0.055	-0.671	0.067	-0.232	-0.126	0.087	0.035	-0.056	0.214	-0.136	-0.068	-0.308	0.044	-0.128	-0.006	0.063
SLCC	0.003	0.132	-0.593	-0.042	0.025	-0.009	0.140	-0.030	-0.038	0.175	-0.011	0.194	-0.168	0.086	0.104	-0.126	-0.012
SYBA	0.366	0.235	-0.055	0.062	-0.050	-0.192	0.060	0.097	0.000	-0.078	-0.146	-0.030	-0.087	0.089	-0.266	-0.077	0.096
SYMX	0.205	-0.031	0.163	0.129	0.098	0.406	0.129	0.187	0.053	0.142	0.199	0.132	0.063	0.288	0.228	0.033	0.054
ZTPO	0.311	0.088	0.230	0.380	0.252	0.423	0.108	0.416	0.151	0.188	0.500	0.211	0.143	0.247	0.163	0.264	0.358
ZTVS	0.311	0.150	-0.006	0.319	0.065	0.358	0.277	0.558	0.222	0.259	0.326	0.116	0.009	0.221	0.003	0.128	0.248
ZTZI	0.246	-0.063	0.124	0.120	0.171	0.197	0.138	0.156	0.005	-0.029	0.282	0.296	0.119	0.218	0.223	0.133	0.093
VSBA	0.371	0.164	0.105	-0.004	-0.088	-0.125	-0.021	0.143	-0.022	-0.030	0.009	-0.138	0.001	-0.083	-0.004	-0.161	0.044
VSSY	0.020	-0.003	-0.119	-0.005	0.085	-0.030	0.130	0.027	-0.030	-0.039	-0.072	0.086	0.031	-0.019	-0.078	0.121	0.000
ZIMX	0.216	0.141	0.041	0.283	0.047	0.173	0.157	0.366	0.168	0.196	0.167	0.054	0.024	0.022	0.033	0.152	0.286
ZSNL	-0.048	-0.020	-0.057	0.128	0.130	0.500	0.068	0.073	-0.128	0.064	-0.021	0.790	0.000	0.678	0.518	0.125	0.048

	NAFM	NA41	NAVS	NAZI	NAZS	BRBA	NALD	DAFM	PLSY	POBA	PM41	41MX	41ZI	PTAS	PTLD	SLBA	SLCC
ACPM	0.098	-0.020	0.081	0.106	0.122	-0.028	-0.019	0.056	-0.045	0.144	0.083	0.005	0.099	0.128	-0.038	-0.127	-0.112
ACSY	0.151	0.258	0.065	0.109	0.075	-0.089	0.102	-0.088	0.650	0.158	0.111	0.379	0.277	0.193	0.050	-0.234	-0.186
PMPM	0.358	-0.022	0.138	0.190	0.103	0.114	0.036	0.278	0.066	0.153	0.344	-0.103	-0.141	0.175	-0.038	-0.145	0.059
ASJP	0.037	0.047	0.095	0.110	0.059	0.054	0.065	-0.135	-0.061	0.000	0.060	-0.076	-0.075	0.260	0.047	-0.218	-0.107
BACC	0.201	0.132	0.176	0.182	0.017	0.215	0.029	0.206	0.032	0.069	0.077	-0.029	-0.087	0.115	0.003	0.150	0.422
BAOP	-0.091	-0.195	-0.109	-0.045	0.088	-0.334	0.062	-0.024	-0.137	0.029	-0.011	-0.217	-0.070	-0.148	0.066	0.052	0.036
ASAS	0.158	0.154	0.078	0.091	0.082	0.083	0.047	0.135	0.034	0.186	0.106	0.107	0.313	-0.163	0.099	0.157	0.063
JPJP	-0.077	0.086	0.195	0.163	0.038	0.312	0.038	0.021	0.105	0.034	-0.064	-0.088	0.013	0.186	-0.003	0.087	0.155
4141	0.325	0.014	0.149	0.226	0.099	0.251	0.058	0.323	0.001	0.244	0.347	-0.151	-0.016	0.120	0.259	0.030	-0.056
POPO	0.366	0.133	0.392	0.294	0.207	0.253	0.275	0.339	0.053	0.662	0.157	0.047	-0.029	0.315	0.264	0.091	0.146
PTPT	0.038	-0.016	0.012	0.187	0.032	0.198	0.220	0.069	0.007	0.335	0.036	0.018	0.099	0.064	0.241	0.112	0.146
STST	0.043	-0.152	-0.235	0.090	-0.045	0.132	-0.073	0.085	-0.281	-0.037	-0.023	-0.211	-0.143	-0.002	-0.016	0.131	0.188
ZTZT	0.489	0.347	0.419	0.402	0.275	0.301	0.356	0.330	0.144	0.459	0.183	0.312	0.293	0.267	0.339	0.105	0.110
BRAS	0.261	0.094	0.306	0.243	0.127	0.595	0.279	0.251	0.031	0.234	0.137	-0.010	-0.064	0.325	0.275	0.092	0.200
BRLD	0.182	-0.002	0.190	0.217	0.094	0.193	0.784	-0.033	-0.090	0.092	0.051	-0.045	-0.109	0.070	0.683	-0.026	0.058
BRNA	0.093	-0.004	0.097	-0.091	0.080	-0.121	0.234	0.088	0.082	0.143	-0.020	0.052	0.029	0.259	0.188	-0.147	-0.121
BRPT	0.060	-0.073	-0.002	0.058	0.028	0.166	0.107	0.093	-0.058	0.106	-0.060	-0.095	-0.094	0.178	0.477	0.037	0.084
NABA	0.366	0.307	0.738	0.456	0.420	0.507	0.327	0.073	0.068	0.100	0.186	0.016	-0.041	0.437	0.236	0.170	0.003
CACP	0.061	0.037	0.089	0.078	-0.020	-0.021	-0.014	0.060	0.002	0.068	0.104	0.017	0.176	0.051	-0.043	0.055	0.132
CPSL	0.060	0.102	0.126	0.145	0.011	0.075	0.142	0.041	0.134	-0.038	-0.085	0.082	-0.058	0.193	0.140	-0.671	-0.593
CPZS	0.121	0.095	0.221	0.124	0.086	0.263	0.153	0.169	0.157	0.196	0.279	-0.133	0.061	0.167	0.167	0.067	-0.042
CNCN	0.118	0.132	0.297	0.128	0.203	0.077	0.082	-0.001	0.043	-0.098	0.047	-0.022	0.013	0.091	0.017	-0.232	0.025
FMPM	0.342	0.581	0.158	0.379	0.025	-0.001	0.124	0.194	0.363	0.137	0.476	0.315	0.403	0.024	0.014	-0.126	-0.009
FMZT	0.051	0.207	0.307	0.450	0.163	0.148	0.131	-0.001	-0.099	0.125	0.053	0.016	0.015	0.241	0.109	0.087	0.140
FMCP	0.526	0.099	0.445	0.200	0.223	0.357	0.258	0.459	0.129	0.502	0.357	-0.082	0.068	0.323	0.227	0.035	-0.030
FMPT	0.035	0.053	0.211	0.049	0.028	-0.064	0.163	-0.009	0.152	0.140	0.056	0.071	0.062	-0.235	-0.291	-0.056	-0.038
LDAS	0.238	0.124	0.163	0.132	0.093	0.238	-0.050	0.307	0.127	0.287	0.105	0.085	0.165	-0.092	0.022	0.214	0.175
LDBA	0.327	0.076	0.413	0.182	0.100	0.520	0.155	0.208	0.207	0.174	0.127	-0.055	-0.142	0.404	0.187	-0.136	-0.011
NANL	0.022	0.474	0.164	0.236	-0.063	-0.077	-0.040	-0.177	0.145	-0.181	0.092	0.101	0.127	0.071	-0.021	-0.068	0.194
NLAC	0.204	0.182	0.056	0.163	0.192	0.074	0.051	0.005	0.022	0.110	0.059	0.024	0.151	-0.005	0.066	-0.308	-0.168
NLVS	0.068	0.324	0.383	0.131	0.152	-0.102	0.114	-0.098	0.374	0.028	0.103	0.330	0.109	0.119	0.018	0.044	0.086
NAAC	0.189	0.715	0.090	0.425	0.088	-0.215	0.043	-0.192	0.266	-0.051	-0.087	0.268	0.178	0.131	0.043	-0.128	0.104
NACA	0.145	-0.049	0.271	-0.035	-0.003	0.344	0.303	0.178	-0.131	0.196	0.146	-0.132	-0.060	0.260	0.331	-0.006	-0.126
NACP	0.279	-0.006	0.423	0.034	0.086	0.272	0.315	0.303	-0.012	0.302	0.346	-0.073	0.120	0.344	0.257	0.063	-0.012
NAFM	1.000	0.258	0.232	0.499	0.459	0.174	0.380	0.696	0.096	0.405	0.261	-0.002	0.020	0.310	0.327	0.026	0.055
NA41	0.258	1.000	0.334	0.581	0.284	0.037	0.086	0.003	0.317	0.176	0.118	0.437	0.312	0.141	0.009	-0.015	0.123
NAVS	0.232	0.334	1.000	0.372	0.404	0.363	0.429	0.070	0.026	0.222	0.134	0.027	-0.093	0.435	0.335	0.029	0.067
NAZI	0.499	0.581	0.372	1.000	0.550	0.203	0.277	0.192	0.122	0.255	0.196	0.007	-0.018	0.323	0.270	0.114	0.162
NAZS	0.459	0.284	0.404	0.550	1.000	0.131	0.232	0.295	0.037	0.284	0.059	-0.045	-0.145	0.240	0.175	0.148	0.161
BRBA	0.174	0.037	0.363	0.203	0.131	1.000	0.096	0.109	-0.034	0.095	0.085	-0.212	-0.264	0.321	0.169	-0.043	0.011
NALD	0.380	0.086	0.429	0.277	0.232	0.096	1.000	0.105	0.063	0.179	0.093	0.072	0.004	0.282	0.840	-0.076	-0.002
DAFM	0.696	0.003	0.070	0.192	0.295	0.109	0.105	1.000	-0.040	0.340	0.277	0.057	0.031	0.141	0.102	-0.003	0.047
PLSY	0.096	0.317	0.026	0.122	0.037	-0.034	0.063	-0.040	1.000	0.155	0.184	0.335	0.189	0.080	0.004	-0.129	-0.184
POBA	0.405	0.176	0.222	0.255	0.284	0.095	0.179	0.340	0.155	1.000	0.294	0.040	0.132	0.139	0.111	0.143	0.105
PM41	0.261	0.118	0.134	0.196	0.059	0.085	0.093	0.277	0.184	0.294	1.000	-0.051	0.150	0.151	0.061	0.144	0.101
41MX	-0.002	0.437	0.027	0.007	-0.045	-0.212	0.072	0.057	0.335	0.040	-0.051	1.000	0.344	-0.043	-0.030	-0.017	-0.033
41ZI	0.020	0.312	-0.093	-0.018	-0.145	-0.264	0.004	0.031	0.189	0.132	0.150	0.344	1.000	-0.285	-0.089	0.142	-0.068
PTAS	0.310	0.141	0.435	0.323	0.240	0.321	0.282	0.141	0.080	0.139	0.151	-0.043	-0.285	1.000	0.400	-0.127	0.024
PTLD	0.327	0.009	0.335	0.270	0.175	0.169	0.840	0.102	0.004	0.111	0.061	-0.030	-0.089	0.400	1.000	-0.073	0.024
SLBA	0.026	-0.015	0.029	0.114	0.148	-0.043	-0.076	-0.003	-0.129	0.143	0.144	-0.017	0.142	-0.127	-0.073	1.000	0.667
SLCC	0.055	0.123	0.067	0.162	0.161	0.011	-0.002	0.047	-0.184	0.105	0.101	-0.033	-0.068	0.024	0.024	0.667	1.000
SYBA	-0.081	-0.252	0.172	-0.037	-0.031	0.008	0.067	0.020	-0.359	-0.043	-0.117	0.000	0.107	-0.004	0.090	0.395	0.070
SYMX	0.242	0.315	0.094	0.179	0.174	0.124	0.051	0.061	0.662	0.246	0.139	0.167	0.207	0.185	0.049	-0.062	-0.054
ZTPO	0.271	0.331	0.384	0.252	0.251	0.323	0.267	0.174	0.245	0.213	0.295	0.258	0.038	0.358	0.236	-0.225	-0.050
ZTVS	0.407	0.351	0.476	0.332	0.277	0.276	0.289	0.317	0.122	0.519	0.201	0.280	0.265	0.181	0.261	0.145	0.142
ZTZI	0.026	0.141	0.363	0.160	0.134	0.297	0.100	-0.063	0.041	-0.188	0.022	0.092	-0.501	0.307	0.161	-0.188	0.056
VSBA	0.184	-0.011	-0.165	0.122	0.054	0.162	-0.081	0.048	0.103	-0.099	0.058	0.045	0.009	0.127	-0.063	0.111	-0.125
VSSY	-0.022	0.020	0.153	0.038	0.044	-0.026	0.082	0.026	-0.591	0.034	-0.095	-0.092	-0.007	-0.038	0.117	0.184	0.203
ZIMX	0.238	0.202	0.152	0.115	0.126	0.114	0.218	0.156	-0.032	0.369	0.190	0.168	0.480	0.142	0.146	0.005	-0.028
ZSNL	0.092	0.291	0.061	0.134	-0.039	-0.221	-0.006	-0.086	0.177	-0.001	0.216	0.086	0.174	-0.021	0.048	-0.027	0.154

	SYBA	SYMX	ZTPO	ZTVS	ZTZI	VSBA	VSSY	ZIMX	ZSNL
ACPM	0.018	-0.079	0.142	0.172	-0.060	-0.101	0.005	0.056	-0.060
ACSY	-0.331	0.573	0.189	0.019	-0.030	0.095	-0.544	0.067	0.352
PMPM	0.149	0.112	0.128	0.229	0.162	0.120	-0.018	-0.028	0.013
ASJP	0.027	0.026	0.133	0.083	0.164	-0.032	0.067	0.058	-0.097
BACC	0.186	0.127	0.199	0.240	0.178	0.174	0.116	0.155	0.083
BAOP	-0.233	-0.111	-0.172	-0.062	-0.194	-0.299	0.102	-0.088	-0.047
ASAS	-0.015	0.118	0.036	0.216	-0.071	-0.088	0.069	0.236	0.017
JPJP	-0.114	0.285	0.304	0.184	0.120	0.010	-0.067	0.182	-0.118
4141	0.246	0.080	0.091	0.256	-0.093	0.096	0.178	0.320	-0.166
POPO	-0.040	0.243	0.308	0.536	0.155	-0.137	0.137	0.192	0.038
PTPT	0.209	0.116	0.163	0.329	-0.009	0.258	0.046	0.196	0.126
STST	-0.131	-0.122	-0.153	-0.144	-0.047	0.110	-0.030	-0.103	-0.166
ZTZT	0.052	0.221	0.303	0.946	0.084	-0.069	0.154	0.546	0.077
BRAS	-0.285	0.080	0.288	0.186	0.059	-0.057	-0.158	0.246	-0.192
BRLD	-0.015	-0.043	0.103	0.125	0.024	-0.115	0.083	0.096	-0.157
BRNA	0.075	0.073	0.206	0.129	0.046	0.057	0.034	0.138	0.033
BRPT	0.125	0.043	0.195	0.169	0.100	0.114	0.076	0.039	0.133
NABA	0.366	0.205	0.311	0.311	0.246	0.371	0.020	0.216	-0.048
CACP	0.235	-0.031	0.088	0.150	-0.063	0.164	-0.003	0.141	-0.020
CPSL	-0.055	0.163	0.230	-0.006	0.124	0.105	-0.119	0.041	-0.057
CPZS	0.062	0.129	0.380	0.319	0.120	-0.004	-0.005	0.283	0.128
CNCN	-0.050	0.098	0.252	0.065	0.171	-0.088	0.085	0.047	0.130
FMPM	-0.192	0.406	0.423	0.358	0.197	-0.125	-0.030	0.173	0.500
FMZT	0.060	0.129	0.108	0.277	0.138	-0.021	0.130	0.157	0.068
FMCP	0.097	0.187	0.416	0.558	0.156	0.143	0.027	0.366	0.073
FMPT	0.000	0.053	0.151	0.222	0.005	-0.022	-0.030	0.168	-0.128
LDAS	-0.078	0.142	0.188	0.259	-0.029	-0.030	-0.039	0.196	0.064
LDBA	-0.146	0.199	0.500	0.326	0.282	0.009	-0.072	0.167	-0.021
NANL	-0.030	0.132	0.211	0.116	0.296	-0.138	0.086	0.054	0.790
NLAC	-0.087	0.063	0.143	0.009	0.119	0.001	0.031	0.024	0.000
NLVS	0.089	0.288	0.247	0.221	0.218	-0.083	-0.019	0.022	0.678
NAAC	-0.266	0.228	0.163	0.003	0.223	-0.004	-0.078	0.033	0.518
NACA	-0.077	0.033	0.264	0.128	0.133	-0.161	0.121	0.152	0.125
NACP	0.096	0.054	0.358	0.248	0.093	0.044	0.000	0.286	0.048
NAFM	-0.081	0.242	0.271	0.407	0.026	0.184	-0.022	0.238	0.092
NA41	-0.252	0.315	0.331	0.351	0.141	-0.011	0.020	0.202	0.291
NAVS	0.172	0.094	0.384	0.476	0.363	-0.165	0.153	0.152	0.061
NAZI	-0.037	0.179	0.252	0.332	0.160	0.122	0.038	0.115	0.134
NAZS	-0.031	0.174	0.251	0.277	0.134	0.054	0.044	0.126	-0.039
BRBA	0.008	0.124	0.323	0.276	0.297	0.162	-0.026	0.114	-0.221
NALD	0.067	0.051	0.267	0.289	0.100	-0.081	0.082	0.218	-0.006
DAFM	0.020	0.061	0.174	0.317	-0.063	0.048	0.026	0.156	-0.086
PLSY	-0.359	0.662	0.245	0.122	0.041	0.103	-0.591	-0.032	0.177
POBA	-0.043	0.246	0.213	0.519	-0.188	-0.099	0.034	0.369	-0.001
PM41	-0.117	0.139	0.295	0.201	0.022	0.058	-0.095	0.190	0.216
41MX	0.000	0.167	0.258	0.280	0.092	0.045	-0.092	0.168	0.086
41ZI	0.107	0.207	0.038	0.265	-0.501	0.009	-0.007	0.480	0.174
PTAS	-0.004	0.185	0.358	0.181	0.307	0.127	-0.038	0.142	-0.021
PTLD	0.090	0.049	0.236	0.261	0.161	-0.063	0.117	0.146	0.048
SLBA	0.395	-0.062	-0.225	0.145	-0.188	0.111	0.184	0.005	-0.027
SLCC	0.070	-0.054	-0.050	0.142	0.056	-0.125	0.203	-0.028	0.154
SYBA	1.000	-0.213	-0.061	0.107	0.035	0.408	0.487	0.237	0.004
SYMX	-0.213	1.000	0.170	0.155	0.020	0.227	-0.524	0.058	0.154
ZTPO	-0.061	0.170	1.000	0.379	0.201	-0.019	0.053	0.191	0.185
ZTVS	0.107	0.155	0.379	1.000	0.067	-0.118	0.257	0.508	0.099
ZTZI	0.035	0.020	0.201	0.067	1.000	-0.054	0.141	-0.251	0.188
VSBA	0.408	0.227	-0.019	-0.118	-0.054	1.000	-0.295	0.204	-0.163
VSSY	0.487	-0.524	0.053	0.257	0.141	-0.295	1.000	0.072	0.001
ZIMX	0.237	0.058	0.191	0.508	-0.251	0.204	0.072	1.000	-0.068
ZSNL	0.004	0.154	0.185	0.099	0.188	-0.163	0.001	-0.068	1.000

Table B5 Environmental Correlation Matrix for Model 2.

	ACPM	ACSY	PMPM	ASJP	BACC	BAOP	ASAS	JPJP	4141	POPO	PTPT	STST	ZTZT	BRAS	BRLD	BRNA	BRPT
ACPM	1.000	0.268	0.475	0.053	0.060	-0.077	0.155	-0.064	0.084	0.018	-0.130	-0.095	0.243	0.134	0.033	-0.139	-0.140
ACSY	0.268	1.000	0.330	0.027	0.033	-0.100	0.107	0.121	0.028	0.084	0.062	-0.236	0.122	0.045	-0.075	0.052	-0.113
PMPM	0.475	0.330	1.000	0.176	0.132	-0.209	0.153	0.091	0.330	0.270	0.138	0.032	0.218	0.130	-0.098	0.111	0.030
ASJP	0.053	0.027	0.176	1.000	0.065	-0.117	0.439	0.077	-0.037	0.161	0.073	-0.034	0.159	-0.121	0.018	0.170	0.046
BACC	0.060	0.033	0.132	0.065	1.000	-0.090	-0.104	0.256	0.168	-0.009	0.180	-0.022	0.178	0.070	0.035	-0.018	0.089
BAOP	-0.077	-0.100	-0.209	-0.117	-0.090	1.000	-0.005	-0.178	-0.425	0.017	-0.033	0.043	-0.095	-0.119	0.091	-0.055	-0.090
ASAS	0.155	0.107	0.153	0.439	-0.104	-0.005	1.000	-0.067	-0.067	0.128	0.160	0.131	0.190	0.162	0.074	-0.015	0.120
JPJP	-0.064	0.121	0.091	0.077	0.256	-0.178	-0.067	1.000	0.131	0.050	0.266	-0.088	0.126	0.258	0.014	-0.036	-0.018
4141	0.084	0.028	0.330	-0.037	0.168	-0.425	-0.067	0.131	1.000	0.078	0.103	0.040	0.152	0.025	0.092	-0.241	0.053
POPO	0.018	0.084	0.270	0.161	-0.009	0.017	0.128	0.050	0.078	1.000	0.305	-0.097	0.425	0.285	0.110	0.020	0.034
PTPT	-0.130	0.062	0.138	0.073	0.180	-0.033	0.160	0.266	0.103	0.305	1.000	0.190	0.287	0.304	0.139	0.277	0.469
STST	-0.095	-0.236	0.032	-0.034	-0.022	0.043	0.131	-0.088	0.040	-0.097	0.190	1.000	-0.100	0.159	0.048	0.064	0.191
ZTZT	0.243	0.122	0.218	0.159	0.178	-0.095	0.190	0.126	0.152	0.425	0.287	-0.100	1.000	0.217	0.149	0.161	0.204
BRAS	0.134	0.045	0.130	-0.121	0.070	-0.119	0.162	0.258	0.025	0.285	0.304	0.159	0.217	1.000	0.432	-0.400	0.014
BRLD	0.033	-0.075	-0.098	0.018	0.035	0.091	0.074	0.014	0.092	0.110	0.139	0.048	0.149	0.432	1.000	-0.283	0.002
BRNA	-0.139	0.052	0.111	0.170	-0.018	-0.055	-0.015	-0.036	-0.241	0.020	0.277	0.064	0.161	-0.400	-0.283	1.000	0.474
BRPT	-0.140	-0.113	0.030	0.046	0.089	-0.090	0.120	-0.018	0.053	0.034	0.469	0.191	0.204	0.014	0.002	0.474	1.000
NABA	0.116	0.062	0.153	0.028	0.234	-0.287	-0.012	0.208	0.218	0.173	0.086	-0.133	0.299	0.248	0.180	-0.008	0.039
CACP	-0.066	-0.025	-0.047	-0.051	0.252	-0.065	0.054	0.256	0.348	0.069	0.048	-0.048	0.227	0.048	-0.034	-0.042	-0.085
CPSL	0.109	0.122	0.033	0.138	-0.040	-0.111	-0.013	0.057	0.099	-0.077	-0.047	-0.005	-0.032	-0.003	0.018	0.047	-0.052
CPZS	0.063	-0.120	0.202	0.067	0.163	-0.169	0.064	0.137	0.215	0.051	0.111	0.006	0.265	0.159	0.072	0.120	0.106
CNCN	0.103	0.140	-0.017	0.046	0.289	0.192	-0.023	0.202	-0.116	-0.033	-0.098	-0.138	0.042	0.076	0.039	0.002	-0.103
FMPM	0.175	0.483	0.225	0.021	0.116	-0.135	0.202	0.080	0.103	0.169	0.099	-0.120	0.383	0.082	-0.077	0.142	0.001
FMZT	-0.054	0.054	0.124	0.078	0.039	-0.174	0.048	0.038	-0.001	0.227	0.288	-0.018	0.362	0.069	-0.024	0.230	0.162
FMCP	0.118	0.029	0.258	0.153	0.193	-0.093	0.111	0.079	0.286	0.486	0.257	-0.053	0.583	0.179	0.057	0.289	0.207
FMPT	-0.061	-0.050	-0.010	0.121	0.122	-0.009	-0.063	0.183	-0.258	0.105	0.148	0.033	0.182	-0.074	0.048	0.148	-0.376
LDAS	0.167	0.150	0.138	-0.288	-0.030	-0.056	0.486	0.063	0.018	0.136	0.153	0.032	0.148	0.467	-0.104	-0.051	0.128
LDBA	0.113	0.223	0.171	0.189	0.111	-0.166	0.020	0.278	0.262	0.250	-0.016	-0.265	0.383	0.333	-0.051	0.102	0.105
NANL	-0.159	0.244	-0.010	-0.085	0.165	-0.157	-0.007	-0.045	-0.150	-0.090	0.017	-0.054	0.135	-0.043	-0.123	0.111	0.095
NLAC	0.247	0.319	0.181	-0.017	0.229	-0.103	0.187	0.146	-0.030	0.041	0.038	0.164	0.018	0.076	-0.004	-0.029	-0.066
NLVS	0.060	0.633	0.166	-0.063	0.053	0.010	0.001	-0.061	-0.029	0.123	0.015	-0.206	0.090	-0.109	-0.063	0.054	-0.098
NAAC	0.021	0.588	0.233	-0.019	0.077	-0.111	0.036	-0.064	-0.183	-0.047	-0.089	-0.105	0.027	-0.159	-0.170	0.137	0.014
NACA	0.032	-0.094	0.193	0.132	-0.044	-0.103	-0.068	-0.186	-0.132	0.181	0.152	0.014	0.106	0.199	0.223	0.153	0.151
NACP	-0.091	-0.069	0.083	0.053	0.107	-0.111	0.065	0.104	0.152	0.270	0.203	-0.057	0.259	0.252	0.158	0.133	0.034
NAFM	0.194	0.216	0.339	0.104	0.226	-0.081	0.227	0.010	0.183	0.268	-0.020	-0.047	0.467	0.249	0.119	0.058	0.012
NA41	-0.041	0.336	0.046	0.062	0.139	-0.175	0.158	0.072	0.009	0.158	-0.016	-0.169	0.326	0.109	-0.037	0.062	-0.026
NAVS	0.063	0.063	0.063	0.094	0.159	-0.063	0.093	0.166	0.122	0.356	-0.030	-0.232	0.368	0.258	0.186	0.057	-0.024
NAZI	0.104	0.128	0.175	0.119	0.169	-0.041	0.078	0.106	0.171	0.211	0.152	0.096	0.397	0.241	0.212	-0.072	0.068
NAZS	0.121	0.113	0.094	0.047	0.026	0.114	0.127	0.054	0.078	0.182	-0.026	-0.060	0.252	0.100	0.072	0.037	-0.008
BRBA	0.019	-0.097	0.104	0.033	0.180	-0.300	0.038	0.338	0.133	0.224	0.161	0.123	0.276	0.579	0.206	-0.075	0.197
NALD	0.018	0.134	0.046	0.102	0.067	0.033	0.106	0.069	0.055	0.266	0.207	-0.059	0.368	0.268	0.789	0.211	0.096
DAFM	0.213	-0.023	0.378	-0.045	0.234	0.031	0.178	0.153	0.363	0.337	0.095	-0.036	0.319	0.263	-0.101	0.066	0.057
PLSY	-0.005	0.675	0.102	-0.015	0.034	-0.116	0.072	0.098	0.048	0.057	0.023	-0.354	0.126	0.021	-0.094	0.062	-0.086
POBA	0.161	0.279	0.163	0.104	-0.004	0.048	0.178	0.075	0.158	0.642	0.299	-0.066	0.400	0.236	0.097	0.143	0.082
PM41	0.129	0.158	0.277	0.100	0.038	0.005	0.101	-0.099	0.286	0.135	0.065	-0.093	0.209	0.096	0.083	0.026	-0.043
41MX	0.022	0.468	0.013	-0.014	0.081	-0.247	0.206	-0.026	-0.024	0.169	0.088	-0.189	0.350	0.022	-0.059	0.010	-0.116
41ZI	1.000	1.000	-0.007	-0.068	-0.070	1.000	0.323	-0.018	1.000	0.076	0.112	-0.160	0.271	-0.005	1.000	1.000	1.000
PTAS	0.185	0.206	0.181	0.257	0.100	-0.137	-0.152	0.181	0.147	0.300	0.063	-0.042	0.286	0.319	0.080	0.249	0.140
PTLD	-0.001	0.104	0.042	0.059	0.025	0.041	0.148	0.009	0.399	0.254	0.225	-0.024	0.312	0.279	0.688	0.162	0.439
SLBA	-0.080	-0.208	-0.150	-0.184	0.187	0.026	0.181	0.100	0.076	0.144	0.139	0.168	0.168	0.159	0.015	-0.147	0.077
SLCC	-0.092	-0.128	0.006	-0.089	0.427	0.047	0.051	0.148	-0.132	0.165	0.163	0.187	0.158	0.212	0.094	-0.111	0.122
SYBA	0.004	-0.439	0.102	-0.004	0.109	-0.240	-0.086	-0.238	0.219	-0.097	0.169	-0.105	-0.028	-0.340	-0.023	0.061	0.103
SYMX	-0.081	0.602	0.081	0.031	0.086	-0.053	0.102	0.252	-0.087	0.196	0.110	-0.165	0.219	0.062	-0.037	0.074	0.054
ZTPO	0.183	0.263	0.103	0.128	0.211	-0.109	0.050	0.334	0.107	0.272	0.214	-0.227	0.350	0.256	0.111	0.205	0.164
ZTVS	0.180	0.064	0.218	0.099	0.183	-0.007	0.156	0.178	0.203	0.476	0.320	-0.166	0.946	0.157	0.131	0.129	0.172
ZTZI	-0.038	0.053	0.171	0.138	0.152	-0.158	-0.103	0.091	-0.147	0.108	-0.041	-0.081	0.090	0.034	0.034	0.062	0.092
VSBA	0.010	0.087	0.115	-0.041	0.116	-0.326	-0.095	0.044	0.092	-0.188	0.271	0.090	-0.036	-0.018	-0.095	0.126	0.125
VSSY	-0.043	-0.564	-0.049	0.047	0.095	0.100	0.022	-0.134	0.120	0.093	-0.013	-0.031	0.124	-0.195	0.040	0.034	0.070
ZIMX	0.054	0.092	-0.017	0.100	0.140	0.006	0.250	0.202	0.340	0.215	0.196	-0.118	0.567	0.219	0.075	0.097	0.023
ZSNL	-0.041	0.436	0.061	-0.095	0.038	-0.088	-0.027	-0.271	-0.194	0.023	0.062	-0.209	0.056	-0.206	-0.160	0.081	0.125

	NABA	CACP	CPSL	CPZS	CNCN	FMPM	FMZT	FMCP	FMPT	LDAS	LDBA	NANL	NLAC	NLVS	NAAC	NACA	NACP
ACPM	0.116	-0.066	0.109	0.063	0.103	0.175	-0.054	0.118	-0.061	0.167	0.113	-0.159	0.247	0.060	0.021	0.032	-0.091
ACSY	0.062	-0.025	0.122	-0.120	0.140	0.483	0.054	0.029	-0.050	0.150	0.223	0.244	0.319	0.633	0.588	-0.094	-0.069
PMPM	0.153	-0.047	0.033	0.202	-0.017	0.225	0.124	0.258	-0.010	0.138	0.171	-0.010	0.181	0.166	0.233	0.193	0.083
ASJP	0.028	-0.051	0.138	0.067	0.046	0.021	0.078	0.153	0.121	-0.288	0.189	-0.085	-0.017	-0.063	-0.019	0.132	0.053
BACC	0.234	0.252	-0.040	0.163	0.289	0.116	0.039	0.193	0.122	-0.030	0.111	0.165	0.229	0.053	0.077	-0.044	0.107
BAOP	-0.287	-0.065	-0.111	-0.169	0.192	-0.135	-0.174	-0.093	-0.009	-0.056	-0.166	-0.157	-0.103	0.010	-0.111	-0.103	-0.111
ASAS	-0.012	0.054	-0.013	0.064	-0.023	0.202	0.048	0.111	-0.063	0.486	0.020	-0.007	0.187	0.001	0.036	-0.068	0.065
JPJP	0.208	0.256	0.057	0.137	0.202	0.080	0.038	0.079	0.183	0.063	0.278	-0.045	0.146	-0.061	-0.064	-0.186	0.104
4141	0.218	0.348	0.099	0.215	-0.116	0.103	-0.001	0.286	-0.258	0.018	0.262	-0.150	-0.030	-0.029	-0.183	-0.132	0.152
POPO	0.173	0.069	-0.077	0.051	-0.033	0.169	0.227	0.486	0.105	0.136	0.250	-0.090	0.041	0.123	-0.047	0.181	0.270
PTPT	0.086	0.048	-0.047	0.111	-0.098	0.099	0.288	0.257	0.148	0.153	-0.016	0.017	0.038	0.015	-0.089	0.152	0.203
STST	-0.133	-0.048	-0.005	0.006	-0.138	-0.120	-0.018	-0.053	0.033	0.032	-0.265	-0.054	0.164	-0.206	-0.105	0.014	-0.057
ZTZT	0.299	0.227	-0.032	0.265	0.042	0.383	0.362	0.583	0.182	0.148	0.383	0.135	0.018	0.090	0.027	0.106	0.259
BRAS	0.248	0.048	-0.003	0.159	0.076	0.082	0.069	0.179	-0.074	0.467	0.333	-0.043	0.076	-0.109	-0.159	0.199	0.252
BRLD	0.180	-0.034	0.018	0.072	0.039	-0.077	-0.024	0.057	0.048	-0.104	-0.051	-0.123	-0.004	-0.063	-0.170	0.223	0.158
BRNA	-0.008	-0.042	0.047	0.120	0.002	0.142	0.230	0.289	0.148	-0.051	0.102	0.111	-0.029	0.054	0.137	0.153	0.133
BRPT	0.039	-0.085	-0.052	0.106	-0.103	0.001	0.162	0.207	-0.376	0.128	0.105	0.095	-0.066	-0.098	0.014	0.151	0.034
NABA	1.000	0.241	0.170	0.207	0.199	0.182	0.256	0.383	0.208	0.115	0.414	0.122	-0.042	0.267	0.160	0.109	0.354
CACP	0.241	1.000	-0.133	0.347	0.085	0.109	0.150	0.241	0.109	0.058	0.045	0.110	-0.034	0.126	0.047	-0.504	0.410
CPSL	0.170	-0.133	1.000	0.054	0.084	0.056	-0.015	-0.003	0.028	-0.064	0.114	0.080	0.174	0.000	0.021	0.162	-0.050
CPZS	0.207	0.347	0.054	1.000	0.100	0.328	0.077	0.528	0.097	0.084	0.224	0.148	0.152	-0.019	-0.074	0.154	0.541
CNCN	0.199	0.085	0.084	0.100	1.000	0.110	0.012	0.160	0.223	0.082	0.278	0.152	0.185	0.177	0.211	-0.010	0.124
FMPM	0.182	0.109	0.056	0.328	0.110	1.000	0.137	0.334	0.091	0.192	0.157	0.538	0.349	0.383	0.641	0.214	0.293
FMZT	0.256	0.150	-0.015	0.077	0.012	0.137	1.000	0.289	0.184	0.004	0.066	0.187	-0.125	0.102	0.087	0.003	0.166
FMCP	0.383	0.241	-0.003	0.528	0.160	0.334	0.289	1.000	0.217	0.174	0.533	0.037	-0.004	0.084	-0.102	0.338	0.656
FMPT	0.208	0.109	0.028	0.097	0.223	0.091	0.184	0.217	1.000	-0.109	0.027	-0.056	-0.046	0.168	-0.206	-0.014	0.097
LDAS	0.115	0.058	-0.064	0.084	0.082	0.192	0.004	0.174	-0.109	1.000	0.424	0.101	0.143	0.058	0.056	0.033	0.143
LDBA	0.414	0.045	0.114	0.224	0.278	0.157	0.066	0.533	0.027	0.424	1.000	0.017	0.028	0.073	-0.038	0.300	0.326
NANL	0.122	0.110	0.080	0.148	0.152	0.538	0.187	0.037	-0.056	0.101	0.017	1.000	0.059	0.550	0.646	0.119	0.139
NLAC	-0.042	-0.034	0.174	0.152	0.185	0.349	-0.125	-0.004	-0.046	0.143	0.028	0.059	1.000	0.040	0.437	0.019	-0.021
NLVS	0.267	0.126	0.000	-0.019	0.177	0.383	0.102	0.084	0.168	0.058	0.073	0.550	0.040	1.000	0.465	-0.095	0.039
NAAC	0.160	0.047	0.021	-0.074	0.211	0.641	0.087	-0.102	-0.206	0.056	-0.038	0.646	0.437	0.465	1.000	-0.106	-0.143
NACA	0.109	-0.504	0.162	0.154	-0.010	0.214	0.003	0.338	-0.014	0.033	0.300	0.119	0.019	-0.095	-0.106	1.000	0.465
NACP	0.354	0.410	-0.050	0.541	0.124	0.293	0.166	0.656	0.097	0.143	0.326	0.139	-0.021	0.039	-0.143	0.465	1.000
NAFM	0.383	0.041	0.060	0.097	0.110	0.384	0.073	0.496	0.111	0.237	0.349	0.120	0.198	0.110	0.291	0.128	0.237
NA41	0.362	0.129	0.059	0.138	0.156	0.619	0.209	0.166	0.035	0.139	0.135	0.512	0.209	0.335	0.733	-0.005	0.098
NAVS	0.720	0.112	0.085	0.227	0.284	0.127	0.290	0.462	0.246	0.147	0.409	0.193	-0.016	0.386	0.079	0.240	0.402
NAZI	0.461	0.114	0.123	0.116	0.134	0.374	0.418	0.236	0.105	0.118	0.205	0.251	0.122	0.134	0.420	0.000	0.062
NAZS	0.394	0.017	-0.067	0.111	0.178	0.014	0.121	0.242	0.055	0.100	0.125	-0.039	0.143	0.213	0.114	-0.047	0.094
BRBA	0.499	-0.042	0.146	0.224	0.092	-0.011	0.122	0.351	-0.021	0.175	0.523	-0.106	0.076	-0.177	-0.228	0.371	0.239
NALD	0.369	0.011	0.100	0.195	0.096	0.152	0.183	0.304	0.185	-0.049	0.178	0.004	-0.002	0.142	0.043	0.303	0.337
DAFM	0.095	0.099	0.026	0.238	-0.008	0.291	0.032	0.485	-0.003	0.305	0.249	-0.078	0.042	-0.049	-0.068	0.183	0.376
PLSY	0.011	-0.017	0.122	0.119	0.065	0.401	-0.064	0.090	0.127	0.137	0.254	0.186	0.080	0.349	0.303	-0.148	-0.062
POBA	0.091	0.106	-0.095	0.212	-0.092	0.261	0.157	0.499	0.104	0.238	0.221	-0.114	0.191	0.071	0.065	0.264	0.402
PM41	0.260	0.081	-0.046	0.297	0.056	0.521	0.120	0.355	0.092	0.048	0.163	0.136	0.100	0.200	-0.004	0.207	0.353
41MX	0.087	0.067	0.037	-0.076	-0.005	0.376	0.053	-0.007	0.042	0.193	-0.001	0.254	0.017	0.413	0.333	-0.144	-0.043
41ZI	0.024	0.227	1.000	0.120	1.000	1.000	0.043	0.118	0.036	1.000	1.000	0.218	1.000	1.000	1.000	-0.004	1.000
PTAS	0.365	0.045	0.150	0.165	0.052	0.026	0.270	0.349	-0.210	-0.112	0.421	0.077	-0.062	0.127	0.127	0.226	0.302
PTLD	0.220	-0.017	0.053	0.210	-0.014	0.076	0.144	0.269	-0.306	0.050	0.207	0.020	0.011	0.040	0.060	0.302	0.282
SLBA	0.183	0.052	-0.677	0.046	-0.170	-0.099	0.087	0.081	-0.069	0.235	-0.101	-0.018	-0.297	0.049	-0.118	0.045	0.101
SLCC	0.035	0.122	-0.593	-0.055	0.046	0.012	0.148	0.009	-0.028	0.150	-0.026	0.188	-0.126	0.083	0.133	-0.072	0.006
SYBA	0.264	0.336	-0.070	0.008	-0.089	-0.244	-0.096	0.024	0.031	-0.114	-0.165	-0.061	-0.218	0.000	-0.351	-0.187	0.055
SYMX	0.153	-0.073	0.180	0.102	0.096	0.454	0.129	0.133	0.039	0.091	0.202	0.217	0.083	0.260	0.303	0.050	0.010
ZTPO	0.353	0.115	0.201	0.425	0.254	0.440	0.136	0.453	0.177	0.165	0.512	0.255	0.126	0.348	0.229	0.240	0.349
ZTVS	0.284	0.236	-0.079	0.343	0.086	0.398	0.307	0.559	0.235	0.160	0.341	0.166	0.014	0.162	0.001	0.086	0.262
ZTZI	0.229	-0.044	0.126	0.100	0.158	0.199	0.108	0.153	0.046	-0.055	0.266	0.241	0.132	0.240	0.214	0.094	0.046
VSBA	0.308	0.172	0.141	-0.082	-0.040	-0.086	-0.045	0.086	-0.001	-0.010	0.092	-0.169	0.036	-0.162	0.009	-0.192	0.011
VSSY	0.026	0.059	-0.120	0.038	0.043	-0.066	0.069	0.048	-0.018	-0.081	-0.117	0.099	-0.041	-0.001	-0.110	0.100	0.025
ZIMX	0.207	0.143	0.046	0.287	0.052	0.239	0.214	0.322	0.127	0.171	0.166	0.160	0.073	0.004	0.158	0.127	0.263
ZSNL	-0.024	0.003	-0.035	0.115	0.082	0.544	0.035	0.093	-0.128	0.031	-0.031	0.794	0.070	0.709	0.559	0.138	0.078

	NAFM	NA41	NAVS	NAZI	NAZS	BRBA	NALD	DAFM	PLSY	POBA	PM41	41MX	41ZI	PTAS	PTLD	SLBA	SLCC
ACPM	0.194	-0.041	0.063	0.104	0.121	0.019	0.018	0.213	-0.005	0.161	0.129	0.022	1.000	0.185	-0.001	-0.080	-0.092
ACSY	0.216	0.336	0.063	0.128	0.113	-0.097	0.134	-0.023	0.675	0.279	0.158	0.468	1.000	0.206	0.104	-0.208	-0.128
PMPM	0.339	0.046	0.063	0.175	0.094	0.104	0.046	0.378	0.102	0.163	0.277	0.013	-0.007	0.181	0.042	-0.150	0.006
ASJP	0.104	0.062	0.094	0.119	0.047	0.033	0.102	-0.045	-0.015	0.104	0.100	-0.014	-0.068	0.257	0.059	-0.184	-0.089
BACC	0.226	0.139	0.159	0.169	0.026	0.180	0.067	0.234	0.034	-0.004	0.038	0.081	-0.070	0.100	0.025	0.187	0.427
BAOP	-0.081	-0.175	-0.063	-0.041	0.114	-0.300	0.033	0.031	-0.116	0.048	0.005	-0.247	1.000	-0.137	0.041	0.026	0.047
ASAS	0.227	0.158	0.093	0.078	0.127	0.038	0.106	0.178	0.072	0.178	0.101	0.206	0.323	-0.152	0.148	0.181	0.051
JPJP	0.010	0.072	0.166	0.106	0.054	0.338	0.069	0.153	0.098	0.075	-0.099	-0.026	-0.018	0.181	0.009	0.100	0.148
4141	0.183	0.009	0.122	0.171	0.078	0.133	0.055	0.363	0.048	0.158	0.286	-0.024	1.000	0.147	0.399	0.076	-0.132
POPO	0.268	0.158	0.356	0.211	0.182	0.224	0.266	0.337	0.057	0.642	0.135	0.169	0.076	0.300	0.254	0.144	0.165
PTPT	-0.020	-0.016	-0.030	0.152	-0.026	0.161	0.207	0.095	0.023	0.299	0.065	0.088	0.112	0.063	0.225	0.139	0.163
STST	-0.047	-0.169	-0.232	0.096	-0.060	0.123	-0.059	-0.036	-0.354	-0.066	-0.093	-0.189	-0.160	-0.042	-0.024	0.168	0.187
ZTZT	0.467	0.326	0.368	0.397	0.252	0.276	0.368	0.319	0.126	0.400	0.209	0.350	0.271	0.286	0.312	0.168	0.158
BRAS	0.249	0.109	0.258	0.241	0.100	0.579	0.268	0.263	0.021	0.236	0.096	0.022	-0.005	0.319	0.279	0.159	0.212
BRLD	0.119	-0.037	0.186	0.212	0.072	0.206	0.789	-0.101	-0.094	0.097	0.083	-0.059	1.000	0.080	0.688	0.015	0.094
BRNA	0.058	0.062	0.057	-0.072	0.037	-0.075	0.211	0.066	0.062	0.143	0.026	0.010	1.000	0.249	0.162	-0.147	-0.111
BRPT	0.012	-0.026	-0.024	0.068	-0.008	0.197	0.096	0.057	-0.086	0.082	-0.043	-0.116	1.000	0.140	0.439	0.077	0.122
NABA	0.383	0.362	0.720	0.461	0.394	0.499	0.369	0.095	0.011	0.091	0.260	0.087	0.024	0.365	0.220	0.183	0.035
CACP	0.041	0.129	0.112	0.114	0.017	-0.042	0.011	0.099	-0.017	0.106	0.081	0.067	0.227	0.045	-0.017	0.052	0.122
CPSL	0.060	0.059	0.085	0.123	-0.067	0.146	0.100	0.026	0.122	-0.095	-0.046	0.037	1.000	0.150	0.053	-0.677	-0.593
CPZS	0.097	0.138	0.227	0.116	0.111	0.224	0.195	0.238	0.119	0.212	0.297	-0.076	0.120	0.165	0.210	0.046	-0.055
CNCN	0.110	0.156	0.284	0.134	0.178	0.092	0.096	-0.008	0.065	-0.092	0.056	-0.005	1.000	0.052	-0.014	-0.170	0.046
FMPM	0.384	0.619	0.127	0.374	0.014	-0.011	0.152	0.291	0.401	0.261	0.521	0.376	1.000	0.026	0.076	-0.099	0.012
FMZT	0.073	0.209	0.290	0.418	0.121	0.122	0.183	0.032	-0.064	0.157	0.120	0.053	0.043	0.270	0.144	0.087	0.148
FMCP	0.496	0.166	0.462	0.236	0.242	0.351	0.304	0.485	0.090	0.499	0.355	-0.007	0.118	0.349	0.269	0.081	0.009
FMPT	0.111	0.035	0.246	0.105	0.055	-0.021	0.185	-0.003	0.127	0.104	0.092	0.042	0.036	-0.210	-0.306	-0.069	-0.028
LDAS	0.237	0.139	0.147	0.118	0.100	0.175	-0.049	0.305	0.137	0.238	0.048	0.193	1.000	-0.112	0.050	0.235	0.150
LDBA	0.349	0.135	0.409	0.205	0.125	0.523	0.178	0.249	0.254	0.221	0.163	-0.001	1.000	0.421	0.207	-0.101	-0.026
NANL	0.120	0.512	0.193	0.251	-0.039	-0.106	0.004	-0.078	0.186	-0.114	0.136	0.254	0.218	0.077	0.020	-0.018	0.188
NLAC	0.198	0.209	-0.016	0.122	0.143	0.076	-0.002	0.042	0.080	0.191	0.100	0.017	1.000	-0.062	0.011	-0.297	-0.126
NLVS	0.110	0.335	0.386	0.134	0.213	-0.177	0.142	-0.049	0.349	0.071	0.200	0.413	1.000	0.127	0.040	0.049	0.083
NAAC	0.291	0.733	0.079	0.420	0.114	-0.228	0.043	-0.068	0.303	0.065	-0.004	0.333	1.000	0.127	0.060	-0.118	0.133
NACA	0.128	-0.005	0.240	0.000	-0.047	0.371	0.303	0.183	-0.148	0.264	0.207	-0.144	-0.004	0.226	0.302	0.045	-0.072
NACP	0.237	0.098	0.402	0.062	0.094	0.239	0.337	0.376	-0.062	0.402	0.353	-0.043	1.000	0.302	0.282	0.101	0.006
NAFM	1.000	0.278	0.240	0.529	0.488	0.149	0.357	0.671	0.076	0.345	0.292	0.033	-0.007	0.297	0.229	0.072	0.112
NA41	0.278	1.000	0.328	0.558	0.261	0.061	0.104	0.046	0.351	0.267	0.164	0.500	0.367	0.127	0.072	-0.007	0.146
NAVS	0.240	0.328	1.000	0.370	0.398	0.354	0.408	0.060	-0.040	0.204	0.198	-0.006	1.000	0.387	0.269	0.039	0.077
NAZI	0.529	0.558	0.370	1.000	0.545	0.199	0.302	0.216	0.136	0.248	0.285	0.029	-0.032	0.304	0.264	0.115	0.185
NAZS	0.488	0.261	0.398	0.545	1.000	0.114	0.202	0.283	0.033	0.244	0.117	-0.068	-0.169	0.195	0.109	0.161	0.186
BRBA	0.149	0.061	0.354	0.199	0.114	1.000	0.126	0.102	-0.041	0.113	0.121	-0.151	-0.268	0.307	0.180	-0.023	0.018
NALD	0.357	0.104	0.408	0.302	0.202	0.126	1.000	0.108	0.065	0.202	0.172	0.066	-0.014	0.276	0.837	-0.041	0.047
DAFM	0.671	0.046	0.060	0.216	0.283	0.102	0.108	1.000	-0.083	0.395	0.248	0.111	1.000	0.152	0.105	0.089	0.120
PLSY	0.076	0.351	-0.040	0.136	0.033	-0.041	0.065	-0.083	1.000	0.193	0.202	0.381	0.202	0.064	0.010	-0.120	-0.150
POBA	0.345	0.267	0.204	0.248	0.244	0.113	0.202	0.395	0.193	1.000	0.213	0.187	1.000	0.138	0.159	0.266	0.172
PM41	0.292	0.164	0.198	0.285	0.117	0.121	0.172	0.248	0.202	0.213	1.000	-0.036	0.194	0.164	0.081	0.176	0.101
41MX	0.033	0.500	-0.006	0.029	-0.068	-0.151	0.066	0.111	0.381	0.187	-0.036	1.000	0.362	-0.037	0.016	0.004	0.035
41ZI	-0.007	0.367	1.000	-0.032	-0.169	-0.268	-0.014	1.000	0.202	1.000	0.194	0.362	1.000	-0.264	-0.031	1.000	-0.036
PTAS	0.297	0.127	0.387	0.304	0.195	0.307	0.276	0.152	0.064	0.138	0.164	-0.037	-0.264	1.000	0.378	-0.098	0.046
PTLD	0.229	0.072	0.269	0.264	0.109	0.180	0.837	0.105	0.010	0.159	0.081	0.016	-0.031	0.378	1.000	-0.008	0.077
SLBA	0.072	-0.007	0.039	0.115	0.161	-0.023	-0.041	0.089	-0.120	0.266	0.176	0.004	1.000	-0.098	-0.008	1.000	0.678
SLCC	0.112	0.146	0.077	0.185	0.186	0.018	0.047	0.120	-0.150	0.172	0.101	0.035	-0.036	0.046	0.077	0.678	1.000
SYBA	-0.215	-0.329	0.046	-0.201	-0.098	-0.146	0.043	0.043	-0.466	-0.085	-0.171	0.053	0.146	-0.137	0.084	0.358	0.020
SYMX	0.236	0.348	0.069	0.170	0.190	0.056	0.076	0.002	0.685	0.224	0.165	0.231	0.213	0.187	0.054	-0.052	-0.019
ZTPO	0.311	0.344	0.373	0.287	0.235	0.356	0.297	0.112	0.243	0.213	0.310	0.282	0.032	0.359	0.200	-0.136	0.003
ZTVS	0.328	0.377	0.422	0.320	0.238	0.220	0.320	0.281	0.089	0.497	0.192	0.406	0.332	0.186	0.302	0.231	0.197
ZTZI	0.081	0.131	0.341	0.124	0.112	0.255	0.141	-0.035	0.077	-0.176	0.071	0.163	-0.473	0.289	0.149	-0.136	0.082
VSBA	0.155	-0.007	-0.240	0.072	0.034	0.136	-0.046	0.083	0.076	-0.174	0.066	0.146	1.000	0.061	-0.024	0.098	-0.143
VSSY	-0.040	0.005	0.156	-0.006	0.023	-0.067	0.059	0.016	-0.565	0.071	-0.099	-0.089	-0.024	-0.036	0.101	0.179	0.190
ZIMX	0.152	0.287	0.078	0.136	0.113	0.091	0.181	0.147	-0.077	0.409	0.155	0.223	0.564	0.104	0.162	0.040	-0.002
ZSNL	0.156	0.353	0.074	0.150	-0.029	-0.289	0.034	-0.014	0.228	0.065	0.275	0.229	1.000	0.006	0.106	0.023	0.152

	SYBA	SYMX	ZTPO	ZTVS	ZTZI	VSBA	VSSY	ZIMX	ZSNL
ACPM	0.004	-0.081	0.183	0.180	-0.038	0.010	-0.043	0.054	-0.041
ACSY	-0.439	0.602	0.263	0.064	0.053	0.087	-0.564	0.092	0.436
PMPM	0.102	0.081	0.103	0.218	0.171	0.115	-0.049	-0.017	0.061
ASJP	-0.004	0.031	0.128	0.099	0.138	-0.041	0.047	0.100	-0.095
BACC	0.109	0.086	0.211	0.183	0.152	0.116	0.095	0.140	0.038
BAOP	-0.240	-0.053	-0.109	-0.007	-0.158	-0.326	0.100	0.006	-0.088
ASAS	-0.086	0.102	0.050	0.156	-0.103	-0.095	0.022	0.250	-0.027
JPJP	-0.238	0.252	0.334	0.178	0.091	0.044	-0.134	0.202	-0.271
4141	0.219	-0.087	0.107	0.203	-0.147	0.092	0.120	0.340	-0.194
POPO	-0.097	0.196	0.272	0.476	0.108	-0.188	0.093	0.215	0.023
PTPT	0.169	0.110	0.214	0.320	-0.041	0.271	-0.013	0.196	0.062
STST	-0.105	-0.165	-0.227	-0.166	-0.081	0.090	-0.031	-0.118	-0.209
ZTZT	-0.028	0.219	0.350	0.946	0.090	-0.036	0.124	0.567	0.056
BRAS	-0.340	0.062	0.256	0.157	0.034	-0.018	-0.195	0.219	-0.206
BRLD	-0.023	-0.037	0.111	0.131	0.034	-0.095	0.040	0.075	-0.160
BRNA	0.061	0.074	0.205	0.129	0.062	0.126	0.034	0.097	0.081
BRPT	0.103	0.054	0.164	0.172	0.092	0.125	0.070	0.023	0.125
NABA	0.264	0.153	0.353	0.284	0.229	0.308	0.026	0.207	-0.024
CACP	0.336	-0.073	0.115	0.236	-0.044	0.172	0.059	0.143	0.003
CPSL	-0.070	0.180	0.201	-0.079	0.126	0.141	-0.120	0.046	-0.035
CPZS	0.008	0.102	0.425	0.343	0.100	-0.082	0.038	0.287	0.115
CNCN	-0.089	0.096	0.254	0.086	0.158	-0.040	0.043	0.052	0.082
FMPM	-0.244	0.454	0.440	0.398	0.199	-0.086	-0.066	0.239	0.544
FMZT	-0.096	0.129	0.136	0.307	0.108	-0.045	0.069	0.214	0.035
FMCP	0.024	0.133	0.453	0.559	0.153	0.086	0.048	0.322	0.093
FMPT	0.031	0.039	0.177	0.235	0.046	-0.001	-0.018	0.127	-0.128
LDAS	-0.114	0.091	0.165	0.160	-0.055	-0.010	-0.081	0.171	0.031
LDBA	-0.165	0.202	0.512	0.341	0.266	0.092	-0.117	0.166	-0.031
NANL	-0.061	0.217	0.255	0.166	0.241	-0.169	0.099	0.160	0.794
NLAC	-0.218	0.083	0.126	0.014	0.132	0.036	-0.041	0.073	0.070
NLVS	0.000	0.260	0.348	0.162	0.240	-0.162	-0.001	0.004	0.709
NAAC	-0.351	0.303	0.229	0.001	0.214	0.009	-0.110	0.158	0.559
NACA	-0.187	0.050	0.240	0.086	0.094	-0.192	0.100	0.127	0.138
NACP	0.055	0.010	0.349	0.262	0.046	0.011	0.025	0.263	0.078
NAFM	-0.215	0.236	0.311	0.328	0.081	0.155	-0.040	0.152	0.156
NA41	-0.329	0.348	0.344	0.377	0.131	-0.007	0.005	0.287	0.353
NAVS	0.046	0.069	0.373	0.422	0.341	-0.240	0.156	0.078	0.074
NAZI	-0.201	0.170	0.287	0.320	0.124	0.072	-0.006	0.136	0.150
NAZS	-0.098	0.190	0.235	0.238	0.112	0.034	0.023	0.113	-0.029
BRBA	-0.146	0.056	0.356	0.220	0.255	0.136	-0.067	0.091	-0.289
NALD	0.043	0.076	0.297	0.320	0.141	-0.046	0.059	0.181	0.034
DAFM	0.043	0.002	0.112	0.281	-0.035	0.083	0.016	0.147	-0.014
PLSY	-0.466	0.685	0.243	0.089	0.077	0.076	-0.565	-0.077	0.228
POBA	-0.085	0.224	0.213	0.497	-0.176	-0.174	0.071	0.409	0.065
PM41	-0.171	0.165	0.310	0.192	0.071	0.066	-0.099	0.155	0.275
41MX	0.053	0.231	0.282	0.406	0.163	0.146	-0.089	0.223	0.229
41ZI	0.146	0.213	0.032	0.332	-0.473	1.000	-0.024	0.564	1.000
PTAS	-0.137	0.187	0.359	0.186	0.289	0.061	-0.036	0.104	0.006
PTLD	0.084	0.054	0.200	0.302	0.149	-0.024	0.101	0.162	0.106
SLBA	0.358	-0.052	-0.136	0.231	-0.136	0.098	0.179	0.040	0.023
SLCC	0.020	-0.019	0.003	0.197	0.082	-0.143	0.190	-0.002	0.152
SYBA	1.000	-0.444	-0.101	0.034	-0.012	0.387	0.514	0.274	-0.020
SYMX	-0.444	1.000	0.229	0.083	0.037	0.172	-0.563	-0.010	0.217
ZTPO	-0.101	0.229	1.000	0.392	0.169	0.028	0.021	0.161	0.230
ZTVS	0.034	0.083	0.392	1.000	0.042	-0.134	0.277	0.539	0.122
ZTZI	-0.012	0.037	0.169	0.042	1.000	-0.072	0.113	-0.249	0.167
VSBA	0.387	0.172	0.028	-0.134	-0.072	1.000	-0.296	0.230	-0.195
VSSY	0.514	-0.563	0.021	0.277	0.113	-0.296	1.000	0.145	-0.014
ZIMX	0.274	-0.010	0.161	0.539	-0.249	0.230	0.145	1.000	0.026
ZSNL	-0.020	0.217	0.230	0.122	0.167	-0.195	-0.014	0.026	1.000

Table B6 Environmental Correlation Matrix for Model 3.

	ACPM	ACSY	PMPM	ASJP	BACC	BAOP	ASAS	JPJP	4141	POPO	PTPT	STST	ZTZT	BRAS	BRLD	BRNA	BRPT
ACPM	1.000	0.182	0.392	0.002	0.016	0.010	0.106	-0.067	0.131	0.003	-0.198	-0.051	0.108	0.070	0.001	-0.135	-0.159
ACSY	0.182	1.000	0.153	-0.086	-0.034	0.050	0.004	0.065	-0.047	-0.131	-0.089	-0.164	-0.288	-0.085	-0.156	-0.061	-0.181
PMPM	0.392	0.153	1.000	0.107	0.007	-0.187	0.064	-0.005	0.169	0.123	0.025	0.102	-0.019	-0.005	-0.170	-0.014	-0.022
ASJP	0.002	-0.086	0.107	1.000	0.021	-0.087	0.417	0.052	-0.056	0.143	0.023	-0.014	0.070	-0.203	-0.009	0.140	0.026
BACC	0.016	-0.034	0.007	0.021	1.000	-0.033	-0.167	0.215	0.076	-0.227	0.095	0.021	0.028	-0.037	-0.010	-0.042	0.060
BAOP	0.010	0.050	-0.187	-0.087	-0.033	1.000	0.050	-0.111	-0.308	0.126	-0.001	0.041	-0.021	-0.073	0.109	0.003	-0.082
ASAS	0.106	0.004	0.064	0.417	-0.167	0.050	1.000	-0.119	-0.097	0.027	0.086	0.164	0.044	0.085	0.042	-0.026	0.093
JPJP	-0.067	0.065	-0.005	0.052	0.215	-0.111	-0.119	1.000	0.082	-0.073	0.200	-0.070	0.015	0.169	-0.022	-0.020	-0.051
4141	0.131	-0.047	0.169	-0.056	0.076	-0.308	-0.097	0.082	1.000	-0.104	-0.003	0.150	-0.099	-0.084	0.034	-0.185	0.028
POPO	0.003	-0.131	0.123	0.143	-0.227	0.126	0.027	-0.073	-0.104	1.000	0.200	-0.047	0.187	0.185	0.126	-0.081	-0.072
PTPT	-0.198	-0.089	0.025	0.023	0.095	-0.001	0.086	0.200	-0.003	0.200	1.000	0.246	0.168	0.223	0.096	0.228	0.459
STST	-0.051	-0.164	0.102	-0.014	0.021	0.041	0.164	-0.070	0.150	-0.047	0.246	1.000	-0.049	0.204	0.065	0.119	0.205
ZTZT	0.108	-0.288	-0.019	0.070	0.028	-0.021	0.044	0.015	-0.099	0.187	0.168	-0.049	1.000	0.036	0.079	0.076	0.163
BRAS	0.070	-0.085	-0.005	-0.203	-0.037	-0.073	0.085	0.169	-0.084	0.185	0.223	0.204	0.036	1.000	0.416	-0.522	-0.030
BRLD	0.001	-0.156	-0.170	-0.009	-0.010	0.109	0.042	-0.022	0.034	0.126	0.096	0.065	0.079	0.416	1.000	-0.340	-0.018
BRNA	-0.135	-0.061	-0.014	0.140	-0.042	0.003	-0.026	-0.020	-0.185	-0.081	0.228	0.119	0.076	-0.522	-0.340	1.000	0.445
BRPT	-0.159	-0.181	-0.022	0.026	0.060	-0.082	0.093	-0.051	0.028	-0.072	0.459	0.205	0.163	-0.030	-0.018	0.445	1.000
NABA	0.047	-0.157	-0.102	-0.037	0.130	-0.209	-0.105	0.160	0.092	-0.144	-0.127	-0.054	-0.040	0.074	0.079	-0.024	-0.040
CACP	-0.130	-0.144	-0.163	-0.093	0.179	-0.044	-0.013	0.197	0.173	-0.086	-0.028	-0.016	0.096	-0.045	-0.070	-0.105	-0.115
CPSL	0.086	0.088	0.025	0.127	-0.055	-0.098	-0.029	0.051	0.075	-0.064	-0.063	0.004	-0.099	-0.023	0.008	0.051	-0.061
CPZS	0.000	-0.321	0.020	-0.004	0.049	-0.075	-0.001	0.045	0.108	-0.210	-0.055	0.123	0.001	0.001	0.003	0.064	0.049
CNCN	0.043	0.081	-0.119	0.005	0.240	0.205	-0.078	0.146	-0.240	-0.182	-0.173	-0.120	-0.086	0.010	0.008	-0.055	-0.128
FMPM	-0.052	0.244	-0.105	-0.125	-0.128	-0.028	0.011	-0.115	-0.157	-0.253	-0.151	-0.020	-0.151	-0.260	-0.242	0.022	-0.108
FMZT	-0.108	-0.126	-0.004	0.029	-0.041	-0.112	-0.048	-0.022	-0.033	0.056	0.201	0.046	0.201	-0.061	-0.083	0.198	0.125
FMCP	0.009	-0.365	-0.002	0.074	0.033	0.003	-0.032	-0.078	0.113	0.231	0.090	0.087	0.350	-0.055	-0.037	0.255	0.173
FMPT	-0.056	-0.042	-0.080	0.102	0.088	0.042	-0.098	0.152	-0.300	0.046	0.085	0.069	0.110	-0.133	0.025	0.154	-0.418
LDAS	0.089	0.025	0.013	-0.382	-0.132	-0.001	0.440	-0.018	-0.076	-0.002	0.056	0.073	-0.041	0.405	-0.155	-0.128	0.091
LDBA	0.009	0.016	-0.020	0.126	-0.019	-0.111	-0.089	0.201	0.041	0.048	-0.194	-0.252	0.166	0.216	-0.134	0.015	0.052
NANL	-0.198	0.170	-0.202	-0.139	0.058	-0.053	-0.102	-0.127	-0.193	-0.350	-0.142	0.049	-0.146	-0.231	-0.195	0.071	0.046
NLAC	0.174	0.235	0.059	-0.068	0.149	-0.026	0.125	0.094	-0.018	-0.095	-0.047	0.191	-0.230	-0.046	-0.056	-0.070	-0.094
NLVS	0.040	0.581	-0.011	-0.129	-0.031	0.106	-0.064	-0.144	-0.058	-0.092	-0.153	-0.160	-0.217	-0.245	-0.128	0.027	-0.159
NAAC	-0.113	0.527	0.009	-0.108	-0.010	0.021	-0.073	-0.113	-0.138	-0.282	-0.245	-0.025	-0.420	-0.326	-0.256	0.048	-0.059
NACA	0.044	-0.210	0.070	0.110	-0.121	0.005	-0.099	-0.225	-0.118	0.069	0.052	0.070	-0.070	0.121	0.201	0.132	0.097
NACP	-0.161	-0.387	-0.170	-0.026	-0.003	-0.009	-0.060	-0.001	0.010	0.004	0.036	0.042	-0.035	0.087	0.108	0.036	-0.038
NAFM	0.140	-0.019	0.141	0.052	0.132	0.044	0.140	-0.074	0.049	0.044	-0.202	0.028	0.258	0.085	0.047	0.055	-0.061
NA41	-0.248	0.073	-0.271	-0.046	-0.037	-0.090	-0.002	-0.067	-0.197	-0.171	-0.266	-0.089	-0.182	-0.171	-0.176	-0.053	-0.132
NAVS	-0.034	-0.222	-0.194	0.020	0.027	0.028	0.026	0.078	-0.045	0.095	-0.237	-0.186	0.127	0.101	0.125	-0.035	-0.099
NAZI	-0.022	-0.137	-0.032	0.055	0.041	0.083	-0.043	-0.004	-0.004	-0.062	-0.003	0.206	0.137	0.063	0.142	-0.148	0.008
NAZS	0.073	-0.043	-0.034	0.003	-0.059	0.174	0.075	-0.033	0.019	0.067	-0.135	-0.022	0.105	0.007	0.036	-0.018	-0.053
BRBA	-0.034	-0.206	-0.032	-0.015	0.107	-0.241	-0.009	0.287	0.077	0.079	0.077	0.168	0.122	0.527	0.175	-0.116	0.167
NALD	-0.093	-0.129	-0.158	0.034	-0.053	0.128	0.031	-0.013	-0.109	0.144	0.094	-0.003	0.167	0.147	0.808	0.136	0.046
DAFM	0.123	-0.213	0.215	-0.111	0.126	0.131	0.092	0.095	0.269	0.179	-0.030	0.029	0.087	0.125	-0.181	0.042	0.005
PLSY	-0.072	0.644	-0.025	-0.076	-0.046	-0.028	-0.004	0.021	-0.018	-0.067	-0.079	-0.310	-0.109	-0.095	-0.150	-0.004	-0.132
POBA	0.033	0.021	-0.111	0.033	-0.181	0.160	0.063	-0.043	-0.004	0.502	0.165	0.018	0.087	0.049	0.011	0.050	0.034
PM41	0.048	0.015	0.140	0.036	-0.089	0.087	-0.001	-0.203	0.182	-0.064	-0.053	-0.023	-0.060	-0.045	0.022	-0.050	-0.102
41MX	-0.082	0.343	-0.200	-0.086	-0.009	-0.146	0.092	-0.111	-0.087	-0.032	-0.055	-0.105	0.039	-0.152	-0.137	-0.020	-0.167
41ZI	0.001	0.168	-0.222	-0.148	-0.174	0.023	0.244	-0.096	-0.031	-0.142	-0.017	-0.092	-0.026	-0.183	-0.218	-0.004	-0.157
PTAS	0.084	-0.007	0.031	0.214	-0.011	-0.109	-0.254	0.094	0.003	0.153	-0.040	-0.012	0.132	0.220	0.034	0.175	0.114
PTLD	-0.125	-0.162	-0.143	-0.003	-0.108	0.077	0.052	-0.113	0.203	0.088	0.131	0.018	0.094	0.161	0.684	0.072	0.434
SLBA	-0.103	-0.211	-0.223	-0.200	0.153	0.052	0.123	0.084	0.064	0.084	0.082	0.181	0.103	0.094	-0.010	-0.148	0.056
SLCC	-0.119	-0.117	-0.080	-0.121	0.394	0.081	-0.011	0.124	-0.130	0.065	0.106	0.206	0.071	0.140	0.057	-0.131	0.095
SYBA	0.105	-0.352	0.053	0.013	0.118	-0.174	-0.052	-0.200	0.365	-0.120	0.119	-0.045	-0.052	-0.315	-0.033	0.122	0.082
SYMX	-0.149	0.511	-0.055	-0.029	0.006	0.028	0.032	0.185	-0.195	0.086	0.008	-0.119	0.045	-0.054	-0.101	0.005	0.008
ZTPO	0.033	-0.002	-0.107	0.044	0.056	-0.069	-0.093	0.250	-0.236	0.016	0.111	-0.182	0.104	0.103	0.030	0.093	0.152
ZTVS	0.025	-0.356	-0.035	-0.011	0.008	0.088	-0.007	0.067	-0.055	0.218	0.188	-0.137	0.925	-0.061	0.051	-0.006	0.117
ZTZI	-0.100	-0.006	0.107	0.102	0.099	-0.144	-0.160	0.047	-0.202	0.002	-0.104	-0.062	-0.010	-0.030	0.010	0.026	0.069
VSBA	0.068	0.130	0.055	-0.047	0.120	-0.284	-0.096	0.065	0.137	-0.231	0.232	0.126	-0.103	-0.030	-0.103	0.157	0.112
VSSY	-0.036	-0.600	-0.075	0.042	0.092	0.124	0.026	-0.126	0.174	0.088	-0.035	-0.011	0.117	-0.217	0.033	0.057	0.062
ZIMX	-0.107	-0.243	-0.220	-0.004	-0.002	0.044	0.141	0.112	0.129	0.002	0.088	-0.076	0.418	0.072	-0.005	-0.015	-0.031
ZSNL	-0.053	0.397	-0.093	-0.174	-0.043	0.000	-0.127	-0.281	-0.217	-0.216	-0.096	-0.094	-0.217	-0.341	-0.215	0.045	0.037

	NABA	CACP	CPSL	CPZS	CNCN	FMPM	FMZT	FMCP	FMPT	LDAS	LDBA	NANL	NLAC	NLVS	NAAC	NACA	NACP
ACPM	0.047	-0.130	0.086	0.000	0.043	-0.052	-0.108	0.009	-0.056	0.089	0.009	-0.198	0.174	0.040	-0.113	0.044	-0.161
ACSY	-0.157	-0.144	0.088	-0.321	0.081	0.244	-0.126	-0.365	-0.042	0.025	0.016	0.170	0.235	0.581	0.527	-0.210	-0.387
PMPM	-0.102	-0.163	0.025	0.020	-0.119	-0.105	-0.004	-0.002	-0.080	0.013	-0.020	-0.202	0.059	-0.011	0.009	0.070	-0.170
ASJP	-0.037	-0.093	0.127	-0.004	0.005	-0.125	0.029	0.074	0.102	-0.382	0.126	-0.139	-0.068	-0.129	-0.108	0.110	-0.026
BACC	0.130	0.179	-0.055	0.049	0.240	-0.128	-0.041	0.033	0.088	-0.132	-0.019	0.058	0.149	-0.031	-0.010	-0.121	-0.003
BAOP	-0.209	-0.044	-0.098	-0.075	0.205	-0.028	-0.112	0.003	0.042	-0.001	-0.111	-0.053	-0.026	0.106	0.021	0.005	-0.009
ASAS	-0.105	-0.013	-0.029	-0.001	-0.078	0.011	-0.048	-0.032	-0.098	0.440	-0.089	-0.102	0.125	-0.064	-0.073	-0.099	-0.060
JPJP	0.160	0.197	0.051	0.045	0.146	-0.115	-0.022	-0.078	0.152	-0.018	0.201	-0.127	0.094	-0.144	-0.113	-0.225	-0.001
4141	0.092	0.173	0.075	0.108	-0.240	-0.157	-0.033	0.113	-0.300	-0.076	0.041	-0.193	-0.018	-0.058	-0.138	-0.118	0.010
POPO	-0.144	-0.086	-0.064	-0.210	-0.182	-0.253	0.056	0.231	0.046	-0.002	0.048	-0.350	-0.095	-0.092	-0.282	0.069	0.004
PTPT	-0.127	-0.028	-0.063	-0.055	-0.173	-0.151	0.201	0.090	0.085	0.056	-0.194	-0.142	-0.047	-0.153	-0.245	0.052	0.036
STST	-0.054	-0.016	0.004	0.123	-0.120	-0.020	0.046	0.087	0.069	0.073	-0.252	0.049	0.191	-0.160	-0.025	0.070	0.042
ZTZT	-0.040	0.096	-0.099	0.001	-0.086	-0.151	0.201	0.350	0.110	-0.041	0.166	-0.146	-0.230	-0.217	-0.420	-0.070	-0.035
BRAS	0.074	-0.045	-0.023	0.001	0.010	-0.260	-0.061	-0.055	-0.133	0.405	0.216	-0.231	-0.046	-0.245	-0.326	0.121	0.087
BRLD	0.079	-0.070	0.008	0.003	0.008	-0.242	-0.083	-0.037	0.025	-0.155	-0.134	-0.195	-0.056	-0.128	-0.256	0.201	0.108
BRNA	-0.024	-0.105	0.051	0.064	-0.055	0.022	0.198	0.255	0.154	-0.128	0.015	0.071	-0.070	0.027	0.048	0.132	0.036
BRPT	-0.040	-0.115	-0.061	0.049	-0.128	-0.108	0.125	0.173	-0.418	0.091	0.052	0.046	-0.094	-0.159	-0.059	0.097	-0.038
NABA	1.000	0.082	0.155	-0.031	0.069	-0.455	0.106	0.084	0.177	-0.058	0.206	-0.125	-0.196	0.107	-0.126	0.011	0.094
CACP	0.082	1.000	-0.163	0.273	0.040	-0.096	0.046	0.097	0.048	-0.021	-0.089	0.006	-0.112	-0.009	-0.085	-0.650	0.347
CPSL	0.155	-0.163	1.000	0.043	0.076	0.027	-0.032	-0.081	0.024	-0.094	0.090	0.062	0.158	-0.042	-0.004	0.138	-0.083
CPZS	-0.031	0.273	0.043	1.000	-0.039	-0.002	-0.074	0.333	0.044	-0.060	-0.009	-0.019	0.022	-0.196	-0.263	0.055	0.405
CNCN	0.069	0.040	0.076	-0.039	1.000	-0.081	-0.067	0.005	0.180	0.020	0.204	0.023	0.123	0.048	0.108	-0.098	-0.022
FMPM	-0.455	-0.096	0.027	-0.002	-0.081	1.000	-0.150	-0.238	-0.074	-0.040	-0.284	0.395	0.253	0.127	0.484	0.004	-0.136
FMZT	0.106	0.046	-0.032	-0.074	-0.067	-0.150	1.000	0.131	0.135	-0.125	-0.109	0.052	-0.200	-0.047	-0.056	-0.050	-0.012
FMCP	0.084	0.097	-0.081	0.333	0.005	-0.238	0.131	1.000	0.171	-0.031	0.340	-0.293	-0.241	-0.224	-0.546	0.230	0.477
FMPT	0.177	0.048	0.024	0.044	0.180	-0.074	0.135	0.171	1.000	-0.179	-0.068	-0.109	-0.091	0.138	-0.203	0.000	0.031
LDAS	-0.058	-0.021	-0.094	-0.060	0.020	-0.040	-0.125	-0.031	-0.179	1.000	0.347	-0.044	0.051	-0.051	-0.059	-0.053	-0.032
LDBA	0.206	-0.089	0.090	-0.009	0.204	-0.284	-0.109	0.340	-0.068	0.347	1.000	-0.213	-0.121	-0.148	-0.262	0.189	0.068
NANL	-0.125	0.006	0.062	-0.019	0.023	0.395	0.052	-0.293	-0.109	-0.044	-0.213	1.000	-0.053	0.495	0.591	0.040	0.013
NLAC	-0.196	-0.112	0.158	0.022	0.123	0.253	-0.200	-0.241	-0.091	0.051	-0.121	-0.053	1.000	-0.094	0.340	-0.026	-0.140
NLVS	0.107	-0.009	-0.042	-0.196	0.048	0.127	-0.047	-0.224	0.138	-0.051	-0.148	0.495	-0.094	1.000	0.434	-0.099	-0.165
NAAC	-0.126	-0.085	-0.004	-0.263	0.108	0.484	-0.056	-0.546	-0.203	-0.059	-0.262	0.591	0.340	0.434	1.000	-0.219	-0.383
NACA	0.011	-0.650	0.138	0.055	-0.098	0.004	-0.050	0.230	0.000	-0.053	0.189	0.040	-0.026	-0.099	-0.219	1.000	0.407
NACP	0.094	0.347	-0.083	0.405	-0.022	-0.136	-0.012	0.477	0.031	-0.032	0.068	0.013	-0.140	-0.165	-0.383	0.407	1.000
NAFM	0.167	-0.159	0.019	-0.159	-0.027	-0.055	-0.072	0.269	0.085	0.094	0.158	-0.125	0.089	-0.065	0.058	0.047	-0.041
NA41	-0.056	-0.059	0.023	-0.223	0.021	0.337	0.001	-0.430	-0.099	-0.060	-0.240	0.372	0.075	0.119	0.627	-0.235	-0.357
NAVS	0.612	-0.050	0.051	0.007	0.192	-0.388	0.138	0.229	0.209	-0.006	0.223	-0.004	-0.168	0.239	-0.187	0.131	0.159
NAZI	0.249	-0.062	0.094	-0.134	0.010	-0.045	0.288	-0.115	0.020	-0.059	-0.067	0.083	-0.011	-0.102	0.249	-0.136	-0.312
NAZS	0.273	-0.064	-0.094	-0.044	0.116	-0.277	0.018	0.067	0.007	0.012	-0.022	-0.189	0.063	0.036	-0.029	-0.132	-0.093
BRBA	0.415	-0.136	0.141	0.090	0.025	-0.326	0.024	0.234	-0.066	0.099	0.448	-0.229	-0.022	-0.287	-0.348	0.296	0.090
NALD	0.156	-0.116	0.076	-0.001	0.020	-0.274	0.020	0.047	0.142	-0.226	-0.033	-0.208	-0.149	-0.022	-0.234	0.217	0.101
DAFM	-0.167	-0.059	-0.004	0.027	-0.122	-0.055	-0.085	0.293	-0.038	0.190	0.068	-0.325	-0.046	-0.233	-0.249	0.097	0.189
PLSY	-0.197	-0.121	0.122	-0.042	0.008	0.269	-0.183	-0.138	0.095	0.046	0.134	0.101	0.012	0.293	0.228	-0.221	-0.299
POBA	-0.279	-0.063	-0.144	-0.049	-0.256	-0.212	-0.045	0.217	0.016	0.088	-0.049	-0.386	0.024	-0.203	-0.224	0.131	0.109
PM41	0.079	-0.032	-0.064	0.141	-0.044	0.340	-0.003	0.156	0.036	-0.093	-0.034	-0.033	0.011	0.039	-0.170	0.147	0.182
41MX	-0.199	-0.061	0.008	-0.309	-0.102	0.162	-0.074	-0.390	-0.014	0.065	-0.225	0.156	-0.058	0.341	0.215	-0.232	-0.309
41ZI	-0.293	0.142	-0.101	-0.050	-0.084	0.199	-0.119	-0.204	-0.021	0.120	-0.366	0.113	0.054	-0.048	0.060	-0.112	-0.022
PTAS	0.195	-0.037	0.136	-0.026	-0.014	-0.308	0.162	0.155	-0.282	-0.253	0.309	-0.098	-0.180	-0.051	-0.099	0.115	0.107
PTLD	-0.039	-0.112	0.031	-0.010	-0.090	-0.276	-0.004	-0.016	-0.423	-0.086	0.033	-0.182	-0.113	-0.177	-0.173	0.162	0.040
SLBA	0.163	0.008	-0.694	-0.025	-0.212	-0.267	0.045	0.029	-0.076	0.181	-0.168	-0.059	-0.317	0.044	-0.120	0.007	0.021
SLCC	-0.050	0.061	-0.622	-0.155	-0.004	-0.209	0.092	-0.104	-0.046	0.081	-0.111	0.122	-0.174	0.083	0.062	-0.119	-0.109
SYBA	0.422	0.269	-0.061	0.050	-0.125	-0.243	-0.026	0.022	0.075	-0.112	-0.162	0.002	-0.120	0.116	-0.130	-0.100	0.129
SYMX	-0.018	-0.186	0.162	-0.065	0.022	0.294	0.030	-0.088	-0.016	-0.005	0.062	0.116	-0.002	0.162	0.155	-0.017	-0.192
ZTPO	0.033	-0.009	0.212	0.206	0.183	0.066	-0.066	0.158	0.090	0.006	0.361	-0.001	-0.057	0.099	-0.106	0.083	0.077
ZTVS	-0.181	0.100	-0.158	0.059	-0.041	-0.121	0.115	0.266	0.174	-0.043	0.074	-0.187	-0.229	-0.218	-0.460	-0.151	-0.111
ZTZI	0.118	-0.099	0.122	-0.006	0.131	0.112	0.039	0.026	-0.004	-0.121	0.205	0.144	0.089	0.147	0.124	0.047	-0.052
VSBA	0.396	0.132	0.134	-0.117	-0.079	-0.156	-0.034	0.020	0.025	-0.020	0.090	-0.170	0.032	-0.140	0.063	-0.168	-0.026
VSSY	0.025	0.040	-0.127	0.054	0.024	-0.104	0.059	0.044	-0.020	-0.098	-0.156	0.123	-0.036	0.017	-0.074	0.121	0.074
ZIMX	-0.150	0.049	0.027	0.057	-0.029	-0.175	0.005	0.032	0.042	0.027	-0.073	-0.081	-0.110	-0.279	-0.175	-0.074	-0.020
ZSNL	-0.204	-0.108	-0.035	-0.003	-0.037	0.406	-0.098	-0.183	-0.146	-0.087	-0.249	0.773	-0.068	0.684	0.523	0.098	-0.075

	NAFM	NA41	NAVS	NAZI	NAZS	BRBA	NALD	DAFM	PLSY	POBA	PM41	41MX	41ZI	PTAS	PTLD	SLBA	SLCC
ACPM	0.140	-0.248	-0.034	-0.022	0.073	-0.034	-0.093	0.123	-0.072	0.033	0.048	-0.082	0.001	0.084	-0.125	-0.103	-0.119
ACSY	-0.019	0.073	-0.222	-0.137	-0.043	-0.206	-0.129	-0.213	0.644	0.021	0.015	0.343	0.168	-0.007	-0.162	-0.211	-0.117
PMPM	0.141	-0.271	-0.194	-0.032	-0.034	-0.032	-0.158	0.215	-0.025	-0.111	0.140	-0.200	-0.222	0.031	-0.143	-0.223	-0.080
ASJP	0.052	-0.046	0.020	0.055	0.003	-0.015	0.034	-0.111	-0.076	0.033	0.036	-0.086	-0.148	0.214	-0.003	-0.200	-0.121
BACC	0.132	-0.037	0.027	0.041	-0.059	0.107	-0.053	0.126	-0.046	-0.181	-0.089	-0.009	-0.174	-0.011	-0.108	0.153	0.394
BAOP	0.044	-0.090	0.028	0.083	0.174	-0.241	0.128	0.131	-0.028	0.160	0.087	-0.146	0.023	-0.109	0.077	0.052	0.081
ASAS	0.140	-0.002	0.026	-0.043	0.075	-0.009	0.031	0.092	-0.004	0.063	-0.001	0.092	0.244	-0.254	0.052	0.123	-0.011
JPJP	-0.074	-0.067	0.078	-0.004	-0.033	0.287	-0.013	0.095	0.021	-0.043	-0.203	-0.111	-0.096	0.094	-0.113	0.084	0.124
4141	0.049	-0.197	-0.045	-0.004	0.019	0.077	-0.109	0.269	-0.018	-0.004	0.182	-0.087	-0.031	0.003	0.203	0.064	-0.130
POPO	0.044	-0.171	0.095	-0.062	0.067	0.079	0.144	0.179	-0.067	0.502	-0.064	-0.032	-0.142	0.153	0.088	0.084	0.065
PTPT	-0.202	-0.266	-0.237	-0.003	-0.135	0.077	0.094	-0.030	-0.079	0.165	-0.053	-0.055	-0.017	-0.040	0.131	0.082	0.106
STST	0.028	-0.089	-0.186	0.206	-0.022	0.168	-0.003	0.029	-0.310	0.018	-0.023	-0.105	-0.092	-0.012	0.018	0.181	0.206
ZTZT	0.258	-0.182	0.127	0.137	0.105	0.122	0.167	0.087	-0.109	0.087	-0.060	0.039	-0.026	0.132	0.094	0.103	0.071
BRAS	0.085	-0.171	0.101	0.063	0.007	0.527	0.147	0.125	-0.095	0.049	-0.045	-0.152	-0.183	0.220	0.161	0.094	0.140
BRLD	0.047	-0.176	0.125	0.142	0.036	0.175	0.808	-0.181	-0.150	0.011	0.022	-0.137	-0.218	0.034	0.684	-0.010	0.057
BRNA	0.055	-0.053	-0.035	-0.148	-0.018	-0.116	0.136	0.042	-0.004	0.050	-0.050	-0.020	-0.004	0.175	0.072	-0.148	-0.131
BRPT	-0.061	-0.132	-0.099	0.008	-0.053	0.167	0.046	0.005	-0.132	0.034	-0.102	-0.167	-0.157	0.114	0.434	0.056	0.095
NABA	0.167	-0.056	0.612	0.249	0.273	0.415	0.156	-0.167	-0.197	-0.279	0.079	-0.199	-0.293	0.195	-0.039	0.163	-0.050
CACP	-0.159	-0.059	-0.050	-0.062	-0.064	-0.136	-0.116	-0.059	-0.121	-0.063	-0.032	-0.061	0.142	-0.037	-0.112	0.008	0.061
CPSL	0.019	0.023	0.051	0.094	-0.094	0.141	0.076	-0.004	0.122	-0.144	-0.064	0.008	-0.101	0.136	0.031	-0.694	-0.622
CPZS	-0.159	-0.223	0.007	-0.134	-0.044	0.090	-0.001	0.027	-0.042	-0.049	0.141	-0.309	-0.050	-0.026	-0.010	-0.025	-0.155
CNCN	-0.027	0.021	0.192	0.010	0.116	0.025	0.020	-0.122	0.008	-0.256	-0.044	-0.102	-0.084	-0.014	-0.090	-0.212	-0.004
FMPM	-0.055	0.337	-0.388	-0.045	-0.277	-0.326	-0.274	-0.055	0.269	-0.212	0.340	0.162	0.199	-0.308	-0.276	-0.267	-0.209
FMZT	-0.072	0.001	0.138	0.288	0.018	0.024	0.020	-0.085	-0.183	-0.045	-0.003	-0.074	-0.119	0.162	-0.004	0.045	0.092
FMCP	0.269	-0.430	0.229	-0.115	0.067	0.234	0.047	0.293	-0.138	0.217	0.156	-0.390	-0.204	0.155	-0.016	0.029	-0.104
FMPT	0.085	-0.099	0.209	0.020	0.007	-0.066	0.142	-0.038	0.095	0.016	0.036	-0.014	-0.021	-0.282	-0.423	-0.076	-0.046
LDAS	0.094	-0.060	-0.006	-0.059	0.012	0.099	-0.226	0.190	0.046	0.088	-0.093	0.065	0.120	-0.253	-0.086	0.181	0.081
LDBA	0.158	-0.240	0.223	-0.067	-0.022	0.448	-0.033	0.068	0.134	-0.049	-0.034	-0.225	-0.366	0.309	0.033	-0.168	-0.111
NANL	-0.125	0.372	-0.004	0.083	-0.189	-0.229	-0.208	-0.325	0.101	-0.386	-0.033	0.156	0.113	-0.098	-0.182	-0.059	0.122
NLAC	0.089	0.075	-0.168	-0.011	0.063	-0.022	-0.149	-0.046	0.012	0.024	0.011	-0.058	0.054	-0.180	-0.113	-0.317	-0.174
NLVS	-0.065	0.119	0.239	-0.102	0.036	-0.287	-0.022	-0.233	0.293	-0.203	0.039	0.341	-0.048	-0.051	-0.177	0.044	0.083
NAAC	0.058	0.627	-0.187	0.249	-0.029	-0.348	-0.234	-0.249	0.228	-0.224	-0.170	0.215	0.060	-0.099	-0.173	-0.120	0.062
NACA	0.047	-0.235	0.131	-0.136	-0.132	0.296	0.217	0.097	-0.221	0.131	0.147	-0.232	-0.112	0.115	0.162	0.007	-0.119
NACP	-0.041	-0.357	0.159	-0.312	-0.093	0.090	0.101	0.189	-0.299	0.109	0.182	-0.309	-0.022	0.107	0.040	0.021	-0.109
NAFM	1.000	-0.118	-0.006	0.374	0.393	0.036	0.183	0.627	-0.095	0.042	0.119	-0.213	-0.271	0.140	-0.003	0.048	0.062
NA41	-0.118	1.000	-0.011	0.312	0.093	-0.179	-0.268	-0.323	0.214	-0.155	-0.160	0.343	0.156	-0.119	-0.231	-0.123	0.014
NAVS	-0.006	-0.011	1.000	0.152	0.279	0.241	0.220	-0.219	-0.243	-0.113	-0.011	-0.278	-0.407	0.238	0.068	-0.012	-0.007
NAZI	0.374	0.312	0.152	1.000	0.487	0.050	0.071	0.004	-0.055	-0.106	0.086	-0.248	-0.333	0.148	0.053	0.074	0.125
NAZS	0.393	0.093	0.279	0.487	1.000	0.029	0.084	0.163	-0.072	0.088	0.007	-0.220	-0.310	0.096	-0.021	0.131	0.145
BRBA	0.036	-0.179	0.241	0.050	0.029	1.000	-0.020	-0.020	-0.143	-0.048	0.002	-0.299	-0.431	0.213	0.069	-0.040	-0.034
NALD	0.183	-0.268	0.220	0.071	0.084	-0.020	1.000	-0.103	-0.110	-0.080	-0.013	-0.162	-0.239	0.142	0.800	-0.137	-0.046
DAFM	0.627	-0.323	-0.219	0.004	0.163	-0.020	-0.103	1.000	-0.215	0.189	0.100	-0.077	-0.084	-0.013	-0.094	0.041	0.058
PLSY	-0.095	0.214	-0.243	-0.055	-0.072	-0.143	-0.110	-0.215	1.000	0.024	0.107	0.286	0.082	-0.059	-0.135	-0.165	-0.212
POBA	0.042	-0.155	-0.113	-0.106	0.088	-0.048	-0.080	0.189	0.024	1.000	-0.012	-0.100	0.102	-0.075	-0.095	0.210	0.077
PM41	0.119	-0.160	-0.011	0.086	0.007	0.002	-0.013	0.100	0.107	-0.012	1.000	-0.286	-0.001	0.007	-0.115	0.103	0.010
41MX	-0.213	0.343	-0.278	-0.248	-0.220	-0.299	-0.162	-0.077	0.286	-0.100	-0.286	1.000	0.247	-0.211	-0.179	-0.069	-0.065
41ZI	-0.271	0.156	-0.407	-0.333	-0.310	-0.431	-0.239	-0.084	0.082	0.102	-0.001	0.247	1.000	-0.480	-0.225	0.077	-0.139
PTAS	0.140	-0.119	0.238	0.148	0.096	0.213	0.142	-0.013	-0.059	-0.075	0.007	-0.211	-0.480	1.000	0.290	-0.162	-0.028
PTLD	-0.003	-0.231	0.068	0.053	-0.021	0.069	0.800	-0.094	-0.135	-0.095	-0.115	-0.179	-0.225	0.290	1.000	-0.078	-0.013
SLBA	0.048	-0.123	-0.012	0.074	0.131	-0.040	-0.137	0.041	-0.165	0.210	0.103	-0.069	0.077	-0.162	-0.078	1.000	0.666
SLCC	0.062	0.014	-0.007	0.125	0.145	-0.034	-0.046	0.058	-0.212	0.077	0.010	-0.065	-0.139	-0.028	-0.013	0.666	1.000
SYBA	-0.073	-0.253	0.048	-0.129	-0.080	-0.068	0.049	0.110	-0.393	-0.045	-0.131	0.114	0.206	-0.174	0.024	0.363	0.048
SYMX	0.103	0.169	-0.119	-0.013	0.102	-0.045	-0.092	-0.144	0.643	0.032	0.049	0.105	0.083	0.069	-0.106	-0.097	-0.067
ZTPO	-0.010	-0.035	0.134	-0.007	0.106	0.232	0.079	-0.214	0.081	-0.126	0.108	0.020	-0.253	0.230	-0.016	-0.276	-0.131
ZTVS	-0.074	-0.068	0.127	-0.063	0.035	0.014	0.068	-0.020	-0.161	0.216	-0.085	0.160	0.089	-0.045	0.053	0.158	0.096
ZTZI	-0.033	0.025	0.268	0.028	0.054	0.196	0.076	-0.133	0.031	-0.339	0.003	0.070	-0.613	0.236	0.091	-0.178	0.037
VSBA	0.236	-0.022	-0.340	0.104	0.029	0.161	-0.041	0.090	0.128	-0.211	0.065	0.165	0.091	0.017	-0.083	0.114	-0.122
VSSY	-0.053	0.004	0.178	0.000	0.023	-0.078	0.040	0.019	-0.578	0.073	-0.125	-0.086	-0.014	-0.059	0.074	0.174	0.187
ZIMX	-0.181	-0.049	-0.214	-0.202	-0.030	-0.096	-0.046	-0.090	-0.278	0.170	-0.064	-0.020	0.424	-0.067	-0.017	-0.085	-0.141
ZSNL	0.004	0.164	-0.113	-0.026	-0.182	-0.363	-0.155	-0.177	0.188	-0.206	0.123	0.151	0.136	-0.172	-0.120	0.001	0.113

	SYBA	SYMX	ZTPO	ZTVS	ZTZI	VSBA	VSSY	ZIMX	ZSNL
ACPM	0.105	-0.149	0.033	0.025	-0.100	0.068	-0.036	-0.107	-0.053
ACSY	-0.352	0.511	-0.002	-0.356	-0.006	0.130	-0.600	-0.243	0.397
PMPM	0.053	-0.055	-0.107	-0.035	0.107	0.055	-0.075	-0.220	-0.093
ASJP	0.013	-0.029	0.044	-0.011	0.102	-0.047	0.042	-0.004	-0.174
BACC	0.118	0.006	0.056	0.008	0.099	0.120	0.092	-0.002	-0.043
BAOP	-0.174	0.028	-0.069	0.088	-0.144	-0.284	0.124	0.044	0.000
ASAS	-0.052	0.032	-0.093	-0.007	-0.160	-0.096	0.026	0.141	-0.127
JPJP	-0.200	0.185	0.250	0.067	0.047	0.065	-0.126	0.112	-0.281
4141	0.365	-0.195	-0.236	-0.055	-0.202	0.137	0.174	0.129	-0.217
POPO	-0.120	0.086	0.016	0.218	0.002	-0.231	0.088	0.002	-0.216
PTPT	0.119	0.008	0.111	0.188	-0.104	0.232	-0.035	0.088	-0.096
STST	-0.045	-0.119	-0.182	-0.137	-0.062	0.126	-0.011	-0.076	-0.094
ZTZT	-0.052	0.045	0.104	0.925	-0.010	-0.103	0.117	0.418	-0.217
BRAS	-0.315	-0.054	0.103	-0.061	-0.030	-0.030	-0.217	0.072	-0.341
BRLD	-0.033	-0.101	0.030	0.051	0.010	-0.103	0.033	-0.005	-0.215
BRNA	0.122	0.005	0.093	-0.006	0.026	0.157	0.057	-0.015	0.045
BRPT	0.082	0.008	0.152	0.117	0.069	0.112	0.062	-0.031	0.037
NABA	0.422	-0.018	0.033	-0.181	0.118	0.396	0.025	-0.150	-0.204
CACP	0.269	-0.186	-0.009	0.100	-0.099	0.132	0.040	0.049	-0.108
CPSL	-0.061	0.162	0.212	-0.158	0.122	0.134	-0.127	0.027	-0.035
CPZS	0.050	-0.065	0.206	0.059	-0.006	-0.117	0.054	0.057	-0.003
CNCN	-0.125	0.022	0.183	-0.041	0.131	-0.079	0.024	-0.029	-0.037
FMPM	-0.243	0.294	0.066	-0.121	0.112	-0.156	-0.104	-0.175	0.406
FMZT	-0.026	0.030	-0.066	0.115	0.039	-0.034	0.059	0.005	-0.098
FMCP	0.022	-0.088	0.158	0.266	0.026	0.020	0.044	0.032	-0.183
FMPT	0.075	-0.016	0.090	0.174	-0.004	0.025	-0.020	0.042	-0.146
LDAS	-0.112	-0.005	0.006	-0.043	-0.121	-0.020	-0.098	0.027	-0.087
LDBA	-0.162	0.062	0.361	0.074	0.205	0.090	-0.156	-0.073	-0.249
NANL	0.002	0.116	-0.001	-0.187	0.144	-0.170	0.123	-0.081	0.773
NLAC	-0.120	-0.002	-0.057	-0.229	0.089	0.032	-0.036	-0.110	-0.068
NLVS	0.116	0.162	0.099	-0.218	0.147	-0.140	0.017	-0.279	0.684
NAAC	-0.130	0.155	-0.106	-0.460	0.124	0.063	-0.074	-0.175	0.523
NACA	-0.100	-0.017	0.083	-0.151	0.047	-0.168	0.121	-0.074	0.098
NACP	0.129	-0.192	0.077	-0.111	-0.052	-0.026	0.074	-0.020	-0.075
NAFM	-0.073	0.103	-0.010	-0.074	-0.033	0.236	-0.053	-0.181	0.004
NA41	-0.253	0.169	-0.035	-0.068	0.025	-0.022	0.004	-0.049	0.164
NAVS	0.048	-0.119	0.134	0.127	0.268	-0.340	0.178	-0.214	-0.113
NAZI	-0.129	-0.013	-0.007	-0.063	0.028	0.104	0.000	-0.202	-0.026
NAZS	-0.080	0.102	0.106	0.035	0.054	0.029	0.023	-0.030	-0.182
BRBA	-0.068	-0.045	0.232	0.014	0.196	0.161	-0.078	-0.096	-0.363
NALD	0.049	-0.092	0.079	0.068	0.076	-0.041	0.040	-0.046	-0.155
DAFM	0.110	-0.144	-0.214	-0.020	-0.133	0.090	0.019	-0.090	-0.177
PLSY	-0.393	0.643	0.081	-0.161	0.031	0.128	-0.578	-0.278	0.188
POBA	-0.045	0.032	-0.126	0.216	-0.339	-0.211	0.073	0.170	-0.206
PM41	-0.131	0.049	0.108	-0.085	0.003	0.065	-0.125	-0.064	0.123
41MX	0.114	0.105	0.020	0.160	0.070	0.165	-0.086	-0.020	0.151
41ZI	0.206	0.083	-0.253	0.089	-0.613	0.091	-0.014	0.424	0.136
PTAS	-0.174	0.069	0.230	-0.045	0.236	0.017	-0.059	-0.067	-0.172
PTLD	0.024	-0.106	-0.016	0.053	0.091	-0.083	0.074	-0.017	-0.120
SLBA	0.363	-0.097	-0.276	0.158	-0.178	0.114	0.174	-0.085	0.001
SLCC	0.048	-0.067	-0.131	0.096	0.037	-0.122	0.187	-0.141	0.113
SYBA	1.000	-0.403	-0.226	0.025	-0.034	0.437	0.517	0.195	0.047
SYMX	-0.403	1.000	0.070	-0.199	-0.018	0.191	-0.610	-0.213	0.131
ZTPO	-0.226	0.070	1.000	0.099	0.086	-0.049	-0.019	-0.057	-0.015
ZTVS	0.025	-0.199	0.099	1.000	-0.080	-0.254	0.323	0.376	-0.214
ZTZI	-0.034	-0.018	0.086	-0.080	1.000	-0.101	0.098	-0.376	0.079
VSBA	0.437	0.191	-0.049	-0.254	-0.101	1.000	-0.267	0.176	-0.164
VSSY	0.517	-0.610	-0.019	0.323	0.098	-0.267	1.000	0.120	0.002
ZIMX	0.195	-0.213	-0.057	0.376	-0.376	0.176	0.120	1.000	-0.248
ZSNL	0.047	0.131	-0.015	-0.214	0.079	-0.164	0.002	-0.248	1.000

Table B7 Phenotypic Correlation Matrix for Model 1.

	ACPM	ACSY	PMPM	ASJP	BACC	BAOP	ASAS	JPJP	4141	POPO	PTPT	STST	ZTZT	BRAS	BRLD	BRNA	BRPT
ACPM	1.000	0.404	0.550	0.139	0.087	0.047	0.198	0.169	0.389	0.150	0.162	-0.034	0.241	0.167	0.121	0.207	0.088
ACSY	0.404	1.000	0.177	0.028	0.139	0.056	0.197	0.181	0.259	0.239	0.015	-0.088	0.213	0.153	0.033	0.152	-0.024
PMPM	0.550	0.177	1.000	0.120	0.066	0.054	0.144	0.101	0.438	0.101	0.143	-0.043	0.151	0.156	0.056	0.110	0.014
ASJP	0.139	0.028	0.120	1.000	0.090	0.023	0.428	0.001	0.105	0.151	0.093	-0.044	0.192	-0.044	0.071	0.230	0.080
BACC	0.087	0.139	0.066	0.090	1.000	-0.024	0.135	0.391	0.196	0.301	0.145	-0.002	0.334	0.116	0.052	0.133	0.023
BAOP	0.047	0.056	0.054	0.023	-0.024	1.000	0.079	0.095	0.095	0.078	-0.007	-0.131	0.032	-0.013	0.042	0.034	-0.048
ASAS	0.198	0.197	0.144	0.428	0.135	0.079	1.000	0.208	0.184	0.352	0.092	-0.009	0.330	0.284	0.005	0.139	0.057
JPJP	0.169	0.181	0.101	0.001	0.391	0.095	0.208	1.000	0.151	0.269	0.151	0.048	0.209	0.144	0.023	0.142	0.044
4141	0.389	0.259	0.438	0.105	0.196	0.095	0.184	0.151	1.000	0.228	0.167	-0.020	0.371	0.240	0.091	0.220	-0.002
POPO	0.150	0.239	0.101	0.151	0.301	0.078	0.352	0.269	0.228	1.000	0.236	0.174	0.501	0.260	0.046	0.226	0.092
PTPT	0.162	0.015	0.143	0.093	0.145	-0.007	0.092	0.151	0.167	0.236	1.000	0.351	0.212	0.260	0.127	0.291	0.460
STST	-0.034	-0.088	-0.043	-0.044	-0.002	-0.131	-0.009	0.048	-0.020	0.174	0.351	1.000	-0.054	0.158	0.008	0.176	0.364
ZTZT	0.241	0.213	0.151	0.192	0.334	0.032	0.330	0.209	0.371	0.501	0.212	-0.054	1.000	0.282	0.151	0.221	0.029
BRAS	0.167	0.153	0.156	-0.044	0.116	-0.013	0.284	0.144	0.240	0.260	0.260	0.158	0.282	1.000	0.445	-0.126	0.028
BRLD	0.121	0.033	0.056	0.071	0.052	0.042	0.005	0.023	0.091	0.046	0.127	0.008	0.151	0.445	1.000	-0.199	0.013
BRNA	0.207	0.152	0.110	0.230	0.133	0.034	0.139	0.142	0.220	0.226	0.291	0.176	0.221	-0.126	-0.199	1.000	0.469
BRPT	0.088	-0.024	0.014	0.080	0.023	-0.048	0.057	0.044	-0.002	0.092	0.460	0.364	0.029	0.028	0.013	0.469	1.000
NABA	0.321	0.401	0.217	0.220	0.354	-0.063	0.214	0.174	0.307	0.239	0.072	-0.068	0.353	0.215	0.061	0.269	0.038
CACP	0.149	0.152	0.059	0.077	0.077	-0.005	0.055	0.036	0.009	-0.061	-0.028	-0.073	0.000	-0.025	-0.019	0.055	0.010
CPSL	0.005	0.058	-0.034	0.047	0.081	-0.041	-0.058	0.010	-0.083	-0.017	0.000	0.111	0.020	-0.017	-0.033	0.099	0.042
CPZS	0.277	0.274	0.214	0.144	0.220	0.048	0.246	0.196	0.352	0.214	0.107	-0.010	0.342	0.179	0.086	0.184	0.000
CNCN	0.023	0.091	0.023	0.047	0.312	0.343	0.013	0.220	0.113	0.036	-0.032	-0.064	0.024	0.028	-0.020	0.044	0.003
FMPM	0.221	0.531	0.154	0.126	0.095	0.058	0.140	0.142	0.260	0.184	0.025	-0.110	0.266	0.083	0.042	0.148	-0.024
FMZT	0.156	0.175	0.139	0.213	0.133	-0.005	0.201	0.126	0.165	0.220	0.160	0.050	0.465	0.197	0.017	0.250	0.078
FMCP	0.329	0.330	0.207	0.163	0.257	0.053	0.278	0.226	0.371	0.357	0.160	-0.023	0.520	0.250	0.117	0.336	0.092
FMPT	0.149	0.162	0.135	0.102	0.154	0.143	0.113	0.106	0.260	0.162	0.189	-0.152	0.283	0.180	0.052	0.195	-0.414
LDAS	0.139	0.229	0.150	-0.210	0.091	0.036	0.575	0.130	0.219	0.277	0.064	-0.053	0.289	0.553	-0.106	0.055	-0.003
LDBA	0.234	0.203	0.212	0.316	0.192	0.105	0.195	0.101	0.229	0.246	0.057	-0.149	0.356	0.364	0.079	0.292	0.066
NANL	0.104	0.475	0.035	0.065	0.117	0.068	0.128	0.154	0.144	0.158	-0.016	-0.088	0.158	0.050	-0.013	0.036	-0.068
NLAC	0.223	0.412	0.151	0.079	0.114	0.112	0.112	0.104	0.193	0.043	0.021	-0.105	0.091	0.060	0.050	0.081	0.044
NLVS	0.309	0.711	0.126	0.020	0.185	0.024	0.179	0.226	0.177	0.233	-0.004	-0.065	0.245	0.151	0.021	0.128	-0.018
NAAC	0.184	0.649	0.102	0.103	0.102	0.139	0.123	0.163	0.196	0.166	0.006	-0.108	0.179	0.059	0.014	0.097	-0.011
NACA	0.214	0.190	0.157	0.144	0.117	0.090	0.217	0.185	0.310	0.304	0.125	-0.036	0.319	0.232	0.105	0.230	0.019
NACP	0.330	0.335	0.189	0.194	0.205	0.034	0.294	0.212	0.332	0.306	0.102	-0.080	0.339	0.237	0.064	0.338	0.081
NAFM	0.302	0.382	0.231	0.109	0.210	0.106	0.238	0.256	0.295	0.360	0.243	0.045	0.410	0.203	0.058	0.280	0.092
NA41	0.163	0.424	0.100	0.144	0.132	0.059	0.165	0.188	0.238	0.201	0.063	-0.074	0.262	0.107	0.033	0.166	-0.016
NAVS	0.278	0.334	0.143	0.128	0.147	0.016	0.162	0.175	0.215	0.215	0.090	0.015	0.267	0.192	0.070	0.269	0.131
NAZI	0.228	0.356	0.171	0.170	0.199	0.084	0.243	0.241	0.253	0.288	0.183	-0.023	0.406	0.194	0.065	0.226	0.060
NAZS	0.159	0.163	0.100	0.052	0.107	0.160	0.150	0.142	0.096	0.248	0.169	0.044	0.230	0.106	0.063	0.123	0.095
BRBA	0.184	0.104	0.106	0.279	0.235	-0.086	0.114	0.032	0.164	0.163	0.248	0.212	0.271	0.465	0.231	0.293	0.283
NALD	0.316	0.256	0.189	0.231	0.168	0.117	0.147	0.140	0.279	0.260	0.203	-0.071	0.333	0.322	0.702	0.409	0.185
DAFM	0.182	0.281	0.162	0.038	0.136	0.062	0.132	0.127	0.210	0.274	0.219	0.071	0.349	0.090	0.012	0.181	0.101
PLSY	0.136	0.627	0.046	-0.033	0.034	-0.065	0.050	0.089	0.110	0.089	-0.007	0.002	0.127	0.047	-0.005	0.079	-0.052
POBA	0.247	0.248	0.108	0.234	0.307	0.128	0.313	0.243	0.273	0.711	0.175	0.025	0.501	0.182	0.100	0.199	0.067
PM41	0.286	0.386	0.284	0.080	0.138	0.124	0.175	0.127	0.403	0.179	0.087	-0.026	0.128	0.137	0.017	0.042	0.035
41MX	0.133	0.475	0.049	0.013	0.112	0.043	0.111	0.116	0.248	0.179	-0.001	-0.058	0.204	0.091	0.039	0.195	-0.051
41ZI	1.000	1.000	0.002	0.081	0.001	1.000	0.156	0.131	1.000	0.159	0.035	-0.077	0.190	0.028	1.000	1.000	1.000
PTAS	0.138	0.113	0.082	0.329	0.113	-0.012	-0.039	0.135	0.121	0.167	-0.066	0.069	0.164	0.248	0.192	0.242	0.267
PTLD	0.149	0.080	0.052	0.143	0.056	0.053	0.057	0.067	0.066	0.137	0.118	0.102	0.143	0.211	0.657	0.210	0.528
SLBA	0.170	0.114	0.110	0.069	0.198	-0.042	0.040	-0.013	0.253	0.010	0.065	-0.058	0.154	0.011	0.100	0.069	0.011
SLCC	0.150	0.109	0.162	0.068	0.460	0.045	0.102	0.225	0.304	0.166	0.143	-0.034	0.186	0.111	0.031	0.115	-0.007
SYBA	0.083	0.047	0.110	0.016	0.249	-0.012	0.093	0.092	0.219	0.145	-0.052	-0.072	0.197	0.075	-0.018	0.020	-0.056
SYMX	0.114	0.496	0.041	0.028	0.113	-0.099	0.123	0.149	0.148	0.126	0.036	-0.018	0.243	0.147	0.027	0.134	-0.012
ZTPO	0.095	0.205	0.066	0.051	0.203	0.012	0.058	0.093	0.201	0.131	0.012	-0.108	0.297	0.201	0.068	0.163	0.013
ZTVS	0.164	0.228	0.109	0.074	0.298	0.021	0.275	0.195	0.332	0.448	0.169	0.003	0.921	0.259	0.104	0.193	0.030
ZTZI	-0.031	0.028	0.066	0.136	0.200	-0.055	-0.024	0.051	0.089	0.045	-0.006	-0.048	0.224	0.043	-0.023	0.041	-0.045
VSBA	0.068	0.198	0.114	0.115	0.333	-0.106	0.128	0.059	0.157	0.154	-0.051	-0.108	0.205	0.042	-0.039	0.022	-0.105
VSSY	0.032	-0.199	0.063	0.018	0.035	0.122	0.036	0.056	0.082	0.039	0.027	-0.037	0.069	0.052	0.023	0.110	0.072
ZIMX	0.242	0.179	0.096	0.091	0.081	-0.037	0.172	0.031	0.232	0.144	0.131	-0.014	0.426	0.104	0.057	0.217	0.080
ZSNL	0.231	0.575	0.129	0.090	0.101	0.073	0.158	0.170	0.197	0.219	-0.010	-0.123	0.199	0.085	0.026	0.117	-0.050

	NABA	CACP	CPSL	CPZS	CNCN	FMPM	FMZT	FMCP	FMPT	LDAS	LDBA	NANL	NLAC	NLVS	NAAC	NACA	NACP
ACPM	0.321	0.149	0.005	0.277	0.023	0.221	0.156	0.329	0.149	0.139	0.234	0.104	0.223	0.309	0.184	0.214	0.330
ACSY	0.401	0.152	0.058	0.274	0.091	0.531	0.175	0.330	0.162	0.229	0.203	0.475	0.412	0.711	0.649	0.190	0.335
PMPM	0.217	0.059	-0.034	0.214	0.023	0.154	0.139	0.207	0.135	0.150	0.212	0.035	0.151	0.126	0.102	0.157	0.189
ASJP	0.220	0.077	0.047	0.144	0.047	0.126	0.213	0.163	0.102	-0.210	0.316	0.065	0.079	0.020	0.103	0.144	0.194
BACC	0.354	0.077	0.081	0.220	0.312	0.095	0.133	0.257	0.154	0.091	0.192	0.117	0.114	0.185	0.102	0.117	0.205
BAOP	-0.063	-0.005	-0.041	0.048	0.343	0.058	-0.005	0.053	0.143	0.036	0.105	0.068	0.112	0.024	0.139	0.090	0.034
ASAS	0.214	0.055	-0.058	0.246	0.013	0.140	0.201	0.278	0.113	0.575	0.195	0.128	0.112	0.179	0.123	0.217	0.294
JPJP	0.174	0.036	0.010	0.196	0.220	0.142	0.126	0.226	0.106	0.130	0.101	0.154	0.104	0.226	0.163	0.185	0.212
4141	0.307	0.009	-0.083	0.352	0.113	0.260	0.165	0.371	0.260	0.219	0.229	0.144	0.193	0.177	0.196	0.310	0.332
POPO	0.239	-0.061	-0.017	0.214	0.036	0.184	0.220	0.357	0.162	0.277	0.246	0.158	0.043	0.233	0.166	0.304	0.306
PTPT	0.072	-0.028	0.000	0.107	-0.032	0.025	0.160	0.160	0.189	0.064	0.057	-0.016	0.021	-0.004	0.006	0.125	0.102
STST	-0.068	-0.073	0.111	-0.010	-0.064	-0.110	0.050	-0.023	-0.152	-0.053	-0.149	-0.088	-0.105	-0.065	-0.108	-0.036	-0.080
ZTZT	0.353	0.000	0.020	0.342	0.024	0.266	0.465	0.520	0.283	0.289	0.356	0.158	0.091	0.245	0.179	0.319	0.339
BRAS	0.215	-0.025	-0.017	0.179	0.028	0.083	0.197	0.250	0.180	0.553	0.364	0.050	0.060	0.151	0.059	0.232	0.237
BRLD	0.061	-0.019	-0.033	0.086	-0.020	0.042	0.017	0.117	0.052	-0.106	0.079	-0.013	0.050	0.021	0.014	0.105	0.064
BRNA	0.269	0.055	0.099	0.184	0.044	0.148	0.250	0.336	0.195	0.055	0.292	0.036	0.081	0.128	0.097	0.230	0.338
BRPT	0.038	0.010	0.042	0.000	0.003	-0.024	0.078	0.092	-0.414	-0.003	0.066	-0.068	0.044	-0.018	-0.011	0.019	0.081
NABA	1.000	0.201	0.133	0.389	0.158	0.220	0.310	0.512	0.264	0.180	0.387	0.179	0.117	0.464	0.244	0.433	0.614
CACP	0.201	1.000	0.003	0.255	0.034	0.131	0.059	0.169	0.012	-0.016	0.049	0.133	0.091	0.135	0.137	-0.399	0.335
CPSL	0.133	0.003	1.000	0.067	0.148	0.120	0.030	0.006	-0.014	-0.038	0.082	0.086	0.074	0.101	0.114	-0.038	-0.047
CPZS	0.389	0.255	0.067	1.000	0.096	0.319	0.261	0.655	0.296	0.172	0.222	0.264	0.185	0.368	0.257	0.406	0.634
CNCN	0.158	0.034	0.148	0.096	1.000	0.026	-0.004	0.066	0.071	0.029	0.138	0.073	0.101	0.084	0.094	0.034	0.063
FMPM	0.220	0.131	0.120	0.319	0.026	1.000	0.276	0.266	0.087	0.150	0.241	0.667	0.459	0.463	0.776	0.190	0.315
FMZT	0.310	0.059	0.030	0.261	-0.004	0.276	1.000	0.351	0.221	0.142	0.257	0.217	0.129	0.202	0.261	0.230	0.286
FMCP	0.512	0.169	0.006	0.655	0.066	0.266	0.351	1.000	0.410	0.269	0.349	0.124	0.183	0.381	0.196	0.562	0.735
FMPT	0.264	0.012	-0.014	0.296	0.071	0.087	0.221	0.410	1.000	0.202	0.291	0.115	-0.014	0.216	0.119	0.289	0.290
LDAS	0.180	-0.016	-0.038	0.172	0.029	0.150	0.142	0.269	0.202	1.000	0.490	0.151	0.077	0.238	0.158	0.237	0.266
LDBA	0.387	0.049	0.082	0.222	0.138	0.241	0.257	0.349	0.291	0.490	1.000	0.180	0.101	0.214	0.250	0.249	0.334
NANL	0.179	0.133	0.086	0.264	0.073	0.667	0.217	0.124	0.115	0.151	0.180	1.000	0.106	0.582	0.802	0.127	0.267
NLAC	0.117	0.091	0.074	0.185	0.101	0.459	0.129	0.183	-0.014	0.077	0.101	0.106	1.000	0.130	0.464	0.076	0.173
NLVS	0.464	0.135	0.101	0.368	0.084	0.463	0.202	0.381	0.216	0.238	0.214	0.582	0.130	1.000	0.572	0.237	0.394
NAAC	0.244	0.137	0.114	0.257	0.094	0.776	0.261	0.196	0.119	0.158	0.250	0.802	0.464	0.572	1.000	0.111	0.259
NACA	0.433	-0.399	-0.038	0.406	0.034	0.190	0.230	0.562	0.289	0.237	0.249	0.127	0.076	0.237	0.111	1.000	0.669
NACP	0.614	0.335	-0.047	0.634	0.063	0.315	0.286	0.735	0.290	0.266	0.334	0.267	0.173	0.394	0.259	0.669	1.000
NAFM	0.531	0.085	0.020	0.322	0.072	0.263	0.145	0.459	0.148	0.186	0.215	0.110	0.238	0.296	0.243	0.372	0.475
NA41	0.316	0.116	0.115	0.281	0.059	0.780	0.348	0.264	0.163	0.147	0.282	0.644	0.334	0.364	0.804	0.196	0.309
NAVS	0.722	0.079	0.100	0.338	0.085	0.207	0.238	0.483	0.196	0.174	0.316	0.150	0.126	0.515	0.232	0.456	0.562
NAZI	0.446	0.042	0.047	0.315	-0.008	0.431	0.472	0.333	0.183	0.199	0.279	0.401	0.234	0.325	0.537	0.333	0.387
NAZS	0.368	-0.030	-0.013	0.148	0.095	0.083	0.155	0.229	0.135	0.124	0.162	0.114	0.131	0.147	0.228	0.236	0.248
BRBA	0.493	0.073	0.181	0.151	0.062	0.095	0.239	0.290	0.127	0.165	0.624	0.028	0.088	0.141	0.053	0.142	0.233
NALD	0.407	0.057	0.015	0.284	0.077	0.220	0.189	0.411	0.270	0.039	0.406	0.106	0.125	0.212	0.192	0.355	0.417
DAFM	0.350	0.034	-0.004	0.250	0.032	0.233	0.115	0.389	0.016	0.093	0.040	0.067	0.200	0.223	0.140	0.276	0.342
PLSY	0.218	0.066	0.056	0.164	-0.039	0.465	0.130	0.186	0.100	0.117	0.117	0.306	0.199	0.360	0.419	0.110	0.175
POBA	0.344	0.058	-0.031	0.169	-0.017	0.260	0.203	0.357	0.161	0.243	0.385	0.213	0.063	0.218	0.231	0.280	0.334
PM41	0.288	0.125	0.052	0.274	0.121	0.343	0.077	0.248	0.119	0.195	0.173	0.241	0.220	0.338	0.245	0.203	0.274
41MX	0.209	0.073	0.097	0.231	0.041	0.623	0.208	0.295	0.160	0.106	0.136	0.362	0.289	0.390	0.476	0.170	0.261
41ZI	0.162	0.164	1.000	0.239	1.000	1.000	0.135	0.252	0.113	1.000	1.000	0.433	1.000	1.000	1.000	0.157	1.000
PTAS	0.286	0.076	0.054	0.122	0.108	0.123	0.234	0.215	-0.334	-0.146	0.223	0.049	0.082	0.114	0.099	0.148	0.222
PTLD	0.129	0.011	0.020	0.072	0.060	0.095	0.073	0.183	-0.359	-0.053	0.205	0.016	0.096	0.045	0.088	0.119	0.135
SLBA	0.451	0.060	-0.522	0.042	-0.056	0.049	0.089	0.085	0.075	-0.029	0.102	0.023	0.023	0.111	-0.001	0.102	0.114
SLCC	0.364	0.057	-0.464	0.118	0.076	0.034	0.131	0.128	0.140	0.057	0.109	0.055	0.028	0.129	0.035	0.163	0.180
SYBA	0.520	0.089	0.121	0.296	0.140	0.148	0.152	0.279	0.166	0.116	0.071	0.156	0.093	0.349	0.157	0.164	0.273
SYMX	0.250	0.033	-0.043	0.167	-0.065	0.311	0.231	0.239	0.113	0.155	0.165	0.219	0.143	0.307	0.291	0.165	0.215
ZTPO	0.234	0.022	0.132	0.298	0.200	0.311	0.133	0.331	0.169	0.177	0.267	0.223	0.128	0.263	0.187	0.213	0.260
ZTVS	0.310	-0.042	0.026	0.306	0.047	0.242	0.337	0.529	0.256	0.309	0.251	0.104	0.100	0.331	0.145	0.307	0.304
ZTZI	0.120	-0.059	0.155	0.153	0.184	0.121	0.202	0.096	0.078	0.014	0.164	0.073	0.173	0.047	0.073	0.050	0.007
VSBA	0.498	0.099	0.096	0.082	0.134	0.100	0.122	0.079	0.112	0.058	0.107	0.172	0.029	0.083	0.167	0.053	0.140
VSSY	0.047	0.047	0.070	0.229	0.085	0.153	0.114	0.201	0.122	0.073	0.086	0.103	0.098	0.246	0.129	0.105	0.159
ZIMX	0.214	0.183	0.014	0.243	-0.020	0.246	0.127	0.313	0.132	0.134	0.213	0.143	0.104	0.148	0.201	0.104	0.285
ZSNL	0.264	0.144	0.095	0.281	0.018	0.673	0.219	0.256	0.172	0.182	0.245	0.861	0.111	0.713	0.727	0.194	0.341

	NAFM	NA41	NAVS	NAZI	NAZS	BRBA	NALD	DAFM	PLSY	POBA	PM41	41MX	41ZI	PTAS	PTLD	SLBA	SLCC
ACPM	0.302	0.163	0.278	0.228	0.159	0.184	0.316	0.182	0.136	0.247	0.286	0.133	1.000	0.138	0.149	0.170	0.150
ACSY	0.382	0.424	0.334	0.356	0.163	0.104	0.256	0.281	0.627	0.248	0.386	0.475	1.000	0.113	0.080	0.114	0.109
PMPM	0.231	0.100	0.143	0.171	0.100	0.106	0.189	0.162	0.046	0.108	0.284	0.049	0.002	0.082	0.052	0.110	0.162
ASJP	0.109	0.144	0.128	0.170	0.052	0.279	0.231	0.038	-0.033	0.234	0.080	0.013	0.081	0.329	0.143	0.069	0.068
BACC	0.210	0.132	0.147	0.199	0.107	0.235	0.168	0.136	0.034	0.307	0.138	0.112	0.001	0.113	0.056	0.198	0.460
BAOP	0.106	0.059	0.016	0.084	0.160	-0.086	0.117	0.062	-0.065	0.128	0.124	0.043	1.000	-0.012	0.053	-0.042	0.045
ASAS	0.238	0.165	0.162	0.243	0.150	0.114	0.147	0.132	0.050	0.313	0.175	0.111	0.156	-0.039	0.057	0.040	0.102
JPJP	0.256	0.188	0.175	0.241	0.142	0.032	0.140	0.127	0.089	0.243	0.127	0.116	0.131	0.135	0.067	-0.013	0.225
4141	0.295	0.238	0.215	0.253	0.096	0.164	0.279	0.210	0.110	0.273	0.403	0.248	1.000	0.121	0.066	0.253	0.304
POPO	0.360	0.201	0.215	0.288	0.248	0.163	0.260	0.274	0.089	0.711	0.179	0.179	0.159	0.167	0.137	0.010	0.166
PTPT	0.243	0.063	0.090	0.183	0.169	0.248	0.203	0.219	-0.007	0.175	0.087	-0.001	0.035	-0.066	0.118	0.065	0.143
STST	0.045	-0.074	0.015	-0.023	0.044	0.212	-0.071	0.071	0.002	0.025	-0.026	-0.058	-0.077	0.069	0.102	-0.058	-0.034
ZTZT	0.410	0.262	0.267	0.406	0.230	0.271	0.333	0.349	0.127	0.501	0.128	0.204	0.190	0.164	0.143	0.154	0.186
BRAS	0.203	0.107	0.192	0.194	0.106	0.465	0.322	0.090	0.047	0.182	0.137	0.091	0.028	0.248	0.211	0.011	0.111
BRLD	0.058	0.033	0.070	0.065	0.063	0.231	0.702	0.012	-0.005	0.100	0.017	0.039	1.000	0.192	0.657	0.100	0.031
BRNA	0.280	0.166	0.269	0.226	0.123	0.293	0.409	0.181	0.079	0.199	0.042	0.195	1.000	0.242	0.210	0.069	0.115
BRPT	0.092	-0.016	0.131	0.060	0.095	0.283	0.185	0.101	-0.052	0.067	0.035	-0.051	1.000	0.267	0.528	0.011	-0.007
NABA	0.531	0.316	0.722	0.446	0.368	0.493	0.407	0.350	0.218	0.344	0.288	0.209	0.162	0.286	0.129	0.451	0.364
CACP	0.085	0.116	0.079	0.042	-0.030	0.073	0.057	0.034	0.066	0.058	0.125	0.073	0.164	0.076	0.011	0.060	0.057
CPSL	0.020	0.115	0.100	0.047	-0.013	0.181	0.015	-0.004	0.056	-0.031	0.052	0.097	1.000	0.054	0.020	-0.522	-0.464
CPZS	0.322	0.281	0.338	0.315	0.148	0.151	0.284	0.250	0.164	0.169	0.274	0.231	0.239	0.122	0.072	0.042	0.118
CNCN	0.072	0.059	0.085	-0.008	0.095	0.062	0.077	0.032	-0.039	-0.017	0.121	0.041	1.000	0.108	0.060	-0.056	0.076
FMPM	0.263	0.780	0.207	0.431	0.083	0.095	0.220	0.233	0.465	0.260	0.343	0.623	1.000	0.123	0.095	0.049	0.034
FMZT	0.145	0.348	0.238	0.472	0.155	0.239	0.189	0.115	0.130	0.203	0.077	0.208	0.135	0.234	0.073	0.089	0.131
FMCP	0.459	0.264	0.483	0.333	0.229	0.290	0.411	0.389	0.186	0.357	0.248	0.295	0.252	0.215	0.183	0.085	0.128
FMPT	0.148	0.163	0.196	0.183	0.135	0.127	0.270	0.016	0.100	0.161	0.119	0.160	0.113	-0.334	-0.359	0.075	0.140
LDAS	0.186	0.147	0.174	0.199	0.124	0.165	0.039	0.093	0.117	0.243	0.195	0.106	1.000	-0.146	-0.053	-0.029	0.057
LDBA	0.215	0.282	0.316	0.279	0.162	0.624	0.406	0.040	0.117	0.385	0.173	0.136	1.000	0.223	0.205	0.102	0.109
NANL	0.110	0.644	0.150	0.401	0.114	0.028	0.106	0.067	0.306	0.213	0.241	0.362	0.433	0.049	0.016	0.023	0.055
NLAC	0.238	0.334	0.126	0.234	0.131	0.088	0.125	0.200	0.199	0.063	0.220	0.289	1.000	0.082	0.096	0.023	0.028
NLVS	0.296	0.364	0.515	0.325	0.147	0.141	0.212	0.223	0.360	0.218	0.338	0.390	1.000	0.114	0.045	0.111	0.129
NAAC	0.243	0.804	0.232	0.537	0.228	0.053	0.192	0.140	0.419	0.231	0.245	0.476	1.000	0.099	0.088	-0.001	0.035
NACA	0.372	0.196	0.456	0.333	0.236	0.142	0.355	0.276	0.110	0.280	0.203	0.170	0.157	0.148	0.119	0.102	0.163
NACP	0.475	0.309	0.562	0.387	0.248	0.233	0.417	0.342	0.175	0.334	0.274	0.261	1.000	0.222	0.135	0.114	0.180
NAFM	1.000	0.304	0.467	0.549	0.492	0.170	0.337	0.827	0.253	0.337	0.263	0.235	0.191	0.175	0.099	0.200	0.264
NA41	0.304	1.000	0.338	0.643	0.314	0.124	0.250	0.172	0.438	0.276	0.116	0.646	0.620	0.136	0.096	0.021	0.075
NAVS	0.467	0.338	1.000	0.455	0.447	0.322	0.379	0.315	0.206	0.255	0.192	0.209	1.000	0.229	0.181	0.144	0.159
NAZI	0.549	0.643	0.455	1.000	0.524	0.136	0.306	0.349	0.300	0.296	0.202	0.299	0.219	0.215	0.114	0.100	0.220
NAZS	0.492	0.314	0.447	0.524	1.000	0.082	0.228	0.308	0.078	0.187	0.099	0.081	0.088	0.092	0.109	0.011	0.075
BRBA	0.170	0.124	0.322	0.136	0.082	1.000	0.314	0.071	0.056	0.292	0.087	0.089	0.059	0.239	0.227	0.259	0.125
NALD	0.337	0.250	0.379	0.306	0.228	0.314	1.000	0.188	0.105	0.293	0.142	0.217	0.196	0.350	0.745	0.178	0.180
DAFM	0.827	0.172	0.315	0.349	0.308	0.071	0.188	1.000	0.214	0.247	0.172	0.192	1.000	0.111	0.087	0.169	0.195
PLSY	0.253	0.438	0.206	0.300	0.078	0.056	0.105	0.214	1.000	0.131	0.173	0.362	0.316	0.058	0.015	0.063	-0.006
POBA	0.337	0.276	0.255	0.296	0.187	0.292	0.293	0.247	0.131	1.000	0.194	0.188	1.000	0.141	0.161	0.247	0.258
PM41	0.263	0.116	0.192	0.202	0.099	0.087	0.142	0.172	0.173	0.194	1.000	-0.001	0.011	0.059	0.058	0.106	0.181
41MX	0.235	0.646	0.209	0.299	0.081	0.089	0.217	0.192	0.362	0.188	-0.001	1.000	0.642	0.086	0.059	0.038	0.009
41ZI	0.191	0.620	1.000	0.219	0.088	0.059	0.196	1.000	0.316	1.000	0.011	0.642	1.000	0.013	0.069	1.000	-0.066
PTAS	0.175	0.136	0.229	0.215	0.092	0.239	0.350	0.111	0.058	0.141	0.059	0.086	0.013	1.000	0.564	0.078	0.105
PTLD	0.099	0.096	0.181	0.114	0.109	0.227	0.745	0.087	0.015	0.161	0.058	0.059	0.069	0.564	1.000	0.062	-0.002
SLBA	0.200	0.021	0.144	0.100	0.011	0.259	0.178	0.169	0.063	0.247	0.106	0.038	1.000	0.078	0.062	1.000	0.693
SLCC	0.264	0.075	0.159	0.220	0.075	0.125	0.180	0.195	-0.006	0.258	0.181	0.009	-0.066	0.105	-0.002	0.693	1.000
SYBA	0.184	0.091	0.130	0.068	0.078	0.141	0.077	0.124	-0.152	0.094	0.237	0.149	0.108	0.050	-0.020	0.235	0.162
SYMX	0.259	0.386	0.202	0.375	0.163	0.133	0.172	0.172	0.578	0.158	0.057	0.221	0.232	0.189	0.050	0.124	0.132
ZTPO	0.129	0.239	0.213	0.207	0.033	0.154	0.253	0.104	0.164	0.111	0.131	0.204	0.022	0.238	0.118	-0.022	0.105
ZTVS	0.298	0.232	0.379	0.323	0.165	0.211	0.272	0.289	0.146	0.415	0.134	0.224	0.142	0.105	0.141	0.087	0.133
ZTZI	0.026	0.063	0.042	0.098	0.039	0.139	0.035	0.047	0.024	-0.113	0.047	0.013	-0.391	0.127	-0.015	-0.059	0.070
VSBA	0.178	0.079	-0.171	0.103	0.040	0.207	0.065	0.096	0.077	0.154	0.179	0.073	1.000	0.089	-0.064	0.326	0.219
VSSY	0.015	0.170	0.151	0.079	0.053	0.042	0.078	-0.007	-0.324	0.017	0.067	0.157	0.144	0.004	0.042	-0.037	0.024
ZIMX	0.160	0.311	0.210	0.138	0.019	0.169	0.246	0.152	0.159	0.261	0.071	0.249	0.429	0.050	0.133	0.120	0.059
ZSNL	0.203	0.545	0.208	0.350	0.099	0.108	0.188	0.116	0.322	0.299	0.339	0.426	1.000	0.060	0.038	0.070	0.070

	SYBA	SYMX	ZTPO	ZTVS	ZTZI	VSBA	VSSY	ZIMX	ZSNL
ACPM	0.083	0.114	0.095	0.164	-0.031	0.068	0.032	0.242	0.231
ACSY	0.047	0.496	0.205	0.228	0.028	0.198	-0.199	0.179	0.575
PMPM	0.110	0.041	0.066	0.109	0.066	0.114	0.063	0.096	0.129
ASJP	0.016	0.028	0.051	0.074	0.136	0.115	0.018	0.091	0.090
BACC	0.249	0.113	0.203	0.298	0.200	0.333	0.035	0.081	0.101
BAOP	-0.012	-0.099	0.012	0.021	-0.055	-0.106	0.122	-0.037	0.073
ASAS	0.093	0.123	0.058	0.275	-0.024	0.128	0.036	0.172	0.158
JPJP	0.092	0.149	0.093	0.195	0.051	0.059	0.056	0.031	0.170
4141	0.219	0.148	0.201	0.332	0.089	0.157	0.082	0.232	0.197
POPO	0.145	0.126	0.131	0.448	0.045	0.154	0.039	0.144	0.219
PTPT	-0.052	0.036	0.012	0.169	-0.006	-0.051	0.027	0.131	-0.010
STST	-0.072	-0.018	-0.108	0.003	-0.048	-0.108	-0.037	-0.014	-0.123
ZTZT	0.197	0.243	0.297	0.921	0.224	0.205	0.069	0.426	0.199
BRAS	0.075	0.147	0.201	0.259	0.043	0.042	0.052	0.104	0.085
BRLD	-0.018	0.027	0.068	0.104	-0.023	-0.039	0.023	0.057	0.026
BRNA	0.020	0.134	0.163	0.193	0.041	0.022	0.110	0.217	0.117
BRPT	-0.056	-0.012	0.013	0.030	-0.045	-0.105	0.072	0.080	-0.050
NABA	0.520	0.250	0.234	0.310	0.120	0.498	0.047	0.214	0.264
CACP	0.089	0.033	0.022	-0.042	-0.059	0.099	0.047	0.183	0.144
CPSL	0.121	-0.043	0.132	0.026	0.155	0.096	0.070	0.014	0.095
CPZS	0.296	0.167	0.298	0.306	0.153	0.082	0.229	0.243	0.281
CNCN	0.140	-0.065	0.200	0.047	0.184	0.134	0.085	-0.020	0.018
FMPM	0.148	0.311	0.311	0.242	0.121	0.100	0.153	0.246	0.673
FMZT	0.152	0.231	0.133	0.337	0.202	0.122	0.114	0.127	0.219
FMCP	0.279	0.239	0.331	0.529	0.096	0.079	0.201	0.313	0.256
FMPT	0.166	0.113	0.169	0.256	0.078	0.112	0.122	0.132	0.172
LDAS	0.116	0.155	0.177	0.309	0.014	0.058	0.073	0.134	0.182
LDBA	0.071	0.165	0.267	0.251	0.164	0.107	0.086	0.213	0.245
NANL	0.156	0.219	0.223	0.104	0.073	0.172	0.103	0.143	0.861
NLAC	0.093	0.143	0.128	0.100	0.173	0.029	0.098	0.104	0.111
NLVS	0.349	0.307	0.263	0.331	0.047	0.083	0.246	0.148	0.713
NAAC	0.157	0.291	0.187	0.145	0.073	0.167	0.129	0.201	0.727
NACA	0.164	0.165	0.213	0.307	0.050	0.053	0.105	0.104	0.194
NACP	0.273	0.215	0.260	0.304	0.007	0.140	0.159	0.285	0.341
NAFM	0.184	0.259	0.129	0.298	0.026	0.178	0.015	0.160	0.203
NA41	0.091	0.386	0.239	0.232	0.063	0.079	0.170	0.311	0.545
NAVS	0.130	0.202	0.213	0.379	0.042	-0.171	0.151	0.210	0.208
NAZI	0.068	0.375	0.207	0.323	0.098	0.103	0.079	0.138	0.350
NAZS	0.078	0.163	0.033	0.165	0.039	0.040	0.053	0.019	0.099
BRBA	0.141	0.133	0.154	0.211	0.139	0.207	0.042	0.169	0.108
NALD	0.077	0.172	0.253	0.272	0.035	0.065	0.078	0.246	0.188
DAFM	0.124	0.172	0.104	0.289	0.047	0.096	-0.007	0.152	0.116
PLSY	-0.152	0.578	0.164	0.146	0.024	0.077	-0.324	0.159	0.322
POBA	0.094	0.158	0.111	0.415	-0.113	0.154	0.017	0.261	0.299
PM41	0.237	0.057	0.131	0.134	0.047	0.179	0.067	0.071	0.339
41MX	0.149	0.221	0.204	0.224	0.013	0.073	0.157	0.249	0.426
41ZI	0.108	0.232	0.022	0.142	-0.391	1.000	0.144	0.429	1.000
PTAS	0.050	0.189	0.238	0.105	0.127	0.089	0.004	0.050	0.060
PTLD	-0.020	0.050	0.118	0.141	-0.015	-0.064	0.042	0.133	0.038
SLBA	0.235	0.124	-0.022	0.087	-0.059	0.326	-0.037	0.120	0.070
SLCC	0.162	0.132	0.105	0.133	0.070	0.219	0.024	0.059	0.070
SYBA	1.000	-0.117	0.147	0.175	0.096	0.604	0.520	0.031	0.226
SYMX	-0.117	1.000	0.246	0.215	0.063	0.085	-0.295	0.132	0.225
ZTPO	0.147	0.246	1.000	0.377	0.209	0.045	0.111	0.183	0.234
ZTVS	0.175	0.215	0.377	1.000	0.158	0.020	0.187	0.413	0.169
ZTZI	0.096	0.063	0.209	0.158	1.000	0.086	0.062	-0.243	0.020
VSBA	0.604	0.085	0.045	0.020	0.086	1.000	-0.167	0.025	0.198
VSSY	0.520	-0.295	0.111	0.187	0.062	-0.167	1.000	0.073	0.133
ZIMX	0.031	0.132	0.183	0.413	-0.243	0.025	0.073	1.000	0.124
ZSNL	0.226	0.225	0.234	0.169	0.020	0.198	0.133	0.124	1.000

Table B8 Phenotypic Correlation Matrix for Model 2.

	ACPM	ACSY	PMPM	ASJP	BACC	BAOP	ASAS	JPJP	4141	POPO	PTPT	STST	ZTZT	BRAS	BRLD	BRNA	BRPT
ACPM	1.000	0.404	0.550	0.139	0.087	0.047	0.198	0.169	0.389	0.150	0.162	-0.034	0.241	0.167	0.121	0.207	0.088
ACSY	0.404	1.000	0.177	0.028	0.139	0.056	0.197	0.181	0.259	0.239	0.015	-0.088	0.213	0.153	0.033	0.152	-0.024
PMPM	0.550	0.177	1.000	0.120	0.066	0.054	0.144	0.101	0.438	0.101	0.143	-0.043	0.151	0.156	0.056	0.110	0.014
ASJP	0.139	0.028	0.120	1.000	0.090	0.023	0.428	0.001	0.105	0.151	0.093	-0.044	0.192	-0.044	0.071	0.230	0.080
BACC	0.087	0.139	0.066	0.090	1.000	-0.024	0.135	0.391	0.196	0.301	0.145	-0.002	0.334	0.116	0.052	0.133	0.023
BAOP	0.047	0.056	0.054	0.023	-0.024	1.000	0.079	0.095	0.095	0.078	-0.007	-0.131	0.032	-0.013	0.042	0.034	-0.048
ASAS	0.198	0.197	0.144	0.428	0.135	0.079	1.000	0.208	0.184	0.352	0.092	-0.009	0.330	0.284	0.005	0.139	0.057
JPJP	0.169	0.181	0.101	0.001	0.391	0.095	0.208	1.000	0.151	0.269	0.151	0.048	0.209	0.144	0.023	0.142	0.044
4141	0.389	0.259	0.438	0.105	0.196	0.095	0.184	0.151	1.000	0.228	0.167	-0.020	0.371	0.240	0.091	0.220	-0.002
POPO	0.150	0.239	0.101	0.151	0.301	0.078	0.352	0.269	0.228	1.000	0.236	0.174	0.501	0.260	0.046	0.226	0.092
PTPT	0.162	0.015	0.143	0.093	0.145	-0.007	0.092	0.151	0.167	0.236	1.000	0.351	0.212	0.260	0.127	0.291	0.460
STST	-0.034	-0.088	-0.043	-0.044	-0.002	-0.131	-0.009	0.048	-0.020	0.174	0.351	1.000	-0.054	0.158	0.008	0.176	0.364
ZTZT	0.241	0.213	0.151	0.192	0.334	0.032	0.330	0.209	0.371	0.501	0.212	-0.054	1.000	0.282	0.151	0.221	0.029
BRAS	0.167	0.153	0.156	-0.044	0.116	-0.013	0.284	0.144	0.240	0.260	0.260	0.158	0.282	1.000	0.445	-0.126	0.028
BRLD	0.121	0.033	0.056	0.071	0.052	0.042	0.005	0.023	0.091	0.046	0.127	0.008	0.151	0.445	1.000	-0.199	0.013
BRNA	0.207	0.152	0.110	0.230	0.133	0.034	0.139	0.142	0.220	0.226	0.291	0.176	0.221	-0.126	-0.199	1.000	0.469
BRPT	0.088	-0.024	0.014	0.080	0.023	-0.048	0.057	0.044	-0.002	0.092	0.460	0.364	0.029	0.028	0.013	0.469	1.000
NABA	0.321	0.401	0.217	0.220	0.354	-0.063	0.214	0.174	0.307	0.239	0.072	-0.068	0.353	0.215	0.061	0.269	0.038
CACP	0.149	0.152	0.059	0.077	0.077	-0.005	0.055	0.036	0.009	-0.061	-0.028	-0.073	0.000	-0.025	-0.019	0.055	0.010
CPSL	0.005	0.058	-0.034	0.047	0.081	-0.041	-0.058	0.010	-0.083	-0.017	0.000	0.111	0.020	-0.017	-0.033	0.099	0.042
CPZS	0.277	0.274	0.214	0.144	0.220	0.048	0.246	0.196	0.352	0.214	0.107	-0.010	0.342	0.179	0.086	0.184	0.000
CNCN	0.023	0.091	0.023	0.047	0.312	0.343	0.013	0.220	0.113	0.036	-0.032	-0.064	0.024	0.028	-0.020	0.044	0.003
FMPM	0.221	0.531	0.154	0.126	0.095	0.058	0.140	0.142	0.260	0.184	0.025	-0.110	0.266	0.083	0.042	0.148	-0.024
FMZT	0.156	0.175	0.139	0.213	0.133	-0.005	0.201	0.126	0.165	0.220	0.160	0.050	0.465	0.197	0.017	0.250	0.078
FMCP	0.329	0.330	0.207	0.163	0.257	0.053	0.278	0.226	0.371	0.357	0.160	-0.023	0.520	0.250	0.117	0.336	0.092
FMPT	0.149	0.162	0.135	0.102	0.154	0.143	0.113	0.106	0.260	0.162	0.189	-0.152	0.283	0.180	0.052	0.195	-0.414
LDAS	0.139	0.229	0.150	-0.210	0.091	0.036	0.575	0.130	0.219	0.277	0.064	-0.053	0.289	0.553	-0.106	0.055	-0.003
LDBA	0.234	0.203	0.212	0.316	0.192	0.105	0.195	0.101	0.229	0.246	0.057	-0.149	0.356	0.364	0.079	0.292	0.066
NANL	0.104	0.475	0.035	0.065	0.117	0.068	0.128	0.154	0.144	0.158	-0.016	-0.088	0.158	0.050	-0.013	0.036	-0.068
NLAC	0.223	0.412	0.151	0.079	0.114	0.112	0.112	0.104	0.193	0.043	0.021	-0.105	0.091	0.060	0.050	0.081	0.044
NLVS	0.309	0.711	0.126	0.020	0.185	0.024	0.179	0.226	0.177	0.233	-0.004	-0.065	0.245	0.151	0.021	0.128	-0.018
NAAC	0.184	0.649	0.102	0.103	0.102	0.139	0.123	0.163	0.196	0.166	0.006	-0.108	0.179	0.059	0.014	0.097	-0.011
NACA	0.214	0.190	0.157	0.144	0.117	0.090	0.217	0.185	0.310	0.304	0.125	-0.036	0.319	0.232	0.105	0.230	0.019
NACP	0.330	0.335	0.189	0.194	0.205	0.034	0.294	0.212	0.332	0.306	0.102	-0.080	0.339	0.237	0.064	0.338	0.081
NAFM	0.302	0.382	0.231	0.109	0.210	0.106	0.238	0.256	0.295	0.360	0.243	0.045	0.410	0.203	0.058	0.280	0.092
NA41	0.163	0.424	0.100	0.144	0.132	0.059	0.165	0.188	0.238	0.201	0.063	-0.074	0.262	0.107	0.033	0.166	-0.016
NAVS	0.278	0.334	0.143	0.128	0.147	0.016	0.162	0.175	0.215	0.215	0.090	0.015	0.267	0.192	0.070	0.269	0.131
NAZI	0.228	0.356	0.171	0.170	0.199	0.084	0.243	0.241	0.253	0.288	0.183	-0.023	0.406	0.194	0.065	0.226	0.060
NAZS	0.159	0.163	0.100	0.052	0.107	0.160	0.150	0.142	0.096	0.248	0.169	0.044	0.230	0.106	0.063	0.123	0.095
BRBA	0.184	0.104	0.106	0.279	0.235	-0.086	0.114	0.032	0.164	0.163	0.248	0.212	0.271	0.465	0.231	0.293	0.283
NALD	0.316	0.256	0.189	0.231	0.168	0.117	0.147	0.140	0.279	0.260	0.203	-0.071	0.333	0.322	0.702	0.409	0.185
DAFM	0.182	0.281	0.162	0.038	0.136	0.062	0.132	0.127	0.210	0.274	0.219	0.071	0.349	0.090	0.012	0.181	0.101
PLSY	0.136	0.627	0.046	-0.033	0.034	-0.065	0.050	0.089	0.110	0.089	-0.007	0.002	0.127	0.047	-0.005	0.079	-0.052
POBA	0.247	0.248	0.108	0.234	0.307	0.128	0.313	0.243	0.273	0.711	0.175	0.025	0.501	0.182	0.100	0.199	0.067
PM41	0.286	0.386	0.284	0.080	0.138	0.124	0.175	0.127	0.403	0.179	0.087	-0.026	0.128	0.137	0.017	0.042	0.035
41MX	0.133	0.475	0.049	0.013	0.112	0.043	0.111	0.116	0.248	0.179	-0.001	-0.058	0.204	0.091	0.039	0.195	-0.051
41ZI	1.000	1.000	0.002	0.081	0.001	1.000	0.156	0.131	1.000	0.159	0.035	-0.077	0.190	0.028	1.000	1.000	1.000
PTAS	0.138	0.113	0.082	0.329	0.113	-0.012	-0.039	0.135	0.121	0.167	-0.066	0.069	0.164	0.248	0.192	0.242	0.267
PTLD	0.149	0.080	0.052	0.143	0.056	0.053	0.057	0.067	0.066	0.137	0.118	0.102	0.143	0.211	0.657	0.210	0.528
SLBA	0.170	0.114	0.110	0.069	0.198	-0.042	0.040	-0.013	0.253	0.010	0.065	-0.058	0.154	0.011	0.100	0.069	0.011
SLCC	0.150	0.109	0.162	0.068	0.460	0.045	0.102	0.225	0.304	0.166	0.143	-0.034	0.186	0.111	0.031	0.115	-0.007
SYBA	0.083	0.047	0.110	0.016	0.249	-0.012	0.093	0.092	0.219	0.145	-0.052	-0.072	0.197	0.075	-0.018	0.020	-0.056
SYMX	0.114	0.496	0.041	0.028	0.113	-0.099	0.123	0.149	0.148	0.126	0.036	-0.018	0.243	0.147	0.027	0.134	-0.012
ZTPO	0.095	0.205	0.066	0.051	0.203	0.012	0.058	0.093	0.201	0.131	0.012	-0.108	0.297	0.201	0.068	0.163	0.013
ZTVS	0.164	0.228	0.109	0.074	0.298	0.021	0.275	0.195	0.332	0.448	0.169	0.003	0.921	0.259	0.104	0.193	0.030
ZTZI	-0.031	0.028	0.066	0.136	0.200	-0.055	-0.024	0.051	0.089	0.045	-0.006	-0.048	0.224	0.043	-0.023	0.041	-0.045
VSBA	0.068	0.198	0.114	0.115	0.333	-0.106	0.128	0.059	0.157	0.154	-0.051	-0.108	0.205	0.042	-0.039	0.022	-0.105
VSSY	0.032	-0.199	0.063	0.018	0.035	0.122	0.036	0.056	0.082	0.039	0.027	-0.037	0.069	0.052	0.023	0.110	0.072
ZIMX	0.242	0.179	0.096	0.091	0.081	-0.037	0.172	0.031	0.232	0.144	0.131	-0.014	0.426	0.104	0.057	0.217	0.080
ZSNL	0.231	0.575	0.129	0.090	0.101	0.073	0.158	0.170	0.197	0.219	-0.010	-0.123	0.199	0.085	0.026	0.117	-0.050

	NABA	CACP	CPSL	CPZS	CNCN	FMPM	FMZT	FMCP	FMPT	LDAS	LDBA	NANL	NLAC	NLVS	NAAC	NACA	NACP
ACPM	0.321	0.149	0.005	0.277	0.023	0.221	0.156	0.329	0.149	0.139	0.234	0.104	0.223	0.309	0.184	0.214	0.330
ACSY	0.401	0.152	0.058	0.274	0.091	0.531	0.175	0.330	0.162	0.229	0.203	0.475	0.412	0.711	0.649	0.190	0.335
PMPM	0.217	0.059	-0.034	0.214	0.023	0.154	0.139	0.207	0.135	0.150	0.212	0.035	0.151	0.126	0.102	0.157	0.189
ASJP	0.220	0.077	0.047	0.144	0.047	0.126	0.213	0.163	0.102	-0.210	0.316	0.065	0.079	0.020	0.103	0.144	0.194
BACC	0.354	0.077	0.081	0.220	0.312	0.095	0.133	0.257	0.154	0.091	0.192	0.117	0.114	0.185	0.102	0.117	0.205
BAOP	-0.063	-0.005	-0.041	0.048	0.343	0.058	-0.005	0.053	0.143	0.036	0.105	0.068	0.112	0.024	0.139	0.090	0.034
ASAS	0.214	0.055	-0.058	0.246	0.013	0.140	0.201	0.278	0.113	0.575	0.195	0.128	0.112	0.179	0.123	0.217	0.294
JPJP	0.174	0.036	0.010	0.196	0.220	0.142	0.126	0.226	0.106	0.130	0.101	0.154	0.104	0.226	0.163	0.185	0.212
4141	0.307	0.009	-0.083	0.352	0.113	0.260	0.165	0.371	0.260	0.219	0.229	0.144	0.193	0.177	0.196	0.310	0.332
POPO	0.239	-0.061	-0.017	0.214	0.036	0.184	0.220	0.357	0.162	0.277	0.246	0.158	0.043	0.233	0.166	0.304	0.306
PTPT	0.072	-0.028	0.000	0.107	-0.032	0.025	0.160	0.160	0.189	0.064	0.057	-0.016	0.021	-0.004	0.006	0.125	0.102
STST	-0.068	-0.073	0.111	-0.010	-0.064	-0.110	0.050	-0.023	-0.152	-0.053	-0.149	-0.088	-0.105	-0.065	-0.108	-0.036	-0.080
ZTZT	0.353	0.000	0.020	0.342	0.024	0.266	0.465	0.520	0.283	0.289	0.356	0.158	0.091	0.245	0.179	0.319	0.339
BRAS	0.215	-0.025	-0.017	0.179	0.028	0.083	0.197	0.250	0.180	0.553	0.364	0.050	0.060	0.151	0.059	0.232	0.237
BRLD	0.061	-0.019	-0.033	0.086	-0.020	0.042	0.017	0.117	0.052	-0.106	0.079	-0.013	0.050	0.021	0.014	0.105	0.064
BRNA	0.269	0.055	0.099	0.184	0.044	0.148	0.250	0.336	0.195	0.055	0.292	0.036	0.081	0.128	0.097	0.230	0.338
BRPT	0.038	0.010	0.042	0.000	0.003	-0.024	0.078	0.092	-0.414	-0.003	0.066	-0.068	0.044	-0.018	-0.011	0.019	0.081
NABA	1.000	0.201	0.133	0.389	0.158	0.220	0.310	0.512	0.264	0.180	0.387	0.179	0.117	0.464	0.244	0.433	0.614
CACP	0.201	1.000	0.003	0.255	0.034	0.131	0.059	0.169	0.012	-0.016	0.049	0.133	0.091	0.135	0.137	-0.399	0.335
CPSL	0.133	0.003	1.000	0.067	0.148	0.120	0.030	0.006	-0.014	-0.038	0.082	0.086	0.074	0.101	0.114	-0.038	-0.047
CPZS	0.389	0.255	0.067	1.000	0.096	0.319	0.261	0.655	0.296	0.172	0.222	0.264	0.185	0.368	0.257	0.406	0.634
CNCN	0.158	0.034	0.148	0.096	1.000	0.026	-0.004	0.066	0.071	0.029	0.138	0.073	0.101	0.084	0.094	0.034	0.063
FMPM	0.220	0.131	0.120	0.319	0.026	1.000	0.276	0.266	0.087	0.150	0.241	0.667	0.459	0.463	0.776	0.190	0.315
FMZT	0.310	0.059	0.030	0.261	-0.004	0.276	1.000	0.351	0.221	0.142	0.257	0.217	0.129	0.202	0.261	0.230	0.286
FMCP	0.512	0.169	0.006	0.655	0.066	0.266	0.351	1.000	0.410	0.269	0.349	0.124	0.183	0.381	0.196	0.562	0.735
FMPT	0.264	0.012	-0.014	0.296	0.071	0.087	0.221	0.410	1.000	0.202	0.291	0.115	-0.014	0.216	0.119	0.289	0.290
LDAS	0.180	-0.016	-0.038	0.172	0.029	0.150	0.142	0.269	0.202	1.000	0.490	0.151	0.077	0.238	0.158	0.237	0.266
LDBA	0.387	0.049	0.082	0.222	0.138	0.241	0.257	0.349	0.291	0.490	1.000	0.180	0.101	0.214	0.250	0.249	0.334
NANL	0.179	0.133	0.086	0.264	0.073	0.667	0.217	0.124	0.115	0.151	0.180	1.000	0.106	0.582	0.802	0.127	0.267
NLAC	0.117	0.091	0.074	0.185	0.101	0.459	0.129	0.183	-0.014	0.077	0.101	0.106	1.000	0.130	0.464	0.076	0.173
NLVS	0.464	0.135	0.101	0.368	0.084	0.463	0.202	0.381	0.216	0.238	0.214	0.582	0.130	1.000	0.572	0.237	0.394
NAAC	0.244	0.137	0.114	0.257	0.094	0.776	0.261	0.196	0.119	0.158	0.250	0.802	0.464	0.572	1.000	0.111	0.259
NACA	0.433	-0.399	-0.038	0.406	0.034	0.190	0.230	0.562	0.289	0.237	0.249	0.127	0.076	0.237	0.111	1.000	0.669
NACP	0.614	0.335	-0.047	0.634	0.063	0.315	0.286	0.735	0.290	0.266	0.334	0.267	0.173	0.394	0.259	0.669	1.000
NAFM	0.531	0.085	0.020	0.322	0.072	0.263	0.145	0.459	0.148	0.186	0.215	0.110	0.238	0.296	0.243	0.372	0.475
NA41	0.316	0.116	0.115	0.281	0.059	0.780	0.348	0.264	0.163	0.147	0.282	0.644	0.334	0.364	0.804	0.196	0.309
NAVS	0.722	0.079	0.100	0.338	0.085	0.207	0.238	0.483	0.196	0.174	0.316	0.150	0.126	0.515	0.232	0.456	0.562
NAZI	0.446	0.042	0.047	0.315	-0.008	0.431	0.472	0.333	0.183	0.199	0.279	0.401	0.234	0.325	0.537	0.333	0.387
NAZS	0.368	-0.030	-0.013	0.148	0.095	0.083	0.155	0.229	0.135	0.124	0.162	0.114	0.131	0.147	0.228	0.236	0.248
BRBA	0.493	0.073	0.181	0.151	0.062	0.095	0.239	0.290	0.127	0.165	0.624	0.028	0.088	0.141	0.053	0.142	0.233
NALD	0.407	0.057	0.015	0.284	0.077	0.220	0.189	0.411	0.270	0.039	0.406	0.106	0.125	0.212	0.192	0.355	0.417
DAFM	0.350	0.034	-0.004	0.250	0.032	0.233	0.115	0.389	0.016	0.093	0.040	0.067	0.200	0.223	0.140	0.276	0.342
PLSY	0.218	0.066	0.056	0.164	-0.039	0.465	0.130	0.186	0.100	0.117	0.117	0.306	0.199	0.360	0.419	0.110	0.175
POBA	0.344	0.058	-0.031	0.169	-0.017	0.260	0.203	0.357	0.161	0.243	0.385	0.213	0.063	0.218	0.231	0.280	0.334
PM41	0.288	0.125	0.052	0.274	0.121	0.343	0.077	0.248	0.119	0.195	0.173	0.241	0.220	0.338	0.245	0.203	0.274
41MX	0.209	0.073	0.097	0.231	0.041	0.623	0.208	0.295	0.160	0.106	0.136	0.362	0.289	0.390	0.476	0.170	0.261
41ZI	0.162	0.164	1.000	0.239	1.000	1.000	0.135	0.252	0.113	1.000	1.000	0.433	1.000	1.000	1.000	0.157	1.000
PTAS	0.286	0.076	0.054	0.122	0.108	0.123	0.234	0.215	-0.334	-0.146	0.223	0.049	0.082	0.114	0.099	0.148	0.222
PTLD	0.129	0.011	0.020	0.072	0.060	0.095	0.073	0.183	-0.359	-0.053	0.205	0.016	0.096	0.045	0.088	0.119	0.135
SLBA	0.451	0.060	-0.522	0.042	-0.056	0.049	0.089	0.085	0.075	-0.029	0.102	0.023	0.023	0.111	-0.001	0.102	0.114
SLCC	0.364	0.057	-0.464	0.118	0.076	0.034	0.131	0.128	0.140	0.057	0.109	0.055	0.028	0.129	0.035	0.163	0.180
SYBA	0.520	0.089	0.121	0.296	0.140	0.148	0.152	0.279	0.166	0.116	0.071	0.156	0.093	0.349	0.157	0.164	0.273
SYMX	0.250	0.033	-0.043	0.167	-0.065	0.311	0.231	0.239	0.113	0.155	0.165	0.219	0.143	0.307	0.291	0.165	0.215
ZTPO	0.234	0.022	0.132	0.298	0.200	0.311	0.133	0.331	0.169	0.177	0.267	0.223	0.128	0.263	0.187	0.213	0.260
ZTVS	0.310	-0.042	0.026	0.306	0.047	0.242	0.337	0.529	0.256	0.309	0.251	0.104	0.100	0.331	0.145	0.307	0.304
ZTZI	0.120	-0.059	0.155	0.153	0.184	0.121	0.202	0.096	0.078	0.014	0.164	0.073	0.173	0.047	0.073	0.050	0.007
VSBA	0.498	0.099	0.096	0.082	0.134	0.100	0.122	0.079	0.112	0.058	0.107	0.172	0.029	0.083	0.167	0.053	0.140
VSSY	0.047	0.047	0.070	0.229	0.085	0.153	0.114	0.201	0.122	0.073	0.086	0.103	0.098	0.246	0.129	0.105	0.159
ZIMX	0.214	0.183	0.014	0.243	-0.020	0.246	0.127	0.313	0.132	0.134	0.213	0.143	0.104	0.148	0.201	0.104	0.285
ZSNL	0.264	0.144	0.095	0.281	0.018	0.673	0.219	0.256	0.172	0.182	0.245	0.861	0.111	0.713	0.727	0.194	0.341

	NAFM	NA41	NAVS	NAZI	NAZS	BRBA	NALD	DAFM	PLSY	POBA	PM41	41MX	41ZI	PTAS	PTLD	SLBA	SLCC
ACPM	0.302	0.163	0.278	0.228	0.159	0.184	0.316	0.182	0.136	0.247	0.286	0.133	1.000	0.138	0.149	0.170	0.150
ACSY	0.382	0.424	0.334	0.356	0.163	0.104	0.256	0.281	0.627	0.248	0.386	0.475	1.000	0.113	0.080	0.114	0.109
PMPM	0.231	0.100	0.143	0.171	0.100	0.106	0.189	0.162	0.046	0.108	0.284	0.049	0.002	0.082	0.052	0.110	0.162
ASJP	0.109	0.144	0.128	0.170	0.052	0.279	0.231	0.038	-0.033	0.234	0.080	0.013	0.081	0.329	0.143	0.069	0.068
BACC	0.210	0.132	0.147	0.199	0.107	0.235	0.168	0.136	0.034	0.307	0.138	0.112	0.001	0.113	0.056	0.198	0.460
BAOP	0.106	0.059	0.016	0.084	0.160	-0.086	0.117	0.062	-0.065	0.128	0.124	0.043	1.000	-0.012	0.053	-0.042	0.045
ASAS	0.238	0.165	0.162	0.243	0.150	0.114	0.147	0.132	0.050	0.313	0.175	0.111	0.156	-0.039	0.057	0.040	0.102
JPJP	0.256	0.188	0.175	0.241	0.142	0.032	0.140	0.127	0.089	0.243	0.127	0.116	0.131	0.135	0.067	-0.013	0.225
4141	0.295	0.238	0.215	0.253	0.096	0.164	0.279	0.210	0.110	0.273	0.403	0.248	1.000	0.121	0.066	0.253	0.304
POPO	0.360	0.201	0.215	0.288	0.248	0.163	0.260	0.274	0.089	0.711	0.179	0.179	0.159	0.167	0.137	0.010	0.166
PTPT	0.243	0.063	0.090	0.183	0.169	0.248	0.203	0.219	-0.007	0.175	0.087	-0.001	0.035	-0.066	0.118	0.065	0.143
STST	0.045	-0.074	0.015	-0.023	0.044	0.212	-0.071	0.071	0.002	0.025	-0.026	-0.058	-0.077	0.069	0.102	-0.058	-0.034
ZTZT	0.410	0.262	0.267	0.406	0.230	0.271	0.333	0.349	0.127	0.501	0.128	0.204	0.190	0.164	0.143	0.154	0.186
BRAS	0.203	0.107	0.192	0.194	0.106	0.465	0.322	0.090	0.047	0.182	0.137	0.091	0.028	0.248	0.211	0.011	0.111
BRLD	0.058	0.033	0.070	0.065	0.063	0.231	0.702	0.012	-0.005	0.100	0.017	0.039	1.000	0.192	0.657	0.100	0.031
BRNA	0.280	0.166	0.269	0.226	0.123	0.293	0.409	0.181	0.079	0.199	0.042	0.195	1.000	0.242	0.210	0.069	0.115
BRPT	0.092	-0.016	0.131	0.060	0.095	0.283	0.185	0.101	-0.052	0.067	0.035	-0.051	1.000	0.267	0.528	0.011	-0.007
NABA	0.531	0.316	0.722	0.446	0.368	0.493	0.407	0.350	0.218	0.344	0.288	0.209	0.162	0.286	0.129	0.451	0.364
CACP	0.085	0.116	0.079	0.042	-0.030	0.073	0.057	0.034	0.066	0.058	0.125	0.073	0.164	0.076	0.011	0.060	0.057
CPSL	0.020	0.115	0.100	0.047	-0.013	0.181	0.015	-0.004	0.056	-0.031	0.052	0.097	1.000	0.054	0.020	-0.522	-0.464
CPZS	0.322	0.281	0.338	0.315	0.148	0.151	0.284	0.250	0.164	0.169	0.274	0.231	0.239	0.122	0.072	0.042	0.118
CNCN	0.072	0.059	0.085	-0.008	0.095	0.062	0.077	0.032	-0.039	-0.017	0.121	0.041	1.000	0.108	0.060	-0.056	0.076
FMPM	0.263	0.780	0.207	0.431	0.083	0.095	0.220	0.233	0.465	0.260	0.343	0.623	1.000	0.123	0.095	0.049	0.034
FMZT	0.145	0.348	0.238	0.472	0.155	0.239	0.189	0.115	0.130	0.203	0.077	0.208	0.135	0.234	0.073	0.089	0.131
FMCP	0.459	0.264	0.483	0.333	0.229	0.290	0.411	0.389	0.186	0.357	0.248	0.295	0.252	0.215	0.183	0.085	0.128
FMPT	0.148	0.163	0.196	0.183	0.135	0.127	0.270	0.016	0.100	0.161	0.119	0.160	0.113	-0.334	-0.359	0.075	0.140
LDAS	0.186	0.147	0.174	0.199	0.124	0.165	0.039	0.093	0.117	0.243	0.195	0.106	1.000	-0.146	-0.053	-0.029	0.057
LDBA	0.215	0.282	0.316	0.279	0.162	0.624	0.406	0.040	0.117	0.385	0.173	0.136	1.000	0.223	0.205	0.102	0.109
NANL	0.110	0.644	0.150	0.401	0.114	0.028	0.106	0.067	0.306	0.213	0.241	0.362	0.433	0.049	0.016	0.023	0.055
NLAC	0.238	0.334	0.126	0.234	0.131	0.088	0.125	0.200	0.199	0.063	0.220	0.289	1.000	0.082	0.096	0.023	0.028
NLVS	0.296	0.364	0.515	0.325	0.147	0.141	0.212	0.223	0.360	0.218	0.338	0.390	1.000	0.114	0.045	0.111	0.129
NAAC	0.243	0.804	0.232	0.537	0.228	0.053	0.192	0.140	0.419	0.231	0.245	0.476	1.000	0.099	0.088	-0.001	0.035
NACA	0.372	0.196	0.456	0.333	0.236	0.142	0.355	0.276	0.110	0.280	0.203	0.170	0.157	0.148	0.119	0.102	0.163
NACP	0.475	0.309	0.562	0.387	0.248	0.233	0.417	0.342	0.175	0.334	0.274	0.261	1.000	0.222	0.135	0.114	0.180
NAFM	1.000	0.304	0.467	0.549	0.492	0.170	0.337	0.827	0.253	0.337	0.263	0.235	0.191	0.175	0.099	0.200	0.264
NA41	0.304	1.000	0.338	0.643	0.314	0.124	0.250	0.172	0.438	0.276	0.116	0.646	0.620	0.136	0.096	0.021	0.075
NAVS	0.467	0.338	1.000	0.455	0.447	0.322	0.379	0.315	0.206	0.255	0.192	0.209	1.000	0.229	0.181	0.144	0.159
NAZI	0.549	0.643	0.455	1.000	0.524	0.136	0.306	0.349	0.300	0.296	0.202	0.299	0.219	0.215	0.114	0.100	0.220
NAZS	0.492	0.314	0.447	0.524	1.000	0.082	0.228	0.308	0.078	0.187	0.099	0.081	0.088	0.092	0.109	0.011	0.075
BRBA	0.170	0.124	0.322	0.136	0.082	1.000	0.314	0.071	0.056	0.292	0.087	0.089	0.059	0.239	0.227	0.259	0.125
NALD	0.337	0.250	0.379	0.306	0.228	0.314	1.000	0.188	0.105	0.293	0.142	0.217	0.196	0.350	0.745	0.178	0.180
DAFM	0.827	0.172	0.315	0.349	0.308	0.071	0.188	1.000	0.214	0.247	0.172	0.192	1.000	0.111	0.087	0.169	0.195
PLSY	0.253	0.438	0.206	0.300	0.078	0.056	0.105	0.214	1.000	0.131	0.173	0.362	0.316	0.058	0.015	0.063	-0.006
POBA	0.337	0.276	0.255	0.296	0.187	0.292	0.293	0.247	0.131	1.000	0.194	0.188	1.000	0.141	0.161	0.247	0.258
PM41	0.263	0.116	0.192	0.202	0.099	0.087	0.142	0.172	0.173	0.194	1.000	-0.001	0.011	0.059	0.058	0.106	0.181
41MX	0.235	0.646	0.209	0.299	0.081	0.089	0.217	0.192	0.362	0.188	-0.001	1.000	0.642	0.086	0.059	0.038	0.009
41ZI	0.191	0.620	1.000	0.219	0.088	0.059	0.196	1.000	0.316	1.000	0.011	0.642	1.000	0.013	0.069	1.000	-0.066
PTAS	0.175	0.136	0.229	0.215	0.092	0.239	0.350	0.111	0.058	0.141	0.059	0.086	0.013	1.000	0.564	0.078	0.105
PTLD	0.099	0.096	0.181	0.114	0.109	0.227	0.745	0.087	0.015	0.161	0.058	0.059	0.069	0.564	1.000	0.062	-0.002
SLBA	0.200	0.021	0.144	0.100	0.011	0.259	0.178	0.169	0.063	0.247	0.106	0.038	1.000	0.078	0.062	1.000	0.693
SLCC	0.264	0.075	0.159	0.220	0.075	0.125	0.180	0.195	-0.006	0.258	0.181	0.009	-0.066	0.105	-0.002	0.693	1.000
SYBA	0.184	0.091	0.130	0.068	0.078	0.141	0.077	0.124	-0.152	0.094	0.237	0.149	0.108	0.050	-0.020	0.235	0.162
SYMX	0.259	0.386	0.202	0.375	0.163	0.133	0.172	0.172	0.578	0.158	0.057	0.221	0.232	0.189	0.050	0.124	0.132
ZTPO	0.129	0.239	0.213	0.207	0.033	0.154	0.253	0.104	0.164	0.111	0.131	0.204	0.022	0.238	0.118	-0.022	0.105
ZTVS	0.298	0.232	0.379	0.323	0.165	0.211	0.272	0.289	0.146	0.415	0.134	0.224	0.142	0.105	0.141	0.087	0.133
ZTZI	0.026	0.063	0.042	0.098	0.039	0.139	0.035	0.047	0.024	-0.113	0.047	0.013	-0.391	0.127	-0.015	-0.059	0.070
VSBA	0.178	0.079	-0.171	0.103	0.040	0.207	0.065	0.096	0.077	0.154	0.179	0.073	1.000	0.089	-0.064	0.326	0.219
VSSY	0.015	0.170	0.151	0.079	0.053	0.042	0.078	-0.007	-0.324	0.017	0.067	0.157	0.144	0.004	0.042	-0.037	0.024
ZIMX	0.160	0.311	0.210	0.138	0.019	0.169	0.246	0.152	0.159	0.261	0.071	0.249	0.429	0.050	0.133	0.120	0.059
ZSNL	0.203	0.545	0.208	0.350	0.099	0.108	0.188	0.116	0.322	0.299	0.339	0.426	1.000	0.060	0.038	0.070	0.070

	SYBA	SYMX	ZTPO	ZTVS	ZTZI	VSBA	VSSY	ZIMX	ZSNL
ACPM	0.083	0.114	0.095	0.164	-0.031	0.068	0.032	0.242	0.231
ACSY	0.047	0.496	0.205	0.228	0.028	0.198	-0.199	0.179	0.575
PMPM	0.110	0.041	0.066	0.109	0.066	0.114	0.063	0.096	0.129
ASJP	0.016	0.028	0.051	0.074	0.136	0.115	0.018	0.091	0.090
BACC	0.249	0.113	0.203	0.298	0.200	0.333	0.035	0.081	0.101
BAOP	-0.012	-0.099	0.012	0.021	-0.055	-0.106	0.122	-0.037	0.073
ASAS	0.093	0.123	0.058	0.275	-0.024	0.128	0.036	0.172	0.158
JPJP	0.092	0.149	0.093	0.195	0.051	0.059	0.056	0.031	0.170
4141	0.219	0.148	0.201	0.332	0.089	0.157	0.082	0.232	0.197
POPO	0.145	0.126	0.131	0.448	0.045	0.154	0.039	0.144	0.219
PTPT	-0.052	0.036	0.012	0.169	-0.006	-0.051	0.027	0.131	-0.010
STST	-0.072	-0.018	-0.108	0.003	-0.048	-0.108	-0.037	-0.014	-0.123
ZTZT	0.197	0.243	0.297	0.921	0.224	0.205	0.069	0.426	0.199
BRAS	0.075	0.147	0.201	0.259	0.043	0.042	0.052	0.104	0.085
BRLD	-0.018	0.027	0.068	0.104	-0.023	-0.039	0.023	0.057	0.026
BRNA	0.020	0.134	0.163	0.193	0.041	0.022	0.110	0.217	0.117
BRPT	-0.056	-0.012	0.013	0.030	-0.045	-0.105	0.072	0.080	-0.050
NABA	0.520	0.250	0.234	0.310	0.120	0.498	0.047	0.214	0.264
CACP	0.089	0.033	0.022	-0.042	-0.059	0.099	0.047	0.183	0.144
CPSL	0.121	-0.043	0.132	0.026	0.155	0.096	0.070	0.014	0.095
CPZS	0.296	0.167	0.298	0.306	0.153	0.082	0.229	0.243	0.281
CNCN	0.140	-0.065	0.200	0.047	0.184	0.134	0.085	-0.020	0.018
FMPM	0.148	0.311	0.311	0.242	0.121	0.100	0.153	0.246	0.673
FMZT	0.152	0.231	0.133	0.337	0.202	0.122	0.114	0.127	0.219
FMCP	0.279	0.239	0.331	0.529	0.096	0.079	0.201	0.313	0.256
FMPT	0.166	0.113	0.169	0.256	0.078	0.112	0.122	0.132	0.172
LDAS	0.116	0.155	0.177	0.309	0.014	0.058	0.073	0.134	0.182
LDBA	0.071	0.165	0.267	0.251	0.164	0.107	0.086	0.213	0.245
NANL	0.156	0.219	0.223	0.104	0.073	0.172	0.103	0.143	0.861
NLAC	0.093	0.143	0.128	0.100	0.173	0.029	0.098	0.104	0.111
NLVS	0.349	0.307	0.263	0.331	0.047	0.083	0.246	0.148	0.713
NAAC	0.157	0.291	0.187	0.145	0.073	0.167	0.129	0.201	0.727
NACA	0.164	0.165	0.213	0.307	0.050	0.053	0.105	0.104	0.194
NACP	0.273	0.215	0.260	0.304	0.007	0.140	0.159	0.285	0.341
NAFM	0.184	0.259	0.129	0.298	0.026	0.178	0.015	0.160	0.203
NA41	0.091	0.386	0.239	0.232	0.063	0.079	0.170	0.311	0.545
NAVS	0.130	0.202	0.213	0.379	0.042	-0.171	0.151	0.210	0.208
NAZI	0.068	0.375	0.207	0.323	0.098	0.103	0.079	0.138	0.350
NAZS	0.078	0.163	0.033	0.165	0.039	0.040	0.053	0.019	0.099
BRBA	0.141	0.133	0.154	0.211	0.139	0.207	0.042	0.169	0.108
NALD	0.077	0.172	0.253	0.272	0.035	0.065	0.078	0.246	0.188
DAFM	0.124	0.172	0.104	0.289	0.047	0.096	-0.007	0.152	0.116
PLSY	-0.152	0.578	0.164	0.146	0.024	0.077	-0.324	0.159	0.322
POBA	0.094	0.158	0.111	0.415	-0.113	0.154	0.017	0.261	0.299
PM41	0.237	0.057	0.131	0.134	0.047	0.179	0.067	0.071	0.339
41MX	0.149	0.221	0.204	0.224	0.013	0.073	0.157	0.249	0.426
41ZI	0.108	0.232	0.022	0.142	-0.391	1.000	0.144	0.429	1.000
PTAS	0.050	0.189	0.238	0.105	0.127	0.089	0.004	0.050	0.060
PTLD	-0.020	0.050	0.118	0.141	-0.015	-0.064	0.042	0.133	0.038
SLBA	0.235	0.124	-0.022	0.087	-0.059	0.326	-0.037	0.120	0.070
SLCC	0.162	0.132	0.105	0.133	0.070	0.219	0.024	0.059	0.070
SYBA	1.000	-0.117	0.147	0.175	0.096	0.604	0.520	0.031	0.226
SYMX	-0.117	1.000	0.246	0.215	0.063	0.085	-0.295	0.132	0.225
ZTPO	0.147	0.246	1.000	0.377	0.209	0.045	0.111	0.183	0.234
ZTVS	0.175	0.215	0.377	1.000	0.158	0.020	0.187	0.413	0.169
ZTZI	0.096	0.063	0.209	0.158	1.000	0.086	0.062	-0.243	0.020
VSBA	0.604	0.085	0.045	0.020	0.086	1.000	-0.167	0.025	0.198
VSSY	0.520	-0.295	0.111	0.187	0.062	-0.167	1.000	0.073	0.133
ZIMX	0.031	0.132	0.183	0.413	-0.243	0.025	0.073	1.000	0.124
ZSNL	0.226	0.225	0.234	0.169	0.020	0.198	0.133	0.124	1.000

Table B9 Phenotypic Correlation Matrix for Model 3.

	ACPM	ACSY	PMPM	ASJP	BACC	BAOP	ASAS	JPJP	4141	POPO	PTPT	STST	ZTZT	BRAS	BRLD	BRNA	BRPT
ACPM	1.000	0.182	0.392	0.002	0.016	0.010	0.106	-0.067	0.131	0.003	-0.198	-0.051	0.108	0.070	0.001	-0.135	-0.159
ACSY	0.182	1.000	0.153	-0.086	-0.034	0.050	0.004	0.065	-0.047	-0.131	-0.089	-0.164	-0.288	-0.085	-0.156	-0.061	-0.181
PMPM	0.392	0.153	1.000	0.107	0.007	-0.187	0.064	-0.005	0.169	0.123	0.025	0.102	-0.019	-0.005	-0.170	-0.014	-0.022
ASJP	0.002	-0.086	0.107	1.000	0.021	-0.087	0.417	0.052	-0.056	0.143	0.023	-0.014	0.070	-0.203	-0.009	0.140	0.026
BACC	0.016	-0.034	0.007	0.021	1.000	-0.033	-0.167	0.215	0.076	-0.227	0.095	0.021	0.028	-0.037	-0.010	-0.042	0.060
BAOP	0.010	0.050	-0.187	-0.087	-0.033	1.000	0.050	-0.111	-0.308	0.126	-0.001	0.041	-0.021	-0.073	0.109	0.003	-0.082
ASAS	0.106	0.004	0.064	0.417	-0.167	0.050	1.000	-0.119	-0.097	0.027	0.086	0.164	0.044	0.085	0.042	-0.026	0.093
JPJP	-0.067	0.065	-0.005	0.052	0.215	-0.111	-0.119	1.000	0.082	-0.073	0.200	-0.070	0.015	0.169	-0.022	-0.020	-0.051
4141	0.131	-0.047	0.169	-0.056	0.076	-0.308	-0.097	0.082	1.000	-0.104	-0.003	0.150	-0.099	-0.084	0.034	-0.185	0.028
POPO	0.003	-0.131	0.123	0.143	-0.227	0.126	0.027	-0.073	-0.104	1.000	0.200	-0.047	0.187	0.185	0.126	-0.081	-0.072
PTPT	-0.198	-0.089	0.025	0.023	0.095	-0.001	0.086	0.200	-0.003	0.200	1.000	0.246	0.168	0.223	0.096	0.228	0.459
STST	-0.051	-0.164	0.102	-0.014	0.021	0.041	0.164	-0.070	0.150	-0.047	0.246	1.000	-0.049	0.204	0.065	0.119	0.205
ZTZT	0.108	-0.288	-0.019	0.070	0.028	-0.021	0.044	0.015	-0.099	0.187	0.168	-0.049	1.000	0.036	0.079	0.076	0.163
BRAS	0.070	-0.085	-0.005	-0.203	-0.037	-0.073	0.085	0.169	-0.084	0.185	0.223	0.204	0.036	1.000	0.416	-0.522	-0.030
BRLD	0.001	-0.156	-0.170	-0.009	-0.010	0.109	0.042	-0.022	0.034	0.126	0.096	0.065	0.079	0.416	1.000	-0.340	-0.018
BRNA	-0.135	-0.061	-0.014	0.140	-0.042	0.003	-0.026	-0.020	-0.185	-0.081	0.228	0.119	0.076	-0.522	-0.340	1.000	0.445
BRPT	-0.159	-0.181	-0.022	0.026	0.060	-0.082	0.093	-0.051	0.028	-0.072	0.459	0.205	0.163	-0.030	-0.018	0.445	1.000
NABA	0.047	-0.157	-0.102	-0.037	0.130	-0.209	-0.105	0.160	0.092	-0.144	-0.127	-0.054	-0.040	0.074	0.079	-0.024	-0.040
CACP	-0.130	-0.144	-0.163	-0.093	0.179	-0.044	-0.013	0.197	0.173	-0.086	-0.028	-0.016	0.096	-0.045	-0.070	-0.105	-0.115
CPSL	0.086	0.088	0.025	0.127	-0.055	-0.098	-0.029	0.051	0.075	-0.064	-0.063	0.004	-0.099	-0.023	0.008	0.051	-0.061
CPZS	0.000	-0.321	0.020	-0.004	0.049	-0.075	-0.001	0.045	0.108	-0.210	-0.055	0.123	0.001	0.001	0.003	0.064	0.049
CNCN	0.043	0.081	-0.119	0.005	0.240	0.205	-0.078	0.146	-0.240	-0.182	-0.173	-0.120	-0.086	0.010	0.008	-0.055	-0.128
FMPM	-0.052	0.244	-0.105	-0.125	-0.128	-0.028	0.011	-0.115	-0.157	-0.253	-0.151	-0.020	-0.151	-0.260	-0.242	0.022	-0.108
FMZT	-0.108	-0.126	-0.004	0.029	-0.041	-0.112	-0.048	-0.022	-0.033	0.056	0.201	0.046	0.201	-0.061	-0.083	0.198	0.125
FMCP	0.009	-0.365	-0.002	0.074	0.033	0.003	-0.032	-0.078	0.113	0.231	0.090	0.087	0.350	-0.055	-0.037	0.255	0.173
FMPT	-0.056	-0.042	-0.080	0.102	0.088	0.042	-0.098	0.152	-0.300	0.046	0.085	0.069	0.110	-0.133	0.025	0.154	-0.418
LDAS	0.089	0.025	0.013	-0.382	-0.132	-0.001	0.440	-0.018	-0.076	-0.002	0.056	0.073	-0.041	0.405	-0.155	-0.128	0.091
LDBA	0.009	0.016	-0.020	0.126	-0.019	-0.111	-0.089	0.201	0.041	0.048	-0.194	-0.252	0.166	0.216	-0.134	0.015	0.052
NANL	-0.198	0.170	-0.202	-0.139	0.058	-0.053	-0.102	-0.127	-0.193	-0.350	-0.142	0.049	-0.146	-0.231	-0.195	0.071	0.046
NLAC	0.174	0.235	0.059	-0.068	0.149	-0.026	0.125	0.094	-0.018	-0.095	-0.047	0.191	-0.230	-0.046	-0.056	-0.070	-0.094
NLVS	0.040	0.581	-0.011	-0.129	-0.031	0.106	-0.064	-0.144	-0.058	-0.092	-0.153	-0.160	-0.217	-0.245	-0.128	0.027	-0.159
NAAC	-0.113	0.527	0.009	-0.108	-0.010	0.021	-0.073	-0.113	-0.138	-0.282	-0.245	-0.025	-0.420	-0.326	-0.256	0.048	-0.059
NACA	0.044	-0.210	0.070	0.110	-0.121	0.005	-0.099	-0.225	-0.118	0.069	0.052	0.070	-0.070	0.121	0.201	0.132	0.097
NACP	-0.161	-0.387	-0.170	-0.026	-0.003	-0.009	-0.060	-0.001	0.010	0.004	0.036	0.042	-0.035	0.087	0.108	0.036	-0.038
NAFM	0.140	-0.019	0.141	0.052	0.132	0.044	0.140	-0.074	0.049	0.044	-0.202	0.028	0.258	0.085	0.047	0.055	-0.061
NA41	-0.248	0.073	-0.271	-0.046	-0.037	-0.090	-0.002	-0.067	-0.197	-0.171	-0.266	-0.089	-0.182	-0.171	-0.176	-0.053	-0.132
NAVS	-0.034	-0.222	-0.194	0.020	0.027	0.028	0.026	0.078	-0.045	0.095	-0.237	-0.186	0.127	0.101	0.125	-0.035	-0.099
NAZI	-0.022	-0.137	-0.032	0.055	0.041	0.083	-0.043	-0.004	-0.004	-0.062	-0.003	0.206	0.137	0.063	0.142	-0.148	0.008
NAZS	0.073	-0.043	-0.034	0.003	-0.059	0.174	0.075	-0.033	0.019	0.067	-0.135	-0.022	0.105	0.007	0.036	-0.018	-0.053
BRBA	-0.034	-0.206	-0.032	-0.015	0.107	-0.241	-0.009	0.287	0.077	0.079	0.077	0.168	0.122	0.527	0.175	-0.116	0.167
NALD	-0.093	-0.129	-0.158	0.034	-0.053	0.128	0.031	-0.013	-0.109	0.144	0.094	-0.003	0.167	0.147	0.808	0.136	0.046
DAFM	0.123	-0.213	0.215	-0.111	0.126	0.131	0.092	0.095	0.269	0.179	-0.030	0.029	0.087	0.125	-0.181	0.042	0.005
PLSY	-0.072	0.644	-0.025	-0.076	-0.046	-0.028	-0.004	0.021	-0.018	-0.067	-0.079	-0.310	-0.109	-0.095	-0.150	-0.004	-0.132
POBA	0.033	0.021	-0.111	0.033	-0.181	0.160	0.063	-0.043	-0.004	0.502	0.165	0.018	0.087	0.049	0.011	0.050	0.034
PM41	0.048	0.015	0.140	0.036	-0.089	0.087	-0.001	-0.203	0.182	-0.064	-0.053	-0.023	-0.060	-0.045	0.022	-0.050	-0.102
41MX	-0.082	0.343	-0.200	-0.086	-0.009	-0.146	0.092	-0.111	-0.087	-0.032	-0.055	-0.105	0.039	-0.152	-0.137	-0.020	-0.167
41ZI	0.001	0.168	-0.222	-0.148	-0.174	0.023	0.244	-0.096	-0.031	-0.142	-0.017	-0.092	-0.026	-0.183	-0.218	-0.004	-0.157
PTAS	0.084	-0.007	0.031	0.214	-0.011	-0.109	-0.254	0.094	0.003	0.153	-0.040	-0.012	0.132	0.220	0.034	0.175	0.114
PTLD	-0.125	-0.162	-0.143	-0.003	-0.108	0.077	0.052	-0.113	0.203	0.088	0.131	0.018	0.094	0.161	0.684	0.072	0.434
SLBA	-0.103	-0.211	-0.223	-0.200	0.153	0.052	0.123	0.084	0.064	0.084	0.082	0.181	0.103	0.094	-0.010	-0.148	0.056
SLCC	-0.119	-0.117	-0.080	-0.121	0.394	0.081	-0.011	0.124	-0.130	0.065	0.106	0.206	0.071	0.140	0.057	-0.131	0.095
SYBA	0.105	-0.352	0.053	0.013	0.118	-0.174	-0.052	-0.200	0.365	-0.120	0.119	-0.045	-0.052	-0.315	-0.033	0.122	0.082
SYMX	-0.149	0.511	-0.055	-0.029	0.006	0.028	0.032	0.185	-0.195	0.086	0.008	-0.119	0.045	-0.054	-0.101	0.005	0.008
ZTPO	0.033	-0.002	-0.107	0.044	0.056	-0.069	-0.093	0.250	-0.236	0.016	0.111	-0.182	0.104	0.103	0.030	0.093	0.152
ZTVS	0.025	-0.356	-0.035	-0.011	0.008	0.088	-0.007	0.067	-0.055	0.218	0.188	-0.137	0.925	-0.061	0.051	-0.006	0.117
ZTZI	-0.100	-0.006	0.107	0.102	0.099	-0.144	-0.160	0.047	-0.202	0.002	-0.104	-0.062	-0.010	-0.030	0.010	0.026	0.069
VSBA	0.068	0.130	0.055	-0.047	0.120	-0.284	-0.096	0.065	0.137	-0.231	0.232	0.126	-0.103	-0.030	-0.103	0.157	0.112
VSSY	-0.036	-0.600	-0.075	0.042	0.092	0.124	0.026	-0.126	0.174	0.088	-0.035	-0.011	0.117	-0.217	0.033	0.057	0.062
ZIMX	-0.107	-0.243	-0.220	-0.004	-0.002	0.044	0.141	0.112	0.129	0.002	0.088	-0.076	0.418	0.072	-0.005	-0.015	-0.031
ZSNL	-0.053	0.397	-0.093	-0.174	-0.043	0.000	-0.127	-0.281	-0.217	-0.216	-0.096	-0.094	-0.217	-0.341	-0.215	0.045	0.037

	NABA	CACP	CPSL	CPZS	CNCN	FMPM	FMZT	FMCP	FMPT	LDAS	LDBA	NANL	NLAC	NLVS	NAAC	NACA	NACP
ACPM	0.047	-0.130	0.086	0.000	0.043	-0.052	-0.108	0.009	-0.056	0.089	0.009	-0.198	0.174	0.040	-0.113	0.044	-0.161
ACSY	-0.157	-0.144	0.088	-0.321	0.081	0.244	-0.126	-0.365	-0.042	0.025	0.016	0.170	0.235	0.581	0.527	-0.210	-0.387
PMPM	-0.102	-0.163	0.025	0.020	-0.119	-0.105	-0.004	-0.002	-0.080	0.013	-0.020	-0.202	0.059	-0.011	0.009	0.070	-0.170
ASJP	-0.037	-0.093	0.127	-0.004	0.005	-0.125	0.029	0.074	0.102	-0.382	0.126	-0.139	-0.068	-0.129	-0.108	0.110	-0.026
BACC	0.130	0.179	-0.055	0.049	0.240	-0.128	-0.041	0.033	0.088	-0.132	-0.019	0.058	0.149	-0.031	-0.010	-0.121	-0.003
BAOP	-0.209	-0.044	-0.098	-0.075	0.205	-0.028	-0.112	0.003	0.042	-0.001	-0.111	-0.053	-0.026	0.106	0.021	0.005	-0.009
ASAS	-0.105	-0.013	-0.029	-0.001	-0.078	0.011	-0.048	-0.032	-0.098	0.440	-0.089	-0.102	0.125	-0.064	-0.073	-0.099	-0.060
JPJP	0.160	0.197	0.051	0.045	0.146	-0.115	-0.022	-0.078	0.152	-0.018	0.201	-0.127	0.094	-0.144	-0.113	-0.225	-0.001
4141	0.092	0.173	0.075	0.108	-0.240	-0.157	-0.033	0.113	-0.300	-0.076	0.041	-0.193	-0.018	-0.058	-0.138	-0.118	0.010
POPO	-0.144	-0.086	-0.064	-0.210	-0.182	-0.253	0.056	0.231	0.046	-0.002	0.048	-0.350	-0.095	-0.092	-0.282	0.069	0.004
PTPT	-0.127	-0.028	-0.063	-0.055	-0.173	-0.151	0.201	0.090	0.085	0.056	-0.194	-0.142	-0.047	-0.153	-0.245	0.052	0.036
STST	-0.054	-0.016	0.004	0.123	-0.120	-0.020	0.046	0.087	0.069	0.073	-0.252	0.049	0.191	-0.160	-0.025	0.070	0.042
ZTZT	-0.040	0.096	-0.099	0.001	-0.086	-0.151	0.201	0.350	0.110	-0.041	0.166	-0.146	-0.230	-0.217	-0.420	-0.070	-0.035
BRAS	0.074	-0.045	-0.023	0.001	0.010	-0.260	-0.061	-0.055	-0.133	0.405	0.216	-0.231	-0.046	-0.245	-0.326	0.121	0.087
BRLD	0.079	-0.070	0.008	0.003	0.008	-0.242	-0.083	-0.037	0.025	-0.155	-0.134	-0.195	-0.056	-0.128	-0.256	0.201	0.108
BRNA	-0.024	-0.105	0.051	0.064	-0.055	0.022	0.198	0.255	0.154	-0.128	0.015	0.071	-0.070	0.027	0.048	0.132	0.036
BRPT	-0.040	-0.115	-0.061	0.049	-0.128	-0.108	0.125	0.173	-0.418	0.091	0.052	0.046	-0.094	-0.159	-0.059	0.097	-0.038
NABA	1.000	0.082	0.155	-0.031	0.069	-0.455	0.106	0.084	0.177	-0.058	0.206	-0.125	-0.196	0.107	-0.126	0.011	0.094
CACP	0.082	1.000	-0.163	0.273	0.040	-0.096	0.046	0.097	0.048	-0.021	-0.089	0.006	-0.112	-0.009	-0.085	-0.650	0.347
CPSL	0.155	-0.163	1.000	0.043	0.076	0.027	-0.032	-0.081	0.024	-0.094	0.090	0.062	0.158	-0.042	-0.004	0.138	-0.083
CPZS	-0.031	0.273	0.043	1.000	-0.039	-0.002	-0.074	0.333	0.044	-0.060	-0.009	-0.019	0.022	-0.196	-0.263	0.055	0.405
CNCN	0.069	0.040	0.076	-0.039	1.000	-0.081	-0.067	0.005	0.180	0.020	0.204	0.023	0.123	0.048	0.108	-0.098	-0.022
FMPM	-0.455	-0.096	0.027	-0.002	-0.081	1.000	-0.150	-0.238	-0.074	-0.040	-0.284	0.395	0.253	0.127	0.484	0.004	-0.136
FMZT	0.106	0.046	-0.032	-0.074	-0.067	-0.150	1.000	0.131	0.135	-0.125	-0.109	0.052	-0.200	-0.047	-0.056	-0.050	-0.012
FMCP	0.084	0.097	-0.081	0.333	0.005	-0.238	0.131	1.000	0.171	-0.031	0.340	-0.293	-0.241	-0.224	-0.546	0.230	0.477
FMPT	0.177	0.048	0.024	0.044	0.180	-0.074	0.135	0.171	1.000	-0.179	-0.068	-0.109	-0.091	0.138	-0.203	0.000	0.031
LDAS	-0.058	-0.021	-0.094	-0.060	0.020	-0.040	-0.125	-0.031	-0.179	1.000	0.347	-0.044	0.051	-0.051	-0.059	-0.053	-0.032
LDBA	0.206	-0.089	0.090	-0.009	0.204	-0.284	-0.109	0.340	-0.068	0.347	1.000	-0.213	-0.121	-0.148	-0.262	0.189	0.068
NANL	-0.125	0.006	0.062	-0.019	0.023	0.395	0.052	-0.293	-0.109	-0.044	-0.213	1.000	-0.053	0.495	0.591	0.040	0.013
NLAC	-0.196	-0.112	0.158	0.022	0.123	0.253	-0.200	-0.241	-0.091	0.051	-0.121	-0.053	1.000	-0.094	0.340	-0.026	-0.140
NLVS	0.107	-0.009	-0.042	-0.196	0.048	0.127	-0.047	-0.224	0.138	-0.051	-0.148	0.495	-0.094	1.000	0.434	-0.099	-0.165
NAAC	-0.126	-0.085	-0.004	-0.263	0.108	0.484	-0.056	-0.546	-0.203	-0.059	-0.262	0.591	0.340	0.434	1.000	-0.219	-0.383
NACA	0.011	-0.650	0.138	0.055	-0.098	0.004	-0.050	0.230	0.000	-0.053	0.189	0.040	-0.026	-0.099	-0.219	1.000	0.407
NACP	0.094	0.347	-0.083	0.405	-0.022	-0.136	-0.012	0.477	0.031	-0.032	0.068	0.013	-0.140	-0.165	-0.383	0.407	1.000
NAFM	0.167	-0.159	0.019	-0.159	-0.027	-0.055	-0.072	0.269	0.085	0.094	0.158	-0.125	0.089	-0.065	0.058	0.047	-0.041
NA41	-0.056	-0.059	0.023	-0.223	0.021	0.337	0.001	-0.430	-0.099	-0.060	-0.240	0.372	0.075	0.119	0.627	-0.235	-0.357
NAVS	0.612	-0.050	0.051	0.007	0.192	-0.388	0.138	0.229	0.209	-0.006	0.223	-0.004	-0.168	0.239	-0.187	0.131	0.159
NAZI	0.249	-0.062	0.094	-0.134	0.010	-0.045	0.288	-0.115	0.020	-0.059	-0.067	0.083	-0.011	-0.102	0.249	-0.136	-0.312
NAZS	0.273	-0.064	-0.094	-0.044	0.116	-0.277	0.018	0.067	0.007	0.012	-0.022	-0.189	0.063	0.036	-0.029	-0.132	-0.093
BRBA	0.415	-0.136	0.141	0.090	0.025	-0.326	0.024	0.234	-0.066	0.099	0.448	-0.229	-0.022	-0.287	-0.348	0.296	0.090
NALD	0.156	-0.116	0.076	-0.001	0.020	-0.274	0.020	0.047	0.142	-0.226	-0.033	-0.208	-0.149	-0.022	-0.234	0.217	0.101
DAFM	-0.167	-0.059	-0.004	0.027	-0.122	-0.055	-0.085	0.293	-0.038	0.190	0.068	-0.325	-0.046	-0.233	-0.249	0.097	0.189
PLSY	-0.197	-0.121	0.122	-0.042	0.008	0.269	-0.183	-0.138	0.095	0.046	0.134	0.101	0.012	0.293	0.228	-0.221	-0.299
POBA	-0.279	-0.063	-0.144	-0.049	-0.256	-0.212	-0.045	0.217	0.016	0.088	-0.049	-0.386	0.024	-0.203	-0.224	0.131	0.109
PM41	0.079	-0.032	-0.064	0.141	-0.044	0.340	-0.003	0.156	0.036	-0.093	-0.034	-0.033	0.011	0.039	-0.170	0.147	0.182
41MX	-0.199	-0.061	0.008	-0.309	-0.102	0.162	-0.074	-0.390	-0.014	0.065	-0.225	0.156	-0.058	0.341	0.215	-0.232	-0.309
41ZI	-0.293	0.142	-0.101	-0.050	-0.084	0.199	-0.119	-0.204	-0.021	0.120	-0.366	0.113	0.054	-0.048	0.060	-0.112	-0.022
PTAS	0.195	-0.037	0.136	-0.026	-0.014	-0.308	0.162	0.155	-0.282	-0.253	0.309	-0.098	-0.180	-0.051	-0.099	0.115	0.107
PTLD	-0.039	-0.112	0.031	-0.010	-0.090	-0.276	-0.004	-0.016	-0.423	-0.086	0.033	-0.182	-0.113	-0.177	-0.173	0.162	0.040
SLBA	0.163	0.008	-0.694	-0.025	-0.212	-0.267	0.045	0.029	-0.076	0.181	-0.168	-0.059	-0.317	0.044	-0.120	0.007	0.021
SLCC	-0.050	0.061	-0.622	-0.155	-0.004	-0.209	0.092	-0.104	-0.046	0.081	-0.111	0.122	-0.174	0.083	0.062	-0.119	-0.109
SYBA	0.422	0.269	-0.061	0.050	-0.125	-0.243	-0.026	0.022	0.075	-0.112	-0.162	0.002	-0.120	0.116	-0.130	-0.100	0.129
SYMX	-0.018	-0.186	0.162	-0.065	0.022	0.294	0.030	-0.088	-0.016	-0.005	0.062	0.116	-0.002	0.162	0.155	-0.017	-0.192
ZTPO	0.033	-0.009	0.212	0.206	0.183	0.066	-0.066	0.158	0.090	0.006	0.361	-0.001	-0.057	0.099	-0.106	0.083	0.077
ZTVS	-0.181	0.100	-0.158	0.059	-0.041	-0.121	0.115	0.266	0.174	-0.043	0.074	-0.187	-0.229	-0.218	-0.460	-0.151	-0.111
ZTZI	0.118	-0.099	0.122	-0.006	0.131	0.112	0.039	0.026	-0.004	-0.121	0.205	0.144	0.089	0.147	0.124	0.047	-0.052
VSBA	0.396	0.132	0.134	-0.117	-0.079	-0.156	-0.034	0.020	0.025	-0.020	0.090	-0.170	0.032	-0.140	0.063	-0.168	-0.026
VSSY	0.025	0.040	-0.127	0.054	0.024	-0.104	0.059	0.044	-0.020	-0.098	-0.156	0.123	-0.036	0.017	-0.074	0.121	0.074
ZIMX	-0.150	0.049	0.027	0.057	-0.029	-0.175	0.005	0.032	0.042	0.027	-0.073	-0.081	-0.110	-0.279	-0.175	-0.074	-0.020
ZSNL	-0.204	-0.108	-0.035	-0.003	-0.037	0.406	-0.098	-0.183	-0.146	-0.087	-0.249	0.773	-0.068	0.684	0.523	0.098	-0.075

	NAFM	NA41	NAVS	NAZI	NAZS	BRBA	NALD	DAFM	PLSY	POBA	PM41	41MX	41ZI	PTAS	PTLD	SLBA	SLCC
ACPM	0.140	-0.248	-0.034	-0.022	0.073	-0.034	-0.093	0.123	-0.072	0.033	0.048	-0.082	0.001	0.084	-0.125	-0.103	-0.119
ACSY	-0.019	0.073	-0.222	-0.137	-0.043	-0.206	-0.129	-0.213	0.644	0.021	0.015	0.343	0.168	-0.007	-0.162	-0.211	-0.117
PMPM	0.141	-0.271	-0.194	-0.032	-0.034	-0.032	-0.158	0.215	-0.025	-0.111	0.140	-0.200	-0.222	0.031	-0.143	-0.223	-0.080
ASJP	0.052	-0.046	0.020	0.055	0.003	-0.015	0.034	-0.111	-0.076	0.033	0.036	-0.086	-0.148	0.214	-0.003	-0.200	-0.121
BACC	0.132	-0.037	0.027	0.041	-0.059	0.107	-0.053	0.126	-0.046	-0.181	-0.089	-0.009	-0.174	-0.011	-0.108	0.153	0.394
BAOP	0.044	-0.090	0.028	0.083	0.174	-0.241	0.128	0.131	-0.028	0.160	0.087	-0.146	0.023	-0.109	0.077	0.052	0.081
ASAS	0.140	-0.002	0.026	-0.043	0.075	-0.009	0.031	0.092	-0.004	0.063	-0.001	0.092	0.244	-0.254	0.052	0.123	-0.011
JPJP	-0.074	-0.067	0.078	-0.004	-0.033	0.287	-0.013	0.095	0.021	-0.043	-0.203	-0.111	-0.096	0.094	-0.113	0.084	0.124
4141	0.049	-0.197	-0.045	-0.004	0.019	0.077	-0.109	0.269	-0.018	-0.004	0.182	-0.087	-0.031	0.003	0.203	0.064	-0.130
POPO	0.044	-0.171	0.095	-0.062	0.067	0.079	0.144	0.179	-0.067	0.502	-0.064	-0.032	-0.142	0.153	0.088	0.084	0.065
PTPT	-0.202	-0.266	-0.237	-0.003	-0.135	0.077	0.094	-0.030	-0.079	0.165	-0.053	-0.055	-0.017	-0.040	0.131	0.082	0.106
STST	0.028	-0.089	-0.186	0.206	-0.022	0.168	-0.003	0.029	-0.310	0.018	-0.023	-0.105	-0.092	-0.012	0.018	0.181	0.206
ZTZT	0.258	-0.182	0.127	0.137	0.105	0.122	0.167	0.087	-0.109	0.087	-0.060	0.039	-0.026	0.132	0.094	0.103	0.071
BRAS	0.085	-0.171	0.101	0.063	0.007	0.527	0.147	0.125	-0.095	0.049	-0.045	-0.152	-0.183	0.220	0.161	0.094	0.140
BRLD	0.047	-0.176	0.125	0.142	0.036	0.175	0.808	-0.181	-0.150	0.011	0.022	-0.137	-0.218	0.034	0.684	-0.010	0.057
BRNA	0.055	-0.053	-0.035	-0.148	-0.018	-0.116	0.136	0.042	-0.004	0.050	-0.050	-0.020	-0.004	0.175	0.072	-0.148	-0.131
BRPT	-0.061	-0.132	-0.099	0.008	-0.053	0.167	0.046	0.005	-0.132	0.034	-0.102	-0.167	-0.157	0.114	0.434	0.056	0.095
NABA	0.167	-0.056	0.612	0.249	0.273	0.415	0.156	-0.167	-0.197	-0.279	0.079	-0.199	-0.293	0.195	-0.039	0.163	-0.050
CACP	-0.159	-0.059	-0.050	-0.062	-0.064	-0.136	-0.116	-0.059	-0.121	-0.063	-0.032	-0.061	0.142	-0.037	-0.112	0.008	0.061
CPSL	0.019	0.023	0.051	0.094	-0.094	0.141	0.076	-0.004	0.122	-0.144	-0.064	0.008	-0.101	0.136	0.031	-0.694	-0.622
CPZS	-0.159	-0.223	0.007	-0.134	-0.044	0.090	-0.001	0.027	-0.042	-0.049	0.141	-0.309	-0.050	-0.026	-0.010	-0.025	-0.155
CNCN	-0.027	0.021	0.192	0.010	0.116	0.025	0.020	-0.122	0.008	-0.256	-0.044	-0.102	-0.084	-0.014	-0.090	-0.212	-0.004
FMPM	-0.055	0.337	-0.388	-0.045	-0.277	-0.326	-0.274	-0.055	0.269	-0.212	0.340	0.162	0.199	-0.308	-0.276	-0.267	-0.209
FMZT	-0.072	0.001	0.138	0.288	0.018	0.024	0.020	-0.085	-0.183	-0.045	-0.003	-0.074	-0.119	0.162	-0.004	0.045	0.092
FMCP	0.269	-0.430	0.229	-0.115	0.067	0.234	0.047	0.293	-0.138	0.217	0.156	-0.390	-0.204	0.155	-0.016	0.029	-0.104
FMPT	0.085	-0.099	0.209	0.020	0.007	-0.066	0.142	-0.038	0.095	0.016	0.036	-0.014	-0.021	-0.282	-0.423	-0.076	-0.046
LDAS	0.094	-0.060	-0.006	-0.059	0.012	0.099	-0.226	0.190	0.046	0.088	-0.093	0.065	0.120	-0.253	-0.086	0.181	0.081
LDBA	0.158	-0.240	0.223	-0.067	-0.022	0.448	-0.033	0.068	0.134	-0.049	-0.034	-0.225	-0.366	0.309	0.033	-0.168	-0.111
NANL	-0.125	0.372	-0.004	0.083	-0.189	-0.229	-0.208	-0.325	0.101	-0.386	-0.033	0.156	0.113	-0.098	-0.182	-0.059	0.122
NLAC	0.089	0.075	-0.168	-0.011	0.063	-0.022	-0.149	-0.046	0.012	0.024	0.011	-0.058	0.054	-0.180	-0.113	-0.317	-0.174
NLVS	-0.065	0.119	0.239	-0.102	0.036	-0.287	-0.022	-0.233	0.293	-0.203	0.039	0.341	-0.048	-0.051	-0.177	0.044	0.083
NAAC	0.058	0.627	-0.187	0.249	-0.029	-0.348	-0.234	-0.249	0.228	-0.224	-0.170	0.215	0.060	-0.099	-0.173	-0.120	0.062
NACA	0.047	-0.235	0.131	-0.136	-0.132	0.296	0.217	0.097	-0.221	0.131	0.147	-0.232	-0.112	0.115	0.162	0.007	-0.119
NACP	-0.041	-0.357	0.159	-0.312	-0.093	0.090	0.101	0.189	-0.299	0.109	0.182	-0.309	-0.022	0.107	0.040	0.021	-0.109
NAFM	1.000	-0.118	-0.006	0.374	0.393	0.036	0.183	0.627	-0.095	0.042	0.119	-0.213	-0.271	0.140	-0.003	0.048	0.062
NA41	-0.118	1.000	-0.011	0.312	0.093	-0.179	-0.268	-0.323	0.214	-0.155	-0.160	0.343	0.156	-0.119	-0.231	-0.123	0.014
NAVS	-0.006	-0.011	1.000	0.152	0.279	0.241	0.220	-0.219	-0.243	-0.113	-0.011	-0.278	-0.407	0.238	0.068	-0.012	-0.007
NAZI	0.374	0.312	0.152	1.000	0.487	0.050	0.071	0.004	-0.055	-0.106	0.086	-0.248	-0.333	0.148	0.053	0.074	0.125
NAZS	0.393	0.093	0.279	0.487	1.000	0.029	0.084	0.163	-0.072	0.088	0.007	-0.220	-0.310	0.096	-0.021	0.131	0.145
BRBA	0.036	-0.179	0.241	0.050	0.029	1.000	-0.020	-0.020	-0.143	-0.048	0.002	-0.299	-0.431	0.213	0.069	-0.040	-0.034
NALD	0.183	-0.268	0.220	0.071	0.084	-0.020	1.000	-0.103	-0.110	-0.080	-0.013	-0.162	-0.239	0.142	0.800	-0.137	-0.046
DAFM	0.627	-0.323	-0.219	0.004	0.163	-0.020	-0.103	1.000	-0.215	0.189	0.100	-0.077	-0.084	-0.013	-0.094	0.041	0.058
PLSY	-0.095	0.214	-0.243	-0.055	-0.072	-0.143	-0.110	-0.215	1.000	0.024	0.107	0.286	0.082	-0.059	-0.135	-0.165	-0.212
POBA	0.042	-0.155	-0.113	-0.106	0.088	-0.048	-0.080	0.189	0.024	1.000	-0.012	-0.100	0.102	-0.075	-0.095	0.210	0.077
PM41	0.119	-0.160	-0.011	0.086	0.007	0.002	-0.013	0.100	0.107	-0.012	1.000	-0.286	-0.001	0.007	-0.115	0.103	0.010
41MX	-0.213	0.343	-0.278	-0.248	-0.220	-0.299	-0.162	-0.077	0.286	-0.100	-0.286	1.000	0.247	-0.211	-0.179	-0.069	-0.065
41ZI	-0.271	0.156	-0.407	-0.333	-0.310	-0.431	-0.239	-0.084	0.082	0.102	-0.001	0.247	1.000	-0.480	-0.225	0.077	-0.139
PTAS	0.140	-0.119	0.238	0.148	0.096	0.213	0.142	-0.013	-0.059	-0.075	0.007	-0.211	-0.480	1.000	0.290	-0.162	-0.028
PTLD	-0.003	-0.231	0.068	0.053	-0.021	0.069	0.800	-0.094	-0.135	-0.095	-0.115	-0.179	-0.225	0.290	1.000	-0.078	-0.013
SLBA	0.048	-0.123	-0.012	0.074	0.131	-0.040	-0.137	0.041	-0.165	0.210	0.103	-0.069	0.077	-0.162	-0.078	1.000	0.666
SLCC	0.062	0.014	-0.007	0.125	0.145	-0.034	-0.046	0.058	-0.212	0.077	0.010	-0.065	-0.139	-0.028	-0.013	0.666	1.000
SYBA	-0.073	-0.253	0.048	-0.129	-0.080	-0.068	0.049	0.110	-0.393	-0.045	-0.131	0.114	0.206	-0.174	0.024	0.363	0.048
SYMX	0.103	0.169	-0.119	-0.013	0.102	-0.045	-0.092	-0.144	0.643	0.032	0.049	0.105	0.083	0.069	-0.106	-0.097	-0.067
ZTPO	-0.010	-0.035	0.134	-0.007	0.106	0.232	0.079	-0.214	0.081	-0.126	0.108	0.020	-0.253	0.230	-0.016	-0.276	-0.131
ZTVS	-0.074	-0.068	0.127	-0.063	0.035	0.014	0.068	-0.020	-0.161	0.216	-0.085	0.160	0.089	-0.045	0.053	0.158	0.096
ZTZI	-0.033	0.025	0.268	0.028	0.054	0.196	0.076	-0.133	0.031	-0.339	0.003	0.070	-0.613	0.236	0.091	-0.178	0.037
VSBA	0.236	-0.022	-0.340	0.104	0.029	0.161	-0.041	0.090	0.128	-0.211	0.065	0.165	0.091	0.017	-0.083	0.114	-0.122
VSSY	-0.053	0.004	0.178	0.000	0.023	-0.078	0.040	0.019	-0.578	0.073	-0.125	-0.086	-0.014	-0.059	0.074	0.174	0.187
ZIMX	-0.181	-0.049	-0.214	-0.202	-0.030	-0.096	-0.046	-0.090	-0.278	0.170	-0.064	-0.020	0.424	-0.067	-0.017	-0.085	-0.141
ZSNL	0.004	0.164	-0.113	-0.026	-0.182	-0.363	-0.155	-0.177	0.188	-0.206	0.123	0.151	0.136	-0.172	-0.120	0.001	0.113

	SYBA	SYMX	ZTPO	ZTVS	ZTZI	VSBA	VSSY	ZIMX	ZSNL
ACPM	0.105	-0.149	0.033	0.025	-0.100	0.068	-0.036	-0.107	-0.053
ACSY	-0.352	0.511	-0.002	-0.356	-0.006	0.130	-0.600	-0.243	0.397
PMPM	0.053	-0.055	-0.107	-0.035	0.107	0.055	-0.075	-0.220	-0.093
ASJP	0.013	-0.029	0.044	-0.011	0.102	-0.047	0.042	-0.004	-0.174
BACC	0.118	0.006	0.056	0.008	0.099	0.120	0.092	-0.002	-0.043
BAOP	-0.174	0.028	-0.069	0.088	-0.144	-0.284	0.124	0.044	0.000
ASAS	-0.052	0.032	-0.093	-0.007	-0.160	-0.096	0.026	0.141	-0.127
JPJP	-0.200	0.185	0.250	0.067	0.047	0.065	-0.126	0.112	-0.281
4141	0.365	-0.195	-0.236	-0.055	-0.202	0.137	0.174	0.129	-0.217
POPO	-0.120	0.086	0.016	0.218	0.002	-0.231	0.088	0.002	-0.216
PTPT	0.119	0.008	0.111	0.188	-0.104	0.232	-0.035	0.088	-0.096
STST	-0.045	-0.119	-0.182	-0.137	-0.062	0.126	-0.011	-0.076	-0.094
ZTZT	-0.052	0.045	0.104	0.925	-0.010	-0.103	0.117	0.418	-0.217
BRAS	-0.315	-0.054	0.103	-0.061	-0.030	-0.030	-0.217	0.072	-0.341
BRLD	-0.033	-0.101	0.030	0.051	0.010	-0.103	0.033	-0.005	-0.215
BRNA	0.122	0.005	0.093	-0.006	0.026	0.157	0.057	-0.015	0.045
BRPT	0.082	0.008	0.152	0.117	0.069	0.112	0.062	-0.031	0.037
NABA	0.422	-0.018	0.033	-0.181	0.118	0.396	0.025	-0.150	-0.204
CACP	0.269	-0.186	-0.009	0.100	-0.099	0.132	0.040	0.049	-0.108
CPSL	-0.061	0.162	0.212	-0.158	0.122	0.134	-0.127	0.027	-0.035
CPZS	0.050	-0.065	0.206	0.059	-0.006	-0.117	0.054	0.057	-0.003
CNCN	-0.125	0.022	0.183	-0.041	0.131	-0.079	0.024	-0.029	-0.037
FMPM	-0.243	0.294	0.066	-0.121	0.112	-0.156	-0.104	-0.175	0.406
FMZT	-0.026	0.030	-0.066	0.115	0.039	-0.034	0.059	0.005	-0.098
FMCP	0.022	-0.088	0.158	0.266	0.026	0.020	0.044	0.032	-0.183
FMPT	0.075	-0.016	0.090	0.174	-0.004	0.025	-0.020	0.042	-0.146
LDAS	-0.112	-0.005	0.006	-0.043	-0.121	-0.020	-0.098	0.027	-0.087
LDBA	-0.162	0.062	0.361	0.074	0.205	0.090	-0.156	-0.073	-0.249
NANL	0.002	0.116	-0.001	-0.187	0.144	-0.170	0.123	-0.081	0.773
NLAC	-0.120	-0.002	-0.057	-0.229	0.089	0.032	-0.036	-0.110	-0.068
NLVS	0.116	0.162	0.099	-0.218	0.147	-0.140	0.017	-0.279	0.684
NAAC	-0.130	0.155	-0.106	-0.460	0.124	0.063	-0.074	-0.175	0.523
NACA	-0.100	-0.017	0.083	-0.151	0.047	-0.168	0.121	-0.074	0.098
NACP	0.129	-0.192	0.077	-0.111	-0.052	-0.026	0.074	-0.020	-0.075
NAFM	-0.073	0.103	-0.010	-0.074	-0.033	0.236	-0.053	-0.181	0.004
NA41	-0.253	0.169	-0.035	-0.068	0.025	-0.022	0.004	-0.049	0.164
NAVS	0.048	-0.119	0.134	0.127	0.268	-0.340	0.178	-0.214	-0.113
NAZI	-0.129	-0.013	-0.007	-0.063	0.028	0.104	0.000	-0.202	-0.026
NAZS	-0.080	0.102	0.106	0.035	0.054	0.029	0.023	-0.030	-0.182
BRBA	-0.068	-0.045	0.232	0.014	0.196	0.161	-0.078	-0.096	-0.363
NALD	0.049	-0.092	0.079	0.068	0.076	-0.041	0.040	-0.046	-0.155
DAFM	0.110	-0.144	-0.214	-0.020	-0.133	0.090	0.019	-0.090	-0.177
PLSY	-0.393	0.643	0.081	-0.161	0.031	0.128	-0.578	-0.278	0.188
POBA	-0.045	0.032	-0.126	0.216	-0.339	-0.211	0.073	0.170	-0.206
PM41	-0.131	0.049	0.108	-0.085	0.003	0.065	-0.125	-0.064	0.123
41MX	0.114	0.105	0.020	0.160	0.070	0.165	-0.086	-0.020	0.151
41ZI	0.206	0.083	-0.253	0.089	-0.613	0.091	-0.014	0.424	0.136
PTAS	-0.174	0.069	0.230	-0.045	0.236	0.017	-0.059	-0.067	-0.172
PTLD	0.024	-0.106	-0.016	0.053	0.091	-0.083	0.074	-0.017	-0.120
SLBA	0.363	-0.097	-0.276	0.158	-0.178	0.114	0.174	-0.085	0.001
SLCC	0.048	-0.067	-0.131	0.096	0.037	-0.122	0.187	-0.141	0.113
SYBA	1.000	-0.403	-0.226	0.025	-0.034	0.437	0.517	0.195	0.047
SYMX	-0.403	1.000	0.070	-0.199	-0.018	0.191	-0.610	-0.213	0.131
ZTPO	-0.226	0.070	1.000	0.099	0.086	-0.049	-0.019	-0.057	-0.015
ZTVS	0.025	-0.199	0.099	1.000	-0.080	-0.254	0.323	0.376	-0.214
ZTZI	-0.034	-0.018	0.086	-0.080	1.000	-0.101	0.098	-0.376	0.079
VSBA	0.437	0.191	-0.049	-0.254	-0.101	1.000	-0.267	0.176	-0.164
VSSY	0.517	-0.610	-0.019	0.323	0.098	-0.267	1.000	0.120	0.002
ZIMX	0.195	-0.213	-0.057	0.376	-0.376	0.176	0.120	1.000	-0.248
ZSNL	0.047	0.131	-0.015	-0.214	0.079	-0.164	0.002	-0.248	1.000

Table B10 Developmental Correlation Matrix (D).

	ACPM	ACSY	PMPM	ASJP	BACC	BAOP	ASAS	JPJP	4141	POPO	PTPT	STST	ZTZT	BRAS	BRLD	BRNA	BRPT	NABA
ACPM	1.00	1.00	1.00	0.00	0.00	0.00	0.00	0.00	1.00	0.00	0.50	0.50	1.00	0.50	0.50	0.50	0.50	0.50
ACSY	1.00	1.00	1.00	0.00	0.00	0.00	0.00	0.00	1.00	0.00	0.50	0.50	1.00	0.50	0.50	0.50	0.50	0.50
PMPM	1.00	1.00	1.00	0.00	0.00	0.00	0.00	0.00	1.00	0.00	0.50	0.50	1.00	0.50	0.50	0.50	0.50	0.50
ASJP	0.00	0.00	0.00	1.00	1.00	1.00	1.00	1.00	0.00	1.00	0.50	0.50	0.00	0.50	0.50	0.50	0.50	0.50
BACC	0.00	0.00	0.00	1.00	1.00	1.00	1.00	1.00	0.00	1.00	0.50	0.50	0.00	0.50	0.50	0.50	0.50	0.50
BAOP	0.00	0.00	0.00	1.00	1.00	1.00	1.00	1.00	0.00	1.00	0.50	0.50	0.00	0.50	0.50	0.50	0.50	0.50
ASAS	0.00	0.00	0.00	1.00	1.00	1.00	1.00	1.00	0.00	1.00	0.50	0.50	0.00	0.50	0.50	0.50	0.50	0.50
JPJP	0.00	0.00	0.00	1.00	1.00	1.00	1.00	1.00	0.00	1.00	0.50	0.50	0.00	0.50	0.50	0.50	0.50	0.50
4141	1.00	1.00	1.00	0.00	0.00	0.00	0.00	0.00	1.00	0.00	0.50	0.50	1.00	0.50	0.50	0.50	0.50	0.50
POPO	0.00	0.00	0.00	1.00	1.00	1.00	1.00	1.00	0.00	1.00	0.50	0.50	0.00	0.50	0.50	0.50	0.50	0.50
PTPT	0.50	0.50	0.50	0.50	0.50	0.50	0.50	0.50	0.50	0.50	1.00	0.25	0.50	0.25	0.25	0.25	0.25	0.25
STST	0.50	0.50	0.50	0.50	0.50	0.50	0.50	0.50	0.50	0.50	0.25	1.00	0.50	0.25	0.25	0.25	0.25	0.25
ZTZT	1.00	1.00	1.00	0.00	0.00	0.00	0.00	0.00	1.00	0.00	0.50	0.50	1.00	0.50	0.50	0.50	0.50	0.50
BRAS	0.50	0.50	0.50	0.50	0.50	0.50	0.50	0.50	0.50	0.50	0.25	0.25	0.50	1.00	0.25	0.25	0.25	0.25
BRLD	0.50	0.50	0.50	0.50	0.50	0.50	0.50	0.50	0.50	0.50	0.25	0.25	0.50	0.25	1.00	0.25	0.25	0.25
BRNA	0.50	0.50	0.50	0.50	0.50	0.50	0.50	0.50	0.50	0.50	0.25	0.25	0.50	0.25	0.25	1.00	0.25	0.25
BRPT	0.50	0.50	0.50	0.50	0.50	0.50	0.50	0.50	0.50	0.50	0.25	0.25	0.50	0.25	0.25	0.25	1.00	0.25
NABA	0.50	0.50	0.50	0.50	0.50	0.50	0.50	0.50	0.50	0.50	0.25	0.25	0.50	0.25	0.25	0.25	0.25	1.00
CACP	1.00	1.00	1.00	0.00	0.00	0.00	0.00	0.00	1.00	0.00	0.50	0.50	1.00	0.50	0.50	0.50	0.50	0.50
CPSL	0.50	0.50	0.50	0.50	0.50	0.50	0.50	0.50	0.50	0.50	0.25	0.25	0.50	0.25	0.25	0.25	0.25	0.25
CPZS	1.00	1.00	1.00	0.00	0.00	0.00	0.00	0.00	1.00	0.00	0.50	0.50	1.00	0.50	0.50	0.50	0.50	0.50
CNCN	0.00	0.00	0.00	1.00	1.00	1.00	1.00	1.00	0.00	1.00	0.50	0.50	0.00	0.50	0.50	0.50	0.50	0.50
FMPM	1.00	1.00	1.00	0.00	0.00	0.00	0.00	0.00	1.00	0.00	0.50	0.50	1.00	0.50	0.50	0.50	0.50	0.50
FMZT	1.00	1.00	1.00	0.00	0.00	0.00	0.00	0.00	1.00	0.00	0.50	0.50	1.00	0.50	0.50	0.50	0.50	0.50
FMCP	1.00	1.00	1.00	0.00	0.00	0.00	0.00	0.00	1.00	0.00	0.50	0.50	1.00	0.50	0.50	0.50	0.50	0.50
FMPT	0.50	0.50	0.50	0.50	0.50	0.50	0.50	0.50	0.50	0.50	0.25	0.25	0.50	0.25	0.25	0.25	0.25	0.25
LDAS	0.00	0.00	0.00	1.00	1.00	1.00	1.00	1.00	0.00	1.00	0.50	0.50	0.00	0.50	0.50	0.50	0.50	0.50
LDBA	0.00	0.00	0.00	1.00	1.00	1.00	1.00	1.00	0.00	1.00	0.50	0.50	0.00	0.50	0.50	0.50	0.50	0.50
NANL	1.00	1.00	1.00	0.00	0.00	0.00	0.00	0.00	1.00	0.00	0.50	0.50	1.00	0.50	0.50	0.50	0.50	0.50
NLAC	1.00	1.00	1.00	0.00	0.00	0.00	0.00	0.00	1.00	0.00	0.50	0.50	1.00	0.50	0.50	0.50	0.50	0.50
NLVS	1.00	1.00	1.00	0.00	0.00	0.00	0.00	0.00	1.00	0.00	0.50	0.50	1.00	0.50	0.50	0.50	0.50	0.50
NAAC	1.00	1.00	1.00	0.00	0.00	0.00	0.00	0.00	1.00	0.00	0.50	0.50	1.00	0.50	0.50	0.50	0.50	0.50
NACA	1.00	1.00	1.00	0.00	0.00	0.00	0.00	0.00	1.00	0.00	0.50	0.50	1.00	0.50	0.50	0.50	0.50	0.50
NACP	1.00	1.00	1.00	0.00	0.00	0.00	0.00	0.00	1.00	0.00	0.50	0.50	1.00	0.50	0.50	0.50	0.50	0.50
NAFM	1.00	1.00	1.00	0.00	0.00	0.00	0.00	0.00	1.00	0.00	0.50	0.50	1.00	0.50	0.50	0.50	0.50	0.50
NA41	1.00	1.00	1.00	0.00	0.00	0.00	0.00	0.00	1.00	0.00	0.50	0.50	1.00	0.50	0.50	0.50	0.50	0.50
NAVS	1.00	1.00	1.00	0.00	0.00	0.00	0.00	0.00	1.00	0.00	0.50	0.50	1.00	0.50	0.50	0.50	0.50	0.50
NAZI	1.00	1.00	1.00	0.00	0.00	0.00	0.00	0.00	1.00	0.00	0.50	0.50	1.00	0.50	0.50	0.50	0.50	0.50
NAZS	1.00	1.00	1.00	0.00	0.00	0.00	0.00	0.00	1.00	0.00	0.50	0.50	1.00	0.50	0.50	0.50	0.50	0.50
BRBA	0.50	0.50	0.50	0.50	0.50	0.50	0.50	0.50	0.50	0.50	0.25	0.25	0.50	0.25	0.25	0.25	0.25	0.25
NALD	0.50	0.50	0.50	0.50	0.50	0.50	0.50	0.50	0.50	0.50	0.25	0.25	0.50	0.25	0.25	0.25	0.25	0.25
DAFM	1.00	1.00	1.00	0.00	0.00	0.00	0.00	0.00	1.00	0.00	0.50	0.50	1.00	0.50	0.50	0.50	0.50	0.50
PLSY	1.00	1.00	1.00	0.00	0.00	0.00	0.00	0.00	1.00	0.00	0.50	0.50	1.00	0.50	0.50	0.50	0.50	0.50
POBA	0.00	0.00	0.00	1.00	1.00	1.00	1.00	1.00	0.00	1.00	0.50	0.50	0.00	0.50	0.50	0.50	0.50	0.50
PM41	1.00	1.00	1.00	0.00	0.00	0.00	0.00	0.00	1.00	0.00	0.50	0.50	1.00	0.50	0.50	0.50	0.50	0.50
41MX	1.00	1.00	1.00	0.00	0.00	0.00	0.00	0.00	1.00	0.00	0.50	0.50	1.00	0.50	0.50	0.50	0.50	0.50
41ZI	1.00	1.00	1.00	0.00	0.00	0.00	0.00	0.00	1.00	0.00	0.50	0.50	1.00	0.50	0.50	0.50	0.50	0.50
PTAS	0.50	0.50	0.50	0.50	0.50	0.50	0.50	0.50	0.50	0.50	0.25	0.25	0.50	0.25	0.25	0.25	0.25	0.25
PTLD	0.50	0.50	0.50	0.50	0.50	0.50	0.50	0.50	0.50	0.50	0.25	0.25	0.50	0.25	0.25	0.25	0.25	0.25
SLBA	0.50	0.50	0.50	0.50	0.50	0.50	0.50	0.50	0.50	0.50	0.25	0.25	0.50	0.25	0.25	0.25	0.25	0.25
SLCC	0.50	0.50	0.50	0.50	0.50	0.50	0.50	0.50	0.50	0.50	0.25	0.25	0.50	0.25	0.25	0.25	0.25	0.25
SYBA	0.50	0.50	0.50	0.50	0.50	0.50	0.50	0.50	0.50	0.50	0.25	0.25	0.50	0.25	0.25	0.25	0.25	0.25
SYMX	1.00	1.00	1.00	0.00	0.00	0.00	0.00	0.00	1.00	0.00	0.50	0.50	1.00	0.50	0.50	0.50	0.50	0.50
ZTPO	0.50	0.50	0.50	0.50	0.50	0.50	0.50	0.50	0.50	0.50	0.25	0.25	0.50	0.25	0.25	0.25	0.25	0.25
ZTVS	1.00	1.00	1.00	0.00	0.00	0.00	0.00	0.00	1.00	0.00	0.50	0.50	1.00	0.50	0.50	0.50	0.50	0.50
ZTZI	1.00	1.00	1.00	0.00	0.00	0.00	0.00	0.00	1.00	0.00	0.50	0.50	1.00	0.50	0.50	0.50	0.50	0.50
VSBA	0.50	0.50	0.50	0.50	0.50	0.50	0.50	0.50	0.50	0.50	0.25	0.25	0.50	0.25	0.25	0.25	0.25	0.25
VSSY	1.00	1.00	1.00	0.00	0.00	0.00	0.00	0.00	1.00	0.00	0.50	0.50	1.00	0.50	0.50	0.50	0.50	0.50
ZIMX	1.00	1.00	1.00	0.00	0.00	0.00	0.00	0.00	1.00	0.00	0.50	0.50	1.00	0.50	0.50	0.50	0.50	0.50
ZSNL	1.00	1.00	1.00	0.00	0.00	0.00	0.00	0.00	1.00	0.00	0.50	0.50	1.00	0.50	0.50	0.50	0.50	0.50

	CACP	CPSL	CPZS	CNCN	FMPM	FMZT	FMCP	FMPT	LDAS	LDBA	NANL	NLAC	NLVS	NAAC	NACA	NACP	NAFM	NA41
ACPM	1.00	0.50	1.00	0.00	1.00	1.00	1.00	0.50	0.00	0.00	1.00	1.00	1.00	1.00	1.00	1.00	1.00	1.00
ACSY	1.00	0.50	1.00	0.00	1.00	1.00	1.00	0.50	0.00	0.00	1.00	1.00	1.00	1.00	1.00	1.00	1.00	1.00
PMPM	1.00	0.50	1.00	0.00	1.00	1.00	1.00	0.50	0.00	0.00	1.00	1.00	1.00	1.00	1.00	1.00	1.00	1.00
ASJP	0.00	0.50	0.00	1.00	0.00	0.00	0.00	0.50	1.00	1.00	0.00	0.00	0.00	0.00	0.00	0.00	0.00	0.00
BACC	0.00	0.50	0.00	1.00	0.00	0.00	0.00	0.50	1.00	1.00	0.00	0.00	0.00	0.00	0.00	0.00	0.00	0.00
BAOP	0.00	0.50	0.00	1.00	0.00	0.00	0.00	0.50	1.00	1.00	0.00	0.00	0.00	0.00	0.00	0.00	0.00	0.00
ASAS	0.00	0.50	0.00	1.00	0.00	0.00	0.00	0.50	1.00	1.00	0.00	0.00	0.00	0.00	0.00	0.00	0.00	0.00
JPJP	0.00	0.50	0.00	1.00	0.00	0.00	0.00	0.50	1.00	1.00	0.00	0.00	0.00	0.00	0.00	0.00	0.00	0.00
4141	1.00	0.50	1.00	0.00	1.00	1.00	1.00	0.50	0.00	0.00	1.00	1.00	1.00	1.00	1.00	1.00	1.00	1.00
POPO	0.00	0.50	0.00	1.00	0.00	0.00	0.00	0.50	1.00	1.00	0.00	0.00	0.00	0.00	0.00	0.00	0.00	0.00
PTPT	0.50	0.25	0.50	0.50	0.50	0.50	0.50	0.25	0.50	0.50	0.50	0.50	0.50	0.50	0.50	0.50	0.50	0.50
STST	0.50	0.25	0.50	0.50	0.50	0.50	0.50	0.25	0.50	0.50	0.50	0.50	0.50	0.50	0.50	0.50	0.50	0.50
ZTZT	1.00	0.50	1.00	0.00	1.00	1.00	1.00	0.50	0.00	0.00	1.00	1.00	1.00	1.00	1.00	1.00	1.00	1.00
BRAS	0.50	0.25	0.50	0.50	0.50	0.50	0.50	0.25	0.50	0.50	0.50	0.50	0.50	0.50	0.50	0.50	0.50	0.50
BRLD	0.50	0.25	0.50	0.50	0.50	0.50	0.50	0.25	0.50	0.50	0.50	0.50	0.50	0.50	0.50	0.50	0.50	0.50
BRNA	0.50	0.25	0.50	0.50	0.50	0.50	0.50	0.25	0.50	0.50	0.50	0.50	0.50	0.50	0.50	0.50	0.50	0.50
BRPT	0.50	0.25	0.50	0.50	0.50	0.50	0.50	0.25	0.50	0.50	0.50	0.50	0.50	0.50	0.50	0.50	0.50	0.50
NABA	0.50	0.25	0.50	0.50	0.50	0.50	0.50	0.25	0.50	0.50	0.50	0.50	0.50	0.50	0.50	0.50	0.50	0.50
CACP	1.00	0.50	1.00	0.00	1.00	1.00	1.00	0.50	0.00	0.00	1.00	1.00	1.00	1.00	1.00	1.00	1.00	1.00
CPSL	0.50	1.00	0.50	0.50	0.50	0.50	0.50	0.25	0.50	0.50	0.50	0.50	0.50	0.50	0.50	0.50	0.50	0.50
CPZS	1.00	0.50	1.00	0.00	1.00	1.00	1.00	0.50	0.00	0.00	1.00	1.00	1.00	1.00	1.00	1.00	1.00	1.00
CNCN	0.00	0.50	0.00	1.00	0.00	0.00	0.00	0.50	1.00	1.00	0.00	0.00	0.00	0.00	0.00	0.00	0.00	0.00
FMPM	1.00	0.50	1.00	0.00	1.00	1.00	1.00	0.50	0.00	0.00	1.00	1.00	1.00	1.00	1.00	1.00	1.00	1.00
FMZT	1.00	0.50	1.00	0.00	1.00	1.00	1.00	0.50	0.00	0.00	1.00	1.00	1.00	1.00	1.00	1.00	1.00	1.00
FMCP	1.00	0.50	1.00	0.00	1.00	1.00	1.00	0.50	0.00	0.00	1.00	1.00	1.00	1.00	1.00	1.00	1.00	1.00
FMPT	0.50	0.25	0.50	0.50	0.50	0.50	0.50	1.00	0.50	0.50	0.50	0.50	0.50	0.50	0.50	0.50	0.50	0.50
LDAS	0.00	0.50	0.00	1.00	0.00	0.00	0.00	0.50	1.00	1.00	0.00	0.00	0.00	0.00	0.00	0.00	0.00	0.00
LDBA	0.00	0.50	0.00	1.00	0.00	0.00	0.00	0.50	1.00	1.00	0.00	0.00	0.00	0.00	0.00	0.00	0.00	0.00
NANL	1.00	0.50	1.00	0.00	1.00	1.00	1.00	0.50	0.00	0.00	1.00	1.00	1.00	1.00	1.00	1.00	1.00	1.00
NLAC	1.00	0.50	1.00	0.00	1.00	1.00	1.00	0.50	0.00	0.00	1.00	1.00	1.00	1.00	1.00	1.00	1.00	1.00
NLVS	1.00	0.50	1.00	0.00	1.00	1.00	1.00	0.50	0.00	0.00	1.00	1.00	1.00	1.00	1.00	1.00	1.00	1.00
NAAC	1.00	0.50	1.00	0.00	1.00	1.00	1.00	0.50	0.00	0.00	1.00	1.00	1.00	1.00	1.00	1.00	1.00	1.00
NACA	1.00	0.50	1.00	0.00	1.00	1.00	1.00	0.50	0.00	0.00	1.00	1.00	1.00	1.00	1.00	1.00	1.00	1.00
NACP	1.00	0.50	1.00	0.00	1.00	1.00	1.00	0.50	0.00	0.00	1.00	1.00	1.00	1.00	1.00	1.00	1.00	1.00
NAFM	1.00	0.50	1.00	0.00	1.00	1.00	1.00	0.50	0.00	0.00	1.00	1.00	1.00	1.00	1.00	1.00	1.00	1.00
NA41	1.00	0.50	1.00	0.00	1.00	1.00	1.00	0.50	0.00	0.00	1.00	1.00	1.00	1.00	1.00	1.00	1.00	1.00
NAVS	1.00	0.50	1.00	0.00	1.00	1.00	1.00	0.50	0.00	0.00	1.00	1.00	1.00	1.00	1.00	1.00	1.00	1.00
NAZI	1.00	0.50	1.00	0.00	1.00	1.00	1.00	0.50	0.00	0.00	1.00	1.00	1.00	1.00	1.00	1.00	1.00	1.00
NAZS	1.00	0.50	1.00	0.00	1.00	1.00	1.00	0.50	0.00	0.00	1.00	1.00	1.00	1.00	1.00	1.00	1.00	1.00
BRBA	0.50	0.25	0.50	0.50	0.50	0.50	0.50	0.25	0.50	0.50	0.50	0.50	0.50	0.50	0.50	0.50	0.50	0.50
NALD	0.50	0.25	0.50	0.50	0.50	0.50	0.50	0.25	0.50	0.50	0.50	0.50	0.50	0.50	0.50	0.50	0.50	0.50
DAFM	1.00	0.50	1.00	0.00	1.00	1.00	1.00	0.50	0.00	0.00	1.00	1.00	1.00	1.00	1.00	1.00	1.00	1.00
PLSY	1.00	0.50	1.00	0.00	1.00	1.00	1.00	0.50	0.00	0.00	1.00	1.00	1.00	1.00	1.00	1.00	1.00	1.00
POBA	0.00	0.50	0.00	1.00	0.00	0.00	0.00	0.50	1.00	1.00	0.00	0.00	0.00	0.00	0.00	0.00	0.00	0.00
PM41	1.00	0.50	1.00	0.00	1.00	1.00	1.00	0.50	0.00	0.00	1.00	1.00	1.00	1.00	1.00	1.00	1.00	1.00
41MX	1.00	0.50	1.00	0.00	1.00	1.00	1.00	0.50	0.00	0.00	1.00	1.00	1.00	1.00	1.00	1.00	1.00	1.00
41ZI	1.00	0.50	1.00	0.00	1.00	1.00	1.00	0.50	0.00	0.00	1.00	1.00	1.00	1.00	1.00	1.00	1.00	1.00
PTAS	0.50	0.25	0.50	0.50	0.50	0.50	0.50	0.25	0.50	0.50	0.50	0.50	0.50	0.50	0.50	0.50	0.50	0.50
PTLD	0.50	0.25	0.50	0.50	0.50	0.50	0.50	0.25	0.50	0.50	0.50	0.50	0.50	0.50	0.50	0.50	0.50	0.50
SLBA	0.50	0.25	0.50	0.50	0.50	0.50	0.50	0.25	0.50	0.50	0.50	0.50	0.50	0.50	0.50	0.50	0.50	0.50
SLCC	0.50	0.25	0.50	0.50	0.50	0.50	0.50	0.25	0.50	0.50	0.50	0.50	0.50	0.50	0.50	0.50	0.50	0.50
SYBA	0.50	0.25	0.50	0.50	0.50	0.50	0.50	0.25	0.50	0.50	0.50	0.50	0.50	0.50	0.50	0.50	0.50	0.50
SYMX	1.00	0.50	1.00	0.00	1.00	1.00	1.00	0.50	0.00	0.00	1.00	1.00	1.00	1.00	1.00	1.00	1.00	1.00
ZTPO	0.50	0.25	0.50	0.50	0.50	0.50	0.50	0.25	0.50	0.50	0.50	0.50	0.50	0.50	0.50	0.50	0.50	0.50
ZTVS	1.00	0.50	1.00	0.00	1.00	1.00	1.00	0.50	0.00	0.00	1.00	1.00	1.00	1.00	1.00	1.00	1.00	1.00
ZTZI	1.00	0.50	1.00	0.00	1.00	1.00	1.00	0.50	0.00	0.00	1.00	1.00	1.00	1.00	1.00	1.00	1.00	1.00
VSBA	0.50	0.25	0.50	0.50	0.50	0.50	0.50	0.25	0.50	0.50	0.50	0.50	0.50	0.50	0.50	0.50	0.50	0.50
VSSY	1.00	0.50	1.00	0.00	1.00	1.00	1.00	0.50	0.00	0.00	1.00	1.00	1.00	1.00	1.00	1.00	1.00	1.00
ZIMX	1.00	0.50	1.00	0.00	1.00	1.00	1.00	0.50	0.00	0.00	1.00	1.00	1.00	1.00	1.00	1.00	1.00	1.00
ZSNL	1.00	0.50	1.00	0.00	1.00	1.00	1.00	0.50	0.00	0.00	1.00	1.00	1.00	1.00	1.00	1.00	1.00	1.00

	NAVS	NAZI	NAZS	BRBA	NALD	DAFM	PLSY	POBA	PM41	41MX	41ZI	PTAS	PTLD	SLBA	SLCC	SYBA	SYMX	ZTPO
ACPM	1.00	1.00	1.00	0.50	0.50	1.00	1.00	0.00	1.00	1.00	1.00	0.50	0.50	0.50	0.50	0.50	1.00	0.50
ACSY	1.00	1.00	1.00	0.50	0.50	1.00	1.00	0.00	1.00	1.00	1.00	0.50	0.50	0.50	0.50	0.50	1.00	0.50
PMPM	1.00	1.00	1.00	0.50	0.50	1.00	1.00	0.00	1.00	1.00	1.00	0.50	0.50	0.50	0.50	0.50	1.00	0.50
ASJP	0.00	0.00	0.00	0.50	0.50	0.00	0.00	1.00	0.00	0.00	0.00	0.50	0.50	0.50	0.50	0.50	0.00	0.50
BACC	0.00	0.00	0.00	0.50	0.50	0.00	0.00	1.00	0.00	0.00	0.00	0.50	0.50	0.50	0.50	0.50	0.00	0.50
BAOP	0.00	0.00	0.00	0.50	0.50	0.00	0.00	1.00	0.00	0.00	0.00	0.50	0.50	0.50	0.50	0.50	0.00	0.50
ASAS	0.00	0.00	0.00	0.50	0.50	0.00	0.00	1.00	0.00	0.00	0.00	0.50	0.50	0.50	0.50	0.50	0.00	0.50
JPJP	0.00	0.00	0.00	0.50	0.50	0.00	0.00	1.00	0.00	0.00	0.00	0.50	0.50	0.50	0.50	0.50	0.00	0.50
4141	1.00	1.00	1.00	0.50	0.50	1.00	1.00	0.00	1.00	1.00	1.00	0.50	0.50	0.50	0.50	0.50	1.00	0.50
POPO	0.00	0.00	0.00	0.50	0.50	0.00	0.00	1.00	0.00	0.00	0.00	0.50	0.50	0.50	0.50	0.50	0.00	0.50
PTPT	0.50	0.50	0.50	0.25	0.25	0.50	0.50	0.50	0.50	0.50	0.50	0.25	0.25	0.25	0.25	0.25	0.50	0.25
STST	0.50	0.50	0.50	0.25	0.25	0.50	0.50	0.50	0.50	0.50	0.50	0.25	0.25	0.25	0.25	0.25	0.50	0.25
ZTZT	1.00	1.00	1.00	0.50	0.50	1.00	1.00	0.00	1.00	1.00	1.00	0.50	0.50	0.50	0.50	0.50	1.00	0.50
BRAS	0.50	0.50	0.50	0.25	0.25	0.50	0.50	0.50	0.50	0.50	0.50	0.25	0.25	0.25	0.25	0.25	0.50	0.25
BRLD	0.50	0.50	0.50	0.25	0.25	0.50	0.50	0.50	0.50	0.50	0.50	0.25	0.25	0.25	0.25	0.25	0.50	0.25
BRNA	0.50	0.50	0.50	0.25	0.25	0.50	0.50	0.50	0.50	0.50	0.50	0.25	0.25	0.25	0.25	0.25	0.50	0.25
BRPT	0.50	0.50	0.50	0.25	0.25	0.50	0.50	0.50	0.50	0.50	0.50	0.25	0.25	0.25	0.25	0.25	0.50	0.25
NABA	0.50	0.50	0.50	0.25	0.25	0.50	0.50	0.50	0.50	0.50	0.50	0.25	0.25	0.25	0.25	0.25	0.50	0.25
CACP	1.00	1.00	1.00	0.50	0.50	1.00	1.00	0.00	1.00	1.00	1.00	0.50	0.50	0.50	0.50	0.50	1.00	0.50
CPSL	0.50	0.50	0.50	0.25	0.25	0.50	0.50	0.50	0.50	0.50	0.50	0.25	0.25	0.25	0.25	0.25	0.50	0.25
CPZS	1.00	1.00	1.00	0.50	0.50	1.00	1.00	0.00	1.00	1.00	1.00	0.50	0.50	0.50	0.50	0.50	1.00	0.50
CNCN	0.00	0.00	0.00	0.50	0.50	0.00	0.00	1.00	0.00	0.00	0.00	0.50	0.50	0.50	0.50	0.50	0.00	0.50
FMPM	1.00	1.00	1.00	0.50	0.50	1.00	1.00	0.00	1.00	1.00	1.00	0.50	0.50	0.50	0.50	0.50	1.00	0.50
FMZT	1.00	1.00	1.00	0.50	0.50	1.00	1.00	0.00	1.00	1.00	1.00	0.50	0.50	0.50	0.50	0.50	1.00	0.50
FMCP	1.00	1.00	1.00	0.50	0.50	1.00	1.00	0.00	1.00	1.00	1.00	0.50	0.50	0.50	0.50	0.50	1.00	0.50
FMPT	0.50	0.50	0.50	0.25	0.25	0.50	0.50	0.50	0.50	0.50	0.50	0.25	0.25	0.25	0.25	0.25	0.50	0.25
LDAS	0.00	0.00	0.00	0.50	0.50	0.00	0.00	1.00	0.00	0.00	0.00	0.50	0.50	0.50	0.50	0.50	0.00	0.50
LDBA	0.00	0.00	0.00	0.50	0.50	0.00	0.00	1.00	0.00	0.00	0.00	0.50	0.50	0.50	0.50	0.50	0.00	0.50
NANL	1.00	1.00	1.00	0.50	0.50	1.00	1.00	0.00	1.00	1.00	1.00	0.50	0.50	0.50	0.50	0.50	1.00	0.50
NLAC	1.00	1.00	1.00	0.50	0.50	1.00	1.00	0.00	1.00	1.00	1.00	0.50	0.50	0.50	0.50	0.50	1.00	0.50
NLVS	1.00	1.00	1.00	0.50	0.50	1.00	1.00	0.00	1.00	1.00	1.00	0.50	0.50	0.50	0.50	0.50	1.00	0.50
NAAC	1.00	1.00	1.00	0.50	0.50	1.00	1.00	0.00	1.00	1.00	1.00	0.50	0.50	0.50	0.50	0.50	1.00	0.50
NACA	1.00	1.00	1.00	0.50	0.50	1.00	1.00	0.00	1.00	1.00	1.00	0.50	0.50	0.50	0.50	0.50	1.00	0.50
NACP	1.00	1.00	1.00	0.50	0.50	1.00	1.00	0.00	1.00	1.00	1.00	0.50	0.50	0.50	0.50	0.50	1.00	0.50
NAFM	1.00	1.00	1.00	0.50	0.50	1.00	1.00	0.00	1.00	1.00	1.00	0.50	0.50	0.50	0.50	0.50	1.00	0.50
NA41	1.00	1.00	1.00	0.50	0.50	1.00	1.00	0.00	1.00	1.00	1.00	0.50	0.50	0.50	0.50	0.50	1.00	0.50
NAVS	1.00	1.00	1.00	0.50	0.50	1.00	1.00	0.00	1.00	1.00	1.00	0.50	0.50	0.50	0.50	0.50	1.00	0.50
NAZI	1.00	1.00	1.00	0.50	0.50	1.00	1.00	0.00	1.00	1.00	1.00	0.50	0.50	0.50	0.50	0.50	1.00	0.50
NAZS	1.00	1.00	1.00	0.50	0.50	1.00	1.00	0.00	1.00	1.00	1.00	0.50	0.50	0.50	0.50	0.50	1.00	0.50
BRBA	0.50	0.50	0.50	1.00	0.25	0.50	0.50	0.50	0.50	0.50	0.50	0.25	0.25	0.25	0.25	0.25	0.50	0.25
NALD	0.50	0.50	0.50	0.25	1.00	0.50	0.50	0.50	0.50	0.50	0.50	0.25	0.25	0.25	0.25	0.25	0.50	0.25
DAFM	1.00	1.00	1.00	0.50	0.50	1.00	1.00	0.00	1.00	1.00	1.00	0.50	0.50	0.50	0.50	0.50	1.00	0.50
PLSY	1.00	1.00	1.00	0.50	0.50	1.00	1.00	0.00	1.00	1.00	1.00	0.50	0.50	0.50	0.50	0.50	1.00	0.50
POBA	0.00	0.00	0.00	0.50	0.50	0.00	0.00	1.00	0.00	0.00	0.00	0.50	0.50	0.50	0.50	0.50	0.00	0.50
PM41	1.00	1.00	1.00	0.50	0.50	1.00	1.00	0.00	1.00	1.00	1.00	0.50	0.50	0.50	0.50	0.50	1.00	0.50
41MX	1.00	1.00	1.00	0.50	0.50	1.00	1.00	0.00	1.00	1.00	1.00	0.50	0.50	0.50	0.50	0.50	1.00	0.50
41ZI	1.00	1.00	1.00	0.50	0.50	1.00	1.00	0.00	1.00	1.00	1.00	0.50	0.50	0.50	0.50	0.50	1.00	0.50
PTAS	0.50	0.50	0.50	0.25	0.25	0.50	0.50	0.50	0.50	0.50	0.50	1.00	0.25	0.25	0.25	0.25	0.50	0.25
PTLD	0.50	0.50	0.50	0.25	0.25	0.50	0.50	0.50	0.50	0.50	0.50	0.25	1.00	0.25	0.25	0.25	0.50	0.25
SLBA	0.50	0.50	0.50	0.25	0.25	0.50	0.50	0.50	0.50	0.50	0.50	0.25	0.25	1.00	0.25	0.25	0.50	0.25
SLCC	0.50	0.50	0.50	0.25	0.25	0.50	0.50	0.50	0.50	0.50	0.50	0.25	0.25	0.25	1.00	0.25	0.50	0.25
SYBA	0.50	0.50	0.50	0.25	0.25	0.50	0.50	0.50	0.50	0.50	0.50	0.25	0.25	0.25	0.25	1.00	0.50	0.25
SYMX	1.00	1.00	1.00	0.50	0.50	1.00	1.00	0.00	1.00	1.00	1.00	0.50	0.50	0.50	0.50	0.50	1.00	0.50
ZTPO	0.50	0.50	0.50	0.25	0.25	0.50	0.50	0.50	0.50	0.50	0.50	0.25	0.25	0.25	0.25	0.25	0.50	1.00
ZTVS	1.00	1.00	1.00	0.50	0.50	1.00	1.00	0.00	1.00	1.00	1.00	0.50	0.50	0.50	0.50	0.50	1.00	0.50
ZTZI	1.00	1.00	1.00	0.50	0.50	1.00	1.00	0.00	1.00	1.00	1.00	0.50	0.50	0.50	0.50	0.50	1.00	0.50
VSBA	0.50	0.50	0.50	0.25	0.25	0.50	0.50	0.50	0.50	0.50	0.50	0.25	0.25	0.25	0.25	0.25	0.50	0.25
VSSY	1.00	1.00	1.00	0.50	0.50	1.00	1.00	0.00	1.00	1.00	1.00	0.50	0.50	0.50	0.50	0.50	1.00	0.50
ZIMX	1.00	1.00	1.00	0.50	0.50	1.00	1.00	0.00	1.00	1.00	1.00	0.50	0.50	0.50	0.50	0.50	1.00	0.50
ZSNL	1.00	1.00	1.00	0.50	0.50	1.00	1.00	0.00	1.00	1.00	1.00	0.50	0.50	0.50	0.50	0.50	1.00	0.50

	ZTVS	ZTZI	VSBA	VSSY	ZIMX	ZSNL
ACPM	1.00	1.00	0.50	1.00	1.00	1.00
ACSY	1.00	1.00	0.50	1.00	1.00	1.00
PMPM	1.00	1.00	0.50	1.00	1.00	1.00
ASJP	0.00	0.00	0.50	0.00	0.00	0.00
BACC	0.00	0.00	0.50	0.00	0.00	0.00
BAOP	0.00	0.00	0.50	0.00	0.00	0.00
ASAS	0.00	0.00	0.50	0.00	0.00	0.00
JPJP	0.00	0.00	0.50	0.00	0.00	0.00
4141	1.00	1.00	0.50	1.00	1.00	1.00
POPO	0.00	0.00	0.50	0.00	0.00	0.00
PTPT	0.50	0.50	0.25	0.50	0.50	0.50
STST	0.50	0.50	0.25	0.50	0.50	0.50
ZTZT	1.00	1.00	0.50	1.00	1.00	1.00
BRAS	0.50	0.50	0.25	0.50	0.50	0.50
BRLD	0.50	0.50	0.25	0.50	0.50	0.50
BRNA	0.50	0.50	0.25	0.50	0.50	0.50
BRPT	0.50	0.50	0.25	0.50	0.50	0.50
NABA	0.50	0.50	0.25	0.50	0.50	0.50
CACP	1.00	1.00	0.50	1.00	1.00	1.00
CPSL	0.50	0.50	0.25	0.50	0.50	0.50
CPZS	1.00	1.00	0.50	1.00	1.00	1.00
CNCN	0.00	0.00	0.50	0.00	0.00	0.00
FMPM	1.00	1.00	0.50	1.00	1.00	1.00
FMZT	1.00	1.00	0.50	1.00	1.00	1.00
FMCP	1.00	1.00	0.50	1.00	1.00	1.00
FMPT	0.50	0.50	0.25	0.50	0.50	0.50
LDAS	0.00	0.00	0.50	0.00	0.00	0.00
LDBA	0.00	0.00	0.50	0.00	0.00	0.00
NANL	1.00	1.00	0.50	1.00	1.00	1.00
NLAC	1.00	1.00	0.50	1.00	1.00	1.00
NLVS	1.00	1.00	0.50	1.00	1.00	1.00
NAAC	1.00	1.00	0.50	1.00	1.00	1.00
NACA	1.00	1.00	0.50	1.00	1.00	1.00
NACP	1.00	1.00	0.50	1.00	1.00	1.00
NAFM	1.00	1.00	0.50	1.00	1.00	1.00
NA41	1.00	1.00	0.50	1.00	1.00	1.00
NAVS	1.00	1.00	0.50	1.00	1.00	1.00
NAZI	1.00	1.00	0.50	1.00	1.00	1.00
NAZS	1.00	1.00	0.50	1.00	1.00	1.00
BRBA	0.50	0.50	0.25	0.50	0.50	0.50
NALD	0.50	0.50	0.25	0.50	0.50	0.50
DAFM	1.00	1.00	0.50	1.00	1.00	1.00
PLSY	1.00	1.00	0.50	1.00	1.00	1.00
POBA	0.00	0.00	0.50	0.00	0.00	0.00
PM41	1.00	1.00	0.50	1.00	1.00	1.00
41MX	1.00	1.00	0.50	1.00	1.00	1.00
41ZI	1.00	1.00	0.50	1.00	1.00	1.00
PTAS	0.50	0.50	0.25	0.50	0.50	0.50
PTLD	0.50	0.50	0.25	0.50	0.50	0.50
SLBA	0.50	0.50	0.25	0.50	0.50	0.50
SLCC	0.50	0.50	0.25	0.50	0.50	0.50
SYBA	0.50	0.50	0.25	0.50	0.50	0.50
SYMX	1.00	1.00	0.50	1.00	1.00	1.00
ZTPO	0.50	0.50	0.25	0.50	0.50	0.50
ZTVS	1.00	1.00	0.50	1.00	1.00	1.00
ZTZI	1.00	1.00	0.50	1.00	1.00	1.00
VSBA	0.50	0.50	1.00	0.50	0.50	0.50
VSSY	1.00	1.00	0.50	1.00	1.00	1.00
ZIMX	1.00	1.00	0.50	1.00	1.00	1.00
ZSNL	1.00	1.00	0.50	1.00	1.00	1.00

Table B11 General Functional Matrix (Fg).

	ACPM	ACSY	PMPM	ASJP	BACC	BAOP	ASAS	JPJP	4141	POPO	PTPT	STST	ZTZT	BRAS	BRLD	BRNA	BRPT	NABA
ACPM	1	1	1	0	0	0	0	0	1	0	0	0	1	0	0	0	0	0
ACSY	1	1	1	0	0	0	0	0	1	0	0	0	1	0	0	0	0	0
PMPM	1	1	1	0	0	0	0	0	1	0	0	0	1	0	0	0	0	0
ASJP	0	0	0	1	0	0	1	0	0	1	1	1	0	1	1	1	1	0
BACC	0	0	0	0	1	1	0	1	0	0	0	0	0	0	0	0	0	1
BAOP	0	0	0	0	1	1	0	1	0	0	0	0	0	0	0	0	0	1
ASAS	0	0	0	1	0	0	1	0	0	1	1	1	0	1	1	1	1	0
JPJP	0	0	0	0	1	1	0	1	0	0	0	0	0	0	0	0	0	1
4141	1	1	1	0	0	0	0	0	1	0	0	0	1	0	0	0	0	0
POPO	0	0	0	1	0	0	1	0	0	1	1	1	0	1	1	1	1	0
PTPT	0	0	0	1	0	0	1	0	0	1	1	1	0	1	1	1	1	0
STST	0	0	0	1	0	0	1	0	0	1	1	1	0	1	1	1	1	0
ZTZT	1	1	1	0	0	0	0	0	1	0	0	0	1	0	0	0	0	0
BRAS	0	0	0	1	0	0	1	0	0	1	1	1	0	1	1	1	1	0
BRLD	0	0	0	1	0	0	1	0	0	1	1	1	0	1	1	1	1	0
BRNA	0	0	0	1	0	0	1	0	0	1	1	1	0	1	1	1	1	0
BRPT	0	0	0	1	0	0	1	0	0	1	1	1	0	1	1	1	1	0
NABA	0	0	0	0	1	1	0	1	0	0	0	0	0	0	0	0	0	1
CACP	0	0	0	0	1	1	0	1	0	0	0	0	0	0	0	0	0	1
CPSL	0	0	0	0	1	1	0	1	0	0	0	0	0	0	0	0	0	1
CPZS	0	0	0	0	1	1	0	1	0	0	0	0	0	0	0	0	0	1
CNCN	0	0	0	0	1	1	0	1	0	0	0	0	0	0	0	0	0	1
FMPM	1	1	1	0	0	0	0	0	1	0	0	0	1	0	0	0	0	0
FMZT	1	1	1	0	0	0	0	0	1	0	0	0	1	0	0	0	0	0
FMCP	1	1	1	0	0	0	0	0	1	0	0	0	1	0	0	0	0	0
FMPT	1	1	1	0	0	0	0	0	1	0	0	0	1	0	0	0	0	0
LDAS	0	0	0	1	0	0	1	0	0	1	1	1	0	1	1	1	1	0
LDBA	0	0	0	1	0	0	1	0	0	1	1	1	0	1	1	1	1	0
NANL	1	1	1	0	0	0	0	0	1	0	0	0	1	0	0	0	0	0
NLAC	1	1	1	0	0	0	0	0	1	0	0	0	1	0	0	0	0	0
NLVS	1	1	1	0	0	0	0	0	1	0	0	0	1	0	0	0	0	0
NAAC	1	1	1	0	0	0	0	0	1	0	0	0	1	0	0	0	0	0
NACA	1	1	1	0	0	0	0	0	1	0	0	0	1	0	0	0	0	0
NACP	1	1	1	0	0	0	0	0	1	0	0	0	1	0	0	0	0	0
NAFM	1	1	1	0	0	0	0	0	1	0	0	0	1	0	0	0	0	0
NA41	1	1	1	0	0	0	0	0	1	0	0	0	1	0	0	0	0	0
NAVS	0	0	0	0	1	1	0	1	0	0	0	0	0	0	0	0	0	1
NAZI	1	1	1	0	0	0	0	0	1	0	0	0	1	0	0	0	0	0
NAZS	1	1	1	0	0	0	0	0	1	0	0	0	1	0	0	0	0	0
BRBA	0	0	0	1	0	0	1	0	0	1	1	1	0	1	1	1	1	0
NALD	0	0	0	1	0	0	1	0	0	1	1	1	0	1	1	1	1	0
DAFM	1	1	1	0	0	0	0	0	1	0	0	0	1	0	0	0	0	0
PLSY	1	1	1	0	0	0	0	0	1	0	0	0	1	0	0	0	0	0
POBA	0	0	0	0	1	1	0	1	0	0	0	0	0	0	0	0	0	1
PM41	1	1	1	0	0	0	0	0	1	0	0	0	1	0	0	0	0	0
41MX	1	1	1	0	0	0	0	0	1	0	0	0	1	0	0	0	0	0
41ZI	1	1	1	0	0	0	0	0	1	0	0	0	1	0	0	0	0	0
PTAS	0	0	0	1	0	0	1	0	0	1	1	1	0	1	1	1	1	0
PTLD	0	0	0	1	0	0	1	0	0	1	1	1	0	1	1	1	1	0
SLBA	0	0	0	0	1	1	0	1	0	0	0	0	0	0	0	0	0	1
SLCC	0	0	0	0	1	1	0	1	0	0	0	0	0	0	0	0	0	1
SYBA	0	0	0	0	1	1	0	1	0	0	0	0	0	0	0	0	0	1
SYMX	1	1	1	0	0	0	0	0	1	0	0	0	1	0	0	0	0	0
ZTPO	0	0	0	1	0	0	1	0	0	1	1	1	0	1	1	1	1	0
ZTVS	1	1	1	0	0	0	0	0	1	0	0	0	1	0	0	0	0	0
ZTZI	1	1	1	0	0	0	0	0	1	0	0	0	1	0	0	0	0	0
VSBA	0	0	0	0	1	1	0	1	0	0	0	0	0	0	0	0	0	1
VSSY	1	1	1	0	0	0	0	0	1	0	0	0	1	0	0	0	0	0
ZIMX	1	1	1	0	0	0	0	0	1	0	0	0	1	0	0	0	0	0
ZSNL	1	1	1	0	0	0	0	0	1	0	0	0	1	0	0	0	0	0

	CACP	CPSL	CPZS	CNCN	FMPM	FMZT	FMCP	FMPT	LDAS	LDBA	NANL	NLAC	NLVS	NAAC	NACA	NACP	NAFM	NA41
ACPM	0	0	0	0	1	1	1	1	0	0	1	1	1	1	1	1	1	1
ACSY	0	0	0	0	1	1	1	1	0	0	1	1	1	1	1	1	1	1
PMPM	0	0	0	0	1	1	1	1	0	0	1	1	1	1	1	1	1	1
ASJP	0	0	0	0	0	0	0	0	1	1	0	0	0	0	0	0	0	0
BACC	1	1	1	1	0	0	0	0	0	0	0	0	0	0	0	0	0	0
BAOP	1	1	1	1	0	0	0	0	0	0	0	0	0	0	0	0	0	0
ASAS	0	0	0	0	0	0	0	0	1	1	0	0	0	0	0	0	0	0
JPJP	1	1	1	1	0	0	0	0	0	0	0	0	0	0	0	0	0	0
4141	0	0	0	0	1	1	1	1	0	0	1	1	1	1	1	1	1	1
POPO	0	0	0	0	0	0	0	0	1	1	0	0	0	0	0	0	0	0
PTPT	0	0	0	0	0	0	0	0	1	1	0	0	0	0	0	0	0	0
STST	0	0	0	0	0	0	0	0	1	1	0	0	0	0	0	0	0	0
ZTZT	0	0	0	0	1	1	1	1	0	0	1	1	1	1	1	1	1	1
BRAS	0	0	0	0	0	0	0	0	1	1	0	0	0	0	0	0	0	0
BRLD	0	0	0	0	0	0	0	0	1	1	0	0	0	0	0	0	0	0
BRNA	0	0	0	0	0	0	0	0	1	1	0	0	0	0	0	0	0	0
BRPT	0	0	0	0	0	0	0	0	1	1	0	0	0	0	0	0	0	0
NABA	1	1	1	1	0	0	0	0	0	0	0	0	0	0	0	0	0	0
CACP	1	1	1	1	0	0	0	0	0	0	0	0	0	0	0	0	0	0
CPSL	1	1	1	1	0	0	0	0	0	0	0	0	0	0	0	0	0	0
CPZS	1	1	1	1	0	0	0	0	0	0	0	0	0	0	0	0	0	0
CNCN	1	1	1	1	0	0	0	0	0	0	0	0	0	0	0	0	0	0
FMPM	0	0	0	0	1	1	1	1	0	0	1	1	1	1	1	1	1	1
FMZT	0	0	0	0	1	1	1	1	0	0	1	1	1	1	1	1	1	1
FMCP	0	0	0	0	1	1	1	1	0	0	1	1	1	1	1	1	1	1
FMPT	0	0	0	0	1	1	1	1	0	0	1	1	1	1	1	1	1	1
LDAS	0	0	0	0	0	0	0	0	1	1	0	0	0	0	0	0	0	0
LDBA	0	0	0	0	0	0	0	0	1	1	0	0	0	0	0	0	0	0
NANL	0	0	0	0	1	1	1	1	0	0	1	1	1	1	1	1	1	1
NLAC	0	0	0	0	1	1	1	1	0	0	1	1	1	1	1	1	1	1
NLVS	0	0	0	0	1	1	1	1	0	0	1	1	1	1	1	1	1	1
NAAC	0	0	0	0	1	1	1	1	0	0	1	1	1	1	1	1	1	1
NACA	0	0	0	0	1	1	1	1	0	0	1	1	1	1	1	1	1	1
NACP	0	0	0	0	1	1	1	1	0	0	1	1	1	1	1	1	1	1
NAFM	0	0	0	0	1	1	1	1	0	0	1	1	1	1	1	1	1	1
NA41	0	0	0	0	1	1	1	1	0	0	1	1	1	1	1	1	1	1
NAVS	1	1	1	1	0	0	0	0	0	0	0	0	0	0	0	0	0	0
NAZI	0	0	0	0	1	1	1	1	0	0	1	1	1	1	1	1	1	1
NAZS	0	0	0	0	1	1	1	1	0	0	1	1	1	1	1	1	1	1
BRBA	0	0	0	0	0	0	0	0	1	1	0	0	0	0	0	0	0	0
NALD	0	0	0	0	0	0	0	0	1	1	0	0	0	0	0	0	0	0
DAFM	0	0	0	0	1	1	1	1	0	0	1	1	1	1	1	1	1	1
PLSY	0	0	0	0	1	1	1	1	0	0	1	1	1	1	1	1	1	1
POBA	1	1	1	1	0	0	0	0	0	0	0	0	0	0	0	0	0	0
PM41	0	0	0	0	1	1	1	1	0	0	1	1	1	1	1	1	1	1
41MX	0	0	0	0	1	1	1	1	0	0	1	1	1	1	1	1	1	1
41ZI	0	0	0	0	1	1	1	1	0	0	1	1	1	1	1	1	1	1
PTAS	0	0	0	0	0	0	0	0	1	1	0	0	0	0	0	0	0	0
PTLD	0	0	0	0	0	0	0	0	1	1	0	0	0	0	0	0	0	0
SLBA	1	1	1	1	0	0	0	0	0	0	0	0	0	0	0	0	0	0
SLCC	1	1	1	1	0	0	0	0	0	0	0	0	0	0	0	0	0	0
SYBA	1	1	1	1	0	0	0	0	0	0	0	0	0	0	0	0	0	0
SYMX	0	0	0	0	1	1	1	1	0	0	1	1	1	1	1	1	1	1
ZTPO	0	0	0	0	0	0	0	0	1	1	0	0	0	0	0	0	0	0
ZTVS	0	0	0	0	1	1	1	1	0	0	1	1	1	1	1	1	1	1
ZTZI	0	0	0	0	1	1	1	1	0	0	1	1	1	1	1	1	1	1
VSBA	1	1	1	1	0	0	0	0	0	0	0	0	0	0	0	0	0	0
VSSY	0	0	0	0	1	1	1	1	0	0	1	1	1	1	1	1	1	1
ZIMX	0	0	0	0	1	1	1	1	0	0	1	1	1	1	1	1	1	1
ZSNL	0	0	0	1	1	1	1	0	0	1	1	1	1	1	1	1	1	0

	NAVS	NAZI	NAZS	BRBA	NALD	DAFM	PLSY	POBA	PM41	41MX	41ZI	PTAS	PTLD	SLBA	SLCC	SYBA	SYMX	ZTPO
ACPM	0	1	1	0	0	1	1	0	1	1	1	0	0	0	0	0	1	0
ACSY	0	1	1	0	0	1	1	0	1	1	1	0	0	0	0	0	1	0
PMPM	0	1	1	0	0	1	1	0	1	1	1	0	0	0	0	0	1	0
ASJP	0	0	0	1	1	0	0	0	0	0	0	1	1	0	0	0	0	1
BACC	1	0	0	0	0	0	0	1	0	0	0	0	0	1	1	1	0	0
BAOP	1	0	0	0	0	0	0	1	0	0	0	0	0	1	1	1	0	0
ASAS	0	0	0	1	1	0	0	0	0	0	0	1	1	0	0	0	0	1
JPJP	1	0	0	0	0	0	0	1	0	0	0	0	0	1	1	1	0	0
4141	0	1	1	0	0	1	1	0	1	1	1	0	0	0	0	0	1	0
POPO	0	0	0	1	1	0	0	0	0	0	0	1	1	0	0	0	0	1
PTPT	0	0	0	1	1	0	0	0	0	0	0	1	1	0	0	0	0	1
STST	0	0	0	1	1	0	0	0	0	0	0	1	1	0	0	0	0	1
ZTZT	0	1	1	0	0	1	1	0	1	1	1	0	0	0	0	0	1	0
BRAS	0	0	0	1	1	0	0	0	0	0	0	1	1	0	0	0	0	1
BRLD	0	0	0	1	1	0	0	0	0	0	0	1	1	0	0	0	0	1
BRNA	0	0	0	1	1	0	0	0	0	0	0	1	1	0	0	0	0	1
BRPT	0	0	0	1	1	0	0	0	0	0	0	1	1	0	0	0	0	1
NABA	1	0	0	0	0	0	0	1	0	0	0	0	0	1	1	1	0	0
CACP	1	0	0	0	0	0	0	1	0	0	0	0	0	1	1	1	0	0
CPSL	1	0	0	0	0	0	0	1	0	0	0	0	0	1	1	1	0	0
CPZS	1	0	0	0	0	0	0	1	0	0	0	0	0	1	1	1	0	0
CNCN	1	0	0	0	0	0	0	1	0	0	0	0	0	1	1	1	0	0
FMPM	0	1	1	0	0	1	1	0	1	1	1	0	0	0	0	0	1	0
FMZT	0	1	1	0	0	1	1	0	1	1	1	0	0	0	0	0	1	0
FMCP	0	1	1	0	0	1	1	0	1	1	1	0	0	0	0	0	1	0
FMPT	0	1	1	0	0	1	1	0	1	1	1	0	0	0	0	0	1	0
LDAS	0	0	0	1	1	0	0	0	0	0	0	1	1	0	0	0	0	1
LDBA	0	0	0	1	1	0	0	0	0	0	0	1	1	0	0	0	0	1
NANL	0	1	1	0	0	1	1	0	1	1	1	0	0	0	0	0	1	0
NLAC	0	1	1	0	0	1	1	0	1	1	1	0	0	0	0	0	1	0
NLVS	0	1	1	0	0	1	1	0	1	1	1	0	0	0	0	0	1	0
NAAC	0	1	1	0	0	1	1	0	1	1	1	0	0	0	0	0	1	0
NACA	0	1	1	0	0	1	1	0	1	1	1	0	0	0	0	0	1	0
NACP	0	1	1	0	0	1	1	0	1	1	1	0	0	0	0	0	1	0
NAFM	0	1	1	0	0	1	1	0	1	1	1	0	0	0	0	0	1	0
NA41	0	1	1	0	0	1	1	0	1	1	1	0	0	0	0	0	1	0
NAVS	1	0	0	0	0	0	0	1	0	0	0	0	0	1	1	1	0	0
NAZI	0	1	1	0	0	1	1	0	1	1	1	0	0	0	0	0	1	0
NAZS	0	1	1	0	0	1	1	0	1	1	1	0	0	0	0	0	1	0
BRBA	0	0	0	1	1	0	0	0	0	0	0	1	1	0	0	0	0	1
NALD	0	0	0	1	1	0	0	0	0	0	0	1	1	0	0	0	0	1
DAFM	0	1	1	0	0	1	1	0	1	1	1	0	0	0	0	0	1	0
PLSY	0	1	1	0	0	1	1	0	1	1	1	0	0	0	0	0	1	0
POBA	1	0	0	0	0	0	0	1	0	0	0	0	0	1	1	1	0	0
PM41	0	1	1	0	0	1	1	0	1	1	1	0	0	0	0	0	1	0
41MX	0	1	1	0	0	1	1	0	1	1	1	0	0	0	0	0	1	0
41ZI	0	1	1	0	0	1	1	0	1	1	1	0	0	0	0	0	1	0
PTAS	0	0	0	1	1	0	0	0	0	0	0	1	1	0	0	0	0	1
PTLD	0	0	0	1	1	0	0	0	0	0	0	1	1	0	0	0	0	1
SLBA	1	0	0	0	0	0	0	1	0	0	0	0	0	1	1	1	0	0
SLCC	1	0	0	0	0	0	0	1	0	0	0	0	0	1	1	1	0	0
SYBA	1	0	0	0	0	0	0	1	0	0	0	0	0	1	1	1	0	0
SYMX	0	1	1	0	0	1	1	0	1	1	1	0	0	0	0	0	1	0
ZTPO	0	0	0	1	1	0	0	0	0	0	0	1	1	0	0	0	0	1
ZTVS	0	1	1	0	0	1	1	0	1	1	1	0	0	0	0	0	1	0
ZTZI	0	1	1	0	0	1	1	0	1	1	1	0	0	0	0	0	1	0
VSBA	1	0	0	0	0	0	0	1	0	0	0	0	0	1	1	1	0	0
VSSY	0	1	1	0	0	1	1	0	1	1	1	0	0	0	0	0	1	0
ZIMX	0	1	1	0	0	1	1	0	1	1	1	0	0	0	0	0	1	0
ZSNL	1	1	0	0	1	1	0	1	1	1	0	0	0	0	0	1	0	1

	ZTVS	ZTZI	VSBA	VSSY	ZIMX	ZSNL
ACPM	1	1	0	1	1	1
ACSY	1	1	0	1	1	1
PMPM	1	1	0	1	1	1
ASJP	0	0	0	0	0	0
BACC	0	0	1	0	0	0
BAOP	0	0	1	0	0	0
ASAS	0	0	0	0	0	0
JPJP	0	0	1	0	0	0
4141	1	1	0	1	1	1
POPO	0	0	0	0	0	0
PTPT	0	0	0	0	0	0
STST	0	0	0	0	0	0
ZTZT	1	1	0	1	1	1
BRAS	0	0	0	0	0	0
BRLD	0	0	0	0	0	0
BRNA	0	0	0	0	0	0
BRPT	0	0	0	0	0	0
NABA	0	0	1	0	0	0
CACP	0	0	1	0	0	0
CPSL	0	0	1	0	0	0
CPZS	0	0	1	0	0	0
CNCN	0	0	1	0	0	0
FMPM	1	1	0	1	1	1
FMZT	1	1	0	1	1	1
FMCP	1	1	0	1	1	1
FMPT	1	1	0	1	1	1
LDAS	0	0	0	0	0	0
LDBA	0	0	0	0	0	0
NANL	1	1	0	1	1	1
NLAC	1	1	0	1	1	1
NLVS	1	1	0	1	1	1
NAAC	1	1	0	1	1	1
NACA	1	1	0	1	1	1
NACP	1	1	0	1	1	1
NAFM	1	1	0	1	1	1
NA41	1	1	0	1	1	1
NAVS	0	0	1	0	0	0
NAZI	1	1	0	1	1	1
NAZS	1	1	0	1	1	1
BRBA	0	0	0	0	0	0
NALD	0	0	0	0	0	0
DAFM	1	1	0	1	1	1
PLSY	1	1	0	1	1	1
POBA	0	0	1	0	0	0
PM41	1	1	0	1	1	1
41MX	1	1	0	1	1	1
41ZI	1	1	0	1	1	1
PTAS	0	0	0	0	0	0
PTLD	0	0	0	0	0	0
SLBA	0	0	1	0	0	0
SLCC	0	0	1	0	0	0
SYBA	0	0	1	0	0	0
SYMX	1	1	0	1	1	1
ZTPO	0	0	0	0	0	0
ZTVS	1	1	0	1	1	1
ZTZI	1	1	0	1	1	1
VSBA	0	0	1	0	0	0
VSSY	1	1	0	1	1	1
ZIMX	1	1	0	1	1	1
ZSNL	1	0	1	1	1	

Table B12 Specific Functional Matrix (Fs).

	ACPM	ACSY	PMPM	ASJP	BACC	BAOP	ASAS	JPJP	4141	POPO	PTPT	STST	ZTZT	BRAS	BRLD	BRNA	BRPT	NABA
ACPM	1.0	0.5	1.0	0.0	0.0	0.0	0.0	0.0	1.0	0.0	0.0	0.0	0.5	0.0	0.0	0.0	0.0	0.0
ACSY	0.5	1.0	0.5	0.0	0.0	0.0	0.0	0.0	0.5	0.0	0.0	0.0	0.5	0.0	0.0	0.0	0.0	0.0
PMPM	1.0	0.5	1.0	0.0	0.0	0.0	0.0	0.0	1.0	0.0	0.0	0.0	0.5	0.0	0.0	0.0	0.0	0.0
ASJP	0.0	0.0	0.0	1.0	0.0	0.0	1.0	0.0	0.0	1.0	0.5	0.5	0.0	0.5	1.0	0.5	0.5	0.0
BACC	0.0	0.0	0.0	0.0	1.0	1.0	0.0	1.0	0.0	0.0	0.0	0.0	0.0	0.0	0.0	0.0	0.0	0.5
BAOP	0.0	0.0	0.0	0.0	1.0	1.0	0.0	1.0	0.0	0.0	0.0	0.0	0.0	0.0	0.0	0.0	0.0	0.5
ASAS	0.0	0.0	0.0	1.0	0.0	0.0	1.0	0.0	0.0	1.0	0.5	0.5	0.0	0.5	1.0	0.5	0.5	0.0
JPJP	0.0	0.0	0.0	0.0	1.0	1.0	0.0	1.0	0.0	0.0	0.0	0.0	0.0	0.0	0.0	0.0	0.0	0.5
4141	1.0	0.5	1.0	0.0	0.0	0.0	0.0	0.0	1.0	0.0	0.0	0.0	0.5	0.0	0.0	0.0	0.0	0.0
POPO	0.0	0.0	0.0	1.0	0.0	0.0	1.0	0.0	0.0	1.0	0.5	0.5	0.0	0.5	1.0	0.5	0.5	0.0
PTPT	0.0	0.0	0.0	0.5	0.0	0.0	0.5	0.0	0.0	0.5	1.0	1.0	0.0	1.0	0.5	1.0	1.0	0.0
STST	0.0	0.0	0.0	0.5	0.0	0.0	0.5	0.0	0.0	0.5	1.0	1.0	0.0	1.0	0.5	1.0	1.0	0.0
ZTZT	0.5	0.5	0.5	0.0	0.0	0.0	0.0	0.0	0.5	0.0	0.0	0.0	1.0	0.0	0.0	0.0	0.0	0.0
BRAS	0.0	0.0	0.0	0.5	0.0	0.0	0.5	0.0	0.0	0.5	1.0	1.0	0.0	1.0	0.5	1.0	1.0	0.0
BRLD	0.0	0.0	0.0	1.0	0.0	0.0	1.0	0.0	0.0	1.0	0.5	0.5	0.0	0.5	1.0	0.5	0.5	0.0
BRNA	0.0	0.0	0.0	0.5	0.0	0.0	0.5	0.0	0.0	0.5	1.0	1.0	0.0	1.0	0.5	1.0	1.0	0.0
BRPT	0.0	0.0	0.0	0.5	0.0	0.0	0.5	0.0	0.0	0.5	1.0	1.0	0.0	1.0	0.5	1.0	1.0	0.0
NABA	0.0	0.0	0.0	0.0	0.5	0.5	0.0	0.5	0.0	0.0	0.0	0.0	0.0	0.0	0.0	0.0	0.0	1.0
CACP	0.0	0.0	0.0	0.0	0.5	0.5	0.0	0.5	0.0	0.0	0.0	0.0	0.0	0.0	0.0	0.0	0.0	1.0
CPSL	0.0	0.0	0.0	0.0	0.5	0.5	0.0	0.5	0.0	0.0	0.0	0.0	0.0	0.0	0.0	0.0	0.0	1.0
CPZS	0.0	0.0	0.0	0.0	0.5	0.5	0.0	0.5	0.0	0.0	0.0	0.0	0.0	0.0	0.0	0.0	0.0	1.0
CNCN	0.0	0.0	0.0	0.0	1.0	1.0	0.0	1.0	0.0	0.0	0.0	0.0	0.0	0.0	0.0	0.0	0.0	0.5
FMPM	0.5	1.0	0.5	0.0	0.0	0.0	0.0	0.0	0.5	0.0	0.0	0.0	0.5	0.0	0.0	0.0	0.0	0.0
FMZT	0.5	0.5	0.5	0.0	0.0	0.0	0.0	0.0	0.5	0.0	0.0	0.0	1.0	0.0	0.0	0.0	0.0	0.0
FMCP	0.5	0.5	0.5	0.0	0.0	0.0	0.0	0.0	0.5	0.0	0.0	0.0	0.5	0.0	0.0	0.0	0.0	0.0
FMPT	0.5	0.5	0.5	0.0	0.0	0.0	0.0	0.0	0.5	0.0	0.0	0.0	0.5	0.0	0.0	0.0	0.0	0.0
LDAS	0.0	0.0	0.0	1.0	0.0	0.0	1.0	0.0	0.0	1.0	0.5	0.5	0.0	0.5	1.0	0.5	0.5	0.0
LDBA	0.0	0.0	0.0	1.0	0.0	0.0	1.0	0.0	0.0	1.0	0.5	0.5	0.0	0.5	1.0	0.5	0.5	0.0
NANL	0.5	1.0	0.5	0.0	0.0	0.0	0.0	0.0	0.5	0.0	0.0	0.0	0.5	0.0	0.0	0.0	0.0	0.0
NLAC	0.5	1.0	0.5	0.0	0.0	0.0	0.0	0.0	0.5	0.0	0.0	0.0	0.5	0.0	0.0	0.0	0.0	0.0
NLVS	0.5	1.0	0.5	0.0	0.0	0.0	0.0	0.0	0.5	0.0	0.0	0.0	0.5	0.0	0.0	0.0	0.0	0.0
NAAC	0.5	1.0	0.5	0.0	0.0	0.0	0.0	0.0	0.5	0.0	0.0	0.0	0.5	0.0	0.0	0.0	0.0	0.0
NACA	0.5	0.5	0.5	0.0	0.0	0.0	0.0	0.0	0.5	0.0	0.0	0.0	0.5	0.0	0.0	0.0	0.0	0.0
NACP	0.5	0.5	0.5	0.0	0.0	0.0	0.0	0.0	0.5	0.0	0.0	0.0	0.5	0.0	0.0	0.0	0.0	0.0
NAFM	0.5	0.5	0.5	0.0	0.0	0.0	0.0	0.0	0.5	0.0	0.0	0.0	0.5	0.0	0.0	0.0	0.0	0.0
NA41	0.5	1.0	0.5	0.0	0.0	0.0	0.0	0.0	0.5	0.0	0.0	0.0	0.5	0.0	0.0	0.0	0.0	0.0
NAVS	0.0	0.0	0.0	0.0	0.5	0.5	0.0	0.5	0.0	0.0	0.0	0.0	0.0	0.0	0.0	0.0	0.0	1.0
NAZI	0.5	0.5	0.5	0.0	0.0	0.0	0.0	0.0	0.5	0.0	0.0	0.0	1.0	0.0	0.0	0.0	0.0	0.0
NAZS	0.5	0.5	0.5	0.0	0.0	0.0	0.0	0.0	0.5	0.0	0.0	0.0	0.5	0.0	0.0	0.0	0.0	0.0
BRBA	0.0	0.0	0.0	0.5	0.0	0.0	0.5	0.0	0.0	0.5	0.5	0.5	0.0	0.5	0.5	0.5	0.5	0.0
NALD	0.0	0.0	0.0	0.5	0.0	0.0	0.5	0.0	0.0	0.5	0.5	0.5	0.0	0.5	0.5	0.5	0.5	0.0
DAFM	0.5	0.5	0.5	0.0	0.0	0.0	0.0	0.0	0.5	0.0	0.0	0.0	0.5	0.0	0.0	0.0	0.0	0.0
PLSY	1.0	0.5	1.0	0.0	0.0	0.0	0.0	0.0	1.0	0.0	0.0	0.0	0.5	0.0	0.0	0.0	0.0	0.0
POBA	0.0	0.0	0.0	0.0	1.0	1.0	0.0	1.0	0.0	0.0	0.0	0.0	0.0	0.0	0.0	0.0	0.0	0.5
PM41	1.0	0.5	1.0	0.0	0.0	0.0	0.0	0.0	1.0	0.0	0.0	0.0	0.5	0.0	0.0	0.0	0.0	0.0
41MX	1.0	0.5	1.0	0.0	0.0	0.0	0.0	0.0	1.0	0.0	0.0	0.0	0.5	0.0	0.0	0.0	0.0	0.0
41ZI	1.0	0.5	1.0	0.0	0.0	0.0	0.0	0.0	1.0	0.0	0.0	0.0	0.5	0.0	0.0	0.0	0.0	0.0
PTAS	0.0	0.0	0.0	0.5	0.0	0.0	0.5	0.0	0.0	0.5	0.5	0.5	0.0	0.5	0.5	0.5	0.5	0.0
PTLD	0.0	0.0	0.0	0.5	0.0	0.0	0.5	0.0	0.0	0.5	0.5	0.5	0.0	0.5	0.5	0.5	0.5	0.0
SLBA	0.0	0.0	0.0	0.0	0.5	0.5	0.0	0.5	0.0	0.0	0.0	0.0	0.0	0.0	0.0	0.0	0.0	1.0
SLCC	0.0	0.0	0.0	0.0	0.5	0.5	0.0	0.5	0.0	0.0	0.0	0.0	0.0	0.0	0.0	0.0	0.0	1.0
SYBA	0.0	0.0	0.0	0.0	1.0	1.0	0.0	1.0	0.0	0.0	0.0	0.0	0.0	0.0	0.0	0.0	0.0	0.5
SYMX	1.0	0.5	1.0	0.0	0.0	0.0	0.0	0.0	1.0	0.0	0.0	0.0	0.5	0.0	0.0	0.0	0.0	0.0
ZTPO	0.0	0.0	0.0	1.0	0.0	0.0	1.0	0.0	0.0	1.0	0.5	0.5	0.0	0.5	1.0	0.5	0.5	0.0
ZTVS	0.5	0.5	0.5	0.0	0.0	0.0	0.0	0.0	0.5	0.0	0.0	0.0	1.0	0.0	0.0	0.0	0.0	0.0
ZTZI	0.5	0.5	0.5	0.0	0.0	0.0	0.0	0.0	0.5	0.0	0.0	0.0	1.0	0.0	0.0	0.0	0.0	0.0
VSBA	0.0	0.0	0.0	0.0	1.0	1.0	0.0	1.0	0.0	0.0	0.0	0.0	0.0	0.0	0.0	0.0	0.0	0.5
VSSY	1.0	0.5	1.0	0.0	0.0	0.0	0.0	0.0	1.0	0.0	0.0	0.0	0.5	0.0	0.0	0.0	0.0	0.0
ZIMX	1.0	0.5	1.0	0.0	0.0	0.0	0.0	0.0	1.0	0.0	0.0	0.0	0.5	0.0	0.0	0.0	0.0	0.0
ZSNL	0.5	1.0	0.5	0.0	0.0	0.0	0.0	0.0	0.5	0.0	0.0	0.0	0.5	0.0	0.0	0.0	0.0	0.0

	CACP	CPSL	CPZS	CNCN	FMPM	FMZT	FMCP	FMPT	LDAS	LDBA	NANL	NLAC	NLVS	NAAC	NACA	NACP	NAFM	NA41
ACPM	0.0	0.0	0.0	0.0	0.5	0.5	0.5	0.5	0.0	0.0	0.5	0.5	0.5	0.5	0.5	0.5	0.5	0.5
ACSY	0.0	0.0	0.0	0.0	1.0	0.5	0.5	0.5	0.0	0.0	1.0	1.0	1.0	1.0	0.5	0.5	0.5	1.0
PMPM	0.0	0.0	0.0	0.0	0.5	0.5	0.5	0.5	0.0	0.0	0.5	0.5	0.5	0.5	0.5	0.5	0.5	0.5
ASJP	0.0	0.0	0.0	0.0	0.0	0.0	0.0	0.0	1.0	1.0	0.0	0.0	0.0	0.0	0.0	0.0	0.0	0.0
BACC	0.5	0.5	0.5	1.0	0.0	0.0	0.0	0.0	0.0	0.0	0.0	0.0	0.0	0.0	0.0	0.0	0.0	0.0
BAOP	0.5	0.5	0.5	1.0	0.0	0.0	0.0	0.0	0.0	0.0	0.0	0.0	0.0	0.0	0.0	0.0	0.0	0.0
ASAS	0.0	0.0	0.0	0.0	0.0	0.0	0.0	0.0	1.0	1.0	0.0	0.0	0.0	0.0	0.0	0.0	0.0	0.0
JPJP	0.5	0.5	0.5	1.0	0.0	0.0	0.0	0.0	0.0	0.0	0.0	0.0	0.0	0.0	0.0	0.0	0.0	0.0
4141	0.0	0.0	0.0	0.0	0.5	0.5	0.5	0.5	0.0	0.0	0.5	0.5	0.5	0.5	0.5	0.5	0.5	0.5
POPO	0.0	0.0	0.0	0.0	0.0	0.0	0.0	0.0	1.0	1.0	0.0	0.0	0.0	0.0	0.0	0.0	0.0	0.0
PTPT	0.0	0.0	0.0	0.0	0.0	0.0	0.0	0.0	0.5	0.5	0.0	0.0	0.0	0.0	0.0	0.0	0.0	0.0
STST	0.0	0.0	0.0	0.0	0.0	0.0	0.0	0.0	0.5	0.5	0.0	0.0	0.0	0.0	0.0	0.0	0.0	0.0
ZTZT	0.0	0.0	0.0	0.0	0.5	1.0	0.5	0.5	0.0	0.0	0.5	0.5	0.5	0.5	0.5	0.5	0.5	0.5
BRAS	0.0	0.0	0.0	0.0	0.0	0.0	0.0	0.0	0.5	0.5	0.0	0.0	0.0	0.0	0.0	0.0	0.0	0.0
BRLD	0.0	0.0	0.0	0.0	0.0	0.0	0.0	0.0	1.0	1.0	0.0	0.0	0.0	0.0	0.0	0.0	0.0	0.0
BRNA	0.0	0.0	0.0	0.0	0.0	0.0	0.0	0.0	0.5	0.5	0.0	0.0	0.0	0.0	0.0	0.0	0.0	0.0
BRPT	0.0	0.0	0.0	0.0	0.0	0.0	0.0	0.0	0.5	0.5	0.0	0.0	0.0	0.0	0.0	0.0	0.0	0.0
NABA	1.0	1.0	1.0	0.5	0.0	0.0	0.0	0.0	0.0	0.0	0.0	0.0	0.0	0.0	0.0	0.0	0.0	0.0
CACP	1.0	1.0	1.0	0.5	0.0	0.0	0.0	0.0	0.0	0.0	0.0	0.0	0.0	0.0	0.0	0.0	0.0	0.0
CPSL	1.0	1.0	1.0	0.5	0.0	0.0	0.0	0.0	0.0	0.0	0.0	0.0	0.0	0.0	0.0	0.0	0.0	0.0
CPZS	1.0	1.0	1.0	0.5	0.0	0.0	0.0	0.0	0.0	0.0	0.0	0.0	0.0	0.0	0.0	0.0	0.0	0.0
CNCN	0.5	0.5	0.5	1.0	0.0	0.0	0.0	0.0	0.0	0.0	0.0	0.0	0.0	0.0	0.0	0.0	0.0	0.0
FMPM	0.0	0.0	0.0	0.0	1.0	0.5	0.5	0.5	0.0	0.0	1.0	1.0	1.0	1.0	0.5	0.5	0.5	1.0
FMZT	0.0	0.0	0.0	0.0	0.5	1.0	0.5	0.5	0.0	0.0	0.5	0.5	0.5	0.5	0.5	0.5	0.5	0.5
FMCP	0.0	0.0	0.0	0.0	0.5	0.5	1.0	1.0	0.0	0.0	0.5	0.5	0.5	0.5	1.0	1.0	1.0	0.5
FMPT	0.0	0.0	0.0	0.0	0.5	0.5	1.0	1.0	0.0	0.0	0.5	0.5	0.5	0.5	1.0	1.0	1.0	0.5
LDAS	0.0	0.0	0.0	0.0	0.0	0.0	0.0	0.0	1.0	1.0	0.0	0.0	0.0	0.0	0.0	0.0	0.0	0.0
LDBA	0.0	0.0	0.0	0.0	0.0	0.0	0.0	0.0	1.0	1.0	0.0	0.0	0.0	0.0	0.0	0.0	0.0	0.0
NANL	0.0	0.0	0.0	0.0	1.0	0.5	0.5	0.5	0.0	0.0	1.0	1.0	1.0	1.0	0.5	0.5	0.5	1.0
NLAC	0.0	0.0	0.0	0.0	1.0	0.5	0.5	0.5	0.0	0.0	1.0	1.0	1.0	1.0	0.5	0.5	0.5	1.0
NLVS	0.0	0.0	0.0	0.0	1.0	0.5	0.5	0.5	0.0	0.0	1.0	1.0	1.0	1.0	0.5	0.5	0.5	1.0
NAAC	0.0	0.0	0.0	0.0	1.0	0.5	0.5	0.5	0.0	0.0	1.0	1.0	1.0	1.0	0.5	0.5	0.5	1.0
NACA	0.0	0.0	0.0	0.0	0.5	0.5	1.0	1.0	0.0	0.0	0.5	0.5	0.5	0.5	1.0	1.0	1.0	0.5
NACP	0.0	0.0	0.0	0.0	0.5	0.5	1.0	1.0	0.0	0.0	0.5	0.5	0.5	0.5	1.0	1.0	1.0	0.5
NAFM	0.0	0.0	0.0	0.0	0.5	0.5	1.0	1.0	0.0	0.0	0.5	0.5	0.5	0.5	1.0	1.0	1.0	0.5
NA41	0.0	0.0	0.0	0.0	1.0	0.5	0.5	0.5	0.0	0.0	1.0	1.0	1.0	1.0	0.5	0.5	0.5	1.0
NAVS	1.0	1.0	1.0	0.5	0.0	0.0	0.0	0.0	0.0	0.0	0.0	0.0	0.0	0.0	0.0	0.0	0.0	0.0
NAZI	0.0	0.0	0.0	0.0	0.5	1.0	0.5	0.5	0.0	0.0	0.5	0.5	0.5	0.5	0.5	0.5	0.5	0.5
NAZS	0.0	0.0	0.0	0.0	0.5	0.5	1.0	1.0	0.0	0.0	0.5	0.5	0.5	0.5	1.0	1.0	1.0	0.5
BRBA	0.0	0.0	0.0	0.0	0.0	0.0	0.0	0.0	0.5	0.5	0.0	0.0	0.0	0.0	0.0	0.0	0.0	0.0
NALD	0.0	0.0	0.0	0.0	0.0	0.0	0.0	0.0	0.5	0.5	0.0	0.0	0.0	0.0	0.0	0.0	0.0	0.0
DAFM	0.0	0.0	0.0	0.0	0.5	0.5	1.0	1.0	0.0	0.0	0.5	0.5	0.5	0.5	1.0	1.0	1.0	0.5
PLSY	0.0	0.0	0.0	0.0	0.5	0.5	0.5	0.5	0.0	0.0	0.5	0.5	0.5	0.5	0.5	0.5	0.5	0.5
POBA	0.5	0.5	0.5	1.0	0.0	0.0	0.0	0.0	0.0	0.0	0.0	0.0	0.0	0.0	0.0	0.0	0.0	0.0
PM41	0.0	0.0	0.0	0.0	0.5	0.5	0.5	0.5	0.0	0.0	0.5	0.5	0.5	0.5	0.5	0.5	0.5	0.5
41MX	0.0	0.0	0.0	0.0	0.5	0.5	0.5	0.5	0.0	0.0	0.5	0.5	0.5	0.5	0.5	0.5	0.5	0.5
41ZI	0.0	0.0	0.0	0.0	0.5	0.5	0.5	0.5	0.0	0.0	0.5	0.5	0.5	0.5	0.5	0.5	0.5	0.5
PTAS	0.0	0.0	0.0	0.0	0.0	0.0	0.0	0.0	0.5	0.5	0.0	0.0	0.0	0.0	0.0	0.0	0.0	0.0
PTLD	0.0	0.0	0.0	0.0	0.0	0.0	0.0	0.0	0.5	0.5	0.0	0.0	0.0	0.0	0.0	0.0	0.0	0.0
SLBA	1.0	1.0	1.0	0.5	0.0	0.0	0.0	0.0	0.0	0.0	0.0	0.0	0.0	0.0	0.0	0.0	0.0	0.0
SLCC	1.0	1.0	1.0	0.5	0.0	0.0	0.0	0.0	0.0	0.0	0.0	0.0	0.0	0.0	0.0	0.0	0.0	0.0
SYBA	0.5	0.5	0.5	1.0	0.0	0.0	0.0	0.0	0.0	0.0	0.0	0.0	0.0	0.0	0.0	0.0	0.0	0.0
SYMX	0.0	0.0	0.0	0.0	0.5	0.5	0.5	0.5	0.0	0.0	0.5	0.5	0.5	0.5	0.5	0.5	0.5	0.5
ZTPO	0.0	0.0	0.0	0.0	0.0	0.0	0.0	0.0	1.0	1.0	0.0	0.0	0.0	0.0	0.0	0.0	0.0	0.0
ZTVS	0.0	0.0	0.0	0.0	0.5	1.0	0.5	0.5	0.0	0.0	0.5	0.5	0.5	0.5	0.5	0.5	0.5	0.5
ZTZI	0.0	0.0	0.0	0.0	0.5	1.0	0.5	0.5	0.0	0.0	0.5	0.5	0.5	0.5	0.5	0.5	0.5	0.5
VSBA	0.5	0.5	0.5	1.0	0.0	0.0	0.0	0.0	0.0	0.0	0.0	0.0	0.0	0.0	0.0	0.0	0.0	0.0
VSSY	0.0	0.0	0.0	0.0	0.5	0.5	0.5	0.5	0.0	0.0	0.5	0.5	0.5	0.5	0.5	0.5	0.5	0.5
ZIMX	0.0	0.0	0.0	0.0	0.5	0.5	0.5	0.5	0.0	0.0	0.5	0.5	0.5	0.5	0.5	0.5	0.5	0.5
ZSNL	0.0	0.0	0.0	0.0	1.0	0.5	0.5	0.5	0.0	0.0	1.0	1.0	1.0	1.0	0.5	0.5	0.5	1.0

	NAVS	NAZI	NAZS	BRBA	NALD	DAFM	PLSY	POBA	PM41	41MX	41ZI	PTAS	PTLD	SLBA	SLCC	SYBA	SYMX	ZTPO
ACPM	0.0	0.5	0.5	0.0	0.0	0.5	1.0	0.0	1.0	1.0	1.0	0.0	0.0	0.0	0.0	0.0	1.0	0.0
ACSY	0.0	0.5	0.5	0.0	0.0	0.5	0.5	0.0	0.5	0.5	0.5	0.0	0.0	0.0	0.0	0.0	0.5	0.0
PMPM	0.0	0.5	0.5	0.0	0.0	0.5	1.0	0.0	1.0	1.0	1.0	0.0	0.0	0.0	0.0	0.0	1.0	0.0
ASJP	0.0	0.0	0.0	0.5	0.5	0.0	0.0	0.0	0.0	0.0	0.0	0.5	0.5	0.0	0.0	0.0	0.0	1.0
BACC	0.5	0.0	0.0	0.0	0.0	0.0	0.0	1.0	0.0	0.0	0.0	0.0	0.0	0.5	0.5	1.0	0.0	0.0
BAOP	0.5	0.0	0.0	0.0	0.0	0.0	0.0	1.0	0.0	0.0	0.0	0.0	0.0	0.5	0.5	1.0	0.0	0.0
ASAS	0.0	0.0	0.0	0.5	0.5	0.0	0.0	0.0	0.0	0.0	0.0	0.5	0.5	0.0	0.0	0.0	0.0	1.0
JPJP	0.5	0.0	0.0	0.0	0.0	0.0	0.0	1.0	0.0	0.0	0.0	0.0	0.0	0.5	0.5	1.0	0.0	0.0
4141	0.0	0.5	0.5	0.0	0.0	0.5	1.0	0.0	1.0	1.0	1.0	0.0	0.0	0.0	0.0	0.0	1.0	0.0
POPO	0.0	0.0	0.0	0.5	0.5	0.0	0.0	0.0	0.0	0.0	0.0	0.5	0.5	0.0	0.0	0.0	0.0	1.0
PTPT	0.0	0.0	0.0	0.5	0.5	0.0	0.0	0.0	0.0	0.0	0.0	0.5	0.5	0.0	0.0	0.0	0.0	0.5
STST	0.0	0.0	0.0	0.5	0.5	0.0	0.0	0.0	0.0	0.0	0.0	0.5	0.5	0.0	0.0	0.0	0.0	0.5
ZTZT	0.0	1.0	0.5	0.0	0.0	0.5	0.5	0.0	0.5	0.5	0.5	0.0	0.0	0.0	0.0	0.0	0.5	0.0
BRAS	0.0	0.0	0.0	0.5	0.5	0.0	0.0	0.0	0.0	0.0	0.0	0.5	0.5	0.0	0.0	0.0	0.0	0.5
BRLD	0.0	0.0	0.0	0.5	0.5	0.0	0.0	0.0	0.0	0.0	0.0	0.5	0.5	0.0	0.0	0.0	0.0	1.0
BRNA	0.0	0.0	0.0	0.5	0.5	0.0	0.0	0.0	0.0	0.0	0.0	0.5	0.5	0.0	0.0	0.0	0.0	0.5
BRPT	0.0	0.0	0.0	0.5	0.5	0.0	0.0	0.0	0.0	0.0	0.0	0.5	0.5	0.0	0.0	0.0	0.0	0.5
NABA	1.0	0.0	0.0	0.0	0.0	0.0	0.0	0.5	0.0	0.0	0.0	0.0	0.0	1.0	1.0	0.5	0.0	0.0
CACP	1.0	0.0	0.0	0.0	0.0	0.0	0.0	0.5	0.0	0.0	0.0	0.0	0.0	1.0	1.0	0.5	0.0	0.0
CPSL	1.0	0.0	0.0	0.0	0.0	0.0	0.0	0.5	0.0	0.0	0.0	0.0	0.0	1.0	1.0	0.5	0.0	0.0
CPZS	1.0	0.0	0.0	0.0	0.0	0.0	0.0	0.5	0.0	0.0	0.0	0.0	0.0	1.0	1.0	0.5	0.0	0.0
CNCN	0.5	0.0	0.0	0.0	0.0	0.0	0.0	1.0	0.0	0.0	0.0	0.0	0.0	0.5	0.5	1.0	0.0	0.0
FMPM	0.0	0.5	0.5	0.0	0.0	0.5	0.5	0.0	0.5	0.5	0.5	0.0	0.0	0.0	0.0	0.0	0.5	0.0
FMZT	0.0	1.0	0.5	0.0	0.0	0.5	0.5	0.0	0.5	0.5	0.5	0.0	0.0	0.0	0.0	0.0	0.5	0.0
FMCP	0.0	0.5	1.0	0.0	0.0	1.0	0.5	0.0	0.5	0.5	0.5	0.0	0.0	0.0	0.0	0.0	0.5	0.0
FMPT	0.0	0.5	1.0	0.0	0.0	1.0	0.5	0.0	0.5	0.5	0.5	0.0	0.0	0.0	0.0	0.0	0.5	0.0
LDAS	0.0	0.0	0.0	0.5	0.5	0.0	0.0	0.0	0.0	0.0	0.0	0.5	0.5	0.0	0.0	0.0	0.0	1.0
LDBA	0.0	0.0	0.0	0.5	0.5	0.0	0.0	0.0	0.0	0.0	0.0	0.5	0.5	0.0	0.0	0.0	0.0	1.0
NANL	0.0	0.5	0.5	0.0	0.0	0.5	0.5	0.0	0.5	0.5	0.5	0.0	0.0	0.0	0.0	0.0	0.5	0.0
NLAC	0.0	0.5	0.5	0.0	0.0	0.5	0.5	0.0	0.5	0.5	0.5	0.0	0.0	0.0	0.0	0.0	0.5	0.0
NLVS	0.0	0.5	0.5	0.0	0.0	0.5	0.5	0.0	0.5	0.5	0.5	0.0	0.0	0.0	0.0	0.0	0.5	0.0
NAAC	0.0	0.5	0.5	0.0	0.0	0.5	0.5	0.0	0.5	0.5	0.5	0.0	0.0	0.0	0.0	0.0	0.5	0.0
NACA	0.0	0.5	1.0	0.0	0.0	1.0	0.5	0.0	0.5	0.5	0.5	0.0	0.0	0.0	0.0	0.0	0.5	0.0
NACP	0.0	0.5	1.0	0.0	0.0	1.0	0.5	0.0	0.5	0.5	0.5	0.0	0.0	0.0	0.0	0.0	0.5	0.0
NAFM	0.0	0.5	1.0	0.0	0.0	1.0	0.5	0.0	0.5	0.5	0.5	0.0	0.0	0.0	0.0	0.0	0.5	0.0
NA41	0.0	0.5	0.5	0.0	0.0	0.5	0.5	0.0	0.5	0.5	0.5	0.0	0.0	0.0	0.0	0.0	0.5	0.0
NAVS	1.0	0.0	0.0	0.0	0.0	0.0	0.0	0.5	0.0	0.0	0.0	0.0	0.0	1.0	1.0	0.5	0.0	0.0
NAZI	0.0	1.0	0.5	0.0	0.0	0.5	0.5	0.0	0.5	0.5	0.5	0.0	0.0	0.0	0.0	0.0	0.5	0.0
NAZS	0.0	0.5	1.0	0.0	0.0	1.0	0.5	0.0	0.5	0.5	0.5	0.0	0.0	0.0	0.0	0.0	0.5	0.0
BRBA	0.0	0.0	0.0	1.0	1.0	0.0	0.0	0.0	0.0	0.0	0.0	1.0	1.0	0.0	0.0	0.0	0.0	0.5
NALD	0.0	0.0	0.0	1.0	1.0	0.0	0.0	0.0	0.0	0.0	0.0	1.0	1.0	0.0	0.0	0.0	0.0	0.5
DAFM	0.0	0.5	1.0	0.0	0.0	1.0	0.5	0.0	0.5	0.5	0.5	0.0	0.0	0.0	0.0	0.0	0.5	0.0
PLSY	0.0	0.5	0.5	0.0	0.0	0.5	1.0	0.0	1.0	1.0	1.0	0.0	0.0	0.0	0.0	0.0	1.0	0.0
POBA	0.5	0.0	0.0	0.0	0.0	0.0	0.0	1.0	0.0	0.0	0.0	0.0	0.0	0.5	0.5	1.0	0.0	0.0
PM41	0.0	0.5	0.5	0.0	0.0	0.5	1.0	0.0	1.0	1.0	1.0	0.0	0.0	0.0	0.0	0.0	1.0	0.0
41MX	0.0	0.5	0.5	0.0	0.0	0.5	1.0	0.0	1.0	1.0	1.0	0.0	0.0	0.0	0.0	0.0	1.0	0.0
41ZI	0.0	0.5	0.5	0.0	0.0	0.5	1.0	0.0	1.0	1.0	1.0	0.0	0.0	0.0	0.0	0.0	1.0	0.0
PTAS	0.0	0.0	0.0	1.0	1.0	0.0	0.0	0.0	0.0	0.0	0.0	1.0	1.0	0.0	0.0	0.0	0.0	0.5
PTLD	0.0	0.0	0.0	1.0	1.0	0.0	0.0	0.0	0.0	0.0	0.0	1.0	1.0	0.0	0.0	0.0	0.0	0.5
SLBA	1.0	0.0	0.0	0.0	0.0	0.0	0.0	0.5	0.0	0.0	0.0	0.0	0.0	1.0	1.0	0.5	0.0	0.0
SLCC	1.0	0.0	0.0	0.0	0.0	0.0	0.0	0.5	0.0	0.0	0.0	0.0	0.0	1.0	1.0	0.5	0.0	0.0
SYBA	0.5	0.0	0.0	0.0	0.0	0.0	0.0	1.0	0.0	0.0	0.0	0.0	0.0	0.5	0.5	1.0	0.0	0.0
SYMX	0.0	0.5	0.5	0.0	0.0	0.5	1.0	0.0	1.0	1.0	1.0	0.0	0.0	0.0	0.0	0.0	1.0	0.0
ZTPO	0.0	0.0	0.0	0.5	0.5	0.0	0.0	0.0	0.0	0.0	0.0	0.5	0.5	0.0	0.0	0.0	0.0	1.0
ZTVS	0.0	1.0	0.5	0.0	0.0	0.5	0.5	0.0	0.5	0.5	0.5	0.0	0.0	0.0	0.0	0.0	0.5	0.0
ZTZI	0.0	1.0	0.5	0.0	0.0	0.5	0.5	0.0	0.5	0.5	0.5	0.0	0.0	0.0	0.0	0.0	0.5	0.0
VSBA	0.5	0.0	0.0	0.0	0.0	0.0	0.0	1.0	0.0	0.0	0.0	0.0	0.0	0.5	0.5	1.0	0.0	0.0
VSSY	0.0	0.5	0.5	0.0	0.0	0.5	1.0	0.0	1.0	1.0	1.0	0.0	0.0	0.0	0.0	0.0	1.0	0.0
ZIMX	0.0	0.5	0.5	0.0	0.0	0.5	1.0	0.0	1.0	1.0	1.0	0.0	0.0	0.0	0.0	0.0	1.0	0.0
ZSNL	0.0	0.5	0.5	0.0	0.0	0.5	0.5	0.0	0.5	0.5	0.5	0.0	0.0	0.0	0.0	0.0	0.5	0.0

	ZTVS	ZTZI	VSBA	VSSY	ZIMX	ZSNL
ACPM	0.5	0.5	0.0	1.0	1.0	0.5
ACSY	0.5	0.5	0.0	0.5	0.5	1.0
PMPM	0.5	0.5	0.0	1.0	1.0	0.5
ASJP	0.0	0.0	0.0	0.0	0.0	0.0
BACC	0.0	0.0	1.0	0.0	0.0	0.0
BAOP	0.0	0.0	1.0	0.0	0.0	0.0
ASAS	0.0	0.0	0.0	0.0	0.0	0.0
JPJP	0.0	0.0	1.0	0.0	0.0	0.0
4141	0.5	0.5	0.0	1.0	1.0	0.5
POPO	0.0	0.0	0.0	0.0	0.0	0.0
PTPT	0.0	0.0	0.0	0.0	0.0	0.0
STST	0.0	0.0	0.0	0.0	0.0	0.0
ZTZT	1.0	1.0	0.0	0.5	0.5	0.5
BRAS	0.0	0.0	0.0	0.0	0.0	0.0
BRLD	0.0	0.0	0.0	0.0	0.0	0.0
BRNA	0.0	0.0	0.0	0.0	0.0	0.0
BRPT	0.0	0.0	0.0	0.0	0.0	0.0
NABA	0.0	0.0	0.5	0.0	0.0	0.0
CACP	0.0	0.0	0.5	0.0	0.0	0.0
CPSL	0.0	0.0	0.5	0.0	0.0	0.0
CPZS	0.0	0.0	0.5	0.0	0.0	0.0
CNCN	0.0	0.0	1.0	0.0	0.0	0.0
FMPM	0.5	0.5	0.0	0.5	0.5	1.0
FMZT	1.0	1.0	0.0	0.5	0.5	0.5
FMCP	0.5	0.5	0.0	0.5	0.5	0.5
FMPT	0.5	0.5	0.0	0.5	0.5	0.5
LDAS	0.0	0.0	0.0	0.0	0.0	0.0
LDBA	0.0	0.0	0.0	0.0	0.0	0.0
NANL	0.5	0.5	0.0	0.5	0.5	1.0
NLAC	0.5	0.5	0.0	0.5	0.5	1.0
NLVS	0.5	0.5	0.0	0.5	0.5	1.0
NAAC	0.5	0.5	0.0	0.5	0.5	1.0
NACA	0.5	0.5	0.0	0.5	0.5	0.5
NACP	0.5	0.5	0.0	0.5	0.5	0.5
NAFM	0.5	0.5	0.0	0.5	0.5	0.5
NA41	0.5	0.5	0.0	0.5	0.5	1.0
NAVS	0.0	0.0	0.5	0.0	0.0	0.0
NAZI	1.0	1.0	0.0	0.5	0.5	0.5
NAZS	0.5	0.5	0.0	0.5	0.5	0.5
BRBA	0.0	0.0	0.0	0.0	0.0	0.0
NALD	0.0	0.0	0.0	0.0	0.0	0.0
DAFM	0.5	0.5	0.0	0.5	0.5	0.5
PLSY	0.5	0.5	0.0	1.0	1.0	0.5
POBA	0.0	0.0	1.0	0.0	0.0	0.0
PM41	0.5	0.5	0.0	1.0	1.0	0.5
41MX	0.5	0.5	0.0	1.0	1.0	0.5
41ZI	0.5	0.5	0.0	1.0	1.0	0.5
PTAS	0.0	0.0	0.0	0.0	0.0	0.0
PTLD	0.0	0.0	0.0	0.0	0.0	0.0
SLBA	0.0	0.0	0.5	0.0	0.0	0.0
SLCC	0.0	0.0	0.5	0.0	0.0	0.0
SYBA	0.0	0.0	1.0	0.0	0.0	0.0
SYMX	0.5	0.5	0.0	1.0	1.0	0.5
ZTPO	0.0	0.0	0.0	0.0	0.0	0.0
ZTVS	1.0	1.0	0.0	0.5	0.5	0.5
ZTZI	1.0	1.0	0.0	0.5	0.5	0.5
VSBA	0.0	0.0	1.0	0.0	0.0	0.0
VSSY	0.5	0.5	0.0	1.0	1.0	0.5
ZIMX	0.5	0.5	0.0	1.0	1.0	0.5
ZSNL	0.5	0.5	0.0	0.5	0.5	1.0

APPENDIX C
LOD SCORE PLOTS

Figure C1 QTL Locations and Their Corresponding Phenotypes. For each QTL the LOD score is plotted against the genetic map distance for an individual chromosome (left panel). To minimize the number of superimposed lines, only QTLs with LOD ≥ 1.53 are shown (refer to Appendix E, Table E1 for a complete list of all QTLs). Next to each trait name is the model for which the linkage was identified. Traits linked to that QTL are color coded, with the colors corresponding to the depiction of the trait on a CT reconstruction of a baboon cranium (right panel). ECV is indicated by an ellipse drawn on the neural vault, and EIDs for which the endpoint(s) is not visible are drawn with a dashed line to approximate their location. No QTLs were defined for the X-chromosome so there is no LOD score plot, but all the traits that map to it are displayed. For *Cfs12.3* NAVS is indicated by two filled circles, one at *nasion* and the other at *vomerosphenoid junction* on the superior and inferior views of the cranium, respectively.

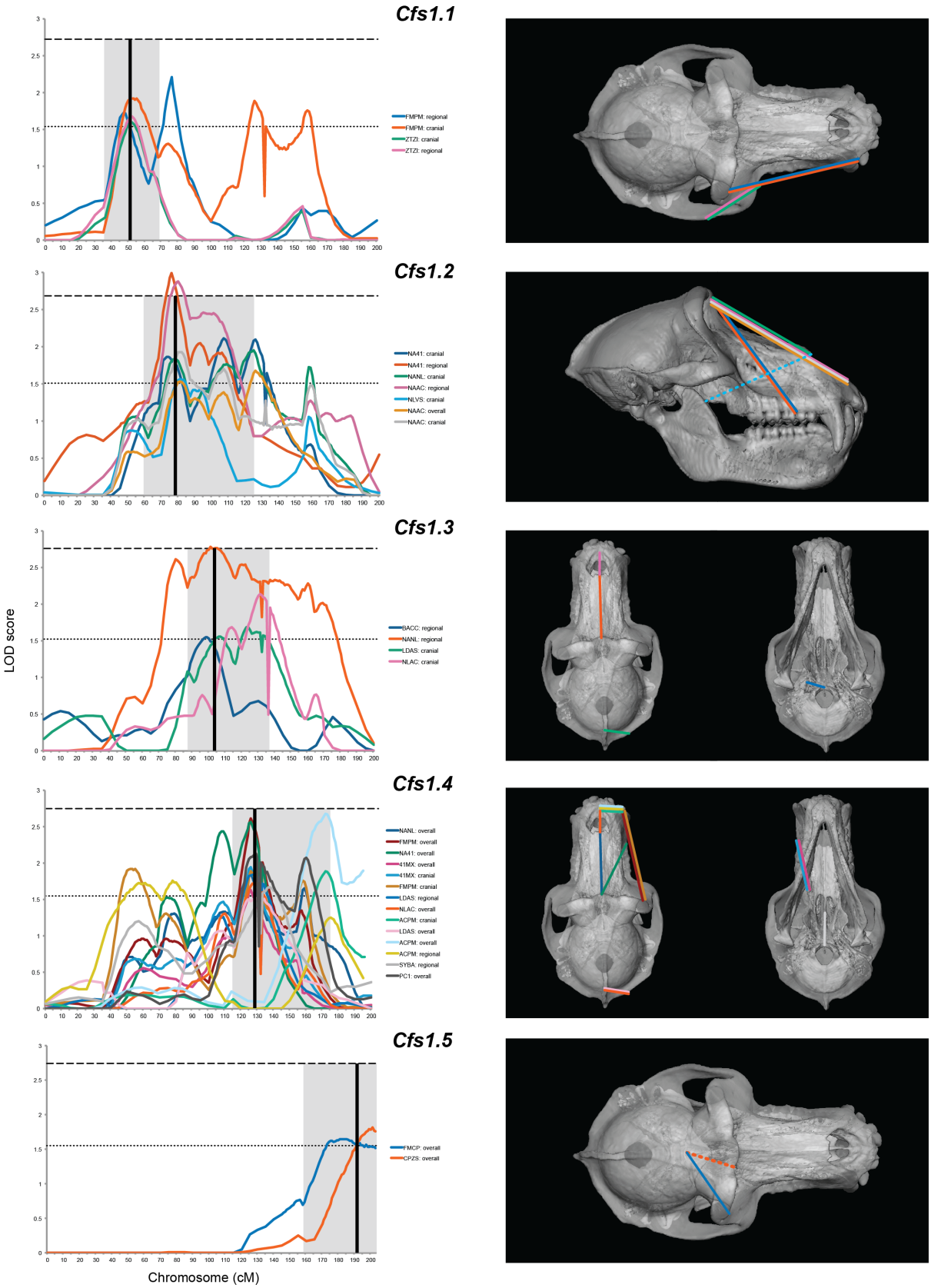
Cfs1.1
FMPM: regional
FMPM: cranial
ZTZI: cranial
ZTZI: regional
Cfs1.2
NA41: cranial
NA41: regional
NANL: cranial
NAAC: regional
NLVS: cranial
NAAC: overall
NAAC: cranial
Cfs1.3
BACC: regional
NANL: regional
LDAS: cranial
NLAC: cranial
Cfs1.4
NANL: overall
FMPM: overall
NA41: overall
41MX: overall
41MX: cranial
FMPM: cranial
LDAS: regional
NLAC: overall
ACPM: cranial
LDAS: overall
ACPM: overall
ACPM: regional
SYBA: regional
PC1: overall
Cfs1.5
FMCP: overall
CPZS: overall
LOD score
Chromosome (cM)

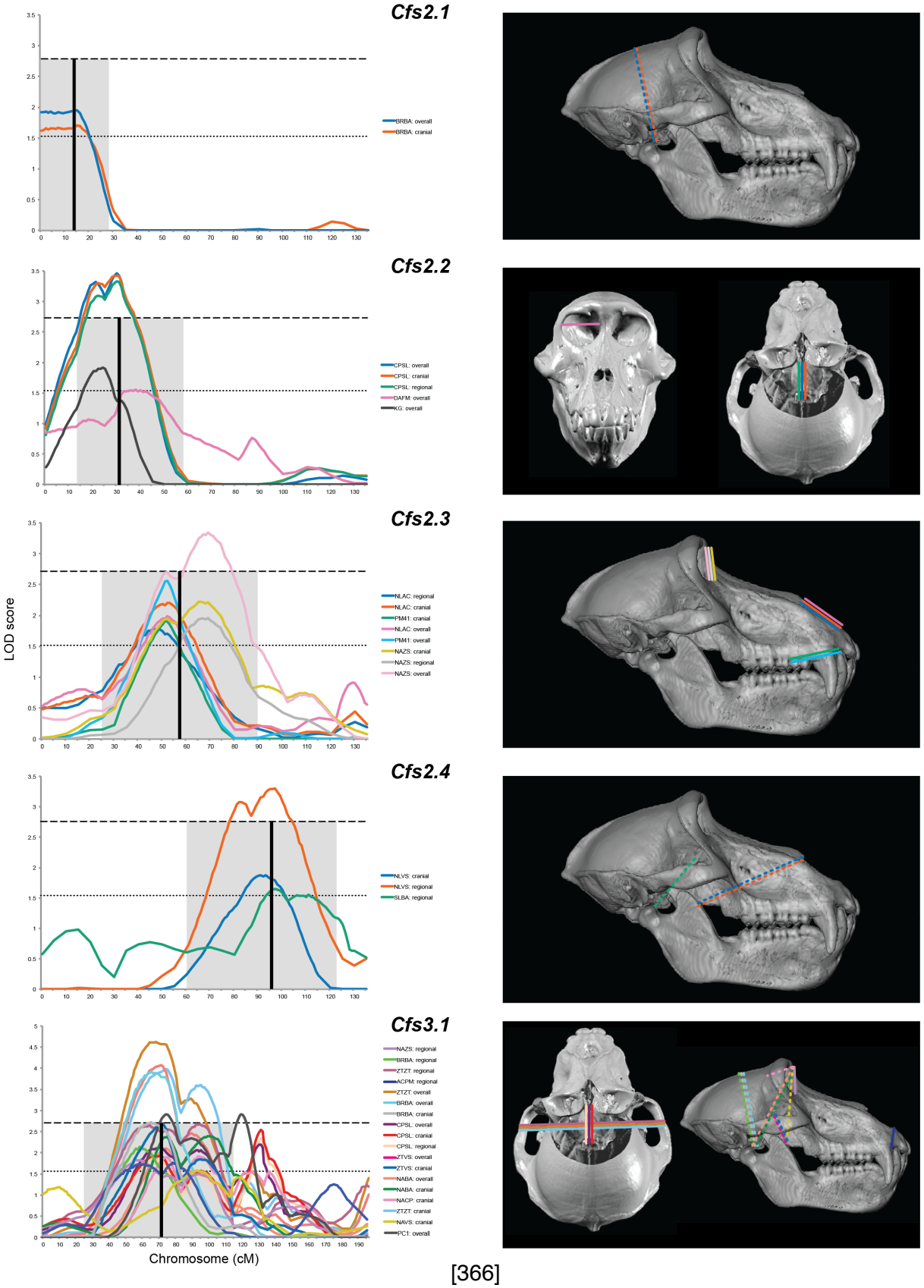
Cfs2.1
BRBA: overall
BRBA: cranial
Cfs2.2
CPSL: overall
CPSL: cranial
CPSL: regional
DAFM: overall
KG: overall
Cfs2.3
NLAC: regional
NLAC: cranial
PM41: cranial
NLAC: overall
PM41: overall
NAZS: cranial
NAZS: regional
NAZS: overall
Cfs2.4
NLVS: cranial
NLVS: regional
SLBA: regional
Cfs3.1
NAZS: regional
BRBA: regional
ZTZT: regional
ACPM: regional
ZTZT: overall
BRBA: overall
BRBA: cranial
CPSL: overall
CPSL: cranial
CPSL: regional
ZTVS: overall
ZTVS: cranial
NABA: overall
NABA: cranial
NACP: cranial
ZTZT: cranial
NAVS: cranial
PC1: overall
LOD score
Chromosome (cM)

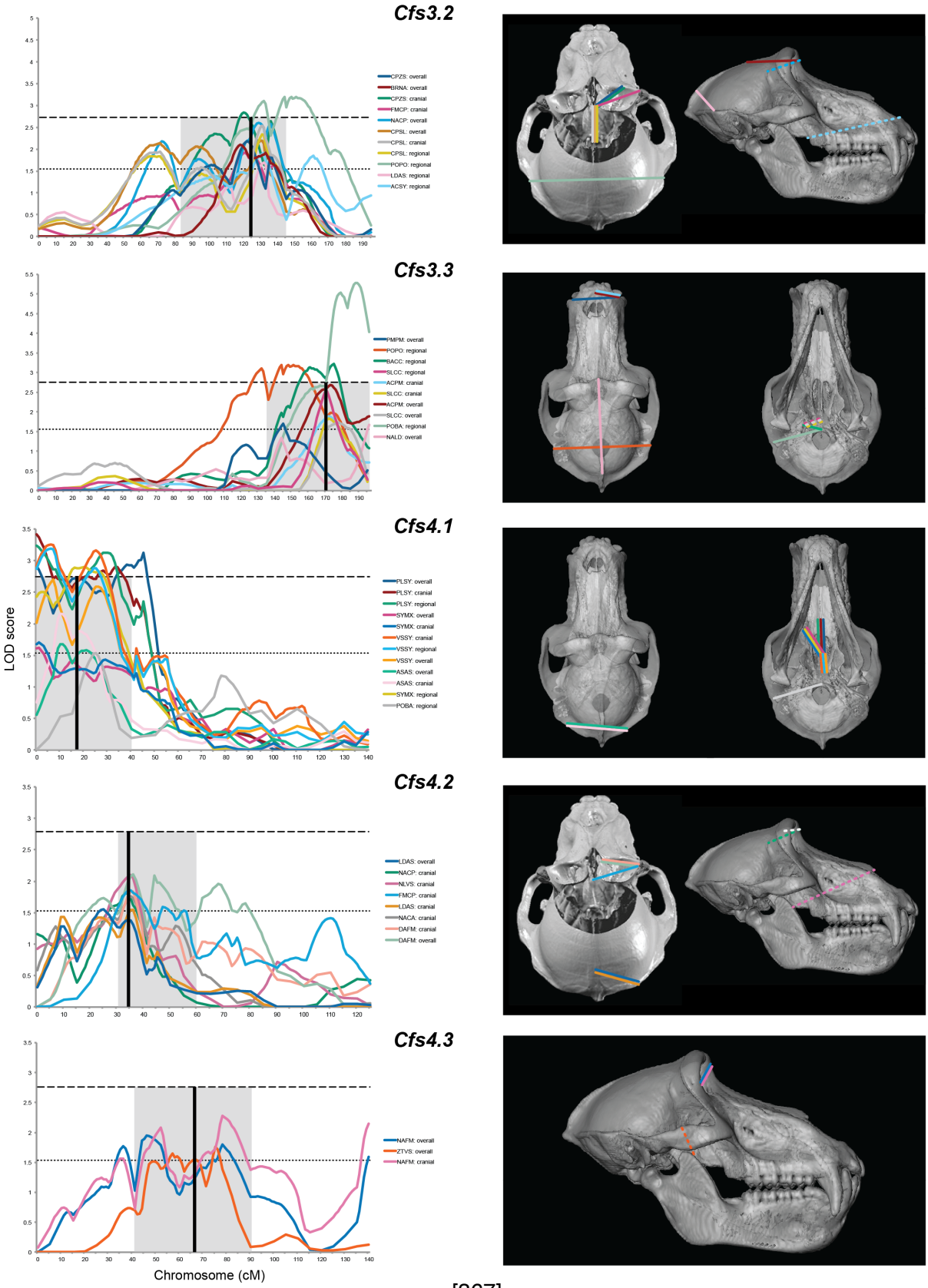
Cfs3.2
CPZS: overall
BRNA: overall
CPZS: cranial
FMCP: cranial
NACP: overall
CPSL: overall
CPSL: cranial
CPSL: regional
POPO: regional
LDAS: regional
ACSY: regional
Cfs3.3
PMPM: overall
POPO: regional
BACC: regional
SLCC: regional
ACPM: cranial
SLCC: cranial
ACPM: overall
SLCC: overall
POBA: regional
NALD: overall
Cfs4.1
LOD score
PLSY: overall
PLSY: cranial
PLSY: regional
SYMX: overall
SYMX: cranial
VSSY: cranial
VSSY: regional
VSSY: overall
ASAS: overall
ASAS: cranial
SYMX: regional
POBA: regional
Cfs4.2
LDAS: overall
NACP: cranial
NLVS: cranial
FMCP: cranial
LDAS: cranial
NACA: cranial
DAFM: cranial
DAFM: overall
Cfs4.3
NAFM: overall
ZTVS: overall
NAFM: cranial
Chromosome (cM)

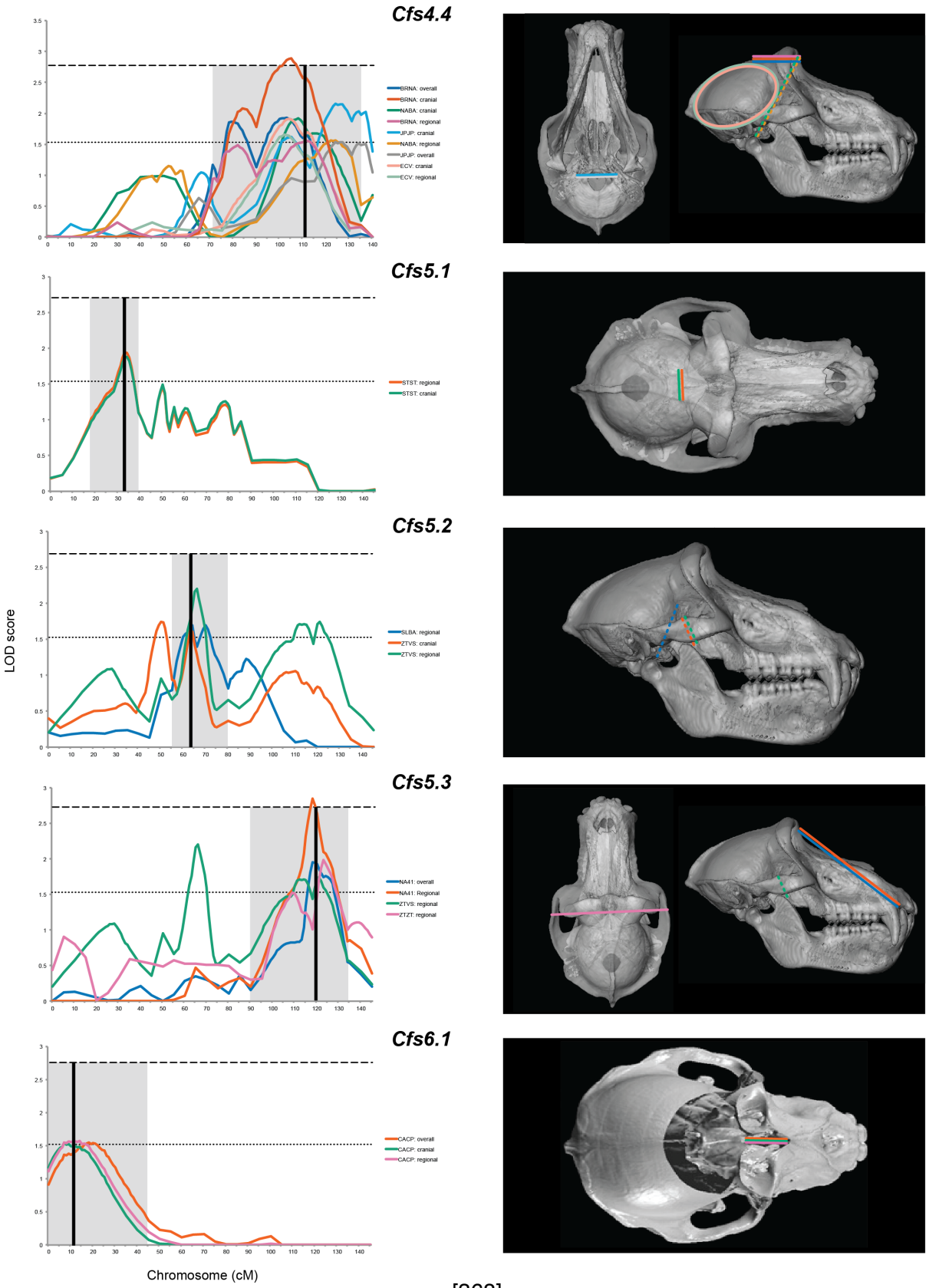
Cfs4.4
BRNA: overall
BRNA: cranial
NABA: cranial
BRNA: regional
JPJP: cranial
NABA: regional
JPJP: overall
ECV: cranial
ECV: regional
Cfs5.1
STST: regional
STST: cranial
Cfs5.2
SLBA: regional
ZTVS: cranial
ZTVS: regional
Cfs5.3
NA41: overall
NA41: Regional
ZTVS: regional
ZTZT: regional
Cfs6.1
CACP: overall
CACP: cranial
CACP: regional
LOD score
Chromosome (cM)

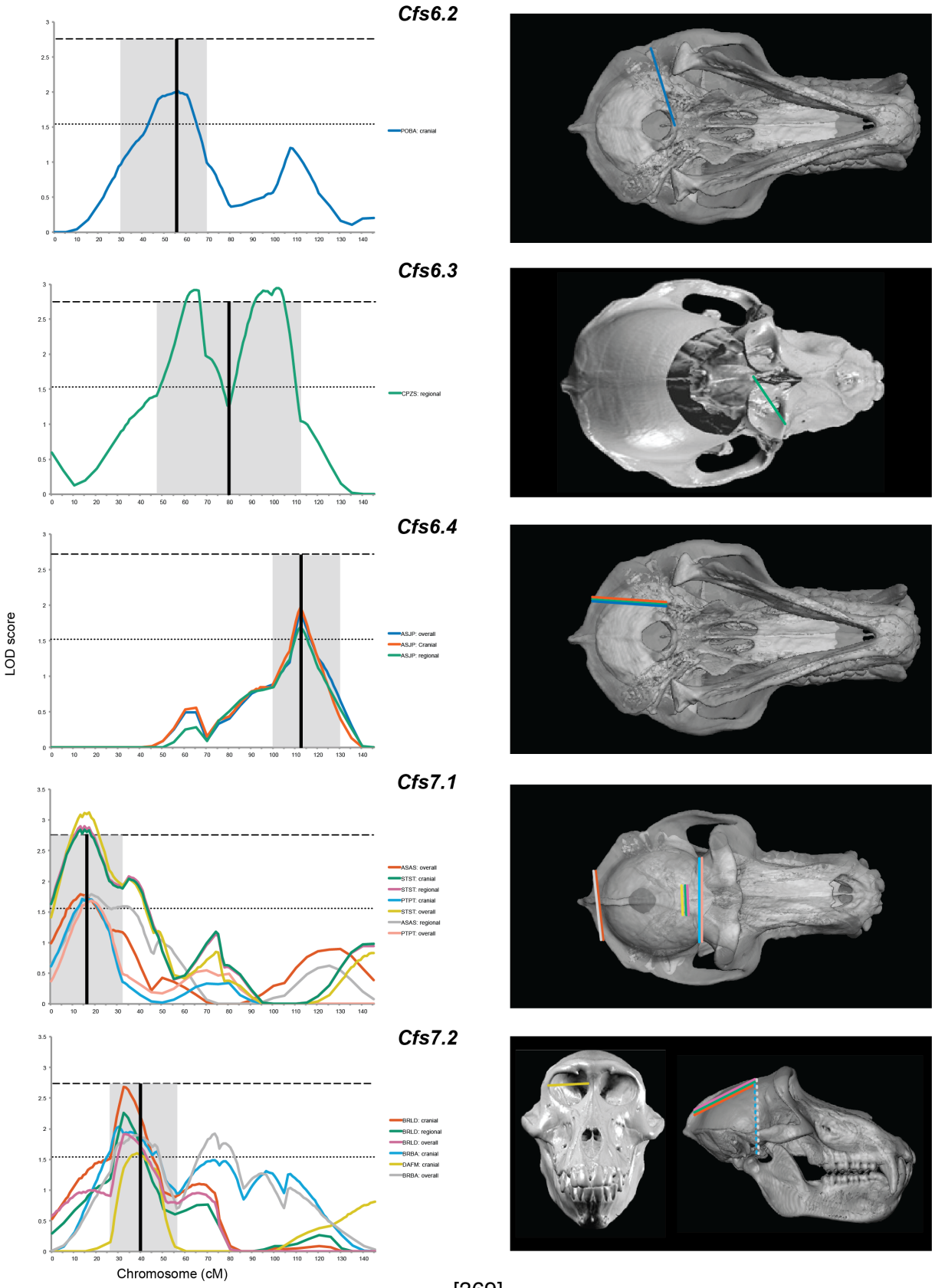
Cfs6.2
POBA: cranial
Cfs6.3
CPZS: regional
Cfs6.4
ASJP: overall
ASJP: Cranial
ASJP: regional
Cfs7.1
ASAS: overall
STST: cranial
STST: regional
PTPT: cranial
STST: overall
ASAS: regional
PTPT: overall
Cfs7.2
BRLD: cranial
BRLD: regional
BRLD: overall
BRBA: cranial
DAFM: cranial
BRBA: overall
LOD score
Chromosome (cM)

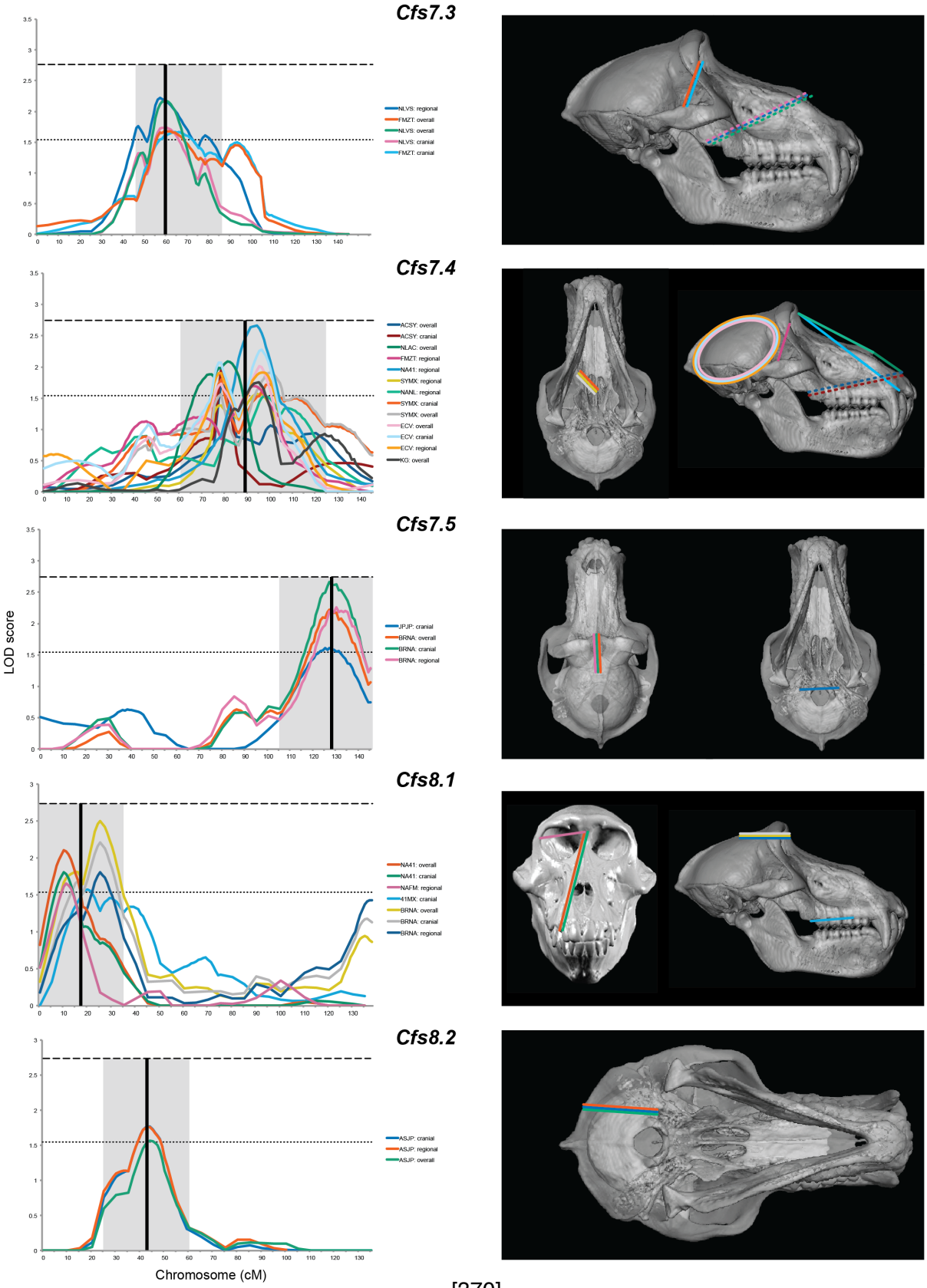
Cfs7.3
NLVS: regional
FMZT: overall
NLVS: overall
NLVS: cranial
FMZT: cranial
Cfs7.4
ACSY: overall
ACSY: cranial
NLAC: overall
FMZT: regional
NA41: regional
SYMX: regional
NANL: regional
SYMX: cranial
SYMX: overall
ECV: overall
ECV: cranial
ECV: regional
KG: overall
Cfs7.5
JPJP: cranial
BRNA: overall
BRNA: cranial
BRNA: regional
LOD score
Cfs8.1
NA41: overall
NA41: cranial
NAFM: regional
41MX: cranial
BRNA: overall
BRNA: cranial
BRNA: regional
Cfs8.2
ASJP: cranial
ASJP: regional
ASJP: overall
Chromosome (cM)

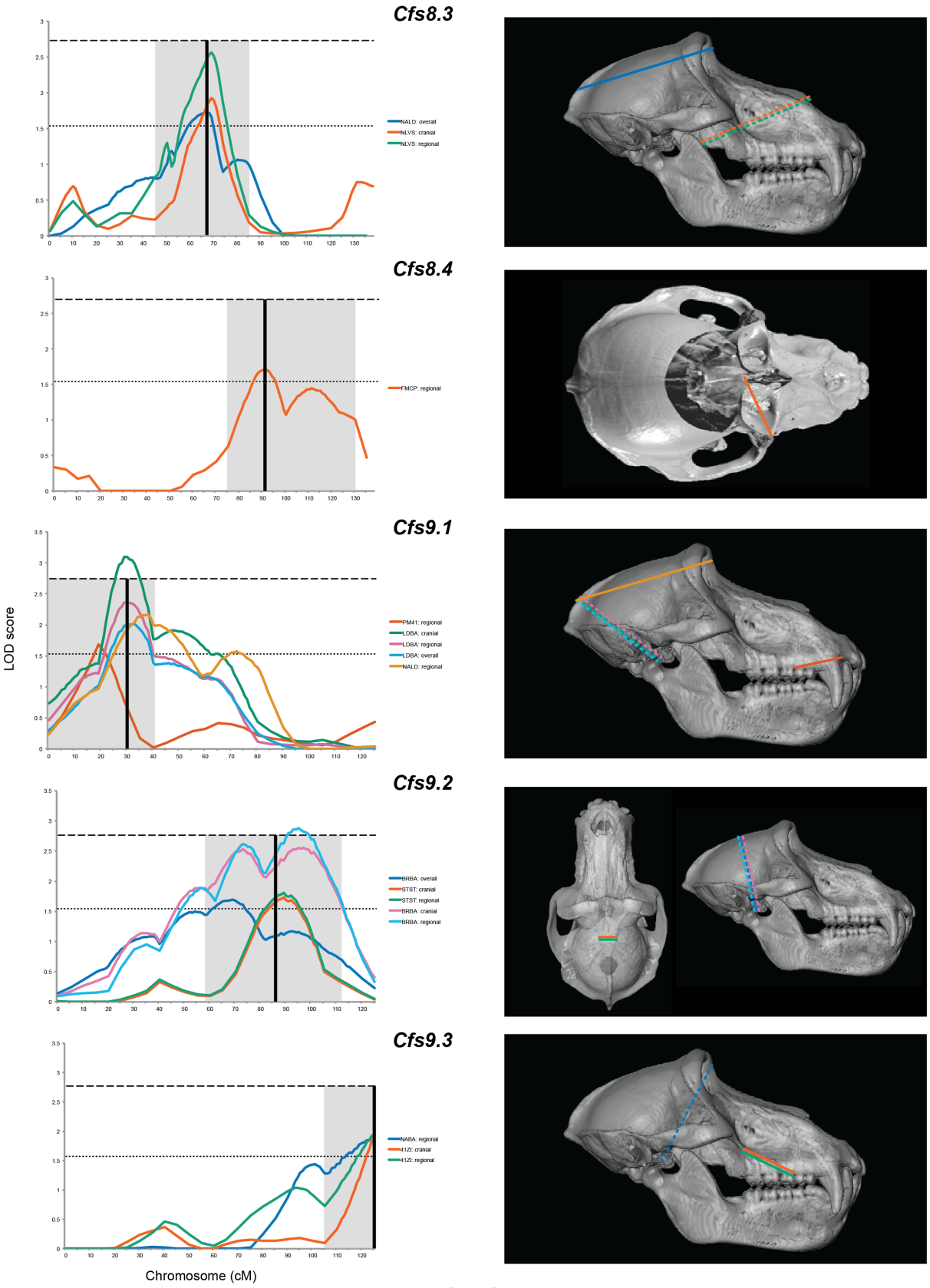
Cfs8.3
NALD: overall
NLVS: cranial
NLVS: regional
Cfs8.4
FMCP: regional
Cfs9.1
PM41: regional
LDBA: cranial
LDBA: regional
LDBA: overall
NALD: regional
Cfs9.2
BRBA: overall
STST: cranial
STST: regional
BRBA: cranial
BRBA: regional
Cfs9.3
NABA: regional
41ZI: cranial
41ZI: regional
LOD score
Chromosome (cM)

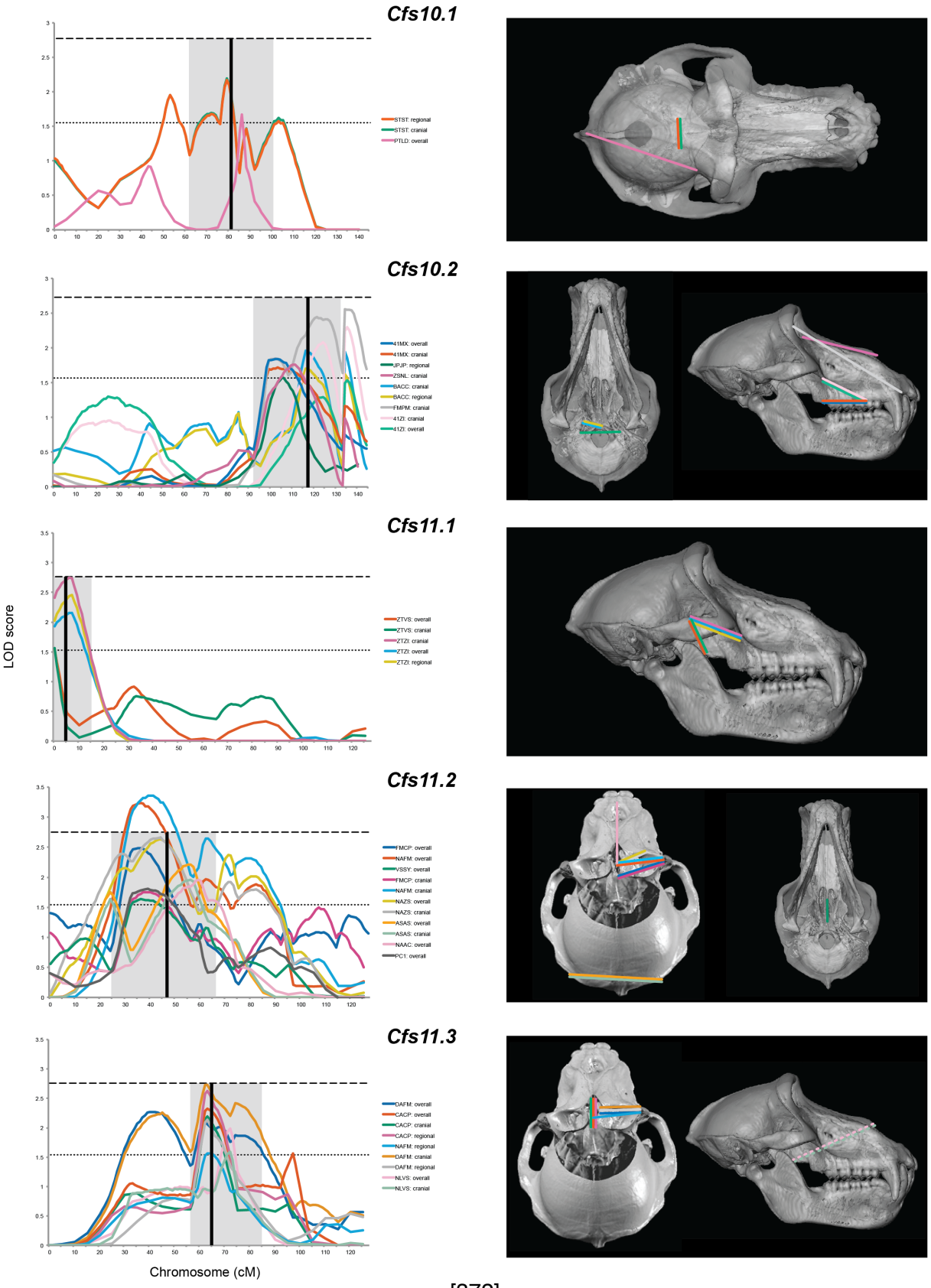
Cfs10.1
STST: regional
STST: cranial
PTLD: overall
Cfs10.2
41MX: overall
41MX: cranial
JPJP: regional
ZSNL: cranial
BACC: cranial
BACC: regional
FMPM: cranial
41ZI: cranial
41ZI: overall
Cfs11.1
ZTVS: overall
ZTVS: cranial
ZTZI: cranial
ZTZI: overall
ZTZI: regional
Cfs11.2
FMCP: overall
NAFM: overall
VSSY: overall
FMCP: cranial
NAFM: cranial
NAZS: overall
NAZS: cranial
ASAS: overall
ASAS: cranial
NAAC: overall
PC1: overall
Cfs11.3
DAFM: overall
CACP: overall
CACP: cranial
CACP: regional
NAFM: regional
DAFM: cranial
DAFM: regional
NLVS: overall
NLVS: cranial
LOD score
Chromosome (cM)

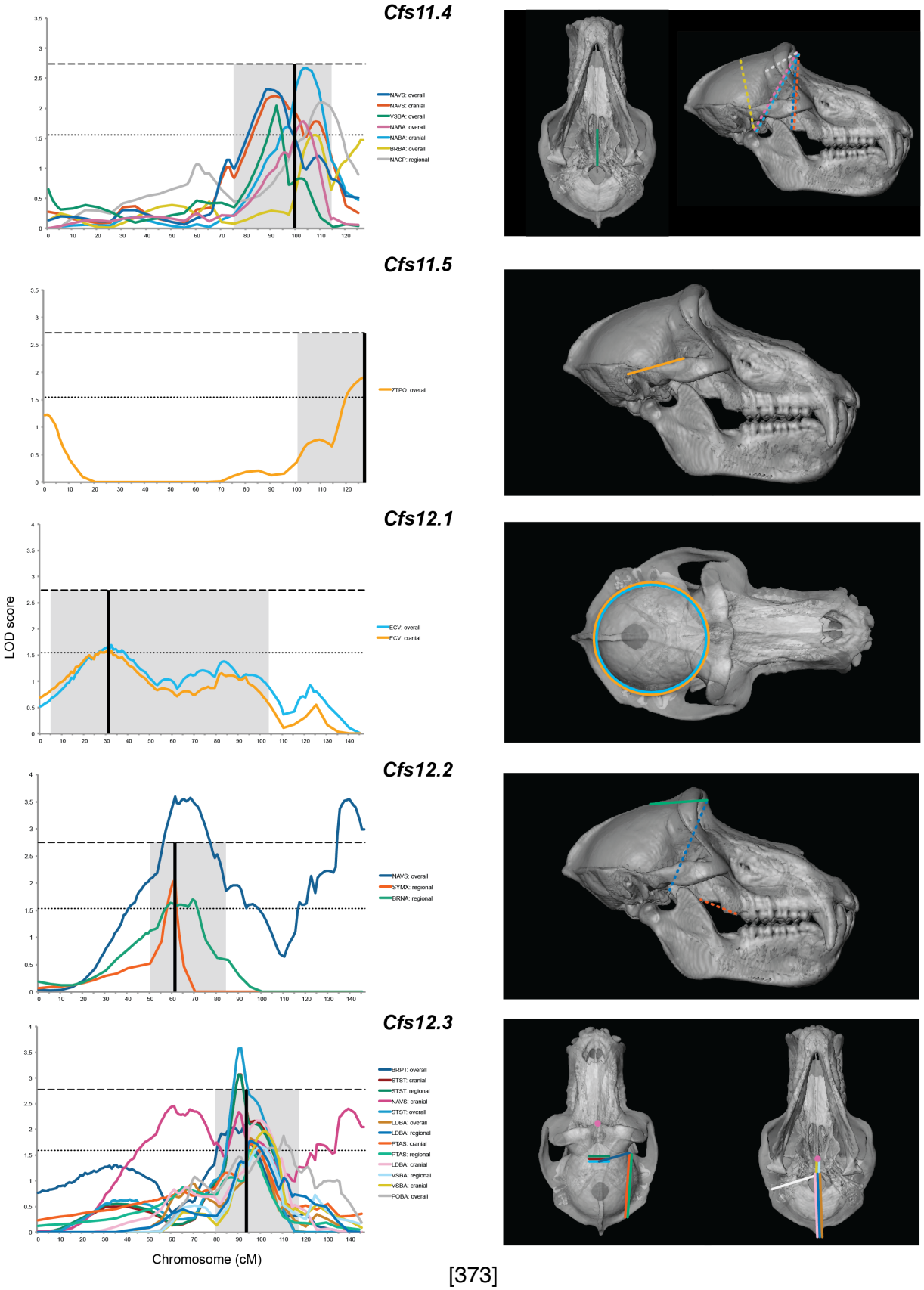
Cfs11.4
NAVS: overall
NAVS: cranial
VSBA: overall
NABA: overall
NABA: cranial
BRBA: overall
NACP: regional
Cfs11.5
ZTPO: overall
Cfs12.1
ECV: overall
ECV: cranial
LOD score
Cfs12.2
NAVS: overall
SYMX: regional
BRNA: regional
Cfs12.3
BRPT: overall
STST: cranial
STST: regional
NAVS: cranial
STST: overall
LDBA: overall
LDBA: regional
PTAS: cranial
PTAS: regional
LDBA: cranial
VSBA: regional
VSBA: cranial
POBA: overall
Chromosome (cM)

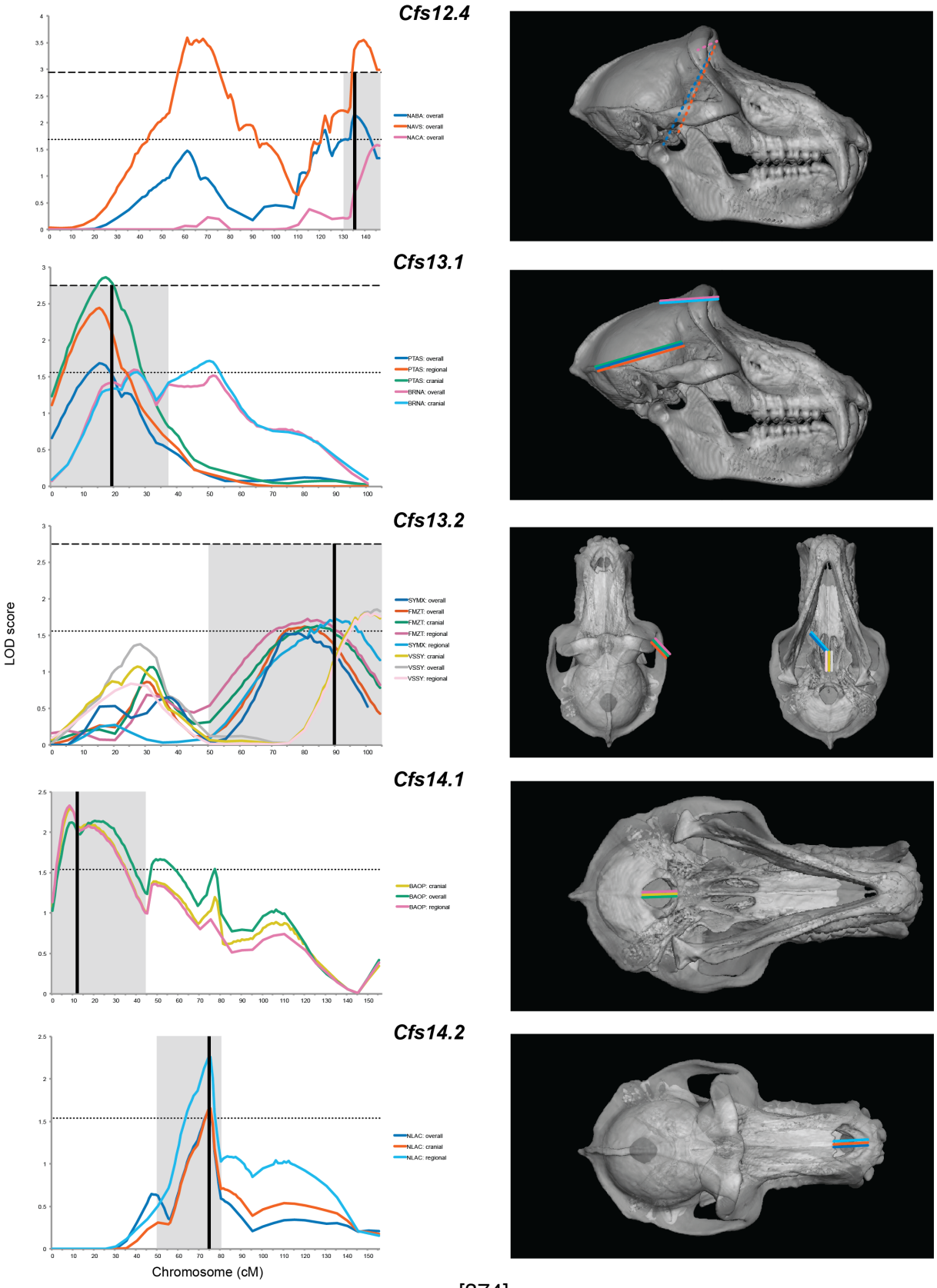
Cfs12.4
NABA: overall
NAVS: overall
NACA: overall
Cfs13.1
PTAS: overall
PTAS: regional
PTAS: cranial
BRNA: overall
BRNA: cranial
Cfs13.2
SYMX: overall
FMZT: overall
FMZT: cranial
FMZT: regional
SYMX: regional
VSSY: cranial
VSSY: overall
VSSY: regional
Cfs14.1
BAOP: cranial
BAOP: overall
BAOP: regional
Cfs14.2
NLAC: overall
NLAC: cranial
NLAC: regional
LOD score
Chromosome (cM)

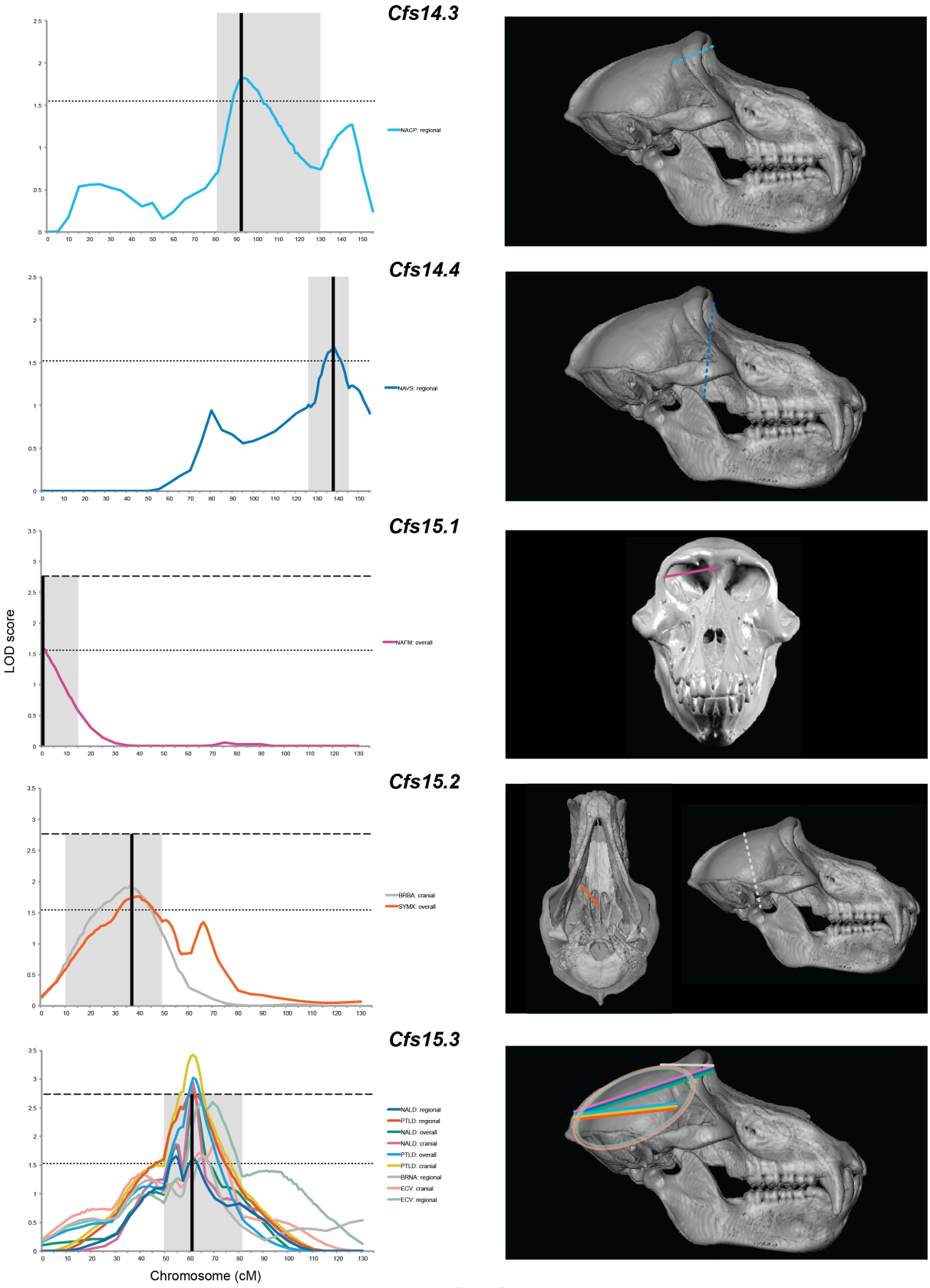
Cfs14.3
NACP: regional
Cfs14.4
NAVS: regional
Cfs15.1
NAFM: overall
Cfs15.2
BRBA: cranial
SYMX: overall
Cfs15.3
NALD: regional
PTLD: regional
NALD: overall
NALD: cranial
PTLD: overall
PTLD: cranial
BRNA: regional
ECV: cranial
ECV: regional
LOD score
Chromosome (cM)

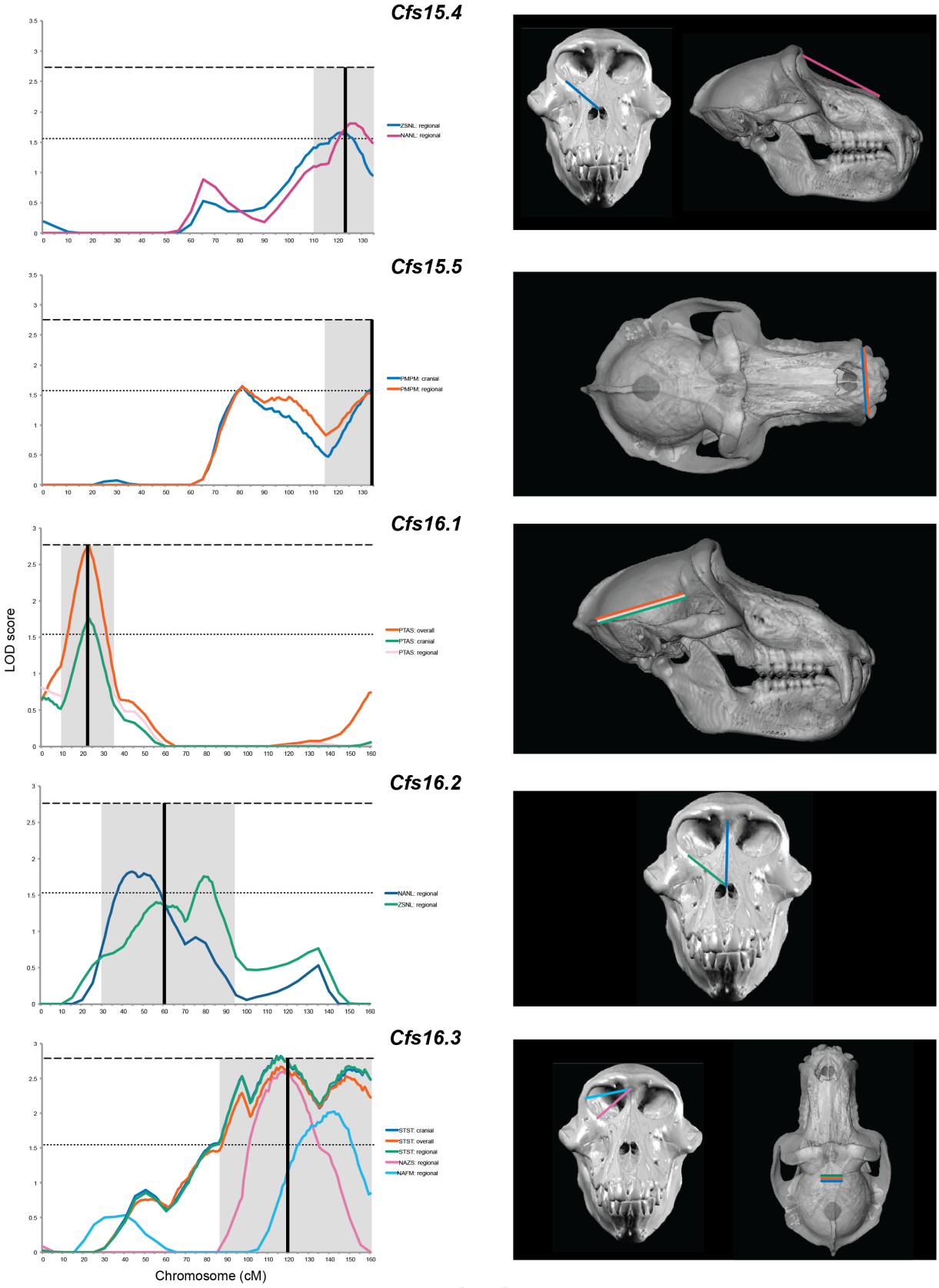
Cfs15.4
ZSNL: regional
NANL: regional
Cfs15.5
PMPM: cranial
PMPM: regional
Cfs16.1
PTAS: overall
PTAS: cranial
PTAS: regional
Cfs16.2
NANL: regional
ZSNL: regional
Cfs16.3
STST: cranial
STST: overall
STST: regional
NAZS: regional
NAFM: regional
LOD score
Chromosome (cM)

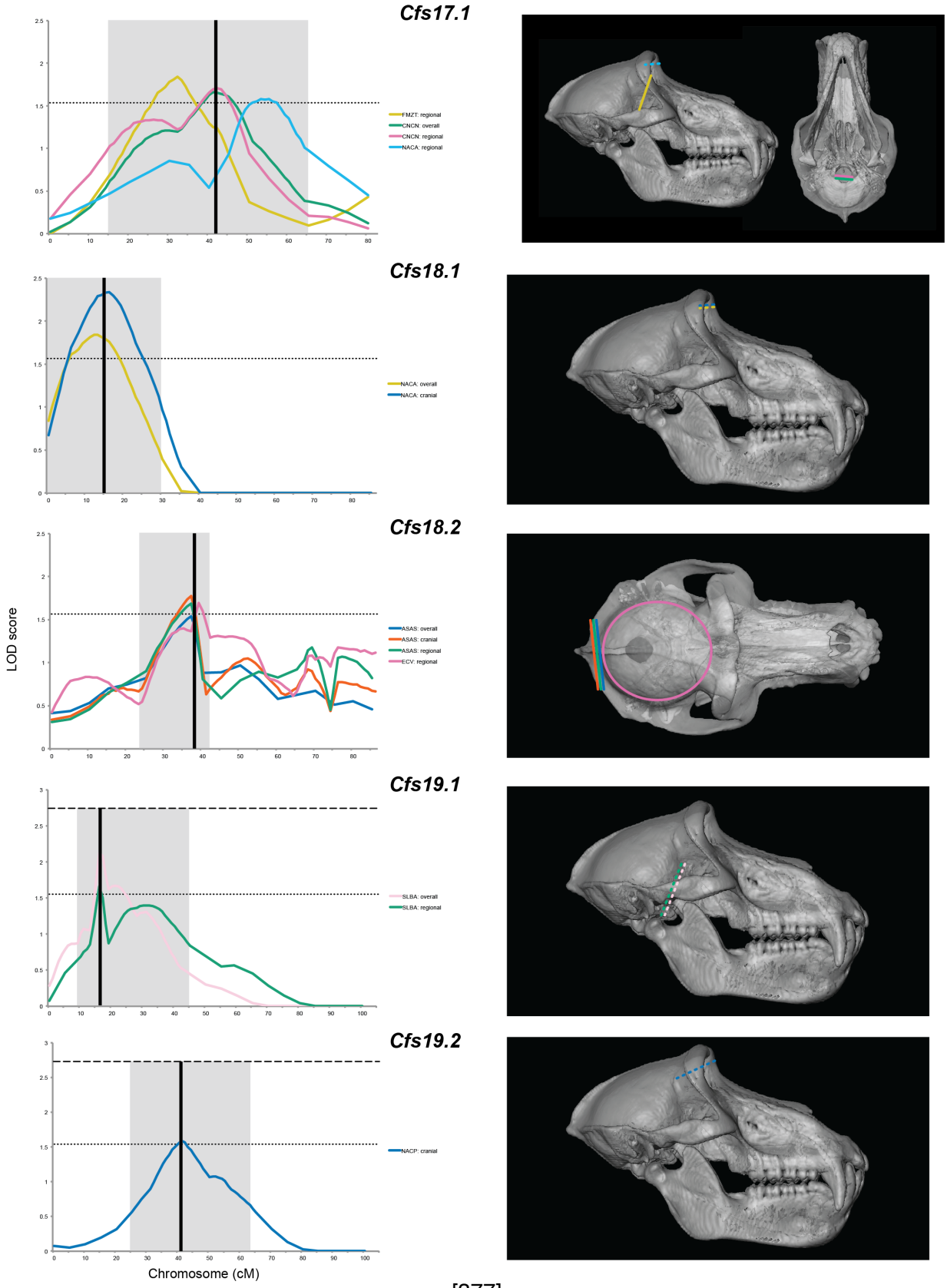
Cfs17.1
FMZT: regional
CNCN: overall
CNCN: regional
NACA: regional
Cfs18.1
NACA: overall
NACA: cranial
Cfs18.2
ASAS: overall
ASAS: cranial
ASAS: regional
ECV: regional
Cfs19.1
SLBA: overall
SLBA: regional
Cfs19.2
NACP: cranial
LOD score
Chromosome (cM)

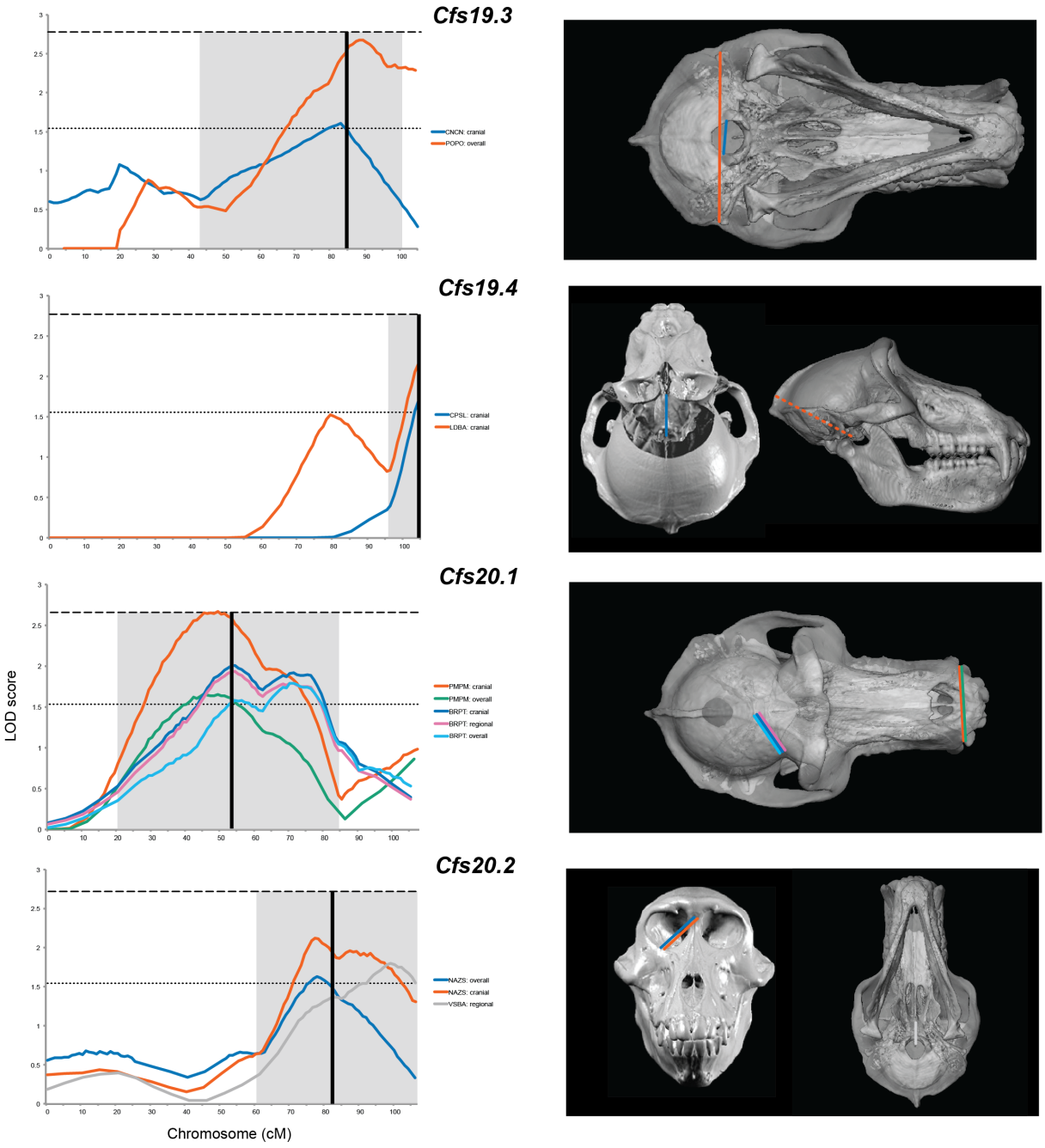
Cfs19.3
CNCN: cranial
POPO: overall
Cfs19.4
CPSL: cranial
LDBA: cranial
Cfs20.1
PMPM: cranial
PMPM: overall
BRPT: cranial
BRPT: regional
BRPT: overall
Cfs20.2
NAZS: overall
NAZS: cranial
VSBA: regional
LOD score
Chromosome (cM)
X Chromosome
CNCN: cranial
CNCN: regional
NACA: cranial
FMZT: cranial
LDAS: cranial
LDAS: regional
ASAS: regional
41ZI: regional
ZIMX: cranial
ZIMX: regional
ZTZT: overall
FMZT: overall
FMZT: regional
ZTZT: regional
FMCP: regional
NACP: regional
ZTZT: cranial
ZTVS: cranial
ZTVS: regional
BRNA: regional
STST: cranial
STST: regional
BRNA: cranial
BRNA: overall
ZSNL: regional
NANL: overall
ZSNL: overall
PM41: regional
CPZS: regional
CNCN: overall
NACP: regional
NA41: overall
NA41: cranial
BRPT: overall

APPENDIX D

THE Q-SET

Table D1 QTL Gene List. All genes contained within the support interval of QTLs with peak LOD ≥ 2.75. Genes shown in bold red typeface are genes known to affect craniofacial variation when mutated.

Cfs1.2					
ABCA4	AMY1C	B3GALT2	CCDC190	CHD1L	CTSS
ABCD3	AMY2A	B4GALT3	CCNJP2	CHI3L2	CTTNBP2NL
ABHD17AP1	AMY2B	BANF1P4	CCNT2P1	CHIA	CYB561D1
ABL2	AMYP1	BARHL2	CCT3	CHIAP1	CYCSP51
ACADM	ANGPTL1	BCAN	CCT8P1	CHIAP2	CYCSP52
ACBD6	ANKRD34A	BCAR3	CD101	CHRNB2	CYCSP53
ACKR1	ANKRD35	BCAS2	CD160	CHTOP	CYMP
ACP6	ANKRD36BP1	BCAS2P2	CD1A	CIART	CYR61
ACTBP12	ANKRD45	BCL10	CD1B	CICP13	DAP3
ACTG1P21	ANP32E	BCL2L15	CD1C	CKS1B	DAP3P1
ACTG1P4	ANXA9	BCL9	CD1D	CLCA1	DARS2
ADAM15	AP4B1	BGLAP	CD1E	CLCA2	DBT
ADAM30	APCS	BLZF1	CD2	CLCA3P	DCAF6
ADAMTS4	APH1A	BNIPL	CD244	CLCA4	DCAF8
ADAMTSL4	APOA1BP	BOLA1	CD247	CLCC1	DCLRE1B
ADAR	APOA2	BPNT1	CD48	CLK2	DCST1
ADCY10	APOBEC4	BRDT	CD53	CNN2P10	DCST2
ADGRL2	AQP10	BRI3P1	CD58	CNN3	DDAH1
ADGRL4	ARF4P5	BRINP2	CD5L	CNOT7P2	DDR2
ADH5P2	ARHGAP29	BRINP3	CD84	**COL11A1**	DDX20
ADORA3	ARHGAP30	BROX	CDC14A	COL24A1	DEDD
AGL	ARHGEF11	BTBD8	CDC42SE1	COLGALT2	DENND2C
AHCYL1	ARHGEF2	C2CD4D	CDC7	COPA	DENND2D
AIDA	ARNT	CA14	CDC73	COX5BP8	DENND4B
AIM2	ARPC5	CACNA1E	CDCA4P2	COX6A1P1	DHX9
AIMP1P2	ASB17	CACYBP	CDK4PS	CRABP2	DISP1
AK5	ASH1L	CADM3	CELF3	CRCT1	DLSTP1
AKNAD1	ASTN1	CAPN2	CELSR2	CREB3L4	DNAJA1P5
AKR1D1P1	ATF6	CAPN8	CENPL	CREG1	DNAJB4
AKR7A2P1	ATP1A1	CAPN8	CEP350	CRNN	DNASE2B
ALDH9A1	ATP1A2	CAPNS1P1	CEPT1	**CRP**	DNM3
ALG14	ATP1A4	CAPZA1	CERS2	CRPP1	DNM3OS
ALX3	ATP1B1	CASQ1	CFAP126	CRTC2	DNTTIP2
AMIGO1	ATP5F1	CASQ2	CFAP45	CRYZ	DPH5
AMPD1	ATP8B2	CCBL2	CGN	CSDE1	DPM3
AMPD2	ATXN7L2	CCDC18	CH17-125A10	CSF1	DPT
AMY1A	AURKAPS1	CCDC181	CH17-408M7	CTBS	**DPYD**
AMY1B	AXDND1	CCDC185	CHCHD2P5	CTSK	

Cfs1.2 cont.					
DR1	FCER1G	GAPDHP64	GSTM5	HSD3B1	KRT8P28
DRAM2	**FCGR1A**	GAPDHP74	GTF2B	HSD3B2	KRT8P45
DRD5P2	FCGR1B	GAPDHP75	HAO2	HSD3BP1	KRTCAP2
DUSP10	FCGR1C	GAS5	HAPLN2	HSD3BP2	LAMC1
DUSP12	FCGR2A	GATAD2B	HAUS4P1	HSD3BP3	LAMC2
DUSP23	FCGR2B	GBA	HAX1	HSD3BP4	LAMTOR2
DUSP27	FCGR2C	GBAP1	HCN3	HSD3BP5	LAMTOR5
DUTP6	FCGR3A	GBAT2	HDAC1P2	HSP90AA3P	LAPTM4BP1
ECM1	FCGR3B	GBP1	HDGF	HSP90B3P	LCE1A
EDEM3	FCRL1	GBP1P1	HENMT1	HSPA6	LCE1B
EEF1A1P11	FCRL2	GBP2	HFE2	HSPA7	LCE1C
EFNA1	FCRL3	GBP3	HFM1	HYDIN2	LCE1D
EFNA3	FCRL4	GBP4	HHIPL2	IARS2	LCE1E
EFNA4	FCRL5	GBP5	HIGD1AP12	IER5	LCE1F
EI24P2	FCRL6	GBP6	HIPK1	IFI16	LCE2A
EIF1P3	FCRL6P1	GBP7	HIPK1-AS1	IFI44	LCE2B
EIF2S2P5	FCRLA	GCLM	HIST2H2AA3	IFI44L	LCE2C
EIF4A1P11	FCRLB	GCSHP5	HIST2H2AA4	IGSF3	LCE2D
ELL2P1	FDPS	GDAP2	HIST2H2AB	IGSF8	LCE3A
EMBP1	FDPSP1	GEMIN2P1	HIST2H2AC	IGSF9	LCE3B
ENSA	FEN1P1	GEMIN8P4	HIST2H2BA	IL6R	LCE3C
EPHX4	FLAD1	GFI1	HIST2H2BB	ILDR2	LCE3D
EPRS	FLG	GIPC2	HIST2H2BC	ILF2	LCE3E
EPS8L3	FLG-AS1	GJA5	HIST2H2BD	INSRR	LCE4A
ERICH3	FLG2	GJA8	HIST2H2BE	INTS3	LCE5A
ETV3	FLJ23867	GLMN	HIST2H2BF	IQGAP3	LCE6A
ETV3L	FLJ27354	GLMP	HIST2H3A	ISCUP1	LCEP1
EVI5	FLJ31662	GLRX2	HIST2H3C	ISG20L2	LCEP2
EXTL2	FMO1	GLUL	HIST2H3D	ITGA10	LCEP3
F11R	FMO10P	GM140	HIST2H3PS2	ITLN1	LCEP4
F3	FMO11P	GM2AP2	HIST2H4A	ITLN2	LELP1
F5	FMO2	**GNAI3**	HIST2H4B	IVL	LENEP
FALEC	FMO3	GNAT2	HLX	IVNS1ABP	LHX4
FAM102B	FMO4	GNG5	HMCN1	JTB	**LHX8**
FAM129A	FMO5	GNRHR2	HMGB1P11	KATNBL1P2	LINGO4
FAM163A	FMO6P	GOLPH3L	HMGB1P18	KCNA10	LIX1L
FAM177B	FMO7P	GON4L	HMGB3P10	KCNA2	**LMNA**
FAM189B	FMO8P	GORAB	HMGB3P6	KCNA3	LMO4
FAM19A3	FMO9P	GOT2P2	HMGB3P9	KCNC4	LMX1A
FAM20B	FNBP1L	GPA33	HMGCS2	KCND3	LOR
FAM212B	FNDC7	GPATCH4	HMGN1P4	KCNJ10	LPAR3
FAM231D	FPGT	GPR161	HMGN1P5	KCNJ9	LPCAT2BP
FAM46C	FRRS1	GPR52	HMGN2P18	KCNN3	LRIF1
FAM63A	FTH1P22	GPR61	HMGN3P1	KIAA0040	LRIG2
FAM69A	FTH1P25	GPR88	HNRNPA1P43	KIAA0907	LRRC39
FAM72B	FTLP17	GPR89A	HNRNPA1P46	KIAA1107	LRRC52
FAM72C	FUBP1	GPR89B	HNRNPA1P54	KIAA1324	LRRC71
FAM72D	GABPB2	GPSM2	HNRNPA1P64	KIAA1614	LRRC8B
FAM73A	GAPDHP23	GS1-120K12	HNRNPA1P68	KIFAP3	LRRC8C
FAM78B	GAPDHP27	GS1-204I12	HNRNPA3P14	KIRREL	LRRC8D
FAM91A2P	GAPDHP29	GS1-279B7	HORMAD1	KLHDC9	LRRIQ3
FAM91A3P	GAPDHP32	GSTM1	HP08777	KLHL20	LY9
FAM91A4P	GAPDHP33	GSTM2	HRNR	KPRP	LYSMD1
FASLG	GAPDHP46	GSTM3	HS2ST1	KRT18P28	MAB21L3
FCER1A	GAPDHP58	GSTM4	HSD17B7	KRT18P57	MAEL

Cfs1.2 cont.						
MAGI3	NBPF11	NUDT4P2	PDC	PPIAL4G	RBMXL1	RNU7-13P
MAN1A2	NBPF12	NUF2	PDE4DIP	PPIAP7	RC3H1	RNU7-57P
MARC1	NBPF13P	NUP210L	PDE4DIPP1	PPM1J	RCSD1	RNU7-70P
MARC2	NBPF14	NUTF2P4	PDIA3P1	PPOX	REG4	RNU7-78P
MARK1	NBPF15	OAZ3	PDZK1	PRCC	RFWD2	RNU7-8P
MCL1	NBPF17P	OCLM	PDZK1P1	PRDX6	RFX5	RNVU1-1
MCOLN2	NBPF18P	ODF2L	PEA15	PRELID3BP1	RGL1	RNVU1-11
MCOLN3	NBPF19	OLFM3	PEAR1	PRG4	RGS1	RNVU1-14
MEF2AP1	NBPF20	OLFML2B	PEX11B	PRKAB2	RGS13	RNVU1-15
MEF2D	NBPF25P	OLFML3	PEX19	PRKACB	RGS16	RNVU1-17
METTL11B	NBPF26	OR10AA1P	PFDN2	PRKAR1AP	RGS18	RNVU1-18
METTL13	NBPF4	OR10AE1P	PFN1P1	PRMT6	RGS2	RNVU1-19
METTL18	NBPF5P	OR10J1	PFN1P12	PROK1	RGS21	RNVU1-3
MEX3A	NBPF6	OR10J2P	PFN1P2	PRPF3	RGS4	RNVU1-4
MFSD14A	NBPF7	OR10J3	PFN1P3	PRPF38B	RGS5	RNVU1-6
MGC27382	NBPF8	OR10J4	PFN1P4	PRR9	RGS8	RNVU1-7
MGST3	NBPF9	OR10J5	PFN1P6	PRRC2C	RGSL1	RNVU1-8
MIA3	NCF2	OR10J6P	PFN1P8	**PRRX1**	RHBG	RNY4P25
MLLT11	NCSTN	OR10J7P	PFN1P9	PRUNE	RHOC	RORC
MNDA	NDE1P1	OR10J8P	PGBD4P7	PSAT1P3	RIIAD1	RP11-216N14
MORF4L1P1	NDUFA4P1	OR10J9P	PGCP1	PSMA5	RIT1	RPAP2
MORF4L1P7	NDUFA5P10	OR10K1	PGLYRP3	PSMB4	RLIMP2	RPF1
MOV10	NDUFAF4P4	OR10K2	PGLYRP4	PSMC1P12	RNA5SP20	RPL10AP4
MPC2	NDUFB1P2	OR10R1P	PHGDH	PSMD4	RNA5SP21	RPL13AP10
MPTX1	NDUFB3P1	OR10R2	PHKA1P1	PSMD8P1	RNA5SP22	RPL13P7
MPZ	NDUFS2	OR10R3P	PHTF1	PSRC1	RNA5SP23	RPL17P5
MPZL1	NDUFS5P2	OR10T1P	PI4KB	PTBP2	RNA5SP51	RPL17P6
MR1	NEFHP1	OR10T2	PIAS3	PTGES3P1	RNA5SP52	RPL17P7
MR1P1	NES	OR10X1	PIFO	PTGFR	RNA5SP53	RPL18P2
MROH9	NEXN	OR10Z1	PIGC	PTGFRN	RNA5SP54	RPL21P26
MRPL24	NFU1P2	OR11I1P	PIGK	PTGS2	RNA5SP55	RPL21P27
MRPL53P1	NGF	OR13Z1P	PIGM	PTP4A1P7	RNA5SP56	RPL22P5
MRPL57P1	NHLH1	OR13Z2P	PIP5K1A	PTPN22	RNA5SP60	RPL22P6
MRPL9	NHLH2	OR13Z3P	PKLR	PTPN2P1	RNA5SP61	RPL23AP22
MRPS10P1	NIT1	OR2AQ1P	PKMP1	PUDPP2	RNA5SP62	RPL23P3
MRPS14	NKAIN1P1	OR6K1P	PKN2	PVRL4	RNA5SP63	RPL26P10
MRPS21	NME7	OR6K2	PKN2-AS1	PYGO2	RNA5SP64	RPL26P11
MRPS21P2	NMNAT1P2	OR6K3	PLA2G4A	PYHIN1	RNA5SP65	RPL26P12
MRPS33P1	NMNAT2	OR6K4P	PLEKHO1	PYHIN5P	RNA5SP66	RPL26P9
MSH4	NOS1AP	OR6K5P	PLPPR4	QRSL1P1	RNA5SP67	RPL27AP2
MSTO1	NOTCH2	OR6K6	PLPPR5	QRSL1P2	RNA5SP68	RPL27P2
MSTO2P	NOTCH2NL	OR6N1	PMF1	QSOX1	RNA5SP69	RPL29P5
MTF2	NOTCH2P1	OR6N2	PMVK	RAB13	RNA5SP71	RPL29P7
MTIF2P1	NPHS2	OR6P1	PNRC2P1	RAB25	RNA5SP72	RPL30P1
MTMR11	NPL	OR6Y1	POGK	RAB3GAP2	RNA5SP73	RPL31P11
MTND2P30	NPR1	OTUD7B	POGZ	RABGAP1L	RNA5SP76	RPL34P1
MTND4P11	NR1H5P	OVAAL	POLR3C	RABGGTB	RNASEL	RPL34P5
MTND5P20	NR1I3	OVGP1	POLR3GL	RAD1P2	RNF115	RPL35AP7
MTX1	NRAS	PACERR	POU2F1	RALGPS2	RNF2	RPL36AP10
MTX1P1	NRBF2P3	PALMD	POU5F1P4	RANP5	RNFT1P2	RPL36AP11
MUC1	NSRP1P1	PAPPA2	PPIAL4A	RAP1A	RNPC3	RPL36AP12
MYBPHL	NTNG1	PAQR6	PPIAL4C	RASAL2	RNU1-13P	RPL39P11
MYOC	NTRK1	PBX1	PPIAL4D	RBM15	RNU5F-2P	RPL39P13
NAP1L4P1	NUDT17	PBXIP1	PPIAL4E	RBM8A	RNU5F-6P	RPL39P8
NBPF10	NUDT4P1	PCP4L1	PPIAL4F	RBMX2P3	RNU6V	RPL39P9

Cfs1.2 cont.					
RPL4P2	RRM2P2	**SF3B4**	SNORD80	TARS2	TRF-GAA10-1
RPL4P3	RRNAD1	SFT2D2	SNORD81	TBX15	TRF-GAA9-1
RPL5	RSBN1	SH2D1B	SNRPEP10	TBX19	TRG-CCC6-1
RPL5P5	RTCA	SH2D2A	SNX27	TCEB1P19	TRG-GCC1-1
RPL5P6	RUSC1	SH3GLB1	SNX2P1	TCEB1P20	TRG-GCC1-2
RPL6P2	RWDD3	SHC1	SNX7	TCHH	TRG-GCC1-3
RPL7AP15	RXFP4	SHCBP1L	SOAT1	TCHHL1	TRG-GCC1-4
RPL7AP17	RXRG	SHE	SOD2P1	TDRD10	TRG-GCC2-1
RPL7AP19	S100A1	SIGLEC30P	SONP1	TDRD5	TRG-GCC4-1
RPL7AP21	S100A10	SIKE1	SORT1	TDRKH	TRG-TCC2-1
RPL7P10	S100A11	SLAMF1	SPAG17	TEDDM1	TRG-TCC2-2
RPL7P8	S100A12	SLAMF6	SPATA1	TEDDM2P	TRG-TCC2-3
RPL7P9	S100A13	SLAMF6P1	SPATA42	TEX35	TRG-TCC2-4
RPLP0P4	S100A14	SLAMF7	SPRR1A	TGFBR3	TRG-TCC2-5
RPLP0P5	S100A16	SLAMF8	SPRR1B	THBS3	TRG-TCC2-6
RPLP1P3	S100A2	SLAMF9	SPRR2A	THEM4	TRG-TCC4-1
RPRD2	S100A3	SLC16A1	SPRR2B	THEM5	TRH-GTG1-1
RPS10P6	S100A4	SLC16A4	SPRR2C	TIPRL	TRH-GTG1-2
RPS10P8	S100A5	SLC19A2	SPRR2D	TLR5	TRH-GTG1-3
RPS11P3	S100A6	SLC22A15	SPRR2E	TMCO1	TRH-GTG1-4
RPS13P1	S100A7	SLC25A24	SPRR2F	TMED5	TRIM33
RPS14P2	S100A7A	SLC25A24P1	SPRR2G	TMEM167B	TRIM45
RPS15AP12	S100A7L2	SLC25A24P2	SPRR3	TMEM56	TRIM46
RPS15AP9	S100A7P1	SLC25A38P1	SPRR4	TMEM79	TRK-CTT13-1
RPS15P1	S100A7P2	SLC25A44	**SPTA1**	TMIGD3	TRK-CTT2-1
RPS15P3	S100A8	SLC27A3	SPTLC1P4	TMOD4	TRL-CAA6-1
RPS17P6	S100A9	SLC30A10	SRGAP2-AS1	TNFAIP8L2	TRL-CAG1-1
RPS18P4	S1PR1	SLC30A7	SRGAP2B	TNFSF4	TRL-CAG1-2
RPS19P2	SAMD13	SLC35A3	SRGAP2C	TNN	TRL-CAG1-3
RPS20P6	SARS	SLC39A1	SRGAP2D	TNNI3K	TRL-CAG1-4
RPS20P7	SASS6	SLC44A3	SSR2	TNR	TRL-CAG1-5
RPS23P10	SCAMP3	SLC44A5	SSX2IP	TOMM40L	TRL-CAG1-6
RPS23P9	SCARNA2	SLC4A1APP2	ST13P20	TOP1P1	TRMT13
RPS24P5	SCARNA3	SLC50A1	ST13P21	TOR1AIP1	TRMT1L
RPS26P12	SCARNA4	SLC6A17	ST6GALNAC3	TOR1AIP2	TRN-GTT1-1
RPS26P16	SCNM1	SLC9C2	ST6GALNAC5	TOR3A	TRN-GTT11-2
RPS27	SCYL3	SMCP	ST7L	TPI1P1	TRN-GTT11-2
RPS27AP5	SDCCAG3P2	SMG5	STRIP1	**TPM3**	TRN-GTT12-1
RPS27AP6	SDHC	SMG7	STX6	TPR	TRN-GTT2-1
RPS27P6	SEC16B	SNAPIN	STXBP3	TRD-GTC10-1	TRN-GTT2-2
RPS27P7	SEC22B	SNORA36B	SUCO	TRD-GTC2-1	TRN-GTT22-1
RPS29P4	SEC63P1	SNORA66	SUMO1P2	TRD-GTC2-2	TRN-GTT23-1
RPS29P5	SELE	SNORA80E	SUMO1P3	TRD-GTC2-3	TRN-GTT3-1
RPS2P10	SELENBP1	SNORD21	SUSD4	TRD-GTC2-4	TRN-GTT3-2
RPS2P14	SELL	SNORD44	SV2A	TRD-GTC2-5	TRN-GTT6-1
RPS3AP10	SELP	SNORD45A	SWT1	TRE-CTC1-1	TRN-GTT7-1
RPS3AP12	SEMA4A	SNORD45B	SYCP1	TRE-CTC1-2	TRN-GTT7-1
RPS3AP8	SEMA6C	SNORD45C	SYDE2	TRE-CTC1-3	TRN-GTT8-1
RPS3AP9	SEPT15	SNORD47	SYPL2	TRE-CTC1-4	TRN-GTT9-2
RPS7P2	SEPT2P1	SNORD74	SYT11	TRE-CTC1-5	TRNAC-GCA
RPSAP16	SERPINC1	SNORD75	SYT6	TRE-TTC10-1	TRNAG-CCC
RPSAP17	SETDB1	SNORD76	TADA1	TRE-TTC14-1	TRNAN-GUU
RPSAP18	SETP10	SNORD77	TAF13	TRE-TTC4-2	TRNAN-GUU
RPSAP19	SETP9	SNORD78	TAF1A	TRE-TTC6-1	TRNAN-GUU
RPTN	SETSIP	SNORD79	TAGLN2	TRE-TTC7-1	TRNAN-GUU

			***Cfs1.2* cont.**			
TRNAN-GUU	TRQ-CTG7-1	TSACC	UBE2Q1	VAMP4	VSIG8	YPEL5P1
TRNAQ-CUG	TRQ-CTG9-1	TSEN15	UBE2WP1	VANGL1	VTCN1	YY1AP1
TRNAV-CAC	TRR-CCT6-2	TSHB	UBL4B	VANGL2	WARS2	ZBTB37
TRNAV-CAC	TRR-CCT7-1	TTC24	UBQLN4	VAV3	WDR3	ZBTB7B
TRNAV-CAC	TRR-CCT8-1	TTF2	UCHL5	VAV3-AS1	WDR47	ZC3H11B
TRNAV-CAC	TRR-TCT1-1	TTLL7	UCK2	VCAM1	WDR63	ZNF101P2
TROVE2	TRR-TCT4-1	TUFT1	UFC1	VDAC1P4	WDR77	ZNF644
TRP-AGG2-1	TRT-TGT2-1	TXNIP	UHMK1	VDAC1P9	WDR82P2	ZNF648
TRP-CGG1-1	TRV-CAC1-1	TXNP3	UOX	VDAC2P3	WNT2B	ZNF687
TRQ-CTG11-1	TRV-CAC4-1	TYW3	UQCRBP2	VHLL	XCL1	ZNF697
TRQ-CTG3-2	TRV-CAC5-1	UAP1	USF1	VPS25P1	XCL2	ZNHIT6
TRQ-CTG4-1	TRV-CAC8-1	UBAP2L	USP21	VPS45	XPR1	ZZZ3
TRQ-CTG4-2	TRX-CAT1-1	UBE2D3P3	USP33	VPS72	XRCC6P3	
			Cfs1.3			
ABHD17AP1	ATP1A4	CD244	CYCSP53	FALEC	FLJ23867	GPA33
ABL2	ATP1B1	CD247	DAP3	FAM129A	FMO1	GPATCH4
ACBD6	ATP8B2	CD48	DAP3P1	FAM163A	FMO10P	GPR161
ACKR1	AURKAPS1	CD58	DARS2	FAM177B	FMO11P	GPR52
ACP6	AXDND1	CD5L	DCAF6	FAM189B	FMO2	GPR89A
ADAM15	B4GALT3	CD84	DCAF8	FAM20B	FMO3	GPR89B
ADAM30	BANF1P4	CDC42SE1	DCST1	FAM231D	FMO4	GS1-120K12
ADAMTS4	BCAN	CELF3	DCST2	FAM46C	FMO5	GS1-204I12
ADAMTSL4	BCAS2	CENPL	DDR2	FAM63A	FMO6P	GS1-279B7
ADAMTSL4-AS1	BCL9	CEP350	DEDD	FAM72B	FMO7P	HAO2
ADAR	BGLAP	CERS2	DENND2C	FAM72C	FMO8P	HAO2-IT1
ADCY10	BLZF1	CFAP126	DENND4B	FAM72D	FMO9P	HAPLN2
AIDA	BNIPL	CFAP45	DHX9	FAM78B	FTH1P22	HAUS4P1
AIM2	BOLA1	CGN	DISP1	FAM91A2P	FTH1P25	HAX1
AIMP1P2	BPNT1	CH17-125A10	DNM3	FAM91A3P	GABPB2	HCN3
AKR1D1P1	BRINP2	CH17-408M7	DNM3OS	FAM91A4P	GAPDHP23	HDAC1P2
ALDH9A1	BROX	CHD1L	DPM3	FASLG	GAPDHP27	HDGF
AMPD1	C2CD4D	CHRNB2	DPT	FCER1A	GAPDHP32	HFE2
ANGPTL1	CA14	CHTOP	DRD5P2	FCER1G	GAPDHP33	HHIPL2
ANKRD34A	CACNA1E	CIART	DUSP10	**FCGR1A**	GAPDHP58	HIST2H2AA3
ANKRD35	CACYBP	CICP13	DUSP12	FCGR1B	GAPDHP64	HIST2H2AA4
ANKRD36BP1	CADM3	CKS1B	DUSP23	FCGR1C	GAPDHP74	HIST2H2AB
ANKRD45	CADM3-AS1	CLK2	DUSP27	FCGR2A	GAS5	HIST2H2AC
ANP32E	CAPN2	CNN2P10	DUTP6	FCGR2B	GATAD2B	HIST2H2BA
ANXA9	CAPN8	CNOT7P2	ECM1	FCGR2C	GBA	HIST2H2BB
APCS	CAPN8	COLGALT2	EDEM3	FCGR3A	GBAP1	HIST2H2BC
APH1A	CASQ1	COPA	EFNA1	FCGR3B	GBAT2	HIST2H2BD
APOA1BP	CASQ2	COX5BP8	EFNA3	FCRL1	GCSHP5	HIST2H2BE
APOA2	CCDC181	CRABP2	EFNA4	FCRL2	GDAP2	HIST2H2BF
APOBEC4	CCDC185	CRCT1	EI24P2	FCRL3	GEMIN2P1	HIST2H3A
AQP10	CCDC190	CREB3L4	EIF1P3	FCRL4	GJA5	HIST2H3C
ARHGAP30	CCT3	CREG1	EIF2S2P5	FCRL5	GJA8	HIST2H3D
ARHGEF11	CCT8P1	CRNN	EIF4A1P11	FCRL6	GLMP	HIST2H3PS2
ARHGEF2	CD101	**CRP**	ELL2P1	FCRL6P1	GLUL	HIST2H4A
ARNT	CD160	CRPP1	EMBP1	FCRLA	GM140	HIST2H4B
ARPC5	CD1A	CRTC2	ENSA	FCRLB	GM2AP2	HLX
ASH1L	CD1B	CSDE1	EPRS	FDPS	GNRHR2	HMCN1
ASTN1	CD1C	CTSK	ETV3	FDPSP1	GOLPH3L	HMGB1P11
ATF6	CD1D	CTSS	ETV3L	FLAD1	GON4L	HMGB3P6
ATP1A1	CD1E	CYCSP51	F11R	FLG	GORAB	HMGCS2
ATP1A2	CD2	CYCSP52	F5	FLG2	GOT2P2	HMGN1P4

Cfs1.3 cont.						
HMGN1P5	LAMC2	MORF4L1P7	NOS1AP	PACERR	PRELID3BP1	RNA5SP66
HMGN2P18	LAMTOR2	MPC2	NOTCH2	PAPPA2	PRG4	RNA5SP67
HMGN3P1	LAPTM4BP1	MPTX1	NOTCH2NL	PAQR6	PRKAB2	RNA5SP68
HNRNPA1P43	LCE1A	MPZ	NOTCH2P1	PBX1	PRPF3	RNA5SP69
HNRNPA1P54	LCE1B	MPZL1	NPHS2	PBXIP1	PRR9	RNA5SP71
HORMAD1	LCE1C	MR1	NPL	PCP4L1	PRRC2C	RNA5SP72
HRNR	LCE1D	MR1P1	NPR1	PDC	**PRRX1**	RNA5SP76
HSD17B7	LCE1E	MROH9	NR1H5P	PDE4DIP	PRUNE	RNASEL
HSD3B1	LCE1F	MRPL24	NR1I3	PDE4DIPP1	PSMB4	RNF115
HSD3B2	LCE2A	MRPL57P1	NRAS	PDIA3P1	PSMC1P12	RNF2
HSD3BP1	LCE2B	MRPL9	NTRK1	PDZK1	PSMD4	RNU1-13P
HSD3BP2	LCE2C	MRPS10P1	NUDT17	PDZK1P1	PSMD8P1	RNU5F-2P
HSD3BP3	LCE2D	MRPS14	NUDT4P1	PEA15	PTGFRN	RNU5F-6P
HSD3BP4	LCE3A	MRPS21	NUDT4P2	PEAR1	PTGS2	RNU7-13P
HSD3BP5	LCE3B	MRPS21P2	NUF2	PEX11B	PTP4A1P7	RNU7-57P
HSP90AA3P	LCE3C	MRPS33P1	NUP210L	PEX19	PTPN2P1	RNU7-78P
HSPA6	LCE3D	MSTO1	OAZ3	PFDN2	PUDPP2	RNVU1-1
HSPA7	LCE3E	MSTO2P	OCLM	PFN1P1	PVRL4	RNVU1-11
HYDIN2	LCE4A	MTIF2P1	OLFML2B	PFN1P12	PYGO2	RNVU1-14
IARS2	LCE5A	MTMR11	OR10AA1P	PFN1P2	PYHIN1	RNVU1-15
IER5	LCE6A	MTX1	OR10AE1P	PFN1P3	PYHIN5P	RNVU1-17
IFI16	LCEP1	MTX1P1	OR10J1	PFN1P4	QRSL1P1	RNVU1-18
IGSF3	LCEP2	MUC1	OR10J2P	PFN1P6	QRSL1P2	RNVU1-19
IGSF8	LCEP3	MYOC	OR10J3	PFN1P8	QSOX1	RNVU1-3
IGSF9	LCEP4	NAP1L4P1	OR10J4	PFN1P9	RAB13	RNVU1-4
IL6R	LELP1	NBPF10	OR10J5	PGLYRP3	RAB25	RNVU1-6
ILDR2	LENEP	NBPF11	OR10J6P	PGLYRP4	RAB3GAP2	RNVU1-7
ILF2	**LHX4**	NBPF12	OR10J7P	PHGDH	RABGAP1L	RNVU1-8
INSRR	LINGO4	NBPF13P	OR10J8P	PI4KB	RAD1P2	RNY4P25
INTS3	LIX1L	NBPF14	OR10J9P	PIAS3	RALGPS2	RORC
IQGAP3	LMNA	NBPF15	OR10K1	PIGC	RASAL2	RP11-216N14
ISCUP1	LMX1A	NBPF17P	OR10K2	PIGM	RBM8A	RPL13AP10
ISG20L2	LOR	NBPF18P	OR10R1P	PIP5K1A	RBMX2P3	RPL13P7
ITGA10	LRRC52	NBPF19	OR10R2	PKLR	RC3H1	RPL18P2
ITLN1	LRRC71	NBPF20	OR10R3P	PKMP1	RCSD1	RPL21P27
ITLN2	LY9	NBPF25P	OR10T1P	PLA2G4A	REG4	RPL22P5
IVL	LYSMD1	NBPF26	OR10T2	PLEKHO1	RFWD2	RPL22P6
IVNS1ABP	MAB21L3	NBPF7	OR10X1	PMF1	RFX5	RPL26P10
JTB	MAEL	NBPF8	OR10Z1	PMVK	RGL1	RPL26P11
KCNJ10	MAN1A2	NBPF9	OR13Z1P	PNRC2P1	RGS16	RPL26P12
KCNJ9	MARC1	NCF2	OR13Z2P	POGK	RGS4	RPL27AP2
KCNN3	MARC2	NCSTN	OR13Z3P	POGZ	RGS5	RPL27P2
KIAA0040	MARK1	NDUFAF4P4	OR2AQ1P	POLR3C	RGS8	RPL29P7
KIAA0907	MCL1	NDUFB1P2	OR6K1P	POLR3GL	RGSL1	RPL30P1
KIAA1614	MEF2AP1	NDUFS2	OR6K2	POU2F1	RHBG	RPL31P11
KIFAP3	MEF2D	NEFHP1	OR6K3	POU5F1P4	RIIAD1	RPL34P1
KIRREL	METTL11B	NES	OR6K4P	PPIAL4A	RIT1	RPL34P5
KLHDC9	METTL13	NGF	OR6K5P	PPIAL4C	RNA5SP55	RPL35AP7
KLHL20	METTL18	NHLH1	OR6K6	PPIAL4D	RNA5SP56	RPL39P11
KPRP	MEX3A	NHLH2	OR6N1	PPIAL4E	RNA5SP60	RPL4P2
KRT18P28	MGST3	NIT1	OR6N2	PPIAL4F	RNA5SP61	RPL4P3
KRT8P28	MIA3	NKAIN1P1	OR6P1	PPIAL4G	RNA5SP62	RPL5P5
KRT8P45	MLLT11	NME7	OR6Y1	PPOX	RNA5SP63	RPL6P2
KRTCAP2	MNDA	NMNAT1P2	OTUD7B	PRCC	RNA5SP64	RPL7AP15
LAMC1	MORF4L1P1	NMNAT2	OVAAL	PRDX6	RNA5SP65	RPL7AP19

Cfs1.3 cont.					
RPL7AP21	S100A7P2	SNORD74	TEX35	TRH-GTG1-3	TRV-CAC4-1
RPLP0P4	S100A8	SNORD75	THBS3	TRH-GTG1-4	TRV-CAC5-1
RPLP0P5	S100A9	SNORD76	THEM4	TRIM33	TRV-CAC8-1
RPLP1P3	SCAMP3	SNORD77	THEM5	TRIM45	TRX-CAT1-1
RPRD2	SCARNA3	SNORD78	TIPRL	TRIM46	TSACC
RPS10P6	SCARNA4	SNORD79	TLR5	TRK-CTT13-1	TSEN15
RPS10P8	SCNM1	SNORD80	TMCO1	TRK-CTT2-1	TSHB
RPS11P3	SCYL3	SNORD81	TMEM79	TRL-CAA6-1	TSPAN2
RPS13P1	SDCCAG3P2	SNRPEP10	TMOD4	TRL-CAG1-1	TSTD1
RPS14P2	SDHC	SNX27	TNFAIP8L2	TRL-CAG1-2	TTC24
RPS15AP12	SEC16B	SNX2P1	TNFSF18	TRL-CAG1-3	TTF2
RPS15AP9	SEC22B	SOAT1	TNFSF4	TRL-CAG1-4	TUFT1
RPS15P3	SELE	SONP1	TNN	TRL-CAG1-5	TXNIP
RPS17P6	SELENBP1	SPAG17	TNR	TRL-CAG1-6	UAP1
RPS18P4	SELL	SPRR1A	TOMM40L	TRMT1L	UBAP2L
RPS23P10	SELP	SPRR1B	TOP1P1	TRN-GTT1-1	UBE2D3P3
RPS23P9	SEMA4A	SPRR2A	TOR1AIP1	TRN-GTT11-2	UBE2Q1
RPS24P5	SEMA6C	SPRR2B	TOR1AIP2	TRN-GTT11-2	UBQLN4
RPS26P12	SERPINC1	SPRR2C	TOR3A	TRN-GTT12-1	UCK2
RPS26P16	SETDB1	SPRR2D	**TPM3**	TRN-GTT2-1	UFC1
RPS27	SETP10	SPRR2E	TPR	TRN-GTT2-2	UHMK1
RPS27AP6	SETP9	SPRR2F	TRD-GTC10-1	TRN-GTT22-1	UQCRBP2
RPS27P7	**SF3B4**	SPRR2G	TRD-GTC2-1	TRN-GTT23-1	USF1
RPS29P4	SFT2D2	SPRR3	TRD-GTC2-2	TRN-GTT3-1	USP21
RPS29P5	SH2D1B	SPRR4	TRD-GTC2-3	TRN-GTT3-2	VAMP4
RPS2P10	SH2D2A	**SPTA1**	TRD-GTC2-4	TRN-GTT6-1	VANGL1
RPS3AP10	SHC1	SPTLC1P4	TRD-GTC2-5	TRN-GTT7-1	VANGL2
RPS3AP12	SHCBP1L	SRGAP2B	TRE-CTC1-1	TRN-GTT7-1	VDAC1P4
RPS3AP8	SHE	SRGAP2C	TRE-CTC1-2	TRN-GTT8-1	VDAC1P9
RPS7P2	SIGLEC30P	SRGAP2D	TRE-CTC1-3	TRN-GTT9-2	VDAC2P3
RPSAP16	SIKE1	SSR2	TRE-CTC1-4	TRNAG-CCC	VHLL
RPSAP17	SLAMF1	STX6	TRE-CTC1-5	TRNAN-GUU	VPS25P1
RPSAP18	SLAMF6	SUCO	TRE-TTC10-1	TRNAN-GUU	VPS45
RPTN	SLAMF6P1	SUMO1P2	TRE-TTC14-1	TRNAN-GUU	VPS72
RRM2P2	SLAMF7	SUMO1P3	TRE-TTC4-2	TRNAN-GUU	VSIG8
RRNAD1	SLAMF8	SUSD4	TRE-TTC6-1	TRNAN-GUU	VTCN1
RUSC1	SLAMF9	SV2A	TRE-TTC7-1	TRNAQ-CUG	WARS2
RXFP4	SLC19A2	SWT1	TRF-GAA10-1	TRNAV-CAC	WDR3
RXRG	SLC22A15	SYCP1	TRF-GAA9-1	TRNAV-CAC	XCL1
S100A1	SLC25A38P1	SYT11	TRG-CCC6-1	TRNAV-CAC	XCL2
S100A10	SLC25A44	SYT6	TRG-GCC1-1	TRNAV-CAC	XPR1
S100A11	SLC27A3	TADA1	TRG-GCC1-2	TRP-AGG2-1	XRCC6P3
S100A12	SLC30A10	TAF1A	TRG-GCC1-3	TRP-CGG1-1	YPEL5P1
S100A13	SLC39A1	TAGLN2	TRG-GCC1-4	TRQ-CTG11-1	YY1AP1
S100A14	SLC4A1APP2	TARS2	TRG-GCC2-1	TRQ-CTG3-2	ZBTB37
S100A16	SLC50A1	TBX15	TRG-GCC4-1	TRQ-CTG4-1	ZBTB7B
S100A2	SLC9C2	TBX19	TRG-TCC2-1	TRQ-CTG4-2	ZC3H11B
S100A3	SMCP	TCEB1P20	TRG-TCC2-2	TRQ-CTG7-1	ZNF648
S100A4	SMG5	TCHH	TRG-TCC2-3	TRQ-CTG9-1	ZNF687
S100A5	SMG7	TCHHL1	TRG-TCC2-4	TRR-CCT6-2	ZNF697
S100A6	SNAPIN	TDRD10	TRG-TCC2-5	TRR-CCT7-1	
S100A7	SNORA36B	TDRD5	TRG-TCC2-6	TRR-CCT8-1	
S100A7A	SNORA80E	TDRKH	TRG-TCC4-1	TRR-TCT4-1	
S100A7L2	SNORD44	TEDDM1	TRH-GTG1-1	TRT-TGT2-1	
S100A7P1	SNORD47	TEDDM2P	TRH-GTG1-2	TRV-CAC1-1	

Cfs2.2					
A4GNT	ANKUB1	CP	GPR160	KRT18P34	OR7E21P
AADAC	ARGFX	CPA3	GPR171	KRT18P35	OR7E29P
AADACL2	**ARHGAP31**	CPB1	GPR79	KRT18P43	OR7E53P
AADACP1	ARHGEF26	CPHL1P	GPR87	KRT8P12	OR7E93P
ABHD10	ARL14	CPNE4	GRAMD1C	KRT8P13	OR7E97P
CCDC54	ARMC8	CSRP2P1	GRK7	KRT8P36	OSBPL11
CCDC58	ASTE1	CSTA	GSK3B	LRRIQ4	OTOL1
CCDC80	ATG3	DBR1	GSTO3P	LSAMP	P2RY1
CCNL1	ATP1B3	DDX50P2	GTF2E1	LXN	P2RY12
CD200	ATP2C1	DHX36	GTPBP8	MAATS1	P2RY13
EEF1A1P25	ATP5G1P3	DIRC2	GUCA1C	MARK2P17	P2RY14
EEF1GP4	ATP5LP5	DNAJB8	GYG1	MARK2P3	PA2G4P4
EEFSEC	ATP6V1A	DNAJC13	H1FOO	MARK2P6	PABPC1P10
EFCAB12	ATR	DPPA2	H1FX	MARK2P8	PAQR9
EFCC1	B3GALNT1	DPPA4	H3F3AP3	MARK3P3	PARP14
EGFEM1P	B3GAT3P1	**DRD3**	HACD2	MBD4	PARP15
HCLS1	B4GALT4	DTX3L	HMCES	MBNL1	PARP9
HEG1	BBX	DUBR	HMGB1P30	MCM2	PBX2P1
HGD	BCHE	DUTP1	HMGB3P13	MECOM	PCCB
HHLA2	BFSP2	DZIP1L	HMGB3P14	MED12L	PCOLCE2
HLTF	BOC	DZIP3	HMGN1P10	MEMO1P3	PDCD10
KY	BPESC1	EAF2	HMGN1P8	METTL15P1	PDIA5
LARP7P4	BRD7P2	EIF2A	HMGN1P9	MFSD1	PFN2
LEKR1	BTLA	EIF4BP8	HMGN2P13	MGLL	PHBP8
LRRC31	BZW1P2	EIF4E2P2	HMGN2P25	MLF1	PHC3
LRRC34	CASR	ENO1P3	HMGN2P26	MME	PHF5DP
LRRC58	CBX1P5	ENPP7P4	HNRNPA1P17	MORC1	PHLDB2
NPM1P29	CCDC14	EPHB1	HNRNPA1P20	MRAS	PIK3CB
NR1I2	CCDC191	ERICH6	HNRNPA1P23	MRE11B	PIK3R4
NUDT16	CD200R1	ESYT3	HNRNPA1P24	MRPL3	PISRT1
NUDT16P1	CD200R1L	FAIM	HPS3	MRPS22	PLA1A
NUP210P1	CD47	FAM162A	HSPA8P19	MSL2	PLCH1
NUP210P3	CD80	FAM86HP	HSPA8P9	MTAPP1	PLCXD2
POU5F1P6	CD86	FAM86JP	HSPBAP1	MTND3P7	PLOD2
PPIAP15	CD96	FBXO40	**IFT122**	MTND4P17	PLS1
PPM1L	CDV3	FKBP1AP4	IFT57	MUC13	PLSCR1
PPP2R3A	CEP63	FLJ22763	IFT80	MYH15	PLSCR2
PQLC2L	CEP70	**FOXL2**	IGSF10	MYLK	PLSCR4
PRKCI	CFAP100	FOXL2NB	IGSF11	MYNN	PLSCR5
ABTB1	CFAP44	FSTL1	IL12A	NAA50	PLXNA1
ACAD11	CHCHD6	FTH1P4	IL20RB	NAP1L1P3	PLXND1
ACAD9	CHST13	GAP43	ILDR1	NCK1	PODXL2
ACKR4	CHST2	GAPDHP39	IQCB1	NCK1-AS1	POGLUT1
ACPP	CLDN11	GAPDHP47	IQCJ	NDUFB4	POLQ
ACTG1P1	CLDN18	GATA2	ISY1	NEK11	POPDC2
ACTRT3	CLRN1	GCSAM	ITGB5	NIP7P2	PRR23A
ADCY5	CLSTN2	GFM1	KALRN	NMD3	PRR23B
ADPRH	CNBP	GK5	KBTBD12	NME9	PRR23C
AGTR1	COL6A4P2	GM2AP1	KCNAB1	NMNAT3	PSAT1P4
ALDH1L1	COL6A5	GMPS	KIAA1257	NPHP3	PSMC1P7
ALG1L	COL6A6	GOLGB1	KIAA1524	NPM1P17	PTMAP8
ALG1L15P	COMMD2	GOLIM4	KLF15	NPM1P28	PTX3
ALG1L2	COPB2	GP9	KLF3P2	OR7E100P	PVRL3
AMOTL2	COPG1	GPR149	KPNA1	OR7E129P	PXYLP1
ANAPC13	COX17	GPR156	KPNA4	OR7E130P	QTRTD1

Cfs2.2 cont.						
RAB43	RNY4P4	RPL7AP11	SDHDP3	SNORA58	TMED10P2	VN2R1P
RAB6B	ROPN1	RPL7AP24	SEC22A	SNORA7B	TMEM108	VPS26AP1
RAB7A	ROPN1B	RPL7L1P7	SEC61A1	SNRPCP11	TMEM14EP	WDR49
RABL3	RPL10P7	RPL7P15	SEC62	SNRPCP3	TMEM183B	WDR5B
RAD51AP1P1	RPL13P8	RPL7P16	SELT	SNRPCP8	TMEM39A	WWTR1
RAP2B	RPL15P6	RPL8P3	SEMA5B	SNX4	TMPRSS7	XRN1
RARRES1	RPL19P6	RPL9P15	SERP1	SOX14	TOMM22P6	YBX1P3
RASA2	RPL21P39	RPN1	SERPINI1	SPICE1	TOPBP1	YWHAQP6
RBP1	RPL21P42	RPS10P4	SERPINI2	SPSB4	TPRA1	ZBBX
RBP2	RPL21P43	RPS12P7	SETP11	SPTSSB	TPT1P3	ZBED2
RCC2P4	RPL21P71	RPS15AP16	SETP14	SRPRB	TRAT1	ZBTB20
RETNLB	RPL22P1	RPS17P10	SHOX2	SSR3	TRC-GCA6-1	ZBTB38
RFKP2	RPL23AP40	RPS17P9	SI	ST13P15	TRC-GCA9-1	ZDHHC23
RHO	RPL23AP41	RPS24P9	SIAH2	STAG1	TRH	ZIC1
RNA5SP137	RPL23AP42	RPS25P5	SIDT1	STXBP5L	TRIM42	ZIC4
RNA5SP138	RPL28P1	RPS26P21	SKIL	SUCLG2P1	TRIM59	ZNF148
RNA5SP139	RPL31P21	RPS26P22	SLC12A8	SUCNR1	TRPC1	ZNF80
RNA5SP141	RPL31P23	RPS27P12	SLC15A2	TAGLN3	TRV-AAC1-1	ZXDC
RNA5SP142	RPL32P3	RPS2P19	SLC25A36	TDGF1P6	TSC22D2	
RNA5SP143	RPL32P8	RPS3AP14	SLC33A1	TERC	TUSC7	
RNA5SP144	RPL32P9	RPS6P4	SLC35A5	TF	TXNRD3	
RNA5SP145	RPL34P9	RPSAP29	SLC35G2	TFDP2	TXNRD3NB	
RNA5SP146	RPL35AP10	RPSAP33	SLC41A3	TFP1	U2SURP	
RNF13	RPL35AP9	RSRC1	SLC7A14	TIGIT	UBA5	
RNF7	RPL38P1	RUVBL1	SLC9A9	TIMMDC1	UBQLN4P1	
RNU5E-8P	RPL39P5	RYK	SLC9C1	TIPARP	UMPS	
RNU7-32P	RPL6P7	SAMD7	SLCO2A1	TM4SF18	UPK1B	
RNU7-47P	RPL6P8	SCARNA7	SLITRK3	TM4SF4	UROC1	
RNU7-82P	RPL6P9	SCHIP1	SMC4	TMCC1	USF3	

Cfs2.3						
A4GNT	CCDC37-AS1	EEFSEC	HMGB3P13	MRAS	OR7E21P	RCC2P4
ABTB1	CDV3	EFCAB12	HMGB3P14	MRPL3	OR7E29P	**RHO**
ACAD11	CEP63	EFCC1	HMGN1P10	MRPS22	OR7E53P	RNA5SP137
ACAD9	CEP70	ENO1P3	HMGN1P9	MSL2	OR7E93P	RNA5SP138
ACKR4	CFAP100	ENPP7P4	HSPA8P19	MUC13	OR7E97P	RNA5SP139
ACPP	CHCHD6	EPHB1	HSPA8P9	MYLK	OSBPL11	RNA5SP141
ACTG1P1	CHST13	ESYT3	**IFT122**	MYLK-AS1	PCCB	RNA5SP142
ADCY5	CLDN18	FAIM	IL20RB	MYLK-AS2	PIK3CB	RNY4P4
ALDH1L1	CLSTN2	FAM86HP	ISY1	NCK1	PIK3R4	ROPN1
ALDH1L1-AS1	CLSTN2-AS1	FAM86JP	ISY1-RAB43	NCK1-AS1	PISRT1	ROPN1B
ALDH1L1-AS2	CNBP	**FOXL2**	ITGB5	NEK11	PLXNA1	RPL23AP40
ALG1L	COL6A4P2	FOXL2NB	KALRN	NIP7P2	PLXND1	RPL23AP41
ALG1L2	COL6A5	FTH1P4	KBTBD12	NME9	PODXL2	RPL31P23
AMOTL2	COL6A6	GAPDHP39	KIAA1257	NMNAT3	POU5F1P6	RPL32P3
ANAPC13	COPB2	GATA2	KLF15	NPHP3	PPP2R3A	RPL39P5
ARMC8	COPG1	GATA2-AS1	KRT8P36	NPHP3-ACAD11	PRR23A	RPL7L1P7
ASTE1	CPNE4	GP9	KY	NPHP3-AS1	PRR23B	RPL7P15
ATP2C1	DBR1	GSTO3P	MARK2P17	NPM1P17	PRR23C	RPL7P16
ATP5G1P3	DNAJB8	H1FOO	MARK2P3	NUDT16	RAB43	RPN1
BCL2L12P1	DNAJB8-AS1	H1FX	MARK2P6	NUDT16P1	RAB6B	RPS15AP16
BFSP2	DNAJC13	H1FX-AS1	MARK2P8	NUP210P1	RAB7A	RPS17P9
BFSP2-AS1	DUTP1	HACD2	MARK3P3	NUP210P3	RAD51AP1P1	RPS24P9
BPESC1	DZIP1L	HEG1	MBD4	OR7E129P	RBP1	RPS26P22
CCDC14	EEF1A1P25	HMCES	MCM2	OR7E130P	RBP2	RPS27P12

Cfs2.3 cont.					
RPS3AP14	SLC25A36	SNRPCP8	TF	TOPBP1	TXNRD3NB
RUVBL1	SLC35G2	SNX4	TFP1	TPRA1	UBA5
RUVBL1-AS1	SLC41A3	SOX14	TMCC1	TRC-GCA6-1	UMPS
RYK	SLCO2A1	SPSB4	TMCC1-AS1	TRC-GCA9-1	UROC1
SEC22A	SNORA58	SRPRB	TMED10P2	TRH	ZNF148
SEC61A1	SNORA7B	STAG1	TMEM108	TRIM42	ZXDC
SLC12A8	SNRPCP11	TDGF1P6	TMEM108-AS1	TXNRD3	

Cfs2.4					
AADAC	CAMP	DHX30	GPX1	KIAA1143	MST1R
AADACL2	CCDC12	DHX36	GRK7	KIF15	MTAPP1
AADACL2-AS1	CCDC13	DLEC1	GRM2	KIF9	MUSTN1
AADACP1	CCDC13-AS1	DLEC1P1	GYG1	KIF9-AS1	MYD88
ABHD14A	CCDC36	DNAH1	HEMK1	KLF3P2	MYL3
ABHD14A-ACY1	CCDC51	DOCK3	HHATL	KLHDC8B	MYRIP
ABHD14B	CCDC71	DSTNP4	HIGD1A	KLHL18	NAT6
ABHD5	CCK	DUSP7	HLTF	KLHL40	NBEAL2
ACAA1	CCNL1	EEF1A1P24	HLTF-AS1	KPNA4	NBPF21P
ACKR2	CCR1	EEF1GP3	HMGB1P30	KRBOX1	NCKIPSD
ACTBP13	CCR2	EEF1GP4	HMGN2P13	KRBOX1-AS1	NDUFAF3
ACTR8	CCR3	EI24P3	HMGN2P24	KRT18P34	NDUFAF4P3
ACVR2B	CCR5	EIF1B	HMGN2P25	KRT18P35	NDUFB1P1
ACVR2B-AS1	CCR8	ENTPD3-AS1	HNRNPA1P20	KRT8P12	NEK4
ACY1	CCR9	EPM2AIP1	HNRNPA1P21	KRT8P18	NFU1P1
ADAD1P1	CCRL2	ERICH6	HNRNPA1P22	LAMB2	NICN1
AGTR1	CDC25A	ERICH6-AS1	HNRNPA1P24	LAMB2P1	NISCH
ALAS1	CDCP1	EXOG	HNRNPA1P77	LARP7P4	NKTR
ALDOAP1	CDHR4	EXOSC7	HPS3	LARS2	NMD3
ALG1L15P	CELSR3	FAM198A	HSPD1P6	LARS2-AS1	NME6
ALS2CL	CELSR3-AS1	FAM212A	IGSF10	LEKR1	NPM1P28
AMIGO3	**CHDH**	FBXW12	IL12A	LIMD1	NPM1P29
AMT	CHST2	FECHP1	IL12A-AS1	LIMD1-AS1	NPRL2
ANKUB1	CISH	FKBP1AP4	IL17RB	LRRC2	NRADDP
ANO10	CLEC3B	FLT1P1	IMPDH2	LRRC2-AS1	NRBF2P2
APEH	CLRN1	FYCO1	IP6K1	LRRFIP2	NT5DC2
ARHGEF26	CLRN1-AS1	GAPDHP47	IP6K2	LSMEM2	OTOL1
ARHGEF26-AS1	COL7A1	GEMIN2P2	IQCF1	MAP4	OXSR1
ARIH2	COMMD2	GFM1	IQCF2	MAPKAPK3	P2RY1
ARIH2OS	CP	GK5	IQCF3	MBNL1	P2RY12
ARL14	CPA3	GLT8D1	IQCF4	MBNL1-AS1	P2RY13
ARPP21	CPB1	GLYCTK	IQCF5	MED12L	P2RY14
ATP1B3	CPHL1P	GLYCTK-AS1	IQCF5-AS1	METTL15P1	P4HTM
ATP5LP5	CSPG5	GM2AP1	IQCF6	MFSD1	PA2G4P4
ATP6V0E1P2	CSRNP1	GMPPB	IQCJ	MIRLET7G	PBX2P1
ATR	CTDSPL	GMPS	IQCJ-SCHIP1	MLF1	PCBP4
ATRIP	CTNNB1	GNAI2	IQCJ-SCHIP1-AS1	MLH1	PCOLCE2
B3GALNT1	CX3CR1	GNAT1	ITGA9	MME	PFKFB4
B3GAT3P1	CXCR6	GNL3	ITGA9-AS1	MOBP	PFN2
BAP1	CYB561D2	GOLGA4	ITIH1	MON1A	PGAM1P3
BRD7P2	CYP8B1	GORASP1	ITIH3	MPRIPP1	PHF5EP
BSN	DAG1	GPR149	ITIH4	MRE11B	PHF7
BSN-AS2	DALRD3	GPR171	ITIH4-AS1	MRPL57P3	PLCD1
CACNA1D	DCLK3	GPR62	KCNAB1	MRPS18AP1	PLCH1
CACNA2D2	DCP1A	GPR79	KCNAB1-AS1	MRPS31P1	PLCH1-AS1
CAMKV	DDX50P2	GPR87	KCNAB1-AS2	MST1	PLCH1-AS2

Cfs2.4 cont.					
PLOD2	RNA5SP144	RPL9P15	SLC9A9	TM4SF4	VN2R1P
PLS1	RNA5SP145	RPS12P7	SLC9A9-AS1	TMA7	VPRBP
PLSCR1	RNA5SP146	RPS16P4	SMARCC1	TMEM110	VPS26BP1
PLSCR2	RNF123	RPS17P10	SMC4	TMEM115	WDR48
PLSCR4	RNF13	RPS24P8	SMIM4	TMEM14EP	WDR6
PLSCR5	RNF7	RPS25P4	SNORA6	TMEM158	WDR82
PLXNB1	RNU5B-2P	RPS25P5	SNORA62	TMEM183B	WWTR1
POC1A	RNU5B-3P	RPS27P4	SNORD13P3	TMEM42	XCR1
POMGNT2	RNU6ATAC4P	RPS2P19	SNORD19	TMEM89	XIRP1
PPIAP18	RNU7-47P	RPS6P4	SNORD19B	TMIE	XRN1
PPM1L	RNU7-73P	SALL4P6	SNORD69	TNNC1	XYLB
PPM1M	RNU7-82P	SCAP	SNRK	TOMM22P6	YWHAQP6
PPP2R2DP1	RPL12P44	SCARNA7	SNRK-AS1	TOPAZ1	ZBTB38
PPP2R5CP	RPL14	SCHIP1	SNRPCP3	TPMTP2	ZBTB47
PQLC2L	RPL15P6	SCN10A	SNRPFP4	TPT1P3	ZDHHC3
PRADC1P1	RPL17P16	SCN11A	SOCS5P3	TRAIP	ZIC1
PRKAR2A	RPL18AP7	SCN5A	SPCS1	TRAK1	ZIC4
PRKCD	RPL18AP9	SDHDP4	SPINK8	TRANK1	ZKSCAN7
PRSS42	RPL19P6	SEC22C	SPSB4	TREX1	ZMYND10
PRSS43	RPL21P135	SELT	SPTSSB	TRIM59	ZNF197
PRSS45	RPL21P39	SEMA3B	SS18L2	TRPC1	ZNF35
PRSS46	RPL21P42	SEMA3F	SSR3	TRR-ACG2-1	ZNF445
PRSS50	RPL21P71	SEMA3G	ST13P14	TSC22D2	ZNF501
PSMC1P7	RPL23AP42	SERBP1P3	ST13P15	TTC21A	ZNF502
PTH1R	RPL29	SERP1	STAB1	TUBAP3	ZNF589
PTPN23	RPL29P11	SETD2	STAC	TUSC2	ZNF619
PTX3	RPL31P21	SETP11	SUCLG2P1	TWF2	ZNF620
PXYLP1	RPL32P8	SETP14	SUCNR1	U2SURP	ZNF621
QARS	RPL32P9	SFMBT1	TCAIM	UBA7	ZNF652P1
QRICH1	RPL35AP10	SHISA5	TCEA1P2	UBE2D3P2	ZNF660
RAD54L2	RPL35AP8	SHOX2	TCTA	UBE2FP1	ZNF662
RAP2B	RPL35AP9	SIAH2	**TDGF1**	UBQLN4P1	ZNF852
RARRES1	RPL36AP17	SLC22A13	TEX264	UCN2	
RASA2	RPL36P20	SLC22A14	TFDP2	ULK4	
RASSF1	RPL38P1	SLC25A20	TGM4	UQCRC1	
RBM15B	RPL5P10	SLC25A36	TIPARP	UQCRC2P1	
RBM5	RPL6P7	SLC25A38	TIPARP-AS1	USP19	
RBM5-AS1	RPL6P8	SLC26A6	TKT	USP4	
RBM6	RPL6P9	SLC33A1	TLR9	VEPH1	
RNA5SP132	RPL7AP24	SLC38A3	TM4SF1	VILL	
RNA5SP143	RPL8P3	SLC6A20	TM4SF18	VIPR1	

Cfs3.1					
ABCA13	ADAMTS1	AK3P3	ANKRD30BP2	ARAFP2	ATP5F1P2
ABCB1	ADAMTS5	**AKAP9**	ANKRD61	ARAFP3	ATP5J
ABCB4	ADAP1	ALG1L5P	ANLN	ARF1P1	ATP5J2
ABCB5	ADCY1	ALKBH4	AOAH	ARL4A	ATP5J2-PTCD1
ABCC13	ADCYAP1R1	AMPH	AOAH-IT1	ARMC10	ATP5J2LP
ABCF2P2	AEBP1	AMZ1	AP1S1	ARPC1A	ATP5O
ABHD11	AGFG2	ANKIB1	AP4M1	ARPC1B	ATXN7L1
ABHD11-AS1	AGMO	ANKMY2	AP5Z1	ASB4	AUTS2
ACHE	AGR2	ANKRD20A11P	APP	ASL	AVL9
ACTB	AGR3	ANKRD20A16P	APTR	ASNS	AZGP1
ACTL6B	AHR	ANKRD20A18P	AQP1	ASNSP2	AZGP1P1
ADAM22	AIMP2	ANKRD30BP1	ARAFP1	ASS1P11	AZGP1P2

Cfs3.1 cont.					
BACH1	CDC27P11	CTB-30L5	DSCR10	FAM185A	GLCCI1
BACH1-IT2	CDC27P9	CUX1	DSCR3	FAM185BP	**GLI3**
BAGE2	CDC42P2	CXADR	DSCR4	FAM188B	GNA12
BAIAP2L1	CDCA7L	CXADRP1	DSCR8	FAM200A	GNAI1
BAZ1B	CDHR3	CYCS	DSCR9	FAM207CP	GNAT3
BBS9	CDK13	CYCSP18	DTX2	FAM20C	GNB2
BCAP29	CDK14	CYCSP41	DTX2P1	FAM220A	GNG11
BCL7B	CDK6	CYCSP42	DUS4L	FAM221A	GNGT1
BET1	CFAP69	CYP2W1	DYNC1I1	FAM86LP	GNL2P1
BHLHA15	CH507-145C22	CYP3A4	DYNLL1P7	FBXL13	GPC2
BLVRA	CH507-42P11	CYP3A43	DYRK1A	FBXL18	GPER1
BMPER	CH507-9B2	CYP3A5	EEF1A1P1	FBXO24	GPNMB
BRAT1	CHAF1B	CYP3A51P	EEF1A1P26	FBXW11P1	GPR141
BRI3	CHCHD2	CYP3A7	EEF1A1P27	FCF1P1	GPR146
BRWD1	CHCHD4P1	CYP3A7	EEF1A1P28	FDPSP2	GPR22
BRWD1-AS1	CHN2	CYP3AP2	EEF1A1P6	FDPSP6	GPX1P2
BRWD1-IT2	CHODL	CYP4F29P	EEF1DP4	FDPSP7	GRAMD4P1
BTF3L4P1	CHODL-AS1	CYP51A1	EEPD1	FDX1P2	GRB10
BTF3P6	CHST12	CYP51A1-AS1	EFCAB10	FEM1AP1	GRID2IP
BTG3	CICP11	CYTH3	EGFR	FERD3L	GRIFIN
BUD31	CICP12	CYYR1	EGFR-AS1	FGF7P2	GRIK1
BZW2	CICP17	CYYR1-AS1	EIF2AK1	FGL2	GRIK1-AS1
C1GALT1	CICP20	D21S2088E	EIF3B	FIGNL1	GRIK1-AS2
C1QBPP1	CICP22	DAGLB	EIF3FP1	FIS1	GRM3
CACNA2D1	CICP28	DBF4	EIF4A1P1	FKBP14	GRPEL2P3
CALCR	CICP8	DBNL	EIF4A1P13	FKBP6	GS1-124K5
CALM1P2	CLDN12	DCAF13P1	EIF4BP6	FKBP9	GS1-124K5
CALN1	CLDN14	DDC	EIF4EP4	FKBP9P1	GS1-259H13
CAMK2B	CLDN15	DDC-AS1	EIF4H	FLJ20712	GS1-278J22
CARD11	CLDN17	DDX43P2	EIF4HP1	FOXK1	GSAP
CASD1	CLDN3	DDX56	ELDR	FSCN1	GTF2I
CBR1	CLDN4	DFNA5	ELFN1	FTLP15	GTF2IP1
CBR3	CLDN8	DGAT2L7P	ELFN1-AS1	FTSJ2	GTF2IP2
CBR3-AS1	CLIC6	DGKB	ELK1P1	FZD1	GTF2IP4
CBSL	CLIP2	DKFZp434L192	ELMO1	FZD9	GTF2IP5
CBX3	CLK2P1	DKFZP586I1420	ELMO1-AS1	GABPA	GTF2IRD1
CCDC126	CLUHP7	**DLX5**	ELN	GABPAP	GTF2IRD1P1
CCDC129	CNN2P7	**DLX6**	EPDR1	GAL3ST4	GTF2IRD2
CCDC146	CNPY4	DLX6-AS1	EPHB4	GAPDHP14	GTF2IRD2B
CCDC71L	COA1	DMTF1	EPO	GAPDHP16	GTF2IRD2P1
CCL24	COBL	DNAAF5	EPS15P1	GAPDHP68	GTF3AP5
CCL26	COG5	DNAH11	ERG	GARS	GTPBP10
CCM2	**COL1A2**	DNAJC2	ERLEC1P1	GART	GUSB
CCNB2P1	COL26A1	DNAJC28	ERV3-1	GATAD1	GUSBP10
CCNJP1	COL28A1	DNAJC30	ERVW-1	GATS	GUSBP12
CCT6A	COPS6	DONSON	ETS2	GATSL2	GUSBP6
CCT6P1	COX19	DOPEY2	ETV1	GBAS	GXYLT1P2
CCT6P3	CPSF4	DPRXP5	EVA1C	GCK	H2AFV
CCT8	CPVL	DPY19L1	EVX1	GCNT1P5	HAUS6P1
CCZ1	CRCP	DPY19L1P1	EVX1-AS	GDI2P1	HBP1
CCZ1B	CREB5	DPY19L1P2	EXOSC3P1	GET4	HDAC9
CD36	CRHR2	DPY19L2P1	EZH2P1	GGCT	HECW1
CDC14BL	CROT	DPY19L2P2	FAM126A	GHRHR	HECW1-IT1
CDC14C	CRYZL1	DPY19L2P3	FAM133B	GIGYF1	HEPACAM2
CDC27P10	CRYZP1	DPY19L2P4	FAM183BP	GJC3	HERPUD2

Cfs3.1 cont.					
HGF	IL10RB-AS1	KRTAP19-9P	MBLAC1	NAMPT	OR4K12P
HIBADH	IL6	KRTAP20-1	MCM7	NANOGP4	OR7E136P
HIGD1AP7	INHBA	KRTAP20-2	MDH2	NAPEPLD	OR7E23P
HINT1P2	INHBA-AS1	KRTAP20-3	MEMO1P1	NAT16	OR7E38P
HIP1	INMT	KRTAP20-4	MEOX2	NCAM2	OR7E39P
HLCS	INMT-FAM188B	KRTAP21-1	MEOX2-AS1	NCAPD2P1	OR7E59P
HMGB3P20	INTS1	KRTAP21-2	MEPCE	NCF1	OR7E7P
HMGB3P21	INTS4P1	KRTAP21-3	METTL21AP1	NCF1B	ORAI2
HMGN1	INTS4P2	KRTAP21-4P	MGC16142	NCF1C	ORC5
HMGN1P19	IQCE	KRTAP22-1	MGC39584	NCOR1P3	OSBPL3
HMGN1P2	IRS3P	KRTAP22-2	MGC72080	NCSTNP1	OSBPL9P6
HMGN2P11	ISPD	KRTAP23-1	MICALL2	NDUFA4	PAPOLB
HMGN2P30	ISPD-AS1	KRTAP24-1	MIOS	NDUFAF4P2	PAXBP1
HNRNPA1P8	ITGB8	KRTAP25-1	MIS18A	NECAP1P1	PAXBP1-AS1
HNRNPA1P9	ITSN1	KRTAP26-1	MLXIPL	NEK4P1	PCBP2P1
HNRNPA2B1	JAM2	KRTAP27-1	MMD2	NEUROD6	PCLO
HNRNPCP7	JAZF1	KRTAP6-1	MOGAT3	NF1P3	PCMTD1P3
HOTAIRM1	JAZF1-AS1	KRTAP6-2	MORC3	NFE2L3	PCOLCE
HOTTIP	KBTBD2	KRTAP6-3	MOSPD3	NFE4	PCOLCE-AS1
HOXA-AS2	KCCAT333	KRTAP7-1	MPLKIP	NHP2P2	PDAP1
HOXA-AS3	KCNE1	KRTAP8-1	MPP6	NIPA2P1	PDE1C
HOXA1	KCNE2	KRTAP8-2P	MRAP	NIPA2P3	PDGFA
HOXA10	KCNJ15	KRTAP8-3P	MRPL20P1	NMD3P1	PDK4
HOXA10-AS	KCNJ6	LAMTOR4	MRPL32	NMD3P2	PEG10
HOXA10-HOXA9	KCTD7	LANCL2	MRPL39	NME8	PER4
HOXA11	KDELR2	LAT2	MRPL42P4	NMTRQ-TTG13-1	PEX1
HOXA11-AS	KIAA0087	LCA5L	MRPS17	NOD1	PGAM2
HOXA13	KIAA0895	LFNG	MRPS23P1	NPC1L1	PHBP15
HOXA2	KIAA1324L	LHFPL3	MRPS24	NPM1P11	PHF14
HOXA3	KLHL7	LHFPL3-AS1	MRPS6	NPM1P13	PHKG1
HOXA4	KLHL7-AS1	LHFPL3-AS2	MSANTD2P1	NPM1P18	PHKG1P1
HOXA5	KMT2E	LIMK1	MTCO1P1	NPSR1	PHKG1P2
HOXA6	KMT2E-AS1	LIPI	MTERF1	NPSR1-AS1	PHKG1P4
HOXA7	KPNA7	LMTK2	MTHFD2P5	NPTX2	PHTF2
HOXA9	KRIT1	LRCH4	MTND1P2	NPVF	PIGP
HPVC1	KRT18P2	LRRC17	MTND1P4	NPY	PIK3CG
HRAT92	KRT8P20	LRRC72	MTND2P1	NRIP1	PILRA
HSPA13	KRTAP11-1	LRRD1	MTND2P4	NSUN5	PILRB
HSPA8P16	KRTAP13-1	LRWD1	MTND2P6	NSUN5P1	PKD1L1
HSPA8P8	KRTAP13-2	LSM5	MTND3P2	NSUN5P2	PLEKHA8
HSPB1	KRTAP13-3	LTN1	MTND4P2	NT5C3A	**PLOD3**
HSPD1P7	KRTAP13-4	MACC1	MTND4P3	NUDCD3	PMPCB
HUNK	KRTAP13-5P	MACC1-AS1	MTND4P5	NUDT1	PMS2
HUS1	KRTAP13-6P	MAD1L1	MTND5P6	NUPL2	PMS2CL
ICA1	KRTAP15-1	MAFK	MTND5P7	NUPR2	PMS2P1
IFNAR1	KRTAP19-1	MAGI2	MTURN	NXPH1	PMS2P10
IFNAR2	KRTAP19-10P	MAGI2-AS2	MUC12	NYAP1	PMS2P12
IFNGR2	KRTAP19-11P	MAGI2-AS3	MUC17	OCM	PMS2P2
IFT22	KRTAP19-2	MALSU1	MUC3A	OCM2	PMS2P3
IGF2BP3	KRTAP19-3	MAP3K7CL	MYH16	OGDH	PMS2P4
IGFBP1	KRTAP19-4	MAPK6PS2	MYL10	OLIG1	PMS2P5
IGFBP3	KRTAP19-5	MARCKSP1	MYL7	OLIG2	PMS2P6
IGHV1OR21-1	KRTAP19-6	MARK2P10	MYO1G	OR10AH1P	PMS2P7
IKZF1	KRTAP19-7	MARK2P13	N6AMT1	OR2AE1	PMS2P8
IL10RB	KRTAP19-8	MARK2P7	NACAD	OR4K11P	PMS2P9

Cfs3.1 cont.						
POLD2	RAD23BLP	RP9	RPS10P14	SEMA3A	SNX10	STK17A
POLM	RAD23BP2	RP9P	RPS17P13	SEMA3C	SNX13	STK31
POLR2CP	RADIL	RPA3	RPS20P1	SEMA3D	SNX18P10	STX1A
POLR2J	RALA	RPL10P1	RPS26P1	SEMA3E	SNX18P11	STYXL1
POLR2J2	RAMP3	RPL10P11	RPS26P30	SEPHS1P1	SNX18P12	SUGCT
POLR2J3	RAPGEF5	RPL12P10	RPS26P32	SEPT14	SNX18P13	SUMF2
POLR2J4	RASA4	RPL12P9	RPS26P33	SEPT7	SNX19P1	SUMO2P3
POM121	RASA4B	RPL13AP16	RPS26P5	SEPT7-AS1	SNX2P2	SUN1
POM121B	RASA4CP	RPL13AP17	RPS27P16	SEPT7P2	SNX8	SUN3
POM121C	RASA4DP	RPL13AP7	RPS27P17	SEPT7P3	SOCS5P1	SYNJ1
POM121L12	RBAK	RPL18AP10	RPS28P6	SEPT7P4	**SOD1**	SYPL1
POMZP3	RBAK-RBAKDN	RPL19P12	RPS29P14	SEPT7P5	SON	TAC1
PON1	RBAKDN	RPL21P72	RPS29P15	SERPINE1	SOSTDC1	TAF6
PON2	RBM11	RPL21P74	RPS29P16	SETD4	SP4	TARP
PON3	RBM22P3	RPL21P75	RPS2P30	SFRP4	SP8	TAS2R2P
POP7	RBM48	RPL22P16	RPS2P32	**SGCE**	SPATA20P1	TAX1BP1
POR	RBMX2P1	RPL23AP12	RPS3AP1	SGOL1P2	SPDYE1	TBL2
POTED	RBMX2P4	RPL23AP3	RPS3AP25	SH2B2	SPDYE10P	TBRG4
POU6F2	RBPMSLP	RPL23AP51	RPS3AP26	SH3BGR	SPDYE11	TBX20
POU6F2-AS1	RCAN1	RPL23AP52	RPS3AP29	SHFM1	SPDYE12P	TCP10L
POU6F2-AS2	RELN	RPL23P2	RPS5P2	SIM2	SPDYE13P	TCP1P1
PPIA	RFC2	RPL23P7	RPS5P3	SKAP2	SPDYE14P	TECPR1
PPIAP1	RHBDD2	RPL23P8	RPS9P1	SKP1P1	SPDYE15P	TEKT4P2
PPIAP22	RHOT1P2	RPL26P21	RPSAP46	SLC12A9	SPDYE16	TERF1P1
PPP1R14BP4	RIMKLBP1	RPL31P34	RPSAP64	SLC25A13	SPDYE17	TFAMP1
PPP1R17	RINT1	RPL31P35	RPSAP68	SLC25A15P4	SPDYE18	TFPI2
PPP1R2P2	RIPPLY3	RPL31P38	RSBN1L	SLC25A1P2	SPDYE19P	**TFR2**
PPP1R35	RN7SL7P	RPL32P18	RSL24D1P3	SLC25A1P3	SPDYE2	THSD7A
PPP1R9A	RN7SL8P	RPL34P3	RSPH10B	SLC25A40	SPDYE21P	THUMPD1P1
PPP6R2P1	RNA5SP227	RPL35P4	RSPH10B2	SLC25A5P3	SPDYE2B	THUMPD3P1
PRKAR1B	RNA5SP228	RPL35P5	RUNDC3B	SLC25A5P5	SPDYE3	TIAM1
PRKAR2B	RNA5SP229	RPL36AP26	**RUNX1**	SLC26A5	SPDYE5	TIMM9P2
PRKRIP1	RNA5SP230	RPL36AP27	RUNX1-IT1	SLC29A4	SPDYE6	TMED4
PRPS1L1	RNA5SP231	RPL36AP29	RWDD2B	SLC29A4P1	SPDYE7P	TMEM106B
PRR15	RNA5SP232	RPL36P12	RWDD4P1	SLC29A4P2	SPDYE8P	TMEM120A
PSMA2	RNA5SP233	RPL37AP6	RWDD4P2	SLC5A3	SPDYE9P	TMEM130
PSMC1P2	RNA5SP234	RPL37P3	S100A11P1	SLC6A6P1	SRI	TMEM184A
PSMC2	RNA5SP235	RPL37P4	S100A11P2	SMIM11A	SRPK2	TMEM196
PSMD4P1	RNA5SP236	RPL39P23	SAMD9	SMIM11B	SRRM3	TMEM243
PSMG1	RNA5SP488	RPL39P40	SAMD9L	SMURF1	SRRT	TMEM248
PSMG3	RNA5SP489	RPL3P1	SAMSN1	SNHG15	SRSF9P1	TMEM50B
PSMG3-AS1	RNA5SP490	RPL6P20	SAMSN1-AS1	SNORA14A	SSC4D	TMEM60
PSPH	RNA5SP491	RPL6P21	SAP25	SNORA15	STAG3	TMPRSS15
PSPHP1	RNF138P2	RPL7AP38	SAPCD2P1	SNORA22	STAG3L1	TMSB4XP3
PTCD1	RNF216	RPL7AP39	SAPCD2P2	SNORA5A	STAG3L2	TNRC18
PTP4A1P3	RNF216-IT1	RPL7AP40	SAPCD2P3	SNORA5B	STAG3L3	TNRC18P2
PTPN12	RNF216P1	RPL7AP41	SAPCD2P4	SNORA5C	STAG3L4	TNRC18P3
PURB	RNF6P1	RPL7AP43	SBDS	SNORA80A	STAG3L5P	TNS3
PUS7	RNGTTP1	RPL7L1P2	SBDSP1	SNORA9	STAG3L5P	TOMM7
PVRIG	RNMTL1P2	RPL7L1P3	SCAF4	SNORD13P2	STARD3NL	TP53TG1
PVRIG2P	RNU1-14P	RPL7P30	SCIN	SNORD93	STEAP1	TPM3P4
RABGEF1	RNU1-15P	RPL7P31	SCRN1	SNRPBP1	STEAP1B	TPST1
RAC1	RNU6-10P	RPL7P60	SDHAF3	SNRPCP19	STEAP2	TPT1P1
RAC1P9	RNU7-35P	RPL8P2	SDK1	SNRPCP9	STEAP2-AS1	TPT1P7
RAD17P1	RNU7-76P	RPL9P19	SEC61G	SNRPGP13	STEAP4	TPTE

Cfs3.1 cont.						
TRA2A	TRGVB	**TWIST1**	VKORC1L1	VN2R20P	ZASP	ZNF716
TRG	TRIL	TWISTNB	VN1R109P	VOPP1	ZCWPW1	ZNF727
TRG-AS1	TRIM4	TYW1	VN1R24P	VPS37D	ZDHHC4	ZNF733P
TRG-GCC1-5	TRIM50	TYW1B	VN1R25P	VPS41	ZFAND2A	ZNF734P
TRGC1	TRIM56	U2AF1L5	VN1R26P	VPS50	ZKSCAN1	ZNF735
TRGC2	TRIM60P16	UBA52P1	VN1R27P	VSTM2A	ZKSCAN5	ZNF736
TRGJ1	TRIM60P17	UBE2D4	VN1R28P	VSTM2A-OT1	ZMIZ2	ZNF789
TRGJ2	TRIM60P18	UBE3AP2	VN1R29P	VWC2	ZNF107	ZNF804B
TRGJP	TRIM73	UFSP1	VN1R30P	VWDE	ZNF114P1	ZNF815P
TRGJP1	TRIM74	UMAD1	VN1R31P	WBSCR16	ZNF117	ZNF853
TRGJP2	TRIP6	UNC93B2	VN1R32P	WBSCR17	ZNF12	ZNF890P
TRGV1	TRRAP	UNCX	VN1R33P	WBSCR22	ZNF138	ZNF90P3
TRGV10	TRW-CCA5-1	UPK3BL	VN1R34P	WBSCR27	ZNF273	ZNF92
TRGV11	TSC22D4	UPP1	VN1R35P	WBSCR28	ZNF299P	ZNHIT1
TRGV2	TSL	URB1	VN1R36P	WI2-2373I1	ZNF3	ZNRF2
TRGV3	TSPAN13	URB1-AS1	VN1R37P	WIPF3	ZNF316	ZNRF2P1
TRGV4	TTC3	URGCP	VN1R38P	WIPI2	ZNF394	ZNRF2P2
TRGV5	TTC3-AS1	URGCP-MRPS24	VN1R39P	WRB	ZNF479	ZP3
TRGV5P	TTC4P1	USF1P1	VN1R40P	YAE1D1	ZNF619P1	ZPBP
TRGV6	TTYH3	USP16	VN1R41P	YBX1P2	ZNF655	ZPBP
TRGV7	TUBAP	USP25	VN1R42P	YKT6	ZNF679	ZSCAN21
TRGV8	TUBBP6	USP42	VN1R43P	YWHAEP1	ZNF680	ZSCAN25
TRGV9	TUBG1P	VDAC2P1	VN1R7P	YWHAG	ZNF680P1	
TRGVA	TVP23CP1	VGF	VN1R8P	ZAN	ZNF713	

Cfs3.2						
AASS	AOAH	AZGP1P2	CBLL1	CHCHD3	COPG2	CYP3A51P
ABCA13	AOAH-IT1	BAIAP2L1	CBX3	CHCHD4P1	COPG2IT1	CYP3A7
ABCB1	AP1S1	BANF1P5	CCDC126	CHN2	COPS6	CYP3A7
ABCB4	AP4M1	BAZ1B	CCDC129	CHRM2	COX5BP3	CYP3AP2
ABCF2P2	APTR	BBS9	CCDC136	CICP11	CPA1	CYP51A1
ABHD11	AQP1	BCAP29	CCDC146	CICP12	CPA2	CYP51A1-AS1
ABHD11-AS1	ARAFP1	BCL7B	CCDC71L	CICP14	CPA4	DBF4
ACHE	ARAFP2	BET1	CCL24	CICP17	CPA5	DBNL
ACTL6B	ARAFP3	BHLHA15	CCL26	CICP20	CPED1	DCAF13P1
ADAM22	ARF1P1	BLVRA	CCM2	CICP22	CPSF4	DDC
ADCK2	ARF5	BMPER	CCNJP1	CICP28	CPVL	DDC-AS1
ADCY1	ARMC10	BPGM	CCT4P1	CICP8	CRCP	DDX43P2
ADCYAP1R1	ARPC1A	**BRAF**	CCT6A	CLCN1	CREB3L2	DDX56
AEBP1	ARPC1B	BRI3	CCT6P1	CLDN12	CREB5	DENND2A
AGBL3	ASB15	BUB3P1	CCT6P3	CLDN15	CRHR2	DFNA5
AGFG2	ASB4	BUD31	CD36	CLDN3	CROT	DGAT2L7P
AGK	ASL	CACNA2D1	CDC14BL	CLDN4	CRYZP1	DGKI
AHCYL2	ASNS	CADPS2	CDC14C	CLEC2L	CTAGE15	DLD
AK3P3	ASZ1	CALCR	CDC26P1	CLEC5A	CTAGE6	DLX5
AKAP9	ATP5F1P2	CALD1	CDC42P2	CLIP2	CTB-30L5	DLX6
AKR1B1	ATP5J2	CALM1P2	CDCA7L	CLK2P1	CTTNBP2	DLX6-AS1
AKR1B10	ATP5J2-PTCD1	CALN1	CDHR3	CLUHP7	CUX1	DMTF1
AKR1B15	ATP6V0A4	CALU	CDK13	CNOT4	CYCS	DNAH11
AKR1D1	ATP6V1F	CAMK2B	CDK14	CNPY4	CYCSP18	DNAJB9
ALKBH4	ATXN7L1	CAPZA2	CDK6	COA1	CYCSP19	DNAJC2
AMPH	AUTS2	CASD1	CEP41	COBL	CYCSP20	DNAJC30
ANKIB1	AVL9	CASP2	CFAP69	COG5	CYP3A4	DOCK4
ANKRD7	AZGP1	CAV1	CFTR	**COL1A2**	CYP3A43	DOCK4-AS1
ANLN	AZGP1P1	CAV2	CHCHD2	COL26A1	CYP3A5	DPY19L1

Cfs3.2 cont.						
DPY19L1P1	FAM71F1	GRM8	HOXA10-AS	KLHL7	MGC72080	NDUFAF4P2
DPY19L1P2	FAM71F2	GRPEL2P3	HOXA10	KLHL7-AS1	MIPEPP1	NDUFB2
DPY19L2P1	FBXL13	GS1-124K5	HOXA11	KLRG2	MKLN1	NDUFB2-AS1
DPY19L2P2	FBXO24	GS1-124K5	HOXA11-AS	KMT2E	MKLN1-AS	NDUFB9P2
DPY19L2P3	FCF1P1	GS1-259H13	HOXA13	KMT2E-AS1	MKRN1	NECAP1P1
DPY19L2P4	FCF1P11	GS1-278J22	**HOXA2**	KPNA7	MLXIPL	NEUROD6
DTX2	FDPSP2	GSAP	HOXA3	KRIT1	MOGAT3	NFE2L3
DTX2P1	FDPSP7	GSTK1	HOXA4	KRT8P20	MOSPD3	NFE4
DUS4L	FEZF1	GTF2I	HOXA5	LAMB1	MOXD2P	NHP2P2
DYNC1I1	FEZF1-AS1	GTF2IP1	HOXA6	LAMB4	MPLKIP	NIPA2P1
DYNLL1P7	FGL2	GTF2IP4	HOXA7	LAMTOR4	MPP6	NMD3P1
EEF1A1P28	FIGNL1	GTF2IP5	HOXA9	LANCL2	MRPL32	NMD3P2
EEF1A1P6	FIS1	GTF2IRD1	HPVC1	LAT2	MRPL42P4	NME8
EEF1B2P6	FKBP14	GTF2IRD1P1	HRAT17	LEP	MRPS17	NMTRQ-TTG13-1
EEF1DP4	FKBP6	GTF2IRD2	HSPA8P16	LHFPL3	MRPS23P1	NMTRQ-TTG2-1
EEF1GP1	FKBP9	GTF2IRD2B	HSPB1	LHFPL3-AS1	MRPS24	NOD1
EEPD1	FKBP9P1	GTF2IRD2P1	HUS1	LHFPL3-AS2	MRPS33	NPC1L1
EFCAB10	FLJ20712	GTF3AP6	HYAL4	LIMK1	MTERF1	NPM1P14
EGFR	FLJ40288	GTPBP10	HYALP1	LINC-PINT	MTHFD2P5	NPM1P18
EGFR-AS1	FLNC	GUSB	IFRD1	LMOD2	MTND1P2	NPSR1
EIF3IP1	FOXP2	GUSBP10	IFT22	LMTK2	MTND1P3	NPSR1-AS1
EIF4A1P13	FSCN3	GUSBP12	IGF2BP3	LRCH4	MTND1P4	NPTX2
EIF4BP6	FTLP15	GUSBP6	IGFBP1	LRGUK	MTND2P4	NPVF
EIF4EP4	FZD1	H2AFV	IGFBP3	LRRC17	MTND2P5	NPY
EIF4H	FZD9	HAUS6P1	IKZF1	LRRC4	MTND2P6	NRCAM
EIF4HP1	GABPAP	HBP1	IL6	LRRD1	MTND3P2	NRF1
ELDR	GAL3ST4	HECW1	IMMP2L	LRRN3	MTND4P2	NSUN5
ELK1P1	GARS	HECW1-IT1	IMPDH1	LRWD1	MTND4P3	NSUN5P1
ELMO1	GATAD1	HEPACAM2	IMPDH1P3	LSM5	MTND4P5	NSUN5P2
ELMO1-AS1	GATS	HERPUD2	ING3	LSM8	MTND4P6	NT5C3A
ELN	GATSL2	HGF	INHBA	LSMEM1	MTND5P6	NUDCD3
EPDR1	GBAS	HIBADH	INHBA-AS1	LUC7L2	MTND5P7	NUP205
EPHA1	GCC1	HIGD1AP7	INMT	LUZP6	MTND5P8	NUPL2
EPHA1-AS1	GCK	HILPDA	INMT-FAM188B	LVCAT5	MTPN	NUPR2
EPHB4	GCNT1P5	HINT1P1	INTS4P1	LYPLA1P1	MTRNR2L6	NYAP1
EPHB6	GDI2P1	HINT1P2	INTS4P2	MAGI2	MTURN	OCM2
EPO	GGCT	HIP1	IQUB	MAGI2-AS2	MUC12	ODCP
EPS15P1	GHRHR	HIPK2	IRF5	MAGI2-AS3	MUC17	OGDH
ERHP1	GIGYF1	HMGB3P20	IRS3P	MALSU1	MUC3A	OPN1SW
ERV3-1	GJC3	HMGB3P21	JAZF1	MARK2P10	MYH16	OR10AC1
ERVW-1	**GLI3**	HMGN1P18	JAZF1-AS1	MARK2P13	MYL10	OR2A12
EVX1	GNAI1	HMGN1P19	JHDM1D-AS1	MARK2P7	MYL6P4	OR2A15P
EVX1-AS	GNAT3	HMGN2P11	KBTBD2	MBLAC1	MYL7	OR2A2
EXOC4	GNB2	HMGN2P30	KCND2	MCM7	MYO1G	OR2A25
FAM126A	GNG11	HNRNPA1P8	KCP	MDFIC	NACAD	OR2A41P
FAM131B	GNGT1	HNRNPA1P9	KCTD7	MDH2	NAMPT	OR2A5
FAM133B	GNL2P1	HNRNPA2B1	KDM7A	MEPCE	NANOGP4	OR2AE1
FAM180A	GPC2	HNRNPCP7	KEL	MEST	NAPEPLD	OR2F1
FAM183BP	GPNMB	HOTAIRM1	KIAA0087	MESTIT1	NAT16	OR2F2
FAM185A	GPR141	HOTTIP	KIAA0895	MET	NCAPD2P1	OR2Q1P
FAM185BP	GPR22	HOXA-AS2	KIAA1147	METTL2B	NCF1	OR2R1P
FAM188B	GPR37	HOXA-AS3	KIAA1324L	MGAM	NCF1B	OR6B1
FAM200A	GPR85	**HOXA1**	KIAA1549	MGAM2	NCF1C	OR6V1
FAM221A	GRB10	HOXA9	KLF14	MGC16142	NCOR1P3	OR6W1P
FAM3C	GRM3	HOXA10	KLHDC10	MGC27345	NDUFA5	OR7E38P

Cfs3.2 cont.						
OR7E7P	POLD2	RABGEF1	RPL10P11	RPS26P32	SKAP2	SPDYE2B
OR9A1P	POLM	RAC1P6	RPL12P10	RPS26P33	SKP1P1	SPDYE3
OR9A2	POLR2J	RAC1P9	RPL13AP16	RPS27P16	SLC12A9	SPDYE5
OR9A3P	POLR2J2	RAD23BP2	RPL13AP17	RPS27P17	SLC13A1	SPDYE6
OR9A4	POLR2J3	RALA	RPL15P11	RPS28P6	SLC13A4	SPDYE7P
OR9N1P	POLR2J4	RAMP3	RPL17P27	RPS29P14	SLC16A1P1	SPDYE8P
OR9P1P	POM121	RAPGEF5	RPL17P28	RPS29P15	SLC23A4P	SPDYE9P
ORAI2	POM121B	RASA4	RPL18AP10	RPS29P16	SLC25A13	SRI
ORC5	POM121C	RASA4B	RPL18P4	RPS2P30	SLC25A1P2	SRPK2
OSBPL3	POM121L12	RASA4CP	RPL18P5	RPS2P31	SLC25A1P3	SRRM3
OSBPL9P6	POMZP3	RASA4DP	RPL19P12	RPS2P32	SLC25A40	SRRT
PAICSP5	PON1	RBM22P3	RPL21P73	RPS3AP25	SLC25A5P3	SSBP1
PAICSP6	PON2	RBM28	RPL21P74	RPS3AP26	SLC25A5P5	SSC4D
PARP12	PON3	RBM48	RPL23P7	RPS3AP27	SLC26A3	SSMEM1
PAX4	POP7	RCC2P3	RPL26P22	RPS3AP28	SLC26A4	SSU72P8
PCLO	**POR**	RELN	RPL26P24	RPS3AP29	SLC26A4-AS1	ST13P17
PCMTD1P3	POT1	RFC2	RPL27P11	RPSAP46	SLC26A5	ST13P7
PCOLCE	POT1-AS1	RHBDD2	RPL31P35	RSBN1L	SLC29A4P1	ST7
PCOLCE-AS1	POU6F2	RINT1	RPL31P36	RSL24D1P3	SLC29A4P2	ST7-AS1
PDAP1	POU6F2-AS1	RN7SL7P	RPL31P37	RUNDC3B	SLC35B4	ST7-AS2
PDE1C	POU6F2-AS2	RN7SL8P	RPL31P38	RWDD4P1	SLC37A3	ST7-OT3
PDK4	PPIA	RNA5SP227	RPL31P39	RWDD4P2	SMKR1	ST7-OT4
PEG10	PPP1R14BP4	RNA5SP228	RPL32P18	S100A11P1	SMO	STAG3
PEX1	PPP1R17	RNA5SP229	RPL35P4	S100A11P2	SMURF1	STAG3L1
PGAM2	PPP1R2P6	RNA5SP230	RPL35P5	SAMD9	SND1	STAG3L2
PHBP15	PPP1R35	RNA5SP231	RPL36AP27	SAMD9L	SND1-IT1	STAG3L3
PHKG1	PPP1R3A	RNA5SP232	RPL36P12	SAP25	SNHG15	STAG3L4
PHKG1P1	PPP1R9A	RNA5SP233	RPL36P13	SAPCD2P1	SNORA14A	STAG3L5P
PHKG1P2	PRELID3BP10	RNA5SP234	RPL37AP5	SAPCD2P2	SNORA15	STAG3L5P
PHKG1P4	PRKAR2B	RNA5SP235	RPL37AP6	SAPCD2P3	SNORA22	STARD3NL
PHTF2	PRKRIP1	RNA5SP236	RPL37P16	SAPCD2P4	SNORA5A	STEAP1
PIGCP2	PRR15	RNA5SP237	RPL39P23	SBDS	SNORA5B	STEAP1B
PIK3CG	PRRT4	RNA5SP238	RPL3P8	SBDSP1	SNORA5C	STEAP2
PILRA	PRSS1	RNA5SP239	RPL6P19	SCRN1	SNORA9	STEAP2-AS1
PILRB	PRSS2	RNA5SP240	RPL6P20	SDHAF3	SNORD93	STEAP4
PIP	PRSS37	RNA5SP241	RPL7AP38	SDHDP2	SNRPBP1	STK17A
PKD1L1	PRSS3P1	RNA5SP242	RPL7AP39	SEC61G	SNRPCP19	STK31
PLEKHA8	PRSS3P3	RNA5SP244	RPL7AP40	SEMA3A	SNRPCP9	STRA8
PLOD3	PRSS58	RNA5SP245	RPL7AP41	SEMA3C	SNRPGP3	STRIP2
PLXNA4	PSMA2	RNA5SP246	RPL7AP42	SEMA3D	SNX10	STX1A
PMPCB	PSMC1P2	RNA5SP247	RPL7AP43	SEMA3E	SNX2P2	STYXL1
PMS2P1	PSMC1P3	RNA5SP248	RPL7L1P2	SEPHS1P1	SOCS5P1	SUGCT
PMS2P10	PSMC2	RNF133	RPL7L1P3	SEPT14	SPAM1	SUMF2
PMS2P12	PSPH	RNF138P2	RPL7P30	SEPT7	SPDYE1	SUMO2P3
PMS2P2	PSPHP1	RNF148	RPL7P31	SEPT7-AS1	SPDYE10P	SUN3
PMS2P3	PTCD1	RNU1-14P	RPL7P32	SEPT7P2	SPDYE11	SVOPL
PMS2P4	PTN	RNU6-10P	RPL7P60	SEPT7P3	SPDYE12P	SYPL1
PMS2P5	PTP4A1P3	RNU7-16P	RPS10P14	SEPT7P4	SPDYE13P	TAC1
PMS2P6	PTPN12	RNU7-27P	RPS10P15	SEPT7P5	SPDYE14P	TAF6
PMS2P7	PTPRZ1	RNU7-35P	RPS14P10	SERPINE1	SPDYE15P	TARP
PMS2P8	PURB	RNU7-54P	RPS15AP22	SFRP4	SPDYE16	TAS2R16
PMS2P9	PUS7	RNU7-76P	RPS15AP23	**SGCE**	SPDYE17	TAS2R3
PNPLA8	PVRIG	RNU7-83P	RPS17P12	SGOL1P2	SPDYE18	TAS2R38
PNPT1P2	PVRIG2P	RP9	RPS17P13	SH2B2	SPDYE2	TAS2R39
PODXL	RAB19	RP9P	RPS26P31	SHFM1	SPDYE21P	TAS2R4

Cfs3.2 cont.						
TAS2R40	TOMM7	TRBV14	TRBV7-6	TRIP6	VN1R32P	ZC3HC1
TAS2R41	TP53TG1	TRBV15	TRBV7-7	TRP-AGG2-8	VN1R33P	ZCWPW1
TAS2R5	TPI1P2	TRBV16	TRBV7-9	TRPV5	VN1R34P	ZKSCAN1
TAS2R60	TPM3P1	TRBV17	TRBV8-1	TRPV6	VN1R35P	ZKSCAN5
TAS2R62P	TPM3P4	TRBV18	TRBV8-2	TRR-CCT4-1	VN1R36P	ZMIZ2
TAS2R6P	TPST1	TRBV19	TRBV9	TRRAP	VN1R37P	ZNF107
TAX1BP1	TPT1P7	TRBV2	TRBVA	TRW-CCA5-1	VN1R38P	ZNF117
TBL2	TRA2A	TRBV20-1	TRBVB	TRY2P	VN1R40P	ZNF138
TBRG4	TRB	TRBV21-1	TRG	TSC22D4	VN1R41P	ZNF273
TBX20	TRBC1	TRBV22-1	TRG-AS1	TSGA13	VN1R42P	ZNF277
TBXAS1	TRBC2	TRBV23-1	TRGC1	TSL	VN1R43P	ZNF3
TCAF1	TRBD1	TRBV24-1	TRGC2	TSPAN33	VOPP1	ZNF394
TCAF1P1	TRBD2	TRBV25-1	TRGJ1	TTC26	VPS37D	ZNF479
TCAF2	TRBJ1-1	TRBV26	TRGJ2	TTC4P1	VPS41	ZNF619P1
TCAF2P1	TRBJ1-2	TRBV27	TRGJP	TUBB3P2	VPS50	ZNF655
TCP1P1	TRBJ1-3	TRBV28	TRGJP2	TUBBP6	VSTM2A	ZNF679
TECPR1	TRBJ1-4	TRBV29-1	TRGV1	TUBG1P	VSTM2A-OT1	ZNF680
TES	TRBJ1-5	TRBV3-1	TRGV10	TVP23CP1	VWC2	ZNF680P1
TFEC	TRBJ1-6	TRBV30	TRGV11	TYW1	WASL	ZNF713
TFPI2	TRBJ2-1	TRBV4-1	TRGV2	TYW1B	WBP1LP2	ZNF716
TFR2	TRBJ2-2	TRBV4-2	TRGV3	UBA52P1	WBSCR16	ZNF727
THAP5	TRBJ2-2P	TRBV5-1	TRGV4	UBE2D4	WBSCR17	ZNF733P
THUMPD3P1	TRBJ2-3	TRBV5-2	TRGV5	UBE2H	WBSCR22	ZNF734P
TMED4	TRBJ2-4	TRBV5-3	TRGV5P	UBN2	WBSCR27	ZNF735
TMEM120A	TRBJ2-5	TRBV5-4	TRGV6	UFSP1	WBSCR28	ZNF736
TMEM139	TRBJ2-6	TRBV5-5	TRGV7	UPK3BL	WDR91	ZNF789
TMEM140	TRBJ2-7	TRBV5-6	TRGV8	UPP1	WEE2	ZNF800
TMEM168	TRBV1	TRBV5-7	TRGV9	UQCRFS1P2	WEE2-AS1	ZNF804B
TMEM178B	TRBV10-1	TRBV6-1	TRGVA	URGCP	WIPF3	ZNF90P3
TMEM209	TRBV10-2	TRBV6-2	TRGVB	URGCP-MRPS24	WNT16	ZNF92
TMEM213	TRBV10-3	TRBV6-4	TRIL	VGF	WNT2	ZNHIT1
TMEM229A	TRBV11-1	TRBV6-5	TRIM24	VKORC1L1	YAE1D1	ZNRF2
TMEM243	TRBV11-2	TRBV6-6	TRIM4	VN1R24P	YBX1P2	ZNRF2P1
TMEM248	TRBV11-3	TRBV6-7	TRIM50	VN1R25P	YKT6	ZNRF2P2
TMEM60	TRBV12-1	TRBV6-8	TRIM56	VN1R26P	YWHAEP1	ZP3
TMSB4XP3	TRBV12-2	TRBV7-1	TRIM60P16	VN1R27P	YWHAG	ZPBP
TNPO3	TRBV12-3	TRBV7-2	TRIM60P17	VN1R28P	ZAN	ZSCAN21
TNRC18P2	TRBV12-4	TRBV7-3	TRIM60P18	VN1R29P	ZASP	ZSCAN25
TNRC18P3	TRBV12-5	TRBV7-4	TRIM73	VN1R30P	ZC3HAV1	ZYX
TNS3	TRBV13	TRBV7-5	TRIM74	VN1R31P	ZC3HAV1L	

Cfs3.3						
ABCB8	ALDH7A1P3	ATP6V1F	CEP41	COX5BP3	CYCSP20	EPHA1
ABCF2	AOC1	BET1P1	CHCHD3	COX6B1P1	DENND2A	EPHA1-AS1
ACTR3B	ARF5	BLACE	CHPF2	CPA1	DGKI	EPHB6
ACTR3C	ARHGEF34P	BPGM	CHRM2	CPA2	DNAJB6	ERHP1
ADCK2	ARHGEF35	**BRAF**	CICP14	CPA4	DPP6	ESYT2
AGAP3	ARHGEF5	CALD1	CLCN1	CPA5	DUTP3	ETF1P2
AGBL3	ASB10	CALU	CLEC2L	CREB3L2	EEF1A1P10	EXOC4
AGK	ASIC3	CASP2	CLEC5A	CRYGN	EEF1B2P6	EZH2
AHCYL2	ATG9B	CCDC136	CNOT4	CTAGE15	EI24P4	FABP5P3
AKR1B1	ATP5F1P3	CCT4P1	CNPY1	CTAGE4	EIF2AP1	FAM131B
AKR1B10	ATP6V0A4	CCT8L1P	CNTNAP2	CTAGE6	EIF2AP2	FAM180A
AKR1B15	ATP6V0E2	CDC26P1	COPG2	CTAGE8	EIF2AP3	FAM71F1
AKR1D1	ATP6V0E2-AS1	CDK5	COPG2IT1	CUL1	EN2	FAM71F2

Cfs3.3 cont.						
FCF1P11	MGC27345	OR9A4	RPL17P27	TAS2R41	TRBV15	TRC-GCA18-1
FLJ40288	MKLN1	OR9N1P	RPL17P28	TAS2R5	TRBV16	TRC-GCA19-1
FLNC	MKLN1-AS	OR9P1P	RPL18P5	TAS2R60	TRBV17	TRC-GCA20-1
FSCN3	MKRN1	PAICSP5	RPL21P73	TAS2R62P	TRBV18	TRC-GCA3-1
GALNT11	MNX1	PAICSP6	RPL21P76	TAS2R6P	TRBV19	TRC-GCA9-2
GALNTL5	MNX1-AS1	PARP12	RPL26P22	TBXAS1	TRBV2	TRC-GCA9-3
GBX1	MNX1-AS2	PAX4	RPL26P23	TCAF1	TRBV20-1	TRC-GCA9-4
GCC1	MOXD2P	PAXIP1	RPL26P24	TCAF1P1	TRBV21-1	TRIM24
GHET1	MRPS33	PAXIP1-AS1	RPL27P11	TCAF2	TRBV22-1	TRP-AGG2-8
GIMAP1	MTND1P3	PAXIP1-AS2	RPL31P36	TCAF2P1	TRBV23-1	TRPV5
GIMAP1	MTND2P5	PDIA4	RPL32P17	THAP5P1	TRBV24-1	TRPV6
GIMAP2	MTPN	PIP	RPL36AP28	TMEM139	TRBV25-1	TRR-CCT4-1
GIMAP3P	MTRNR2L6	PIP5K1P2	RPL36AP30	TMEM140	TRBV26	TRS-AGA5-1
GIMAP4	MYL6P4	PLXNA4	RPL37AP5	TMEM176A	TRBV27	TRY-GTA11-1
GIMAP5	NCAPG2	PODXL	RPL37P16	TMEM176B	TRBV28	TRY2P
GIMAP6	NDUFB2	PPP1R2P6	RPL6P19	TMEM178B	TRBV29-1	TSGA13
GIMAP7	NDUFB2-AS1	PRELID3BP10	RPL7P59	TMEM209	TRBV3-1	TSPAN33
GIMAP8	NDUFB9P2	PRKAG2	RPS10P15	TMEM213	TRBV30	TTC26
GRM8	NMTRQ-TTG2-1	PRKAG2-AS1	RPS14P10	TMUB1	TRBV4-1	TUBB3P2
GSTK1	NOBOX	PRRT4	RPS15AP22	TNPO3	TRBV4-2	UBE2H
HILPDA	NOM1	PRSS1	RPS15AP23	TPI1P2	TRBV5-1	UBE3C
HINT1P1	NOS3	PRSS2	RPS17P12	TPK1	TRBV5-2	UBN2
HIPK2	NPM1P12	PRSS37	RPS20P19	TRB	TRBV5-3	UQCRFS1P2
HTR5A	NRF1	PRSS3P1	RPS27AP12	TRBC1	TRBV5-4	VIPR2
HTR5A-AS1	NUB1	PRSS3P3	RPS3AP27	TRBC2	TRBV5-5	WDR60
IMPDH1	NUP205	PRSS58	RPS3AP28	TRBD1	TRBV5-6	WDR86
IMPDH1P3	ODCP	PSMC1P3	SDHDP2	TRBD2	TRBV5-7	WDR86-AS1
INSIG1	OPN1SW	PTN	SEPT7P6	TRBJ1-1	TRBV6-1	WDR91
IQCA1L	OR10AC1	PTPRN2	**SHH**	TRBJ1-2	TRBV6-2	WEE2
IRF5	OR2A1	RAB19	SLC13A4	TRBJ1-3	TRBV6-4	WEE2-AS1
JHDM1D-AS1	OR2A1-AS1	RANP2	SLC16A1P1	TRBJ1-4	TRBV6-5	XRCC2
KCNH2	OR2A12	RARRES2	SLC23A4P	TRBJ1-5	TRBV6-6	YBX1P4
KCP	OR2A13P	RBM28	SLC35B4	TRBJ1-6	TRBV6-7	ZBED6CL
KDM7A	OR2A14	RBM33	SLC37A3	TRBJ2-1	TRBV6-8	ZC3HAV1
KEL	OR2A15P	RCC2P3	SLC4A2	TRBJ2-2	TRBV7-1	ZC3HAV1L
KIAA1147	OR2A2	REPIN1	SMARCD3	TRBJ2-2P	TRBV7-2	ZC3HC1
KIAA1549	OR2A20P	RHEB	SMKR1	TRBJ2-3	TRBV7-3	ZNF212
KLF14	OR2A25	RNA5SP242	SMO	TRBJ2-4	TRBV7-4	ZNF282
KLHDC10	OR2A3P	RNA5SP244	SND1	TRBJ2-5	TRBV7-5	ZNF398
KLRG2	OR2A41P	RNA5SP245	SND1-IT1	TRBJ2-6	TRBV7-6	ZNF425
KMT2C	OR2A42	RNA5SP246	SNRPGP3	TRBJ2-7	TRBV7-7	ZNF467
KRBA1	OR2A5	RNA5SP247	SSBP1	TRBV1	TRBV7-9	ZNF746
LEP	OR2A7	RNA5SP248	SSMEM1	TRBV10-1	TRBV8-1	ZNF767P
LINC-PINT	OR2A9P	RNA5SP249	SSPO	TRBV10-2	TRBV8-2	ZNF775
LMBR1	OR2AO1P	RNA5SP250	ST13P17	TRBV10-3	TRBV9	ZNF777
LRGUK	OR2F1	RNF32	ST13P7	TRBV11-1	TRBVA	ZNF783
LRRC4	OR2F2	RNU7-16P	STRA8	TRBV11-2	TRBVB	ZNF786
LRRC61	OR2Q1P	RNU7-20P	STRADBP1	TRBV11-3	TRC-GCA1-1	ZNF800
LUC7L2	OR2R1P	RNU7-27P	STRIP2	TRBV12-1	TRC-GCA10-1	ZNF862
LUZP6	OR6B1	RNU7-54P	SVOPL	TRBV12-2	TRC-GCA11-1	ZYX
MEST	OR6V1	RNY1	TAS2R3	TRBV12-3	TRC-GCA12-1	
MESTIT1	OR6W1P	RNY3	TAS2R38	TRBV12-4	TRC-GCA13-1	
METTL2B	OR9A1P	RNY4	TAS2R39	TRBV12-5	TRC-GCA15-1	
MGAM	OR9A2	RNY5	TAS2R4	TRBV13	TRC-GCA16-1	
MGAM2	OR9A3P	RPL15P11	TAS2R40	TRBV14	TRC-GCA17-1	

Cfs4.1						
ABT1	FOXCUT	HIST1H2BF	KAAG1	OR2B8P	RPL13P	TBC1D7
ACOT13	FOXF2	HIST1H2BG	KATNBL1P5	OR2E1P	RPL15P3	TDGF1P4
ADTRP	FOXQ1	HIST1H2BH	KDM1B	OR2G1P	RPL21P61	TDP2
ALDH5A1	GABBR1	HIST1H2BI	KIAA0319	OR2H1	RPL21P62	**TFAP2A**
AMD1P4	GCM2	HIST1H2BJ	KIF13A	OR2H2	RPL21P63	TFAP2A-AS1
ARPC3P5	GCNT2	HIST1H2BK	KRT18P1	OR2H4P	RPL21P68	TMEM14B
ASS1P1	GFOD1	HIST1H2BL	KRT18P38	OR2H5P	RPL23AP1	TMEM14C
ATXN1	GLRX3P2	HIST1H2BM	KRT8P43	OR2I1P	RPL29P1	TMEM170B
BLOC1S5	GMDS	HIST1H2BN	KU-MEL-3	OR2J1	RPL29P17	TMEM183AP1
BMP6	GMDS-AS1	HIST1H2BO	LARP1P1	OR2J2	RPL34P16	TOB2P1
BPHL	GMNN	HIST1H2BPS1	LRRC16A	OR2J3	RPL36AP25	TPMT
BTF3P7	GMPR	HIST1H2BPS2	LY86	OR2J4P	RPL5P20	TRA-AGC1-1
BTN1A1	GPLD1	HIST1H3A	LY86-AS1	OR2N1P	RPL6P17	TRA-AGC2-1
BTN1A1P1	GPR53P	HIST1H3B	LYRM4	OR2P1P	RPL6P18	TRA-AGC2-2
BTN2A1	GPR89P	HIST1H3C	LYRM4-AS1	OR2U1P	RPL7AP36	TRA-AGC23-1
BTN2A2	GPX5	HIST1H3D	MAK	OR2U2P	RPL7P26	TRA-AGC3-1
BTN2A3P	GPX6	HIST1H3E	MAS1L	OR2W1	RPL8P1	TRA-AGC4-1
BTN3A1	GUSBP2	HIST1H3F	MAS1LP1	OR2W2P	RPLP2P1	TRA-AGC5-1
BTN3A2	HCG11	HIST1H3G	MBOAT1	OR2W4P	RPP40	TRA-AGC6-1
BTN3A3	HCG14	HIST1H3H	MCFD2P1	OR2W6P	RPS10P1	TRA-AGC7-1
CAGE1	HCG16	HIST1H3I	MCUR1	OR4F1P	RPS12P12	TRA-CGC1-1
CAP2	HCG4P11	HIST1H3J	MICE	OR5V1	RPS17P1	TRA-CGC2-1
CASC15	HCG9P5	HIST1H3PS1	MOG	PAK1IP1	RPS18P8	TRA-CGC4-1
CD83	HDGFL1	HIST1H4A	MRPL35P1	PGBD1	RPS25P7	TRA-CGC5-1
CD83P1	HFE	HIST1H4B	MRPL42P2	PHACTR1	RPS26P29	TRA-TGC1-1
CDKAL1	HIST1H1A	HIST1H4C	MRPL48P1	PIP5K1P1	RPS3P4	TRA-TGC2-1
CDYL	HIST1H1B	HIST1H4D	MRS2	PKMP5	RPS4XP7	TRA-TGC5-1
CICP18	HIST1H1C	HIST1H4E	MYLIP	POM121L2	RPSAP2	TRA-TGC6-1
CMAHP	HIST1H1D	HIST1H4F	MYLK4	POM121L6P	RREB1	TRA-TGC7-1
CNN3P1	HIST1H1E	HIST1H4G	NBAT1	PPIAP29	RSL24D1P1	TRA-TGC9-1
COX11P1	HIST1H1PS1	HIST1H4H	NEDD9	PPP1R3G	SAR1AP1	TRD-GTC2-10
DCDC2	HIST1H1PS2	HIST1H4I	NHLRC1	PRELID1P2	SCARNA27	TRD-GTC2-11
DDX18P3	HIST1H1T	HIST1H4J	NKAPL	PRKRIRP5	SCGN	TRD-GTC3-1
DDX6P1	HIST1H2AA	HIST1H4K	NOL7	PRL	SERPINB1	TRE-CTC1-6
DEK	HIST1H2AB	HIST1H4L	NOP56P1	PRPF4B	SERPINB6	TRF-GAA1-5
DSP	HIST1H2AC	HIST1H4PS1	NQO2	PRSS16	SERPINB8P1	TRF-GAA1-6
DTNBP1	HIST1H2AD	HIVEP1	NRN1	PSMC1P11	SERPINB9	TRF-GAA11-1
DUSP22	HIST1H2AE	HLA-F	NRSN1	PSMG4	SERPINB9P1	TRF-GAA3-1
E2F3	HIST1H2AG	HLA-F-AS1	NUP153	PXDC1	SIRT5	TRF-GAA4-1
ECI2	HIST1H2AH	HMGN2P28	NUP50P2	RANBP9	SLC17A1	TRF-GAA5-1
EDN1	HIST1H2AI	HMGN4	OFCC1	RBM24	SLC17A2	TRG-GCC2-6
EEF1E1	HIST1H2AJ	HNRNPA1P1	OFCC1	RIOK1	SLC17A3	TRH-GTG1-8
ELF2P2	HIST1H2AK	HNRNPA1P37	OR10C1	RIPK1	SLC17A4	TRI-AAT10-1
ELOVL2	HIST1H2AL	HNRNPA1P58	OR11A1	RNA5SP201	SLC22A23	TRI-AAT2-1
ELOVL2-AS1	HIST1H2AM	HNRNPLP1	OR12D1	RNA5SP202	SLC35B3	TRI-AAT3-1
ERVFRD-1	HIST1H2APS1	HTATSF1P2	OR12D2	RNA5SP203	SMIM13	TRI-AAT5-3
EXOC2	HIST1H2APS2	HULC	OR12D3	RNA5SP204	SNAPC5P1	TRI-AAT5-4
F13A1	HIST1H2APS3	HUS1B	OR14J1	RNA5SP205	SNORD32B	TRI-AAT5-5
FAM136BP	HIST1H2APS4	ID4	OR1F12	RNF144B	SNRNP48	TRI-AAT6-1
FAM217A	HIST1H2APS5	IFITM4P	OR2AD1P	RNF182	SOX4	TRI-AAT7-2
FAM50B	HIST1H2BA	IMPDH1P9	OR2B2	RNU1-11P	SPTLC1P2	TRI-AAT8-1
FAM65B	HIST1H2BB	IQCB2P	OR2B3	RNU7-26P	SSR1	TRI-AAT9-1
FAM8A1	HIST1H2BC	IRF4	OR2B4P	RNY5P5	STMND1	TRI-TAT2-2
FARS2	HIST1H2BD	JARID2	OR2B6	RPL10P2	SUMO2P1	TRI-TAT2-3
FOXC1	HIST1H2BE	JARID2-AS1	OR2B7P	RPL13AP	SYCP2L	TRI-TAT3-1

Cfs4.1 cont.						
TRIM27	TRM-CAT4-3	TRR-ACG1-3	TRS-GCT2-1	TRV-CAC1-6	TUBB2BP1	ZNF204P
TRIM38	TRM-CAT5-1	TRR-ACG2-2	TRS-GCT4-3	TRV-CAC2-1	TXNDC5	ZNF311
TRK-CTT2-5	TRM-CAT5-1	TRR-ACG2-3	TRS-GCT5-1	TRV-CAC6-1	UBD	ZNF322
TRK-TTT13-1	TRMEP1	TRR-ACG2-4	TRS-GCT6-1	TRV-CAC7-1	UBDP1	ZNF391
TRK-TTT3-5	TRNAI-AAU	TRR-CCG1-2	TRS-TGA2-1	TRV-CAC9-1	UQCRFS1P3	ZNF601P
TRK-TTT4-1	TRNAL-CAA	TRR-CCG1-3	TRS-TGA3-1	TRV-TAC4-1	VN1R10P	ZNF602P
TRK-TTT6-1	TRNAL47P	TRR-TCG2-1	TRS-TGA4-1	TRW-CCA3-2	VN1R11P	ZNF603P
TRK-TTT7-1	TRNAM-CAU	TRR-TCG4-1	TRT-AGT2-1	TRW-CCA3-3	VN1R12P	ZNF90P2
TRK-TTT9-1	TRP-AGG2-7	TRR-TCG5-1	TRT-AGT2-2	TRX-CAT1-3	VN1R13P	ZNF968P
TRL-AAG2-4	TRP-CGG2-1	TRR-TCT5-1	TRT-AGT3-1	TRX-CAT1-4	VN1R14P	ZSCAN12
TRL-AAG3-1	TRQ-CTG1-3	TRS-ACT1-1	TRT-AGT5-1	TRX-CAT1-5	WRNIP1	ZSCAN12P1
TRL-AAG4-1	TRQ-CTG1-4	TRS-AGA1-1	TRT-AGT6-1	TRX-CAT1-6	ZBED9	ZSCAN16
TRL-CAA1-2	TRQ-CTG1-5	TRS-AGA2-2	TRT-CGT1-1	TRX-CAT1-7	ZDHHC20P1	ZSCAN16-AS1
TRL-CAA2-1	TRQ-CTG2-1	TRS-AGA2-3	TRT-CGT3-1	TRX-CAT1-8	ZFP57	ZSCAN23
TRL-CAA3-1	TRQ-CTG5-1	TRS-AGA2-4	TRT-CGT5-1	TRX-CAT2-1	ZKSCAN3	ZSCAN26
TRL-CAG1-7	TRQ-CTG6-1	TRS-AGA2-5	TRT-TGT1-1	TRY-GTA1-1	ZKSCAN4	ZSCAN31
TRL-TAA2-1	TRQ-TTG2-1	TRS-AGA3-1	TRV-AAC1-5	TRY-GTA3-1	ZKSCAN8	ZSCAN9
TRL-TAA4-1	TRQ-TTG3-1	TRS-AGA4-1	TRV-AAC3-1	TRY-GTA6-1	ZNF165	
TRM-CAT3-1	TRQ-TTG3-2	TRS-CGA2-1	TRV-AAC4-1	TRY-GTA8-1	ZNF184	
TRM-CAT3-2	TRQ-TTG3-3	TRS-CGA3-1	TRV-AAC5-1	TUBB2A	ZNF192P1	
TRM-CAT4-2	TRR-ACG1-2	TRS-GCT1-1	TRV-AAC6-1	TUBB2B	ZNF192P2	

Cfs4.4						
ABRACL	CCRL1P1	FAM120B	HBS1L	KRT8P42	NDUFS5P1	PLG
ACAT2	CENPW	FAM162B	HDAC2	KRT8P44	NEPNP	PLN
ADAT2	CEP85L	FAM184A	HDDC2	L3MBTL3	NHEG1	PNLDC1
ADGB	CHCHD2P4	FAM229B	HEBP2	LAMA2	NHSL1	PPP1R14BP5
ADGRG6	CITED2	FAM26D	HECA	LAMA4	NIP7P3	PRELID1P1
AGPAT4	CLVS2	FAM26E	HEY2	LPA	NKAIN2	PRR18
AGPAT4-IT1	COL10A1	FAM26F	HGC6	LPAL2	NMBR	PSMB1
AHI1	COX5BP2	FAM8A6P	HINT3	LTV1	NT5DC1	PTPRK
AIG1	COX6A1P3	FBXO30	HIVEP2	MAN1A1	NUDT19P3	QKI
AIRN	CTAGE13P	FEM1AP3	HLFP1	MAP3K4	NUS1	RAB32
AKAP7	CTAGE9	FGFR1OP	HMGA1P7	MAP3K5	OLIG3	RAP1BP3
ALDH8A1	CTGF	FLJ34503	HMGB1P13	MAP7	OR2A4	RBM11P1
AMD1	DACT2	FLJ46906	HMGB1P17	MARCKS	OR4F7P	REPS1
AMZ2P2	DCBLD1	FNDC1	HMGB3P18	MARCKSL1P2	OSTCP1	REV3L
ARFGEF3	DLL1	FRK	HMGN2P29	MAS1	PA2G4P5	RFPL4B
ARG1	DNAJA1P4	FRMD1	HNRNPH1P1	MCM9	PACRG	RFX6
ARHGAP18	DSE	FTH1P26	HRAT13	MEAT6	PACRG-AS1	RNA5SP213
ASF1A	DYNLT1	FUCA2	HS3ST5	MED23	PACRG-AS2	RNA5SP214
ATP5F1P6	ECHDC1	FUNDC2P3	HSF2	MEMO1P2	PACRG-AS3	RNA5SP215
ATP5LP2	ECT2L	FYN	HYMAI	MESTP1	PARK2	RNA5SP216
B3GALNT2P1	EEF1A1P36	GAPDHP72	IFNGR1	MLLT4	PBOV1	RNA5SP217
BCLAF1	EEF1DP5	GAPDHP73	IGF2R	MLLT4-AS1	PDCD2	RNA5SP218
BMPR1APS1	ENPP1	**GJA1**	IL20RA	MOXD1	PDE10A	RNA5SP219
BRD7P3	ENPP3	GJE1	IL22RA2	MPC1	PDE7B	RNA5SP220
BRD7P4	EPB41L2	GNG5P1	KATNBL1P6	MRPL18	PERP	RNA5SP222
BTF3L4P3	EPM2A	GOPC	KIAA0408	MRPL42P3	PEX3	RNASET2
BTRCP1	ERMARD	GPR31	KIAA1919	MRPS17P5	PEX7	RNF146
CAHM	EYA4	GPRC6A	KIF25	MTCYBP4	PHACTR2	RNF217
CBX3P9	EZR	GRM1	KIF25-AS1	MTFR2	PHACTR2-AS1	RNF217-AS1
CCDC28A	EZR-AS1	GSTM2P1	KPNA5	MYB	PHF10	RNU1-18P
CCNG1P1	FABP7	GTF3C6	KRT18P22	NCOA7	PKIB	ROS1
CCR6	FAM103A2P	GVQW2	KRT18P65	NCOA7-AS1	PLAGL1	RPF2

Cfs4.4 cont.						
RPL12P23	RPLP1P8	SAMD3	SNORA20	TAAR7P	TPD52L1	VDAC1P8
RPL13AP15	RPS12	SAMD5	SNORA29	TAAR8	TPI1P3	VGLL2
RPL15P9	RPS15AP21	SASH1	SNORA33	TAAR9	TPT1P4	VIM2P
RPL17P23	RPS18P10	SERINC1	SNORD100	TAGAP	TRAF3IP2	VNN1
RPL21P64	RPS27AP11	SF3B5	SNORD101	TARID	TRAF3IP2-AS1	VNN2
RPL21P66	RPS29P13	SFT2D1	SOCS5P5	TATDN2P2	TRAPPC3L	VNN3
RPL21P67	RPS3AP23	SGK1	SOD2	TBC1D32	TRDN	VTA1
RPL21P69	RPS3AP24	SHPRH	SOGA3	TBP	TRE-CTC1-7	WDR27
RPL23AP46	RPS4XP9	SLC16A10	SSXP10	TBPL1	TRE-TTC15-1	WISP3
RPL23AP47	RPS5P1	SLC18B1	STX11	TCF21	TRL-TAA1-1	WTAP
RPL23AP48	RPS6KA2	SLC22A1	STX7	TCP1	TRMT11	YAP1P1
RPL29P4	RPS6KA2-AS1	SLC22A2	STXBP5	TCP10	TRQ-TTG4-1	YAP1P3
RPL30P8	RPS6KA2-IT1	SLC22A3	STXBP5-AS1	TCP10L2	TSPYL1	YWHAZP4
RPL31P27	RPSAP42	SLC25A5P7	SYTL3	TCTE3	TSPYL4	ZC2HC1B
RPL34P15	RPSAP43	SLC2A12	TAAR1	THBS2	TTLL2	ZUFSP
RPL35AP3	RPSAP45	SLC35D3	TAAR2	THEMIS	TUBE1	
RPL37AP4	RSPH3	SLC35F1	TAAR3	TMEM181	TULP4	
RPL5P18	RSPH4A	SMLR1	TAAR4P	TMEM200A	TXLNB	
RPL5P21	RSPO3	SMOC2	TAAR5	TMEM244	UNC93A	
RPL7AP37	RWDD1	SMPDL3A	TAAR6	TNFAIP3	UTRN	

Cfs5.3						
AADAT	CLDN24	FABP5P12	GTF2F2P1	LSM6	NOCT	RBM46
ABCE1	CLGN	FAM149A	GUCY1A3	LVCAT8	NOL8P1	RFPL4AP4
ACSL1	CLUHP4	FAM160A1	GUCY1B3	MAB21L2	NPY1R	RNA5SP165
ADAM20P2	CPE	FAM192BP	GUSBP5	MAML3	NPY2R	RNA5SP166
ADAM20P3	CTSO	FAM198B	GYPA	MAP9	NPY5R	RNA5SP167
ADAM29	CYCSP14	FAM218A	GYPB	MARCH1	NR3C2	RNA5SP168
AGA	CYP4V2	FAM92A1P2	GYPE	MARK2P4	NUDT19P5	RNA5SP169
AGGF1P1	DBET	FAT1	H3F3AP6	MFAP3L	ORAOV1P1	RNA5SP170
AK4P6	DCHS2	FAUP3	HADHAP1	MGARP	OTUD4	RNA5SP171
AKIRIN2P1	DCLK2	FBXO8	HAND2	MGAT4D	PABPC4L	RNA5SP173
ANAPC10	DCTD	FBXW7	HELT	MGST2	PALLD	RNF150
ANKRD37	DDX60	FGA	HHIP	MMAA	PCDH10	RNF175
ANP32C	DDX60L	FGB	HHIP-AS1	MND1	PCDH18	RNY4P17
ANXA10	DEAR	FGG	HMGB2	MORF4	PDGFC	RNY5P4
ANXA2P1	DUX4	FHDC1	HPGD	MRPS36P2	PDLIM3	RPL14P3
APELA	DUX4L1	FLJ38576	HSP90AA4P	MSMO1	PES1P1	RPL19P8
ARFIP1	DUX4L2	FNIP2	HSP90AA6P	MTHFD2P4	PGBD4P4	RPL21P51
ARHGAP10	DUX4L3	FREM3	HSPA8P12	MTND1P22	PHBP14	RPL23AP84
ASB5	DUX4L4	FRG1	HSPD1P5	MTND2P33	PLRG1	RPL26P16
ASIC5	DUX4L5	FRG2	ICE2P1	MTND3P3	POU4F2	RPL31P26
ASS1P8	DUX4L6	FSTL5	IL15	MTND4P8	PPID	RPL35AP12
ATP5LP4	DUX4L7	FTH1P21	ING2	MTND5P9	PPP1R14BP3	RPL5P11
BTF3L4P4	DUX4L8	FTH1P24	INPP4B	MTNR1A	PRIMPOL	RPL5P13
CASP3	DUX4L9	GAB1	IRF2	MYL12BP2	PRMT5P1	RPL6P11
CBR4	EDNRA	GALNT7	KIAA0922	NAA15	PRMT9	RPL6P12
CCDC110	EEF1A1P35	GALNTL6	KLHL2	NACA3P	PRSS48	RPL6P16
CCNHP1	EEF1GP8	GAPDHP56	KLKB1	NAF1	PSME2P3	RPL7AP27
CDKN2AIP	ELF2	GATB	KRT18P51	NDUFB5P1	PTGES3P3	RPL7AP28
CENPU	ELL2P2	GK3P	KRT18P54	NDUFC1	R3HDM2P1	RPL9P16
CEP44	ELMOD2	GLRA3	LRAT	NEIL3	RAB33B	RPS14P6
CFAP97	ENPP6	GLRB	LRBA	NEK1	RANP6	RPS14P7
CLCN3	**ETFDH**	GPM6A	LRP2BP	NMNAT1P4	RAPGEF2	RPS23P2
CLDN22	F11	GRIA2	LSM3P4	NMTRQ-TTG15-1	RARRES2P4	RPS23P4

Cfs5.3 cont.						
RPS2P20	SCOC-AS1	SMAD1	TBC1D9	TMEM184C	TSEN2P1	WDR17
RPS2P27	SCRG1	SMARCA5	TDO2	TMEM192	TTC29	WDR45P
RPS3A	SERF1AP1	SNORD73A	TENM3	TNRC18P1	TUBB7P	WWC2
RPS3AP18	SETD7	SNORD73B	TERF1P3	TOMM22P4	UCP1	WWC2-AS1
RPSAP36	SFRP2	SNX25	TIGD4	TRAPPC11	UFSP2	WWC2-AS2
RPSAP70	SH3D19	SORBS2	TKTL2	TRIM2	USP38	YWHAQP4
RTN3P1	SH3RF1	SPATA4	TLL1	TRIM60	VEGFC	ZBTB8OSP1
RWDD4	SLC10A7	SPCS3	TLR2	TRIM60P14	VTI1BP2	ZFP42
RXFP1	SLC25A4	SPOCK3	TLR3	TRIM61		ZNF330
SAP30	SLC25A5P6	STMN1P2	TMA16	TRIM75P		ZNF827
SCGB1D5P	SLC7A11	STOX2	TMEM144	TRIML1		
SCOC	SLED1	TARS2P1	TMEM154	TRIML2		

Cfs6.3						
ABLIM3	ARHGEF37	CCDC112	CMYA5	DEPDC1B	FAM13B	GCNT4
ACOT12	ARL14EPL	CCDC125	CNOT8	DHFR	FAM151B	GDF9
ACSL6	ARL15	CCDC152	COL4A3BP	DHX29	FAM159B	GEMIN5
ACTBL2	ARL2BPP4	CCDC69	COMMD10	DIAPH1	FAM169A	GFM2
ACTBP2	ARRDC3	CCL28	COQ10BP2	DIMT1	FAM170A	GFRA3
ACTBP4	ARSB	CCNB1	COX7C	DMGDH	FAM172A	GHR
ADAM19	ARSI	CCNH	CRHBP	DMXL1	FAM174A	GIN1
ADAMTS19	ARSK	CCNI2	CRSP8P	DNAJC18	FAM53C	GJA1P1
ADAMTS6	ASS1P10	CCNJL	CSF1R	DND1	FAM71B	**GLRA1**
ADGRV1	ASS1P9	CCNO	CSF2	DPYSL3	FAM81B	GLRX
ADRA1B	ATG10	CCT5P1	CSNK1A1	DTWD2	FAT2	GLRXP3
ADRB2	ATG12	CCT7P2	CSNK1A1P3	EBF1	FAXDC2	GLULP1
AFAP1L1	ATOX1	CD14	CSNK1G3	ECSCR	FBN2	GM2A
AFF4	ATP10B	CD180	CT45B1P	ECSCR	FBXL17	GNL3LP1
AGGF1	ATP6AP1L	CD74	CTB-113P19	EDIL3	FBXL21	GNPDA1
AK3P4	ATP6V0E1P1	CDC20B	CTB-12O2	EEF1A1P19	FBXO38	GPBP1
AK4P2	ATP6V1G1P5	CDC23	CTB-1I21	EEF1A1P20	FBXO4	GPR150
AK6	ATP6V1G1P6	CDC25C	CTB-3M24	EEF1B2P2	FCHO2	GPR151
ALDH7A1	BCLAF1P1	CDC42SE2	CTB-49A3	EEF1GP2	FCHSD1	GPX3
ALDH7A1P1	BDP1	CDH12P1	CTB-99A3	EFNA5	FEM1C	GPX8
AMD1P3	BHMT	CDH12P2	CTBP2P4	EGR1	FER	GRAMD3
ANKDD1B	BHMT2	CDH12P3	CTC-436P18	EIF3KP1	FGF1	GRIA1
ANKHD1	BIN2P2	CDH12P4	CTD-2151A2	EIF4EBP3	FGF10	GRPEL2
ANKHD1	BOLA3P3	CDK7	CTD-2201I18	ELL2	FGF10-AS1	GRXCR2
ANKRA2	BRCAT107	CDKL3	CTNNA1	ELOVL7	FLJ31104	GTF2H2
ANKRD31	BRCAT54	CDKN2AIPNL	CTNNA1P1	EMB	FLJ32255	GTF2H2B
ANKRD34B	BRD8	CDO1	CTXN3	ENC1	FNDC9	GTF2H2C
ANKRD55	BTF3	CDX1	CUL1P1	EPB41L4A	FNIP1	GTF3AP4
ANXA2R	C1GALT1P2	CENPH	CWC27	ERAP1	FOXD1	GUSBP3
ANXA6	C1QTNF2	CENPK	CXCL14	ERAP2	FST	GUSBP7
AP3B1	C6	CEP120	CXXC5	ERBB2IP	FSTL4	GUSBP8
AP3S1	C7	CETN3	CYFIP2	ERCC8	FTMT	GUSBP9
APBB3	CAMK2A	CFL1P5	CYSTM1	ESM1	FUNDC2P1	GZMA
APC	CAMK4	CHCHD2P2	DBIP2	ETF1	G3BP1	GZMK
APOOP1	CAMLG	CHD1	DCANP1	F2R	**GABRA1**	H2AFY
ARAP3	CARD6	CHSY3	DCP2	F2RL1	GABRA6	HAND1
ARGFXP1	CARMN	CIR1P1	DCTN4	F2RL2	GABRB2	**HAPLN1**
ARHGAP26	CARTPT	CKMT2	DDX18P4	FABP5P5	**GABRG2**	HARS
ARHGAP26-AS1	CAST	CKS1BP3	DDX4	FABP5P6	GALNT10	HARS2
ARHGAP26-IT1	CATSPER3	CKS1BP5	DDX43P1	FABP6	GAPDHP40	HAUS1P1
ARHGEF28	CBX3P3	CLINT1	DDX46	FAM114A2	GAPT	HAVCR1

Cfs6.3 cont.						
HAVCR2	IPO11	MARCH3	NLN	PCDHB18P	PLCXD3	RELL2
HBEGF	IQGAP2	MARK2P11	NME5	PCDHB19P	PLK2	RFESD
HCN1	IRF1	MARVELD2	NMUR2	PCDHB2	PLPP1	RGMB
HDAC3	IRGM	MAST4	NNT	PCDHB3	PMCHL2	RGMB-AS1
HEXB	ISCA1P1	MATR3	NPM1P27	PCDHB4	POC5	RGS7BP
HINT1	ISL1	MBLAC2	NPY6R	PCDHB5	POLD2P1	RHOBTB3
HMGB1P21	ISOC1	MCC	NR2F1	PCDHB6	POLK	RIOK2
HMGB1P22	ITGA1	MCCC2	NR3C1	PCDHB7	POLR3G	RNA5SP182
HMGB1P29	ITGA2	MCIDAS	NREP	PCDHB8	POU4F3	RNA5SP183
HMGB1P35	ITK	MCTP1	NRG2	PCDHB9	POU5F2	RNA5SP184
HMGB1P47	JADE2	MED7	NSA2	PCDHG@	PPARGC1B	RNA5SP185
HMGB3P16	JAKMIP2	MEF2C	NUDT12	PCDHGA1	PPIAP11	RNA5SP186
HMGB3P17	JMY	MEF2C-AS1	OCLN	PCDHGA10	PPIC	RNA5SP187
HMGCR	KATNBL1P4	MEGF10	OR7H2P	PCDHGA11	PPIGP1	RNA5SP188
HMGCS1	KCNN2	MEIKIN	OTP	PCDHGA12	PPIP5K2	RNA5SP189
HMGN1P13	KCTD16	MFAP3	OXCT1	PCDHGA2	PPP1R2P3	RNA5SP190
HMGN1P14	KDELC1P1	MGC32805	P4HA2	PCDHGA3	PPP2CA	RNA5SP191
HMGN1P15	KDM3B	MIER3	PAIP1	PCDHGA4	PPP2R2B	RNA5SP192
HMGN1P16	KIAA0141	MOCS2	PAIP2	PCDHGA5	PPP2R2B-IT1	RNA5SP193
HMGN1P17	KIAA0825	MROH2B	PAM	PCDHGA6	PPWD1	RNA5SP194
HMGN2P27	KIAA1024L	MRPL11P2	PAPD4	PCDHGA7	PRDM6	RNA5SP195
HMGN2P4	KIF20A	MRPL22	PARP8	PCDHGA8	PRELID2	RNA5SP196
HMGXB3	KIF2A	MRPL49P1	PART1	PCDHGA9	PRELID3BP4	RNA5SP197
HMHB1	KIF3A	MRPS27	PCBD2	PCDHGB1	PRELID3BP6	RNA5SP198
HNCAT21	KIF4B	MRPS30	PCBP2P3	PCDHGB2	PRELID3BP7	RNF138P1
HNRNPA0	KLHL3	MRPS35P2	PCDH1	PCDHGB3	PRELID3BP9	RNF14
HNRNPA1P12	KRT18P16	MRPS36	PCDH12	PCDHGB4	PRKAA1	RNF145
HNRNPA1P13	KRT18P42	MRPS5P3	PCDHA@	PCDHGB5	PROB1	RNF180
HNRNPA3P7	KRT18P45	MSH3	PCDHA1	PCDHGB6	PRR16	RNU4ATAC2P
HNRNPH1P3	KRT8P31	MTATP6P2	PCDHA10	PCDHGB7	PRRC1	RNU5B-4P
HNRNPKP1	KRT8P32	MTCO2P22	PCDHA11	PCDHGB8P	PSD2	RNU6ATAC2P
HOMER1	KRT8P33	MTCO3P22	PCDHA12	PCDHGB9P	PSMC1P4	RNU7-15P
HRAT56	KRT8P48	MTHFD2P6	PCDHA13	PCDHGC3	PSME2P1	RNU7-34P
HSD17B4	LAMTOR3P2	MTND4P12	PCDHA14	PCDHGC4	PTCD2	RNU7-53P
HSPA4	LARP1	MTND5P10	PCDHA2	PCDHGC5	PTGER4	RPEP1
HSPA8P4	LARS	MTND5P11	PCDHA3	PCSK1	PTMAP2	RPL10AP10
HSPA9	LDHBP3	MTND5P12	PCDHA4	PCYOX1L	PTP4A1P4	RPL10AP8
HSPB3	LEAP2	MTRNR2L2	PCDHA5	PDCD5P2	PTTG1	RPL10AP9
HSPD1P11	LECT2	MTX3	PCDHA6	PDE4D	PURA	RPL11P2
HSPD1P18	LHFPL2	MYOT	PCDHA7	PDE6A	PWWP2A	RPL12P21
HSPD1P22	LINCR-0003	MYOZ3	PCDHA8	PDE8B	RAB3C	RPL13AP13
HSPE1P10	LIX1	MZB1	PCDHA9	PDGFRB	RAB5CP2	RPL13AP14
HTR1A	LMNB1	NAIP	PCDHAC1	PDLIM4	RAB9BP1	RPL13P9
HTR4	LNPEP	NAMPTP2	PCDHAC2	PELO	RAD17	RPL17P21
IGIP	LOX	NBPF22P	PCDHACT	PFDN1	RAD50	RPL17P22
IK	LRRC70	NCRUPAR	PCDHB@	PGAM1P1	RAP1BL	RPL18P3
IL12B	LRRTM2	NDFIP1	PCDHB1	PGAM5P1	RAPGEF6	RPL21P55
IL13	LSM11	NDST1	PCDHB10	PGBD4P3	RASA1	RPL21P57
IL17B	LUCAT1	NDUFA2	PCDHB11	PGGT1B	RASGRF2	RPL21P58
IL3	LVRN	NDUFAF2	PCDHB12	PHAX	RBBP4P6	RPL23AP44
IL31RA	LYRM7	NDUFB4P2	PCDHB13	PIK3R1	RBM22	RPL26P18
IL4	LYSMD3	NDUFS4	PCDHB14	**PITX1**	RBM27	RPL26P19
IL5	MAN2A1	NEUROG1	PCDHB15	PJA2	RBMX2P5	RPL27AP5
IL6ST	MAP1B	NIM1K	PCDHB16	PKD2L2	REEP2	RPL28P3
IL9	MAP3K1	NIPAL4	PCDHB17P	PLAC8L1	REEP5	RPL29P12

Cfs6.3 cont.						
RPL29P14	RPS14	SCARNA18	SLC36A1	SPATA9	TH2LCRR	UTP15
RPL29P15	RPS14P8	SCGB3A2	SLC36A2	SPINK1	THBS4	VCAN
RPL31P8	RPS17P11	SEC24A	SLC36A3	SPINK13	THG1L	VDAC1
RPL34P13	RPS17P2	SEMA6A	SLC38A9	SPINK14	TICAM2	VTRNA1-1
RPL35AP13	RPS18P7	SEMA6A-AS1	SLC4A9	SPINK5	TIFAB	VTRNA1-2
RPL35AP14	RPS19P4	SEPP1	SLC6A7	SPINK6	TIGD6	VTRNA1-3
RPL35AP15	RPS20P16	SEPT8	SLCO4C1	SPINK7	TIMD4	VTRNA2-1
RPL35AP16	RPS20P3	SERBP1P6	SLCO6A1	SPINK9	TMCO6	WDR36
RPL35AP17	RPS20P4	SERF1A	SLF1	SPOCK1	TMED7	WDR41
RPL36AP20	RPS23	SERF1B	SLU7	SPRY4	TMEM161B	WDR55
RPL36P11	RPS25P6	SERINC5	SMA4	SPZ1	TMEM167A	WNT8A
RPL37	RPS26P26	SETD9	SMA5	SRA1	TMEM171	XBP1P1
RPL39P20	RPS26P27	SETP21	SMAD5	SREK1	TMEM173	XRCC4
RPL39P21	RPS27AP10	SETP22	SMAD5-AS1	SREK1IP1	TMEM174	YBX1P5
RPL3P6	RPS27AP9	SGCD	SMIM15	SRFBP1	TMEM232	YIPF5
RPL5P15	RPS27P14	SGTB	SMIM3	SRP19	TNFAIP8	YTHDC2
RPL5P16	RPS2P22	SH3RF2	SMN1	SSBP2	TNIP1	YTHDF1P1
RPL5P17	RPS2P23	SH3TC2	SMN2	ST13P12	TNPO1	ZBED3
RPL6P15	RPS2P24	SHFM1P1	SNCAIP	ST8SIA4	TRAPPC13	ZBED8
RPL7AP32	RPS2P25	SHROOM1	SNHG4	STARD4	TRC-ACA1-1	ZCCHC10
RPL7L1P4	RPS2P26	SIL1	SNORA13	STK32A	TRIM23	ZCCHC9
RPL7P1	RPS3AP20	SKIV2L2	SNORA47	SUMO1P5	TRIM36	ZFYVE16
RPL7P18	RPS3AP21	SKP1	SNORA74A	SUMO2P4	TRPC7	ZMAT2
RPL7P19	RPS3AP22	SLC12A2	SNORD63	SUMO2P5	TRQ-CTG13-1	ZNF131
RPL7P21	RPS9P3	SLC22A4	SNORD72	SV2C	TRQ-TTG7-1	ZNF300
RPL7P22	RPSAP37	SLC22A5	SNRPCP2	SYNPO	TSLP	ZNF300P1
RPL7P23	RPSAP38	SLC23A1	SNRPEP1	TAF7	TSSK1B	ZNF366
RPL7P24	RSL24D1P10	SLC25A2	SNX18	TAF9	TTC1	ZNF474
RPLP1P6	S100Z	SLC25A46	SNX2	TBCA	TTC33	ZNF608
RPLP1P7	SALL4P1	SLC25A48	SNX24	TCERG1	TTC37	ZRSR1
RPLP2P2	SAP30L	SLC25A5P9	SOWAHA	TCF7	TXNDC15	ZSWIM6
RPS10P11	SAP30L-AS1	**SLC26A2**	SOX30	**TCOF1**	UBE2B	
RPS10P12	SAR1B	SLC27A6	SOX30P1	TCP1P2	UBE2D2	
RPS12P10	SCAMP1	SLC30A5	SPARC	TEX43	UBLCP1	
RPS13P6	SCAMP1-AS1	SLC35A4	SPATA24	TGFBI	UQCRQ	

Cfs7.1						
ABCB10P1	ARHGAP11A	BUB1B	CHEK2P2	**CYP19A1**	DUOX1	EPB42
ABCB10P3	ARHGAP11B	C1QBPP3	CHP1	DAPK2	DUOX2	EXD1
ABCB10P4	ARPP19	C2CD4A	CHRFAM7A	DCAF13P3	DUOXA1	FAM189A1
ACTBP7	ATP10A	C2CD4B	CHRM5	DDX18P2	DUOXA2	FAM214A
ACTC1	ATP5HP1	CA12	CHRNA7	DEPDC1P1	DUT	FAM227B
ACTG1P15	ATP8B4	CAPN3	**CHST14**	DISP2	DYX1C1	FAM63B
ADAL	AVEN	CASC4	CKMT1A	DKFZP434L187	EEF1A1P22	FAM81A
ADAM10	B2M	CASC5	CKMT1B	DLL4	EEF1B2P1	FAM92A1P1
AHCYP7	BAHD1	CATSPER2	CNOT6LP1	DMXL2	EHD4	FAM96A
ALDH1A2	BCAR1P1	CATSPER2P1	COPS2	DNAJC17	EID1	FAM98B
ANKRD63	BCAR1P2	CCNB2	COX6CP4	DNM1P28	EIF2AK4	FAN1
ANP32AP1	BCL2L10	CCNDBP1	CSNK1A1P1	DNM1P29	EIF3J	**FBN1**
ANXA2	BLOC1S6	CCPG1	CTDSPL2	DNM1P30	EIF3J-AS1	FBXL22
AP4E1	BMF	CD24P2	CTXN2	DNM1P31	EIF4EBP2P2	FDPSP10
APBA2	BMS1P15	CDAN1	CXADRP2	DNM1P32	ELL3	FDPSP4
APH1B	BMS1P16	CEP152	CYCSP2	DNM1P5	ELMO2P1	FGF7
AQP9	BNIP2	CGNL1	CYCSP38	DPH6	EMC4	FLJ10038
AQR	BNIP3P5	CHAC1	CYFIP1	DTWD1	EMC7	FMN1

Cfs7.1 cont.						
FOXB1	GREM1	LDHAL6B	NUTF2P6	PWARSN	RPL9P27	SPRED1
FRMD5	GTF2A2	LEO1	NUTM1	PWRN1	RPLP0P10	SPTBN5
FSCN1P1	H3F3AP1	LIPC	OCA2	PWRN2	RPS10P22	SQRDL
FSIP1	HAUS2	LPCAT4	OIP5	PWRN3	RPS13P7	SRP14
FTLP11	HDC	LRRC57	OIP5-AS1	PYGO1	RPS13P8	STARD9
GABPB1	HERC1	LTK	ONECUT1	RAB27A	RPS15P8	STRC
GABRA5	HERC2	LYSMD2	OR11H3P	RAB8B	RPS20P34	STRCP1
GABRB3	HERC2P1	MAGEL2	OR11J1P	RAD51	RPS27L	SYNGR2P1
GABRG3	HERC2P10	MAP1A	OR11J2P	RAD51-AS1	RPS27P2	TCEB1P2
GALK2	HERC2P11	MAPK6	OR11J5P	RASGRP1	RPS3AP47	**TCF12**
GANC	HERC2P2	MAPKBP1	OR11J6P	RBM17P4	RPS3AP6	TEX9
GAPDHP43	HERC2P3	MEIS2	OR11J7P	REREP3	RPS8P10	TGM5
GAPDHP55	HERC2P6	MESTP2	OR11K1P	RFX7	RPSAP55	TGM7
GATM	HERC2P7	MFAP1	OR4H6P	RHOV	RPUSD2	THBS1
GCHFR	HERC2P9	MGA	OR4M2	RHPN2P1	RSL24D1	TJP1
GCNT3	HMGB1P33	MGC15885	OR4N3P	RLIMP3	RTF1	TLN2
GCOM1	HMGN1P26	MKRN3	OR4N4	RMDN3	RYR3	TMCO5A
GJD2	HMGN2P46	MNS1	OR4Q1P	RNA5SP390	SCG3	TMCO5B
GLDN	HMGN2P5	MRPL42P5	OTUD7A	RNA5SP391	SCG5	TMEM261P1
GNB5	HNRNPA1P45	MRPS18CP5	PAK6	RNA5SP392	SECISBP2L	TMEM62
GOLGA2P11	HNRNPA1P71	MTMR10	PATL2	RNA5SP393	SEMA6D	TMEM87A
GOLGA6L1	HNRNPA1P74	MYEF2	PDCD6IPP1	RNA5SP394	SERF2	TMOD2
GOLGA6L2	HNRNPA3P11	MYL12BP1	PDCD6IPP2	RNA5SP395	SERINC4	TMOD3
GOLGA6L22	HNRNPLP2	MYO1E	PDIA3	RNA5SP396	SERPINE4P	TNFAIP8L3
GOLGA6L6	HNRNPMP1	MYO5A	PGBD4	RNA5SP397	SHC4	TP53BP1
GOLGA6L7P	HSP90AB4P	MYO5C	PHGR1	RNF111	SHF	TPM1
GOLGA8A	HYPK	MYZAP	PIGB	RNU3P1	SLC12A1	TPST2P1
GOLGA8B	ICE2	NANOGP8	PIGHP1	RNU7-5P	SLC12A6	TRE-TTC2-2
GOLGA8CP	IGHV1OR15-1	NBEAP1	PIN4P1	RORA	SLC20A1P3	TRH-GTG1-5
GOLGA8DP	IGHV1OR15-2	NBEAP4	PIRC66	RORA-AS1	SLC24A5	TRH-GTG1-6
GOLGA8EP	IGHV1OR15-3	NCAPGP2	PLA2G4B	RORA-AS2	SLC27A2	TRH-GTG1-7
GOLGA8F	IGHV1OR15-9	NDN	PLA2G4D	RPAP1	SLC28A2	TRIM69
GOLGA8G	INAFM2	NDUFAF1	PLA2G4E	RPL15P19	SLC30A4	TRPM1
GOLGA8H	INO80	NDUFAF4P1	PLA2G4F	RPL21P113	SLTM	TRPM7
GOLGA8IP	IPW	NDUFB10P1	PLCB2	RPL21P114	SNAP23	TRS-GCT4-1
GOLGA8J	ISCA1P4	NEDD4	POLR2M	RPL21P117	SNRPN	TTBK2
GOLGA8K	ITPKA	NF1P1	POTEB	RPL21P14	SNURF	TUBGCP4
GOLGA8M	IVD	NF1P2	POTEB2	RPL28P4	SNX1	TUBGCP5
GOLGA8N	JMJD7	NF1P9	POTEB3	RPL32P2	SORD	TVP23BP1
GOLGA8O	KATNBL1	NIPA1	PPIP5K1	RPL32P30	SORD2P	TYRO3
GOLGA8Q	KLF13	NIPA2	PPIP5K1P1	RPL36AP44	SPATA31E2P	UBE2CP4
GOLGA8R	KNSTRN	NMNAT1P5	PPP1R14D	RPL36AP8	SPATA31E3P	UBE3A
GOLGA8S	KRT8P24	NOP10	PRELID1P4	RPL41P2	SPATA5L1	UBR1
GOLGA8T	KRT8P50	NPAP1	PRTG	RPL5P1	SPCS2P1	ULK4P1
GPR176	LACTB	NPM1P47	PWAR1	RPL5P32	SPG11	ULK4P2
GRAMD4P5	LARP4P	NSMCE3	PWAR4	RPL7AP62	SPINT1	
GRAMD4P6	LCMT2	NUSAP1	PWAR5	RPL9P26	SPPL2A	

Cfs9.1						
A1CF	ACTR3BP5	AGAP12P	AGAP9	AKR1C1	AKR1C8P	ANK3
ABCD1P2	ADAMTS14	AGAP13P	AHCYP1	AKR1C2	AKR1E2	ANKRD16
ABI1	ADARB2	AGAP14P	AIFM1P1	AKR1C3	ALDH7A1P4	ANKRD26
ACBD5	ADIPOR1P1	AGAP4	AIFM2	AKR1C4	ALOX5	ANKRD30A
ACBD7	ADO	AGAP6	AK3P5	AKR1C6P	AMD1P1	ANKRD30BP3
ACTBP14	AGAP10P	AGAP7P	AKR1B10P1	AKR1C7P	ANAPC16	ANKRD54P1

Cfs9.1 contd.						
ANTXRL	CDNF	EEF1A1P39	H2AFZP5	MASTL	OLAH	PTPN20CP
ANTXRLP1	CELF2	EGR2	HACD1	MBL2	OPTN	RAB18
ANXA2P3	CEP164P1	EIF2AP4	HERC4	MCM10	OR13A1	RASGEF1A
ANXA8	CEP57L1P1	EIF3LP2	HIRAP1	MCU	OR6D1P	RASSF4
ANXA8L1	CH17-360D5	EIF3LP3	HK1	MED28P1	OR7E110P	RBBP6P1
APBB1IP	CHAT	EIF4BP2	HKDC1	MEIG1	OR7E115P	RBM17
ARHGAP12	CHCHD3P1	EIF4EBP2	HMGB1P7	MICU1	OR7E26P	RBP3
ARHGAP21	**CHST3**	ENKUR	HMGN1P20	MKNK2P1	OTUD1	REEP3
ARHGAP22	CICP9	EPC1	HMGN2P34	MKX	PABPC1P12	**RET**
ARID5B	CISD1	**ERCC6**	HNRNPA1P32	MLLT10	PABPC1P8	RHEBP1
ARL4AP1	CKS1BP2	FAM107B	HNRNPA1P33	MPP7	PALD1	RHOBTB1
ARL5B	COL13A1	FAM133CP	HNRNPA3P1	MRC1	PARD3	RNA5SP299
ARL6IP1P2	COMMD3	FAM13C	HNRNPF	MRLN	PARD3-AS1	RNA5SP300
ARMC3	COQ10BP1	FAM170B	HNRNPH3	MRPL35P2	PARG	RNA5SP301
ARMC4	COX20P1	FAM171A1	HNRNPRP1	MRPL50P4	PARGP1	RNA5SP303
ARMC4P1	CREM	FAM188A	HSD17B7P2	MRPS21P5	PBLD	RNA5SP304
ASAH2	CSGALNACT2	FAM208B	HSP90AB7P	MRPS35P3	PCAT5	RNA5SP305
ASAH2B	CSTF2T	FAM210CP	HSPA14	MSMB	PCBD1	RNA5SP306
ASB13	CTNNA3	FAM21A	HSPA8P3	MSRB2	PCDH15	RNA5SP307
ASCC1	CTSLP2	FAM21C	HSPD1P17	MTND1P18	PDSS1	RNA5SP308
ATOH7	CTSLP3	FAM21EP	IDI1	MTND1P20	PFKFB3	RNA5SP309
ATP5C1	CTSLP4	FAM21FP	IDI2	MTND1P21	PFKP	RNA5SP318
ATP5G1P7	CUBN	FAM25BP	IDI2-AS1	MTND2P15	PGBD3	RNA5SP319
ATP6V1G1P4	CUBNP1	FAM25C	IL15RA	MTND2P16	PGGT1BP1	RNA5SP321
ATP8A2P1	CUBNP2	FAM25G	IL2RA	MTND4P18	PHYH	RNMTL1P1
BAMBI	CUBNP3	FAM35BP	IL9RP2	MTND5P17	PHYHIPL	RNU6-15P
BEND3P1	CUL2	FAM35DP	IMPDH1P5	MTPAP	PIP4K2A	RNU6-6P
BEND7	CUX2P1	FBXO18	IPMK	MTRNR2L5	PITRM1	RNU7-12P
BICC1	CXCL12	FRMD4A	ITGA8	MTRNR2L7	PLA2G12B	RNU7-38P
BMI1	DBF4P1	FRMPD2	ITGB1	MYL6P3	PLXDC2	RNU7-77P
BMS1	DCLRE1C	FRMPD2B	ITIH2	MYO3A	POLR3A	RPL12P28
BMS1P5	DDIT4	FTLP19	ITIH5	MYPN	POU5F1P5	RPL12P8
BMS1P6	DDX10P1	FXYD4	JMJD1C	NAMPTP1	PPA1	RPL13AP19
BMS1P7	DDX20P1	FXYD6P1	KCNMA1	NCOA4	PPIAP30	RPL15P14
BTBD7P1	DDX21	FXYD6P2	KIAA1217	NEBL	PPIAP31	RPL17P35
C1DP1	DDX50	FZD8	KIAA1462	NEFMP1	PRDX2P2	RPL21P88
C1QL3	DHTKD1	GAD2	KIF1BP	NEK4P3	PRELID1P3	RPL21P89
CACNB2	DIP2C	GAPDHP21	KIF5B	NET1	PRF1	RPL21P92
CALM2P2	DKK1	GAPDHP45	KIN	NEUROG3	PRKCQ	RPL21P93
CALML3	DLG5	GATA3	KLF6	NIFKP1	PRKG1	RPL23AP61
CALML5	DNA2	GDF10	KRT19P4	NMT2	PRKG1-AS1	RPL23P11
CAMK1D	DNAJB12	GDF2	KRT8P16	NMTRQ-CTG1-1	PRKRIRP3	RPL26P27
CAP1P2	DNAJC1	GDI2	KRT8P37	**NODAL**	PROSER2	RPL26P28
CASC10	DNAJC12	GJD4	LARP4B	NPAP1P1	PRPF18	RPL26P29
CCAR1	DNAJC19P1	GLUD1P2	LRRC18	NPFFR1	PRPF38AP1	RPL31P44
CCDC3	DNM1P17	GLUD1P5	LRRC20	NPM1P24	PRPF38AP2	RPL31P45
CCDC58P2	DPPA5P3	GLUD1P7	LRRC37A6P	NPY4R	PRR26	RPL32P23
CCDC6	DRGX	GLUD1P8	LRRTM3	NRBF2	PRTFDC1	RPL34P19
CCDC7	DUSP8P3	GNAI2P2	LYZL1	NRBF2P5	PSAP	RPL35AP24
CCND3P1	DUSP8P4	GOLGA2P6	LYZL2	NRP1	PSME2P6	RPL35AP25
CCNY	DUXAP3	GPN3P1	MALRD1	NSUN6	PTCHD3	RPL36AP36
CCNYL2	DUXAP4	GPR158	MAP3K8	NUDT5	PTCHD3P1	RPL36AP55
CDC123	DYNC1I2P1	GPRIN2	MAPK6PS6	NUTM2HP	PTER	RPL37P18
CDH23	EBLN1	GTPBP4	MAPK8	OGDHL	PTF1A	RPL5P25
CDK1	ECHDC3	H2AFY2	MARCH8	OIT3	PTPN20	RPL5P26

Cfs9.1 contd.						
RPL6P24	RPSAP7	SLC25A16	SVILP1	TPRKBP1	USP6NL	
RPL7AP50	RSU1	SLC29A3	SYT15	TPT1P10	VIM	ZNF32
RPL7AP51	RSU1P1	SLC39A12	TACC1P1	TRAF6P1	VIM-AS1	ZNF33A
RPL7AP53	RSU1P2	SLC9A3P1	TACR2	TRDMT1	VN1R53P	ZNF33B
RPL7P37	RSU1P3	SLC9A3P3	TAF3	TRIAP1P1	VN1R54P	ZNF33BP1
RPL9P21	RTKN2	SLC9B1P3	TATDN1P1	TRL-CAA7-1	VPS26A	ZNF33CP
RPLP1P10	RUFY2	SNORD98	TBATA	TRN-GTT2-3	VSTM4	ZNF365
RPP38	SAR1A	SNRPEP8	TCEB1P3	TRP-GGG1-1	WAC	ZNF37A
RPS12P16	SDCBPP1	SNRPGP5	TCEB2P4	TRS-TGA1-1	WDFY4	ZNF37BP
RPS12P17	SEC61A2	SNX19P4	TET1	TRV-TAC3-1	WDR37	ZNF37CP
RPS15AP28	SEPHS1	SPAG6	TFAM	TSPAN15	YME1L1	ZNF438
RPS19P7	SEPT7P9	SPOCK2	THNSL1	TUBAL3	YWHAZP3	ZNF485
RPS24	SFMBT2	SPTLC1P1	TIMM23	TUBB8	YY1P1	ZNF487
RPS24P13	SFTA1P	SRGN	TIMM23B	TYSND1	ZEB1	ZNF488
RPS25P9	SGMS1	SS18L2P1	TLK2P2	UBE2D1	ZFAND4	ZWINT
RPS26P40	SGPL1	ST8SIA6	TMEM14DP	UBE2V2P1	ZMYND11	
RPS3AP37	SHQ1P1	STAM	TMEM161BP1	UCMA	ZNF101P1	
RPS3AP38	SIRT1	STOX1	TMEM236	UCN3	ZNF22	
RPS4XP11	SKIDA1	SUPV3L1	TMEM256P1	UNC5B	ZNF239	
RPS6P14	SLC16A9	SUV39H2	TMEM26	UPF2	ZNF248	
RPSAP10	SLC18A3	SVIL	TMEM72	UQCRHP3	ZNF25	

Cfs9.2						
A1CF	AGAP7P	ARL3	BMS1	CCAR1	CLRN3	CWF19L1
ABCC2	AGAP9	ARL4AP1	BMS1P21	CCDC172	CLUHP5	CXCL12
ABCD1P2	AGGF1P2	ARL5AP2	BMS1P3	CCDC186	CNNM1	CYP17A1
ABLIM1	AHCYP1	ARL6IP1P2	BMS1P4	CCDC58P2	CNNM2	CYP17A1-AS1
ACADSB	AIFM2	ARMC4	BMS1P5	CCDC6	COL13A1	CYP26A1
ACBD5	AK3P5	ARMC4P1	BMS1P6	CCDC7	COL17A1	CYP26C1
ACSL5	AKR1B10P1	ARMS2	BMS1P7	CCND3P1	COMTD1	CYP2C115P
ACSM6	ALDH18A1	AS3MT	BNIP3	CCNJ	COX15	CYP2C18
ACTA2	ALDH7A1P4	ASAH2	BORCS7	CCNY	COX20P1	**CYP2C19**
ACTBP14	ALDOAP2	ASAH2B	BTAF1	CCNYL2	CPEB3	CYP2C59P
ACTR1A	ALOX5	ASCC1	BTBD16	CCSER2	**CPN1**	CYP2C8
ACTR3BP5	ANAPC16	ATAD1	BTBD7P2	CDH23	CPXM2	CYP2C9
ADAM12	ANK3	ATE1	BTF3P15	CDHR1	CREM	CYP2E1
ADAM8	ANKRD1	ATOH7	BTRC	CDK1	CRTAC1	DBF4P1
ADAMTS14	ANKRD2	ATP5G1P7	BUB1P1	CEP164P1	CSGALNACT2	DCLRE1A
ADD3	ANKRD22	ATP5G1P8	BUB3	CEP55	CSTF2T	DDIT4
ADD3-AS1	ANKRD26	ATP6V1G1P4	C1DP1	CEP57L1P1	CTAGE7P	DDX10P1
ADGRA1	ANKRD30A	ATP8A2P1	C1DP2	CFAP43	CTBP2	DDX18P6
ADIRF	ANKRD30BP3	ATRNL1	C1DP3	CFAP46	CTBP2P2	DDX21
ADK	ANKRD54P1	AURKAPS2	C1DP4	CFAP58	CTNNA3	DDX50
ADO	ANTXRL	AVPI1	CACUL1	CFAP70	CTSLP1	DHX32
ADRA2A	ANTXRLP1	BAG3	CACYBPP1	CFL1P1	CTSLP2	DKK1
ADRB1	ANXA11	BAMBI	CALHM1	CH17-360D5	CTSLP3	DLG5
AFAP1L2	ANXA2P3	BANF1P2	CALHM2	CH25H	CTSLP4	DMBT1
AGAP10P	ANXA7	BBIP1	CALHM3	CHAT	CTSLP6	DMBT1P1
AGAP11	ANXA8	BCCIP	CALM2P2	CHCHD1	CUBNP1	DNA2
AGAP12P	ANXA8L1	BEND3P1	CALY	CHST15	CUBNP2	DNAJB12
AGAP13P	AP3M1	BEND3P3	CAMK2G	**CHST3**	CUBNP3	DNAJC12
AGAP14P	ARHGAP12	BICC1	CAP1P2	CHUK	CUEDC2	DNAJC19P1
AGAP4	ARHGAP19	BLNK	CASC2	CICP9	CUL2	DNAJC9
AGAP5	ARHGAP22	BLOC1S2	CASP7	CISD1	CUTC	DNM1P17
AGAP6	ARID5B	**BMPR1A**	CC2D2B	CKS1BP2	CUZD1	DNMBP

Cfs9.2 cont.						
DNTT	EXOSC1	GBF1	HPSE2	LRRC27	MTND4P18	NUTM2A
DOCK1	FAF2P1	GDF10	HSD17B7P2	LRRC37A6P	MTND4P19	NUTM2B
DPCD	FAM133CP	GDF2	HSPA12A	LRRTM3	MTND4P20	NUTM2D
DPYSL4	FAM13C	GFRA1	HSPD1P17	LYZL1	MTND5P17	NUTM2E
DRGX	FAM149B1	GHITM	HTR7	LYZL2	MTPAP	NUTM2HP
DUPD1	FAM160B1	GJD4	HTRA1	LZTS2	MTRNR2L5	OAT
DUSP13	FAM170B	GLRX3	IDE	MAP3K8	MTRNR2L7	OATP1
DUSP5	FAM175B	GLUD1	IFIT1	MAPK6PS6	MXI1	OBFC1
DUSP8P3	FAM196A	GLUD1P2	IFIT1B	MAPK8	MYL6P3	OGDHL
DUSP8P4	FAM204A	GLUD1P3	IFIT2	MAPKAPK5P1	MYOF	OIT3
DUX4L10	FAM210CP	GLUD1P5	IFIT3	MARCH5	MYOZ1	OLMALINC
DUX4L11	FAM213A	GLUD1P7	IFIT5	MARCH8	MYPN	OPALIN
DUX4L12	FAM21A	GLUD1P8	IFIT6P	MARCKSL1P1	NACAP2	OPN4
DUX4L13	FAM21C	GNAI2P2	IKZF5	MARK2P15	NAMPTP1	OR13A1
DUX4L14	FAM21EP	GNG10P1	IMPDH1P5	MARK2P16	NANOGP6	OR6D1P
DUX4L15	FAM21FP	GOLGA2P6	INA	MARK2P9	NANOS1	OR6L1P
DUX4L20	FAM24A	GOLGA7B	INPP5A	MARVELD1	NAPGP1	OR6L2P
DUX4L21	FAM24B	GOT1	INPP5F	MASTL	NCOA4	OR7M1P
DUX4L22	FAM25A	GPAM	IPMK	MAT1A	NDST2	P4HA1
DUX4L23	FAM25BP	GPR26	ITGB1	MBL1P	NDUFB8	PABPC1P12
DUX4L24	FAM25C	GPRIN2	ITPRIP	MBL2	NEFMP1	PABPC1P8
DUX4L25	FAM25G	GRID1	JAKMIP3	MBL3P	NEK4P3	PALD1
DUXAP3	FAM32CP	GRK5	JMJD1C	MCMBP	NEURL1	PANK1
DUXAP4	FAM35A	GRK5-IT1	KAT6B	MCU	NEUROG3	PAOX
DYDC1	FAM35BP	GSTO1	KAZALD1	MED28P1	NFKB2	PAPSS2
DYDC2	FAM35DP	GSTO2	KCNIP2	MED6P1	NHLRC2	PARD3
DYNC1I2P1	FAM45A	GUCY2GP	KCNK18	METTL10	NHP2P1	PARD3-AS1
EBAG9P1	FAM53B	H2AFY2	KCNMA1	MFSD13A	NIFKP1	PARG
EBF3	FANK1	H2AFZP5	KIAA1462	MGEA5	NIP7P1	PARGP1
ECD	FARSBP1	HABP2	KIF11	MGMT	NKX1-2	PAWRP1
ECHS1	FAS	HDAC1P1	KIF1BP	MICU1	NKX2-3	**PAX2**
EDRF1	FAS-AS1	HECTD2	KIF20B	MINPP1	NKX6-2	PBLD
EEF1A1P39	FBXL15	HELLS	KIF5B	MKI67	NOC3L	PCAT5
EGR2	FBXW4	HERC4	KLLN	MKNK2P1	**NODAL**	PCBD1
EIF2AP4	FFAR4	HHEX	KNDC1	MKX	NOLC1	PCDH15
EIF2S2P3	**FGF8**	HIF1AN	KRT19P4	MMP21	NPAP1P1	PCGF5
EIF3A	FGFBP3	HK1	KRT8P38	MMRN2	NPAP1P2	PCGF6
EIF3LP2	**FGFR2**	HKDC1	LBX1	MMS19	NPAP1P3	PDCD11
EIF3LP3	FLJ37035	HMGA1P5	LCOR	MORN4	NPFFR1	PDCD4
EIF4A1P8	FLJ37201	HMGB1P7	LDB1	MPP7	NPM1P24	PDE6C
EIF4A2P2	FOXI2	HMGB3P5	LDB3	MRLN	NPM1P25	PDLIM1
EIF4EBP2	FRA10AC1	HMGB3P8	LDHAP5	MRPL35P2	NPM1P26	PDZD7
EIF5AL1	FRAT1	HMGN2P34	LGI1	MRPL35P3	NPM1P31	PDZD8
EIF5AP4	FRAT2	HMGN2P35	LHPP	MRPL43	NPM3	PFN1P11
ELOVL3	FRG2B	HMGN2P8	LIPA	MRPL50P4	NPS	PGAM1
EMX2	FRMPD2	HMX2	LIPF	MRPS16	NPY4R	PGBD3
EMX2OS	FRMPD2B	HMX3	LIPJ	MRPS21P5	NRAP	PGGT1BP1
EMX2OS	FUOM	HNRNPA1P32	LIPK	MRPS21P6	NRBF2	PGGT1BP2
ENO4	FUT11	HNRNPA1P33	LIPM	MRPS35P3	NRG3	PHACTR2P1
ENTPD1	FXYD4	HNRNPA3P1	LIPN	MSMB	NRP1	PHB2P1
ENTPD7	FXYD6P1	HNRNPF	LOXL4	MSS51	NSMCE4A	PHBP9
EPC1	FXYD6P2	HNRNPH3	LRIT1	MTG1	NT5C2	PHYHIPL
ERCC6	FZD8	HOGA1	LRIT2	MTND1P18	NTAN1P1	PI4K2A
ERLIN1	GAPDHP21	HPS1	LRRC18	MTND1P20	NUDT13	PIK3AP1
EXOC6	GAPDHP28	HPS6	LRRC20	MTND2P15	NUDT9P1	PIPSL

Cfs9.2 contd.						
PITX3	RASSF4	RPL21P89	RPS26P42	SLC29A3	TECTB	VSTM4
PKD2L1	RBBP6P1	RPL21P90	RPS27P1	SLC35G1	TET1	VTI1A
PLA2G12B	RBM20	RPL21P91	RPS27P18	SLC9A3P1	TEX36	VWA2
PLAC9	RBP3	RPL21P92	RPS2P36	SLC9A3P3	TFAM	WAC
PLAU	**RBP4**	RPL21P93	RPS3AP36	SLC9B1P3	TIAL1	WAPL
PLCE1	RCBTB2P1	RPL22P17	RPS3AP37	SLF2	TIMM23	WARS2P1
PLPP4	REEP3	RPL22P18	RPS3AP38	SLIT1	TIMM23B	WBP1L
PLEKHA1	**RET**	RPL23AP58	RPS3AP5	SLK	TIMM9P1	WDFY4
PLEKHS1	RGR	RPL23AP59	RPS4XP11	SMC3	TLK2P2	WDR11
PNLIP	RGS10	RPL23AP60	RPS6P14	SMNDC1	TLL2	WNT8B
PNLIPP1	RHEBP1	RPL23AP61	RPS6P15	SNCG	TLX1	XPNPEP1
PNLIPRP1	RHOBTB1	RPL23P11	RPS7P9	SNORA12	TLX1NB	XRCC6P1
PNLIPRP2	RNA5SP308	RPL26P27	RPS8P4	SNORA19	TM9SF3	YBX2P1
PNLIPRP3	RNA5SP309	RPL26P29	RPSAP10	SNORD98	TMEM14DP	YME1L1
POLL	RNA5SP318	RPL26P6	RPSAP6	SNRPD2P1	TMEM161BP1	YWHAZP5
POLR3A	RNA5SP319	RPL31P44	RRP12	SNRPEP8	TMEM254	YY1P1
POLR3DP1	RNA5SP320	RPL34P19	RSU1P1	SNRPGP12	TMEM256P1	ZCCHC24
POU5F1P5	RNA5SP321	RPL34P20	RSU1P2	SNRPGP6	TMEM26	ZDHHC16
PPA1	RNA5SP322	RPL35AP24	RSU1P3	SNX19P4	TMEM72	ZDHHC6
PPIAP13	RNA5SP323	RPL35AP25	RTKN2	SORBS1	TNKS2	ZEB1
PPIAP19	RNA5SP324	RPL36AP55	RUFY2	SORCS1	TNPO1P1	ZFAND4
PPIAP31	RNA5SP325	RPL37P18	SAMD8	SORCS3	TOMM22P5	ZFYVE27
PPIF	RNA5SP326	RPL39P25	SAR1A	SPA17P1	TPM4P1	ZMIZ1
PPP1R3C	RNA5SP327	RPL5P26	SAR1AP2	SPCS2P2	TPRKBP1	ZNF101P1
PPP2R2D	RNA5SP328	RPL5P27	SCART1	SPOCK2	TPRX1P1	ZNF22
PPP3CB	RNLS	RPL5P28	SCD	SPRN	TPT1P10	ZNF239
PPRC1	RNU1-19P	RPL7AP50	SDHCP2	SPRNP1	TRAF6P1	ZNF248
PRAP1	RNU4-5P	RPL7AP51	SEC23IP	SPTLC1P1	TRIAP1P1	ZNF25
PRDX2P2	RNU5B-6P	RPL7AP52	SEC24C	SRGN	TRIM8	ZNF32
PRDX3	RNU7-12P	RPL7AP53	SEC31B	SRP9P1	TRL-CAA7-1	ZNF33A
PRELID1P3	RNU7-38P	RPL7AP8	SEMA4G	SS18L2P1	TRS-TGA1-1	ZNF33B
PRF1	RNU7-77P	RPL7P34	SEPT7P9	ST13P13	TRUB1	ZNF33BP1
PRKG1	RNY4P26	RPL7P35	SFR1	STAMBPL1	TSPAN14	ZNF33CP
PRKRIRP3	RNY5P7	RPL7P36	SFRP5	STK32C	TSPAN15	ZNF365
PRLHR	RPA2P2	RPL7P37	SFTPA1	STOX1	TUBGCP2	ZNF37A
PSAP	RPAP2P1	RPL9P21	SFTPA2	SUFU	TXNP1	ZNF37BP
PSD	RPEL1	RPLP1P10	SFTPA3P	SUPV3L1	TYSND1	ZNF37CP
PSTK	RPL11P3	RPP30	SFTPD	SVIL	UBE2D1	ZNF438
PTCD2P2	RPL11P4	RPS10P18	SFXN2	SVILP1	UBE2V1P5	ZNF485
PTCHD3	RPL12P26	RPS12P16	SFXN3	SYCE1	UBTD1	ZNF487
PTCHD3P1	RPL12P27	RPS12P17	SFXN4	SYNPO2L	UNC5B	ZNF488
PTEN	RPL12P29	RPS12P18	SGMS1	SYT15	UNC5B-AS1	ZNF503
PTPN20	RPL12P8	RPS12P2	SGPL1	TACC1P1	UQCRHP3	ZNF511
PTPN20CP	RPL13AP19	RPS15AP28	SH2D4B	TACC2	**UROS**	ZNF518A
PTPRE	RPL13AP5	RPS15AP29	SH3PXD2A	TACR2	USMG5	ZNF519P1
PWWP2B	RPL13AP6	RPS15AP30	SHOC2	TAF5	USP54	ZNRF2P3
PYROXD2	RPL15P13	RPS15AP5	SHQ1P1	TAF9BP2	UTF1	ZRANB1
R3HCC1L	RPL15P14	RPS19P7	SHTN1	TATDN1P1	VAX1	ZSWIM8
RAB11AP1	RPL17P34	RPS24	SIRT1	TBATA	**VCL**	ZSWIM8-AS1
RAB11FIP2	RPL17P35	RPS24P13	SLC16A12	TBC1D12	VDAC2	ZWINT
RAB18	RPL17P36	RPS25P9	SLC16A9	TCEB2P4	VENTX	
RAB5CP1	RPL17P50	RPS26P38	SLC18A2	TCERG1L	VN1R53P	
RAD1P1	RPL19P16	RPS26P39	SLC18A3	TCF7L2	VN1R54P	
RARRES2P2	RPL21P16	RPS26P40	SLC25A16	TCTN3	VN1R55P	
RASGEF1A	RPL21P88	RPS26P41	SLC25A28	TDRD1	VPS26A	

Cfs11.1						
A2M	CLEC1B	FOXJ2	KLRC2	OR7E148P	RPL19P17	TAS2R15P
A2ML1	CLEC2A	FOXM1	KLRC3	OR7E149P	RPL21P100	TAS2R18P
A2MP1	CLEC2B	GABARAPL1	KLRC4	OTUD4P1	RPL21P136	TAS2R19
ACRBP	CLEC2D	GALNT8	KLRD1	OVOS	RPL23AP14	TAS2R20
ACSM4	CLEC4A	GAPDH	KLRF1	P3H3	RPL23AP66	TAS2R30
ADIPOR2	CLEC4C	GAPDHP31	KLRF2	PARP11	RPL31P10	TAS2R31
AICDA	CLEC4D	GCSHP4	KLRG1	PEX5	RPL37AP9	TAS2R42
AKAP3	CLEC4E	GDF3	KLRK1	PHB2	RPL37P20	TAS2R43
ANO2	CLEC6A	GNB3	KRT17P8	PHC1	RPS15P7	TAS2R46
APOBEC1	CLEC7A	GOT2P3	LAG3	PIANP	RPS20P28	TAS2R50
APOLD1	CLEC9A	GPR162	LAMP1P1	PKP2P1	RPS20P29	TAS2R63P
ATN1	CLECL1	GPR19	LOH12CR2	PLEKHG6	RPS26P44	TAS2R64P
ATP5J2P5	CLSTN3	GPRC5A	LPAR5	POU5F1P3	RPS26P46	TAS2R67P
B4GALNT3	COPS7A	GPRC5D	LPCAT3	PRB1	RPS27P3	TAS2R7
BCL2L14	CRACR2A	GRIN2B	LRP6	PRB2	RPS3AP43	TAS2R8
BORCS5	CREBL2	GSG1	LRRC23	PRB3	RPS4XP14	TAS2R9
BTG1P1	DCP1B	HADHAP2	LRTM2	PRB4	RPS6P1	TEAD4
C1R	DDX11L8	HEBP1	LTBR	PRH1	RPS6P18	THCAT155
C1R	DDX12P	HIGD1AP8	M6PR	PRH1-PRR4	RPSAP51	TIGAR
C1RL	DDX47	HNRNPA1P34	MAGOHB	PRH2	SCARNA10	TMEM52B
C1S	DDX55P1	HNRNPABP1	MANSC1	PRMT8	SCARNA11	TNFRSF1A
C3AR1	DPPA3	HSPA8P5	MFAP5	PRR4	SCARNA12	TPI1
CACNA1C	DSTNP2	HSPD1P12	MLF2	PTMAP4	SCNN1A	TPT1P12
CACNA2D4	DUSP16	HSPE1P12	MORF4L1P2	PTMS	SLC2A14	TSPAN9
CBX3P4	DYRK4	HTR1DP1	MRPL51	PTPN6	SLC2A3	TULP3
CCDC77	EMG1	HTR7P1	NANOG	PZP	SLC6A12	USP5
CCND2	EMP1	IFFO1	NANOGNB	RAD51AP1	SLC6A13	VAMP1
CD163	ENO2	ING4	NANOGP1	RAD52	SMIM10L1	VDAC2P2
CD163L1	ERC1	IQSEC3	NCAPD2	RBP5	SNRPCP7	VWF
CD27	ETV6	IQSEC3P1	NDUFA9	RHNO1	SPSB2	WNK1
CD4	FAM138D	IQSEC3P2	NECAP1	RIMKLB	SRP14P1	WNT5B
CD69	FAM234B	ITFG2	NIFKP3	RNA5SP353	STX8P1	YBX3
CD9	FAM66C	KCNA1	NINJ2	RNU7-1	STYK1	ZNF384
CDCA3	FAM86FP	KCNA5	NOP2	RNU7-60P	SUPT4H1P2	ZNF705A
CDKN1B	FAM90A1	KCNA6	NPM1P7	RPL13AP20	TAPBPL	
CHD4	FBXL14	KDM5A	NRIP2	RPL13AP24	TAS2R10	
CLEC12A	FGF23	KLRAP1	NTF3	RPL13P5	TAS2R12P	
CLEC12B	FGF6	KLRB1	OLR1	RPL15P17	TAS2R13	
CLEC1A	FKBP4	KLRC1	OR7E140P	RPL18P9	TAS2R14	

Cfs11.2						
ABCC9	ANKRD33	ASUN	CAND1	**COL2A1**	DIP2B	ETNK1
ABCD2	ANO6	ATF1	CAPRIN2	COX14	DNAJC22	FAIM2
ACVR1B	ANP32D	ATF7IP	CAPZA3	COX5BP5	DNM1L	FAM186A
ACVRL1	AQP2	ATG101	CASC1	CPNE8	DSPA2D	FAM186B
ADAMTS20	AQP5	ATP5HP4	CCDC184	CSRNP2	DUX4L27	FAM60A
ADCY6	AQP6	BCAT1	CCDC65	DAD1P1	DYRK2	FAR2
AEBP2	ARF3	BCDIN3D	CCDC91	DAZAP2	EEF1A1P16	FGD4
AK4P3	ARHGDIB	BHLHE41	CCNT1	DBX2	EEF1A1P17	FGFR1OP2
AK6P1	ARID2	BICD1	CELA1	DDN	EEF1A1P4	FIGNL2
AK6P2	ARNTL2	BIN2	CENPUP2	DDX11	EGLN3P1	FKBP11
ALG10	ART4	BRI3P2	CERS5	DDX23	ENDOU	FLJ13224
ALG10B	ASB8	C1QL4	CLUHP8	DENND5B	EPS8	FMNL3
AMIGO2	ASIC1	C2CD5	CMAS	DERA	ERGIC2	GALNT6
AMN1	ASS1P14	CACNB3	CNTN1	DHH	ERP27	GGTA2P

Cfs11.2 cont.						
GNAI2P1	KNOP1P2	MRPS18CP4	PIK3C2G	RNA5SP358	SCAF11	SYT10
GOLT1B	**KRAS**	MRPS35	PKP2	RNA5SP359	SCN8A	TCEB1P31
GOT2P4	KRT7	MRPS36P5	PLBD1	RNA5SP360	SENP1	TCP1P3
GPD1	KRT80	MRPS7P2	PLCZ1	RNA5SP361	SKP1P2	TDGP1
GRASP	KRT81	MTND1P24	PLEKHA5	RND1	SLC11A2	TFCP2
GRIN2B	KRT83	MTND2P17	PLEKHA8P1	RNU5F-4P	SLC15A5	THEM4P1
GRIP1	KRT86	MUC19	POLR2KP1	RNU7-39P	SLC2A13	TIMM17BP1
GUCY2C	KRT87P	NCKAP5L	POU6F1	RPAP3	SLC38A1	TM7SF3
GXYLT1	KRT88P	NDFIP1P1	PPFIBP1	RPL10P12	SLC38A2	TMBIM6
GYS2	LALBA	NELL2	PPHLN1	RPL12P32	SLC38A4	TMEM106C
H1FNT	LARP4	NF1P12	PRICKLE1	RPL13AP21	SLC48A1	TMEM117
H2AFJ	LDHB	NMTRQ-TTG6-1	PRKAG1	RPL13AP22	SLC4A8	TMPRSS12
H3F3C	LETMD1	NR4A1	PRPF40B	RPL21P101	SLCO1A2	TMTC1
HDAC7	LIMA1	NTAN1P3	PRPH	RPL21P102	SLCO1B1	TROAP
HIGD1AP9	LMBR1L	OR10AD1	PSMC1P8	RPL21P99	SLCO1B3	TSPAN11
HIGD1C	LMNTD1	OR11M1P	PSMC1P9	RPL26P33	SLCO1B7	TUBA1A
HIST4H4	LMO3	OR5BJ1P	PSMC6P2	RPL29P27	SLCO1C1	TUBA1B
HMGB1P49	LRMP	OR5BK1P	PTHLH	RPL30P11	SMAGP	TUBA1C
HMGN1P23	LRRC34P1	OR5BS1P	PTPRO	RPL30P13	SMARCD1	TUBB8P4
HNRNPA1P70	LRRK2	OR5BT1P	PUS7L	RPL31P50	SMCO2	TUBB8P5
HNRNPA3P10	LSM6P2	OR7A19P	PYROXD1	RPL32P27	SMCO3	TWF1
IAPP	LYRM5	OR7E47P	RACGAP1	RPL34P25	SNORA2A	UBE2L2
IFNG	MANSC4	OR8S1	RACGAP1P	RPL35AP27	SNORA2B	**VDR**
IL22	MARK3P1	OR8S21P	RAP1B	RPL35AP28	SNORA2C	WBP11
IL26	MCRS1	OR8T1P	RAPGEF3	RPL35AP29	SNORA70G	**WNT1**
IPO8	MDM1	OSBPL9P4	RARSP1	RPL37P19	SOX5	WNT10B
IRAK4	MED21	OVCH1	RASSF8	RPL39P27	SPATS2	YAF2
ITPR2	MEF2BNBP1	OVOS2	RECQL	RPL39P28	SPX	YARS2
KANSL2	METTL20	PCED1B	REP15	RPL7P40	SRSF11P1	ZCRB1
KCNH3	METTL7A	PDCD5P1	RERG	RPL7P6	SSPN	ZKSCAN7P1
KCNJ8	METTL7AP1	PDE3A	RERG-AS1	RPLP2P4	ST13P9	ZNF641
KIAA1551	METTL8P1	PDE6H	RERGL	RPS10P20	ST8SIA1	ZNF75BP
KIF21A	MGP	PDZRN4	RHEBL1	RPS27P21	STK38L	ZNF970P
KLHL42	MGST1	PFKM	RNA5SP354	RPS27P22	STMN1P1	
KMT2D	MRPL30P2	PHBP18	RNA5SP356	RPS2P42	STRAP	
KNOP1P1	MRPL40P1	PHBP19	RNA5SP357	RPSAP12	SUPT16HP1	

Cfs12.2						
ABCA12	AOX1	CD28	CALCRL	COQ10B	CYP20A1	DNAJC19P5
ABCB11	AOX2P	CD302	CARF	CPO	CYTIP	DPP4
ABI2	API5P2	CDCA7	CASP10	CPS1	DAP3P2	DPRXP1
ACADL	ARHGAP15	ATP5F1P4	CDK15	CREB1	DAPL1	DSTNP5
ACVR1	ARL5A	ATP5G2P3	CDK7PS	CRYGA	DAZAP2P1	DUSP19
ACVR1C	ARL6IP6	ATP5G3	CERKL	CRYGB	DCAF17	DYNC1I2
ACVR2A	ASNSD1	B3GALT1	CERS6	CRYGC	DFNB59	DYTN
ADAM23	ATF2	BARD1	CERS6-AS1	CRYGD	DHRS9	E2F3P2
AGPS	ATIC	BAZ2B	CFLAR	CRYGEP	DIRC1	EEF1B2
AHCTF1P1	ATP5A1P2	BBS5	CFLAR-AS1	CRYGFP	DIRC3	EIF2S2P4
AHCYP5	CASP8	BICD1P1	CHN1	CSRNP3	DLX1	EIF3EP2
ALDH7A1P2	CBX3P6	BMPR2	**CHRNA1**	CTAGE14P	DLX2	EIF3EP3
ALS2	CCDC141	BOLL	CIR1	CTLA4	DLX2-AS1	ELF2P4
ALS2CR11	CCDC148	BTF3L4P2	CLK1	CWC22	DNAH7	ENO1P4
ALS2CR12	CCDC150	BZW1	COBLL1	CYB5AP2	DNAJA1P2	ENSAP3
ANKAR	CCDC173	CACNB4	**COL3A1**	CYBRD1	DNAJB1P1	EPC2
ANKRD44	CCNYL1	CACYBPP2	COL5A2	CYCTP	DNAJC10	ERBB4

Cfs12.2 cont.						
ERICH2	HNRNPA1P39	LRP2	NOP58	RBM45	RPL7AP22	
ERMN	HNRNPA1P47	LY75	NOSTRIN	RBMS1	RPL7L1P9	SSFA2
EVX2	HNRNPA1P51	LYPD6	NPM1P33	RFTN2	RPL7P14	ST13P2
EXTL2P1	HNRNPA3	LYPD6B	NPM1P46	RIF1	RPL7P61	STAM2
FABP5P10	HNRNPCP2	MAP2	NR4A2	RNA5SP107	RPL9P13	STAT1
FABP5P14	HNRNPDLP2	MAPRE1P3	NRP2	RNA5SP108	RPL9P14	STAT4
FAM117B	HOXD-AS2	MARCH4	NUDCP1	RNA5SP109	RPLP0P7	STIP1P1
FAM126B	HOXD1	MARCH7	NUDCP2	RNA5SP110	RPLP1P4	STK17B
FAM133DP	HOXD10	MARS2	NUP35	RNA5SP111	RPRM	STK39
FAM171B	HOXD11	MBD5	OLA1	RNA5SP112	RPS15AP14	STRADB
FAM8A3P	HOXD12	MDH1B	OR7E28P	RNA5SP113	RPS15P4	SUMO1
FAP	HOXD13	MEAF6P1	OR7E89P	RNA5SP114	RPS16P3	TANC1
FASTKD1	HOXD3	MED28P3	OR7E90P	RNA5SP115	RPS17P8	TANK
FASTKD2	HOXD4	METAP1D	ORC2	RNA5SP116	RPS20P13	TBR1
FIGN	HOXD8	METTL21A	ORC4	RNA5SP117	RPS26P20	TEX41
FKBP7	HOXD9	METTL5	ORMDL1	RNA5SP118	RPS27P10	TFPI
FMNL2	HSPA8P6	METTL8	OSBPL6	RNA5SP119	RPS29P8	TIMM8AP1
FN1	HSPD1	MFSD6	OSGEPL1	RNA5SP120	RPS29P9	TLK1
FRZB	HSPE1	MMADHC	PABPC1P2	RND3	RPS2P16	TMEFF2
FSIP2	ICA1L	MOB4	PARD3B	RNF11P1	RPS2P18	TMEM169
FTCDNL1	ICOS	MPP4	PCED1CP	RNU5E-9P	RPS3AP13	TMEM237
FTH1P20	IDH1	MREG	PCGEM1	RNU6-31P	RPS6P2	TNFAIP6
FUCA1P1	IFIH1	MRPL50P2	PDE11A	RNU7-2P	RPSAP24	TNP1
FZD5	IGFBP2	MSTN	PDE1A	RNU7-44P	RPSAP25	TNS1
FZD7	IGFBP5	MTND1P27	PDK1	RNU7-45P	RPSAP27	TPT1P2
G6PC2	IKZF2	MTND2P19	PECR	RNY5P2	SAP18P2	TRA-CGC3-1
GAD1	IMPDH1P10	MTND2P20	PGAP1	RPE	**SATB2**	TRAK2
GALNT13	IMPDH1P7	MTND2P23	PHBP4	RPL10P6	SCHLAP1	TRE-CTC7-1
GALNT3	INO80D	MTND3P9	PHF5GP	RPL12P16	**SCN1A**	TRE-CTC9-1
GALNT5	INPP1	MTND4P22	PHOSPHO2	RPL12P17	SCN2A	TRE-TTC9-1
GAPDHP59	ITGA4	MTND4P23	PIKFYVE	RPL13AP12	SCN3A	TRG-GCC2-5
GCA	ITGA6	MTND4P28	PKI55	RPL17P10	SCN7A	TTC21B
GCG	ITGAV	MTND4P29	PKP4	RPL17P12	SCN9A	TTC30A
GCSHP3	ITGB6	MTND4P30	PKP4P1	RPL17P13	SCRN3	TTC30B
GLS	KANSL1L	MTND5P24	PLA2R1	RPL21P31	SDHDP5	TTN
GLULP6	KCNH7	MTND5P25	PLCL1	RPL21P32	SDPR	TTN-AS1
GORASP2	KCNJ3	MTND5P30	PLEKHA3	RPL21P38	SEPHS1P6	TXNP5
GPD2	KCTD18	MTND5P31	PLEKHM3	RPL23AP29	SESTD1	TYW5
GPR1	KIAA1715	MTX2	PMS1	RPL23AP30	SF3B1	UBBP3
GPR155	KIAA2012	MYL1	PPIG	RPL23AP33	SGCEP	UBE2E3
GRB14	KIF5C	MYL6BP1	PPIL3	RPL23AP35	SGOL2	UBE2V1P6
GSTM3P2	KLF7	MYO1B	PPP1R14BP2	RPL23AP36	SLC25A12	UBQLN4P2
GTDC1	KLHL23	MYO3B	PPP1R1C	RPL26P14	SLC38A11	UBR3
GTF3C3	KLHL41	NAB1	**PRKRA**	RPL27AP3	SLC39A10	UNC80
GULP1	KRT18P19	NABP1	PRPF40A	RPL27P8	SLC40A1	UPP2
H3F3AP4	KRT18P29	NBEAL1	PRPS1P1	RPL29P8	SLC4A10	VWC2L
HAGLR	KRT18P39	NCKAP1	PSMA2P3	RPL30P2	SMARCAL1	WDR12
HAGLROS	KRT18P46	NDUFB3	PSMB3P2	RPL31P14	SNAI1P1	WDR75
HAT1	KRT8P10	NDUFS1	PSMD14	RPL31P15	SP3	WDSUB1
HECW2	KRT8P15	NEB	PTCHD3P2	RPL37A	SP5	WIPF1
HIBCH	KRT8P40	NEMP2	PTH2R	RPL39P14	SP9	XIRP2
HMGB1P27	KYNU	NEUROD1	PTP4A1P1	RPL5P7	SPAG16	XRCC5
HMGB1P4	LANCL1	NFE2L2	RAPGEF4	RPL5P8	SPATS2L	ZAK
HMGN1P6	LIN28AP1	NIF3L1	RAPH1	RPL6P5	SPC25	ZC3H15
HNRNPA1P35	LRP1B	NMI	RBM43	RPL6P6	SSB	ZDBF2

Cfs12.2 cont.						
ZEB2	ZNF385B	ZNF804A	ZSWIM2			

Cfs12.3						
AAMP	FAM124B	INO80D	NHEJ1	RNA5SP117	RPS2P16	STK36
ABCA12	ALPP	ARMC9	NIF3L1	RNA5SP118	RPSAP27	STRADB
ABCB6	ALPPL2	ARPC2	BCS1L	RNA5SP119	RQCD1	SUMO1
ABI2	ALS2	ASIC4	BICD1P1	RNA5SP120	RUFY4	TDGF1P2
ACADL	ALS2CR11	ATG12P2	BMPR2	CCDC140	CFLAR	COPS7B
ACSL3	ALS2CR12	ATG9A	BZW1	CCL20	CHPF	COX20P2
ADAM23	ANKZF1	ATIC	CAB39	CCNYL1	CHRND	CPO
AGFG1	AOX1	B3GNT7	CARF	CD28	CHRNG	CPS1
ALPI	AOX2P	BANF1P3	CASP10	CDK15	CLK1	CREB1
CRYGC	AP1S3	BARD1	CASP8	CDK5R2	CNPPD1	CRYBA2
CRYGD	FAM126B	IRS1	CATIP	CFAP65	COL4A3	CRYGA
CRYGEP	FAM134A	ITM2C	NMUR1	RNA5SP121	COL4A4	CRYGB
CRYGFP	FARSB	KANSL1L	NOP58	RNF25	**SATB2**	TIGD1
CTDSP1	FASTKD2	KCNE4	NPM1P33	RNU6-31P	SATB2-AS1	TM4SF20
CTLA4	FBXO36	KCNJ13	NPPC	RNU7-45P	SCG2	TMBIM1
CUL3	FEV	KCTD18	NRP2	RNU7-9P	SEPHS1P6	TMEM169
CXCR1	FN1	KIAA2012	NYAP2	RNY4P19	SERPINE2	TMEM198
CXCR2	FTCDNL1	KLF7	OBSL1	RPE	SGOL2	TMEM237
CXCR2P1	FZD5	KRT18P39	ORC2	RPL10P6	SGPP2	TNP1
CYP20A1	FZD7	KRT8P15	PARD3B	RPL12P16	SLC11A1	TNS1
CYP27A1	GAMTP1	KRT8P30	**PAX3**	RPL12P17	SLC16A14	TPM3P8
DAW1	GAPDHP49	LANCL1	PCED1CP	RPL13AP12	SLC19A3	TPT1P2
DAZAP2P1	GCSHP3	MAP2	PDE6D	RPL17P10	SLC23A3	TRAK2
DES	GIGYF2	MARCH4	PECR	RPL17P14	SLC4A3	TRE-TTC9-1
DIRC3	GLB1L	MDH1B	PID1	RPL19P5	SMARCAL1	TRIP12
DIS3L2	GMPPA	MEAF6P1	PIKFYVE	RPL21P35	SNAI1P1	TRK-TTT15-1
DIS3L2P1	GPBAR1	METTL21A	PKI55	RPL23AP26	SNORA41	TRQ-CTG16-1
DNAJB2	GPR1	MFF	PKP4P1	RPL23AP28	SNORA75	TRY-ATA1-1
DNER	GPR55	MOGAT1	PLCD4	RPL23AP30	SNORD11	TTLL4
DNPEP	HIGD1AP4	MPP4	PLCL1	RPL23AP31	SNORD11B	TUBA4A
DOCK10	HMGB1P3	MREG	PLEKHM3	RPL23AP36	SNORD20	TUBA4B
DSTNP5	HMGB1P9	MRPL44	PNKD	RPL23P4	SNORD51	TYW5
DYTN	HMGN1P6	MRPL50P2	PPIL3	RPL23P5	SNORD70	UNC80
ECEL1	HNRNPA1P35	MTND2P23	PPP1R14BP2	RPL27P8	SNORD82	USP37
ECEL1P1	HNRNPA1P51	MTND4P23	PRKAG3	RPL28P2	SNRPGP8	VIL1
ECEL1P2	HSPA8P6	MTND4P29	PRSS56	RPL31P14	SP100	VWC2L
ECEL1P3	HSPA9P1	MTND4P30	PSMA2P3	RPL31P17	SP110	WDFY1
EEF1B2	HTR2B	MTND5P25	PSMB3P2	RPL37A	SP140	WDR12
EEF1B2P7	ICA1L	MTND5P31	PSMD1	RPL39P14	SP140L	WNT10A
EFHD1	ICOS	MYL1	PTH2R	RPL5P8	SPAG16	WNT6
EIF4E2	IDH1	MYL6BP1	PTMA	RPL6P6	SPATA3	XRCC5
ENO1P4	IGFBP2	NANOGP2	PTPRN	RPL7L1P9	SPATS2L	ZBTB8OSP2
ENSAP3	IGFBP5	NBEAL1	RAPH1	RPL7P14	SPEG	ZDBF2
EPHA4	IHH	NCL	RESP18	RPL9P14	SPHKAP	ZFAND2B
ERBB4	IKZF2	NDUFB3	RHBDD1	RPS27P10	STIP1P2	ZNF142
FABP5P14	IMPDH1P10	NDUFS1	RNA5SP115	RPS28P4	STK11IP	
FAM117B	INHA	NGEF	RNA5SP116	RPS29P9	STK16	

Cfs12.4						
ACKR3	ANO7	ASB1	BOK	COL6A3	D2HGDH	ESPNL
AGXT	AQP12A	ASB18	CAPN10	COPS8	DTYMK	FAM132B
ANKMY1	AQP12B	ATG4B	CICP10	CROCC2	DUSP28	FARP2

Cfs12.4 cont.						
FLJ43879	ILKAP	MLPH	OR6B3	PPP1R7	RNPEPL1	STK25
GAL3ST2	ING5	MTERF4	OR9S24P	PRLH	RPL23AP88	THAP4
GPC1	IQCA1	MYEOV2	OTOS	PRR21	RPL3P5	TRAF3IP1
GPR35	KIF1A	NDUFA10	PASK	RAB17	RTP5	TWIST2
HDAC4	KLHL30	NEU4	PDCD1	RAMP1	SCLY	UBE2F
HDLBP	LRRFIP1	OR5S1P	PER2	RBM44	SEPT2	
HES6	MGC16025	OR6B2	PP14571	RNA5SP122	SNED1	

Cfs13.1						
ABCG5	CYS1	GEN1	MFSD2B	PTRHD1	RAD51AP2	TRAPPC12
ABCG8	DCDC2C	GPATCH11	MIR7515HG	PUM2	RASGRP3	TRG-CCC7-1
ABHD1	DDX1	GPN1	MORN2	RDH14	RBKS	TRI-TAT2-1
ACP1	DDX50P1	GREB1	MPV17	RHOB	SDHCP3	TRIB2
ADAM17	DHX57	GRHL1	MRPL33	RMDN2	SF3B6	TRIM54
ADCY3	DNAJC27	GTF3C2	MRPL50P1	RMDN2-AS1	SH3YL1	TRMT112P6
ADGRF3	DNAJC5G	HAAO	MSGN1	RNA5SP84	SLC25A5P2	TRMT61B
ADI1	DNMT3A	HADHA	MTA3	RNA5SP85	SLC30A3	TRY-GTA2-1
AGBL5	DPY30	HADHB	MYADML	RNA5SP86	SLC30A6	TSSC1
AK2P2	DPYSL5	HEATR5B	MYCN	RNA5SP87	SLC35F6	TTC27
ALK	DRC1	HMGB1P25	MYCNOS	RNA5SP88	SLC4A1AP	TTC32
ALLC	DTNB	HMGN2P20	MYCNUT	RNA5SP89	SLC5A6	TTC39DP
APOB	DYNC2LI1	HNRNPA1P57	MYT1L	RNA5SP90	SLC7A15P	TYW1P1
ARHGEF33	E2F6	HNRNPA1P61	NACAP4	RNA5SP91	SLC8A1	UBXN2A
ASAP2	EFR3B	HNRNPLL	NBAS	RNA5SP92	SMARCE1P6	UCN
ASS1P2	EHD3	HPCAL1	NCOA1	RNASEH1	SMC6	UQCRHP2
ASXL2	EIF2AK2	HS1BP3	NDUFAF7	RNF144A	SNORA80B	VDAC1P13
ATAD2B	EIF2B4	IAH1	NLRC4	RNFT1P1	SNORD53	VIT
ATL2	EMILIN1	ID2	NOL10	RNU5E-7P	SNORD92	VSNL1
ATP6V0E1P3	EML4	IFT172	NPM1P48	ROCK2	SNRPEP5	**WDR35**
ATP6V1C2	EPT1	ITGB1BP1	NRBP1	RPL21P36	SNRPGP7	WDR43
ATRAID	FAM110C	ITSN2	NRIR	RPL21P70	SNTG2	XDH
BIRC6	FAM150B	KCNF1	NT5C1B	RPL23AP34	SNX17	YIPF4
BRE	FAM179A	KCNG3	NTSR2	RPL30P3	**SOS1**	YPEL5
C1GALT1C1L	FAM228A	KCNK3	NUTF2P8	RPL31P16	SOX11	YWHAQ
CAD	FAM228B	KCNS3	ODC1	RPL36AP13	SPAST	ZFP36L2
CAPN13	FAM49A	KHK	OSR1	RPL37P11	SPDYA	ZFYVE9P2
CAPN14	FAM84A	KIDINS220	OST4	RPL6P4	SRD5A2	ZNF512
CCDC121	FAM98A	KIF3C	OTOF	RPL7P12	SRSF7	ZNF513
CDC42EP3	FEZ2	KLF11	OXER1	RPLP0P6	ST13P1	ZPAXP
CDKL4	FKBP1B	KLHL29	PDIA6	RPLP1P5	STRN	
CDKN2AIPNLP2	FLJ31356	KRT18P52	PFN4	RPS12P4	SUCLA2P3	
CEBPZ	FLJ33534	KRTCAP3	PGAM1P6	RPS13P3	SULT6B1	
CEBPZOS	FNDC4	LAPTM4A	PKDCC	RPS13P4	SUPT7L	
CENPA	FOSL2	LBH	PLB1	RPS13P5	TAF1B	
CENPO	FTH1P3	LCLAT1	PLEKHH2	RPS16P2	TCF23	
CGREF1	FTOP1	LDAH	POMC	RPS25P3	TDRD15	
CIB4	GACAT3	LDHAP3	PPIL1P1	RPS26P18	THADA	
CISD1P1	GALM	LPIN1	PPM1G	RPS2P15	THUMPD2	
CLIP4	GALNT14	LRPPRC	PPP1CB	RPS7	TMEM178A	
CMPK2	GAPDHP25	LTBP1	PQLC3	RRM2	TMEM18	
COLEC11	GAPDHP48	MAP4K3	PREB	RSAD2	TMEM214	
COX7A2L	GAREM2	MAPRE3	PRKD3	SDC1	TMSB4XP2	
CPSF3	GCKR	MATN3	PRR30	PXDN	TP53I3	
CRIM1	GDF7	MBOAT2	PSMC1P10	QPCT	TPM3P7	
CYP1B1	GEMIN6	MEMO1	PTGES3P2	RAB10	TPO	

Cfs15.3						
AAED1	ATP5A1P5	CHMP5	EBLN3	FKTN	HAUS6	IL11RA
ABCA1	ATP5A1P7	CKS2	ECM2	FLJ43315	HDHD3	IL6RP1
ABHD17B	ATP5A1P8	CLIC4P1	EEF1DP2	FOCAD	HEMGN	IMPDH1P1
ACER2	ATP5J2P3	CLK3P1	EIF4BP3	FOXB2	HINT2	INIP
ACO1	ATP6V1G1	CLTA	ELAVL2	FOXD4L3	HMGB1P37	INVS
ACTG1P19	ATP8B5P	CNN2P2	ELF2P3	FOXD4L4	HMGB3P23	IPPK
ACTL7A	AUH	CNN2P3	ENHO	FOXD4L5	HMGB3P24	ISCA1
ACTL7B	B4GALT1	CNN2P4	EPB41L4B	FOXD4L6	HMGN2P32	IZUMO3
ADAMTSL1	bA255A11	CNTFR	EQTN	**FOXE1**	HMGN2P33	KCTD10P1
ADGRD2	BAAT	CNTLN	ERCC6L2	FRG1HP	HNRNPA1P14	KCTD9P3
ADGRF5P1	BAATP1	CNTNAP3	ERP44	FRG1JP	HNRNPA1P15	KGFLP1
ADGRF5P2	BAG1	CNTNAP3B	ERVFRD-3	FRG1KP	HNRNPK	KGFLP2
AGTPBP1	BANCR	CNTNAP3P1	EXOSC3	FRMD3	HRCT1	KHSRPP1
AHCYP2	BARX1	CNTNAP3P2	FAM120A	FRMPD1	HSD17B3	KIAA0368
AKAP2	BEND3P2	CNTNAP3P5	FAM120AOS	FRRS1L	HSDL2	KIAA1161
AKNA	BICD2	CNTNAP3P6	FAM122A	FSD1L	HSPA5	KIAA1958
ALAD	BMS1P10	CNTNAP3P7	FAM166B	FTLP4	HSPA8P17	KIF12
ALDH1A1	BMS1P11	CNTNAP3P8	FAM189A2	FXN	HSPB1P1	KIF24
ALDH1B1	BMS1P12	CNTRL	FAM201A	FXNP2	HSPE1P22	KIF27
ALDOB	BMS1P13	COL15A1	FAM205A	FYTTD1P1	HSPE1P28	KLF4
ALG2	BMS1P9	COL27A1	FAM205BP	GABBR2	IARS	KLF9
ALOX15P2	BNC2	CORO2A	FAM205C	GADD45G	IDNK	KLHL9
AMBP	BNIP3P4	CRB2	FAM206A	GALNT12	IFNA1	KRT18P13
ANKRD18A	BRINP1	CREB3	FAM214B	GALT	IFNA10	KRT18P24
ANKRD18B	BSPRY	CTAGE12P	FAM219A	GAPDHP26	IFNA11P	KRT18P36
ANKRD19P	BTF3P4	CTNNAL1	FAM220BP	GAPVD1	IFNA12P	KRT18P66
ANKRD20A1	C5	CTSL	FAM220CP	GAS1	IFNA13	KRT18P67
ANKRD20A2	CA9	CTSL3P	FAM221B	GAS1RR	IFNA14	KRT8P11
ANKRD20A20P	CAAP1	CTSLP8	FAM225A	GAS2L1P1	IFNA16	LAGE3P1
ANKRD20A3	CARD19	CTSV	FAM225B	GAS2L1P2	IFNA17	LHX2
ANKRD20A4	CARNMT1	CYCSP24	FAM27B	GBA2	IFNA2	LHX6
ANKRD20A7P	CBWD3	CYLC2	FAM27C	GCNT1	IFNA20P	LINGO2
ANKS6	CBWD4P	CYP1D1P	FAM27E2	GDA	IFNA21	LPAR1
ANP32B	CBWD5	CYP4F25P	FAM27E3	GGTA1P	IFNA22P	LRRC19
ANXA1	CBWD6	CYP4F59P	FAM71BP1	GKAP1	IFNA4	LRRC37A5P
ANXA2P2	CCDC107	DAB2IP	FAM74A1	GLIDR	IFNA5	LSM1P1
APBA1	CCDC180	DAPK1	FAM74A3	GLIPR2	IFNA6	LYPLA2P3
APTX	CCIN	DCAF10	FAM74A4	GLRX3P1	IFNA7	MAMDC2
AQP3	CCL19	DCAF12	FAM74A6	GLULP4	IFNA8	MAP1LC3BP1
AQP7	CCL21	DCTN3	FAM74A7	GNA14	IFNB1	MAPKAP1
AQP7P1	CCL27	DDX58	FAM95B1	GNAQ	IFNE	ME2P1
AQP7P2	CD72	DEC1	FAM95C	GNE	IFNK	MEGF9
AQP7P3	CDC14B	DENND1A	FANCC	GNG10	IFNNP1	MELK
AQP7P4	CDC20P1	DENND4C	FANCG	GOLGA1	IFNW1	MEP1AP1
AQP7P5	CDC26	DEPDC1P2	FBP1	GOLM1	IFNWP15	MEP1AP3
ARHGEF39	CDK20	DFFBP1	FBP2	GPR21	IFNWP18	MEP1AP4
ARID3C	CDK2AP2P1	DFNB31	FBP2P1	GRHPR	IFNWP19	MFSD14B
ARL2BPP7	CDK2AP2P3	DIRAS2	FBXO10	GRIN3A	IFNWP2	MFSD14C
ARMC8P1	CDK5RAP2	DMRTA1	FBXW2	GSN	IFNWP5	MIRLET7A1
ARPC5L	CDKN2A	DNAI1	FGD3	GXYLT1P3	IFNWP9	MIRLET7D
ASPN	CDKN2B	DNAJA1	FKBP15	GXYLT1P4	IFT74	MIRLET7DHG
ASS1P12	CENPP	DNAJB5	FKBP4P2	GXYLT1P5	IGFBPL1	MIRLET7F1
ASS1P3	CEP78	DNAJB5P1	FKBP4P6	GXYLT1P6	IGKV1OR-2	MLLT3
ASTN2	CHCHD2P9	DNAJC25	FKBP4P7	HABP4	IGKV1OR9-1	MOB3B
ATP5A1P10	CHCHD4P2	DPP3P2	FKBP4P8	HACD4	IKBKAP	MORN5

Cfs15.3 cont.						
MRPL50	OR13C1P	PCSK5	RALGAPA1P	RPL31P42	SH3GL2	SUGT1P1
MRPS10P5	OR13C2	PDCL	RAP1BP1	RPL31P43	SHB	SUMO2P2
MRPS21P4	OR13C3	PDK1P1	RBM17P1	RPL32P21	SHC3	SUSD1
MRRF	OR13C4	PGAM1P2	RBM17P2	RPL32P22	SIGMAR1	SUSD3
MSANTD3	OR13C5	PGM5	RBM17P3	RPL35	SIT1	SVEP1
MSMP	OR13C6P	PGM5P2	RBM18	RPL35AP2	SKA2P1	SYF2P2
MT1P1	OR13C7	PHBP7	RBM22P5	RPL35AP21	SKP1P3	SYK
MTAP	OR13C8	PHF19	RBMXP2	RPL35AP22	SLC24A2	SYNGR2P2
MTND2P11	OR13C9	PHF2	RBPJP2	RPL36AP33	SLC25A51	TAF1L
MTND2P8	OR13D1	PHF24	RBPJP5	RPL36AP34	SLC25A5P8	TAL2
MTND3P4	OR13D2P	PIGFP2	RBPJP6	RPL36AP35	SLC25A6P2	TBC1D2
MTND4P15	OR13D3P	PIGO	RBPJP7	RPL36AP6	SLC25A6P5	TCEA1P1
MUPP	OR13E1P	PIGUP1	RC3H2	RPL36P14	SLC28A3	TCEA1P3
MURC	OR13F1	PIP5K1B	RECK	RPL7AP44	SLC31A1	TCEA1P4
MUSK	OR13I1P	PLAA	RFC5P1	RPL7AP45	SLC31A2	TDRD7
MVB12B	OR13J1	PLIN2	RFK	RPL7AP46	SLC35D2	TEK
MYO5BP1	OR1B1	PLPPR1	RGP1	RPL7AP48	SLC44A1	TESK1
MYO5BP2	OR1H1P	POLE3	RGS3	RPL7AP49	SLC46A2	TEX10
MYO5BP3	OR1J1	POLR1E	RMI1	RPP25L	SLC4A1APP1	**TGFBR1**
NAA35	OR1J2	PPP3R2	RMRP	RPS10P17	SMC2	TJP2
NAMA	OR1J4	PPP6C	RNA5-8SP3	RPS10P3	SMC5	TLE4
NANOGP5	OR1K1	PRKACG	RNA5SP280	RPS11P4	SMC5-AS1	TLK1P1
NANS	OR1L1	PRO2852	RNA5SP281	RPS15AP27	SMNP	TLN1
NCBP1	OR1L3	PRPF4	RNA5SP282	RPS20P24	SMU1	**TLR4**
NDUFA5P3	OR1L4	PRPS1P2	RNA5SP283	RPS21P5	SNORA70C	TMC1
NDUFA5P4	OR1L6	PRSS3	RNA5SP284	RPS25P8	SNORA84	TMEFF1
NDUFA8	OR1L8	PRUNE2	RNA5SP285	RPS26P2	SNORD121A	TMEM2
NDUFB3P2	OR1N1	PSAT1	RNA5SP286	RPS26P37	SNORD121B	TMEM215
NDUFB6	OR1N2	PSMA7P	RNA5SP288	RPS27AP15	SNORD90	TMEM245
NEK6	OR1Q1	PSMB7	RNA5SP289	RPS29P17	SNRPCP1	TMEM246
NFIL3	OR2AM1P	PSMC3P	RNA5SP290	RPS29P18	SNX18P2	TMEM252
NFX1	OR2K2	PSMD5	RNA5SP291	RPS2P35	SNX18P3	TMEM38B
NINJ1	OR2S1P	PTAR1	RNA5SP292	RPS6	SNX18P4	TMEM8B
NIPSNAP3A	OR2S2	PTBP3	RNA5SP293	RPS6P10	SNX18P5	TMOD1
NIPSNAP3B	OR5C1	**PTCH1**	RNA5SP294	RPS6P13	SNX18P7	TMX2P1
NMRK1	OR7E108P	PTCSC2	RNA5SP295	RPS8P9	SNX18P8	TNC
NOL6	OR7E109P	PTENP1	RNF183	RPSAP49	SNX18P9	TNFSF15
NOL8	OR7E116P	PTGER4P1	RNF20	RPSAP76	SNX30	TNFSF8
NOP56P2	OR7E31P	PTGER4P2	RNF38	RPSAP9	SPAG8	TOMM5
NPAP1P4	ORM1	PTGER4P3	RNU2-5P	RRAGA	SPATA31A1	TOPORS
NPAP1P5	ORM2	PTGR1	RNU5B-5P	RUSC2	SPATA31A3	TOPORSLP1
NPAP1P6	OSTCP8	PTGS1	RNU7-36P	S1PR3	SPATA31A5	**TPM2**
NPR2	OSTF1	PTPDC1	RNY4P1	SAMM50P1	SPATA31A6	TPT1P9
NR4A3	OTX2P1	PTPN3	RNY4P18	SAXO1	SPATA31A7	TRAF1
NR5A1	PA2G4P6	PTS-P1	**ROR2**	SCAI	SPATA31C1	TRBV20OR9-2
NR6A1	PABPC1P11	PUS7P1	RORB	SCARNA8	SPATA31C2	TRBV21OR9-2
NRON	PAICSP1	RAB14	RPL10P3	SDR42E1P1	SPATA31E1	TRBV22OR9-2
NTRK2	PAICSP2	RAB1C	RPL21P82	SDR42E1P2	SPIN1	TRBV23OR9-2
NUDT2	PALM2	RAB28P1	RPL21P83	SDR42E1P3	SPINK4	TRBV24OR9-2
NUTM2F	PAPPA	RAB28P2	RPL21P84	SDR42E1P4	SPTLC1	TRBV25OR9-2
NUTM2G	PAX5	RAB28P3	RPL21P85	SEC61B	STK33P1	TRBV26OR9-2
NXNL2	PBX3	RAB28P4	RPL21P86	SECISBP2	STOM	TRBV29OR9-2
OGN	PCA3	RABEPK	RPL21P87	SEMA4D	STOML2	TRBVAOR9-2
OLFML2A	PCAT7	RABGAP1	RPL24P8	SEPT7P7	STRBP	TRIM14
OMD	PCNPP2	RAD23B	RPL29P20	SERPINH1P1	STX17	TRIM32

Cfs15.3 cont.						
TRMO	TUBBP4	UGCG	VN1R52P	YBX1P6	ZFAND5	ZNF510
TRMT10B	TUSC1	UNC13B	VN2R3P	YRDCP1	ZFAND6P1	ZNF618
TRMT112P4	TXN	UNQ6494	VN2R6P	YRDCP2	ZFP37	ZNF658
TRPM3	TXNDC8	UPF3AP3	VN2R7P	YWHABP1	ZNF169	ZNF658B
TRPM6	UBA52P6	VCP	VPS13A	YWHAZP6	ZNF189	ZNF782
TRR-TCG6-1	UBAP1	VDAC1P11	WDR31	ZBTB26	ZNF322P1	ZNF883
TSTD2	UBAP2	VN1R47P	WDR38	ZBTB5	ZNF367	ZYG11AP1
TTLL11	UBE2R2	VN1R48P	WNK2	ZBTB6	ZNF462	
TUBB4BP2	UBE2V1P10	VN1R49P	XPA	ZCCHC6	ZNF483	
TUBB8P1	UBQLN1	VN1R51P	YBX1P10	ZCCHC7	ZNF484	

Cfs16.1						
ABR	CTC1	KDM6B	OR1D5	RPAIN	SNORD91A	TRT-AGT4-1
ACADVL	CTDNEP1	KIAA0753	OR1E1	RPL15P21	SNORD91B	TRW-CCA1-1
ACAP1	CTNS	KIF1C	OR1E2	RPL19P18	SOX15	TRW-CCA3-1
ADPRM	CXCL16	KRBA2	OR1E3	RPL21P122	SPAG7	TSR1
AIPL1	CYB5D1	MAGOH2P	OR1G1	RPL21P125	SPATA22	TUSC5
ALOX12	CYB5D2	MAP2K4	OR1P1	RPL23AP73	SPDYE4	TXNDC17
ALOX12B	DERL2	MED11	OR1R1P	RPL26	SPEM1	TXNP4
ALOX12P2	DHRS7C	MED31	OR3A1	RPL29P2	SPNS2	UBE2G1
ALOX15	DHX33	METTL16	OR3A2	RPL7AP64	SPNS3	USP43
ALOX15B	DLG4	MFSD1P1	OR3A3	RPS12P29	SRR	USP6
ALOX15P1	DNAH2	MFSD6L	OR3A4P	RPS26P53	STX8	VAMP2
ALOXE3	DNAH9	MINK1	OR3A5P	RPS27AP1	TAX1BP3	VMO1
ALOXE3P1	DPH1	MIS12	OVCA2	RTN4RL1	TEKT1	WDR81
ANKFY1	DVL2	MNT	P2RX1	RYKP1	TLCD2	WRAP53
ARHGEF15	EFNB3	MPDU1	P2RX5	SAMD11P1	TM4SF5	WSCD1
ARRB2	EIF4A1	MRPL14P1	**PAFAH1B1**	SAT2	TMEM102	XAF1
ASGR1	EIF4A1P9	MYBBP1A	PELP1	SCARF1	TMEM107	YBX2
ASGR2	EIF5A	MYH1	PER1	SCARNA21	TMEM220	YWHAE
ASPA	ELP5	MYH10	PFAS	SCIMP	TMEM256	ZBTB4
ATP1B2	EMC6	MYH13	PFN1	SCO1	TMEM88	ZFP3
ATP2A3	ENO3	MYH2	PHF23	SENP3	TMEM95	ZMYND15
ATP6V0CP1	FAM64A	MYH3	PIK3R5	SERPINF1	TNFSF12	ZNF18
AURKB	FBXO39	MYH4	PIK3R6	SERPINF2	TNFSF13	ZNF232
BCL6B	FGF11	**MYH8**	PIRT	SGSM2	TNK1	ZNF594
BHLHA9	FXR2	MYHAS	PITPNA	SHBG	**TP53**	ZZEF1
BORCS6	GABARAP	MYO1C	PITPNM3	SHISA6	TRAPPC1	
BTF3P14	GAS7	MYOCD	PLD2	SHPK	TRD-GTC2-9	
C1QBP	GGT6	NAA38	PLSCR3	SLC13A5	TRG-GCC2-4	
CAMKK1	GLP2R	NCBP3	POLR2A	SLC16A11	TRG-TCC3-1	
CAMTA2	GLTPD2	NDEL1	PRPF8	SLC16A13	TRI-AAT4-1	
CCDC42	GP1BA	NEURL4	PSMB6	SLC25A11	TRI-AAT5-2	
CCDC90AP1	GPS2	NLGN2	RABEP1	SLC25A35	TRK-TTT3-4	
CD68	GSG1L2	NLRP1	RANGRF	SLC2A4	TRL-TAG1-1	
CFAP52	GSG2	NPM1P45	RAP1GAP2	SLC35G6	TRP-CGG1-3	
CHD3	GUCY2D	NTN1	RCVRN	SLC43A2	TRPV1	
CHRNB1	HES7	NUP88	RILP	SLC52A1	TRPV3	
CHRNE	HIC1	ODF4	RNA5SP434	SMG6	TRQ-CTG1-2	
CLDN7	HNRNPA1P16	OR1A1	RNASEK	SMTNL2	TRR-TCT2-1	
CLEC10A	INCA1	OR1A2	RNF167	SMYD4	TRS-AGA2-1	
CLUH	INPP5K	OR1AC1P	RNF222	SNORA48	TRS-CGA1-1	
CNTROB	ITGAE	OR1D2	RNU7-31P	SNORA67	TRS-GCT4-2	
CRK	KCNAB3	OR1D3P	RNU7-43P	SNORD10	TRT-AGT1-1	
CTB-41I6	KCTD11	OR1D4	RPA1	SNORD118	TRT-AGT1-2	

Cfs16.3						
AANAT	BTBD17	CYCSP40	FSCN2	ITGB4	KRTAP3-3	MGC57346
AARSD1	BZRAP1	CYGB	FTSJ3	JMJD6	KRTAP3-4P	MIF4GD
AATK	C1QL1	CYTH1	FZD2	JUP	KRTAP4-1	MILR1
ABCA10	C1QTNF1	DBF4B	G6PC	KANSL1	KRTAP4-11	MINOS1P2
ABCA5	CA4	DCAF7	G6PC3	KAT2A	KRTAP4-12	MKS1
ABCA6	CACNG1	DCAKD	GAA	KCNH4	KRTAP4-16P	MLX
ABCA8	CACNG4	DCXR	GALK1	KCNH6	KRTAP4-2	MPO
ABCA9	CACNG5	DDX42	GALR2	KCNJ16	KRTAP4-3	MPP2
ACBD4	CALM2P1	DDX5	GAST	**KCNJ2**	KRTAP4-4	MPP3
ACE	CANT1	DHX40	GCGR	KCTD2	KRTAP4-5	MRC2
ACE3P	CARD14	DHX58	GDPD1	KIF18B	KRTAP4-6	MRPL12
ACLY	CASC17	DHX8	GFAP	KIF19	KRTAP4-7	MRPL38
ACOX1	CASKIN2	DNAH17	GGA3	KLHL10	KRTAP4-8	MRPS7
ACTG1	CBX2	DNAI2	GH1	KLHL11	KRTAP4-9	MSX2P1
ADAM11	CBX4	DNAJC7	GH2	KPNA2	KRTAP9-1	MTMR4
AFMID	CBX8	DND1P1	GHDC	**KRT10**	KRTAP9-11P	MXRA7
ALYREF	CCDC103	DND1P2	GJC1	KRT12	KRTAP9-12P	MYADML2
AMZ2	CCDC137	DUS1L	GNA13	KRT13	KRTAP9-2	MYL6P5
AMZ2P1	CCDC40	DUSP3	GPATCH8	KRT14	KRTAP9-3	MYO15B
ANAPC11	CCDC43	EEF1DP7	GPR142	KRT15	KRTAP9-4	NACA2
AOC2	CCDC47	EFCAB3	GPRC5C	KRT16	KRTAP9-6	NAGLU
AOC3	CCDC57	**EFTUD2**	GPS1	**KRT17**	KRTAP9-7	NAGS
AOC4P	CCR10	EIF1	GRB2	KRT18P61	KRTAP9-8	NARF
APOH	CD300A	EIF4A3	GRIN2C	KRT19	KRTAP9-9	NAT9
APPBP2	CD300C	EIF5AP2	GRN	KRT20	LACAT1	NBR1
ARHGAP27	CD300E	ENDOV	H3F3B	KRT23	LGALS3BP	NBR2
ARHGDIA	CD300LB	ENGASE	HAP1	KRT31	LIMD2	NDUFB8P2
ARL16	CD300LD	ENPP7	HCRT	KRT32	LLGL2	NKIRAS2
ARL17A	CD300LF	ENTHD2	HDAC5	KRT33A	LPO	NMT1
ARL17B	CD300LG	EPX	HEATR6	KRT33B	LRRC37A	NOL11
ARL2BPP9	CD7	ERN1	HELZ	KRT34	LRRC37A	NOTUM
ARL4D	CD79B	ETV4	HEXDC	KRT35	LRRC37A10P	NPB
ARMC7	CDC42EP4	EVPL	HEXIM1	KRT36	LRRC37A16P	NPLOC4
ARSG	CDK3	EXOC7	HEXIM2	KRT37	LRRC37A2	NPTX1
ASB16	CDR2L	EZH1	HGS	KRT38	LRRC37A3	NSF
ASPSCR1	CEP112	FAAP100	HID1	KRT39	LRRC37A4P	NSFP1
ATF4P3	CEP131	FADS6	HIGD1B	KRT40	LRRC45	NT5C
ATG12P1	CEP295NL	FAM104A	HMGB3P27	KRT41P	LSM12	NT5C3B
ATP5H	CEP95	FAM106DP	HMGN1P28	KRT42P	MAFG	NUP85
ATP5J2P4	CH17-351M24	FAM134C	HMGN1P29	KRT43P	MAP2K6	OGFOD3
ATP5LP6	CHMP6	FAM171A2	HMGN2P15	KRT9	MAP3K14	OR4D1
ATP5LP7	CLTC	FAM195B	HMGN2P42	KRTAP1-1	MAP3K3	OR4D2
ATP6V0A1	CNP	FAM20A	HMGN2P43	KRTAP1-3	MAPK8IPP	OTOP2
ATXN7L3	CNTD1	FAM215A	HN1	KRTAP1-4	MAPT	OTOP3
AXIN2	CNTNAP1	FASN	HP09025	KRTAP1-5	MAPT-IT1	OXLD1
B3GNTL1	COA3	FBF1	HSD17B1	KRTAP16-1	MAR10	P3H4
BAHCC1	COASY	FBXO36P1	HSD17B1P1	KRTAP17-1	MED13	P4HB
BAIAP2	COG1	FDXR	HSF5	KRTAP2-1	MEIOC	PCYT2
BCAS3	CPSF4L	FKBP10	HSPB9	KRTAP2-2	MEOX1	PDE6G
BECN1	CRHR1	FLJ45079	ICAM2	KRTAP2-3	METRNL	PECAM1
BIRC5	CSH1	FMNL1	ICT1	KRTAP2-4	METTL23	PGS1
BPTF	CSH2	FN3K	IFI35	KRTAP2-5P	METTL2A	PITPNC1
BRCA1	CSHL1	FN3KRP	IGBP1P2	KRTAP29-1	MFSD11	PLCD3
BRCA1P1	CSNK1D	FOXJ1	INTS2	KRTAP3-1	MGAT5B	PLEKHH3
BRIP1	CYB561	FOXK2	ITGA2B	KRTAP3-2	MGC16275	PLEKHM1

Cfs16.3 cont.						
PLEKHM1P1	RAMP2	RPL32P32	SGSH	SOCS3	TEX19	TUBG2
POLG2	PRO1804	RPL32P33	SH3GL1P3	SOST	TEX2	UBALD2
POLR3KP2	PRPSAP1	RPL34P30	SHC1P2	**SOX9**	THA1P	UBE2O
POLRMTP1	RBFOX3	RPL36AP46	SIRT7	SPATA32	TIMP2	UBE2V2P2
PP13	RECQL5	RPL36AP47	SKA2	SPDYE22P	TK1	UBTF
PPM1D	RFNG	RPL36AP48	SLC16A3	SPHK1	TLK2	UNC13D
PPM1E	RGS9	RPL36AP7	SLC16A5	SPPL2C	**TMC6**	UNK
PPP1R27	RHBDF2	RPL38	SLC16A6	SRP68	TMC8	USH1G
PPY	RNA5SP444	RPL6P26	SLC16A6P1	SRSF2	TMEM101	USP32
PRCD	RNA5SP445	RPL7L1P5	SLC25A10	SSTR2	TMEM104	USP32P4
PRELID3BP3	RNA5SP446	RPL7P49	SLC25A19	ST6GALNAC1	TMEM105	USP36
PRKAR1A	RNA5SP447	RPL9P29	SLC25A39	ST6GALNAC2	TMEM106A	UTS2R
PRKCA	RND2	RPLP2P5	SLC26A11	STAT3	TMEM235	VAT1
PRR11	RNF157	RPS10P26	SLC38A10	STAT5A	TMEM94	VMP1
PRR29	RNF157-AS1	RPS12P30	SLC39A11	STAT5B	TMEM99	VPS25
PRR29-AS1	RNF213	RPS23P7	SLC4A1	STH	TMUB2	WBP2
PSMC3IP	RNF43	RPS26P8	SLC9A3R1	STRA13	TNRC6C	WDR45B
PSMC5	RNFT1	RPS29P21	SMARCD2	STRADA	TRIM37	WFDC21P
PSMD12	RNU2-1	RPS6KB1	SMCO4P1	SUMO2	TRIM47	WHSC1L2P
PSMD7P1	RNU2-4P	RPS7P11	SMG8	SUPT4H1	TRIM65	WIPI1
PSME3	RNU7-52P	RPTOR	SMIM5	SYNGR2	TRMT112P3	WNK4
PTGES3L	RNY4P2	RUNDC1	SMIM6	TACO1	TRR-CCG2-1	**WNT3**
PTP4A2P1	RPL12P37	RUNDC3A	SMURF2	TANC2	TRR-CCT1-1	**WNT9B**
PTRF	RPL12P38	SAP30BP	SNHG16	TBC1D16	TRR-CCT2-1	YPEL2
PTRH2	RPL17P41	SCARNA16	SNHG20	TBC1D3P1	TRR-TCG3-1	ZACN
PYCR1	RPL21P4	SCARNA20	SNHG25	TBC1D3P2	TRSUP-TTA1-1	ZNF385C
PYY	RPL23AP74	**SCN4A**	SNORA38B	TBCD	TRX-CAT1-2	ZNF750
QRICH2	RPL23AP87	SDK2	SNORA50C	TBX2	TSEN54	ZNF848P
RAB37	RPL27	SEC14L1	SNORD104	TBX2-AS1	TSPAN10	
RAB40B	RPL29P31	SECTM1	SNORD1A	TBX4	TTC25	
RAB5C	RPL31P57	SEPT4	SNORD1B	TCAM1P	TTYH2	
RAC3	RPL31P7	SEPT9	SNORD1C	TEN1	TUBD1	
RAD51C	RPL32P31	SETP3	SNRPGP4	TEX14	TUBG1	

APPENDIX E

LINKAGE SIGNALS

Table E1 Individual-trait Peaks. Location of both suggestive and significant linkage signals and the corresponding QTLs for ECV and the EIDs for all three models: (1) overall, (2) cranial, and (3) regional.

Trait	Human Ortholog	Covariate Model	LOD Score[a]	Peak Locus (CI)[b]	QTL Name[c]
ECV	2q	Model 1	1.65	30 (4-108)	*Cfs12.1*
		Model 2	1.59	32 (0-104)	
	6	Model 2	1.91	104 (89-122)	*Cfs4.4*
		Model 3	1.66	102 (85-121)	
	9	Model 1	1.34	54 (0-80)	*Cfs15.3*
		Model 2	1.88	71 (30-79)	
		Model 3	2.60	69 (58-80)	
	14_15	Model 1	2.02	95 (64-104)	*Cfs7.4*
		Model 2	2.27	96 (69-104)	
		Model 3	1.91	97 (67-112)	
	18	Model 1	1.44	39 (25-60)	*Cfs18.2*
		Model 2	1.35	39 (25-86)	
		Model 3	1.70	39 (25-63)	
ACPM	1	Model 1	2.49	133 (119-149)	*Cfs1.4*
		Model 2	2.51	130 (119-147)	
		Model 3	2.10	136 (117-154)	
	7_21	Model 3	1.53	70 (30-100)	*Cfs3.1*
	7_21	Model 1	2.68	173 (156-195)	*Cfs3.3*
		Model 2	1.89	172 (155-187)	
ACSY	7_21	Model 3	1.91	132 (77-145)	*Cfs3.2*
	14_15	Model 1	1.71	78 (20-95)	*Cfs7.4*
		Model 2	1.96	78 (75-84)	
		Model 3	1.53	79 (69-95)	
PMPM	7_21	Model 1	1.71	145 (110-170)	*Cfs3.3*
	9	Model 2	1.61	134 (117-134)	*Cfs15.5*
		Model 3	1.56	134 (65-134)	
	16	Model 1	1.65	48 (20-80)	*Cfs20.1*
		Model 2	2.65	44 (27-73)	
		Model 3	1.50	44 (20-80)	
ASJP	5	Model 1	1.89	112 (95-127)	*Cfs6.4*
		Model 2	1.97	112 (100-124)	
		Model 3	1.70	112 (85-130)	
	8	Model 1	1.57	44 (20-60)	*Cfs8.2*
		Model 2	1.77	43 (25-55)	
		Model 3	1.76	43 (20-55)	
BACC	1	Model 2	1.30	100 (65-165)	*Cfs1.3*
		Model 3	1.55	99 (70-120)	
	7_21	Model 2	1.37	175 (162-183)	*Cfs3.3*
		Model 3	3.14	161 (147-182)	
	20_22	Model 2	1.96	116 (109-129)	*Cfs10.2*
		Model 3	1.71	116 (100-130)	
BAOP	11	Model 1	2.05	15 (0-69)	*Cfs14.1*
		Model 2	2.30	8 (1-39)	
		Model 3	2.09	17 (0-43)	
ASAS	6	Model 1	1.68	21 (1-40)	*Cfs4.1*
		Model 2	2.16	10 (3-28)	
	12	Model 1	2.21	56 (38-69)	*Cfs11.2*
		Model 2	1.96	56 (37-73)	
	14_15	Model 1	1.79	13 (0-39)	*Cfs7.1*
		Model 2	1.37	16 (0-43)	
		Model 3	1.79	18 (0-60)	

Trait	Human Ortholog	Covariate Model	LOD Score[a]	Peak Locus (CI)[b]	QTL Name[c]
	18	Model 1	1.54	37 (10-85)	*Cfs18.2*
		Model 2	1.78	37 (24-43)	
		Model 3	1.69	37 (15-45)	
	X	Model 3	1.79	3 (0-42)	---
JPJP	6	Model 1	1.54	127 (95-140)	*Cfs4.4*
		Model 2	2.15	124 (96-140)	
	14_15	Model 1	1.52	131 (105-145)	*Cfs7.5*
		Model 2	1.61	127 (106-145)	
	20_22	Model 3	1.58	105 (95-120)	*Cfs10.2*
4141	---	---	---	---	---
POPO	7-21	Model 3	3.19	151 (113-168)	*Cfs3.3*
	19	Model 1	2.68	88 (68-104)	*Cfs19.3*
PTPT	14_15	Model 1	1.69	18 (3-31)	*Cfs7.1*
		Model 2	1.72	16 (1-30)	
STST	2q	Model 1	3.59	91 (86-97)	*Cfs12.3*
		Model 2	3.07	90 (86-100)	
		Model 3	3.06	90 (86-100)	
	4	Model 2	1.88	34 (16-43)	*Cfs5.1*
		Model 3	1.94	33 (17-42)	
	10	Model 2	1.74	89 (70-104)	*Cfs9.2*
		Model 3	1.81	89 (70-103)	
	14_15	Model 1	3.12	17 (4-28)	*Cfs7.1*
		Model 2	2.85	15 (1-42)	
		Model 3	2.90	15 (1-41)	
	17	Model 1	2.67	116 (88-160)	*Cfs16.3*
		Model 2	2.82	114 (88-160)	
		Model 3	2.82	116 (88-160)	
	20_22	Model 2	1.58	67 (27-85)	*Cfs10.1*
		Model 3	1.95	53 (41-85)	
	X	Model 1	1.46	24 (15-42)	---
		Model 2	1.64	24 (16-40)	
		Model 3	1.64	24 (16-40)	
ZTZT	4	Model 2	1.39	108 (85-135)	*Cfs5.3*
		Model 3	1.98	123 (100-144)	
	7_21	Model 1	4.62	65 (52-81)	*Cfs3.1*
		Model 2	3.98	74 (54-104)	
		Model 3	2.55	76 (43-107)	
	X	Model 1	1.67	6 (0-42)	---
		Model 2	2.64	18 (2-42)	
		Model 3	2.27	16 (2-30)	
BRAS	---	---	---	---	---
BRLD	14_15	Model 1	1.91	33 (10-51)	*Cfs7.2*
		Model 2	2.68	32 (26-44)	
		Model 3	2.26	32 (26-44)	
BRNA	2p	Model 1	1.60	26 (8-85)	*Cfs13.1*
		Model 2	1.56	27 (5-90)	
	2q	Model 2	1.51	58 (20-85)	*Cfs12.1*
		Model 3	1.70	69 (35-80)	
	6	Model 1	1.93	103 (69-118)	*Cfs4.4*
		Model 2	2.89	105 (90-118)	
		Model 3	1.57	111 (65-125)	
	7_21	Model 1	2.10	118 (105-150)	*Cfs3.2*
		Model 2	1.34	117 (100-155)	
	8	Model 1	2.50	25 (8-35)	*Cfs8.1*
		Model 2	2.21	25 (9-35)	
		Model 3	1.81	25 (6-40)	
	9	Model 1	1.43	65 (31-80)	*Cfs15.3*
		Model 2	1.35	66 (30-85)	
		Model 3	1.65	65 (30-80)	
	14_15	Model 1	2.22	127 (114-143)	*Cfs7.5*
		Model 2	2.66	127 (116-141)	
		Model 3	2.26	130 (117-144)	
	X	Model 1	1.85	26 (14-34)	---

Trait	Human Ortholog	Covariate Model	LOD Score[a]	Peak Locus (CI)[b]	QTL Name[c]
		Model 2	1.69	25.5(10-40)	
		Model 3	1.72	22 (10-35)	
BRPT	2q	Model 1	2.04	87 (74-103)	*Cfs12.3*
		Model 2	1.36	93 (75-105)	
		Model 3	1.46	93 (75-105)	
	16	Model 1	1.57	64 (34-89)	*Cfs20.1*
		Model 2	2.01	53 (31-87)	
		Model 3	1.94	53 (31-90)	
	X	Model 1	1.91	42 (24-42)	---
		Model 2	1.45	42 (15-52)	
		Model 3	1.42	42 (15-42)	
NABA	2q	Model 1	1.66	129 (115-146)	*Cfs12.4*
	6	Model 1	1.31	105 (90-130)	*Cfs4.4*
		Model 2	1.92	108 (96-129)	
		Model 3	1.56	124 (95-135)	
	7_21	Model 1	2.10	73 (56-109)	*Cfs3.1*
		Model 2	2.56	75 (63-113)	
		Model 2	2.40	99 (62-120)	
	10	Model 3	1.89	125 (90-125)	*Cfs9.3*
	12	Model 1	1.78	103 (86-111)	*Cfs11.4*
		Model 2	2.67	104 (95-112)	
CACP	5	Model 1	1.55	18 (0-42)	*Cfs6.1*
		Model 2	1.54	7 (0-35)	
		Model 3	1.57	12 (0-40)	
	12	Model 1	2.32	63 (58-74)	*Cfs11.3*
		Model 2	2.19	63 (58-72)	
		Model 3	2.63	63 (59-72)	
CPSL	3	Model 1	3.46	30 (10-40)	*Cfs2.2*
		Model 2	3.43	30 (13-41)	
		Model 3	3.33	30 (14-41)	
	7_21	Model 1	1.77	81 (50-140)	*Cfs3.1*
		Model 2	1.77	71 (42-113)	
		Model 3	1.68	71 (40-112)	
	7_21	Model 1	2.20	130 (113-140)	*Cfs3.2*
		Model 2	2.54	131 (123-143)	
		Model 3	2.34	131 (124-143)	
	19	Model 1	2.16	104 (98-104)	*Cfs19.4*
		Model 2	1.70	104 (98-104)	
CPZS	1	Model 1	1.82	201 (176-203)	*Cfs1.5*
	5	Model 2	1.33	99 (80-131)	*Cfs6.3*
		Model 3	2.91	95 (84-108)	
	7_21	Model 1	1.84	117 (87-133)	*Cfs3.2*
		Model 2	2.84	120 (92-131)	
	X	Model 1	1.68	34 (23-42)	---
		Model 3	1.60	34 (20-42)	
CNCN	13	Model 1	1.66	41 (15-59)	*Cfs17.1*
		Model 2	1.46	42 (5-60)	
		Model 3	1.71	42 (10-55)	
	19	Model 1	1.29	73 (0-100)	*Cfs19.3*
		Model 2	1.61	79 (3-96)	
		Model 3	1.37	79 (0-100)	
	X	Model 1	1.48	0 (0-42)	---
		Model 2	1.81	0 (0-19)	
		Model 3	2.02	0 (0-16)	
	X	Model 1	1.60	34 (0-42)	---
		Model 3	1.30	34 (0-42)	
FMPM	1	Model 2	1.92	52 (41-85)	*Cfs1.1*
		Model 3	1.73	47 (37-90)	
	1	Model 1	2.61	126 (118-138)	*Cfs1.4*
		Model 2	1.89	126 (117-166)	
	20_22	Model 1	1.43	137 (93-144)	*Cfs10.2*
		Model 2	2.44	121 (97-144)	
FMZT	2p	Model 1	1.62	80 (61-101)	*Cfs13.2*

Trait	Human Ortholog	Covariate Model	LOD Score[a]	Peak Locus (CI)[b]	QTL Name[c]
		Model 2	1.62	81 (56-104)	
		Model 3	1.71	84 (50-104)	
	13	Model 3	1.84	32 (16-50)	*Cfs17.1*
	14_15	Model 1	1.68	60 (47-105)	*Cfs7.3*
		Model 2	1.67	64 (47-105)	
		Model 3	1.70	93 (30-110)	
	X	Model 1	2.23	6 (0-21)	---
		Model 2	1.95	2 (0-42)	
		Model 3	1.57	10 (0-40)	
FMCP	1	Model 1	1.65	183 (149-203)	*Cfs1.5*
	6	Model 1	1.49	37 (26-85)	*Cfs4.2*
		Model 2	1.85	35 (25-60)	
		Model 3	1.29	27 (16-42)	
	7_21	Model 1	3.09	129 (118-142)	*Cfs3.2*
		Model 2	1.91	120 (103-149)	
	8	Model 3	1.71	91 (75-135)	*Cfs8.4*
	12	Model 1	2.49	35 (27-51)	*Cfs11.2*
		Model 2	1.75	38 (27-71)	
	X	Model 3	1.29	17 (0-42)	---
FMPT	---	---	---	---	---
LDAS	1	Model 1	1.55	132 (80-157)	*Cfs1.4*
		Model 2	1.55	107 (81-154)	
		Model 3	1.84	128 (95-150)	
	6	Model 1	1.55	25 (2-48)	*Cfs4.2*
		Model 2	1.54	35 (1-49)	
	7_21	Model 3	1.69	132 (100-140)	*Cfs3.2*
	X	Model 1	1.54	0 (0-10)	---
		Model 2	1.64	2 (0-9)	
		Model 3	2.11	2 (0-5)	
LDBA	2q	Model 1	1.83	95 (88-106)	*Cfs12.3*
		Model 2	2.17	100 (91-111)	
		Model 3	1.78	95 (86-114)	
	10	Model 1	2.01	33 (18-68)	*Cfs9.1*
		Model 2	3.10	29 (22-39)	
		Model 3	2.37	29 (20-51)	
	19	Model 1	2.21	104 (97-104)	*Cfs19.4*
		Model 2	2.16	104 (97-104)	
NANL	1	Model 1	1.31	79 (41-189)	*Cfs1.2*
		Model 2	1.83	78 (63-165)	
		Model 3	2.61	80 (71-177)	
	1	Model 1	1.33	109 (41-189)	*Cfs1.3*
		Model 2	1.76	107 (46-168)	
		Model 3	2.78	101 (72-175)	
	1	Model 1	1.87	125 (87-174)	*Cfs1.4*
		Model 2	1.95	125 (64-164)	
		Model 3	2.54	122 (71-178)	
	9	Model 1	1.30	125 (97-134)	*Cfs15.4*
		Model 2	1.28	125 (96-134)	
		Model 3	1.81	125 (100-134)	
	X	Model 1	1.79	29 (21-42)	---
		Model 2	1.33	28 (16-42)	
NLAC	1	Model 1	1.73	128 (102-146)	*Cfs1.4*
		Model 2	1.68	110 (99-150)	
	3	Model 1	1.99	52 (34-68)	*Cfs2.3*
		Model 2	2.19	50 (34-68)	
		Model 3	1.78	47 (24-71)	
	11	Model 1	1.62	74 (59-80)	*Cfs14.2*
		Model 2	1.65	75 (59-86)	
		Model 3	2.26	75 (60-79)	
	14_15	Model 1	2.09	81 (62-91)	*Cfs7.4*
		Model 2	1.43	82 (60-92)	
		Model 3	1.44	83 (55-95)	
NLVS	1	Model 2	1.57	81 (70-109)	*Cfs1.2*

Trait	Human Ortholog	Covariate Model	LOD Score[a]	Peak Locus (CI)[b]	QTL Name[c]
		Model 3	1.32	78 (50-110)	
	3	Model 1	1.42	93 (56-110)	*Cfs2.4*
		Model 2	1.87	93 (71-109)	
		Model 3	3.31	97 (75-109)	
	6	Model 2	2.07	34 (9-45)	*Cfs4.2*
	8	Model 1	1.34	69 (50-80)	*Cfs8.3*
		Model 2	1.93	69 (56-77)	
		Model 3	2.56	69 (56-76)	
	12	Model 1	1.99	72 (65-79)	*Cfs11.3*
		Model 2	1.59	72 (30-82)	
	14_15	Model 1	2.18	60 (46-72)	*Cfs7.3*
		Model 2	1.74	60 (41-83)	
		Model 3	2.22	57 (42-86)	
NAAC	1	Model 1	1.53	81 (60-160)	*Cfs1.2*
		Model 2	1.93	81 (63-135)	
		Model 3	2.88	80 (70-113)	
	12	Model 1	1.96	59 (38-73)	*Cfs11.2*
		Model 2	1.27	53 (25-105)	
NACA	2q	Model 1	1.58	145 (134-146)	*Cfs12.4*
	6	Model 1	1.35	35 (1-66)	*Cfs4.2*
		Model 2	1.76	35 (1-59)	
	13	Model 3	1.58	55 (40-80)	*Cfs17.1*
	18	Model 1	1.84	13 (0-26)	*Cfs18.1*
		Model 2	2.34	16 (3-28)	
	X	Model 2	1.72	1 (0-40)	---
NACP	6	Model 2	1.81	33 (19-44)	*Cfs4.2*
	7_21	Model 1	2.17	72 (58-82)	*Cfs3.1*
		Model 2	1.89	74 (58-147)	
	7_21	Model 1	2.61	129 (117-144)	*Cfs3.2*
		Model 2	1.54	136 (50-165)	
	11	Model 3	1.82	94 (82-125)	*Cfs14.3*
	12	Model 3	2.09	109 (95-123)	*Cfs11.4*
	19	Model 2	1.59	41 (25-65)	*Cfs19.2*
		Model 3	1.22	42 (15-67)	
	X	Model 3	1.56	17 (0-42)	---
		Model 3	1.83	37 (7-42)	
NAFM	6	Model 1	1.02	61 (23-90)	*Cfs4.3*
		Model 2	2.28	78 (61-106)	
	8	Model 3	1.65	11 (1-25)	*Cfs8.1*
	9	Model 1	1.61	0 (0-15)	*Cfs15.1*
	12	Model 1	3.24	36 (27-50)	*Cfs11.2*
		Model 2	3.36	41 (29-54)	
	12	Model 1	1.97	62 (19-94)	*Cfs11.3*
		Model 2	2.65	63 (26-91)	
		Model 3	1.57	63 (25-85)	
	17	Model 2	1.56	157 (137-160)	*Cfs16.3*
		Model 3	2.02	142 (118-157)	
NA41	1	Model 1	1.53	75 (57-147)	*Cfs1.2*
		Model 2	1.87	74 (56-132)	
		Model 3	2.99	76 (68-86)	
	1	Model 1	2.35	111 (92-139)	*Cfs1.4*
		Model 2	1.93	111 (57-144)	
		Model 3	1.68	111 (14-140)	
	4	Model 1	1.95	118 (113-132)	*Cfs5.3*
		Model 2	1.24	119 (50-145)	
		Model 3	2.85	118 (112-128)	
	8	Model 1	2.10	10 (1-23)	*Cfs8.1*
		Model 2	1.81	10 (1-29)	
	14_15	Model 2	1.39	89 (73-145)	*Cfs7.4*
		Model 3	2.66	94 (83-103)	
	X	Model 1	1.60	37 (18-42)	---
		Model 2	1.65	37 (13-42)	
NAVS	2q	Model 1	3.59	61 (54-78)	*Cfs12.2*

Trait	Human Ortholog	Covariate Model	LOD Score[a]	Peak Locus (CI)[b]	QTL Name[c]
		Model 2	2.45	61 (43-84)	
	2q	Model 1	1.96	88 (32-106)	*Cfs12.3*
		Model 2	2.33	90 (39-106)	
		Model 3	1.25	90 (30-146)	
	2q	Model 1	3.55	139 (133-146)	*Cfs12.4*
		Model 2	2.40	139 (124-146)	
		Model 3	2.30	139 (133-146)	
	7_21	Model 1	1.26	87 (44-150)	*Cfs3.1*
		Model 2	1.57	93 (61-132)	
	12	Model 1	2.32	89 (78-101)	*Cfs11.4*
		Model 2	2.20	91 (78-114)	
NAZI	---	---	---	---	---
NAZS	3	Model 1	3.34	69 (46-83)	*Cfs2.3*
		Model 2	2.22	66 (39-84)	
		Model 3	1.95	66 (47-85)	
	7_21	Model 3	1.82	58 (30-108)	*Cfs3.1*
	12	Model 1	1.39	60 (15-95)	*Cfs11.2*
		Model 2	2.67	44 (18-57)	
		Model 3	1.33	42 (13-90)	
	16	Model 1	1.63	77 (53-100)	*Cfs20.2*
		Model 2	2.13	77 (66-106)	
	17	Model 3	2.60	117 (100-134)	*Cfs16.3*
BRBA	3	Model 1	1.95	14 (0-25)	*Cfs2.1*
		Model 2	1.71	15 (0-28)	
		Model 3	1.41	18 (0-35)	
	7_21	Model 1	3.92	65 (51-80)	*Cfs3.1*
		Model 2	2.71	65 (47-82)	
		Model 3	2.14	58 (39-80)	
	9	Model 1	1.41	42 (10-58)	*Cfs15.2*
		Model 2	1.93	36 (13-53)	
		Model 3	1.36	28 (0-65)	
	10	Model 1	1.69	69 (21-113)	*Cfs9.2*
		Model 2	2.53	73 (46-113)	
		Model 2	2.55	97 (46-113)	
		Model 3	2.88	95 (63-110)	
	12	Model 1	1.56	108 (99-127)	*Cfs11.4*
	14_15	Model 1	1.90	39 (19-55)	*Cfs7.2*
		Model 2	1.95	35 (17-56)	
NALD	7_21	Model 1	1.68	196 (189-196)	*Cfs3.3*
	8	Model 1	1.72	69 (35-89)	*Cfs8.3*
		Model 2	1.52	59 (19-90)	
	9	Model 1	2.81	61 (58-66)	*Cfs15.3*
		Model 2	2.94	61 (58-65)	
		Model 3	1.62	61 35-90)	
	10	Model 3	2.16	38 (21-82)	*Cfs9.1*
DAFM	3	Model 1	1.56	38 (0-74)	*Cfs2.2*
	6	Model 1	2.10	36 (13-85)	*Cfs4.2*
		Model 2	1.85	35 (15-55)	
	12	Model 1	2.09	62 (27-89)	*Cfs11.3*
		Model 2	2.73	63 (31-87)	
		Model 3	2.14	63 (58-75)	
	14_15	Model 2	1.60	38 (28-51)	*Cfs7.2*
PLSY	6	Model 1	2.91	0 (0-51)	*Cfs4.1*
		Model 1	3.13	45 (0-50)	
		Model 2	3.42	0 (0-41)	
		Model 2	2.89	33 (0-47)	
		Model 3	3.24	0 (0-39)	
		Model 3	3.13	29 (0-40)	
POBA	2q	Model 1	1.64	105 (66-139)	*Cfs12.3*
		Model 2	1.26	105 (45-140)	
	5	Model 1	1.26	48 (20-85)	*Cfs6.2*
		Model 2	2.01	56 (30-69)	
	6	Model 3	1.54	25 (10-34)	*Cfs4.1*

Trait	Human Ortholog	Covariate Model	LOD Score[a]	Peak Locus (CI)[b]	QTL Name[c]
	7_21	Model 3	5.29	189 (174-195)	*Cfs3.3*
PM41	3	Model 1	2.56	52 (40-61)	*Cfs2.3*
		Model 2	1.91	51 (37-65)	
	10	Model 2	1.46	19 (5-34)	*Cfs9.1*
		Model 3	1.68	19 (5-30)	
	X	Model 3	1.33	30 (0-42)	---
41MX	1	Model 1	1.63	126 (100-155)	*Cfs1.4*
		Model 2	1.95	126 (98-145)	
	8	Model 1	1.46	29 (7-55)	*Cfs8.1*
		Model 2	1.57	20 (6-55)	
		Model 3	1.37	29 (5-50)	
	20_22	Model 1	1.84	103 (93-125)	*Cfs10.2*
		Model 2	1.72	103 (93-132)	
41ZI	10	Model 1	1.35	125 (115-125)	*Cfs9.3*
		Model 2	1.90	125 (116-125)	
		Model 3	1.96	125 (105-125)	
	20_22	Model 1	1.53	135 (106-144)	*Cfs10.2*
		Model 2	1.40	130 (108-142)	
	X	Model 2	1.52	3 (0-14)	---
		Model 3	2.68	3 (0-13)	
PTAS	2p	Model 1	1.68	15 (0-32)	*Cfs13.1*
		Model 2	2.86	17 (4-27)	
		Model 3	2.44	15 (2-26)	
	2q	Model 2	1.72	95 (70-108)	*Cfs12.3*
		Model 3	1.61	95 (55-110)	
	17	Model 1	2.75	23 (13-31)	*Cfs16.1*
		Model 2	1.76	23 (12-34)	
		Model 3	1.78	23 (11-35)	
PTLD	9	Model 1	3.02	61 (54-69)	*Cfs15.3*
		Model 2	3.43	61 (53-67)	
		Model 3	2.72	60 (49-71)	
	20_22	Model 1	1.67	86 (82-91)	*Cfs10.1*
		Model 2	1.22	86 (79-94)	
SLBA	3	Model 1	1.29	106 (80-135)	*Cfs2.4*
		Model 2	1.50	106 (81-128)	
		Model 3	1.64	97 (60-129)	
	4	Model 1	1.33	70 (46-104)	*Cfs5.2*
		Model 2	1.48	70 (48-99)	
		Model 3	1.70	70 (45-100)	
	19	Model 1	2.13	16 (13-35)	*Cfs19.1*
		Model 2	1.39	16 (5-50)	
		Model 3	1.66	16 (9-50)	
SLCC	7_21	Model 1	1.73	178 (163-193)	*Cfs3.3*
		Model 2	1.84	172 (163-190)	
		Model 3	2.53	170 (163-179)	
SYBA	1	Model 2	1.38	137 (90-158)	*Cfs1.4*
		Model 3	1.67	137 (95-160)	
SYMX	2p	Model 1	1.54	78 (62-100)	*Cfs13.2*
		Model 2	1.40	88 (60-104)	
		Model 3	1.72	90 (60-104)	
	2q	Model 3	2.08	61 (55-63)	*Cfs12.2*
	6	Model 1	1.62	1 (0-60)	
		Model 2	1.70	1 (0-57)	
		Model 3	2.91	20 (0-36)	
	9	Model 1	1.76	39 (12-72)	*Cfs15.2*
	14_15	Model 1	1.91	100 (87-138)	*Cfs7.4*
		Model 2	1.80	78 (47-86)	
		Model 3	1.57	94 (70-125)	
ZTPO	12	Model 1	1.91	127 (115-127)	*Cfs11.5*
ZTVS	4	Model 2	1.75	50 (42-71)	*Cfs5.2*
		Model 3	2.20	66 (59-72)	
	4	Model 3	1.74	121 (90-133)	*Cfs5.3*
	6	Model 1	1.54	66 (44-84)	*Cfs4.3*

Trait	Human Ortholog	Covariate Model	LOD Score[a]	Peak Locus (CI)[b]	QTL Name[c]
	7_21	Model 1	4.07	71 (53-79)	*Cfs3.1*
		Model 2	2.71	71 (53-81)	
		Model 3	1.33	71 (30-115)	
	12	Model 1	1.55	0 (0-5)	*Cfs11.1*
		Model 2	1.56	0 (0-4)	
	X	Model 1	1.21	15 (0-42)	---
		Model 2	2.39	19 (12-34)	
		Model 3	2.09	19 (0-29)	
ZTZI	1	Model 1	1.28	51 (35-77)	*Cfs1.1*
		Model 2	1.59	52 (39-70)	
		Model 3	1.67	52 (35-70)	
	12	Model 1	2.16	7 (0-16)	*Cfs11.1*
		Model 2	2.75	6 (0-14)	
		Model 3	2.45	7 (0-15)	
VSBA	2q	Model 2	1.97	102 (88-110)	*Cfs12.3*
		Model 3	1.66	100 (86-110)	
	12	Model 1	2.04	92 (84-96)	*Cfs11.4*
	16	Model 1	1.34	97 (60-106)	*Cfs20.2*
		Model 2	1.47	97 (66-106)	
		Model 3	1.80	97 (65-106)	
VSSY	2p	Model 1	1.85	102 (87-104)	*Cfs13.2*
		Model 2	1.80	99 (86-104)	
		Model 3	1.80	102 (87-104)	
	6	Model 1	2.70	7 (0-35)	*Cfs4.1*
		Model 2	3.25	6 (0-34)	
		Model 3	3.19	6 (0-32)	
	12	Model 1	1.64	36 (26-71)	*Cfs11.2*
ZIMX	X	Model 2	2.04	5 (0-20)	---
		Model 3	1.54	5 (0-40)	
ZSNL	9	Model 3	1.66	123 (95-134)	*Cfs15.4*
	17	Model 3	1.76	79 (35-94)	*Cfs16.2*
	20_22	Model 1	1.47	112 (90-127)	*Cfs10.2*
		Model 2	1.76	110 (94-126)	
	X	Model 1	1.67	29 (21-40)	---
		Model 3	1.78	27 (15-40)	

[a]Traits with LOD scores above the significance threshold (LOD ≥ 2.75) are indicated in red typeface. The gray shading is simply to help with ease of reading by clearly delineating each QTL. [b]Loci are given in cM mapping units. [c]QTL names correspond to those provided in Table 6.3. As individual QTLs were not defined on the X-chromosome, any such linkage signals are designated with a series of three dashes.